Lithostratigraphy and tectonic evolution of the north-eastern Bornu basin, from integrated surface and subsurface interpretation

By

Aminu Abdullahi Isyaku

BSc (Geology), MSc (Engineering Geology)

Thesis submitted in partial fulfilment of the requirements for the award of the degree of

Doctor of Philosophy of the University of Portsmouth
United Kingdom

July 2018

Abstract

Surface and subsurface structural lineaments are important in understanding tectonic movements and oil and gas trapping architecture in sedimentary basins. However, good exposures of these geological features are always lacking in semi-arid regions with extensive surficial sediment cover. An integrated multisource data analysis is applied to constrain the tectonic setting, structure and lithostratigraphy of the north-eastern Bornu basin, which were previously poorly understood. Detailed geological analyses are based on integration and geospatial correlations of surface datasets, including optical, radar and DEM Earth Observation imageries with subsurface datasets, including, seismic, well log, gravity and aeromagnetic. The Bornu basin, situated in the West African Rift System (WARS), overlain by Quaternary - Recent sediments is found herein to contain > 5000 m thick of Cretaceous rocks overlying the Precambrian basement migmatite-gneiss complex. New insights into the basin evolution model from pre-rift to post-rift tectonic settings are developed using deductions from the integrated studies herein. This study outlines additional tectonic regimes that were not identified in the previous tectonic model for the basin including: (1) Barremian (120 Ma), (2) Late Aptian – Early Albian (101 Ma), Late Santonian (84 Ma) and (4) Quaternary – Recent. Furthermore, the research identified that basement control, pre-existing basement lineaments, transfer faulting and upward fault propagation have all influenced the tectonic evolution of the basin. Lithology and stratigraphy of the subsurface formations are mapped using Combined Log Pattern (CLP) method adapted herein involving Gamma Ray, Resistivity, Bulk Density and Sonic logs. Four subsurface stratigraphic formations including Bima, Gongila, Fika and Chad Formations are mapped from validated seismic and well log stratigraphy in the north-eastern Bornu basin. Predictive Spectral Lithological (PSL) units mapped represent the various surface Quaternary-Recent deposits in the area using improved spectral mapping approach involving

combined band combination, band ratio and Spectral Angle Mapper (SAM) supervised classification. Geospatial correlations and interpretations of lineaments indicate that the north-eastern Bornu basin is controlled by two predominant lineament systems trending NE-SW and NW-SE. The geospatial correlation method visually illustrates linkages between subsurface tectonic lineaments and lithostratigraphy with the surface structures. Accordingly, the geospatial correlation has established the relationship between the palaeoshoreline and palaeodrainage systems with the subsurface structural setting of the basin. Relationships of the main structural systems in the north-eastern Bornu basin may have developed potential oil and gas trapping systems associated with the regional pattern. Two potential petroleum systems from pre-rift to post rift tectonic regimes derived from the tectonic evolution model of the basin developed herein are presented. The Tertiary non-deposition in the north-eastern Bornu basin is determined to be due to a pinch out of the Tertiary Kerri-Kerri Formation that extends from the Benue trough and terminated near the Maiduguri area.

Thesis Declaration

“Whilst registered as a candidate for the above degree, I have not been registered for any other research award. The results and conclusions embodied in this thesis are the work of the named candidate and have not been submitted for any other academic award.”

Table of Contents

Chapter 5:

Chapter 7:

Discussions on tectono-lithostratigraphic analysis of the evolution and hydrocarbon potential of the north-eastern Bornu basin from surface and subsurface correlation 237

List of figures

27. Fig. 4.14: Band ratio 3/1 image for the 185/051 path/row Landsat 7 ETM+ image showing the different spectral responses of the lithological compositions in different contrasts.

28. Fig. 4.15: Band ratio 5/7 image for the 185/051 path/row Landsat 7 ETM+ image showing the different spectral responses of the lithological compositions in different contrasts.

29. Fig. 4.16: Band ratio 5/4 image for the 185/051 path/row Landsat 7 ETM+ image showing the different spectral responses of the lithological compositions in different contrasts.

30. Fig 4.17. End member regions of interests (ROIs) 1-6 collected from the study area as training classes for the SAM supervised classification collected from the Landsat 7 ETM+ path/row 185/051 image.

31. Fig 4.18. Spectral profiles of training classes 1 and 2 representing Lake Chad and the vegetation cover respectively shown on Fig 4.17, compared with their corresponding profiles below from the John Hopkins vegetation and lake water Spectral Library samples in ENVI showing high degree of equivalence, thus validating the two non-lithological materials. These materials are however automatically mapped because the SAM supervised classification presents the spectral properties of all pixels in the image.

32. Fig 4.19. Spectral profiles of the remaining four lithological spectral end members (3 - 6) captured from the spectral training classes and representing PSL Units (1-4) respectively in Fig 4.17. The end-members 1 and 2 representing Lake and vegetation are shown on Fig 4.18.

33. Fig. 4.20: Landsat 7 ETM+ path/row 185/051 image indicating the PSL Units interpreted from the selected band ratios. The images are same with those in Figs 4.14 – 4.16 arranged here for comparison.

34. Figures (4.21): (a) Landsat 7 ETM+ image seamless mosaic clip of the north-eastern Bornu basin (b) Result of the SAM classification of various surface lithological materials in the north eastern Bornu basin processed from Fig. 4.21 (a). (c) Digitised version of the SAM classification map showing the surficial geological map of the north eastern Bornu basin produced from Fig. 4.21 (b,) after all image processing edge artefacts are removed. Lithology identified are; (RC): Recent Clayey deposit, (AA): Ancient Alluvium deposit, (LS): Lateritised Silicate deposits. The images are herein compared.

35. Fig 4.22a: lineament map of the north-eastern Bornu basin extracted from the subset mosaic of the Landsat 7 ETM + images using automatic method. Note that areas covered by dunes are masked out.

36. Fig 4.22b: Lineament map of the north-eastern Bornu basin extracted from the subset mosaic of the Landsat 7 ETM + images using automatic method overlain on the raster mosaic image subset. Note that areas covered by dunes are masked out.

37. Fig. 4.23: Surface landforms identified in the north-eastern Bornu basin including palaeoshorelines, dunes and palaeodrainage features. The different map layers are overlain using GIS on the Landsat 7 ETM + mosaic image subset.

38. Fig.4.24. SRTM DEM Hill shade relief image showing the subsurface expressions of the palaeoshorelines and palaeodrainage features

39. Fig 4.25: Four topographic profiles drawn in Fig. (4.24) across the Bama Beach Ridge to determine the elevations of the feature relative to the adjoining areas.

40. Fig 4.26: Manual GIS digitisation of surface lineaments in the north eastern Bornu basin mapped from the Landsat 7 ETM+ mosaic image subset and overlain on the raster image. Dune areas identified are masked out during the manual mapping (lineaments are shown in purple colour).

41. Fig 4.27: Lineament map shapefile of the north eastern Bornu basin extracted from the subset mosaic of the Landsat 7 ETM + images using automatic method overlain using GIS by the dunes map layer shown in beige colour

42. Fig 4.28: Lineament density map showing lineament zones as areas with high lineament concentration mapped in Fig. 4.27. Lineament zones main trend is in NE-SW and NW-SE directions similar to trends of the manual mapped lineaments as well as trends of the individual automatic mapped lineaments in the north eastern Bornu basin. Note that the dune areas were masked out of the lineament analysis.

43. Fig 4.29: Structural trends of surface lineaments in the north eastern Bornu basin from automatic mapping method mapped from the subset of the Landsat 7 ETM+ mosaic

44. Fig. 4.30. Geospatial correlation of the manual digitised surface lineaments and the lineaments mapped from automatic method. The complimentary methods

offer validation of the surface lineament mapping results. Note the predominant trends of the structural lineaments in NE-SW and NW-SE directions.

45. Fig. 5.1. Distribution of seismic and well log data used for this study displayed in the RockDoc software. Krumta and Masu wells shown in blue colour are not analysed due to data error. Well log analysis is based on the remaining 21 wells.

46. Fig. 5.2.Three commonly identified log curve patterns on gamma ray log paired with resistivity log (modified after Krassay, 1998).

47. Fig. 5.3. Showing Kasade_01 well with blocked log intervals and ITT values for sonic log in red colour, (ITT values listed in Table 5.2).

48. Fig. 5.4. N–S oriented cross section of wells as shown in Figure 5.1, showing interpreted subsurface stratigraphic correlation and basin structure. Wells Abbreviations: KAS (Kasade), BUT (Bulte), HRW (Herwa), KAD (Kadaru), ABK (Albarka), FAT (Faltu), MBJ (Mbeji), and KUC (Kuchalli) wells.

49. Fig. 5.5. W-E oriented cross section of wells as shown in Figure 5.1, showing stratigraphic correlation and basin structure. Wells abbreviations: NGA (Ngammaeast), NGN (Ngornorth), GUB (Gubio), WUS (Wushe), SA (Sa), TUM (Tuma), (WAD (Wadi), KND (Kanadi), (GAB (Gaibu), KIN (Kinasar), ZY (Ziye) MUR (Murshe), KEM (Kemar).

50. Fig. 5.6: Typical combined well log interpretation in Albarka_1 well used to delineate subsurface stratigraphy from mirrored gamma ray, resistivity and sonic log. Rest of the well log data interpretation is contained in Appendix.B

51. Fig 5.7: Uninterpreted greyscale seismic line 13 used for the seismic – well toe to validate the stratigraphic analysis.

52. Fig. 5.8. Final correlation of blocked sonic log intervals A – E for Kasade_01 (KAS) well to reflections 1 - 6 on the intersecting seismic line_13 shown on Figure 5.1 (inset figure is part of Fig 5.1) to show intersection between KAS well and seismic Line 13.

53. Fig. 5.9: Uninterpreted multi-coloured seismic line 13.

54. Fig. 5.10. Interpreted NE-SW oriented seismic Line_13 showing stratigraphic horizons correlated from the well logs. Subsurface basin structure indicating horst and graben features with Kasade_01 (KAS) well bottomed on horst and basal facies infilled within grabens. (Inset figure is part of Fig 5.1) section showing preserved extensional geometry

Intrabasinal faults in the gravity and magnetic data showing basement control of the basement-propagated faults with the synrift package. Compare this image with the GIS correlated surface and subsurface structural analysis map on Fig. 7.7.

68. Fig 5.24: Gongila Formation Time-structure map showing fewer faults occurring in the synrift basal Formation. Due to the constraint on the extent of the seismic data, the faults at the synformal and anticlinal boundaries correlate with the Intrabasinal faults in the gravity and magnetic data showing basement control of the basement-propagated faults with the synrift package. Compare this image with the GIS correlated surface and subsurface structural analysis map on Fig. 7.8.

69. Fig 5.25: Fika Formation Time-structure map showing fewer faults occurring in the post rift Formation. Due to the constraint on the extent of the seismic data, the faults at the synformal and anticlinal boundaries correlate with the Intrabasinal faults in the gravity and magnetic data showing basement control of the basement-propagated faults with the synrift package. Compare this image with the GIS correlated surface and subsurface structural analysis map on Fig. 7.9.

70. Fig 5.26: Chad Formation Time-structure map showing fewer faults occurring in the post rift Formation. Due to the constraint on the extent of the seismic data, the faults at the synformal and anticlinal boundaries correlate with the Intrabasinal faults in the gravity and magnetic data showing basement control of the basement-propagated faults with the synrift package. Compare this image with the GIS correlated surface and subsurface structural analysis map on Fig. 7.11.

71. Fig. 5.27. Bima - Gongila (Cenomanian – Turonian) interval isochron map shows an overall south-eastward thickening of sediments indicating a broad synrift depocenters bounded by faults. Bounding faults trends mainly NE-SW and NW-SE.

72. Fig. 5.28 Gongila - Fika (Turonian – Senonian) interval isochron map, showing defines the top of syn-rift and beginning of post-rift represented by the Fika Formation and bounding faults. Bounding faults trends mainly NE-SW and NW-SE.

73. Fig. 5.29. Chad - Fika (Senonian – Quaternary) interval isochron map, which defines the top of Fika Formation, indicates an overall westward thinning and bounding faults, Bounding faults trends mainly NE-SW and NW-SE.

74. Fig. 6.1. Total Magnetic Intensity map of the north-eastern Bornu basin processed from the raw data values

75. Figure 6.2 Bouguer gravity anomaly map of the north eastern Bornu Basin processed from the raw data value

76. Fig. 6.3: Colour shaded relief image map of the regional magnetic anomaly

77. Fig. 6.4: Colour shaded relief image map of the regional gravity anomaly

78. Fig. 6.5. 3 Km Downward Continuation of subset of the magnetic data showing anomalies becoming ductile closer to the sources.

79. Fig. 6.6. 5 km Downward Continuation subset of the magnetic data showing longer and sharpening of anomalies closest to the source

80. Fig. 6.7. Basement relief tectonic map of the north eastern Bornu Basin from regional gravity data

81. Fig 6.8: Rose diagram showing the trends of structural gravity lineaments mapped from Fig 6.10

82. Fig 6.9: Rose diagram showing the trends of structural magnetic lineaments mapped from Fig 6.11

83. Fig. 6.10. Principal gravity lineaments in the north-eastern Bornu Basin. Rose diagram fig 6.8 shows the trends of the gravity lineaments

84. Fig. 6.11. Principal lineaments from magnetic map of the north-eastern Bornu Basin. Rose diagram fig 6.9 shows the trends of the lineament in the north-eastern Bornu basin

85. Fig 6.12. Gravity (basement) lineaments showing the main NE-SW normal faults in relation with the NW-SE faults forming transfer faults similar to the surface structural architecture.

86. Fig 6.13 Magnetic basement lineaments showing the main NE-SW normal faults in relation with the NW-SE faults forming transfer faults from the 5 km downward continued magnetic data. The figure is a subset of Fig 6.11. Data is focused to smaller area for detail analysis.

87. Fig. 6.14. Lineaments same as in Figs. 6.10 and 6.11. Combined herein to form subsurface (basement) lineaments map from gravity (black lines) and magnetic

data (red lines) overlain for geospatial correlation in GIS. Insets are Rose diagrams for the individual lineaments from the two datasets.

88. Fig. 7.1: GIS overlay map of the multiple datasets for georeferenced data correlation analysed herein showing extents of the datasets used in the north eastern Bornu basin within the outline of the entire limits of the Bornu basin as defined by Olugbemiro (1997). Insert are the wells and seismic lines as presented in fig. 5.1

89. Fig. 7.2 a,b: Uninterpreted SRTM DEM hillshade same as Fig. 4.24 and the gravity anomaly map respectively compared for georeferencing of structures in GIS

90. Fig. (7.3 a,b): (a) SRTM Dem hillshade overlain on gravity anomaly map in GIS showing alignment of the NW-SE trending Bama Beach Ridge with basement structural setting (b) Gravity lineament layer overlain on the SRTM DEM hillshade map showing correlation of the Bama Beach Ridge palaeoshoreline with the gravity lineaments. Geospatial boundary of the palaeo-rivers (Fig 4.23) in the southwestern boundary of the SRTM DEM corresponds with the structural boundary of the gravity high anomaly and the gravity lineaments.

91. Fig. 7.4 Combined subsurface lineaments map derived from gravity (black lines) and magnetic data (red lines) showing subsurface (basement) structures in the study area. Insets are Rose diagrams for the individual lineaments from the two datasets. Same as Fig. 6.14.

92. Fig 7.5 a-c: Stress analysis of the extensional rifting in the Bornu basin from the various datasets. Palaeotectonic extension regime showing parallel NW-SE oriented transfer faults that led to the formation of the oblique NE-SW rift. NE-SW neotectonic extension fractures led to the formation of the oblique NW-SE trending

93. Fig. 7.6a. Sketch of the regional early syn-rift to late synrift stages of the north-eastern Bornu basin showing approximate structural architecture. This sketch shows how this work understands the basement control of the rift setting as well as the Intrabasinal transfer faulting. As the rift axis changes paleo stress directions accommodation zones based on relay ramps are formed.

94. 7.6b Sketch diagrams not to scale of fault kinematics and related stress fields in relation to the WARS tectonic framework with emphasis on the two phases of conjugate structural lineaments. with the directions of principal and secondary

stress axes(a) All basement lineaments directions as mapped from gravity data, the NE-SW, NW-SE lineaments trends being dominant. (b) NW-SE initial extension direction that opened up the main NE-SW Bornu basin margin. (c) Later NE-SW extension direction that generated the secondary NW-SE lineaments (d) a simplified tectonic map of the Benue-Bornu-Termit rift syatem with few transfer faults shown in the Bornu basin as revealed from gravity, magnetic and Landsat data. Integrated kinematic and dynamic analyses of the two conjugate structural pairs indicating a continuation of NE-SW rift trend in the Benue trough and continuation of the NW-SE rift trend in the Termit basin hinged at the Bornu basin and forming a rift obliquity at a palaeo-transfer junction.

95. Fig. 7.7 a: Subsurface lineaments linked with surface lineaments using GIS. Landsat 7 ETM+ mapped lineaments (purple), magnetic lineaments (white), gravity lineaments (black) overlain on Landsat 7 ETM+ mosaic subset.

96. Fig. 7.7b.Landsat 7 ETM+ surface mapped lineaments and seismic time structure map mapped faults using GIS. Compare the insert Chad Formation time-structure map overlay with the Fig 5.26 showing detail description of the post-rift Chad Formation time-structure map. Komadugu River that empties into the Lake Chad apparently flows along the conjugate main NE-SW and NW-SE lineament structural alignments.

97. 7.7 c. Landsat 7 ETM+ mapped lineaments (purple), magnetic lineaments (white), gravity lineaments (black) overlain on SRTM DEM hill-shade. Komadugu River that empties into the Lake Chad apparently flows along the conjugate main NE-SW and NW-SE lineament structural alignments.

98. Fig. 7.8. Surface and subsurface faults linked from pre-rift basement gravity and magnetic data mapped lineaments using GIS. Compare the insert syn-rift Bima Formation time-structure map overlay with the Fig 5.23 showing detail description of the Bima Formation time-structure map and correlated subsurface gravity and magnetic lineaments with faults mapped from the seismic time structure map..

99. Fig. 7.9: Subsurface faults mapped from gravity and magnetic maps with Gongila seismic time structure map using GIS. Compare the insert syn-rift Gongila Formation time-structure map overlay with the Fig. 5.24. Showing detail description of the Gongila Formation time-structure map, correlated

subsurface gravity, and magnetic lineaments with faults mapped from the seismic time structure map.

100. Fig. 7.10: Subsurface faults linked from basement gravity and magnetic with seismic mapped lineaments using GIS. Compare the insert post-rift Fika Formation time-structure map overlay with the Fig. 5.25 showing detail description of the Fika Formation time-structure map and correlated subsurface gravity and magnetic lineaments with faults mapped from the seismic time structure map.

101. Fig. 7.11: Post rift surface mapped lineaments mapped from Landsat 7 ETM+ image mosaic and subsurface faults mapped from gravity and magnetic maps with Chad seismic time structure map-using GIS. Compare the insert syn-rift Chad Formation time-structure map overlay with the Fig. 5.26. Showing detail description of the Chad Formation time-structure map, correlated subsurface gravity, magnetic lineaments and surface lineaments with faults mapped from the seismic time structure map.

102. Fig. 7.12 a. Bima Formation time-structure map overlay with subsurface lineaments linked with surface lineaments using GIS. Magnetic lineaments (white), gravity lineaments (black) overlain on magnetic anomaly map. Compare the insert syn-rift Bima Formation time-structure map overlay with the Fig 5.23 showing detail description of the Bima Formation time-structure map.

103. Fig. 7.12 b. Bima Formation time-structure map overlay with subsurface lineaments using GIS. Magnetic lineaments (white), gravity lineaments (black) overlain on gravity anomaly map. Compare the insert syn-rift Bima Formation time-structure map overlay with the Fig 5.23 showing detail description of the Bima Formation time-structure map.

104. Fig 7.13. Major morphotectonic conjugate set of fault zones overlying the north eastern Bornu basin and the proposed model of deformation. Note the drainage structural alignment of the major River Komadugu in the north-western part of the study area, which appears to be flowing along the conjugate NE-SW and NW-SE fractures. Similar structural architecture in the southwestern part of the study area involving river flowing along the NE-SW and NW-SE conjugate fractures are observed.

105. Fig. 7.14: Showing the proposed pre-rift to post-rift tectonic evolution model with additional Barremian 120 Ma, Late Santonian Inversion (84) Ma tectonic

events and Early Aptian – Late Albian (101) Ma events as they affected the Bornu basin within the context of the regional WCARS. (Genik 1993) to include the new tectonic phases that affected the Bornu basin from the integrated data analysis herein improves the existing model given in Fig 2.4.

106. 7.15. A schematic diagram showing the two petroleum systems identified from pre-rift to post-rift in the Bornu basin using the seismic data interpreted in this study and their relation to stages of basin evolution. Conceptual model is derived from the seismic section above with other information derived from gravity and Landsat data analyses.

107. Fig. 7.16. Conceptual model showing schematic geological cross-section of the study area (drawn not to scale) based on the combined well log and seismic data analyses in this research. The regional uplift provided the barrier that prevented the continued deposition of the Tertiary and erosion that removed the formation in the north-eastern Bornu basin.

List of Tables

Appendices:

Acknowledgement

I would like to thank my supervisor Dr Derek Rust for helping me with my PhD work in many inspiring ways. His unique and timely physical and written responses to my request for intervention with my sponsors and property owner have been indispensable. His guidance and academic advice with that of the supervisory team including Dr Richard Teeuw and Dr Malcolm Whithworth are greatly appreciated. The post-viva meetings I had with all the supervisors are indispensable to the success of this work. I appreciate the External Examiner Professor Marin Insley for his critical appraisal of this thesis. Special thanks to Dr Andy Gibson the Internal Examiner, who was my lecturer during my MSc programme. Dr Andy was the Annual Review Examiner for this research and has made important observations during the viva that have improved the standard of this work.

Special appreciation to the Nigerian Government funding of my research through the Petroleum technology Development Fund (PTDF) with particular recognition to Late Ismaila Jauro and Aminu Galadima. I thank the agencies that provided data and software for my research including European Satellite Agency (ESA), NASA, Bureau Gravimetric International (BGI), Department of Petroleum Resources (DPR) Nigeria, Nigerian National Petroleum Corporation (NNPC), Nigerian Geological Survey Agency (NGSA) and Ikon Science (RokDoc). I appreciate ExxonMobil and Society for Exploration Geophysicists (SEG) for training in data interpretation. I would like to thank Dr Adekunle Adepelumi and Professor S. B. Ojo for their support with data and software requisition. Very importantly, I could not have done this work successfully without the support and endurance of my wife Zainab, her love and caring for me and for our two lovely boys Abdurrahman (Hilmi) and Zayed is appreciated. My prayers and that of my surviving mother to Almighty Allah must have kept me going all these times. My prayer and love goes to her as well as my family members and my brother Usman Isyaku. The support my family got from the nice family friends we met in Portsmouth including Ibrahim Labaran, Abubakar Isa and Awwal Bamanga cannot be forgotten. I appreciate the friendship of Ugonna Nkwononwo and the

kindness of Prof. Tony Pointon and Dr Nasos Athanasios who were with me in the PhD Office. I thank Dr Philip Ideawor and Senator Lawal Shuaibu for their kind intervention in resolving my extension funding. I dedicate this work to my Late Father Alhaji Isyaku Abdullahi for his dedication to my studies from kindergarten.

Dissemination

During the course of this research, aspects of this work were presented at various conferences and published as follows:

Academic Journal paper:

A. A. Isyaku., D. Rust, R. Teeuw., M. Whitworth (2016). Integrated well log and 2-D seismic data interpretation to image the subsurface stratigraphy and structure in north-eastern Bornu (Chad) basin. Journal of African Earth Sciences, 121, pp 1-15.

Conference Papers:

1. **A. A. Isyaku**, D. Rust, R. Teeuw and M. Whitworth. Imaging Extensional Systems with Potential Fields and Seismic in Bornu (Chad) basin NE Nigeria. 78th EAGE Conference and Exhibition, 30th May – 2nd June 2016, Vienna, Austria.

2. A. A. Isyaku. Geological remote sensing studies in the Bornu (Chad) Basin in NE Nigeria using Optical-Radar-DEM data integration. Nigerian Association of Petroleum Explorationists (NAPE) 33rd Annual International Conference and Exhibition 8th – 12th November 2015, Lagos, Nigeria.

3. **A. A. Isyaku**. New geophysical interpretations combined with remote sensing and GIS for structural geological studies in the Bornu (Chad) Basin, NE Nigeria, American Association of Petroleum Geologists (AAPG) Convention, 31 May – 3 June 2015, Denver, Colorado USA.

4. A. A. Isyaku, D. Rust, R. Teeuw and M. Whitworth. Remote sensing and geosciences interpretation of lineaments for tectonic and hydrocarbon studies in Bornu Basin, NE Nigeria. Third European Association of Geosciences and Engineers (EAGE) Exploration Workshop: 6th – 9th April 2014. Abu Dhabi, United Arab Emirates.

Chapter 1:

General Introduction

1.1 Research problem

Geoscientists commonly use field geological mapping methods to study lithological and structural geological settings of sedimentary basins. However, the traditional field outcrop mapping method is inadequate in delineating regional geomorphic features in remote areas that are characterised with flat topography and paucity of adequate bedrock exposures (Abdelsalam et al., 2000b). Consequently, the applications of geological remote sensing to study regional geospatial characteristics of surface geological features in such terrains are increasingly recognised (Weng, 2010; Harris et al., 2012; Chaabouni et al., 2012; Abdullah et al., 2013). Moreover, integrating lower-spatial-resolution-higher-confidence subsurface geophysical data with higher-spatial-resolution-lower-confidence Earth Observation (EO) data enhances the reliability of interpretations and correlation of litho-structural features for comprehensive understanding of the geological settings of such basins (Pena and Abdelsalam, 2006; Thurmond et al., 2006; Laake et al., 2008; Saadi et al., 2011; Khatiwada et al,. 2013). In areas where reconnaissance geological maps are lacking, use of Earth Observation (EO) imageries offer the cheapest, quickest and effective tools for generating surface geological maps.

The semi-arid Bornu basin (Fig. 1.1) is one of the most explored inland basins in Nigeria and its hydrocarbon potentials have been well-identified (Petters and Ekweozor, 1982; Avbovbo et al., 1986; Genik, 1992; Genik, 1993; Olugbemiro et al., 1997; Moumouni et al., 2007; Obaje, 2009; Anakwuba and Chinwuko, 2012; Hamza and Hamidu, 2012; Adepelumi et al., 2012). Furthermore, the basin is the most explored inland basin in Nigeria; hence, multiple datasets are available (Table 1.1). Bedrock outcrops in the basin are scarce, mainly covered by thick Quaternary

sediments forming flat terrain at the southwestern shore of the Lake Chad and the southwestern boundary of the Republic of Chad (Isiorho, and Nkereuwem, 1996). However, few rock outcrops are found in the southern part of the basin towards its boundary with the Upper Benue Trough (Obaje, 2009; Boboye and Akaegbobi, 2012; Chinwuko et al., 2012; Hamza and Hamidu, 2012). The restricted outcrops in the southern area previously mapped using traditional field methods were extended to generalise the surface litho-stratigraphy and structure of the entire basin (Hamza and Hamidu, 2012; Adepelumi et al., 2012). The field stratigraphic mapping carried out in the localised southern part of the basin by Hamza and Hamidu (2012) were therefore inadequate since the stratigraphy of the unmapped vast northern part of the basin, which remained constrained by paucity of continuous bedrock outcrops, have not been fully established. Hence, no detail lithological map of the basin is published so far.

Consequently, several discrepancies exist in the literature for the litho-stratigraphic classification of the Bornu basin using available subsurface data (Table 2.1 and Table 2.2). The subsurface stratigraphy in the north-eastern part of the basin towards the south-western shores of the Lake Chad remains uncertain since integrated data analysis, which allows for correlation and multi-data validation is not used. The stratigraphy and tectonic setting of the Bornu basin was thus commonly associated with that of its south adjoining Gongola Basin in the Upper Benue Trough. Previous subsurface studies used mainly single data type in the southern region of the Bornu basin. The previous subsurface studies in the north-eastern part of the basin, including, Moumouni et al., (2007); Boboye and Abimbola, (2009); Alalade and Tyson, (2010); Hamza and Hamidu, (2012); Boboye and Akaegbobi, (2012); Adeigbe and Abimbola, (2013); Adegoke et al., (2014) used only few core samples or segregated ditch cuttings obtained from few wells. Other specific data type analyses, include

gamma ray log analysis; Adepelumi et al., (2012), 2-D seismic data analysis; Avbovbo et al., (1986); Okpikoro and Oluronniwo (2010), gravity analysis; Cratchely et al., (1984), Nwankwo et al., (2012), magnetic analysis; Anakwuba and Chinwuko, (2012). These studies were insufficient in establishing detail subsurface stratigraphy and tectonic structure of the north-eastern part of the Bornu basin from the single datasets utilised. Background geological information from the adjoining Benue Trough were used in these previous studies to generalise the stratigraphy of the entire basin including the constrained northern part.

Surface lineament analysis for structural studies in sedimentary basins is a common approach particularly for several semi-arid basins with inadequate rock outcrops essential for the field survey (Grandjean, et al., 2006; Masoud and Koike, 2006; Leech et al., 2003). Such regional lineament studies become more essential where traditional field mapping is not viable due to presence of thick cover sediments, topographic flatness or remoteness of the study area (Sabins, 1998a; Abdelsalam et al., 2000a; Pena and Abdelsalam, 2006; Saadi, et al,. 2009). Nevertheless, the synoptic view of the geology of the north-eastern Bornu Basin using recent advances in satellite remote sensing and GIS technology have not been presented.

Although, Bornu basin evolved from the Equatorial Atlantic source extensional West African Rift System (WARS) that initiated in the Early Cretaceous and peaked in the Late Cretaceous (Genik, 1992; 1993), no evidence of structural linkages or similarity of surface and subsurface expressions of the rift features in the intracontinental Bornu basin were previously identified. Thus, no geological map of the basin from published literature studies is available. Furthermore, no comprehensive study, which integrates the existing multi-source geophysical datasets for a large-scale litho-stratigraphy and tectono-structural interpretation of the basin is presented.

Integrating Earth Observation data, which imaged the surface geology with geophysical data that image subsurface geological conditions offers reliability and reduces ambiguity of geological interpretations (Saadi et al., 2011). Thus, in the absence of bedrock outcrops and intact core samples from the Bornu basin, an alternative surface geological mapping integrated with multiple subsurface data analysis is required for comprehensive interpretation of the geological setting of the basin.

Therefore, in this study, I used various geophysical data available from the basin including 2D seismic, gravity, aeromagnetic and multi-well log datasets with orbital optical multispectral Landsat 7 ETM+, SRTM DEM and Envisat Advanced synthetic Aperture Radar (ASAR) remote sensing/Earth Observation map layers assembled in GIS to carryout of an integrated geological study of the basin (Fig. 1.2). The study improved on the synergistic use of surface and subsurface datasets for further structural and lithostratigraphic investigations using the north-eastern Bornu basin case study. Furthermore, this study provides new insights into the tectonic development of the basin by deducing the significance of the correlated surface and subsurface structural lineaments to hydrocarbon prospectivity of the basin

1.2 Location of the study area

Bornu basin referred to as the Nigerian sector of the Lake Chad basin makes up approximately ten percent of the 230,000 km^2 of the entire Lake Chad basin, which extends into countries including Chad, Niger, Cameroon and Central African Republic (Fig. 1.1). Bornu basin is an east – west elongated inland sub-basin in the south-western boundary of the Lake Chad Basin in north-eastern Nigeria covering latitudes 11º.00'N – 13º. 45'N and Longitudes 8º 21'E – 14º. 40'E (Olugbemiro, 1997). The Upper Benue Trough bounds the southern flank of the Chad Basin, which constitutes

the Bornu basin (Alalade and Tyson, 2010). This research deals mainly with the north-eastern part of Bornu basin in north-east Nigeria. The area lies within the physiographically flat plain bordering the south-western shores of Lake Chad and southern border of the Republics of Chad and Niger. The geographical boundaries of the area are between latitudes 11° 00' N – 13° 30' N and longitudes 12° 00' E – 14° 30' E as outlined on Figure (1.1). Major localities within the research area include Maiduguri, Kirenowa, Konduga, Bama and Baga. The region of interest in the north-eastern Bornu basin is selected as the study area because it is covered by available Earth Observation datasets as well as with gravity, magnetic, 2-D seismic and well log datasets.

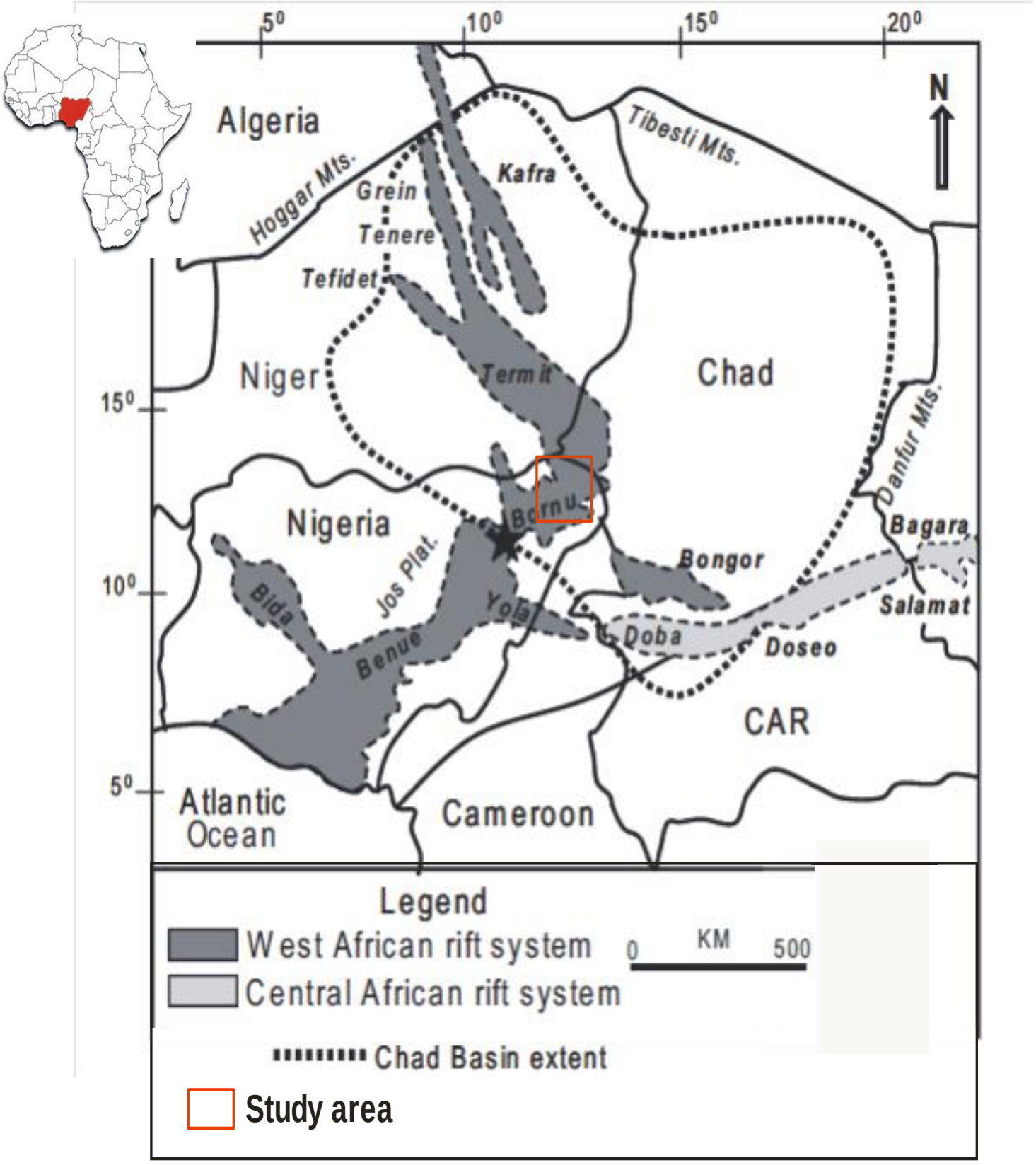

Figure 1.1 Map showing tectonic setting in Nigeria and the adjoining countries within the Lake Chad basin and the location of study area in the Bornu basin (Modified after Alalade and Tyson, 2010).

1.3 Aim and objectives of the research

The primary aim of this research is to constrain the Cretaceous to Recent structure and tectonics of the Bornu basin and determine the significance of lineaments and lithostratigraphy to the hydrocarbon prospectivity of the basin.

This research emphasises that combining multiple data sets will be more reliable in constraining the structural and stratigraphic setting of basins than by using single dataset (Saadi et al., 2011; Laake et al., 2008). The study also analyses the influence of rift tectonics on the stratigraphy and structural framework of the Cretaceous rocks in the north-eastern Bornu basin and their implications for hydrocarbon accumulation in the basin.

Specific objectives are:

1- To review literature on the utility of Earth Observation data for spectral lithological mapping and lineament analysis in semi-arid regions and their potential applicability in the Bornu basin geological setting.

2- To test the utility of combined Earth Observation imageries to address the spatial distribution of cover sediments and their constraints in litho-structural mapping in the basin.

3- To develop new insights into the tectonic framework and evolution of the north-eastern Bornu basin, its tectonic development and analysis of its hydrocarbon prospectivity from correlated surface and subsurface analysis.

4- To determine the synergistic relationship between correlated multiple geophysical datasets in validating the subsurface stratigraphy in the north-eastern Bornu basin.

1.4 Hypothesis and research questions

The rationale for this research is that, as remote sensing/Earth Observation methods are applicable to surface litho-structural studies in topographically flat semi-arid regions to complement traditional field mapping, an integrated study utilizing different subsurface data would provide comprehensive lithostructural and tectonic analysis.

The hypothesis of this study states: Synergistic approach using visual geospatial correlation of optical, radar and DEM Earth Observation datasets integrated with multiple geophysical datasets including gravity, magnetic, seismic and well logs provide better geological interpretation of lithostratigraphy and structural deformations.

Thus, this thesis seeks to address the following questions relating to the characteristics of stratigraphy and structural lineaments in the north-eastern Bornu Basin.

1- How does combined optical, radar and DEM remote sensing datasets apply in geomorphic and structural mapping of regions with flat topography and lack of bedrock outcrops?

2- What synergistic relationship exists in geospatial correlation of multiple subsurface datasets for identifying subsurface stratigraphy and structure?

3- What geotectonic relationships exist between the surface and subsurface structural lineaments and lithostratigraphy in the Bornu basin and how do the relationships influence the petroleum prospectivity of the basin?

1.5 Data and methodology

Table (1.1) presents outline of the datasets used for the research. The research utilised mainly secondary datasets stored in digital database. Details on individual dataset are provided in corresponding data analysis chapters in this thesis.

As this research deals with mapping lithology and structures in the surface and subsurface, Earth Observation and geophysical datasets are considered appropriate.

The justification for including Landsat 7 ETM+, Envisat ASAR and SRTM DEM is based on successful applications of the integrated optical, radar and DEM data sets elsewhere in mapping surface lithology, structures and geomorphic features in contiguous and analogous semi-arid basins by several workers including Thurmond et al., (2006), Abdelsalam et al., (2000b), Pena and Abdelsalam, (2006). Details of system characteristics, concept and applications of Landsat 7 ETM +, SRTM DEM and ASAR are given in Chapter 3 and 4 of this thesis.

The justification for including geophysical data including seismic, well logs, gravity and magnetics is that the datasets present records of the subsurface geology and structures and commonly used for such purposes. Integrating subsurface geophysical datasets for basinal studies is common as presented in Insley et al., (1996); Saadi et al., (2009); Kaymakci et al., (2010); Athanasios, A. (2012); Khatiwada et al., (2013).

Details of characteristics and concepts of the geophysical data sets used are presented in Chapters 5 and 6 of this thesis.

Methodology for this research involves a multidisciplinary approach, which involves analysing and storing individual surface and subsurface interpreted maps as different GIS layers and visually determining their geospatial correlation for geological interpretation. Spectral lithological map is generated from Landsat 7 ETM+ images and geological lineaments are extracted from the Landsat 7 ETM+, gravity data, aeromagnetic data as well as the seismic data. Extracted surface lineaments are

draped on the surface lithological map, while the subsurface lithological cross sections are interpreted from well logs and validated with a corresponding seismic data. The research methodology flow chart is presented in Figure (1.2).

Table 1.1. Showing summary of the different dataset used for the research

Data Type	Data Quantity	Data Source	Analysis and product
2-D Seismic	6 lines	Nigerian National Petroleum Corporation (NNPC)	Basement architecture, structure, stratigraphy
Well log suite (Gamma ray, resistivity, bulk density and sonic)	23 well log suite	Nigerian Department of Petroleum Resources (DPR)	Basement topography, lithology, stratigraphy
Ground Gravity	1334 BAFA Values	Bureau Gravimetric International (BGI) France	Subsurface geometry, gravity lineaments
Aeromagnetic	16384 TMI Values	Geological Survey of Nigeria Agency (GSNA)	Subsurface geometry, magnetic lineaments
Landsat 7 ETM+	4 Images	Earth Explorer (NASA), USA.	Surface lineaments, lithology, geomorphic features
EnviSat ASAR	4 Image mode scenes	European Space Agency (ESA)	Surface structures, palaeodrainage
SRTM DEM	6 image scenes	Earth Explorer (NASA), USA.	Palaeodrainage, Palaeoshorelines, Subsurface structures, topography

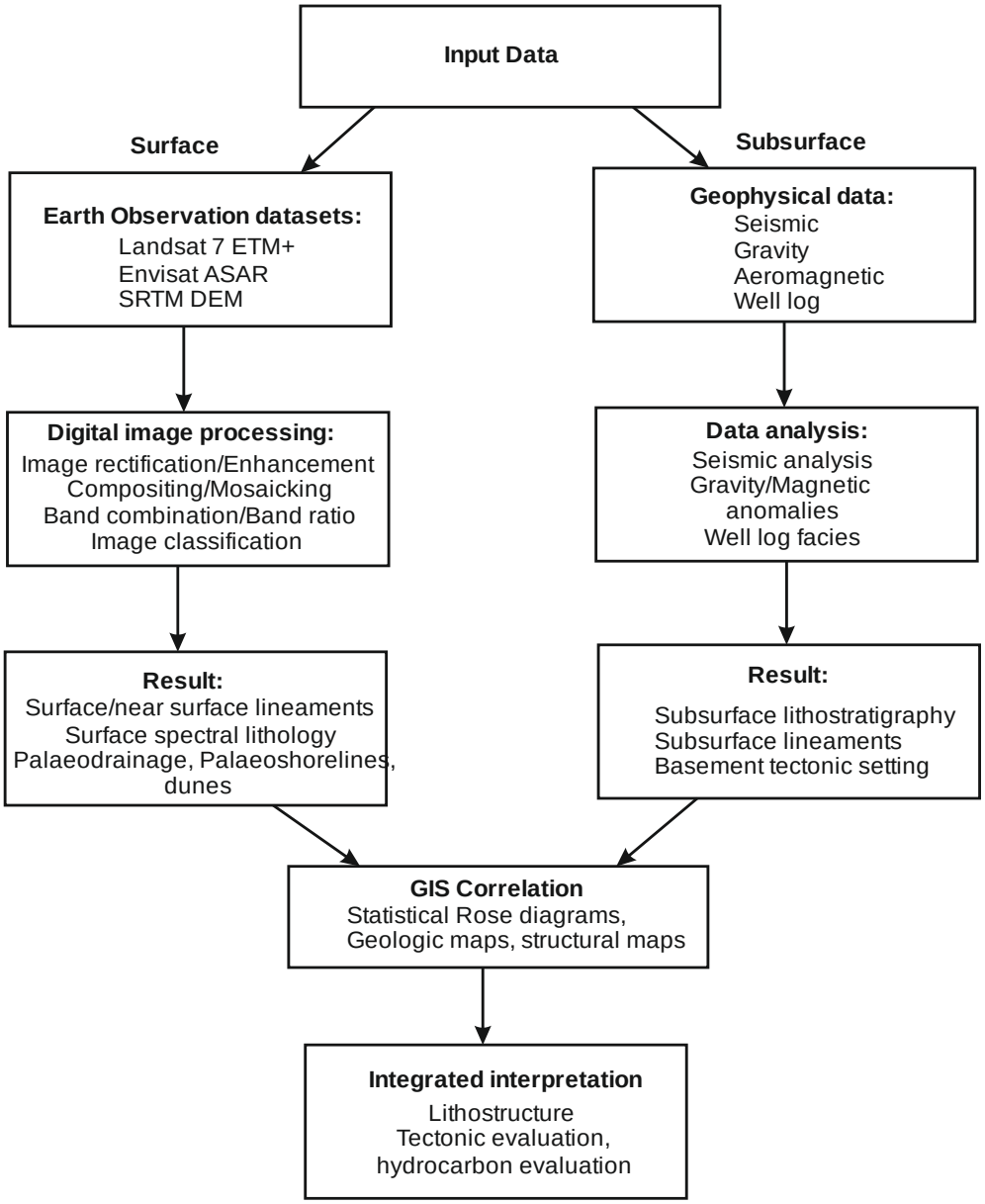

Figure 1.2 Methodology chart illustrating the steps followed for the integrated analysis in the research

1.6 Innovations and contributions of the proposed study

The innovative aspects of the proposed study include:

I. Application of modern Earth Observation data analyses techniques for lithostratigraphic and structural studies using combined Optical – Radar - DEM where traditional field mapping methods previously applied were inadequate.

II. Linking subsurface tectonic lineaments and lithostratigraphy to the surface by correlating between surface and subsurface geologic features using their geospatial relationships for structural analysis and hydrocarbon studies.

III. Developing a systematic technique for detecting structural continuity and trends of faults interpreted from the satellite Earth Observation imageries to constrain the correlation of subsurface faults on geospatially georeferenced seismic time-structure maps and isochron maps.

IV. Application of multi-source data integration methodology for a comprehensive geological study.

V. Developing a new validation technique of structural mapping from manual and automatic lineament mapping methods.

VI. Developing a new spectral mapping methodology for lithological mapping in an area with inadequate previous lithological information using combined band combination, band ratio and Spectral Angle Mapper supervised classification.

VII. Developing a new evolution model for the Bornu basin from pre-rift to post rift tectonic regimes.

VIII. Developing a potential petroleum systems model for the Bornu basin from pre-rift to post-rift setting.

IX. Constraining the subsurface lithostratigraphy of the north-eastern Bornu basin using combined multiple well logs and seismic data, which offers validation than using a single data type.

1.7 Organisation of the thesis

This section presents the structure of the thesis and a summary of each chapter's content. Chapters 1, 2 and 3 represent the introduction, background and literature review for the research. Each of the analysis chapters (4, 5 and 6) deals with an integrated study using two related datasets that deal with specific geological study and they are presented in order; from surface data analysis (Chapter 4) to subsurface analyses (Chapters 5 and 6). The Chapters are designed to use two related datasets in order to deduce validation of the results from each integrated analysis group and can possibly be published individually. As such, Chapter 5 is already published (Appendix B). Chapter 7 is essentially a discussion chapter, which synthesises and critically analyses the overall results of the previous chapters. Specifically:

Chapter 1 is an introduction to the research giving the framework of the overall thesis.

Chapter 2 describes the literature survey of regional geological setting of the study area from continental evolution to the West African tectonic domain of the Lake Chad basin comprising of the Bornu basin. Specific geological aspects of the Bornu basin include; stratigraphy, structure and lithology to provide the status of our present understanding about the basin from previous studies until date.

Chapter 3 provides summary of the geological remote sensing (Earth Observation) method and their potential applications to the north-eastern Bornu basin. The concept of remote sensing for regional geological mapping is adapted in the study area.

Chapter 4 is a combined optical Landsat 7 ETM+, ASAR radar and SRTM DEM remote sensing methodology for surface mapping of lineaments, spectral lithology and tectonic features for geospatial correlation with subsurface features obtained from geophysical analysis.

Chapter 5 is a combined subsurface aspect that deals with mapping of basement structural architecture and stratigraphy using integrated multiple well logs including

gamma ray, bulk density, resistivity and sonic log tied with seismic to validate the subsurface lithostratigraphy and structure.

Chapter 6 is a combined gravity and magnetic analysis that deals with subsurface basement structural setting of the basin, particularly the basement structural geometry for tectonic analysis and for comparison of the subsurface characteristics with corresponding surface expressions.

Chapter 7 is a discussion of the integrated analyses of the results of the surface and subsurface datasets to deduce the tectonic implications of the lineaments and reconstruct the tectonic regimes that have affected the Bornu basin. The chapter also deduces the significance of the tectonic setting to hydrocarbon potential and prospectivity of the north-eastern Bornu basin within the regional tectonic framework from results obtained herein. Chapter 7 also describes the effectiveness of the critical approach to develop informed propositions that justify the hypothesis of the research.

Chapter 8 is the conclusions chapter that presents informed answers to the research questions through evaluating how the research objectives are achieved. Recommendations for further work and limitations are presented.

Chapter 2:

Synthesis of the tectonic evolution and geological aspects of the Bornu basin area

2.1 Cretaceous rift evolution of the South Atlantic - Gulf of Guinea - Benue trough triple junction

Intercontinental separation of the South American and African continents and opening up of the Equatorial Atlantic occurred in response to the break-up of the Gondwanaland (Grant, 1971). Continental separation occurred during the Cretaceous at the triple junction that formed the South Atlantic - Gulf of Guinea and Benue Trough axes (Fig 2.1). The continental separation led to development of transform faults, which extend northeast to the Niger Delta and Benue Trough. The transform fault mechanism, as origin for the continental separation formed an unstable Rift-Rift-Fail (RRF) triple junction where the separation occurred at a divergent continental boundary is located at the margins of West Africa and northern Brazil along the St. Paul and Romanche oceanic transform faults (Grant, 1971) (Fig 2.1, Fig 2.2). The site of the present day Niger Delta in Nigeria is the triple junction of the RRF origin (Fig. 2.1 and Fig. 2.2). Evolution of the Benue Trough is associated with rise and cessation of mantle plumes or hot spots located beneath the present day Niger Delta, which caused doming and rifting in the Benue Trough.

However, while the other two rifted arms continued to spread into the South Atlantic Ocean and the Gulf of Guinea. The Benue Trough as the third rift arm discontinued and formed a rift valley or aulacogen filled with sediments when the associated stress ceased from developing in the Late Cretaceous. However, the failed spreading movement beneath the Benue Trough restored stability to the African plate margins (Olade, 1975)

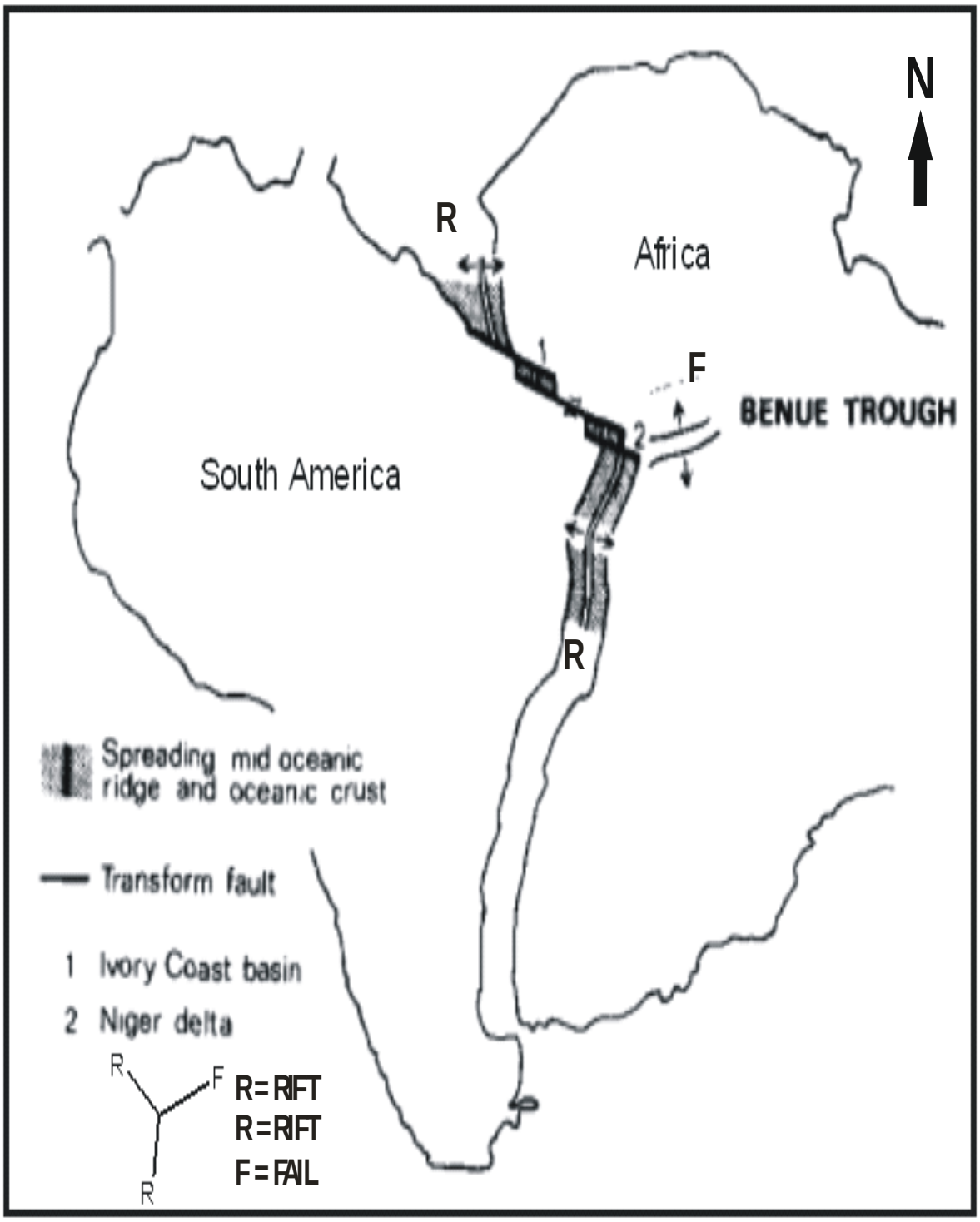

Figure 2.1.Schematic separation of African and South American Continental plates in Albian at the triple rift (RRF) junction (Modified after Grant, 1971). The figure is not to scale.

Precambrian basement rocks in the West African region were categorised into West African Cratons and Mobile Belts (Fig 2.2). Cratonic areas were stable since the Eburnean Orogeny (1900 Ma) while mobile belt areas were affected by the later Pan African Orogeny (500 Ma) as evidenced by the peculiar N-S alignment of Jurassic features mostly in the Younger Granite rocks in Jos and its adjoining areas in north central Nigeria. The underlying basement rocks in Nigeria referred to as the Basement Complex are part of the mobile belt and consist mainly of migmatite, gneisses, granites and schists (Benkhelil, 1982). Intracontinental rifting and basin evolution occurred along lines of crustal weakness created by the intercontinental separation. Such fractures including the South-Atlantic fracture zones relate with deformations within the West African basins (Benkhelil, 1987; Guiraud and Maurin, 1992). Deformational features are evident in the Equatorial Atlantic including the extensive Charcot, Romanche and Chain fracture zones, which link up to the West and Central African Rift System (WCARS) (Fig 2.3) through the Niger Delta and Benue Trough (Fig 2.2).

However, the African and South American continental separation have wider tectonic imprints across North Africa and Arabia particularly in relation to the Santonian compressional events (83 – 85 Ma) (Genik, 1992) (Fig 2.4). Stratigraphic variations across several pull-apart fault bounded sub-basins exist with sediment thickness reaching up to 10 km in the Lake Chad area (Genik, 1992). Sediment thickness ranging from 4 km to 7 km are common in most parts of the rift basins following post-rift subsidence and deposition of Tertiary and Recent sediments over the Cretaceous rifts (Avbovbo, et al., 1986).

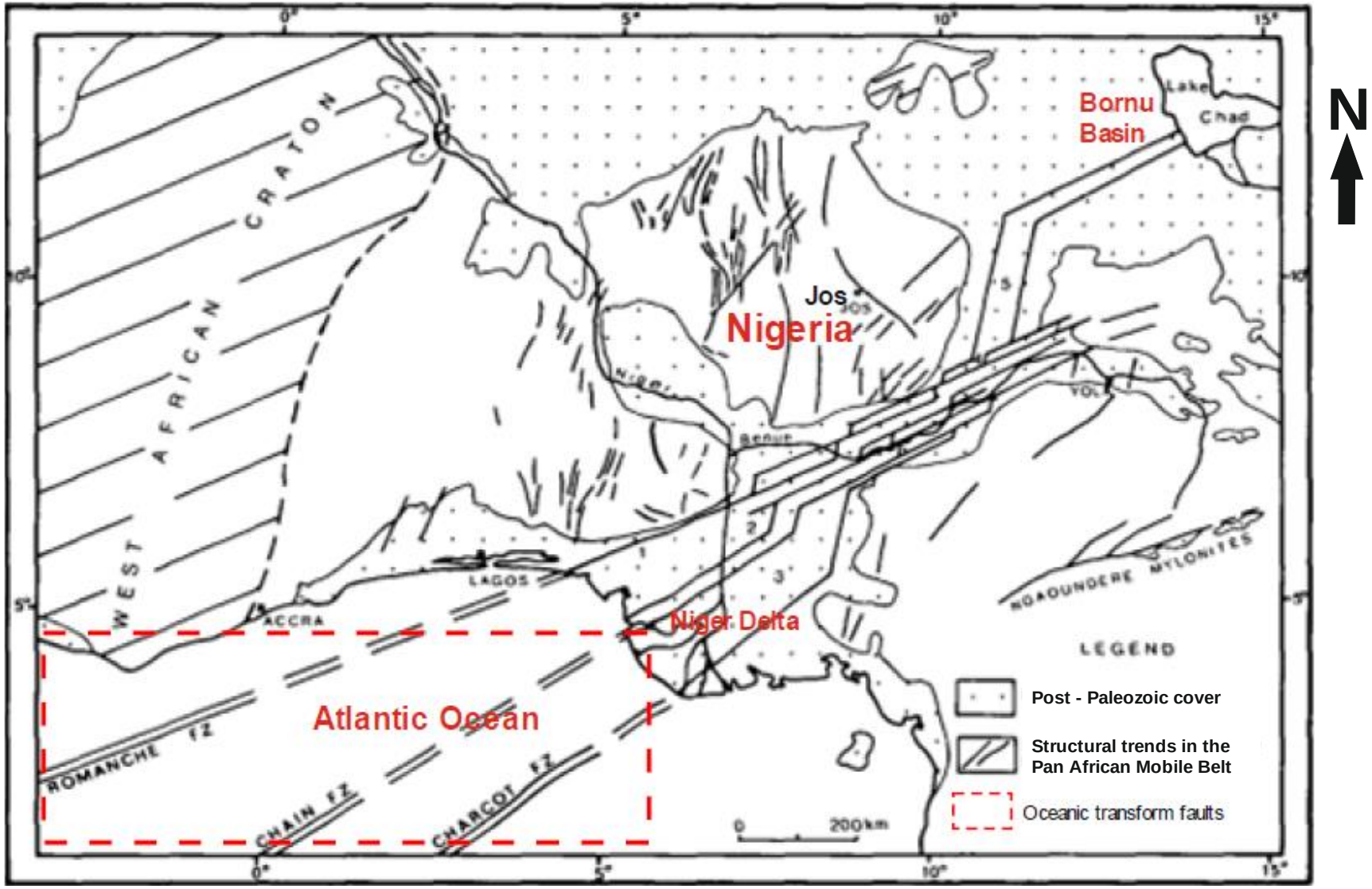

Fig 2.2: Equatorial Atlantic transform faults linking up to the Niger Delta and Benue Trough. West African Craton indicated in the west bordering a mobile belt where the Nigerian basement is located (Modified after Wright, 1976).

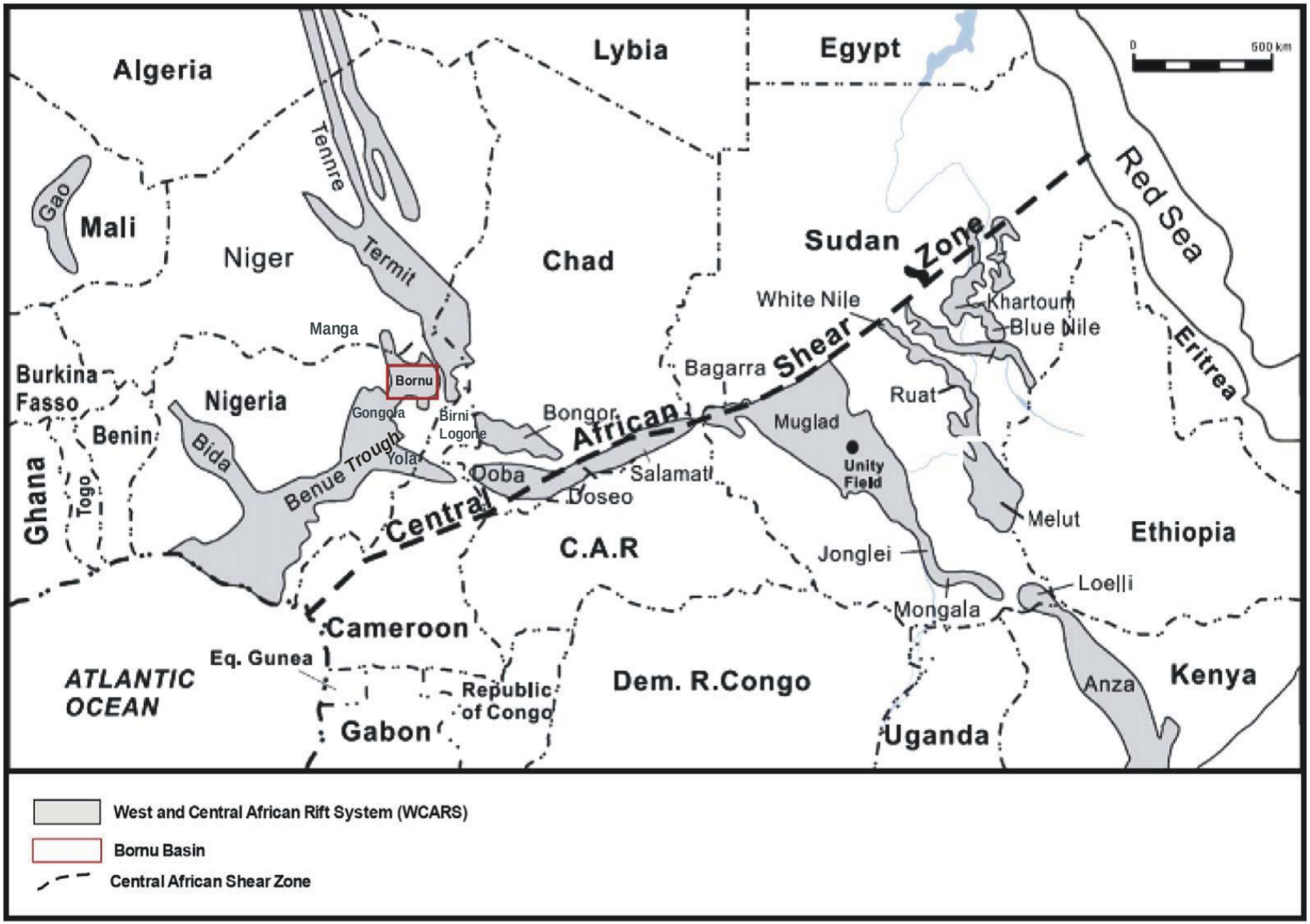

Fig 2.3: West and Central African Rift System (WCARS) basins resulting from the Cretaceous rift through the Benue Trough (Modified after Dou et al., 2007)

2.2 Evolution of the West African Rift System (WARS) basins

The Early Cretaceous continental separation accompanied by rifting at the Equatorial Atlantic produced the West and Central African Rift Systems (WCARS) and associated basins (Fig. 2.3) (Genik 1992; Guiraud and Maurin 1992). The Mesozoic WCARS extend over 4000 km northwards from Nigeria into Niger, Chad and Libya and southwards into Sudan forming both strike-slip and extensional faults. The WCARS basins bifurcate into the West African Rift System (WARS) and the Central African Rift System (CARS). The WARS sub system extends from the Gulf of Guinea through the sinistral (wrench) strike slip system in the Benue Trough, the flanking Yola and Gongola rifts and continued into the Chad Basin. Strike slip faults within the WCARS penetrated well into the African continent forming extensional basins perpendicular to the strike direction of the faults. There are eight contiguous rift basins identified within the WARS including the Bornu basin (Fig 2.3) (Genik, 1993). Five main tectonic phases were responsible for evolution of the structures in WCARS as identified by Genik (1992; 1993) (Figure 2.4). Initially, the Pan African (500 Ma) crustal consolidation phase established the main basement lineaments and faults within the underlying igneous and metamorphic rocks. The basement lineaments controlled subsequent Cretaceous NW-SE rift trend in the Niger-Air axis and the NE-SW rift trend in the Benue-Bornu rift axis of the WARS with similar trends in the CARS (Benkhelil, 1988).

Palaeozoic - Jurassic (550 - 130 Ma) tectonic phase formed a stable platform that was overlain by transgressive sediments (Guiraud et al., 1987). Late Cretaceous main rifting phase occurred in response to the crustal fragmentation and the initial separation of the African and South American plates and subsequently lead to the formation of the WCARS basins. The opening-up of South Atlantic started with wrench faults extending from South America through the Gulf of Guinea into Africa. Cratchley

et al., (1984) reported that the pre-existing openings formed during the Pan African Orogeny controlled the Romanche and Chain faults (Fig. 2.2). The WCARS basins were fully developed following a new rift phase in the Maastrichtian - Palaeogene (75 - 30 Ma). Uplift and arching rejuvenated the Bornu basin due to a tensional deformational regime and created an elongated graben system. The last major tectonic rift phase exist from Palaeogene - Recent with uplift and erosion of volcanic masses in the Cameroon - Nigeria border (Fig 2.3). The WARS basins are mainly separate half grabens with long normal faults that subsided and filled with Tertiary continental and marine sequences. The tensional patterns in the WARS basins consist of rotated synthetic faults and antithetic faults. Some faults are listric linking up with the mantle and the largest displacements, seen in the longest faults in the Termit basin adjoining the Bornu basin. Most common faults in the Termit were the Cainozoic NNW-SSE antithetic fault blocks (Genik, 1993) (Figure 2.3).

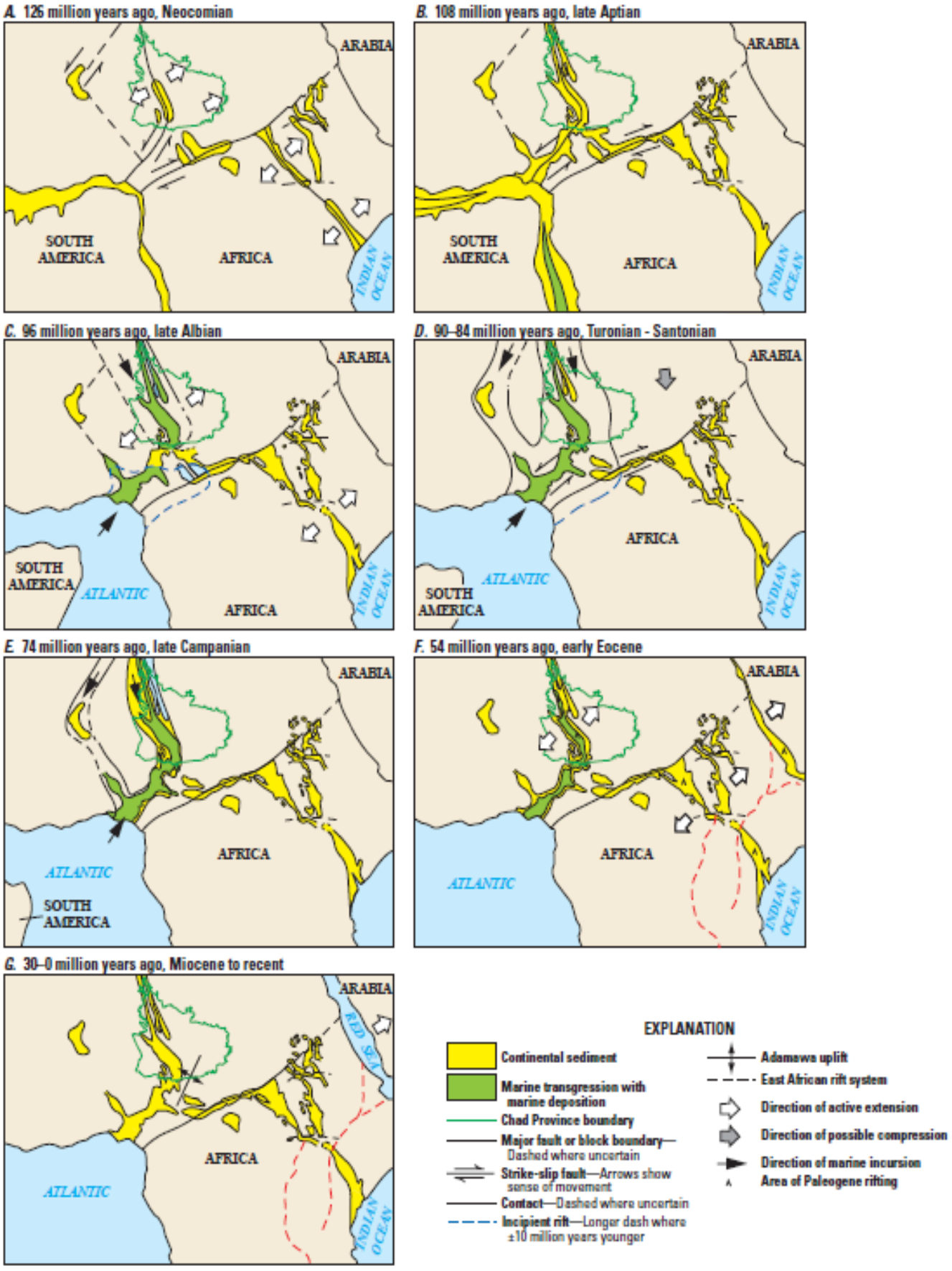

Fig 2.4: Cretaceous - Recent phase rifting due to the African and South American continents and the formation of the WCARS basins (Genik, 1993).

2.3 Outline of the previous geologic studies in the Bornu Basin

2.3.1 Tectonic imprints in the Bornu Basin

The Lake Chad basin and its constituent Bornu basin were classified as rift basins based on several evidences including; presence of basement tensional force indicators, presence of zigzag fault patterns and lack of compressive features (Avbovbo et al., 1986). A regional positive anomaly of 45mgal trending NNE from the Bornu basin to the north of the Lake Chad exists, which is similar to the positive anomalies in the Benue Trough, suggesting that the major regional Atlantic fractures link the Benue Trough and the Bornu Basin (Cratchley et al., 1984). The Equatorial Atlantic fracture zones were linked with Benue Trough and continued beneath it to the Bornu basin include; Romanche Fault zone, Chain Fault zone and the Charcot Fault zone (Fig 2.2). The faults were been controlled by the pre-existing lines of weakness, which developed during the Pan African orogenic events or from older lineaments (McCurry 1971). The Cretaceous tectonic imprints proved herein within the Bornu Basin were not been mapped previously.

2.3.2 Lithostratigraphy

Rock outcrops in the Bornu basin are generally scarce mostly covered by thick Quaternary sediments (Fig. 2.5) mainly forming flat topography (Fig 2.6) (Isiorho, and Nkereuwem, 1996). Most bedrock exposures are been confined in the southern areas and at the Bornu basin – Benue Trough boundary (Hamza and Hamidu, 2012). Carter, (1963) and Avbovbo et al., (1986) presented the generalised stratigraphic scheme for the Bornu basin, which indicated Cenomanian Bima Sandstone as the oldest formation overlying an unnamed Pre Bima Formation on the basement (Table 2.1). The Bima Sandstone is a product of weathering of the basement rocks and represents the Nigerian equivalent of Continental Intercalaire deposit (Adepelumi et al., 2012).

Fig 2.5: Image showing typical thick Quaternary - Recent sediment cover overlying the Chad Formation (Modified after Isiorho and NKereuwem, 1996).

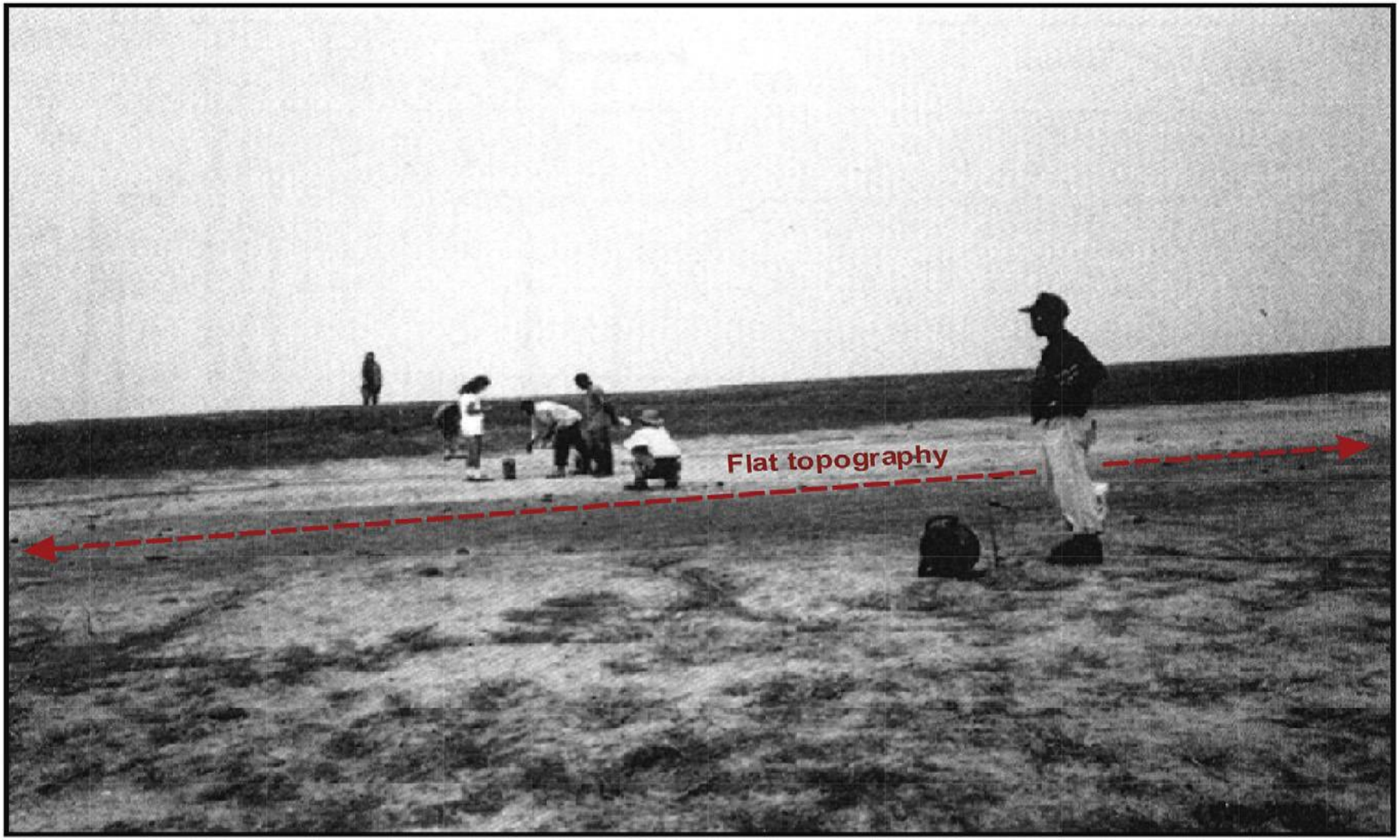

Fig 2.6: Image showing typical flat terrain in the northeast Bornu basin (Modified after Isiorho and Nkereuwem, 1996).

The Bima Sandstone is been overlain by Gongila Formation, which was deposited during the Turonian transgression and comprised of alternating sand and shale layers with occasional limestone interbeds. Senonian marine Fika Shale overlies the Gongila Formation and marks the end of Cretaceous deposition in the basin. Subsequent regression deposited Gombe Sandstone, which was been overlain by Tertiary Kerri-Kerri Formation made up of sandstone and clay and intermittent laterite. Quaternary Chad Formation is the topmost layer consisting of alternating sequence of clay with sand interbeds. Thus, this stratigraphic scheme by Avbovbo et al., (1986) consisted of seven stratigraphic units. However, Umar (1999) and Okpikoro and Olorunniwo, (2010) mapped six stratigraphic units using 2-D seismic data.

Table 2.1: Generalised stratigraphy of the Bornu basin obtained from mainly seismic data by Avbovbo et al., (1986) exposed in the southern part of the basin.

Period/Epoch	**Formation**	**Average thickness (m)**	**Thickness from seismic data (m)**	**Lithology**
Quaternary	Chad	400	800	Clays with sand interbeds
Tertiary	Kerri-Kerri	150		Sandstone and clay with laterite
Maastrichtian	Gombe	315	0-1000	Sandstone, siltstone and clay with coal beds.
Senonian	Fika	430	0-900	Shale, with limestone beds
Turonian	Gongila	420	0-800	Alternating sandstone and shale with limestone
Cenomanian	Bima	3050	2000	Sandstone
Albian	Unnamed	-	3600	-
	Unnamed	-	0-3000	-
Precambrian	Basement			-

Adepelumi et al., (2012) mapped six subsurface stratigraphic units including Gombe Formation and Kerri-Kerri Formation in the north-eastern Bornu basin using gamma ray log data analysis. However, Isiorho and Nkereuwem (1996), indicated that the top most Chad Formation is completely buried at the north-eastern area by an overlying "post Chad Formation" consisting of aeolian, fluvial and lacustrine sediments with thickness of 1 - 6 m (Fig. 2.5). Late Tertiary volcanism was common in the southern and central parts of the basin (Grant, 1971). However, Petters (1978) and Okosun (1995) indicated that only five stratigraphic units including Bima, Gongila, Fika, Kerri-Kerri and Chad Formations were deposited in the basin. Burke (1976) used water well data and established that deposits of Kerri-Kerri Formation in the basin were localised, forming a thickness of 300 m in the north central Nigeria (Fig 2.2) and terminated in the Maiduguri area in the north eastern Bornu basin. This supports earlier study by (Miller et al., 1968) that showed Kerri-Kerri Formation was been exposed only in the western parts of the basin beneath the Chad Formation and absent in the south-western parts. Conversely, four subsurface stratigraphic units including Bima, Gongila, Fika and Chad Formations were recorded in few core samples with no evidence of Gombe Formation and Kerri-Kerri Formation underlying the north-eastern Bornu Basin (Olugbemiro et al., 1997; Obaje et al., 2004; Boboye and Abimbola, 2009; Alalade and Tyson, 2010). The lateral facies distributions of the different stratigraphic formations across the north-eastern area are not investigated so far.

Hamza and Hamidu (2012) produced a different generalised stratigraphic scheme for the basin and added new Formations using segregated ditch cutting samples from four wells in the north-eastern area combined with outcrop mapping in the southern boundary of the basin (Table 2.2). Later stratigraphic classification by Hamza and Hamidu (2012) reclassified the Bima Formation as Bima Group that subdivided into Lower, Middle and Upper Formations while the overlying Gongila Formation

subdivided into Formation 1 and Formation 2. Fika Shale, which overlies the Gongila Formation was subdivided into three; including Formation 3, Formation 4 and Formation 5 (Table 2.2). Gombe Formation and Kerri-Kerri Formation were indicated beneath the uppermost Chad Formation.

Table 2.2: Generalised stratigraphic scheme for Bornu basin by Hamza and Hamidu (2012) indicating additional stratigraphic horizons

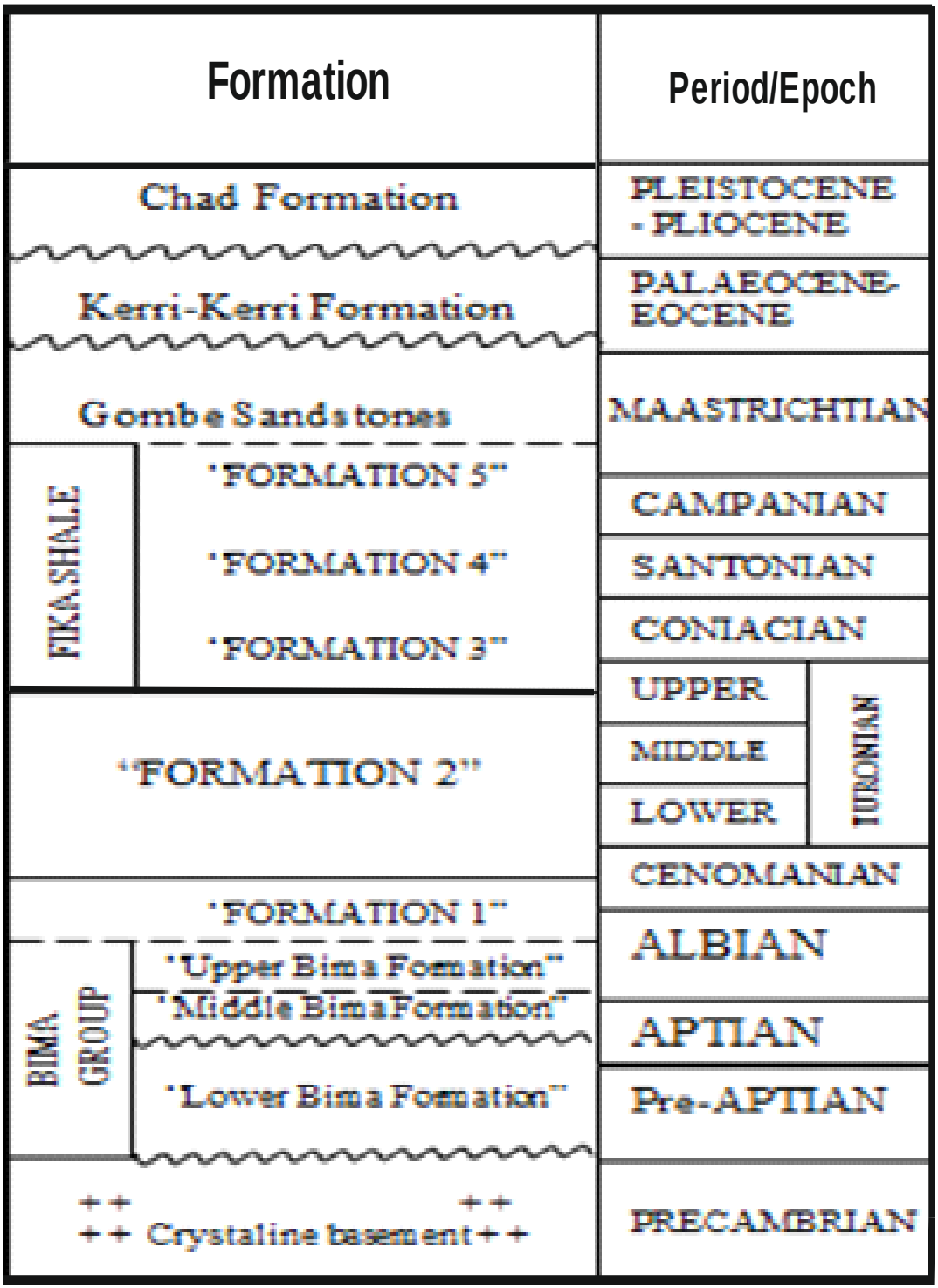

2.3.3 Structural Geology

Structural features in the Bornu basin were poorly understood due to inadequate bedrock outcrops exposures covered by Quaternary sediments (Isiorho, et al., 1992; Obaje, 2009; Adepelumi et al., 2012; Chukwunonso et al., 2012). However, hydrological investigation using remote sensing in the Bornu basin indicated few surface lineaments interpreted from Landsat TM 4 images (Isiorho et al., 1992). Relationship of the lineaments with the groundwater quality and groundwater movements in the south-western area of the Lake Chad Basin was established. A 14 km long lineament observed on a Landsat imagery and validated from resistivity survey delineated the subsurface extent of the lineament (Isiorho and Nkereuwem 1996).

Structural architecture of the Bornu basin from seismic evidence indicates presence of faults and folds. Deformations during the Late Cretaceous, which affected the basement and restructured the basin, had produced uplifts, arching and widespread horsts, grabens and related faults. The faults are mostly high angle normal faults and rarely reverse faults. The faults are related to the tensional regime, which include normal faults and graben or those related to the under-thrusting magmatic intrusives, which include reverse faults and horst associated with symmetrical folds. The folds are mostly low-lying structures dissipating upwards and flattening with depth (Okpikoro and Oluronniwo 2010). However, anticlines and synclines in Dumbulwa and Mutwe in southern part of the basin trending NW-SE are the only fold structures reported in the basin (Carter, 1963; Adepelumi et al., 2012).

Structural elements in the basin mostly terminate at the Maastrichtian upper sequence boundary beneath Tertiary sediments (Okpikoro and Olorunniwo, 2010; Avbovbo et al., 1986). Qualitative interpretation of aeromagnetic data in the basin shows the presence of large magnetic anomalies in the northern part of the basin, which

conforms to the structural axial trend of the basin itself. The various anomalies and structural patterns show narrowly spaced linear and sub parallel patterns of possible faults or local fracture zones. Magnetic susceptibility in the basin is associated with fracture zones due to oxidation of iron and or due to dyke emplacements having magnetic source materials different from the host rocks (Anakwuba et al., 2011).

2.4 Summary of research gaps in the literature

Critical evaluations of the published literatures studied so far on the tectonic structure and lithostratigraphy of the Bornu basin have indicated aspects, which justify further research. The following deductions are presented:

1. Surface expressions of the rift features and the regional scale morphology of the subtle expressions of subsurface horst and graben that may exist in the basin are not mapped.
2. Surface structures and other surface geomorphological features were undetected since traditional field geological mapping is constrained by flat topography and cover sediments.
3. Structural relationship between the surface and subsurface lineaments and their relationship with potential oil and gas trapping features, which would influence petroleum prospectivity in the basin are not established.
4. Lithostratigraphy of the northeast Bornu basin is not investigated using integrated data analysis that allows for validation.
5. The Bornu basin tectonic rift extension setting within the regional WCARS basins is not been evaluated from surface and subsurface perspective.
6. The implication of structural inversion resulting from the regional Santonian compression as it affected the Bornu basin need to be constrained from new analyses,

as the imprints of the Santonian inversion and its hydrocarbon implication in the basin are not presented so far.

7. The characteristics of the geomorphic features including palaeoshorelines and palaeodrainage systems and their structural relationships were not investigated.
8. Quaternary developments of the basin as well as the Tertiary geology were poorly understood.

Chapter 3:

Review of geological remote sensing concept, lineament analysis and their potential applications in the Bornu basin

3.1 Introduction

Surface structural lineaments including fractures, faults and shear zones as well as their relationships with the lithostratigraphy of host rocks are common features in sedimentary basins. From recent technological advances in the field of geosciences, one approach for mapping geologic features in geomorphological settings similar to the Bornu basin is the use of remote sensing or Earth Observation. Mapping of surface lithology and lineaments in several contiguous and analogous basins in the Saharan region indicate the effectiveness of remote sensing in such geological settings. According to Guo et al., (1997) characteristics of structural features and their host rocks, discernible from synoptic view of remote sensing often relate with the distribution of the subsurface structures.

Tectonic history of basins relates to the influence of surface structural lineaments that often reflect the configuration of the basement structure at depth. Understanding of surface and subsurface lineaments is required to ascertain geological features and increase reliability of interpretations. This chapter synthesizes the basic concept of remote sensing and Earth Observation as applied in analogous geological settings with a view to understanding and rationalising the potential applications of spectral mapping and lineament analysis to deduce the characteristics and tectonic relationship of lithology and structures in the north-eastern Bornu basin.

3.2 Imagery sources and acquisition

Detail review of the common datasets used in exploration as well as the most applicable data types used for analyses of the Bornu basin are given in section 3.4. Various orbital optical and radar remote sensing systems with different spectral, spatial and radiometric characteristics were launched globally in the last fifty years and the image data held with governments and private agencies are provided both freely and commercially (Grandjean et al., 2006). The north-eastern Nigeria including the Bornu basin area is covered by various satellite imageries including Landsat 7 ETM+, Envisat ASAR and SRTM DEM. The properties of the datasets used in this research are given in Table (4.1).

Remote sensing is the science and art of studying an object, area or phenomenon from data obtained by instruments that were not directly in contact with the matter under investigation (Lillesand *et al.*, 2007). Satellite remote sensing and Earth Observation deals with acquiring, processing and interpreting images obtained from spacecrafts and satellites by the interaction of emitted electromagnetic energy with the Earth surface (Sabins, 1996). The reflected energy measured by a sensor from an airborne plane or a space-borne platform generates an image of the Earth landscape captured beneath the sensor (Fig 3.1). Satellite imageries are recorded in the ultraviolet, visible and near-mid infrared wavelengths of the electromagnetic spectrum. However, due to significant atmospheric absorption of the radiation, measurements are not been recorded in the ultraviolet wavelength region. Data recorded as imageries, form the primary source of information of the ground covered by the sensor (Richards et al., 2005).

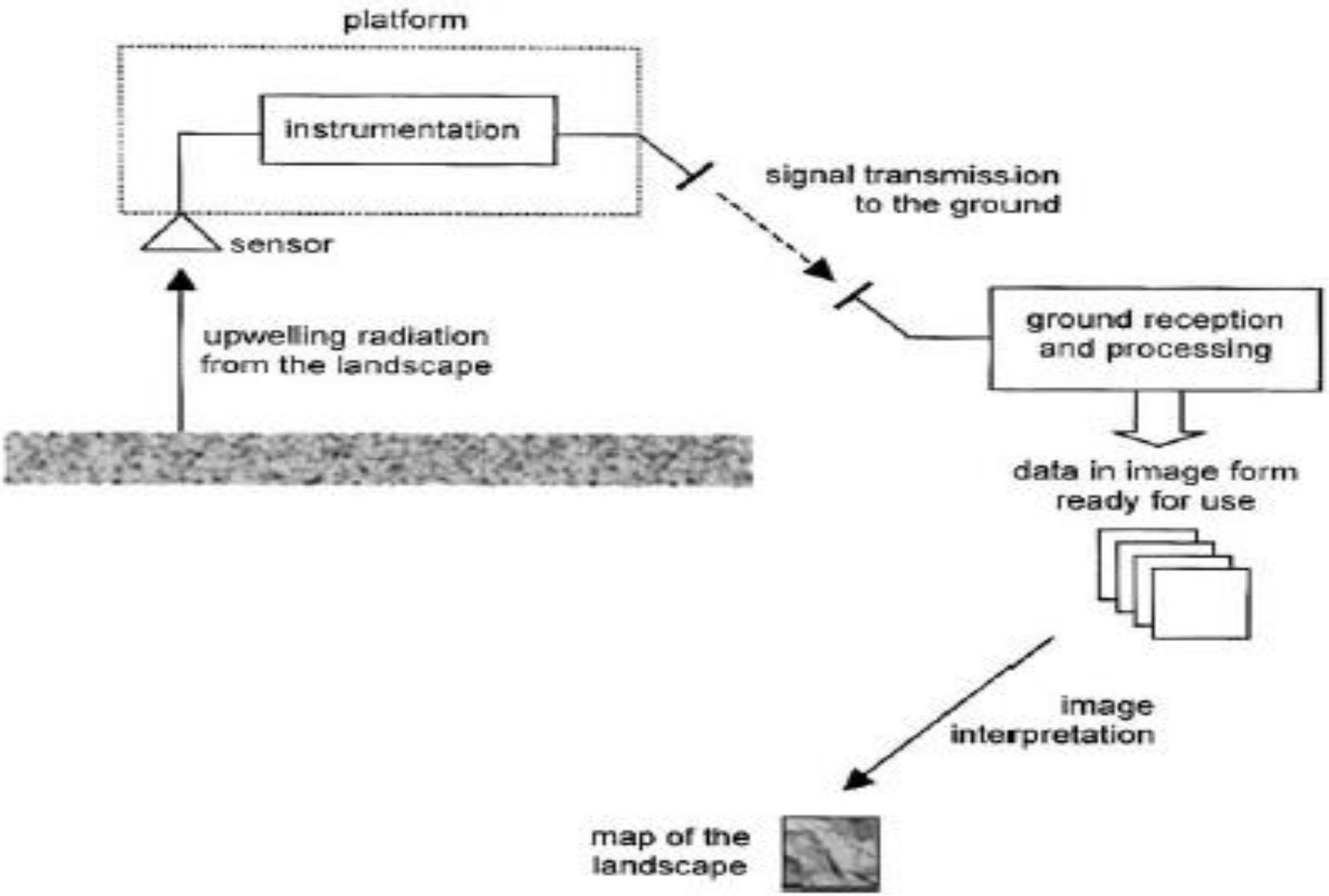

Fig 3.1. Electromagnetic energy flow and generation of imagery in remote sensing (Richards et al., 2005)

The visible region has red, green and blue (RGB) colour bands, which range from 0.4 – 0.7 µm where the optical remote sensing systems are recorded. The infrared (IR) region divides into reflected and thermal sub regions. The reflected IR sub region ranges from 0.7 – 3.0 µm and the thermal sub region ranges from 3.0 – 15 µm while the microwave region wavelength ranges from 10 mm to 100 µm (Sabins, 1996) (Fig. 3.2). A typical satellite image acquired and generated in digital format is spatially composed of discrete picture elements referred to as pixels (Fig 3.3). The main characteristics of a digital image band include its spatial resolution representing its pixel size, its radiometric resolution representing its range of brightness values and its spectral bands, which represent spectral measurements made by individual sensors (Richards et al., 2005). Accordingly, Landsat 7 ETM+ raster images used herein have 30 m with 15 m panchromatic band resolutions spanning 170 x 185 km^2 with three visible bands (1, 2, and 3), three reflected IR bands (4, 5 and 7) while band 6 records energy in the thermal region (Fig. 3.2). Spectral characteristics of different rocks are similar in the visible bands but distinguishable in the optimum reflected IR bands.

Synthetic Aperture Radar (SAR) records day and night images with or without cloud cover. The microwave radar imageries are comparatively more useful for structural mapping and detection of different outcrop signatures and topography due to the strong highlighting and shadowing effects. Accordingly, the C - Band image mode of Envisat ASAR, used herein has a spatial ground resolution of 30m x 30m. The Shuttle Imaging Radar (SIR) is capable of penetrating dry sand with to detect immediate subsurface structural features (Sabins, 1998a). However, the highlighting and shadowing property of the radar signal can be used in the north-eastern Bornu basin to detect surface structure including those few meters beneath sediment cover. In the absence of field-based expressions of structures and lithological characteristics in the

north-eastern Bornu basin, these image characteristics can provide a synoptic view of geomorphic features in the basin.

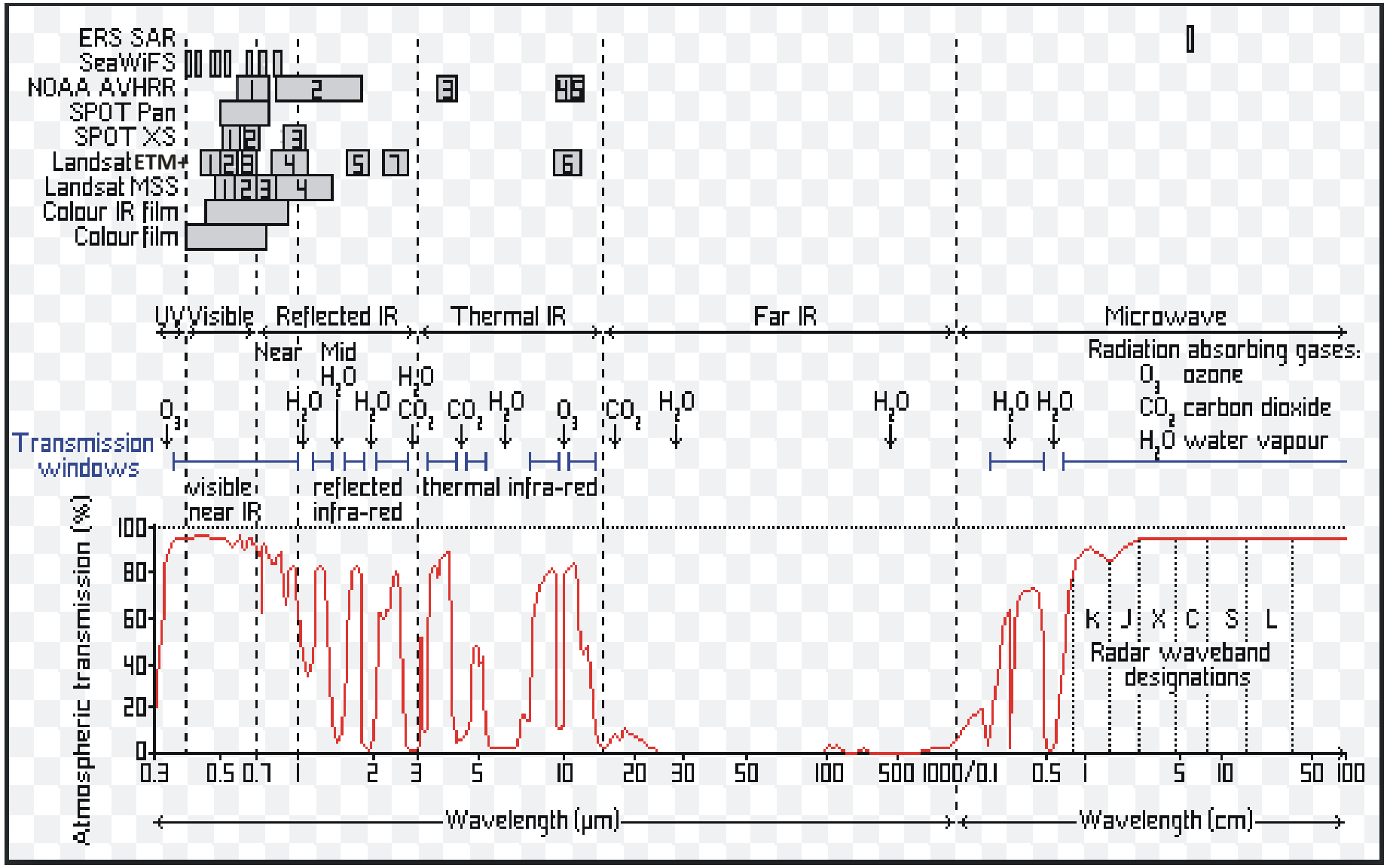

Fig 3.2. Electromagnetic spectrum showing wavelength ranges with corresponding frequencies and energy regions (Harbord n.d).

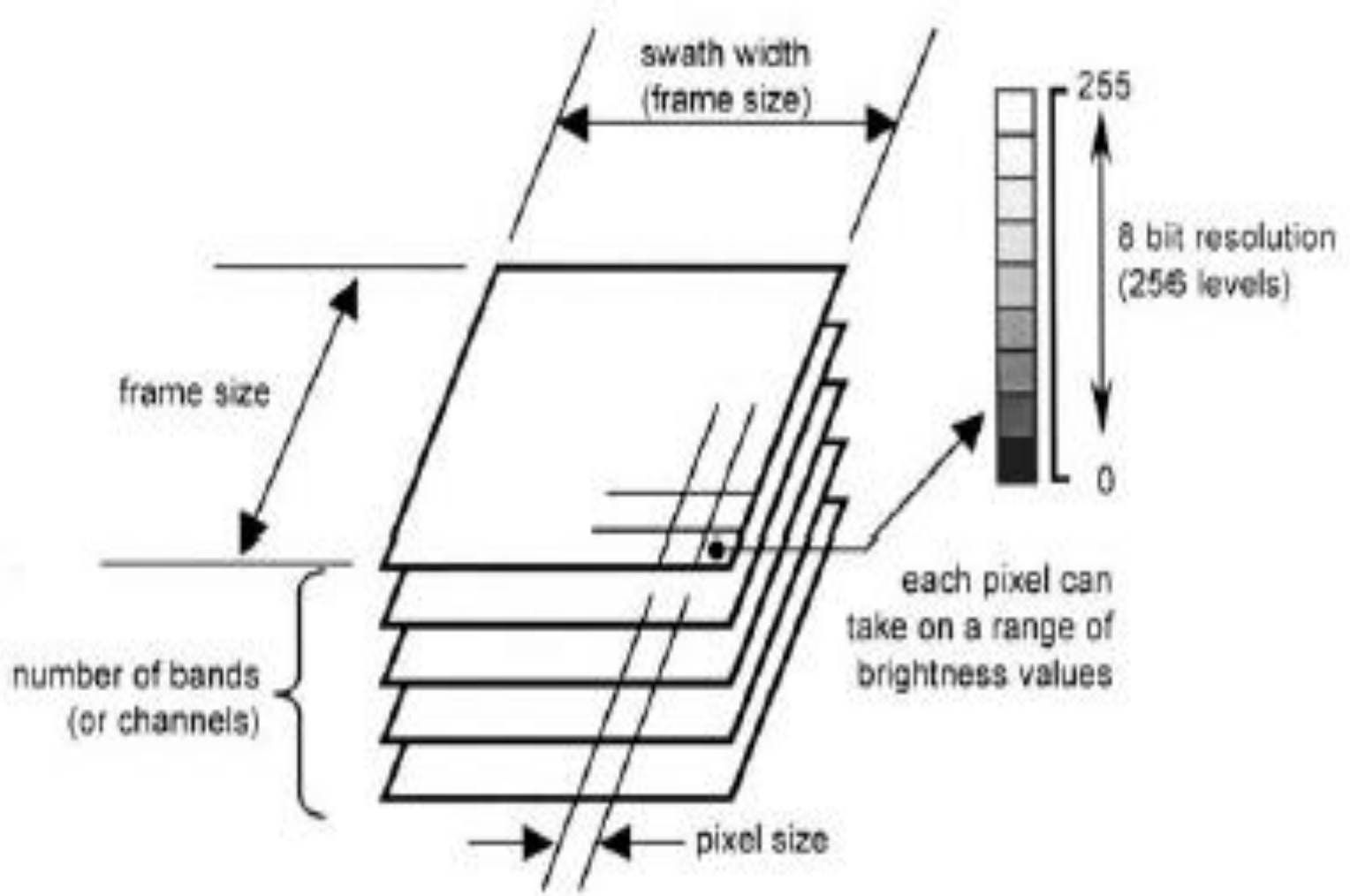

Fig 3.3. Different components of a digital image data showing arrangement of bands (Richards et al., 2005)

3.3 Outline of the geological remote sensing method

The remote sensing digital image analyses involve multiple operations carried out on satellite images to facilitate geological interpretation. Geological remote sensing method is generally carried out in three main stages including; (1) image enhancement for lineament extraction and characterisation of geological structures, (2) image classification for geological mapping and (3) draping of satellite images and multiple data in a GIS environment (Koike et al., 1998). Harris et al., (2012) developed a Remote Predictive Mapping (RPM) approach for acquiring, processing and interpreting geological remote sensed datasets to generate predictive lithological and structural maps in GIS layers. Sequentially, the methodology involves acquiring raw satellite image data; image pre-processing; gridding and geo-referencing; image enhancement; image classification; overlaying existing geology and geophysical data. The resultant images are interpreted using visual or automatic methods (Harris et al., 2012). However, automatic extraction of lineaments using image analysis software complements the hand tracing of lineaments observed on satellite images (Masoud and Koike, 2006). Consequently, the predictive spectral lithological mapping method can be developed for the north-eastern Bornu basin since previous field based studies have not produce geological maps for the area from field studies. Therefore, the manual and automatic lineament extract methods can be developed in the north-eastern Bornu basin to generate a more validated lineament mapping process.

3.3.1 Image pre-processing and correction

Richards et al., (2005) have provided a methodology for image pre-processing, since raw digital image data initially require pre-processing to correct errors in the image geometry (geometrical distortions) and image radiometry (radiometric distortions). Thus, preliminary corrections of integral defects in the system during the data acquisition process are required. The geometric distortions during image acquisition are due to factors including; (1) Earth rotation, (2) wide sensor field of view, (3) Earth curvature, and (4) sensor platform variation in altitude and velocity. Geometric corrections usually involve linking the pixels of an image with the corresponding coordinates of the pixel points on the ground via a map projection system or by performing co-registration of two corresponding images.

Radiometric distortions mechanisms affect the measured brightness values of image pixels causing variation in distribution of the brightness in an image relative to that on the ground. Radiometric distortions lead to variation of the brightness values of the pixels in an image band relative to the spectral reflectance behaviour of the ground area. Radiometric distortions in a remote sensing imagery can be due to the atmospheric effects on electromagnetic radiation and on remote sensing imagery as well as instrumentation errors. Common radiometric corrections including haze removal, caused by scattering or absorption effects of the atmosphere as well as noise reductions are carried out before geometric correction (Richards et al., 2005).

3.3.2 Contrast and histogram stretching

In digital image enhancement, contrast stretching improves the limited number of pixel values that occurred on the image. This is achieved by stretching each of the pixel values out to a display level such that the lowest pixel assigned to values close to 0 and the highest actual pixel values assigned to a display level close to 255 (Fig. 3.4). Each image pixel has a digital number (DN) from zero (dark colours) – 255 (bright colours) and pixel values are displayed on a brightness scale or display level, which are assigned values across the range (Lillesand et al., 2007).

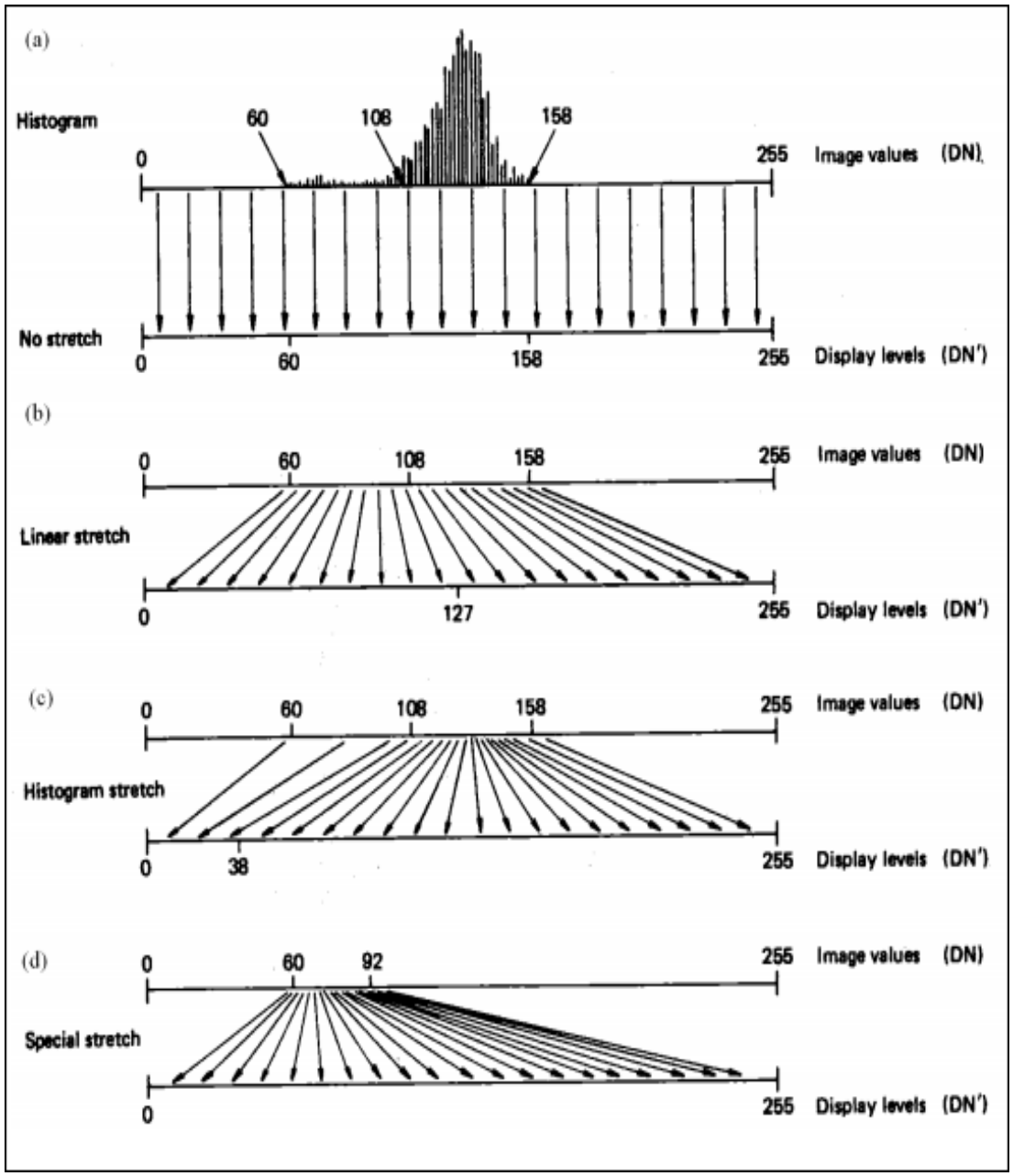

Fig. 3.4. Image contrast and histogram stretching (modified from Lillesand et al., (2004). Such different contrasts can be sampled on images for the Bornu basin to get the most suitable appearance for analysis.

Histogram of an image evaluates its tonal or radiometric quality. The image histogram is a graph displaying the number of pixels with given brightness versus brightness value. An image that utilises all available range of brightness values shows a histogram with bars spread over its full range. Histogram modification refers to the mapping of image brightness values with poor contrast to improve contrast and produce new image with the histogram full of bars spread over the brightness range (Richards et al., 2005).

3.3.3 Band Combination and Band Ratio Images

R-G-B (Red-Green-Blue) band combination and RGB band ratio composite images (Ramadan et al., 2001; Pena and Abdelsalam, 2006) are important image processing and enhancements used in the discrimination of lithology and structures (Kenea, 1997; Drury, 2001). Colour composite images are generated by compositing any three spectral bands to generate RGB colour combination such as bands 7-4-2 which is commonly used for arid and semi - arid regions such as the north-eastern Bornu basin. Teeuw et al., (2005) summarised various RGB band combination and band ratio images from optical remote sensing platforms including the features they highlighted (Table 3.1). Bands 3, 4, 5 and 7 in the near infrared and mid-infrared ranges of the electromagnetic spectrum on Landsat 7 ETM+ differentiate lithological units (Leverington and Moon, 2012).

RGB 7-4-2 combination applies extensively for oil and gas exploration in arid environments (Pena and Abdelsalam, 2006). Band 7 and band 4 in Landsat 7 ETM+ are effective for mapping iron oxides rich rocks dominant in arid regions due to the lack of vegetation, which has relatively high total reflectance in the near infrared region of the electromagnetic spectrum (Jensen, 2000). Discrimination of vegetation results from their low reflection in Landsat 7 ETM+ due to absorption in the blue and

red regions and high reflection in the green region of the energy spectrum (Sabins, 1997). Band 2 of Landsat 7 ETM+ in the visible green portion of the electromagnetic spectrum corresponds with the green reflectance peak of vegetation. Moreover, geological features are commonly discriminated in Landsat 7 ETM+ bands 4, 5 and 7 because the bands highlight most rock types and lineaments (Won-In and Charusiri, 2003). Very Near Infrared (VNIR) and the Short Wave Infrared (SWIR) RGB colour combinations of the Landsat 7 ETM+ are effective in lithological mapping since many sedimentary rocks have distinctive spectral features in this portion of the electromagnetic spectrum (Gaffey, 1987; Evans, 1988).

However, ratio of DN values of pixels with high total reflectance and the DN values of corresponding pixels with low total reflectance image bands of Landsat 7 ETM+ are more useful in distinguishing lithology than the RGB colour combination images (Jensen, 1996; Abdelsalam et al., 2000a, b). Band rationing in remote sensing digital analysis is a technique of displaying various spectral variations in images for effective visualisations (Sabins, 1997). According to Sultan et al., (1986) and Sultan et al., (1987) band ratio images are generated to utilise the maximum potential of the spectral properties of the features in an area. Band ratio images from multi-spectral optical Landsat ETM+ data are applicable to map different lithology better than using RGB band combination images (Abdelsalam et al., 2000 a, b; Pena and Abdelsalam, 2006). Various band ratio combinations were used for lithological mapping in arid areas by many workers including Abrams et al., (1988); Pena and Abdelsalam (2006); Sultan et al., (1986); Kusky and Ramadan, (2002) and Sabins, (1999). Combined band combination and band ratio method is applicable in the north-eastern Bornu basin due to its semi-arid setting and potential for iron oxide rich lateritic sediments as indicated on Table (2.1). Presence of few vegetation cover

around the Lake Chad shore in the north-eastern Bornu basin can be distinguished from the surrounding lithology by the Landsat 7 ETM+ images.

Table 3.1. Table showing various RGB combinations and band ratios for Landsat 7 ETM+ used by several workers (Modified after Teeuw et al., (2005).

RGB Combination	Highlighted features	Band ratio
Landsat 7 ETM+		Landsat 7 ETM+
321	True colour	
432	Vegetation chlorophyll highlighted in red	4/3, (4-3) / (4+3)
463 468 467 741 764 721 742	Soil and rock types	6/7, 4/6 3/1 (6/7) (4/6) (3/1) (3/1) (6/7) 3/6) (4/6) (6/7) (7/6)
641 741	Hydrothermal alteration of volcanic rocks	
761 742	Discrimination between Fe-rich soils and rocks	3/1, 4/6
631 672 234 742	Useful with various vegetation and rock types	

3.3.4 Image classification

As indicated in section (2.3.2) surface lithological characteristics of the sedimentary deposits in the Bornu basin are difficult to map using traditional field traverse methods. As such, in mapping surface geological materials in the basin, spectral classification presents a suitable method owing to the presence of un-differentiated cover sediments. Image classification is a method of attaching labels to image pixels based on their spectral character. Reflectance properties of spectral lithological units including rocks and soils depend on the mineralogical composition of the spectral classes mapped. As such, lithological identification is determined using the differences in reflectance spectra of individual classes (Gaffey, 1987). Classification of images are categorised into supervised and unsupervised methods. Unsupervised classification method involves assigning pixels to previously unknown spectral classes where clusters of pixels determine the number and location of the spectral class of each pixel. The classes identified are matched with corresponding characters of reference spectra in a spectral library or ground data.

Supervised classification is based on statistical and other geometric techniques of separation of spectral classes involving user identified surface cover representative pixels as training classes for automatic mapping of similar signatures in the whole area. Supervised classification consists of three general steps including; (1) selection of training pixels for different spectral class based on a reference data, (2) determination of the mean likely position of the spectral class where a pixel from a class is most likely to be located and, (3) forming the covariance matrix of the distribution representing its directional spread in the pixel space (Richards et al., 2005).

3.4 Review of applications of surface and subsurface structural lineament detection and their applicability to the Bornu basin

3.4.1 Applications of surface lineaments in structural studies

As field mapping in some remote regions is almost impractical due to inaccessibility, cost and time for regional scale studies, arguably, the most important aspect of satellite geological remote sensing for tectonic studies and for oil and gas exploration is lineament analysis (Mabee et al., 1994; Koike et al., 1998). The concepts and geological significance of lineaments are well documented in O'Leary (1977); O'Driscoll (1981); Thurmond et al., (2006); Chaabouni, et al., (2012). Lineaments interpreted from aerial photography and satellite imagery are natural simple or composite pattern of linear or curvilinear features detectable on the Earth surface, which geologically may represent crustal structures or zones of structural weakness. Marghany (2012) defined lineament as a linear feature on the ground surface, which represent an expression of an underlying geological structure including faults expressed as fracture zones, shear zones, aligned valleys, hills or coastlines. Caran et al., (1982) described lineament as a linear and continuous feature in a solid planetary body having definable end-points, relatively high length to width ratio and definite azimuth relating to geologic structure or stratigraphy. The extent of a lineament varies from local to continental scales examples include the Trans-Saharan Belt, Trans-Brazilian Lineament and the San Andreas Fault. Fractures that form in response to lithostatic, tectonic and thermal stresses or high fluid pressures occurring from micro scale to continental scale are important as pathways for fluid flow. Peterson, (1985) and Mah et al., (1995) referred remote sensing lineaments as mostly a reflection of rock fractures observed by vegetation and topographic alignments. Tonal alignments are used for lineaments detection on Landsat 7 ETM+, radar and SPOT images (Masoud and Koike, 2006). Linear features formed by

edges of features marked by subtle tonal differences in an image are often difficult to detect on the image as well as in the field. Lineaments may also represent straight stream channels, alignment of uplifts and depressions, abrupt changes in soil tonal expressions, abrupt changes in topography and changes in the lithology. Wise et al., (1985) described the term “lineaments swarm” to distinguish subparallel lineaments populations numbering in tens to hundreds and ranging in lengths from 20 to 100 km and spacing up to tens of kilometres. O’Driscoll (1981) classified short lineaments as high frequency lineaments while regional lineaments are low frequency lineaments, which form narrow aligned zones.

Lineament features in the Earth crust occurring in rock outcrops show varying orientations and lengths commonly disappearing locally but often with persistent trends in continental scales. However, some linear features on satellite images are very short and identified as synthetic such as fence lines, roads, rails. Such spurious linear features, which are not geological in origin, should be disregarded (Mostafa and Bishta, 2005). Due to scale of observation, some lineaments are difficult to verify by field geology. However, various remote sensed lineaments can be systematically verified using reasoned estimates from field studies (Arlegui and Soriano 1998).

Although, the origin of some lineaments became a subject of argument in modern structural geology since precise data on the ages, tectonic settings and tectonic stress regimes of the lineaments are often misinterpreted (Wise et al., 1985). Major lineaments are lithospheric in origin based on the assumption that a laterally extensive fracture zone could remain within the upper mantle layer over an extended period of time (Lenov, 1991; Dunbar and Sawyer, 1989).

3.4.2 Applications of subsurface lineaments in structural studies

The broader terminology of lineaments also include subsurface structural alignments and fracture systems mapped from seismic, gravity and magnetic anomalies (Guo and George, 1999), which are also referred to as basement lineaments (Prabaharan et al., 2013). The subsurface geophysical anomalies associated with geological structures at basement depths can propagate upward to the surface (Fig 3.5), such that both regional and local tectonic fractures may appear as surface lineaments on satellite images (Gay, 2012). Significant potential exists for surface lineaments that developed from pre-existing fractures in the Bornu basin underlying basement following the Cretaceous rifting. Geological interconnections between basement faults with joints and surface lineaments that extend from basement indicate the association of lineaments with underlying sedimentary deposition. However, in the absence of hydrocarbon extraction from the Bornu basin, Gay, (2012) discovered that lineaments might develop from slight movements of faults in underlying basement rocks in response to the overburden sedimentary deposition. Regional gravity lineaments marking the margins of Bouguer anomalies originate from deeper sourced structures (Dufréchou and Harris 2013). Collinearity of Quaternary lineaments with basement structures, which have topographic expressions at the surface are evidence of tectonic reactivation and rejuvenation of pre-existing zones of weaknesses (Pana et al., 2001).

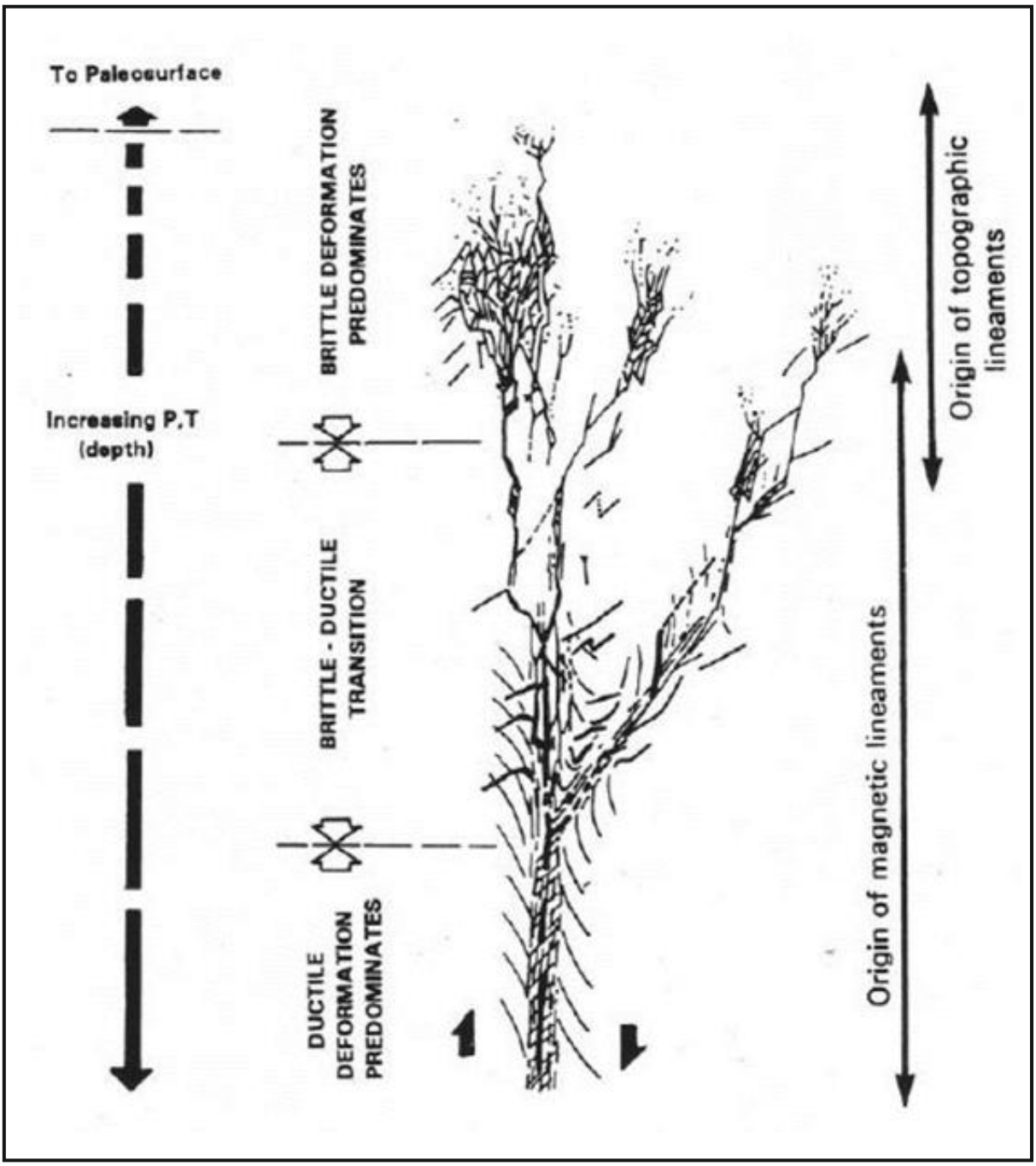

Fig 3.5. Sketch of origin and geologic setting of structural lineaments from the deep subsurface and propagating to the surface (Athanasios, 2012).

3.5 Spectral lithostructural mapping in low relief semi-arid regions

The concepts of lithological mapping in arid regions using Landsat 7 ETM+ images are well established in (Sultan et al., 1986; Sultan et al., 1987; Chavez and Kwarteng 1989; Abrams and Hook, 1995; Sabins, 1998b). Satellite remote sensing imageries have been analysed to generate lithological and structural base maps for hydrocarbon exploration in different geologic terrains for decades. Traditionally, geological maps are prepared using data obtained from field-based traverses at outcrop areas and extrapolated to remote and non-rock outcrop areas. Rock types observed in the field are marked on scaled topographic base maps to generate the final geological maps, which are generally not georeferenced. Traditional field geological mapping is often constrained by inaccuracy of geological boundaries and regional scale observation of subtle structural details (Harris et al., 2012), as obtained in the Bornu basin.

Remote sensing/Earth Observation data provide rapid and relatively cheaper analysis of lithology, structural lineaments and mineral deposits in arid areas, as such the techniques are increasingly been applied to similar areas. Spectral mapping techniques in arid regions utilising systematic mineralogical inferences from Landsat multispectral data are based on identification of spectral reflectance features identical to various rock types (Qaoud, 2014). However, knowledge of the general distributions of the rock outcrops is critical for validating the mapped units. Vegetation cover, which can adversely restrain the spectral reflectance signatures of rocks are commonly absent in arid regions. ASAR imagery as an active system with long wavelengths in the microwave region of the electromagnetic spectrum has a side-looking geometry, which provides complete transmission and enhanced imaging of low relief features similar to the physical setting in the Bornu basin. Some of these

physical conditions including presence of fine-grained sediments cover, dry conditions are available for the Bornu basin.

3.6 Remote sensing and geophysical data integration

Integrating geophysical data with remote sensing imagery for lineament analysis has been carried out by several workers including Laake et al., (2006); Insley et al., (1996); Vesnaver et al., (2009); Kaymakci et al., (2010); Laake and Cutts (2007); Laake et al., (2006); Sandwell and Smith (2009); Laake et al., (2011); Komolafe et al., (2012). Although remote sensing data provides spatial coverage and near surface imaging they do not penetrate the deeper subsurface while geophysical methods provide information at points or along linear patterns and at the deeper subsurface. Geospatial correlation of multiple data visually allows for cross-calibration of the interpreted geological features (Laake *et al*., 2008). The technique of integrating insitu surface and subsurface lineament analysis can be helpful in identifying potential structural anomalies of local and regional extent (Pena and Abdelsalam, 2006). Saadi *et al*., (2008) integrated satellite remote sensing data with gravity and aeromagnetic data and carried out lineament analysis of the surface and subsurface data to delineate an anticlinal structure in Eljufra area of Libya. Saadi *et al*., (2011) combined SRTM DEM, Landsat 7 ETM+, gravity, magnetic and well datasets to study the origin and tectonic setting of the Ghadames Basin in Libya and revealed a fault system, which was active at several stages of the basin development.

Al Fastawi and Van Dijk (1990) have correlated surface lineaments from Landsat TM 5 and Radarsat data with basement lineaments and indicated strong correlations with known oil and gas fields. Mohammed *et al*., (2010) integrated Landsat 7 ETM+,

seismic, magnetic and gravity data to generate surface and subsurface lineaments and evaluated the petroleum potentials the basin.

3.7 Petroleum exploration potentials of lineaments

Over the past 20 years, oil and gas companies have used satellite Earth Observation (EO) technology through the entire project lifecycle from pre-acquisition to full operation including the use of both optical and radar platforms having different wavelengths across the electromagnetic spectrum. Various datasets used include Landsat TM, Landsat 7 ETM+, ERS SAR, Envisat ASAR, SPOT and recent platforms including Landsat 8, Sentinel -1A and PALSAR. Applications of EO data include logistical planning to reconnaissance and detail geological mapping of lithology, structures and hydrocarbon seepage (Laake and Insley 2004) and Ferretti (2014).

SAR interferometry (InSAR) is a developing technology for oil and gas industry used for analysis of surface deformation monitoring due to subsidence arising from subsurface fluid extraction and hydrocarbon seepages and other environmental and risk mitigation measures. However, the Bornu basin is currently not a petroleum-producing basin, as such, use of the InSAR technology for detection of subsidence due to fluid extraction is beyond the scope of this research. However, exploration for oil and gas in the Bornu basin since several years ago remains unsuccessful (Obaje, 2009), partly due to the poor understanding of the relationship of the surface and subsurface structures necessary for trap formations. The applications of structural lineaments in hydrocarbon exploration in various sedimentary basins have already been established (Guo and Carol, 1995; Sabins, 1998 a,b; Zeinalov, 2000; Yassaghi, 2006; Mohammed et al., 2010). Hydrocarbon exploration in areas including the Sahara Desert and adjoining environs in North Africa and the Bornu basin area that have few or no field exposure of insitu geological features is obviously challenging

due to thick sand cover. However, integrated multispectral Landsat 7 ETM+, Advanced Space-borne Thermal Emission and Radiometer (ASTER) with radar and Digital Elevation Models (DEMs) are useful for geological mapping in arid regions characterised with lack of continuous bedrock outcrops to aid oil and gas exploration (Pena and Abdelsalam 2006).

Thus, the concept of using lineaments mapping in structural geology depends on whether the surface anomalies represented by lineaments relate to the subsurface geological features genetically and physically. Oil wells were drilled from leads provided by structural lineaments mapped from interpretation of radar images even without seismic confirmation surveys. Geological maps obtained from Landsat TM remote sensing on the scale of 1:250,000 were used to delineate prospective drilling sites in desert area (Sabins, 1998a). Surface lineaments trends were used as structural contours to delineate areas of fracture-enhanced permeability and detect overlap with subsurface pre-Permian oil and gas reservoirs. Similarly, surface lineaments overlap subsurface oil and gas traps (Guo et al., 1997). Anticlines mapped along basement fault lineaments proved as exploration targets for oil and gas. Recurring patterns of such lineaments associations individually or collectively as lineament zones and lineament areas, which correlate with subsurface structures, could prove important for exploration (Yassaghi, 2006).

Chapter 4:

Optical – Radar – DEM data integration for geological mapping in the north-eastern Bornu basin

4.1 Introduction

Semi-arid tropical regions in sub-Saharan Africa are characterised with flat topography, thick cover sediments and lack of continuous bedrock outcrops (Sabins and Wender, 1991; Jensen, 2000; Abdelsalam et al., 2000b: Pena and Abdelsalam 2006; Laake et al., 2008). Although Late Quaternary events are thought to have had significant effects on the development of the landforms in the northeast Nigeria (Servant, 1983), an alternative approach for identifying regional geomorphic features including surficial deposits and lineaments is to use satellite Earth Observation images to provide a base map data for lithostructural and tectonic characterisation of the north-eastern Bornu basin. This chapter describes the utility of free multispectral Landsat 7 ETM+, SRTM DEM and ASAR Earth Observation data to spectrally characterise the surface geological materials in the north-eastern Bornu basin.

Satellite remote sensing imageries, which generate lithological and structural base maps for hydrocarbon exploration, are used in different sedimentary settings (Sabins, 1998b). Subsurface geophysical anomalies associated with geological structures at depth can propagate upward to the surface such that both regional and local tectonic fractures may appear as surface lineaments on satellite images (Guo and George, 1999). The methodology used in this Chapter develops on the concept and applications of the Earth Observation data presented in Chapter 3 of this thesis.

This chapter presents the methodology for the characterisation of neotectonic surface structures and surface lithology in the north-eastern Bornu basin, which is part of the semi-arid tropical sub-Saharan region. The features including topography, structural lineaments and surface lithology are extracted from optical multispectral

orbital Landsat 7 ETM+ images, Envisat ASAR and SRTM DEM images. Of these methods, the integration of the Earth Observation (EO) datasets in GIS is highly essential. The SRTM DEM data and ASAR images are important tools for mapping ancient desert fluvial features that were buried beneath sand cover (Ghoneim et al., 2007). The radar datasets are selected because of the C-band wavelength that enables penetration into the cover sediments, which can be tested to reveal the near surface palaeodrainage in the study area. Additionally, this chapter presents the palaeohydrological and surface aeolian features of the north-eastern Bornu basin. Accordingly, this chapter has three primary objectives. The first is to evaluate the utility of geological remote sensing/Earth Observation data in predictive drift lithological mapping as an alternative preliminary approach to field based lithological mapping in the north-eastern Bornu basin. The second objective is to map and analyse surface structural lineaments and assembled them in a GIS to determine their geospatial relationships with the underlying structures interpreted from geophysical datasets in subsequent Chapters 5 and 6 of this thesis. The third objective of this chapter is to separate other surface features including palaeoshorelines, palaeodunes and river channels as well as their relationship with the structural setting and Quaternary development of the Bornu basin.

4.2 Datasets

Mosaic of four cloud free multispectral Landsat 7 ETM+ composite (30 m spatial resolution) images (Figs. 4.1 – 4.4) were used for mapping of lithology and surface lineaments to produce a spectral geological map of the study area. The four Landsat 7 ETM+ images were downloaded freely from NASA's *Earth Explorer.* Four corresponding Envisat ASAR images (Fig. 4.5) obtained from *European Space Agency (ESA)* were utilised to delineate the surface and the near surface lineaments due to the ability of the microwave C - band radar that enables the superficial sand layer penetration, which is typical of the conditions in the study area. Although, for the purpose of geospatial correlation of mapped features in the study area from the various datasets, the smaller image sizes of the ASAR datasets are mosaicked to similar map frame coordinates with the mosaicked optical and DEM images, The characteristics of these images are given in Table (4.1). Correct georeferencing of surface and subsurface maps allow for correlation of geologic features. The geographical coordinates of the images used correspond with the geospatial locations of the well log and seismic data as well as the gravity and magnetic datasets used in this study. Six void-filled SRTM tiles were mosaicked to construct a continuous and seamless digital elevation model (DEM) of the entire study area for delineation of features (Fig. 4.6).

Table 4.1. Specifications of the various Earth Observation datasets used in this study.

Data Type	Scene	Date	Analysis Product
Landsat 7 ETM+ Spectral Bands 1-7 are 30 m resolution. Panchromatic Band 8 is 15 m resolution. DATUM = "WGS84" UTM_ZONE = 33 CLOUD_COVER = 0.00%	4 images (each scene is 170 km x 183 km) Path/Row: Image 1: 185/051 Image 2: 185/052 Image 3: 186/051 Image 4: 186/052	2000-03-31	Spectral lithological mapping and structural lineament analysis
ENVISAT1-ASAR 30 spatial resolution, C Band Frequency, VV/HH polarisation 30 m x 30 m	4 L1 Image mode: Image 1: ASA_IMP_1P Pass: Descending Track:93 Orbit: 35718 Image 2: ASA_APP_1P Pass: Descending Track: 395 Orbit: 49116 Image 3: ASA_IMP_1P Pass Descending Track: 95 Orbit: 12171 Image 4: ASA_IMP_1P Pass Descending Track: 395 Orbit: 8435	2000-01-01 2001-07-27 2004-04-28 2011-05-22	Structural lineament analysis
SRTM DEM 1 Arc – second Global. 30 m.	5Image scenes. Entity 1D: SRTM 1N11EO12V3 SRTM 1N11EO13V3 SRTM 1N12EO12V3 SRTM 1N12EO13V3 SRTM 1N13EO12V3 SRTM 1N13EO13V3	11/02/00	DEM Palaeodrainage analysis Palaeoshorelines analysis Structural analysis

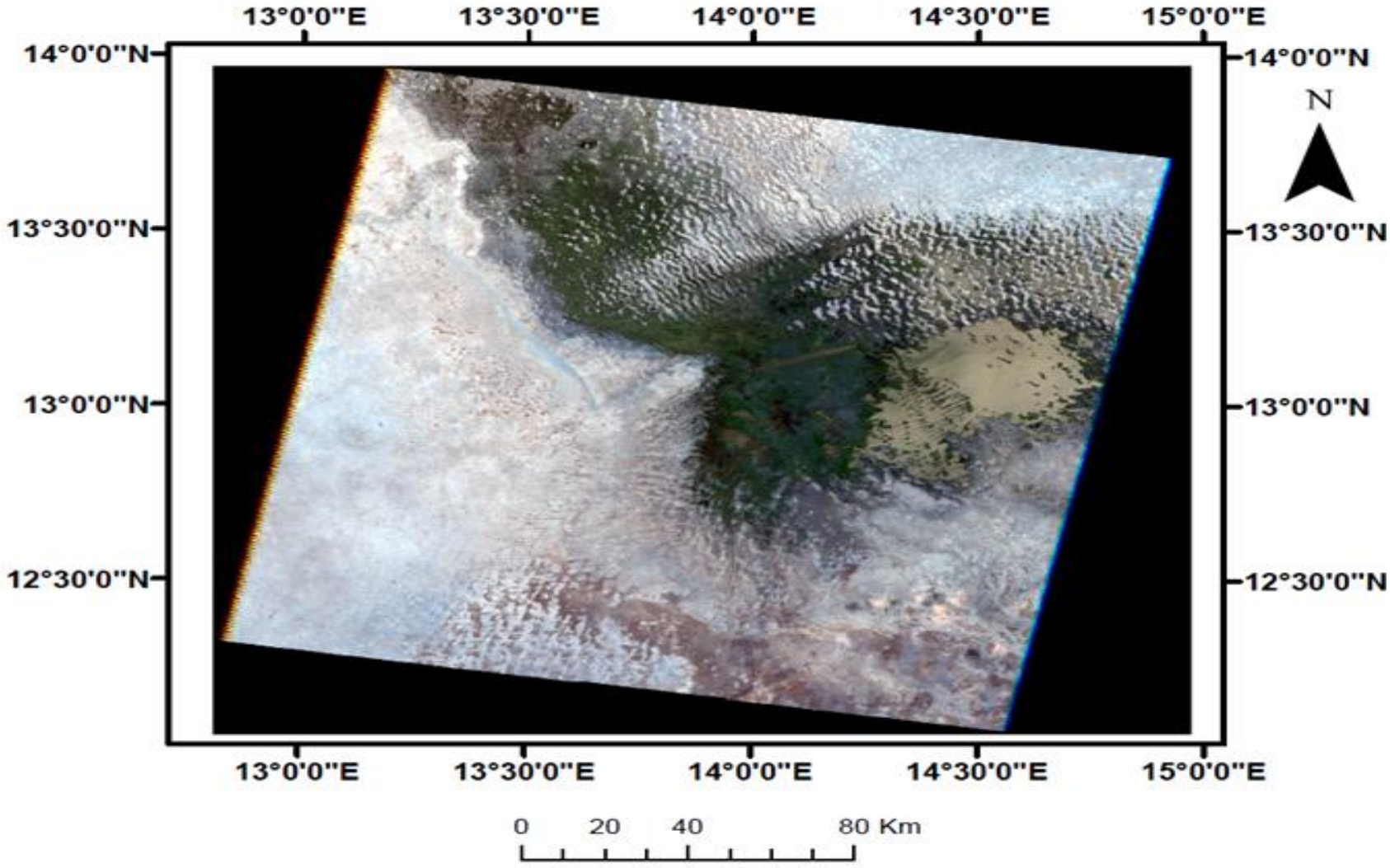

Fig 4.1: Linear stretched RGB 321 Landsat 7 ETM+ composite image. Path/Row: 185/051 of the study area showing Lake Chad.

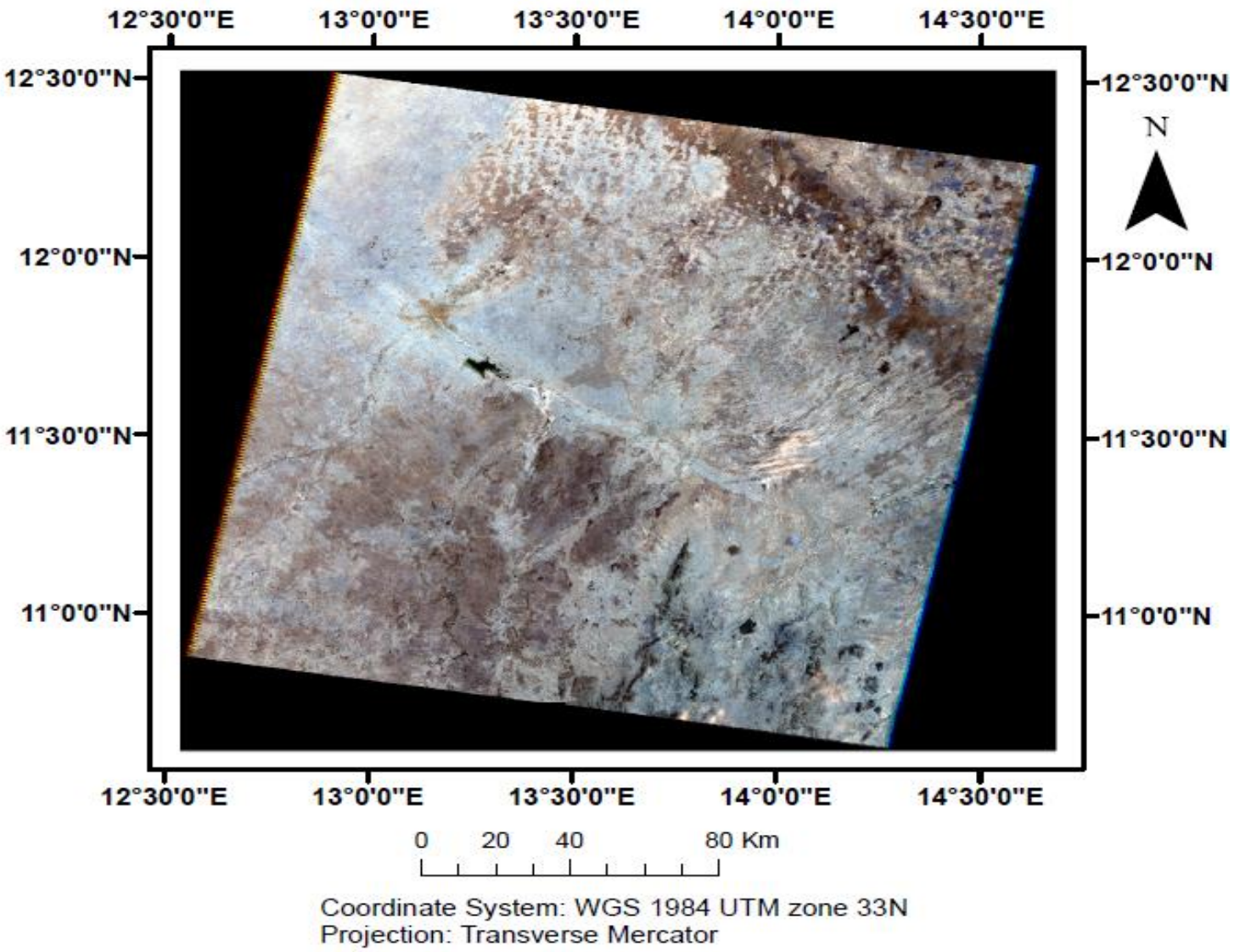

Fig 4.2: Linear stretched RGB 321 Landsat 7 ETM+ composite image. Path/Row: 185/052 of the study area showing Alau Lake along the NW-SE strectched Bama Beach Ridge paleoshoreline.

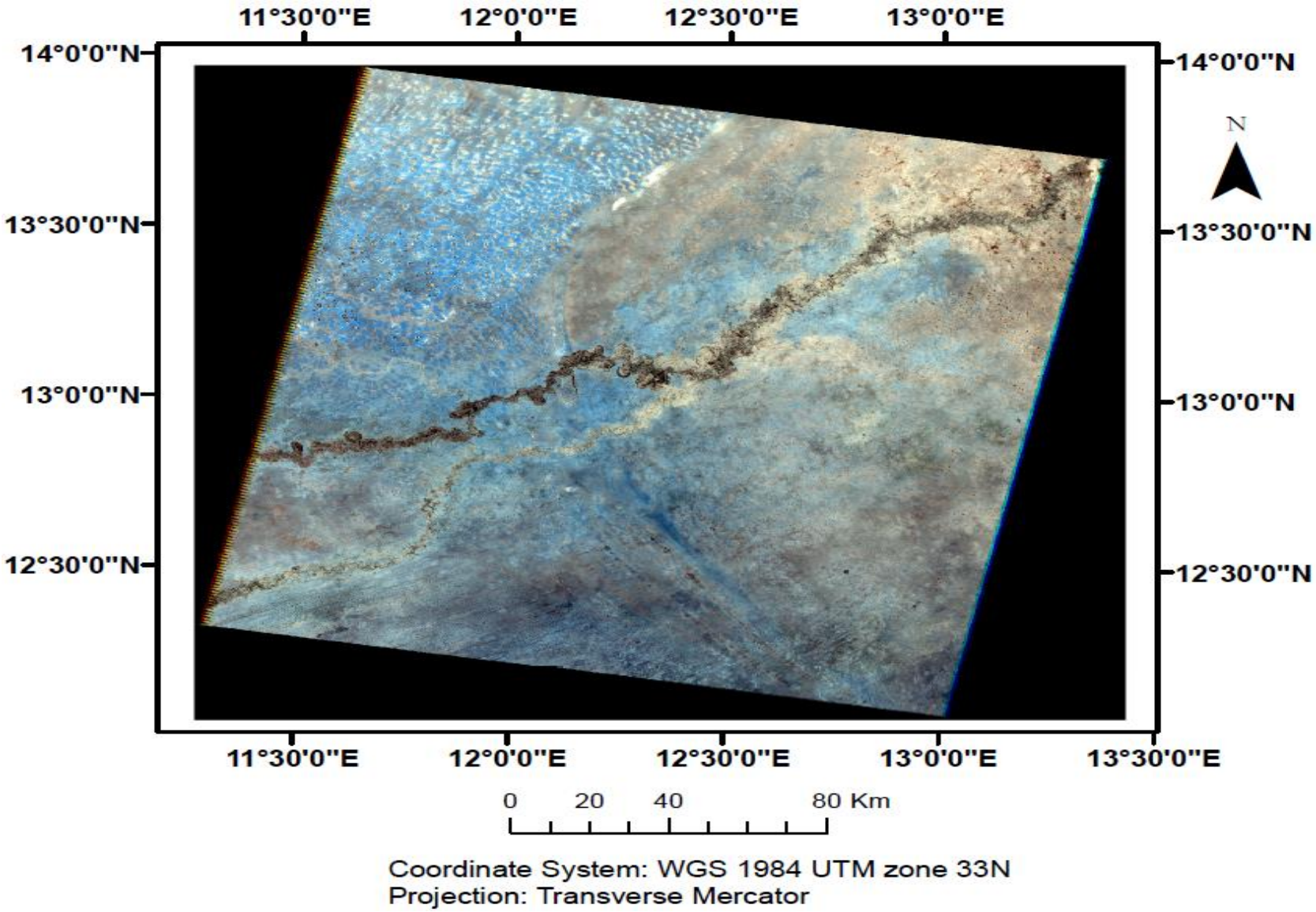

Fig 4.3: Linear stretched RGB 321 Landsat 7 ETM+ composite image. Path/Row: 186/051 of the study area.

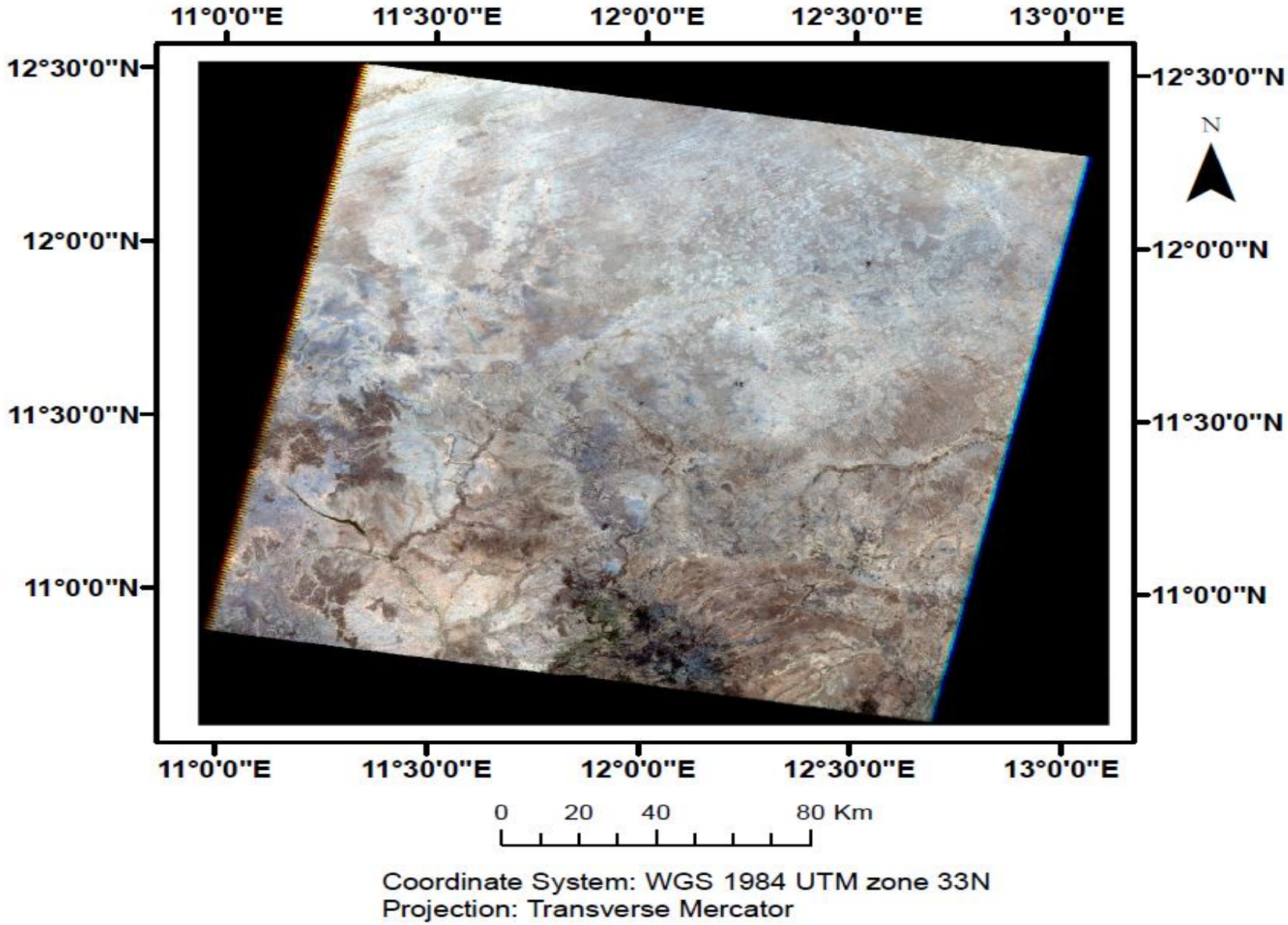

Fig 4.4: Linear stretched RGB 321 Landsat 7 ETM+ composite image. Path/Row: 186/052 of the study area.

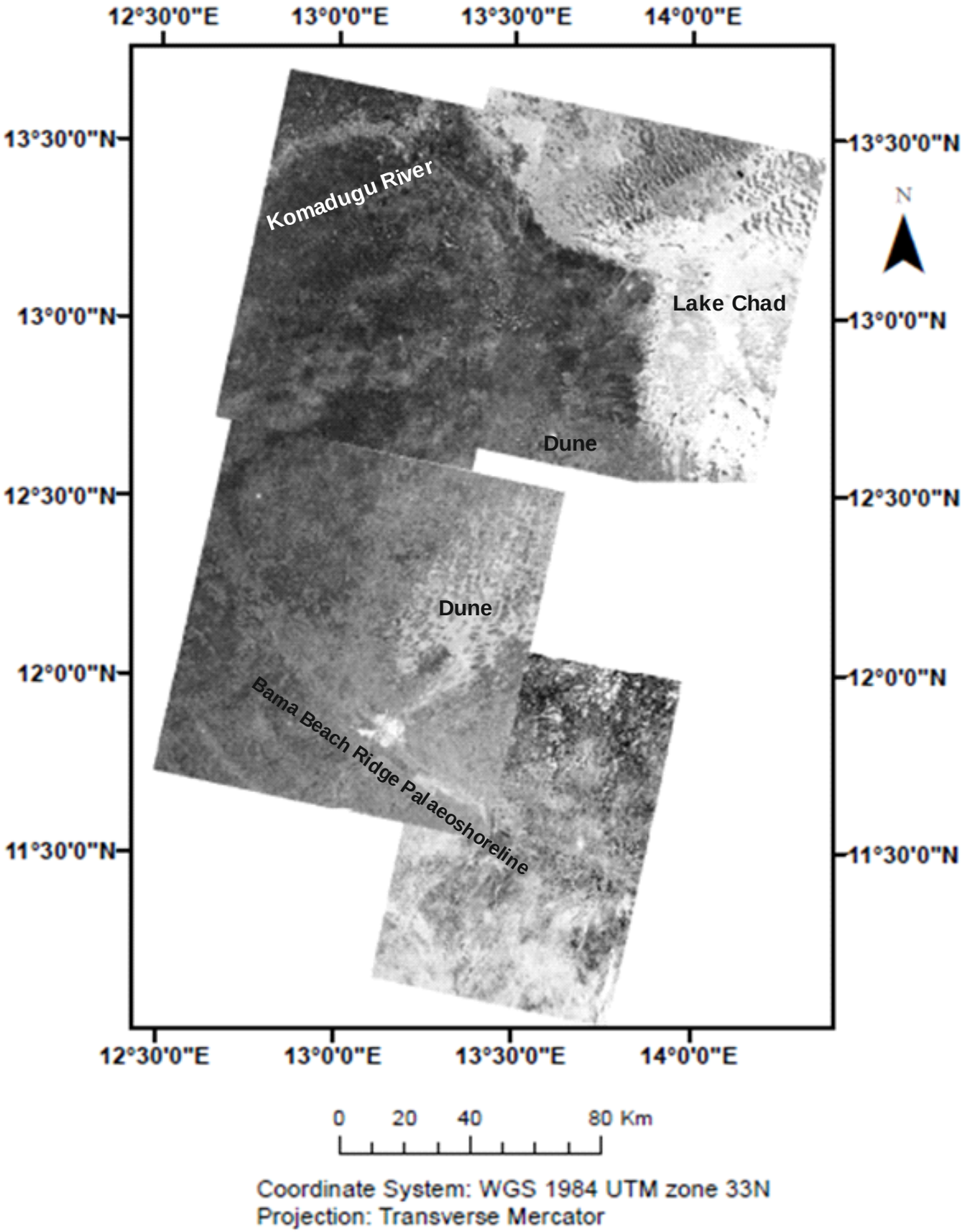

Fig 4.5: Calibrated, speckle filtered, geometrically and radiometrically corrected mosaic of 4 raw (Level 1) Envisat ASAR images. Showing the geomorphic features mapped in the area, hoqwever lineaments are difficult to be discernible.

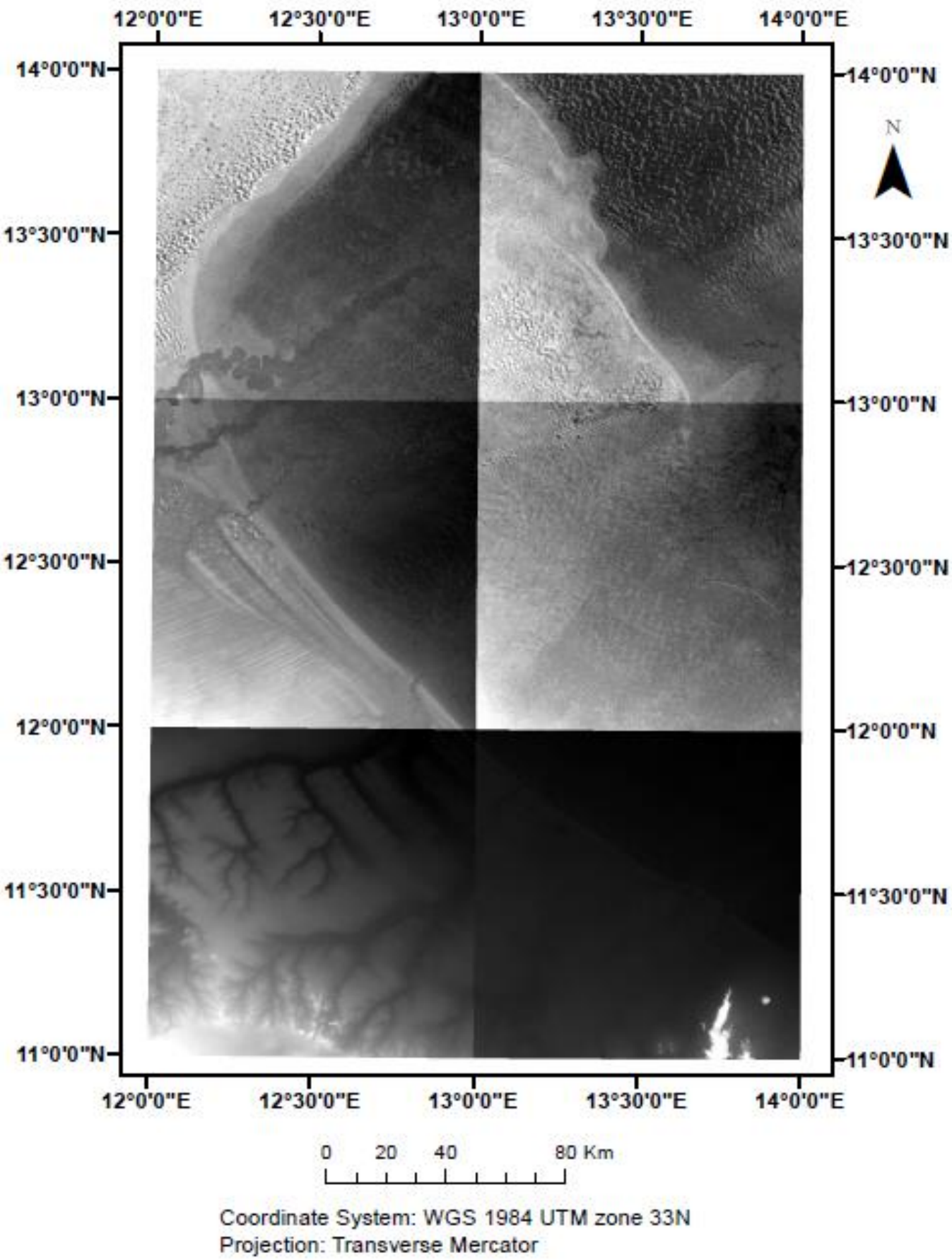

Fig 4.6: The raw (unprocessed) six 1 arc –second SRTM DEM 30 m scenes according to their path and rows and placed within the common map frame covering the study area used in this study.

4.3 Landsat 7 ETM+, ASAR and SRTM DEM Images analysis: Methodology

Details of the Earth Observation image analyses methods are already described in Chapter 3. Standard image processing and analysis procedures described by Koike *et al*., (1995) are applied herein to process and enhance the satellite imageries for interpretation. Accordingly, the images are processed to improve the visual identification of lineaments and other geological features. Processes adopted involved; image rectification pre-processing, image enhancements, image classification, georeferencing, compositing and multi-band selection. The digital image analyses select most appropriate enhancement combination. The flow diagram of the methodology used in this work is given in Figure (4.7).

4.3.1 Image acquisition and pre-processing

Individual bands 1, 2, 3, 4, 5, 6 (1), 6 (2), 7 and 8 were extracted using *7-zip* software from the individual Landsat 7 ETM+ images. The Image pre-processing operations utilised various processing software including *ArcMap 10.2.2* and *ENVI* 5.0. Radiometric and geometric corrections prior to image enhancements were performed. The optical images are geometrically corrected for distortions due to satellite sensor-Earth geometry variations. All images are georeferenced to a common projection of WGS84 Universal Transverse Mercator (UTM) Zone 33N system, which complies with the projection system of other maps used in this study for geospatial correlation in GIS. Details of radiometric correction methods in the image analysis are presented in Mahny and Turner (2007) and Tso et al., (2009).

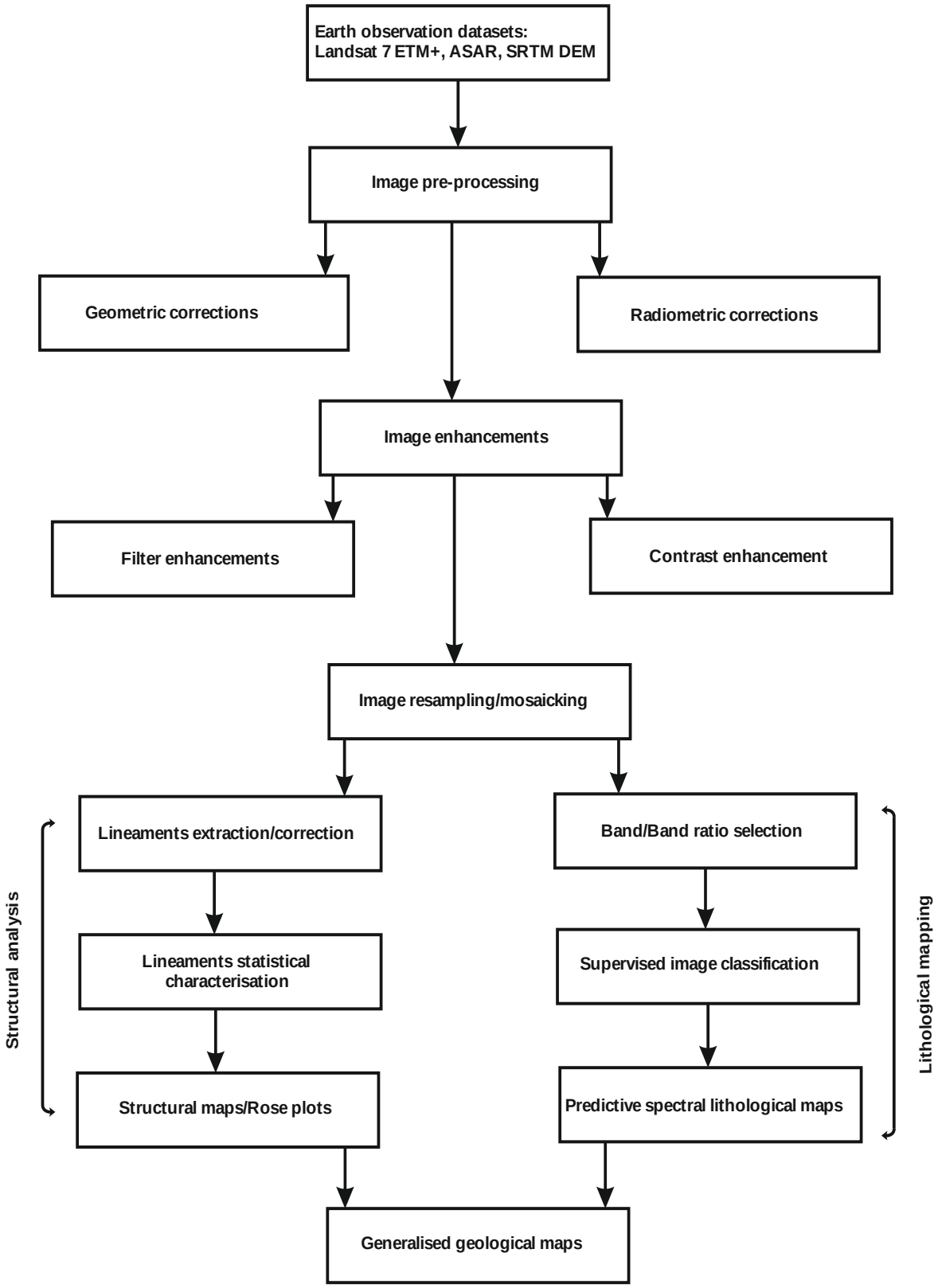

Fig 4.7. Flow chart of the systematic methodology used herein for the remote sensing data analysis

The radiometrically corrected band images for the individual images were stacked and mosaicked into single multiband raster images for further analysis. The standard pre-processing procedures for radar image analysis developed by Mahapatra and Hanssen (2011) were adopted for this study. *SAR toolbox software* is used to further process the level 1 nominal processed images originally delivered in (.N1) format and the resultant images are converted to GeoTiff that is usable in *Envi* and *ArcMap*. The Level-1 images were initially processed into amplitude and intensity dual band greyscale Envisat ASAR imageries (Figure 4.5). Subsets of the amplitude images are formed to remove image black backgrounds and specify the regions of interest. Image restoration and calibration of the ASAR images are performed to produce output images with the pixels corresponding to the radar backscatter of the image scene. Since the Level-1 images were direct products of raw data processing, radiometric corrections performed to correct the pixel values of the radar images to represent the true backscatter of the imaged surfaces. Terrain and geometric corrections were applied on the images to compensate for the geometric distortions, topographic variations and the tilt of the satellite sensor, which caused distortion in the ASAR images. Terrain correction on the images were performed using corresponding reference SRTM DEM of the area using the *Range Doppler Terrain Corrector Operator* in the *SAR toolbox* software to derive precise georeferenced information of the ASAR images.

The corrected ASAR images are in the WGS84 Universal Transverse Mercator (UTM) Zone 33N projection, which covers the study area. The georeferencing allowed the images to be stored in the correct GIS format. In order to further process the images for lineaments analysis, forward Principal Components Analysis (PCA) are performed on the ASAR images in *Envi* software to produce uncorrelated output PC bands that are linear combinations of the original spectral bands, which maximise the variance of

the data (Fig. 4.5). All the radar images are mosaicked with minimal loss to the dynamic contrast by applying image adjustments. The six SRTM DEM images (Fig. 4.6) are mosaicked to generate a continuous and seamless DEM for the entire study area to ensure continuous delineation of structural and hydrological features.

4.3.2 Image enhancements

Various image enhancement techniques are applied to improve the visual impact for surface and near surface lineament mapping on the Landsat 7 ETM+ and Envisat ASAR images. The objective of image enhancement is to adjust the appearance and improve visualisation of the images for analysis and interpretation. Discrimination and identification of lithology and lineaments by the most appropriate enhancement combination are sampled. Linear stretching is applied to produce well contrasting image pairs for optimised feature identification (Fig. 4.8) as outlined in Chapter 3.

Appearance of the images were enhanced using several spatial frequency functions including Gaussian filters, which are capable of suppressing specific features and highlighting other features of interest (Fig. 4.9a and Fig. 4.9b). Landsat 7 ETM+ image clips are mosaicked into single image. Individual images were initially composed into a single image having all the 8 bands stacked on top of each other (Fig. 4.10). A subset RGB 321 image showing the region of interest used for this research is produced from the mosaicked four Landsat 7 ETM+ images covering the north-eastern Bornu basin is shown in Fig (4.11). Fig (4.12) shows the subset grayscale image of the region of interest in north eastern Bornu basin obtained from the mosaicked four images shown on Fig (4.11). Speckle filtering were applied to the Envisat ASAR images to reduce the raw speckled appearance of the ASAR images due to inherent speckle noise while preserving the textural information. Speckles in ASAR images are caused by the

random constructive and destructive interference of de-phased and coherent reflected scattered waves in the image resolution pixels (Richards *et al*., 2005).

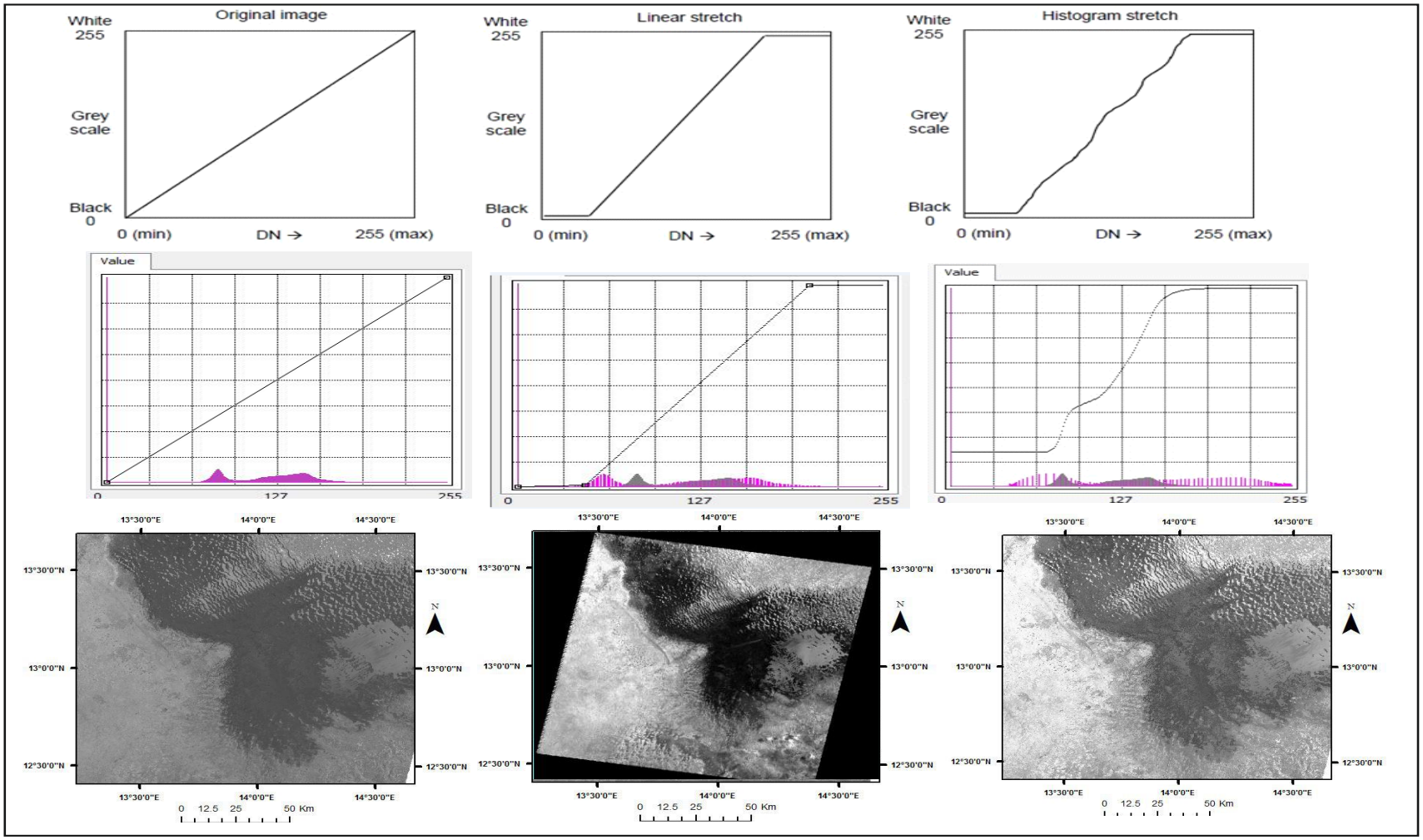

Fig 4.8 a-c: Original Landsat 7 ETM+ band 1 subset of Image 185/051 shows poor contrast since its histogram uses restricted range of brightness values with optimum use of the available display levels and good contrast in figures 4.8b and c.

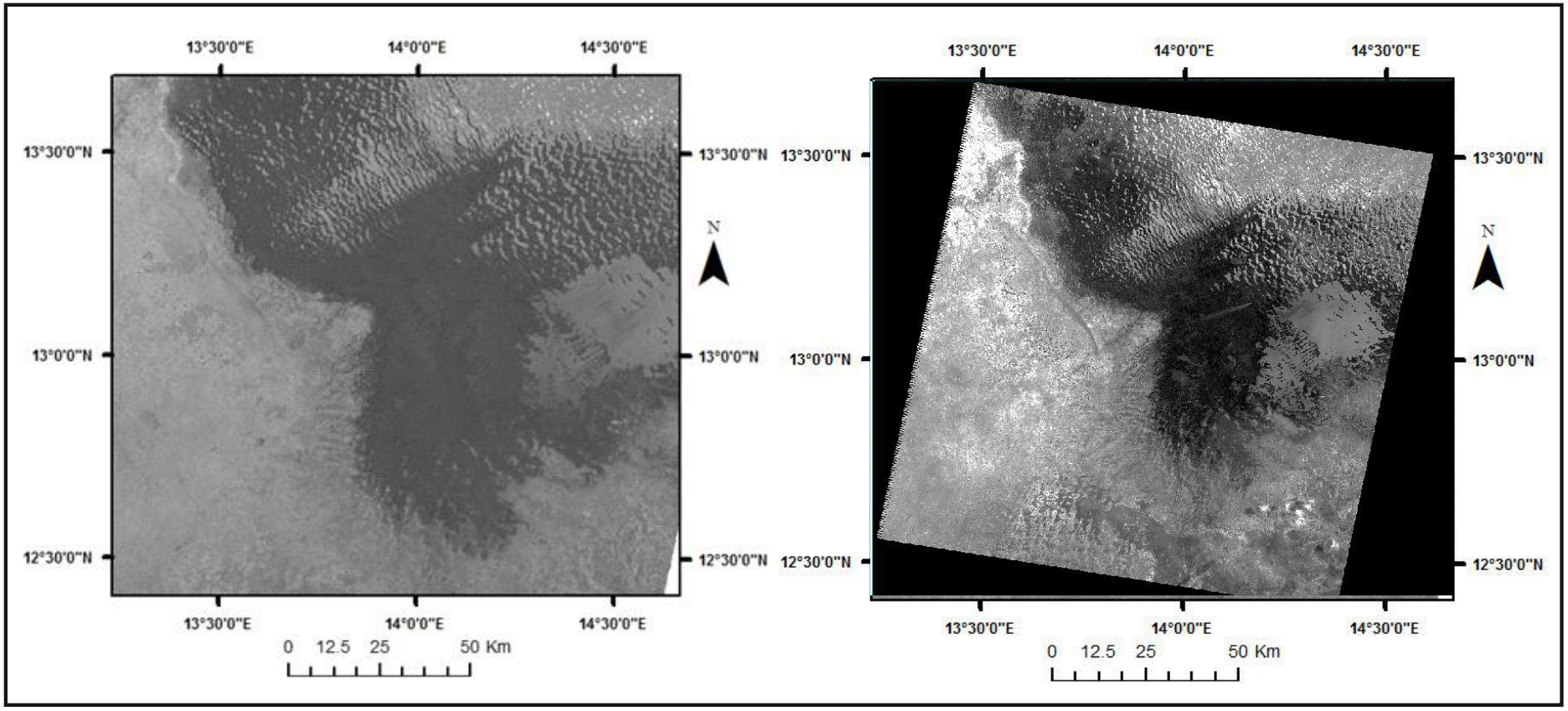

Fig 4.9 a-b: Original Landsat 7 ETM+ band 1 subset of Image 185/051 shows an example of applying lowpass Gaussian filter: (a) original image, (b) filtered image.

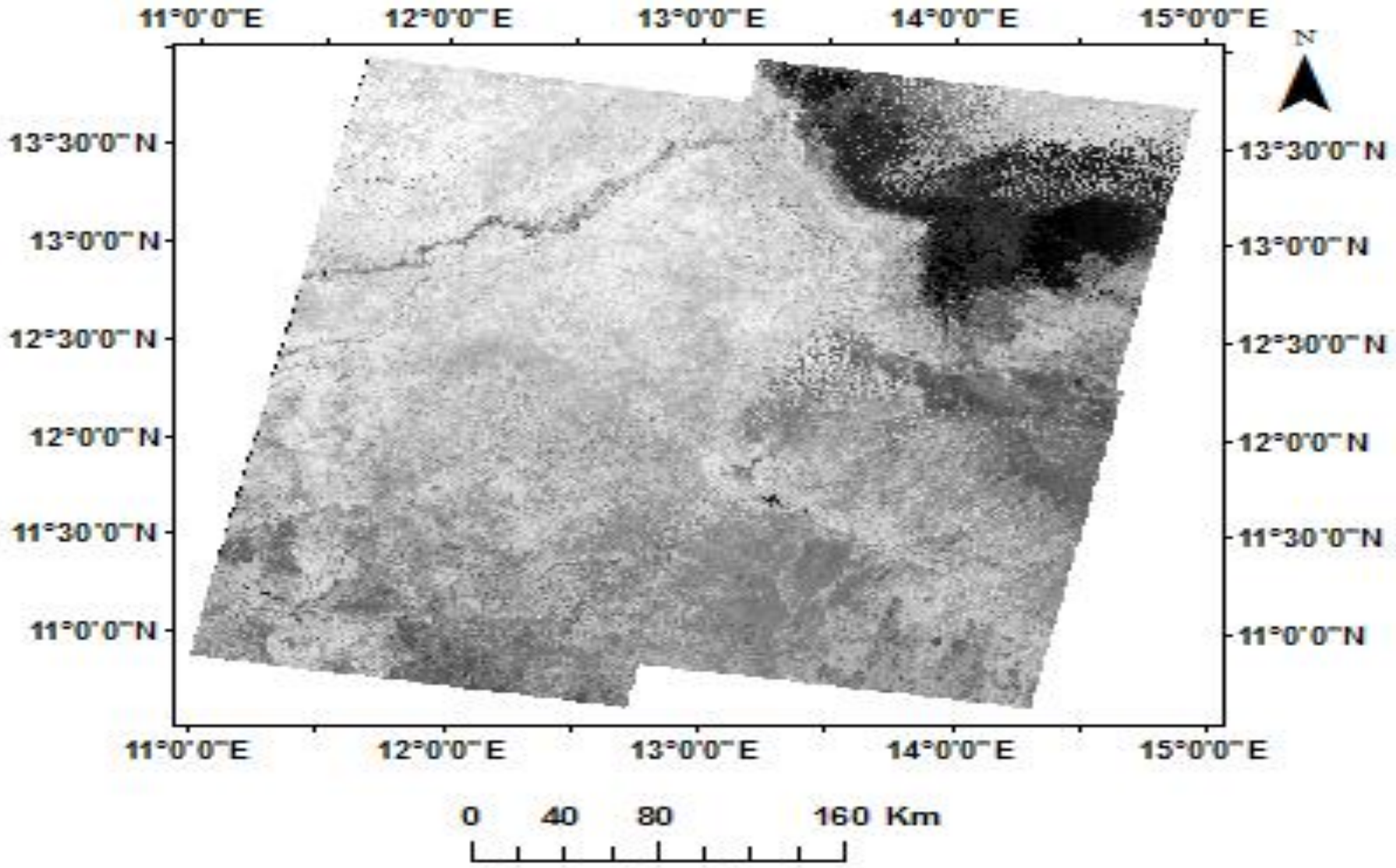

Fig. 4.10: Grayscale mosaicked four image of the Landsat 7 ETM+ images covering the north eastern Bornu basin shown in figures 4.1 – 4.4.

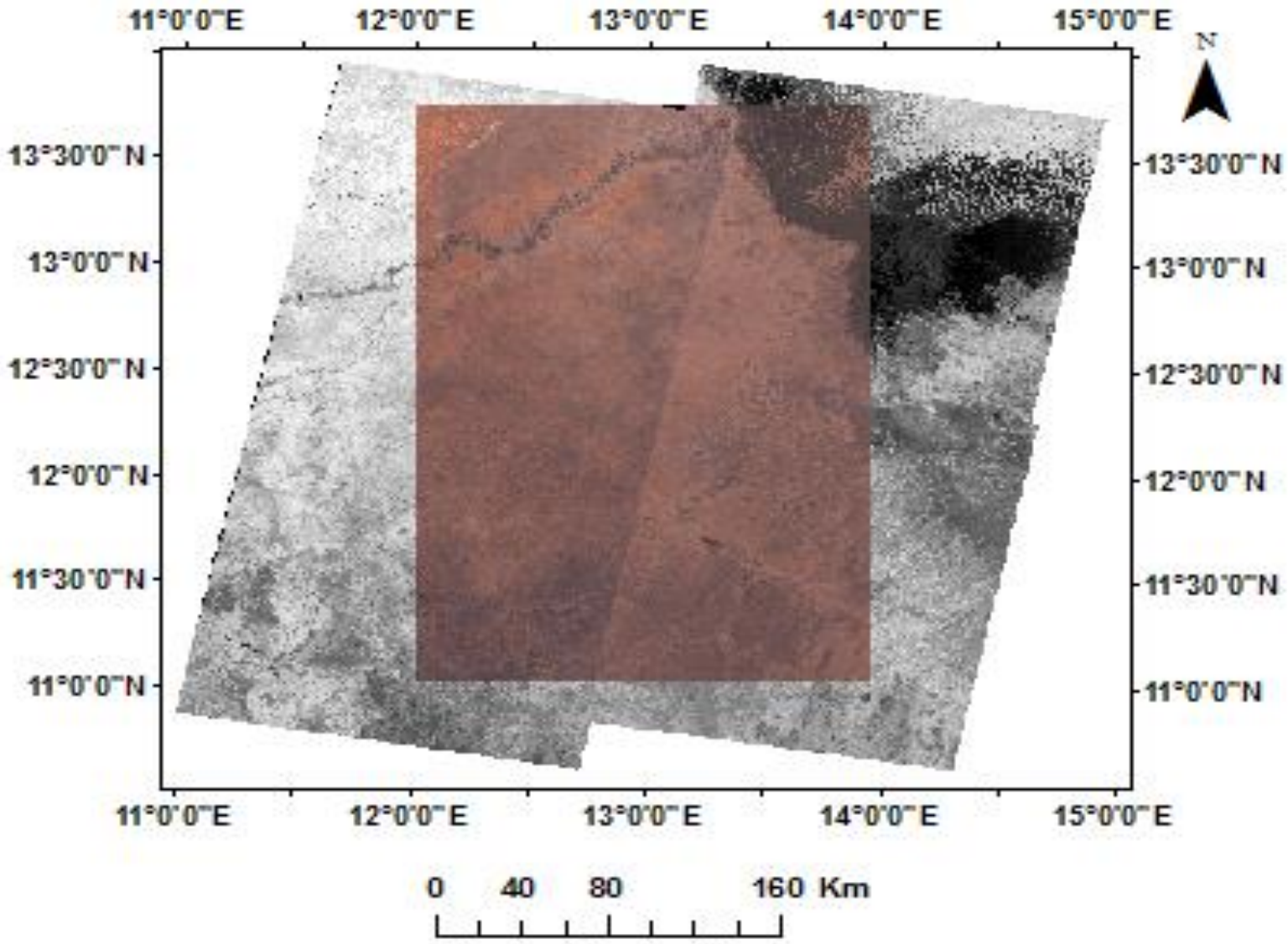

Fig 4.11: Mosaicked four images of the Landsat 7 ETM+ images covering the north eastern Bornu basin overlain by the subset RGB 321 image of the region of interest for this research.

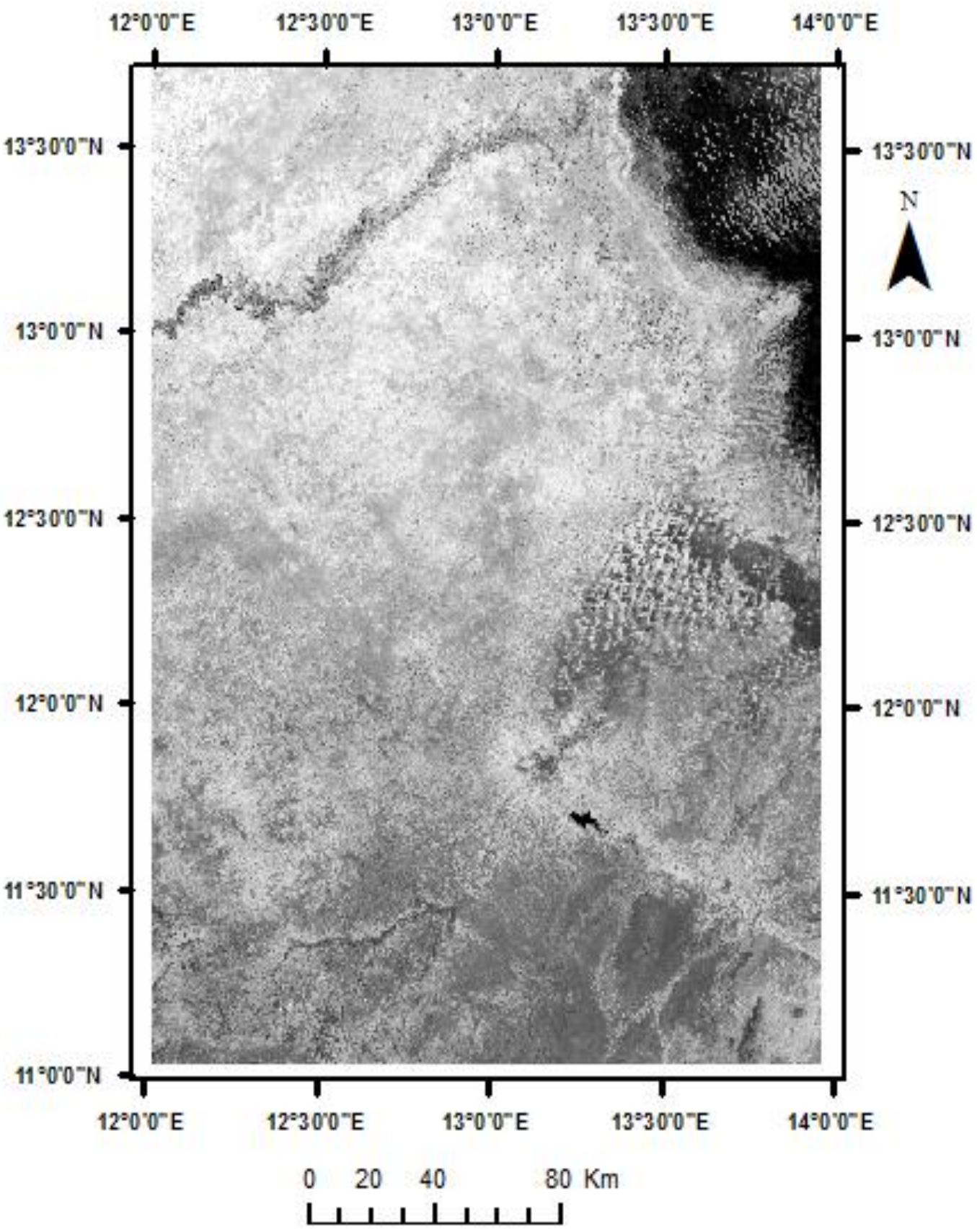

Fig 4.12: Subset grayscale image of the region of interest in north eastern Bornu basin obtained from the mosaicked four images shown on Fig (4.11).

4.4 Predictive spectral lithological mapping: Methodology

The concept of spectral lithological mapping using combined band combination images, band ratio images and supervised classification as presented in this chapter is adapted mainly from Sultan et al., (1987); Kruse et al., (1993); Inzana et al., (2003); Girouard et al., (2004); Gad and Kusky (2006); Misra et al., (2007); Leverington and Moon (2012); Harris et al., (2012); Abdul-Qadir, (2013). However, the authors have variously used only band ratios and supervised classifications for lithological analysis. An alternative spectral lithological mapping is herein developed for the north-eastern Bornu basin using spectral discrimination of the surface features identified on the Landsat 7 ETM+ images to infer on the lithology. The approach involves four steps including: computations of band combination images; computations of band ratio images; supervised image classification and inference of lithological composition.

The specific technique developed herein for the spectral lithological mapping in the north-eastern Bornu basin is detailed as follows;

1. Select most suitable RGB band combination that visually shows clear spatial variability of the unknown surface materials to identify end member training classes in the area.
2. Collect and label training samples of pixels from individual end member training samples representing their wider spectral variability for feature extraction from the radiance based image spectra of the selected RGB band combination image.
3. Generate surface classification map by computing a Spectral Angle Mapper (SAM) supervised classification using the end member training samples.
4. Compute band ratios images by selecting image bands that would emphasise mineralogical components of the potential drift deposits as well as the subsurface lithostratigraphy of the area.

5. Evaluate absorption, reflection and wavelengths characteristics of the spectral curves of the end member classes and compare their selected band ratio characteristics to infer mineralogical composition.
6. Compare characteristics of the mineralogy deduced to infer the surface lithology.

4.4.1 Band combination images

Sabins and Wender (1991); Sabins, (1997) and Abdelsalam et al., (2000a) have used Landsat 7 ETM+ band combination images to distinguish lithological units in arid environments. In this study, Landsat 7 ETM+ image bands were assigned different RGB colour composites to generate false colour images other than the true (natural) image colour (Figs. 4.13 a-f). The natural colour composite RGB 321 assigned colours to bands collected in the red (R) part of the spectrum as band 3, the green (G) part of the spectrum as band 2 and the blue (B) part of the electromagnetic spectrum as band 1. Thus, RGB (3-2-1) natural colour composite image differentiates the vegetation cover, Lake Chad and sedimentary deposits in the north-eastern Bornu basin according to their natural colours (Fig. 4.13a). However, false colour composite RGB 4-3-2 image (Fig 4.13c) is used to validate the vegetation areas in red colour because vegetation is reflective in the infrared region. RGB 7-4-2, which has been used extensively for oil and gas exploration in arid environments (Sabins and Wender, 1991; Pena and Abdelsalam, 2006) was computed in this analysis. The RGB 7-4-2 band combination display morphological and lithological aspects in colour bands in the VNIR and SWIR regions of the electromagnetic spectrum.

However, in this analysis, RGB 7-4-1 Landsat 7 ETM+ band combination images (Fig. 4.13d) from visualisation of the subset image displayed superior geological and morphological features in the north-eastern Bornu Basin. Vegetation have high (50%) total reflectance in the NIR region of the electromagnetic spectrum as such RGB combinations that consist of band 7 of Landsat ETM+7 images are effective in lithological mapping in arid environments where vegetation is lacking (Jensen, 2000). Similarly, Band 7 is useful for mapping hydrothermally altered rocks associated with mineral deposits. Reflectance in band 4 Landsat 7 ETM+ allow for the identification of iron rich soils and rocks in arid environments (Sabins, 1997; Jensen, 2000). Since the shorelines of Lake Chad in the study area have some vegetation cover, reflectance in band 1 Landsat 7 ETM+ that corresponds with the blue-green reflectance of vegetation allows for their distinction from the sedimentary deposits in the basin.

The RGB 7-4-1 Landsat 7 ETM+ band combination (Fig. 4.13d) better highlights the surface materials including superficial deposits and bedrock lithology while preserving the natural colours of the vegetation and the lake. Fine colour variations indicating different lithology, the lake shorelines and the boundary between the light coloured superficial deposits and dark coloured possible bedrock are highlighted. Visual interpretations of these images were used as guide for a supervised classification of the images to produce a spectral lithological map of the study area.

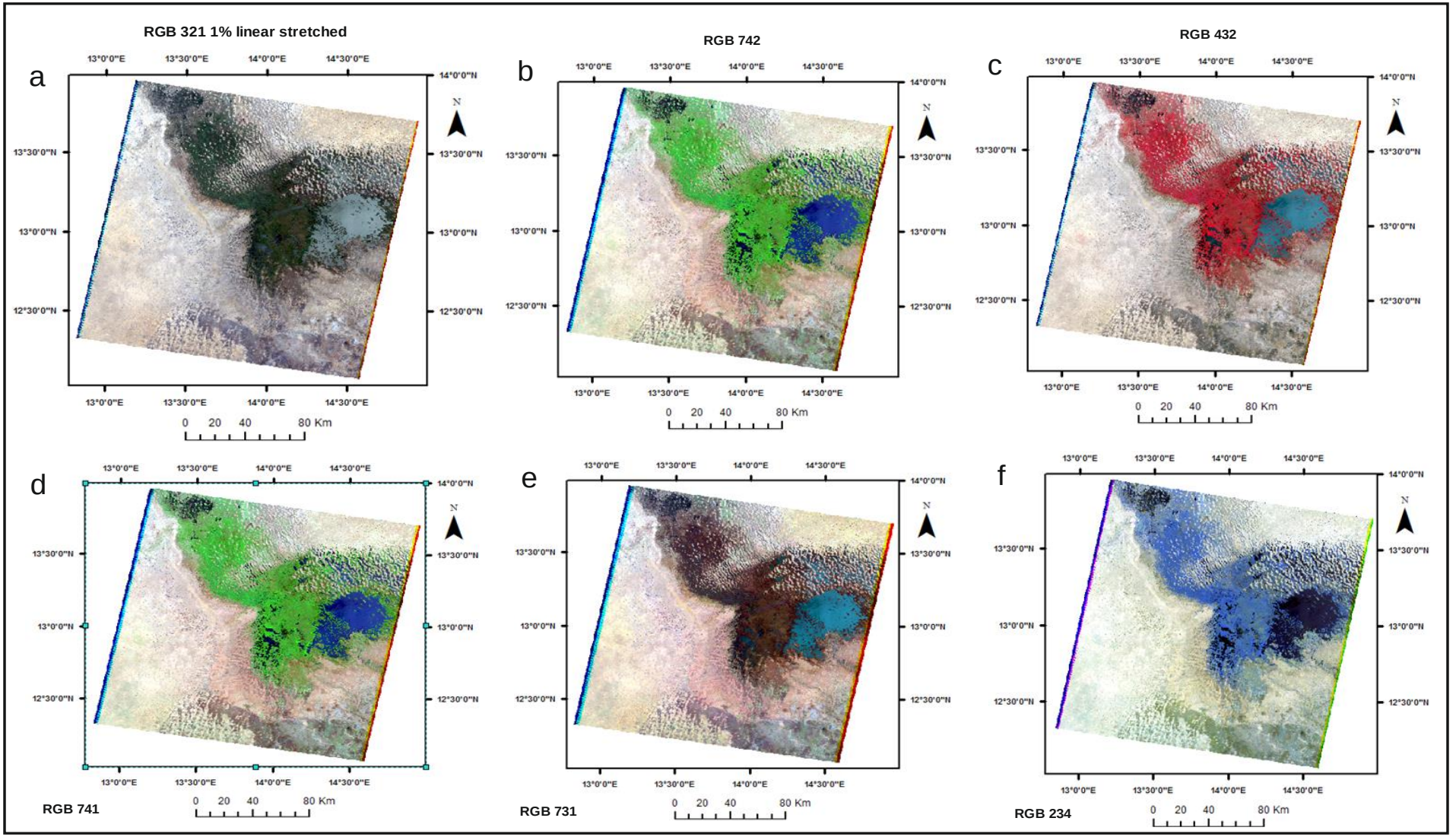

Fig 4.13 (a-f): The different spectral appearances of the Landsat 7 ETM+ images when different band combinations are applied to classify the different surface materials in the area. The RGB variously used by previous workers including Abdelsalam et al., (2000 a,b) is spectrally similar to RGB 741 used herein.

4.4.2 Band ratio images

Band ratio calculations are commonly used for discrimination of lithology in geological remote sensing, since they indicate the spectral characteristics of image elements irrespective of variations in scene illumination conditions (Abdul-Qadir, 2013). Abrams et al., (1988), Sultan et al., (1986), Kusky and Ramadan (2002) have used band ratios to identify specific geological materials and mineral alteration zones in arid and semi-arid environments analogous to the Bornu basin.

The band ratio images were herein generated to further highlight the spectral signature of the geological features in the area. Digital numbers (DN) of pixels in image bands having high total reflectance were divided with the DN values of pixels in a band with low total reflectance as carried out by Jensen, (1996) and Abdelsalam et al., (2000a, b). The RGB 741 band combination images was used to assign band ratio images, which highlight different properties including vegetation cover, soils, rocks and the lake. The band ratios selected were based on the spectral signatures of the lithology of the area, which correspond with bands that have short wave lengths and long wavelengths. The combinations were selected based on spectral variability of the rocks in the area and the band ratios included a combination of; (1) ratio of short wavelength bands (2), ratio of long wavelengths bands and (3) combined ratio of short and long wavelength bands as described in Sultan et al., (1986; 1987). The Landsat 7 ETM+ band ratio images were utilised to discriminate the lithological composition in the basin in terms of clay, iron oxides, hydroxyl and silicate compositions since their potential in the study area are indicated on Table (2.1). In applying band ratios for lithological studies, minerals are best differentiated by a combination of long band ratios or combination of long wavelengths and short wavelengths band ratio groups (Crippen, 1989).

Sultan et al., (1986; 1987) have used various band ratios including 3/1, 5/7, 5/4 and 3/4 to map lithologies in arid areas. However, in this study, band ratio combinations 5/7–5/4–3/1 in greyscale, which maximise the differences between surfaces with higher contrast between the lithologies than the natural and false colour RGB colour combination images were assigned (Figs. 4.14 – 4.16). Details of spectral properties of individual bands used herein and characteristics of the band ratios including the spectral lithological classification, which they represent, is described in Section 4.4.3.

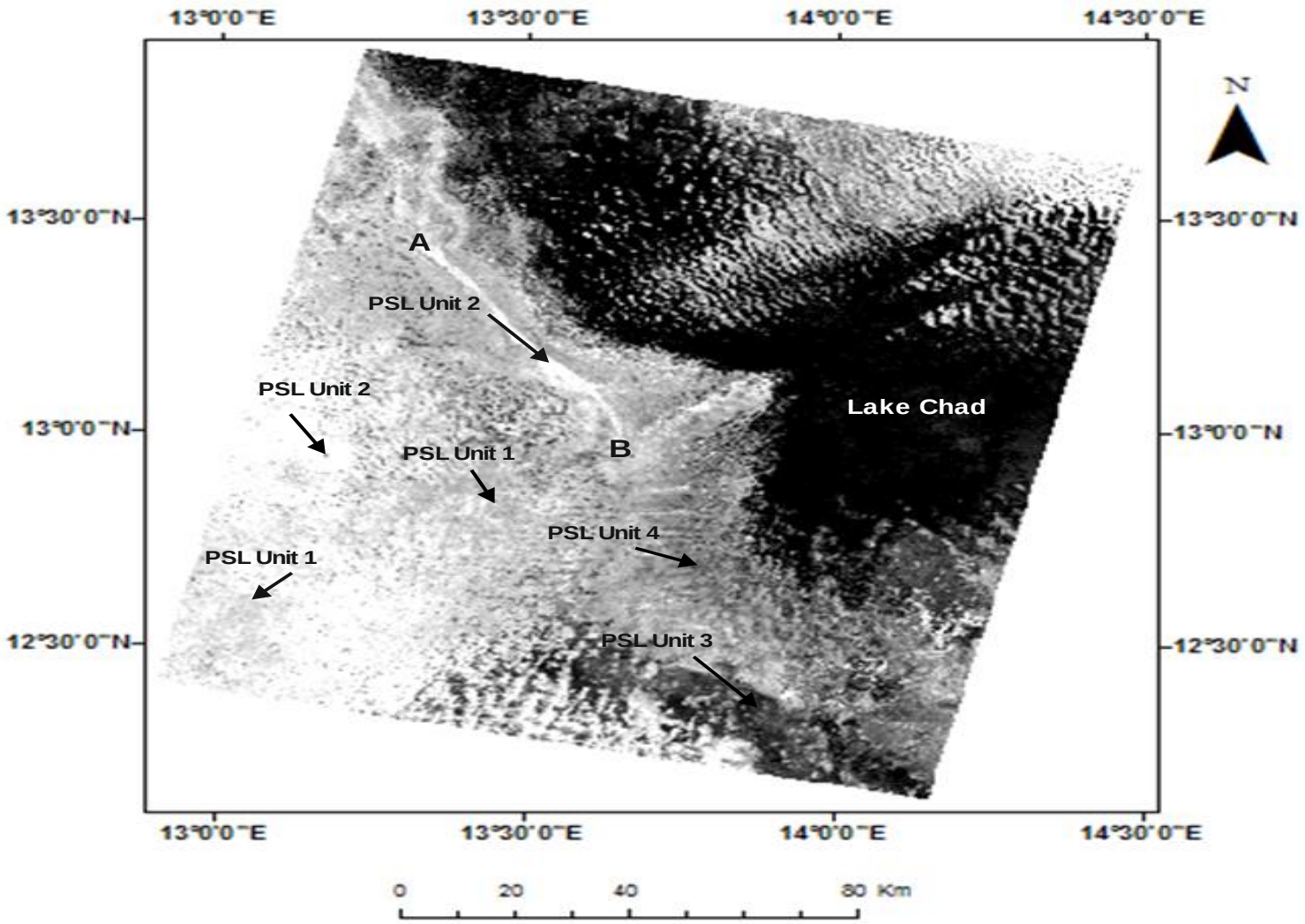

Fig. 4.14: Band ratio 3/1 image for the 185/051 path/row Landsat 7 ETM+ image showing the different spectral responses of the lithological compositions in different contrasts.

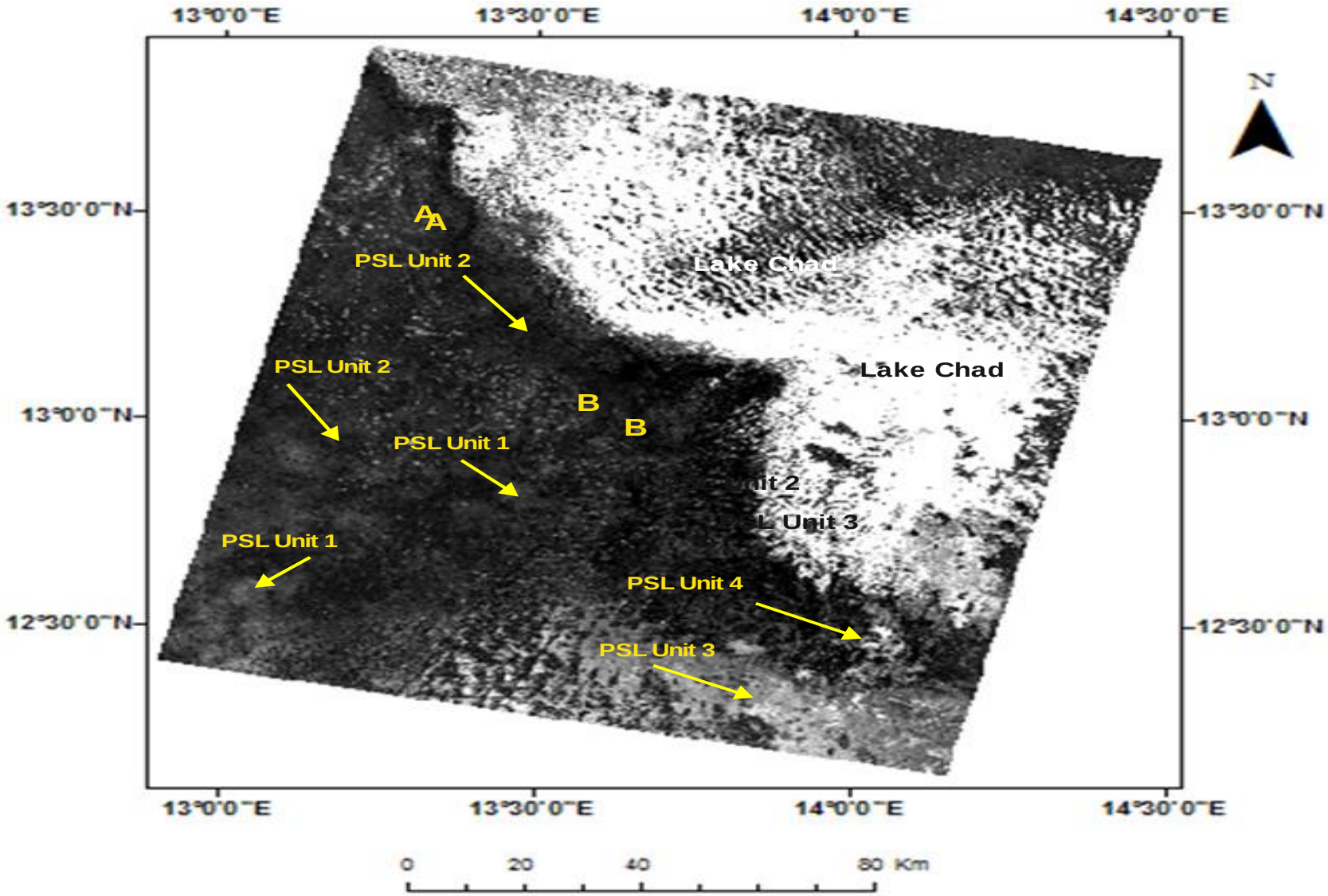

Fig. 4.15: Band ratio 5/7 image for the 185/051 path/row Landsat 7 ETM+ image showing the different spectral responses of the lithological compositions in different contrasts.

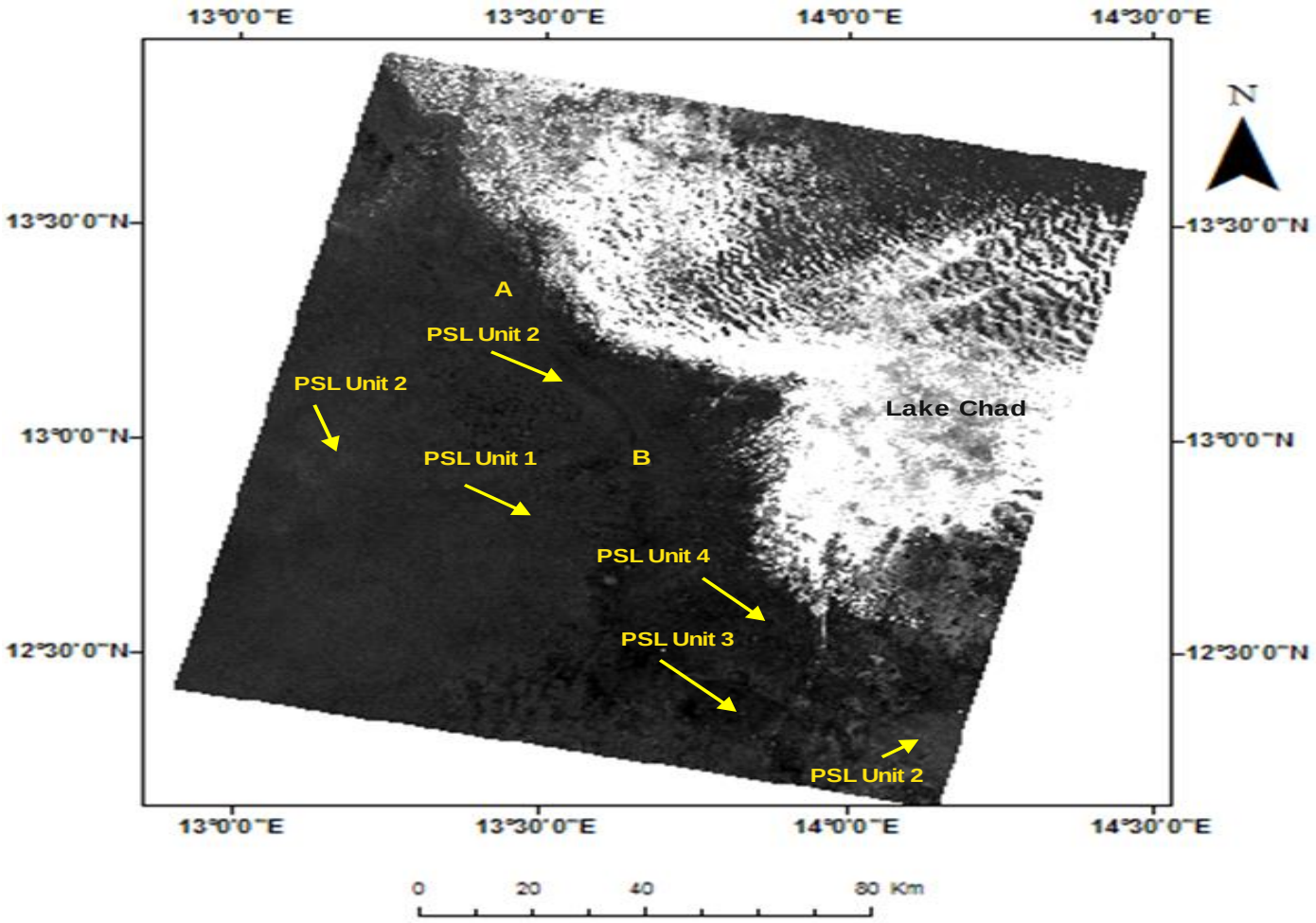

Fig. 4.16: Band ratio 5/4 image for the 185/051 path/row Landsat 7 ETM+ image showing the different spectral responses of the lithological compositions in different contrasts.

o

4.4.3 Supervised classification of surface features

The concept of spectral image classification is presented in section (3.3.4). Band combination and band ratio images presented herein in sections (4.4.1 and 4.4.2) respectively have not explicitly display the variations of the uneven surface sediments and their boundaries were not clearly delineated. Nevertheless, the RGB 7-4-1 band combination, which provides better spatial discrimination of spectral features herein, provides the basis, which supervised image classification is used to map the spatial distribution of the exposed lithological materials in the study area. Supervised classification methods are used to classify the spectral properties of the surface materials in the area into spectral units to produce a superficial geological map of the area. Sultan et al., (1986) indicated that spectral properties of lithological units including rocks and soils depend on the mineralogical composition of the spectral classes mapped. In this research, original radiance spectral data is used to classify the surface materials in the study area using known absorption features to label the training classes. Distinctive pattern recognition of the spectral absorption curves are applied in characterising the spectral units identified. If the results of the classification indicate inadequate inclusion of training pixels of individual end members, pixels representing their wider spectral variability are recollected and the process repeated.

As there are no known surface lithological ground georeferenced targets in the study area from any previous published work, this approach has the advantage of being able to work in areas with inadequate surface geological information whose spectra are undifferentiated and unknown.

Additionally, the Spectral Angle Mapper (SAM) supervised image classification method has been used for lithological mapping in areas with unknown ground targets by several workers including Van Der Meer et al., (1997); Rowan and Mars (2003); Leverington and Moon (2012); Inzana et al., (2003) and Abdul-Qadir, (2013) in

different geological environments including semi-arid terrains. As such, supervised image classification using Spectral Angle Mapper (SAM) in *ENVI* software is used herein to classify the spectral end member classes mapped in the study area. The SAM groups identical pixels into classes and iteratively compares other pixels to the assigned classes (Kruse et al., 1993). The SAM algorithm matches the spectral similarity between two spectra obtained from the images as a test and a reference spectrum in a spectral library to match the pixels to the reference spectra and deduce its mineralogical component. Six end member regions of interests (ROIs) spectral training classes are identified herein from the RGB 7-4-1 band combination image with distinctive spectral appearance (Fig. 4.17). Individual curves were plotted to characterise the spectral behaviour of the six end-member classes extracted (Figs. 4.18 and 4.19). Mapping of mineralogical components of the surface lithological materials in the north eastern Bornu basin using the SAM algorithm in *ENVI* was on the basis of the extracted end-member spectral training classes 1-6 (Figs. 4.18 - 4.19). The SAM classification identifies the different responses for the six end-member classes having unique spectral characteristics with their corresponding spectral curves visually inspected to detect distinctive patterns and identify absorption and reflection peaks with corresponding band wavelengths. Spectral mapping techniques in arid regions utilising systematic mineralogical inferences from Landsat multispectral data is commonly based on identification of spectral reflectance features identical to various rock types (Qaoud, 2014).

The spectral properties of the end member spectral classes relate to the sedimentary materials in the study area as discriminated on the RGB 741 band combination image (Fig. 4.17). The six spectra representing the vegetation, the Lake Chad and the four unknown sedimentary deposits are produced (Fig. 4.20). However, comparison between the spectral property and wavelengths of the end-member classes 1 and 2

representing Lake Chad and the vegetation respectively calculated herein show good similarities with their equivalents from the John Hopkins University spectral libraries in *ENVI* (Fig. 4.18). Identification of the vegetation and the lake is only to distinguish them from the sedimentary materials mapped iteratively by the SAM, thus validating the spectral mapping in the entire study area.

4.4.4 Identification of spectral lithology

This study develops on the SAM approach, which was variously applied for lithological mapping by herein relating the SAM classes with band ratios as described in Sultan et al., (1987); Gad and Kusky (2007) and Kodikara et al., (2016). Additionally, the mineralogical properties of the spectral classes are compared with the subsurface lithostratigraphy of the area to establish whether the surface deposits are directly sourced from the bedrock lithologies. Thus, subsurface analysis obtained from Isyaku et al., (2016) (published Chapter 5 of this thesis), Hamza and Hamidu (2012) and Avbovbo et al., (1986) are used for comparison. As established in (Kruse et al., 1993), patterns of absorption, reflection, slope features of spectral curves and their associated band wavelengths are used in lithological characterisation. Figs. (4.21 b-c) show the result of the SAM classification delineating the various surface lithological materials in the north eastern Bornu basin.

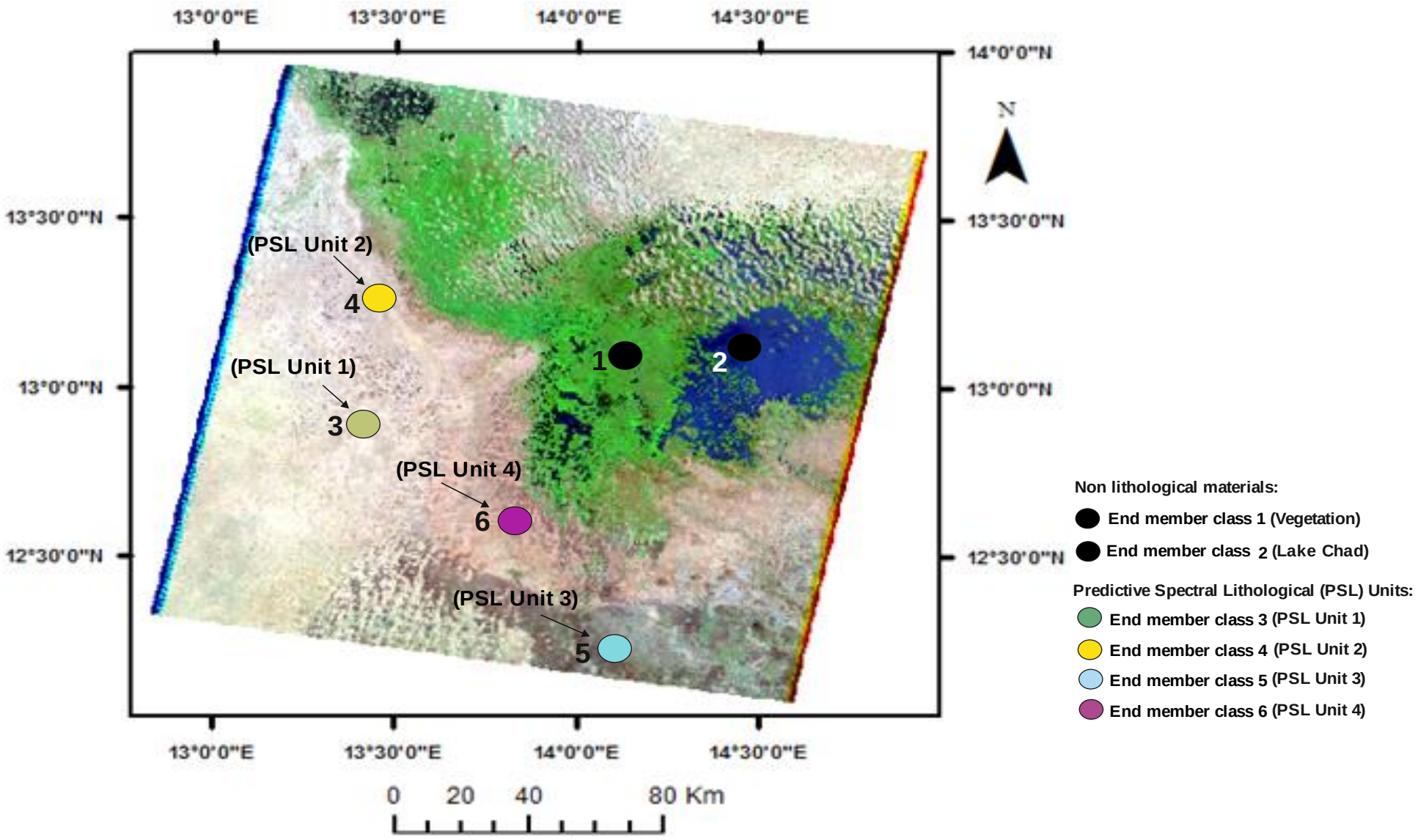

Fig 4.17. End member regions of interests (ROIs) 1-6 collected from the study area as training classes for the SAM supervised classification collected from the Landsat 7 ETM+ path/row 185/051 image.

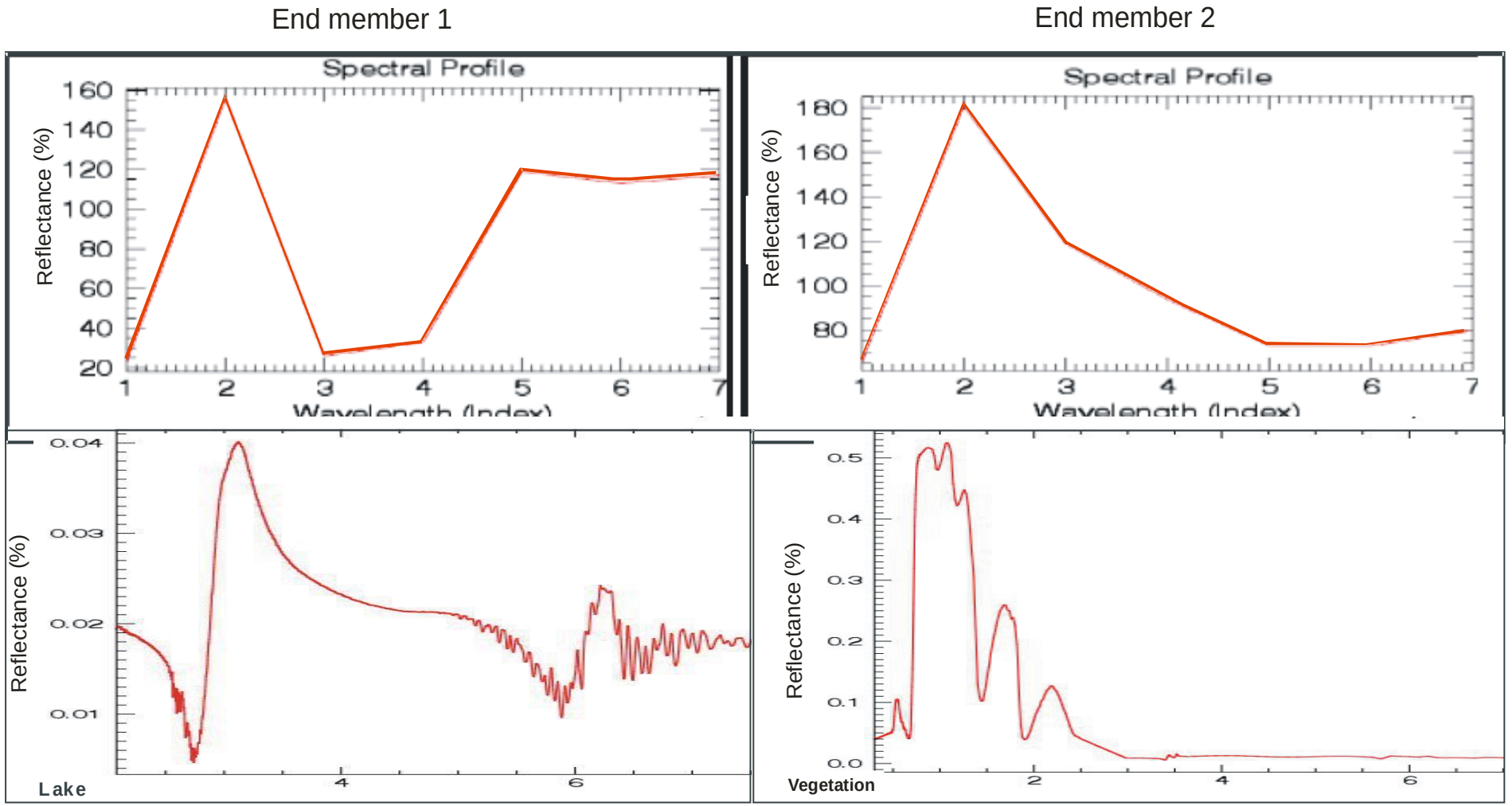

Fig 4.18. Spectral profiles of training classes 1 and 2 representing Lake Chad and the vegetation cover respectively shown on Fig 4.17, compared with their corresponding profiles below from the John Hopkins vegetation and lake water Spectral Library samples in ENVI showing high degree of equivalence, thus validating the two non-lithological materials. These materials are however automatically mapped because the SAM supervised classification presents the spectral properties of all pixels in the image.

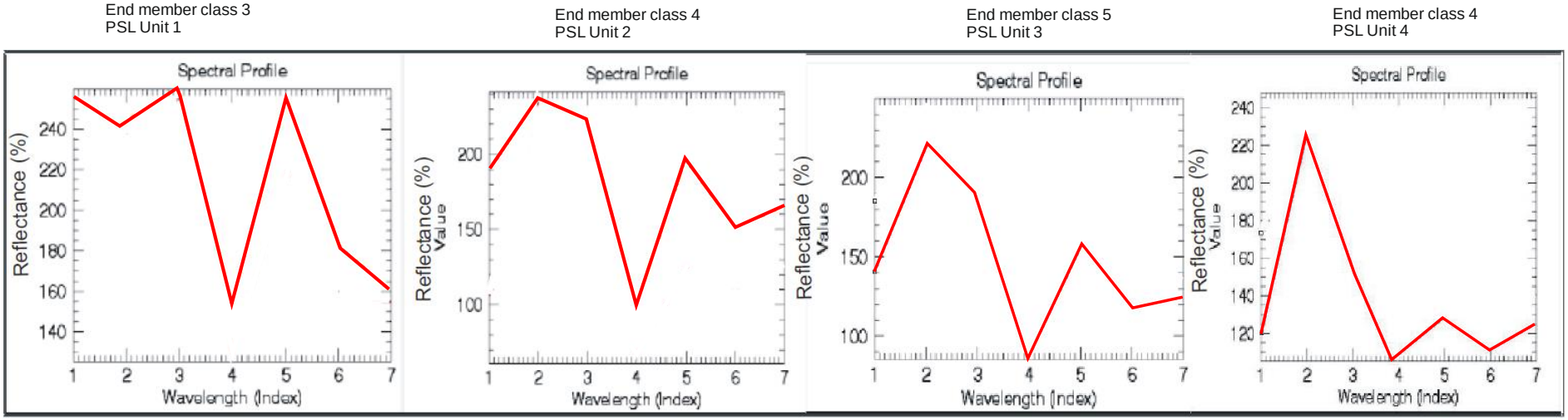

Fig 4.19. Spectral profiles of the remaining four lithological spectral end members (3 - 6) captured from the spectral training classes and representing PSL Units (1-4) respectively in Fig 4.17. The end-members 1 and 2 representing Lake and vegetation are shown on Fig 4.18.

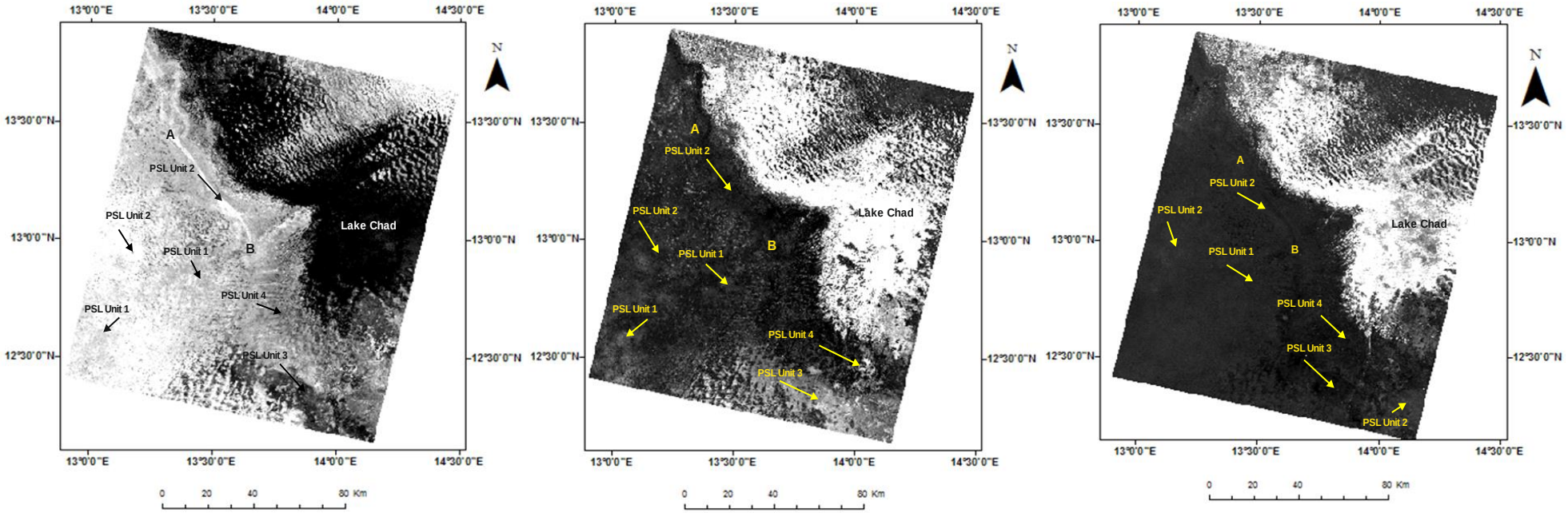

Fig. 4.20: Landsat 7 ETM+ path/row 185/051 image indicating the PSL Units interpreted from the selected band ratios. The images are same with those in Figs 4.14 – 4.16 arranged here for comparison.

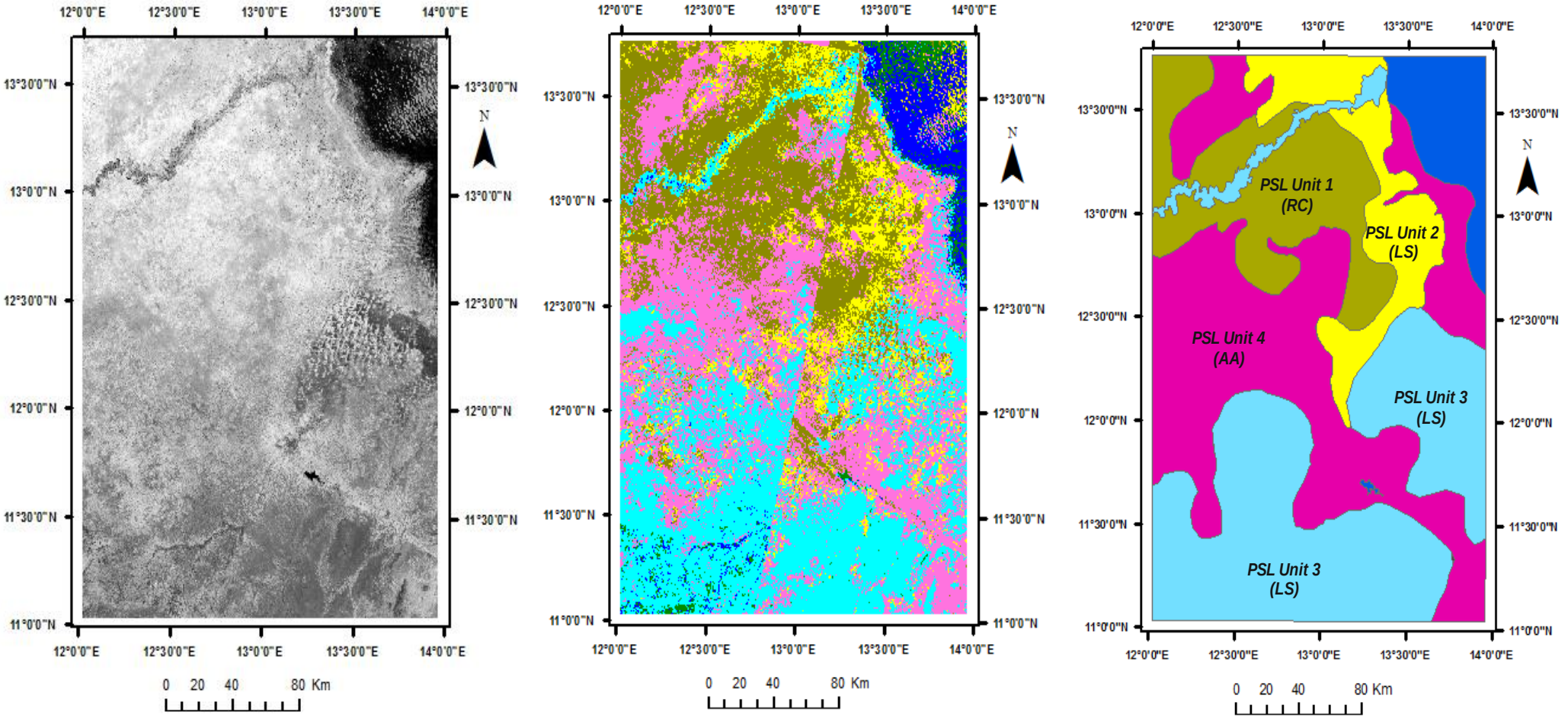

Figures (4.21): (a) Landsat 7 ETM+ image seamless mosaic clip of the north eastern Bornu basin (b) Result of the SAM classification of various surface lithological materials in the north eastern Bornu basin processed from Fig. 4.21 (a). (c) Digitised version of the SAM classification map showing the surficial geological map of the north eastern Bornu basin produced from Fig. 4.21 (b,) after all image processing edge artefacts are removed. Lithology identified are; (RC): Recent Clayey deposit, (AA): Ancient Alluvium deposit, (LS): Lateritised Silicate deposits. The maps are herein compared to appreciate the overall spectral mapping process from the raw image to the final drift geological map. Larger images are reproduced in Appendix A.

4.4.5 Structural lineament extraction and processing

Automatic lineament extraction using *PCI Geomatica* recently been used severally for structural analysis including in; Hubbard et al., (2012); Abdullah et al., (2013); Gannouni and Gabtni (2015); Thannoun, (2013); Rahnama and Gloaguen (2014). Automatic lineaments extraction is a computer aided method that is based on edge filtering and edge detection of morphological features. The method is also suitable for uniform analysis and speed of extraction of lineaments that are not easily discernible manually. The automatic process using the LINE Module algorithm in *PCI Geomatica* software detects lineaments faster and more objectively than the slow and often subjective manual process (Karnieli et al., 1996). All linear features related to human activities including roads, tracks and buildings were masked using the visual correction method. Hung et al., (2005) developed major steps in automatic lineaments correction and the method is adopted herein. Visual lineaments correction was applied to identify and remove all non-geological features as evident on the RGB combination and grey scale images since most linear features are capable of being detected by the *PCI LINE* Module. Residual lineaments mapped are those linear or curvilinear features related to geological structures (faults, joints, line of weaknesses), geomorphological features (terraces, linear valleys and rock cliffs), tonal contrast related to vegetation and rock composition). The automatic lineament extraction retains the coordinates of start and end points including the geometry of each lineament mapped.

The nature of the study area having vast flat terrain with thick sediments cover and paucity of continuous bedrock outcrops merited the use of automatic method to perform uniform extraction of lineaments all over the image subset quickly and map lineaments otherwise obscured during manual extraction. However, the two complementary methods however, offer validation of the results.

Single band optical Landsat 7 ETM+ image subset of the study area is used for the automatic lineament extraction. Lineaments representing spectral reflectance contrast relating to variations in soils and rocks and lithological boundaries, topography, and vegetation alignments were detected and mapped. On completion of the lineaments extraction, the raster image and the corresponding vector lineament layer were exported into *ArcMap* for further analysis. Visual inspection of the mapped lineaments was carried out by overlaying the corresponding vector layer on the raster images to verify geological lineaments from unrelated linear features on the image.

The extracted lineaments map in GIS shape file layer was imported into ArcMap to filter and break polylines into lines (Fig. 4.22a,b). The compound lines were edited and split at vertices into simple straight lines with two end points. The end point coordinates of each line start, line end and mid points were computed. The resulting lines were connected and the filtered lineaments were removed to generate the corrected lineaments map. The resulting lineament map projected to the geographic projection of the original sub set images. Numerical attributes of the extracted lineaments include frequency, density, lengths, azimuths and orientations are presented in Table (4.2). The Envisat ASAR image mosaic is not found to be useful for lineament mapping in this case, which is a limitation of the data.

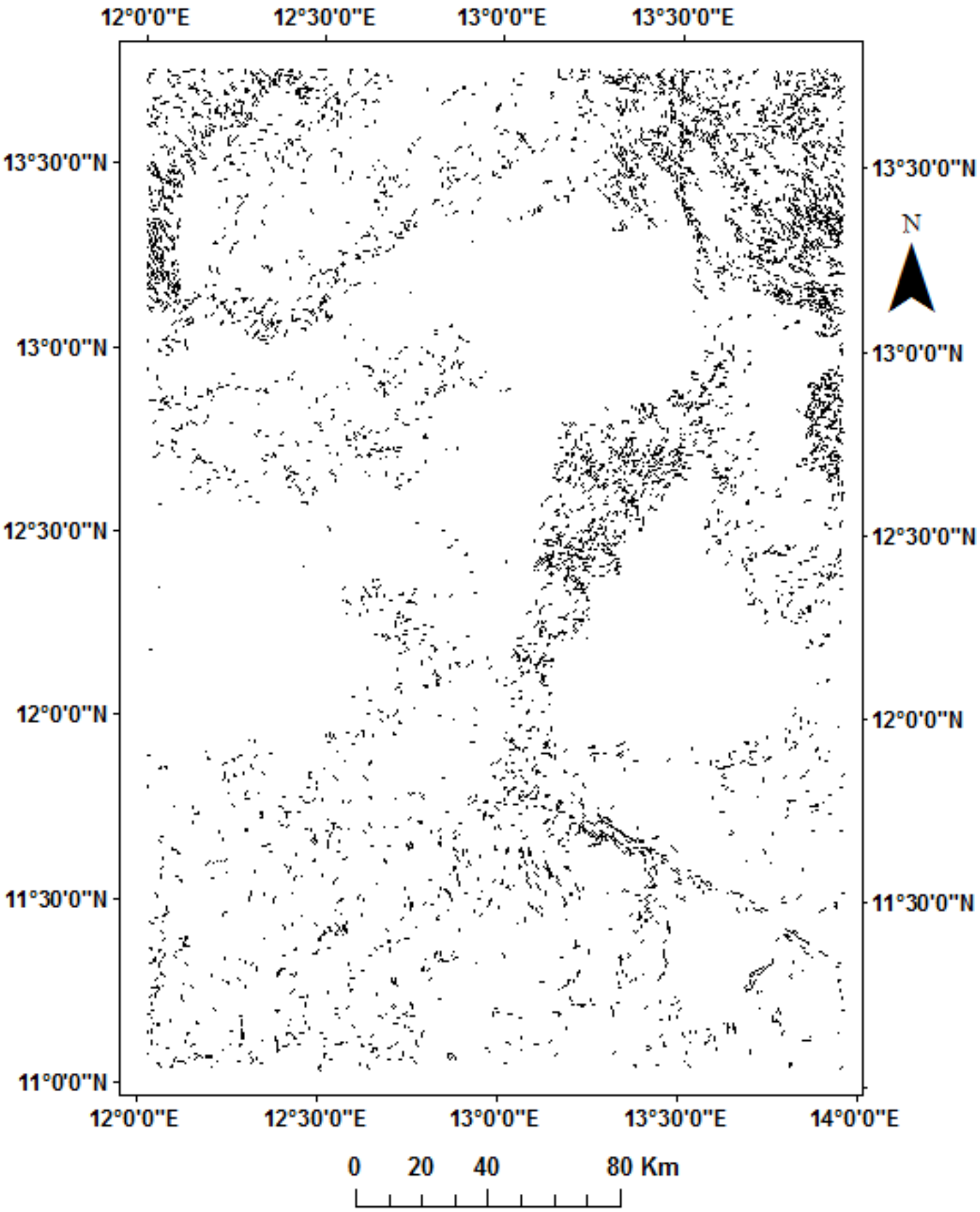

Fig 4.22a: lineament map of the north eastern Bornu basin extracted from the subset mosaic of the Landsat 7 ETM + images using automatic method. Note that areas covered by dunes are masked out.

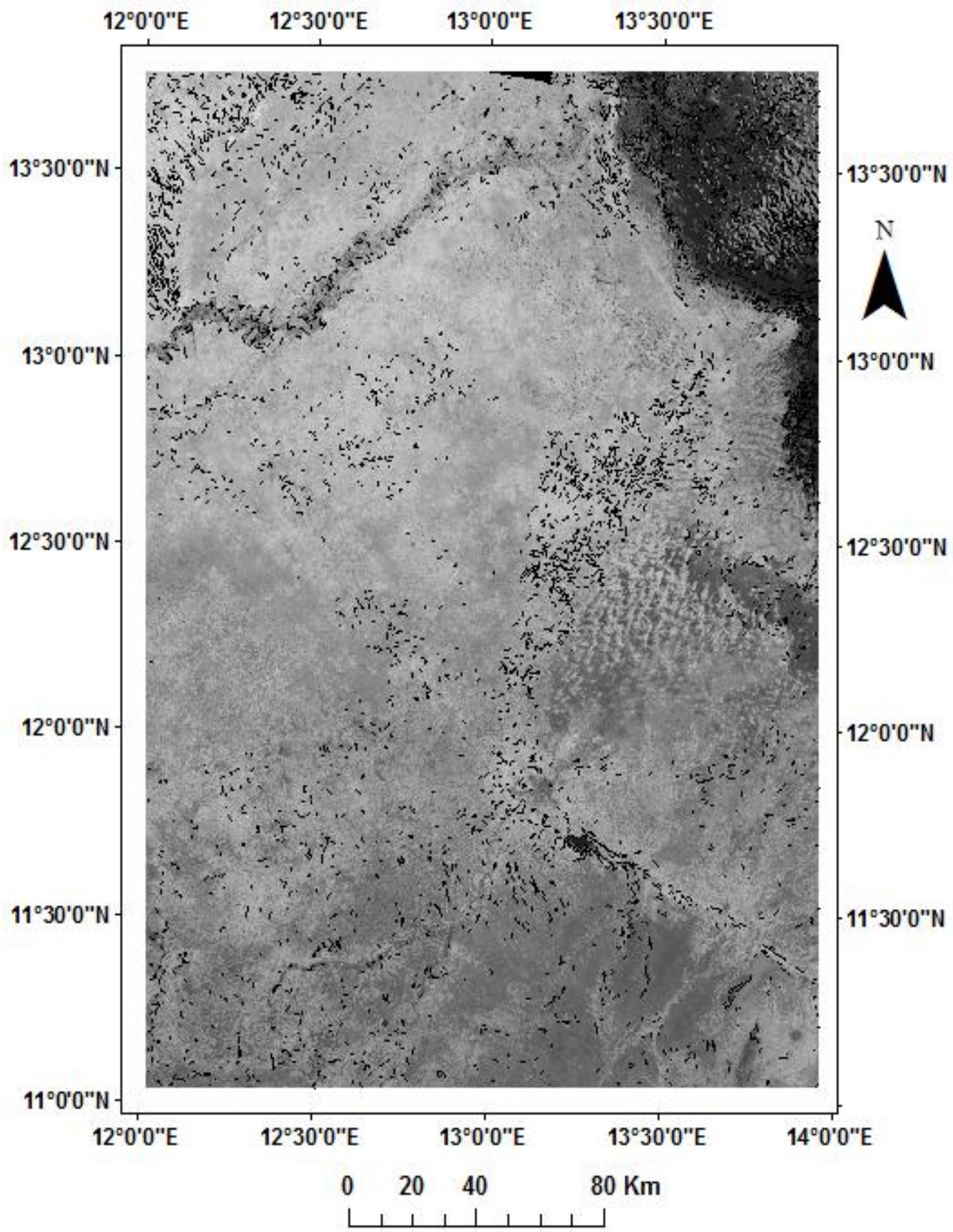

Fig 4.22b: Lineament map of the north eastern Bornu basin extracted from the subset mosaic of the Landsat 7 ETM + images using automatic method overlain on the raster mosaic image subset. Note that areas covered by dunes are masked out.

4.5 Results:

4.5.1 Predictive spectral lithological (PSL) units compositions:

4.5.1.1 Clays and hydroxyl bearing mineral deposit (*Recent clays*)

This lithology is represented by and deduced from the spectral end member training class 3, which represents the PSL Unit 1 (the end member classes 1 and 2 being Lake Chad and the surrounding vegetation respectively, which are non-lithological) (Fig. 4.17). The profile for spectral class 3 (Fig 4.19) indicate high reflection in band 5 relative to band 7. Similarly, the unit appear bright on the band ratio 3/1 image due to the higher reflection values in band 3 relative to band 1 (Fig. 4.20). Band ratio 5/7 is useful in mapping hydroxyl bearing rocks (Sultan et al., 1987) given that clays have high reflectance in band 5 with corresponding lower reflectance in band 7 (Sabins, 1997). As such, band ratio 5/7 emphasises clay deposits since the ratio is a measure of the intensity of hydroxyl absorptions. Consequently, on the band ratio 5/7 image, potential clay alteration areas appear in bright colours since clay minerals including kaolinite, montmorillonite and illites have higher reflection within band 5 and a corresponding lower reflection in band 7 (Abdelsalam et al., 2000a). Reflection in band 7 of Landsat 7 ETM+ depends partially on the hydroxyl composition in rocks. Fig. (4.21) show PSL Unit 1 indicating clay with hydroxyl bearing lithological units relative to the adjoining other lithologic materials. The breakdown of feldspar bearing rocks including from the Bima Sandstone, Gongila and Chad Formations into a variety of clays and other hydroxyl bearing minerals may be the parent rocks for this deposit. However, this lithology could more possibly represent clay components of the overlying Chad Formation. This recent clayey deposit of fluvial character occur mainly east of the Bama Beach Ridge and taking into account that the deposit is mainly restricted in the lagoonal terrace east of the Bama Beach Ridge (Fig. 4.23).

4.5.1.2 Intermediate rocks with minor iron bearing aluminosilicates composition (*Lateritized silicates*)

This lithology is deduced from the spectral end member training classes 4 and 5 representing PSL Units 2 and 3 because the spectral class 4 profile is characteristically similar with the spectral class 5 profile indicating felsic rocks composed of quartzofeldspathic minerals except for the higher reflection at band 3 in spectral profile 4. However, differences exist in the significantly higher reflection values of the PSL Unit 2 in the spectral class 4 profile than in class 5 (Fig. 4.19). Intermediate rocks have compositions between mafic rocks dominated by ferromagnesian minerals and the felsic mineral bearing rocks. Possible mafic rocks are composed of plagioclase feldspar and the ferromagnesian minerals including pyroxene with general absence of quartz and orthoclase feldspars.

The Quaternary setting of the surface sedimentary deposits in the study area suggests that this lithology is likely to be weathered products of the sandy lithologies. Sultan et al., (1987) have described the optical bands reflections for rocks having iron-bearing aluminosilicates to generate a concave-upward spectral reflection pattern in the band 4 wavelength region indicating significant broad absorption because of the presence of iron - bearing lithologies. The drainage feature flowing NW-SE labelled A-B shows zone of possible high haematitic alteration (Fig. 4.20). However, the PSL Unit 2 appears dark on the band ratio 5/7 image while the PSL Unit 3 also appears dark on band ratio 3/1 image (Figure 4.19 – 4.21). Though the band ratio 5/4 image is broadly dark due to the strongest absorption in band 4, the PSL Units 2 and 3 are the relatively black areas on this image. This lithology is also indicated as a conspicuous dark coloured outcropping mass south of the Lake Chad shorelines as shown on the 7-4-1 band combination image (Fig 4.17). The ferruginous composition is possibly indicative of a lateritized silicate deposit. However, the ferromagnesian components of

this surface deposit indicating evidence of laterization of the felsic rocks maybe sourced from the lateritic deposits of the adjoining underlying Kerri-Kerri formation that occurs in the southern part of the Bornu basin and in the Upper Benue Trough as reported by Avbovbo et al., (1986). More so, the deposit occurs characteristically on both sides of the Bama shoreline. The sand components of fluvial origin have been subjected to aeolian reworking and the laterization may be related to the predominant insitu weathering and erosion of dune sands.

4.5.1.3 Felsic rock deposit (*Ancient alluvium*)

This lithology is represented by and deduced from the spectral end member training class 6, which represents PSL Unit 4 (Figs 4.17, 4.19, 4.20, 4.21). On the band ratio 5/4 image, the unit appear dark indicating significant absorption shown on the spectral class 6 profile due to presence of felsic and intermediate rocks composed of quartzofeldspathic minerals. Felsic, intermediate and ultra-mafic rocks, which have low percentage by volume of iron-bearing aluminosilicates would appear dark on band ratio 5/4 images (Sultan et al., 1987). However, the lithological unit appear bright on the band ratio 3/1 image as shown on the spectral class 6 profile indicating high reflection in band 3 relative to absorption in band 1. The spectral class 6 profile show higher reflection in band 5 relative to band 7, as such the unit appear bright in the band ratio 5/7 image (Fig 4.20). Felsic rocks are light coloured low temperature non-ferromagnesian mineral bearing rocks rich in silicates including feldspar, quartz and muscovite (Marshak, 2009). However due to the Quaternary setting of the surface sedimentary deposits in the study area, this lithology is most likely to be weathered products of the sandstone lithologies including Bima Formation, Gongila Formation and Chad Formation present in the Bornu basin.

However, a close observation of the morphological situation in the area indicates that due to the variable climatic history of the area polycyclic ancient alluvial deposition may have occurred, which have been subjected to aeolian and fluvial reworking of dune and beach ridge sediments. This ancient alluvium deposit occurred within a meander besides the inner bank of the Bama beach ridge and mainly in the flood plain towards the Lake.

4.5.2 Palaeohydrological and aeolian landforms in the north eastern Bornu basin

In order not to presume that all linear and curvilinear landforms mapped in the study area are lineaments of structural origin, primary geomorphological and hydrological considerations are necessary to delineate palaeoshorelines, palaeodrainage and sand dunes, which all have the potential to exist in the entire Lake Chad area including in the study area. More so, the potential for structural origin of the palaeoriver channels and palaeoshorelines and their relationship with the structural setting of the area are herein investigated. However, detail arid geomorphological and palaeoenvironmental assessment of the Bornu basin is beyond the scope of this research. The shorelines and geomorphological studies of the entire palaeolake Megachad are presented by Durand (1982); Drake and Bristow (2006); Abafoni et al., (2014).

Mega Lake Chad was affected by lake fluctuations because of climatic changes during the Holocene (Gasse, 2000) forming periodic shoreline beach ridges that were often referred to as fault scarps (Durand, 1982). However, results of GIS based data processing and drainage delineation and palaeodunes identification carried out herein are presented in (Fig 4.23). It is clear that the north eastern Bornu basin hydro system is composed of a few ancient rivers (tributaries) that drain from several directions into a closed topographic depression, which was occupied by the Lake Chad watershed.

SRTM DEM mosaic is used to delineate the drainage and shorelines in the study area. Komadugu-Yobe and Komadugu-Gana rivers are the two main catchments that form major Nigerian tributaries into the Lake Chad are indicated herein (Fig. 4.24). These rivers that originate from the northern Nigeria Basement Complex comprising of migmatite-gniess complex, Older Granites and the Younger Granites of Jos area, form a confluence and developed into a single River Komadugu that empties into the Lake Chad. The major rivers are responsible for bringing in alluvial sediments into large portions of the north eastern Bornu basin. The few shorelines in the area are long and well established indicating the Lake Chad was ephemeral. The shoreline development is influenced by the gentle slope in the area since there was more sediment available for the construction of such features.

Adams and Wesnousky (1998) describe that abundant sediment supply coupled with a relatively long still-stand influences development of the progradational barrier.

A conspicuous palaeobeach shoreline referred to as the Bama Beach Ridge exist within the Bornu basin area formed as a result of the Late Quaternary climatic variations. Thiemeyer, (1992) described the shoreline as the highest energy shoreline along the southwest coast of the Lake Chad having a straight shoreline at 328 m (Figs 4.23 - 4.24) terminating at the Komadugu River which eroded much of the beach ridge complex. The SRTM DEM analysis herein indicates that the Bama Beach Ridge influences the hydrography of the catchment where it forms a major relief feature at 338 m (Figs. 4.24 – 4, 25). The resulting channel network show drainage lines terminating against the paleo lake border and emptying into the Lake Chad from the Bama Beach Ridge palaeoshorelines. Few small channels end up in the watershed where they built their alluvial fans into the depressed area, which would naturally receive fluvial sediments from the small streams.

It can be observed that most of the drainage features in the north eastern Bornu basin may be structurally controlled. The combined arcuate and straight courses of the drainage courses and their relationship to the topographic heights may be related to a structural origin. However, the main Komadugu River in the northern boundary of the study area is probably following along a structural feature breaking and changing courses along NE-SW and NW-SE directions (Fig. 4.26). The drainage lines in the south-eastern part of the study area show close structural origin due to the straightness and trend of the drainage courses comprising of en-echelon NW-SE drainage lines that bisect the main NE-SW paleo-channel.

Few dunes area exists in the study area bordering mainly flat terrain and drainage channels and shorelines. Three main dunes locations are mapped in the eastern, western and north-eastern part of the study area. The surface lineaments mapped also did not correspond with the areas occupied by the dunes. The drainage network did not correspond with all the dune areas mapped. The elongated Bama ridge shoreline is highly visible on all the datasets including the Landsat 7 ETM+ (Fig. 4.23), SRTM DEM (Fig. 4.24) and Envisat ASAR (Fig. 4.5). The shoreline runs NW-SE and curved into NE-SW direction at the north-western end of the study area apparently representing the highest stand of the Lake Chad shoreline. Two other broken segments of shorelines representing different lake still-stands have been recognised and mapped in the study area within the NE graben-like depression. The Ngelewa Ridge is a NW-SE oriented beach ridge similar to the Bama Beach Ridge shoreline and it appear to have been segmented and separated by dunes (Fig. 4.23). However, the extensive Bama Beach Ridge shoreline is herein found not to be at similar altitudes. Profiles 1 - 4 run across different parts of the prominent Bama Beach Ridge palaeoshorelines show different elevations across the feature (Fig. 4.24 – 4.25). The elevation of the shoreline high-stand is higher at the south-eastern end at 351 m than

that at the north-western end, which stands at 345 m. Profile 3 across the Bama Beach Ridge and the Ngelewa Ridge, which stand closest to the present day Lake Chad, show evidence that the Ngelewa ridge is a recent lake stand feature standing at a lower elevation of 300 m. The profiles show that beyond the former lake highstand, the slightly undulating plain east of the Bama Beach Ridge confirmed the relative flatness of the vast topographic areas in the study area.

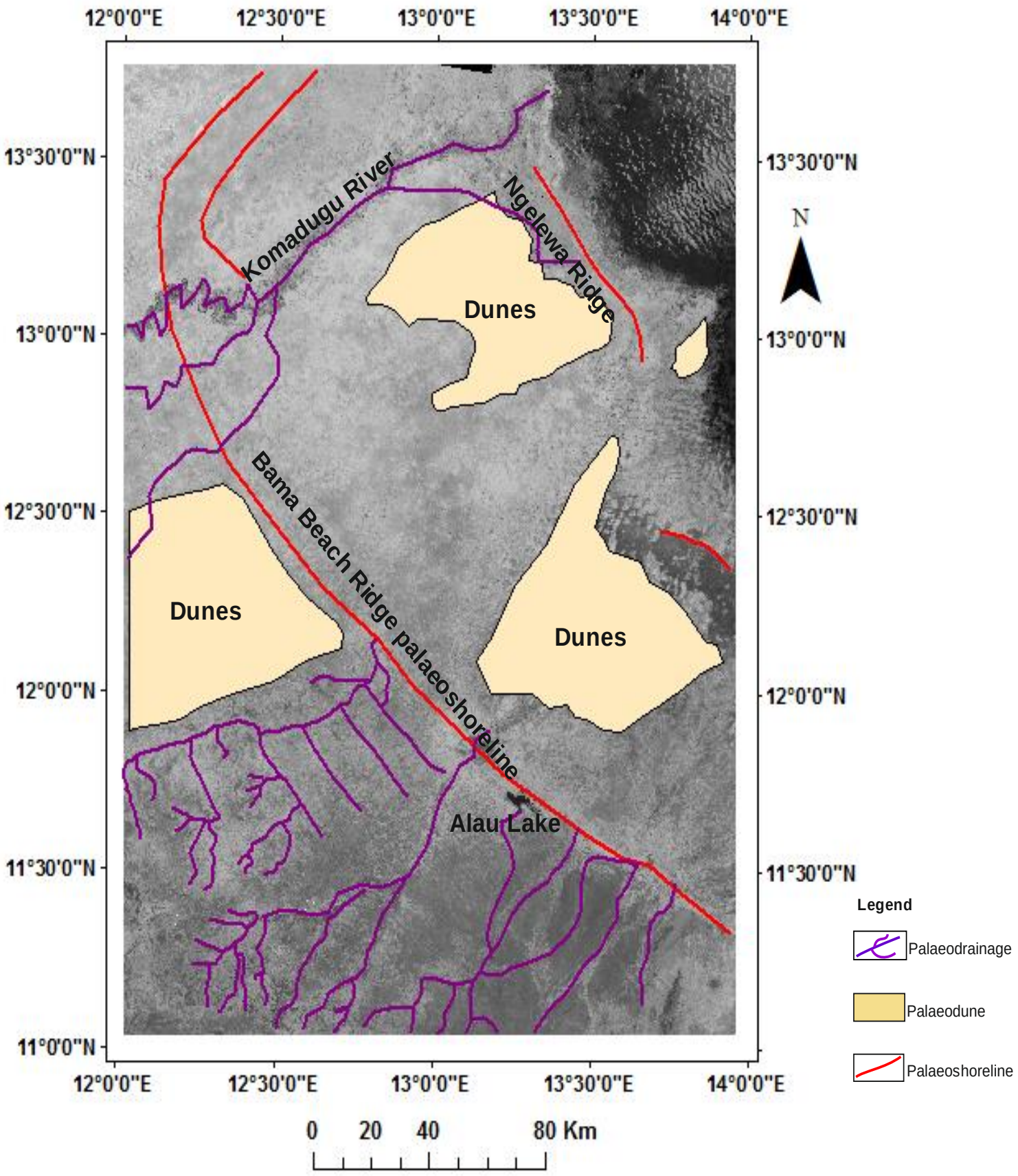

Fig. 4.23: Surface landforms identified in the north-eastern Bornu basin including palaeoshorelines, dunes and palaeodrainage features. The different map layers are overlain using GIS on the Landsat 7 ETM + mosaic image subset.

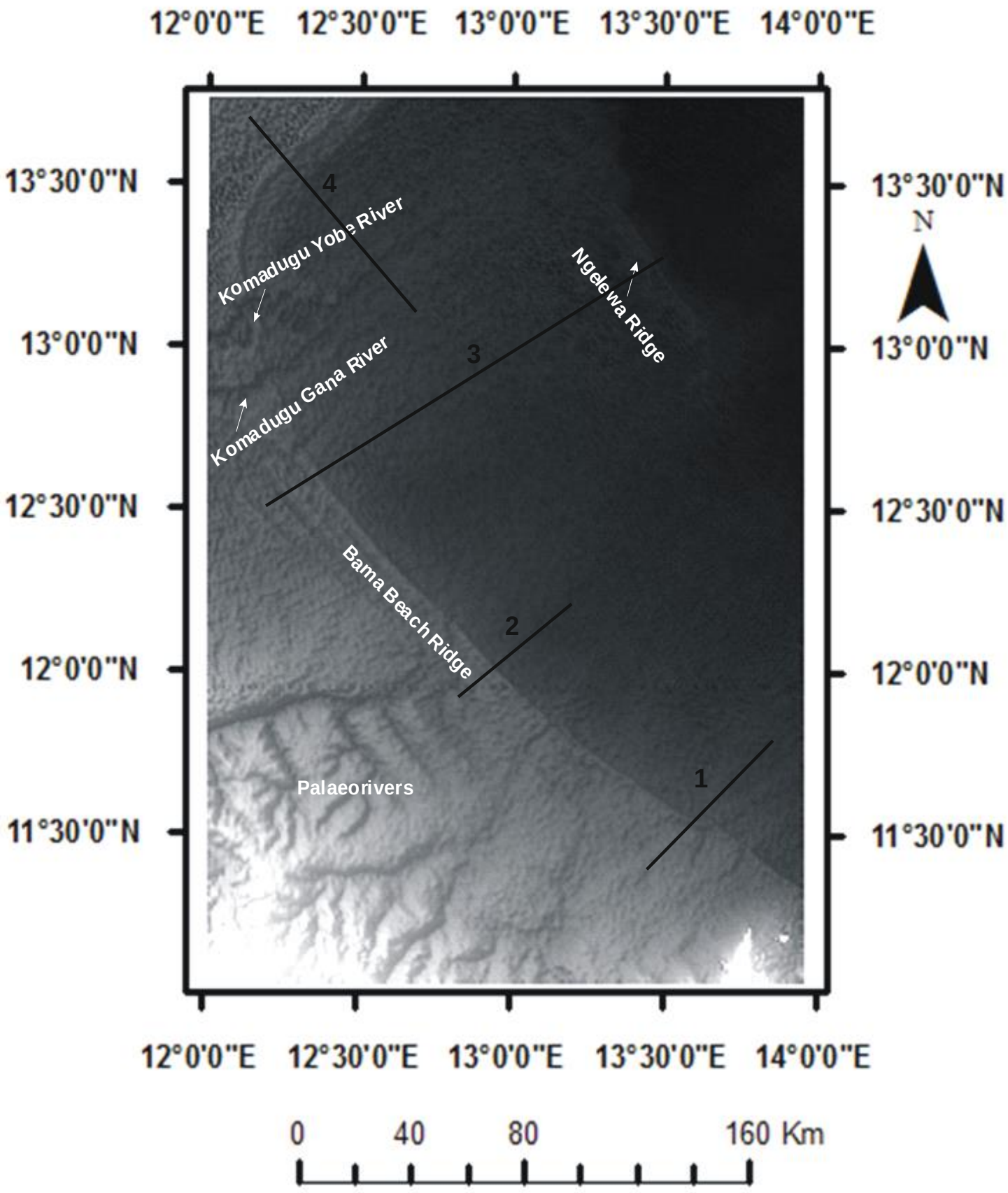

Fig.4.24. SRTM DEM Hill shade relief image showing the subsurface expressions of the palaeoshorelines and palaeodrainage features

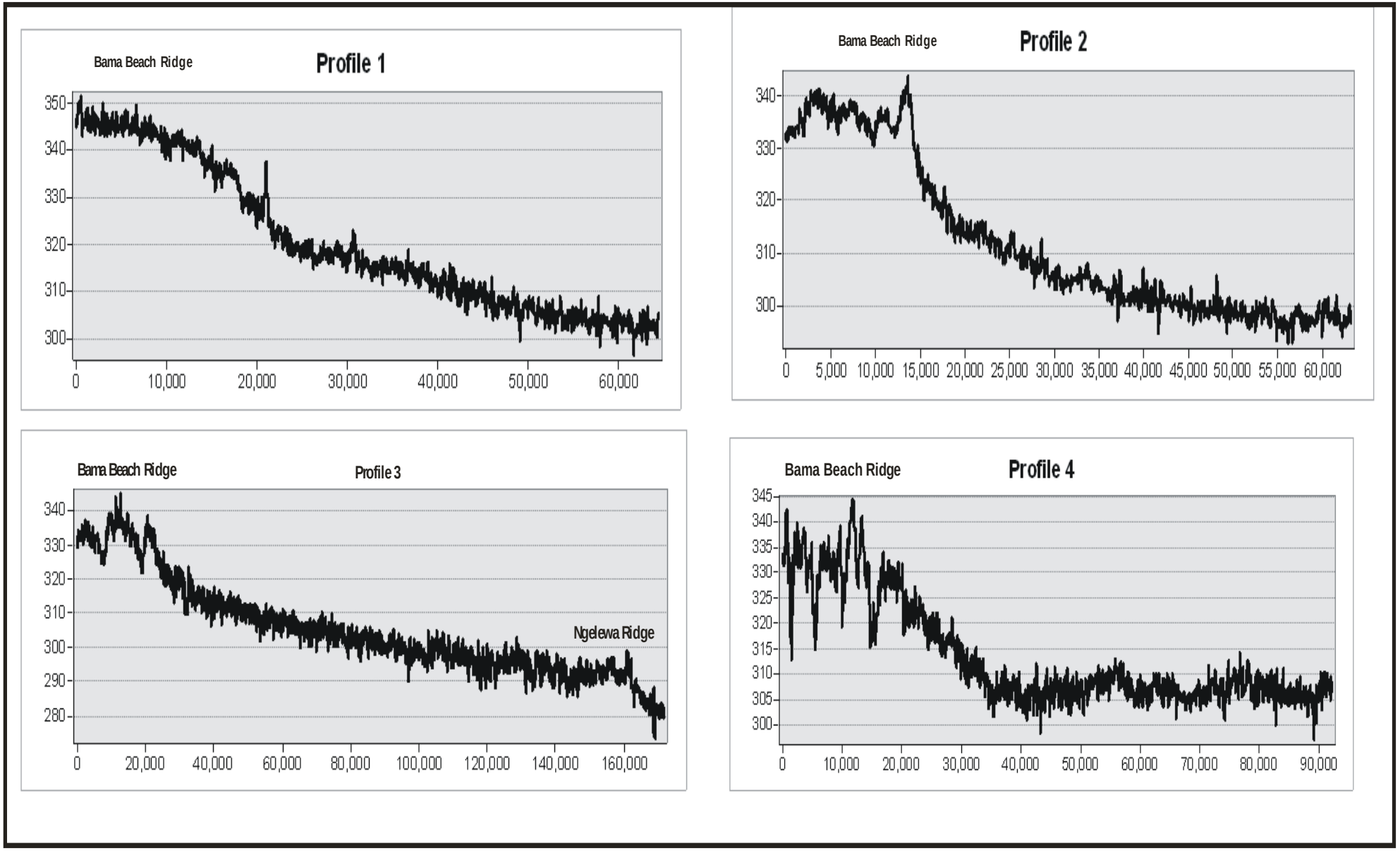

Fig 4.25: Four topographic profiles drawn in Fig. (4.24) across the Bama Beach Ridge to determine the elevations of the feature relative to the adjoining areas.

4.5.3 Lineaments characterisation

Lineaments identification and mapping is important in determining mechanisms of deformation and geological structure (Cortes et al., 1998; De Castro et al., 2002; Morelli and Piana, 2006). Two different comparative approaches to lineaments mapping are carried out in this study involving manual digitization and automatic lineament extraction. Lineaments extracted from the Landsat image mosaic covering the study area are represented as vector maps and overlain on the raster images in GIS (Fig. 4.22b and Fig. 4.26). Lineaments are commonly analysed using their, lengths and orientations (Mostafa and Zakir, 1996; Edet et al., 1998; Zakir et al., 1999). In this study, attributes of the extracted lineaments presented include lineaments lengths, lineaments frequencies and lineaments orientations and populations are computed automatically and presented in Table (4.2). Lineaments metadata were obtained from *Rockwork* software used for the statistical analysis. During the automatic lineament extraction, sand dunes identified in the study area are isolated and masked out.

The GIS overlay of the dunes map on the lineament map is presented as (Fig. 4.27) For ease of analysis and correlation with other thematic maps adjacent numerous lineaments occurring in parallel or continuous were combined to produce lineament zones. Lineament zones are used to simplify correlation with thematic maps than with individual often closely linked and cross cutting lineaments. Lineaments zones are areas of increased lineament occurrences combined to form continuous patterns (Baars, 1995; Caran et al., 1982). Lineament zones display areas of high lineament densities indicating high cumulative concentration of closely occurring lineaments (Kim et al., 2004b; Sharma et al., 2012). Lineament zones thus, consist of individual adjacent lineaments with different properties including length, azimuth and orientation combined together. The aggregation of individual lineaments in this manner produced

lineament zones, which vary in width, length, linearity and pattern distinguishable from adjacent lineaments zones based on their dominant trends and properties.

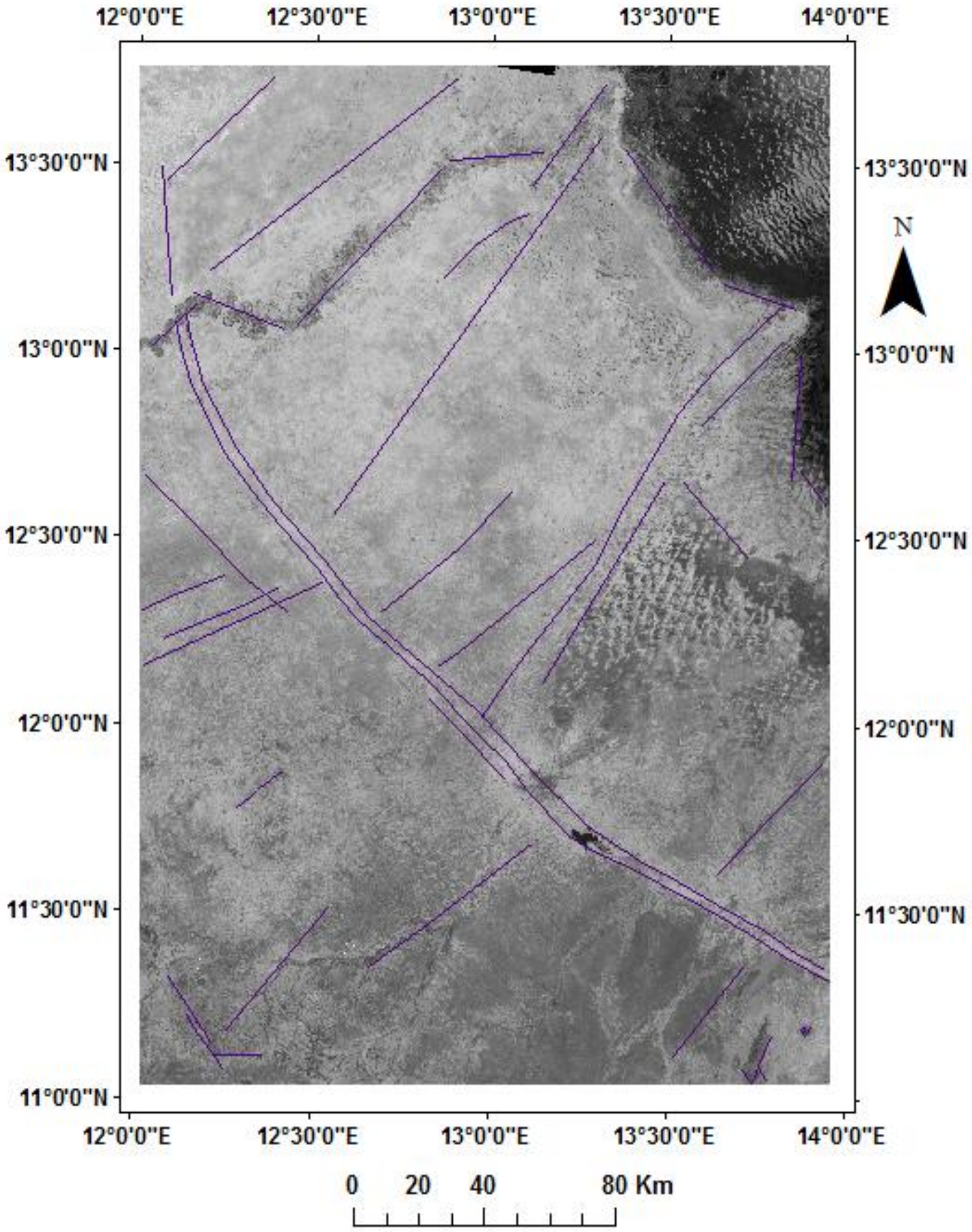

Fig 4.26: Manual GIS digitisation of surface lineaments in the north eastern Bornu basin mapped from the Landsat 7 ETM+ mosaic image subset and overlain on the raster image. Dune areas identified are masked out during the manual mapping (lineaments are shown in purple colour).

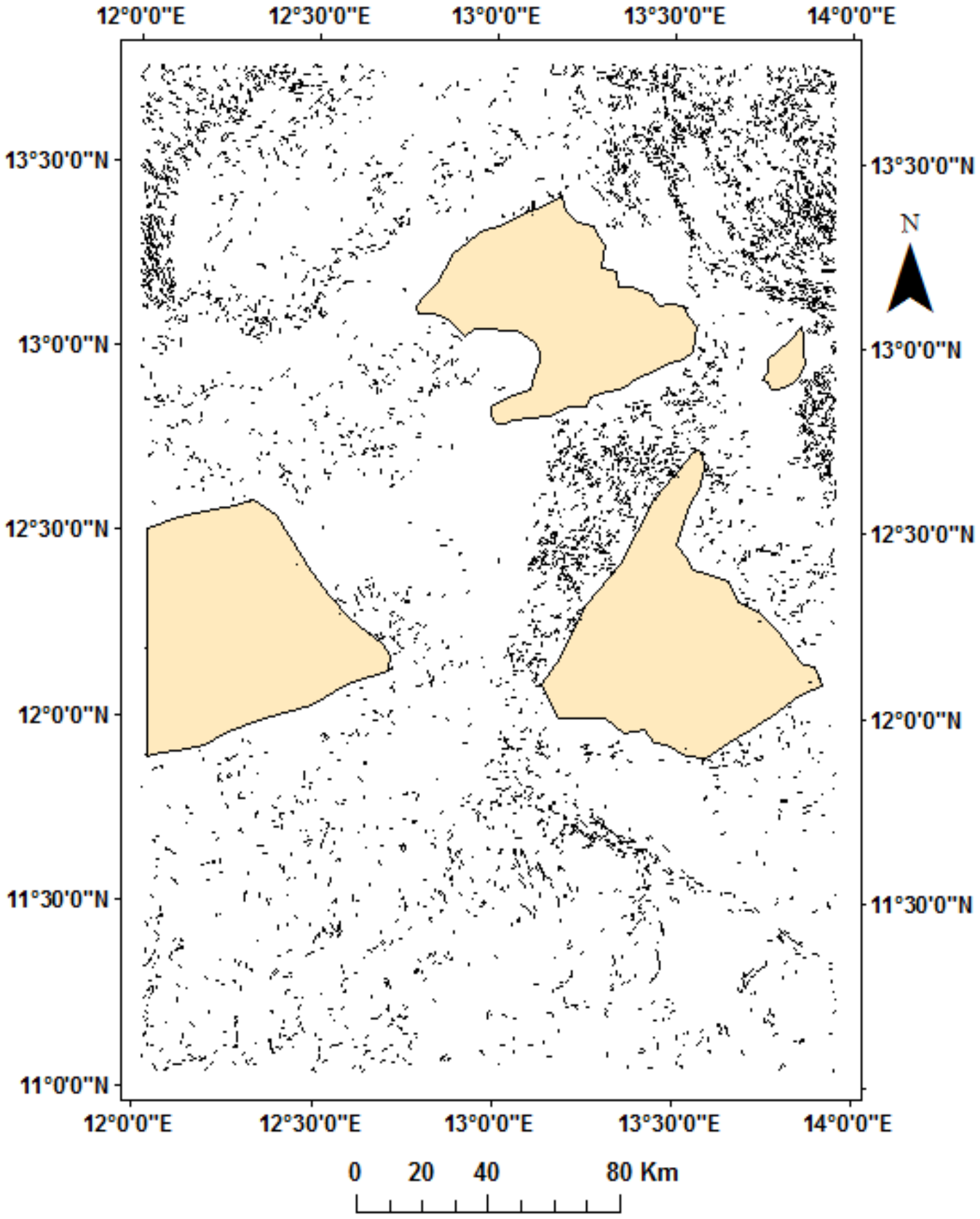

Fig 4.27: Lineament map shapefile of the north eastern Bornu basin extracted from the subset mosaic of the Landsat 7 ETM + images using automatic method overlain using GIS by the dunes map layer shown in beige colour

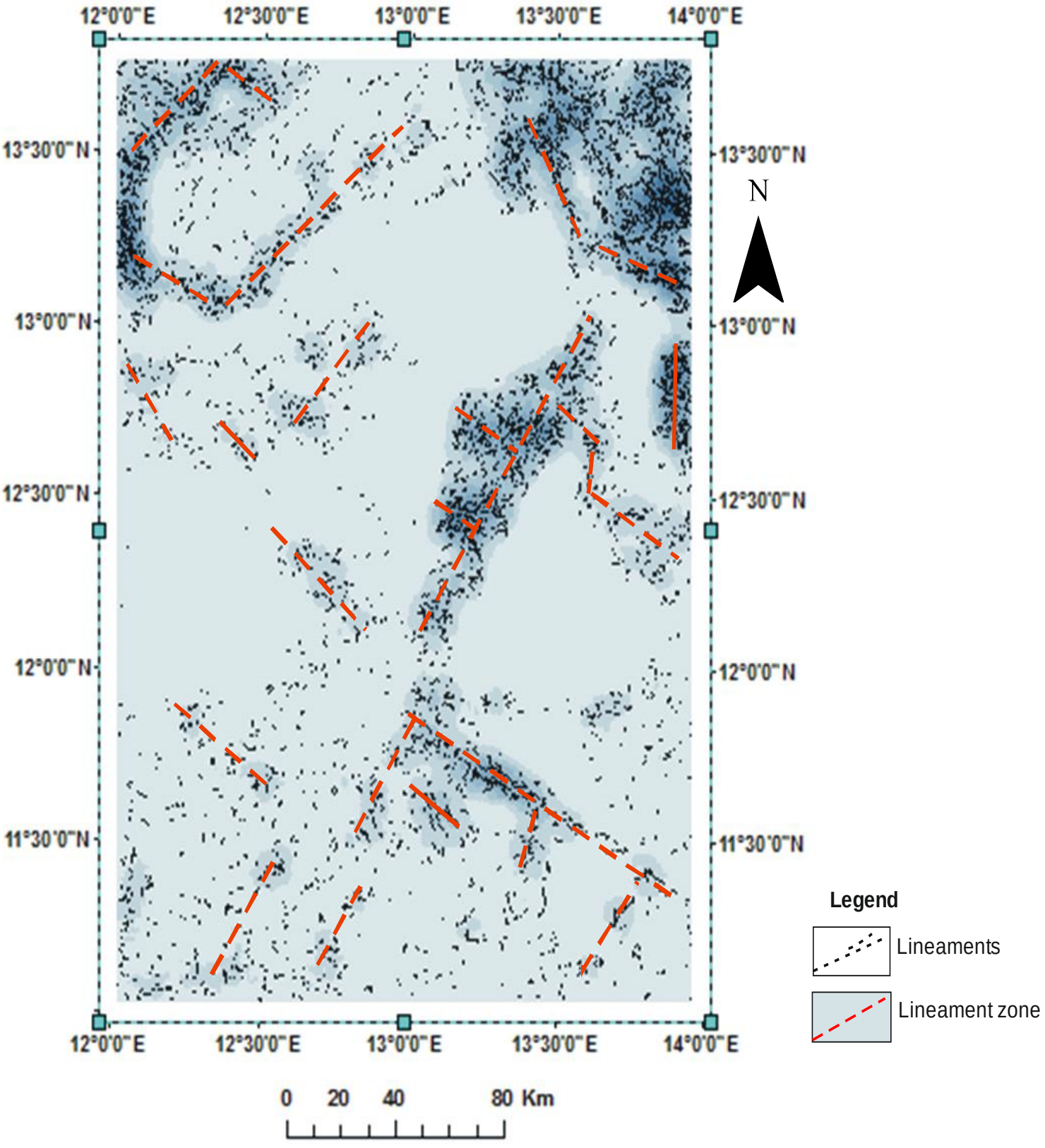

Fig 4.28: Lineament density map showing lineament zones as areas with high lineament concentration mapped in Fig. 4.27. Lineament zones main trend is in NE-SW and NW-SE directions similar to trends of the manual mapped lineaments as well as trends of the individual automatic mapped lineaments in the north eastern Bornu basin. Note that the dune areas were masked out of the lineament analysis.

The lineament zones show major elongated patterns oriented along NW-SE and NE-SW directions. High-density areas representing increased closely occurring lineaments are located throughout the boundary of the lake with the land areas. High lineament zones are displayed at the boundary of the lake where alignments of the vegetation cover exist. The increased anomalies on the lineament map show elongated structural belt trending in NE-SW and NW-SE directions. The high lineament zone areas at the Lake Chad shore in the north-eastern boundary of the map area in Fig. (4.28) are defined by series of elongated continuous lineament zone, which coincide with the intersecting conjugate NW-SE and NE-SW trends of lake shore boundary and along areas covered by the aligned vegetation (Fig. 4.26). The high lineament zone also coincides with the north-eastern edge of the Bornu basin. The terrestrial western part of the map is rather characterised by sparse lineaments aggregates forming narrow low lineament density, which bear much similarity in terms of pattern and orientation. Trends of surface lineaments in the study area mapped from automatic method were displayed on Rose diagram (Fig. 4.29) to identify their preferred orientations. Orientation analysis of the lineaments using the Rose diagram depict the lineaments based on their combined trends and frequency with, the predominant trends of most of the surface lineaments are in the NW-SE and NE-SW lineaments, which potentially suggest that they are more persistent and most related to the major structural trends in the basin. Statistical characteristics of the lineaments trends from automatic mapping method are shown in Table (4.2). Fig. (4.30) shows the geospatial correlation of the manual and automatic lineaments, which shows close agreement in geospatial positions and trends of the lineament zones.

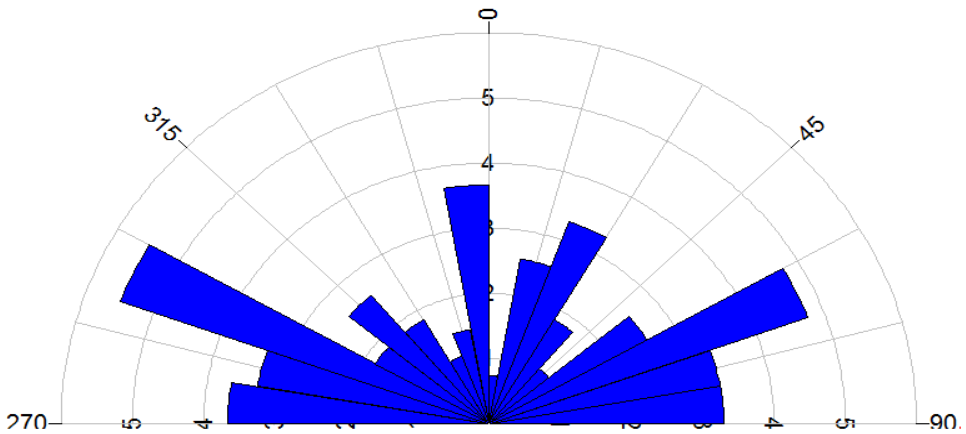

Fig 4.29: Strucural trends of surface lineaments in the north eastern Bornu basin from automatic mapping method mapped from the subset of the Landsat 7 ETM+ mosaic

Table 4.2: Statistical characteristics of the surface lineaments mapped from the subset of the Landsat 7 ETM+ mosaic

Statistical Summary	
Calculation Method:	Frequency
Class Interval:	10.0 Degrees
Azimuth Filtering:	Deactivated
Data Type:	Bidirectional
Rotation Amount:	0
Population:	10,291
Total Length of All Lineations:	273.0
Maximum Bin Population:	16.0
Mean Bin Population:	7.58
Standard Deviation of Bin Population:	3.68
Maximum Bin Population (%):	5.86
Mean Bin Population (%):	2.78
Standard Deviation of Bin Population (%):	1.35
Maximum Bin Length:	16.0
Mean Bin Length:	7.58
Standard Deviation of Bin Lengths:	3.68
Maximum Bin Length (%):	5.86
Mean Bin Length (%):	2.78
Standard Deviation of Bin Lengths (%):	1.35
Vector Mean:	161.7 Degrees
	341.75 Degrees
Confidence Interval:	51.8 Degrees
	(80 Percent)
R-mag:	0.01

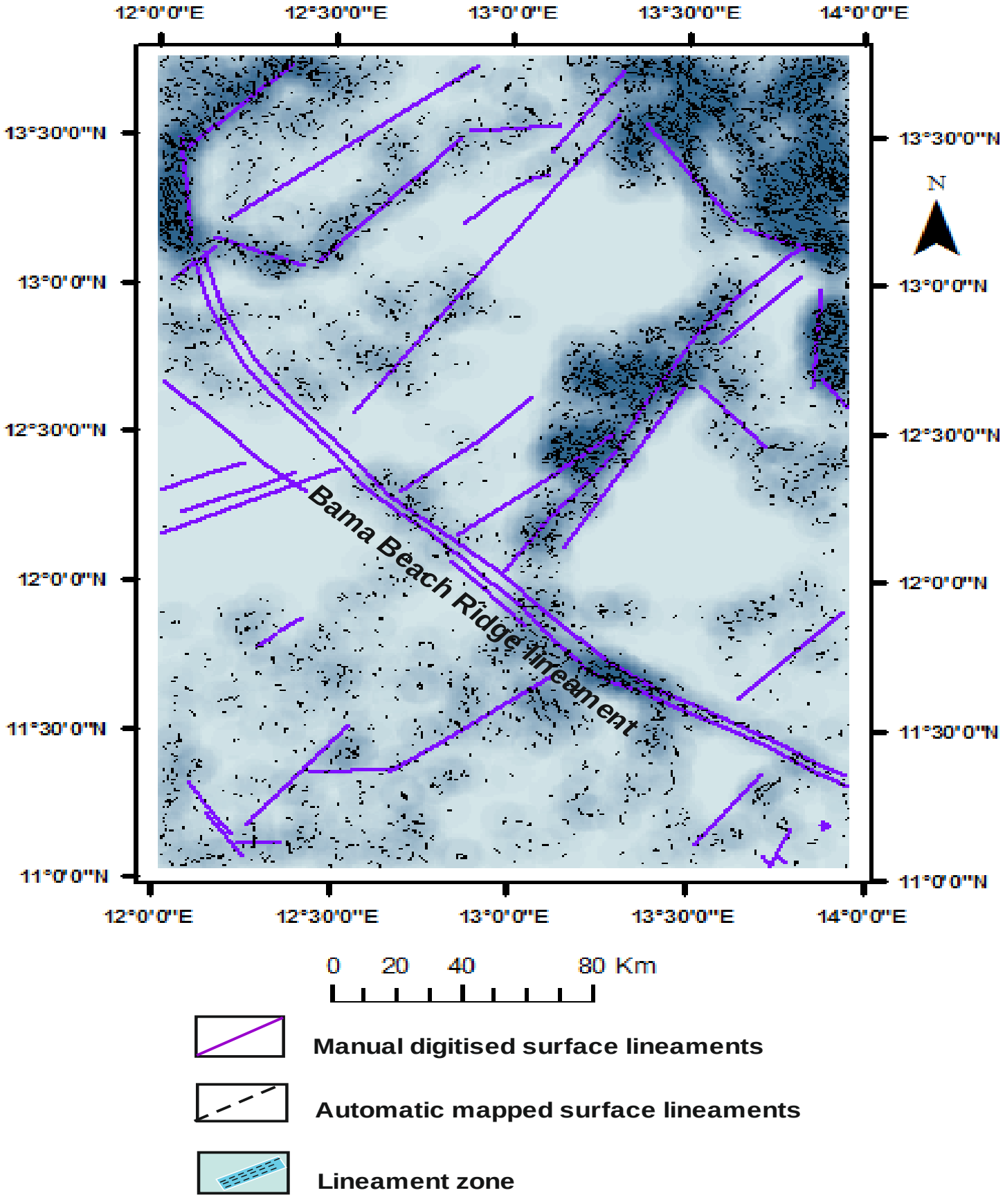

Fig. 4.30. Geospatial correlation of the manual digitised surface lineaments and the lineaments mapped from automatic method. The complimentary methods offer validation of the surface lineament mapping results. Note the predominant trends of the structural lineaments in NE-SW and NW-SE directions.

Chapter 5:

Integrating 2D seismic and well log data to image subsurface litho-stratigraphy and structure in the north-eastern Bornu basin

5.1 Introduction

Several discrepancies exist in the literature for the litho-stratigraphic classification of the Bornu basin. The subsurface stratigraphy in the north-eastern part of the basin towards the south west shores of the Lake Chad remain unclear since specific data were routinely used and not a combination of different datasets, which allow for correlation and validation. The primary objective of this chapter is to constrain the subsurface stratigraphy and structures in the north-eastern Bornu Basin bordering the Lake Chad using combined seismic data and well log data. Specifically, the study aim at (1) correlating the multiple well log datasets, (2) tying well log to seismic data for validation of the stratigraphy, (3) detailed seismic facies interpretation, (4) detailed well log facies interpretation, (5) identifying the sedimentary formations and delineating their thicknesses and lateral variations, (6) deducing the environments of deposition of the formations, (7) characterising the subsurface seismic structures and (8) identifying the synergy between combined application of the different geophysical data types. The main advantage of the integrated data analysis is to provide more detail subsurface analysis, which would enhance reliability of geological interpretations than using any single data in isolation. The most part of this chapter is published already in Isyaku et al., (2016) (Appendix B).

5.2 Well log and seismic analysis: Data and method

The datasets used in this chapter were acquired during the exploration in the Bornu basin by a consortium of oil companies including Halliburton, Landmark and LMK Resources in 1996, which led to the drilling of twenty three (23) exploration wells and several 2-D seismic lines. In this study, the complete suite of available digital well log data from the 23 wells comprising of gamma ray (GR) log, resistivity (ILD) log, bulk density (RHOB) log and sonic (DT) log for each well were obtained for detailed mapping of subsurface stratigraphy and structures. Additional data include post stack time migrated 2D seismic reflection survey data overlapping the wells positions adjoining the Lake Chad in the north-eastern Bornu basin in Nigeria (Fig. 5.1). The datasets were provided by the Nigerian Department of Petroleum Resources (DPR) and Nigerian National Petroleum Corporation (NNPC).

The four different log types including gamma ray, resistivity, bulk density and sonic log were extracted and analysed to establish their synergistic relationships with depth in the wells. The method involved delineating the different geophysical responses of the different log types and their corresponding log curve pattern behaviours in different lithological environments penetrated by each well. Patterns are correlated across different logs at depth in each well and compared across corresponding logs in all wells. The 2-D seismic data are displayed in normal SEG-Y polarity with downward increase in reflection time for a zero phase wavelet reflection wiggle and a positive reflection coefficient having a central wavelength peak. The processed seismic sections possessed high signal-noise (S/N) ratio with smooth and continuous phase reflections, which allow for easy auto tracking of the strong seismic reflections and more reliable manual horizon mapping where necessary. In the absence of rock outcrop and core samples for this study, the universal lithological descriptions of the formations in the basin from published studies were used as guide for identification of

the stratigraphic facies units described herein. Sonic log velocity data were extracted from Kasade_01 (KAS) well, which is directly located at the geospatial position of NE-SW oriented seismic Line_13 was selected for the well-to-seismic tie using their time-depth relationship (Fig. 5.1). NW-SE oriented seismic Line_5, which perpendicularly intersects seismic Line_13, was selected for correlation and validation of the seismic stratigraphy (Fig. 5.1). Well log analysis was carried out using Ikon *RokDoc* software with a free academic license provided by the software company to the School of Earth and Environmental Sciences at the University of Portsmouth UK. Seismic data analysis was carried out using *Petrel 2012* software available on the workstation used installed by the University of Portsmouth.

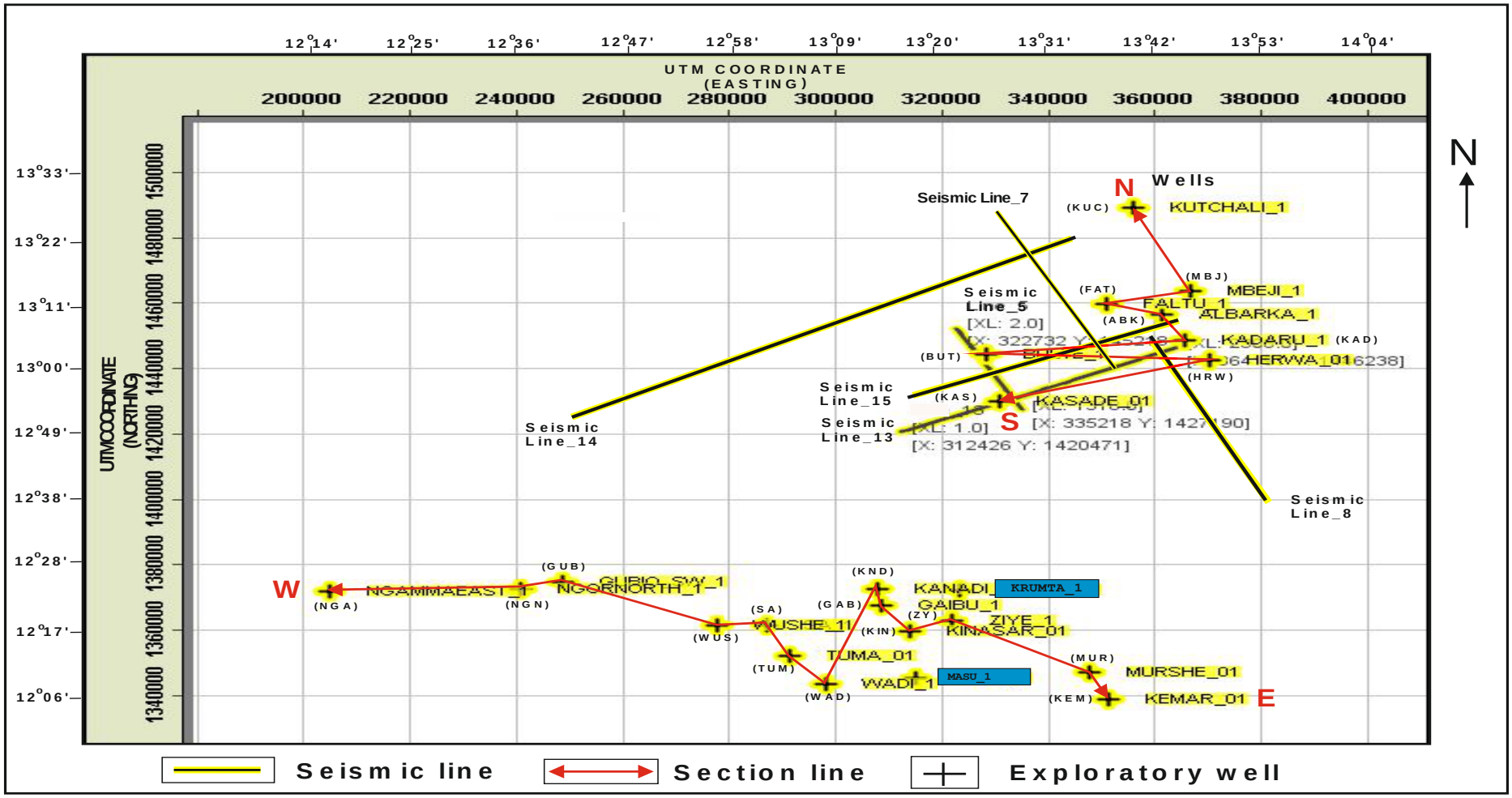

Figure 5.1. Distribution of seismic and well log data used for this study displayed in the RockDoc software. Krumta and Masu wells shown in blue colour are not analysed due to data error. Well log analysis is based on the remaining 21 wells. The seismic lines only corresponds with the geospatial locations of the wells in the north eastern sector of the survey area.

5.2.1 Combined qualitative log pattern analysis

As presented in Railsback (2011), qualitative analysis of the well logs is used in characterisation of the subsurface stratigraphy of the study area into well log facies. Generally, well logs are generated from geophysical instruments lowered down in well bores, which record changes in subsurface physical properties of rocks with depth. Well log data have several applications in the different fields of geology but they are particularly useful in the oil and gas industry for evaluation of hydrocarbon fluids as well as in stratigraphy and structural geology (Asquith and Gibson, 1982). The gamma-ray (GR), resistivity, bulk-density and sonic logs extracted from the 21 wells in the study area wells were all arranged into vertical profiles against common measured depths (MD) to show systematic vertical variations of the sedimentary sequence across different log types at corresponding depths in each well.

Routine smoothing and coarsening of the plotted well logs' scales to fit the data range were applied. Vertical axes or the measured depth (MD) axes of the well logs were adjusted to conform with data-start to data-stop ranges for whole log visualisations. Consistencies in log signatures with depth across different log types in each well were observed by visually recognising and mapping patterns of the logs. Each visual log pattern is associated with a corresponding qualitative indication of the physical property measured by the log. Fine correlations within likely formations as well as at formation boundaries across well sections rather than absolute conformity of the log patterns were considered.

Abrupt changes observed in the overall log patterns with associated changes in individual log values were implied as change in the lithology or stratigraphic boundary. Commonly, in subsurface stratigraphic mapping, correlation relies on the analysis of well log data to build cross sections, subsurface maps and geological models using common correlation methods including use of marker beds, pattern matching and slice

techniques (Madibboyina, 2011). As such, the concept of typical log responses associated with various lithologies described by Railsback (2011) was used herein for the qualitative interpretation of subsurface facies units. Literature descriptions of the main lithologies in the Bornu basin indicated that the formations predominantly contained varying proportions of sand and shale or clay (Table 5.1). As such, qualitative analysis based on the dominance of shale or sand as indicated by their corresponding log responses at any depth within the formation was inferred. Bounding discontinuities as described by Kassenaar (1989) were obtained herein by outlining the intervals within the logs, which display certain characteristic curve shape and deducing the magnitude of the log response within corresponding stratigraphic depth. The well log facies were identified and correlated with their corresponding seismic facies identified from interpreted seismic sections to validate the stratigraphy and structure.

The physical relationship between most geophysical methods including well logging and seismic survey are commonly compared for precise interpretation of subsurface stratigraphy and structures to improve understanding of subsurface heterogeneities (Bueno et al., 2014). In this study, stratigraphic units were identified from qualitative pattern analysis of the different logs and validated with the adjoining seismic data. The methodology involved correlating the time-processed seismic data to the depth-processed sonic log velocity data in order to determine their time-depth relationship. Correspondingly, stratigraphic horizons were mapped from reflection surfaces in the 2D seismic data to represent subsurface lithological interface or sequence stratigraphic boundaries (Appendix B).

5.2.2 Well log facies characteristics

Well log facies were identified and correlated with their corresponding seismic facies identified from interpreted seismic sections to validate the stratigraphy and structure. Log pattern matching can be carried out manually (Schaefer, 2005) or using mathematical, logical, or other advanced computing techniques to recognise patterns in well logs for classification into electrofacies (Igbokwe, 2011). In this study, mapping of stratigraphic intervals were achieved by analysing overall log patterns and their corresponding change in log values, which is consistent with the expected physical and quantitative log behaviour associated with individual lithological properties (Fig. 5.6). Pattern analysis and recognition of log behaviours in different rocks were derived from comparison with the synthetic log response chart developed by Railsback (2011).

5.2.2.1 Gamma ray log

Gamma ray log used herein were analysed mainly to distinguish between shale and non-shales (or sandy) compositions. Conventionally, gamma ray (GR) log is primarily used to detect the presence of radioactive materials that make up clay particles in shales. As such, gamma ray (GR) log is commonly referred to as the 'shale log' (Kenneth and Allan, 2003; Ellis and Singer 2008). The GR log herein were displayed in two narrow columns for measured depths (MD) and the log track recorded in standard American Petroleum Institute (API) units. The scale of 1 – 150 API was used to accommodate the general response range of the gamma ray log data (Appendix B). Sudden changes in GR log curves pattern inferred changes in lithological property or unconformities producing systematic curve trends (Krassay, 1998). However, this does not conclusively imply that all increased gamma ray responses in GR log signify shale content since sand layers may contain radioactive materials (Ellis and Singer, 2008). Gamma ray responses can more reliably be attributed to grain sizes when correlated with outcrop or core samples.

Krassay, (1998) classified three commonly recognised gamma ray log patterns, which infer discrete sedimentary cycles. Funnel-shaped gamma ray log with gamma ray counts decreasing upward indicating progressively coarser or sandy sedimentary sequence denote progradational stacking pattern. Bell-shaped gamma ray log with gamma ray count increasing upward indicating finer or shaly sedimentary sequences denote retrogradational stacking pattern. Block-shaped gamma ray log with regular gamma ray counts indicating uniform sedimentary sequence denote aggradational stacking pattern. These characteristic log shapes are more apparent when the GR log is paired with resistivity log where the patterns are mirrored (Fig. 5.2).

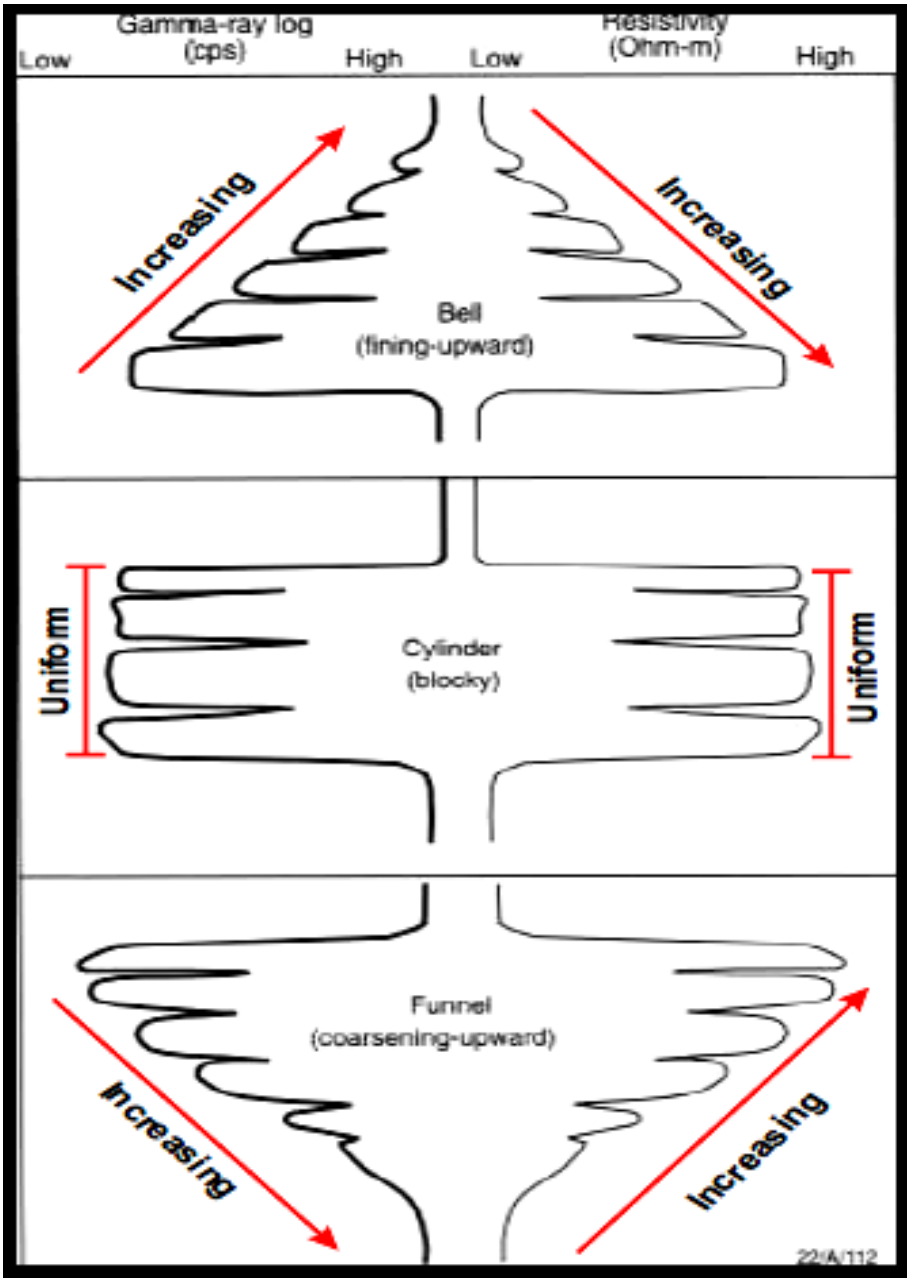

Figure 5.2.Three commonly identified log curve patterns on gamma ray log paired with resistivity log (modified after Krassay, 1998).

5.2.2.2 Resistivity log

Resistivity logs measure electrical properties of rock formations and are usually correlated with gamma ray logs for lithological investigation due to their distinguishing behaviours in sand and shale formations. Quartz and muscovite, which are abundant mineral components in sandstones, have high resistivities while clays in shales have low resistivities. However, resistivity of formations often depends on conductivity due to the presence of water (and its salinity) and hydrocarbons contained within pores spaces of rocks. Resistivity depends on the lithology due to the nature of rock fabric, texture and clay content (Ellis and Singer, 2008). Resistivity method detects mudstone areas having low resistivity and sandstone areas with high resistivity (Chambers et al., 2008).

In this study, the resistivity log type is the deep induction log (ILD), which measures resistivity around the wellbore in the undisturbed deeper zones of the formation that is not invaded by the drilling mud fluid. The log scale was set at a range of 0.2 – 100 Ohms, which fitted the extent of the data. The log tracks have logarithmic grid line scales to accommodate the changes associated with electrical measurements in rocks. The ILD logs are essentially used herein to distinguish between zones of shale and non-shaly (or sand) across the formations. Thus, inverse pattern behaviour was expected between the GR logs and the ILD logs where minimum resistivity readings would indicate high clay and shale content and maximum resistivity readings would indicate the sandy content (in the absence of oil and or associated formation water). The resistivity log responses generally display a consistent contrasting pattern behaviour compared with the GR logs at every defined depth interval in each well. This contrasting pattern behaviour between the GR and ILD log pairs was used to mirror the combined overall log pattern to detect bell, blocky and funnel shapes (Appendix B).

5.2.2.3 Bulk-Density log

Bulk density is an important property of rock formations as it directly relates to in-situ porosity, lithology and pore fluids. Unlike the natural GR log, which measures the in-situ radioactive materials in rocks, bulk density measurements in wireline logging use an active gamma ray source with gamma ray detector device to record Compton scattering interactions (Ellis and Singer, 2008). The bulk density log (presented by default in the RokDoc software as RHOB, showing density unit, RHO and Bulk D) has a unit scale set at 1.45 – 2.65 g/cm^3 according to the range of the data. Changes in RHOB log pattern is based on the result of variation in density of the rock formations due to porosity difference between sandstones and shales is the major distinguishing property used herein for identification of the lithology. Sandy zones display higher bulk density values than the shale zones with even higher values with depth of burial in the sandstone zones.

5.2.2.4 Sonic log

Sonic logs measure the acoustic velocity of the compressional (P) or shear (S) waves travelling through rocks, which primarily depends on the density, porosity, and lithology of the rock medium However, the P waves depend more on the bulk density of the propagating medium. Sonic logs measure the transit time or slowness of the waves in the formations around the well bore such that the wave travel time is lower in high porosity rocks including sandstone and higher in low porosity rocks including shale. The inverse relationship between bulk density and P-wave velocity is qualitatively reflected in their log patterns (Gardner et al., 1974). The sonic log type available in the dataset is the P-sonic with unit scale ranging from 50.8 – 152.4 µs/ft to fit the extent of the data. The sandy zones in this study clearly displayed high density and a corresponding low P-sonic value while other zones with comparative low density values and corresponding high sonic values refer to the shale zones (Appendix B).

5.2.3 Sonic log - seismic data tie

Tying well log to seismic is generally more precise by correlating wiggle traces obtained from well-based reflectivity in vertical seismic profile (VSP) or a synthetic seismogram with reflectivity obtained from the surface seismic data (Herron, 2014). However, in this study, a VSP was not acquired nor processed and a synthetic seismogram for the well log data is not available to match the character of individual well-based reflections with reflections from the 2D seismic data. Since well velocity or check-shot survey data is not available for direct time-depth tying of the seismic to well data the correlation method described by Herron (2014) was tested herein using time-depth components available in the sonic log data. Kasade_01 (KAS) well and seismic Line_13 directly positioned on the same geospatial location are suitable for the well-to-seismic tie. Plotting of the Kasade_01 (KAS) well and the Line _13 seismic data was achieved automatically by the Petrel software used from the geographic coordinates inherent in the two datasets (Fig. 5.1). The 2D seismic Line_13 is a time-processed data in microseconds (µs) and is not converted to depth scale while the well log data from Kasade_1 (KAS) well is depth (MD) processed in metres. Well velocity or check shot survey data were not available and the only source of velocity data in the well log dataset was obtained from the compressional P-wave velocity sonic log, which is a time-depth data.

Thus, the time-depth relationship between the sonic log and seismic datasets were deduced by calculating the two-way-time (TWT) velocity of the sonic log and compared with the seismic data TWT velocity as described by Herron (2011, 2014). The method involves “blocking”, which is referred to visual averaging of the sonic log by delineating discrete log intervals based on distinctive boundaries that mark significant departures from general log patterns and properties. The discrete intervals measured from Kasade_01 (KAS) well sonic log have approximately constant interval

transit time (ITT) corresponding to the constant interval velocity of the log (Fig. 5.3). On the sonic log, the distinct step changes in the overall log patterns were marked and intervals characterised with approximately constant log values were noted. Five major boundary intervals were blocked and labelled A through E having corresponding boundaries 1 through 6 with depth on the sonic log. The ITTs at the top of each boundary interval were measured directly from the sonic log with an average uncertainty of ±6 µs/ft and were used to calculate the TWT in (ms) for each blocked interval using Equation (1).

$$TWT\ (ms) = \frac{\left[2 \times ITT\ (\frac{\mu s}{ft}) \times \text{sonic log interval thickness}\ (ft)\right]}{1000\ (\mu s/ms)}. \quad (1)$$ (Herron, 2014)

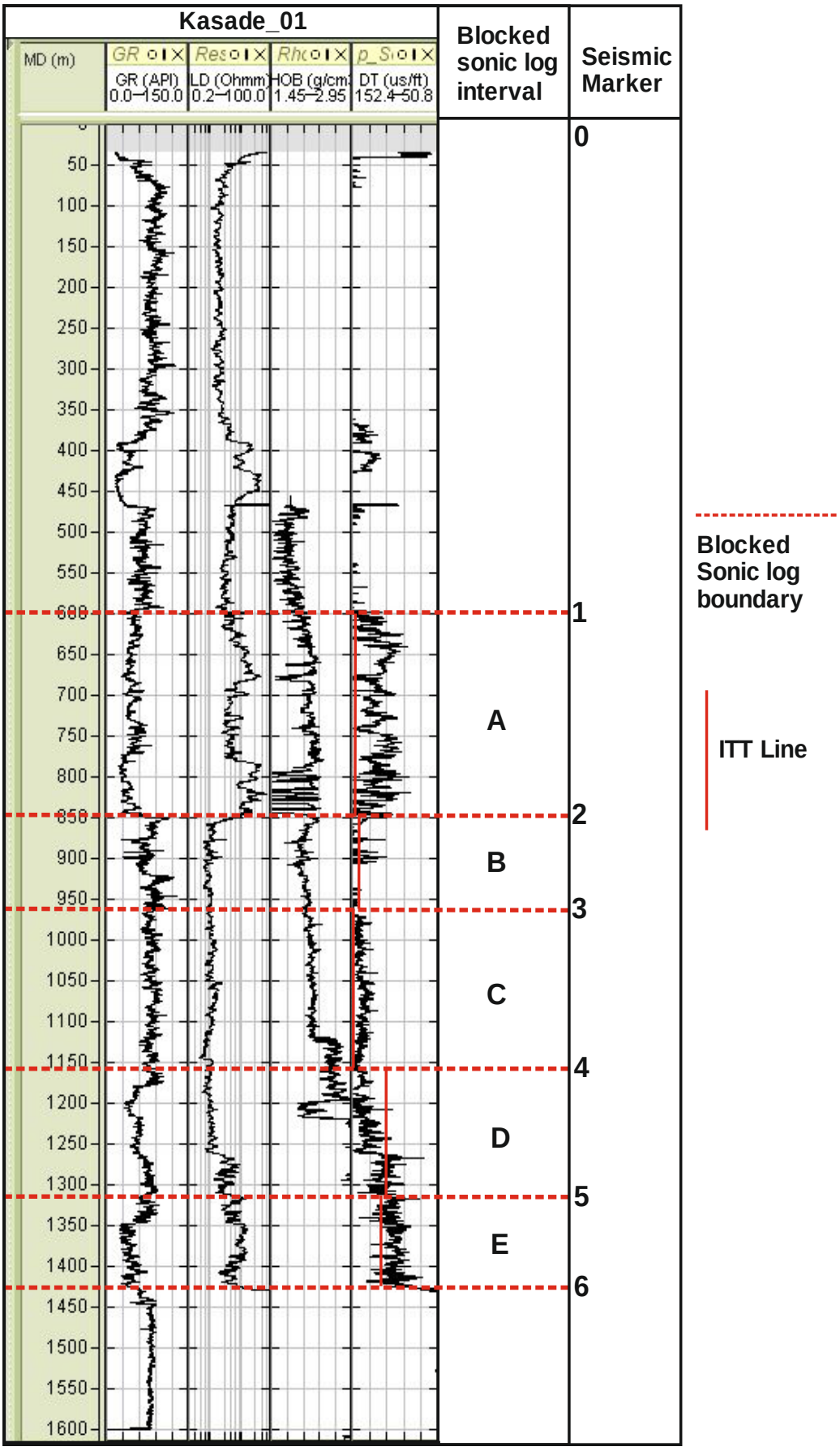

Figure 5.3. Showing Kasade_01 well with blocked log intervals and ITT values for sonic log in red (ITT values listed in Table 5.2).

5.3 Results

5.3.1 Combined well log stratigraphy and basin structure

The gamma ray, resistivity, bulk density and sonic log belonging to individual wells were aligned to establish their synergistic patterns with depth. Well-log facies (WF) interpretation herein utilised mirrored gamma ray and resistivity logs combined with bulk density and sonic logs in each well to delineate the general behaviour of the curves corresponding to overall grain size and mineralogy for correlation. Results indicate four well log facies units WF1, WF2, WF3 and WF4 identified from the combined well log interpretation (Appendix B). The basal well log facies unit 1 (WF1) were associated with closely spaced log curves, less spiky with predominantly low GR log values and regular or blocky overall trend typical of a predominantly sandy unit. The overlying WF2 exhibit very spiky and spread-out log curves associated with alternating sharp increase and decrease in GR log values, which generally decreased upward forming an overall funnel shape typical of alternating sand and shale sequence. WF3 is characterised with very closely spaced GR log curves associated with high GR values with none or occasional spikes and an overall blocky curve trend typical of a dominantly shale unit. The uppermost WF4 is characterised with less closely spaced curves, often spiky and alternating sharp changes in log curves with associated variable log values, which generally increased upward formed overall bell shape curves. WF4 is typical of alternating sand and clay sequence. Log data from two wells namely Masu and Krumta (Fig. 5.1) were not plotted due to high data breaks. Hence, geological interpretations are based on the remaining 21 wells.

The four well log facies WFI, WF2, WF3 and WF4 representing Bima, Gongila, Fika and Chad Formations respectively were identified from the combined well log analysis of the four different log curve characters with depth in the 21 wells (Appendix B). Delineation of corresponding boundary intervals across the different types of well logs

for each well allows for the stratigraphic subdivision of the well log facies into different genetic groups (lithofacies) with lateral relationships. The lithofacies displayed consistent distinct pattern behaviour in the GR and resistivity log pairs and correlated with the bulk-density and sonic logs corresponding to individual sedimentary cycles. Each lithofacies is separated from the other by an observable sudden change in log pattern with associated changes in the multi-log physical properties and log values due to the distinctive change in lithology. In this study, due to the absence of core log samples, which would have provided detailed petrographic and biogenic components in the subsurface rocks, the well log facies analysis relied on the generic lithostratigraphic descriptions of the formations in Bornu basin by Avbovbo et al., (1986) (Table 2.1) to deduce and assign the corresponding lithostratigraphic units. Lithofacies identified were designated into strata and characterised into stratigraphic intervals to interpret the various depositional and stratigraphic framework for the study area from the basal to the upper units. Individual facies characteristics are classified based on their differences in lithological composition, thickness, clay content and stratigraphic position. GR Log profiles were plotted and correlated across the wells along two section lines N-S and E-W (Fig. 5.1) to map the lateral continuous subsurface stratigraphy and structure (Fig. 5.4 and Fig. 5.5). The stratigraphy of the north-eastern Bornu basin obtained from this study is presented in Table (5.1).

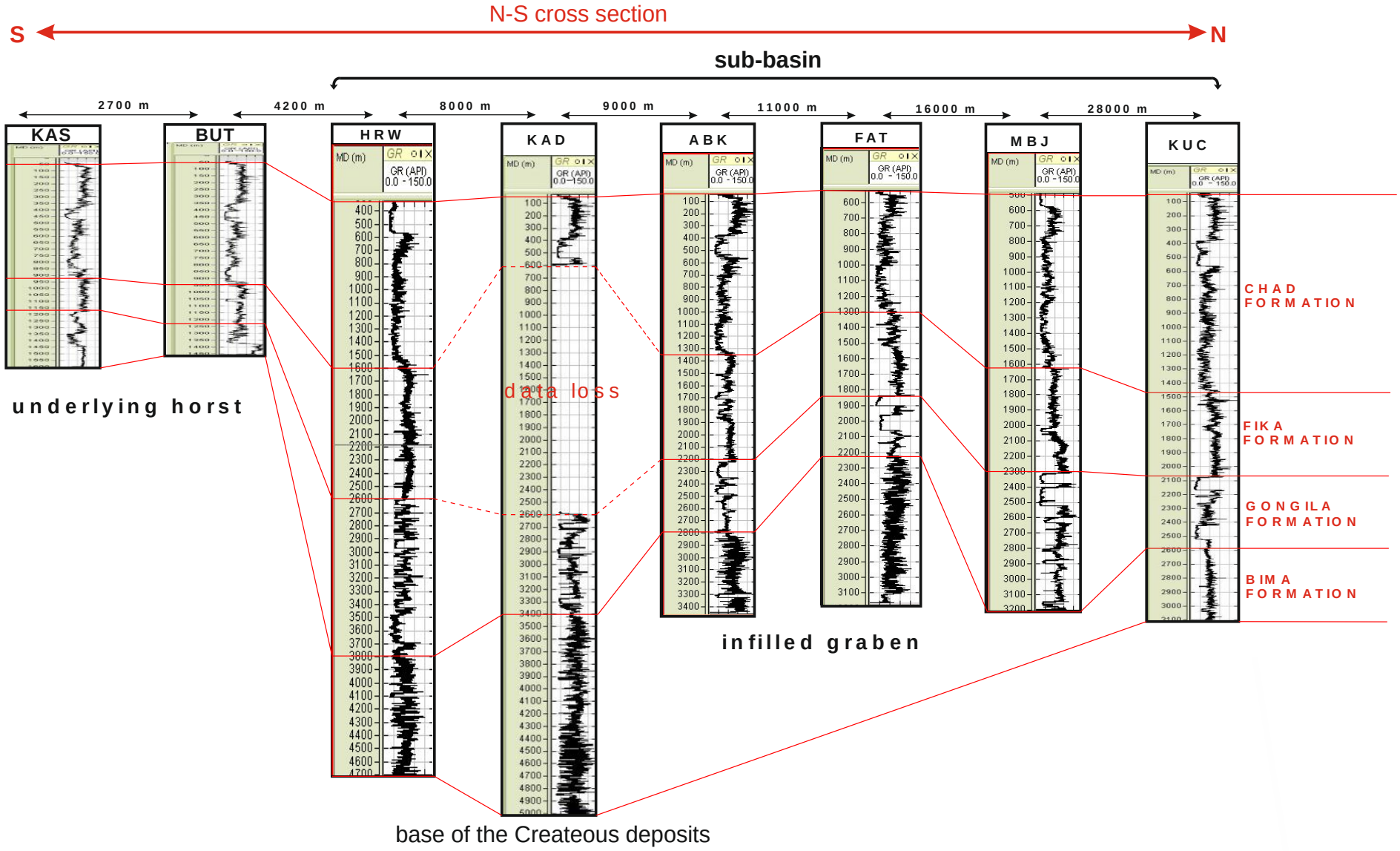

Figure 5.4. N–S oriented cross section of wells as shown in Figure 5.1, showing interpreted subsurface stratigraphic correlation and basin structure. Wells Abbreviations: KAS (Kasade), BUT (Bulte), HRW (Herwa), KAD (Kadaru), ABK (Albarka), FAT (Faltu), MBJ (Mbeji), KUC (Kuchalli) wells. Larger figure is given in Appendix B

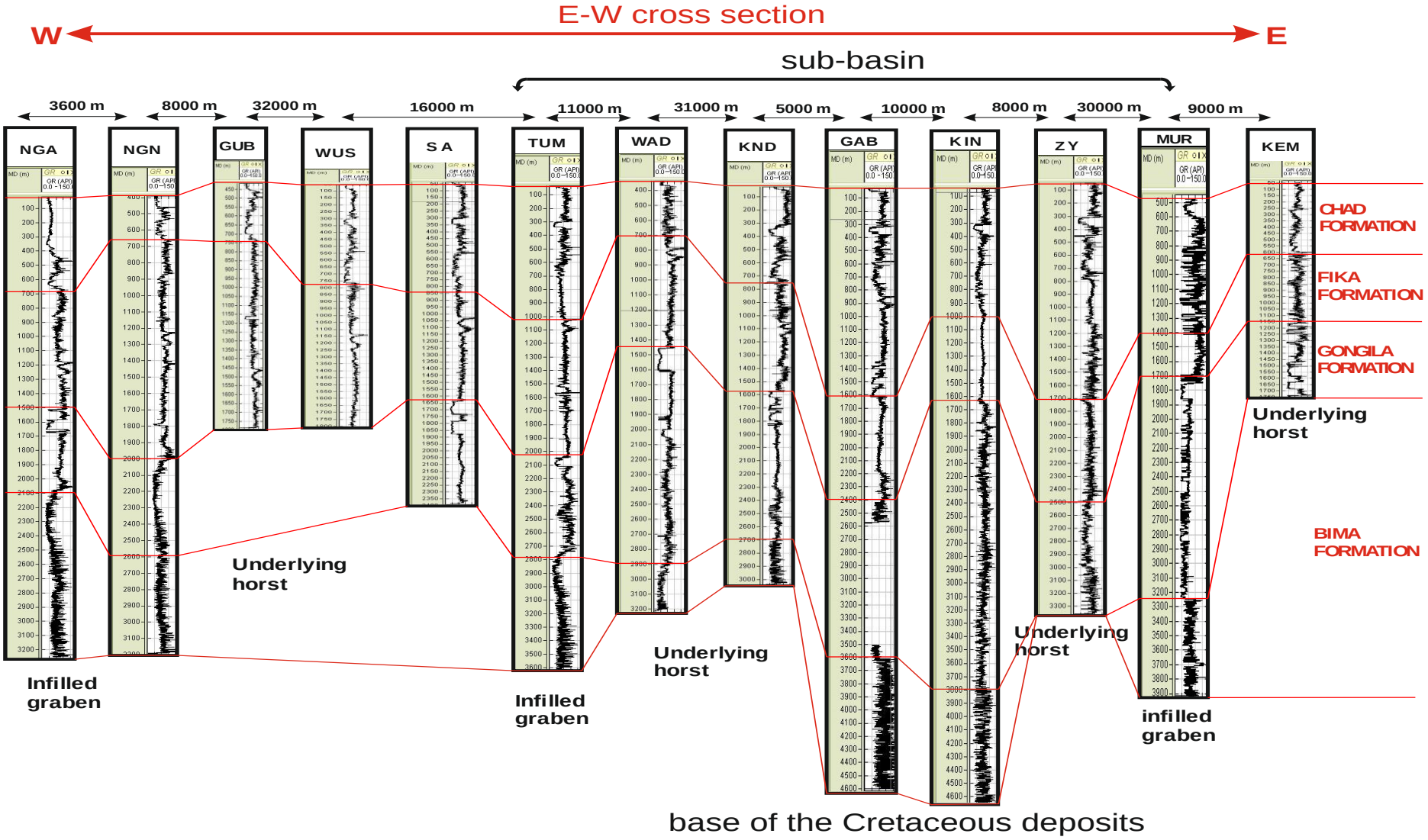

Figure 5.5. W-E oriented cross section of wells as shown in Figure 5.1, showing stratigraphic correlation and basin structure. Wells abbreviations: NGA (Ngammaeast), NGN (Ngornorth), GUB (Gubio), WUS (Wushe), SA (Sa), TUM (Tuma), (WAD (Wadi), KND (Kanadi), (GAB (Gaibu), KIN (Kinasar), ZY (Ziye) MUR (Murshe), KEM (Kemar). Larger figure is given in Appendix B.

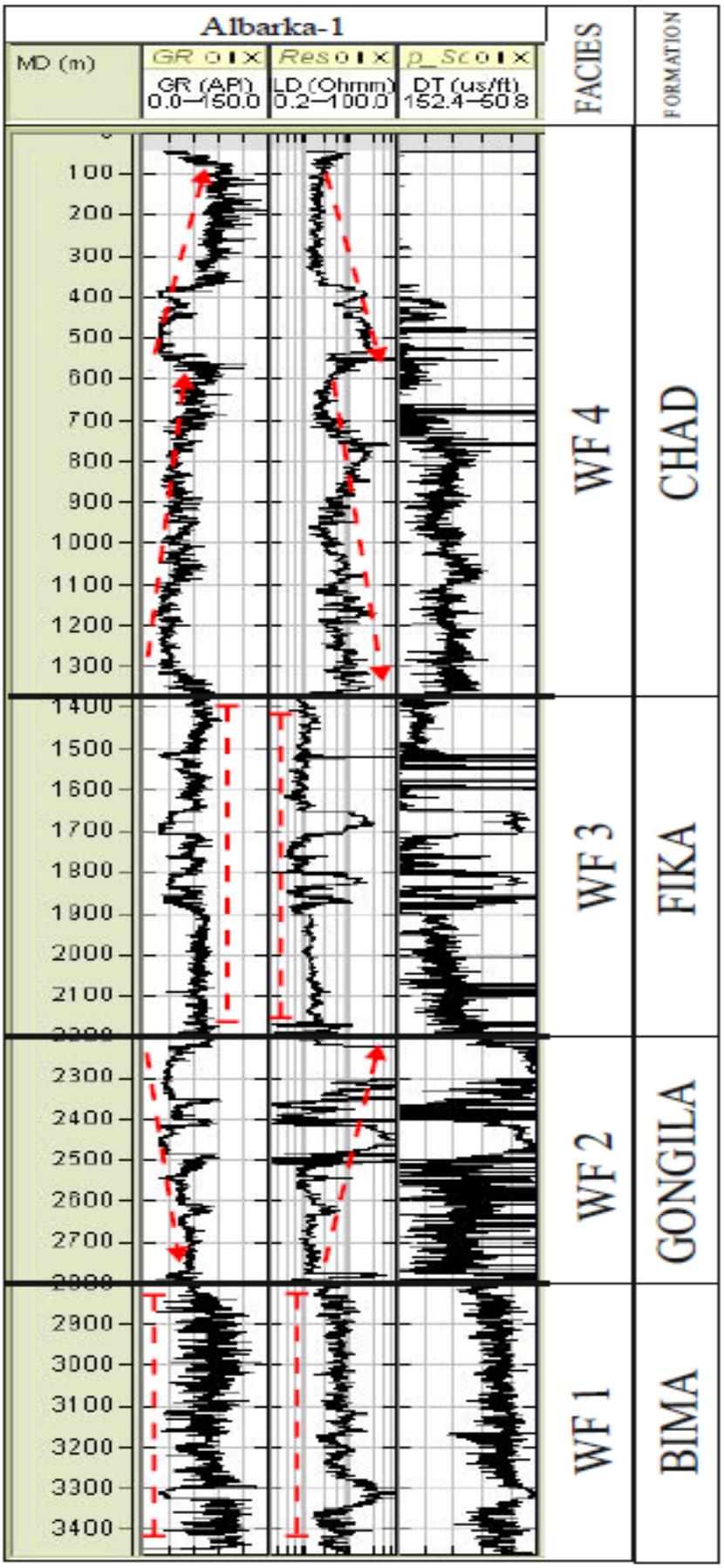

Fig. 5.6: Typical combined well log interpretation in Albarka_1 well used to delineate subsurface stratigraphy from mirrored gamma ray, resistivity and sonic log. Rest of the well log data interpretation is contained in Appendix.B

5.3.2 Well Log Facies 1 (WF1): Bima Formation

WF1 is the basal facies, which displayed characteristic blocky-shaped GR and resistivity curves pair largely having both GR and resistivity values vertically unchanging indicating uniform lithology and lack of overall facies change. This general trend is also observed in the corresponding bulk density and sonic logs. GR API values are generally low, resistivity values are generally high, bulk density values are high and p-sonic velocity values are low indicating sandy unit as the deepest rock formation penetrated by any of the wells. Cross section analysis of the N-S and E-W axes indicate WF1 as the oldest sedimentary unit in the study area with overall thickness ranging from 300 m in Wadi_1 (WAD) well (Fig. 5.5) to 1600 m in Kadaru_1 (KAD) well (Figure 5.4). The maximum depth of the WF1 recorded in the study area is 5000 m from (KAD) Kadaru_1 well, which represent the deepest level drilled in the Bornu Basin. Characteristics of WF1 are consistent with the literature description of the basal facies in the basin and are herein interpreted as the basal Bima Formation, which is the oldest formation in the Bornu basin deposited over the basement rocks. Bima Formation consists of sandstone with even degree of grain size and sediment sorting indicative of a continental depositional environment. The uniform lithology and constant overall facies character indicate an aggradational sedimentary stacking pattern (Appendix B).

.

5.3.3 Well Log Facies 2 (WF2): Gongila Formation

WF2 unit directly overlies the WF1 and it displayed characteristic overall funnel-shape in combined GR and resistivity curves pair often with repeated alternating block intervals of GR and resistivity spikes. Similar distinguishing trend was observed in the bulk density and sonic logs indicating alternating shale - sandstone facies sequence. Cross section analysis of the N-S and E-W axes in the area indicated that this layer overlies the Bima Formation with thickness ranging from 200 m in Bulte_1 (BUT) well (Fig. 5.4) to 1621 m in Kinasar_1 (KIN) well (Fig. 5.5). Characteristics of WF2 are consistent with the literature description of the overlying formation is interpreted as the Gongila Formation. The WF2 curves patterns indicate progressive coarsening upward succession representing progradational regressive sedimentation in transitional lacustrine depositional environment.

5.3.4 Well Log Facies 3 (WF3): Fika Formation

WF3 directly overlies the Gongila Formation and displayed characteristic curve pattern similar to WF1 except for higher GR values with corresponding lower resistivity values, lower density values and higher p-sonic velocity values indicative of uniform shale layer. Cross section analysis of the N-S and E-W axes indicate that the WF3 layer ranges in thickness from 255 m in Kasade_1 (KAS) (Fig. 5.4) well to 1349 m in Ngornorth_1 (NGN) well (Fig. 5.5). Characteristics of WF3 are consistent with the literature description of the overlying formation represents the mudrock facies unit interpreted as the Fika Shale, which consists of predominantly shale. The characteristic blocky shape indicates aggradational sedimentary stacking pattern probably in a transitional lacustrine depositional environment.

5.3.5 Well Log Facies 4 (WF4): Chad Formation

The WF4 unit is the uppermost facies overlying the WF3 displaying characteristic overall bell-shaped GR and resistivity curves pair having GR values increasing upward and resistivity values decreasing upward. Similar patterns were repeated in the corresponding bulk density log and sonic log indicating sequence of sand and clay interbeds. WF4 is interpreted as the Chad Formation, which is consistent with the literature description of the topmost formation in the basin (Table 2.1). Cross section analysis of the N-S and E-W axes indicate the Pleistocene-Pliocene Chad Formation ranges in thickness from 658 m in Ngornorth_1 (NGN) well to 1711 m in Ziye_1 (ZY) well representing the thickest formation in the basin (Fig. 5.5). The combined well log curve pattern indicates a retrogradational and landward movement of shorelines and an overall fining upward succession typical of fluvial and lacustrine depositional environments.

Table 5.1. Litho-stratigraphy of the north-eastern Bornu Basin proposed herein from combined well log and seismic interpretation

Period	Formation	Maximum thickness from well log data (m)	Maximum Depth from well log data (m)	Well log facies lithology	Sediment stacking pattern	Environment of deposition
Quaternary	Chad	1711	1711	Mixed sand and clay (shale) sequence	Retrogradational	Fluvial/ Lacustrine
Senonian	Fika	1349	3180	Shaly	Aggradational	Lacustrine
Turonian	Gongila	1621	3800	Alternating shaly and sandy sequence	Progradational	Lacustrine
Cenomanian	Bima	1600	5000	Sandy	Aggradational	Continental

5.3.6 Well log - seismic correlation

The Two-Way-Times (TWTs) calculated for the sonic log blocked intervals A through E in milliseconds became directly comparable with the seismic data having similar unit. Grey scale colour was selected for the seismic section and contrast adjustment was performed to enhance reflection pattern recognition of the seismic section. Distinctive patterns of prominent seismic reflections on the seismic section with stronger amplitude and reflection continuity around the well location were delineated. On the seismic section Line_13 (Fig. 5.8) six reflection markers 1 through 6 were marked with increasing reflection time. Table (5.2) shows calculated TWTs of the blocked interval boundaries on the depth-processed sonic log, which correlate with

the measured TWTs between corresponding seismic reflections markers on the time-processed seismic data shown in Table (5.3).

For example, the calculated TWT for interval A on the sonic log, which closely compared with the TWT at reflection marker 1 on the seismic data, represented a possible unconformity within the Chad Formation as the top of the formation was not clearly displayed on the sonic log. Close correlation exists between the 272 ms calculated TWT at the sonic boundary interval A with the measured 275 ms TWT between reflections 1 and 2 on the seismic section. Moreover, the calculated 112 ms TWT at interval boundary B closely agrees with the 110 ms TWTs measured between seismic markers 2 to 3 and correlate with the base of the uppermost Chad Formation The calculated TWT for all the blocked interval boundaries on the sonic log correlate with the measured TWT between their corresponding seismic reflection markers.

Table 5.2. Blocked Kasade_01 (KAS) well sonic log data analysis, showing closely matched calculated values with those extracted on the corresponding seismic line_13 in Table 5.3.

Interval Boundary	**Sonic log Depth (m)**	**Interval Thickness (m)**	**Measured Sonic velocity Interval Transit Time (ITT) (µs/ft)**	**Calculated sonic velocity at interval boundary Two-Way-Time (TWT) (ms)**
A	600	256	162	**272**
B	856	119	144	**112**
C	975	181	151	**179**
D	1156	119	122	**95**
E	1275	150	136	**134**
Base E	1425	-	-	**-**

Table 5.3. Time, depth and interval velocity data analysis of Line_13 seismic

Seismic reflection marker	**Direct observed seismic velocity Two-Way-Time (TWT) (ms)**	**Seismic reflection markers interval and correlated sonic interval boundary**	**Interval velocity at seismic reflection marker boundary Two-Way-Time (TWT) (ms)**
1	544	0 - 1	544
2	819	1 – 2 (A)	**275**
3	929	2 – 3 (B)	**110**
4	1105	3 – 4 (C)	**176**
5	1198	4 – 5 (D)	**93**
6	1338	5 – 6 (E)	140

The correlation of corresponding TWTs provides the potential for mapping the stratigraphic horizons around the vicinity of the well on the seismic line and thus validating the boundaries of stratigraphic facies identified from the combined well log data analysis in Appendix B. The correlation further illustrates the potential for extending the continuous stratigraphic horizons across adjoining interconnected seismic lines, which do not directly intersect other well positions in the area. Figures (5.7 and 5.8) show the stratigraphy of the area interpreted from the intersecting seismic Line_13.

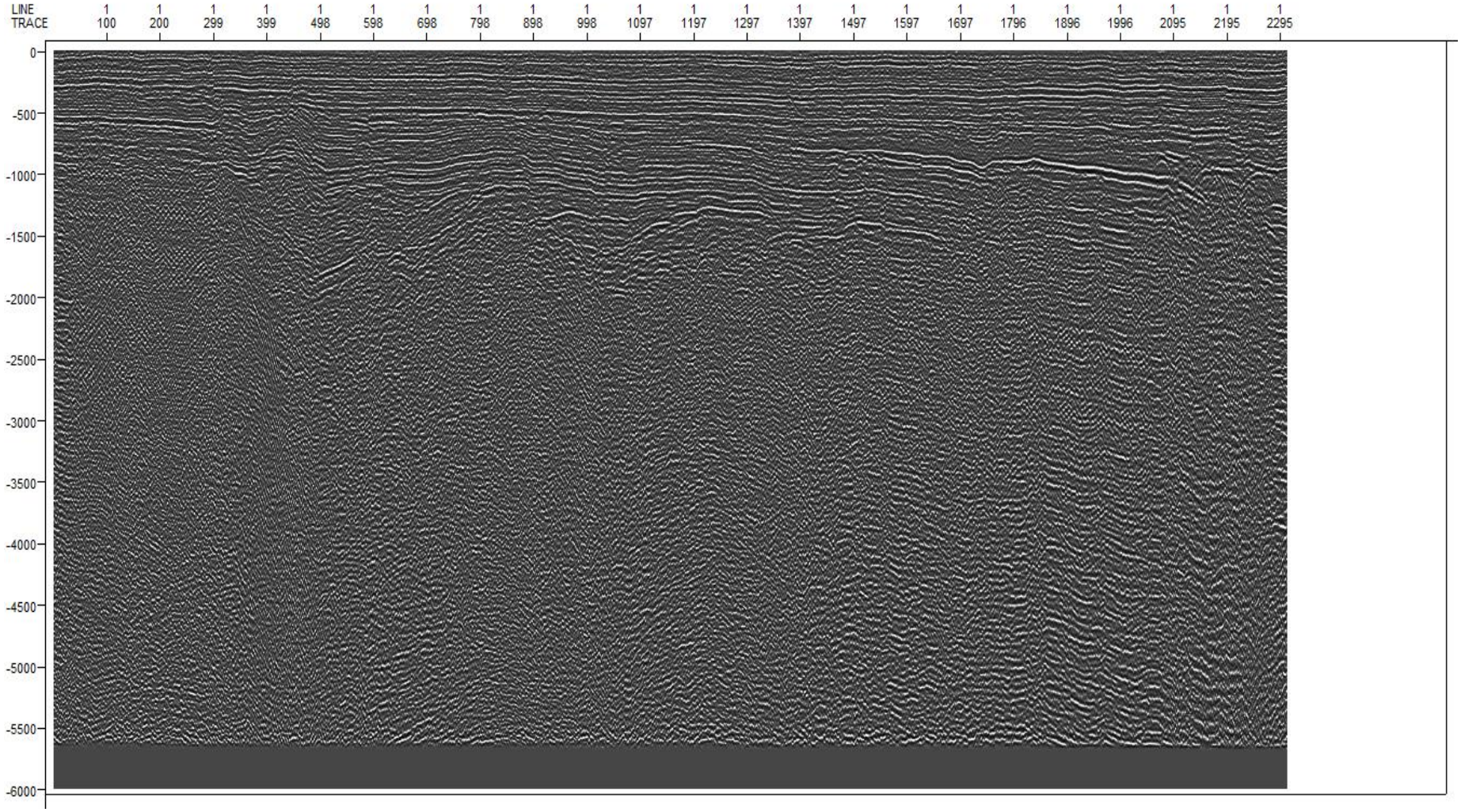

Fig 5.7: Uninterpreted greyscale seismic line 13 used for the seismic – well toe to validate the stratigraphic analysis.

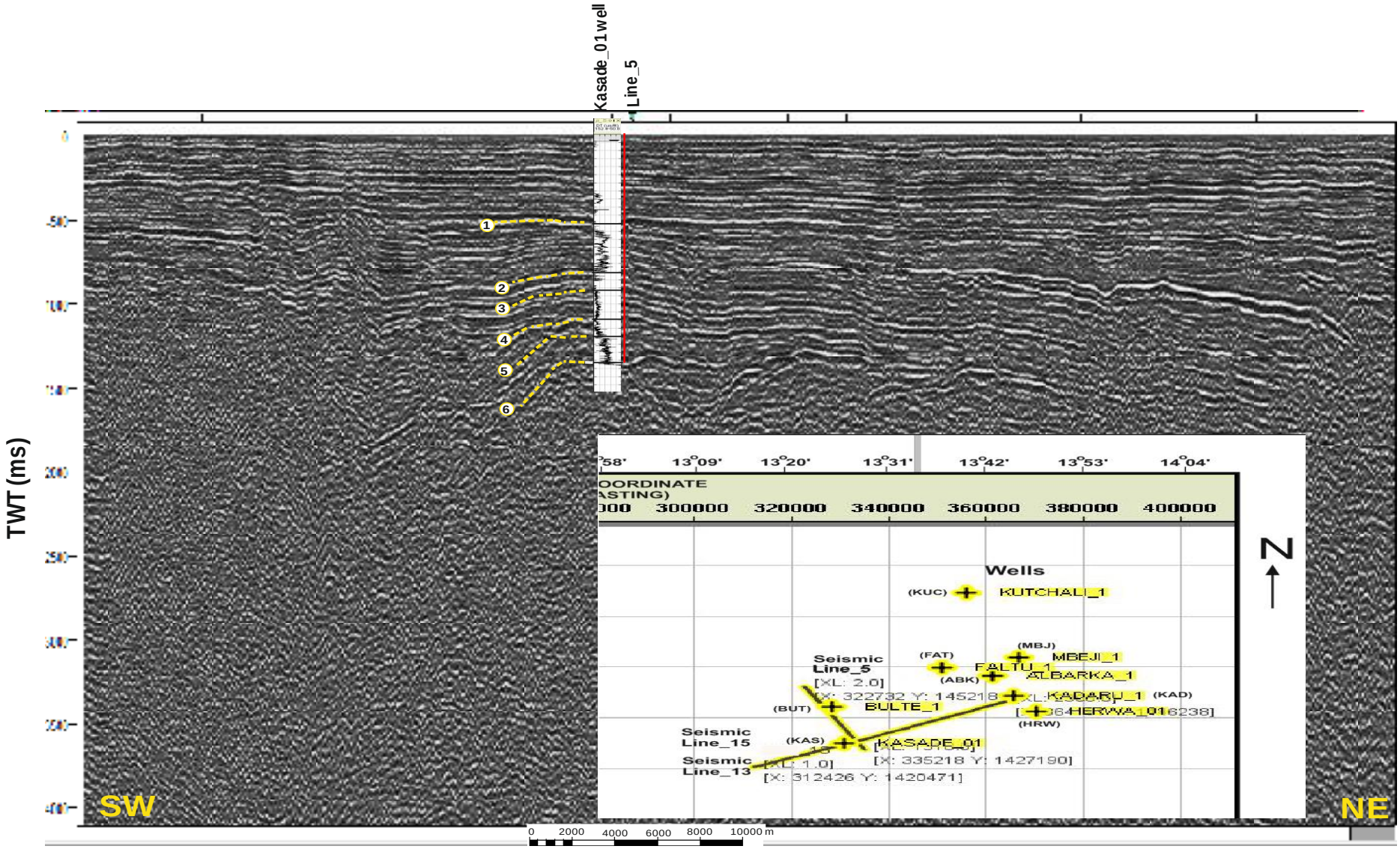

Figure 5.8. Final correlation of blocked sonic log intervals A – E for Kasade_01 (KAS) well to reflections 1 - 6 on the intersecting seismic line_13 shown on Figure 5.1 (inset figure is part of Fig 5.1) to show intersection between KAS well and seismic Line 13.

5.4 Seismic stratigraphy and structure

The seismic stratigraphic analysis was in close agreement with the combined well log analysis. High coherence of reflectors exist in the seismic data, which allowed smooth auto tracking of horizons except where the horizons of interest were tracked along specific weak amplitude peaks or troughs in the seismic section. Correlation of the sonic log interval boundaries with their corresponding seismic reflection markers allowed for the identification of stratigraphic horizons separating the formations delineated. Structural and stratigraphic interpretation of the NE-SW oriented seismic reflection sections Line_13 (Fig. 5.8) and its perpendicular NW-SE oriented intersecting seismic Line_5 (Figs. 5.11 and 5.12) confirmed the four seismic stratigraphic horizons representing the bases of Bima Formation, Gongila Formation, Fika Formation and Chad Formation respectively. The position of correlated Kasade_01 (KAS) well as indicated on the interpreted seismic section (Fig. 5.10) revealed that the well was bottomed at the top of a subsurface horst feature, which confirmed findings from N-S well logs cross section interpretation in (Fig. 5.4) and (Fig. 5.5).

The Cretaceous basin morphology on seismic consist of faults, which form half-graben and graben-and-horst architecture made up of several high angle normal faults affecting mainly the basal units. The basement topography reflected the Cretaceous tectonic and rift evolution of the basin, which controlled the deposition of the basal facies. Relatively shallower depths in the south-western and north-eastern parts exist between a much deeper basin depocenter. Base of the Aptian – Albian is delineated by sub-parallel attenuated weak – moderate amplitude reflector of the basal Bima Formation deposited within the grabens or faulted troughs separated by horsts, which controlled the facies distribution in the Bima, Gongila and Fika Formations.

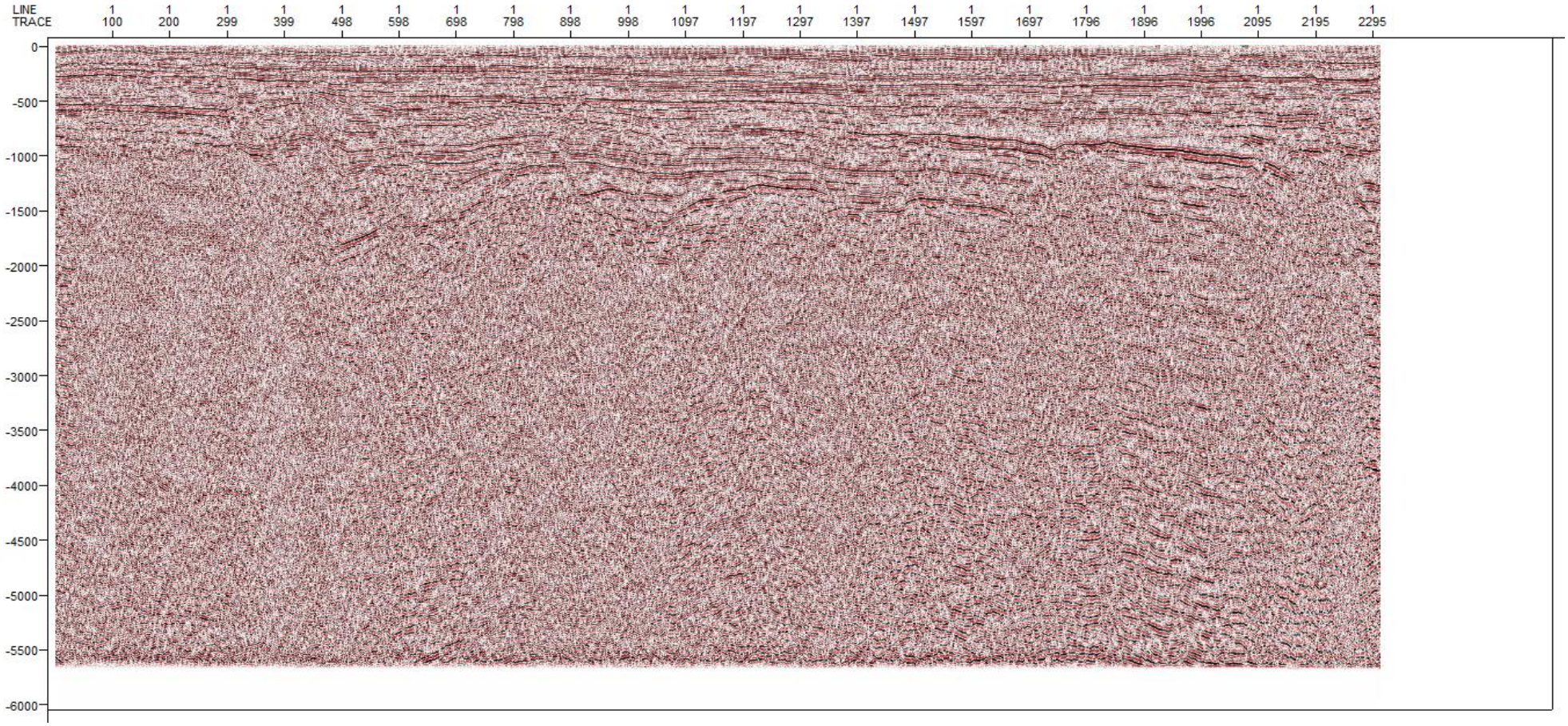

Fig 5.9: Uninterpreted multi-coloured seismic line 13.

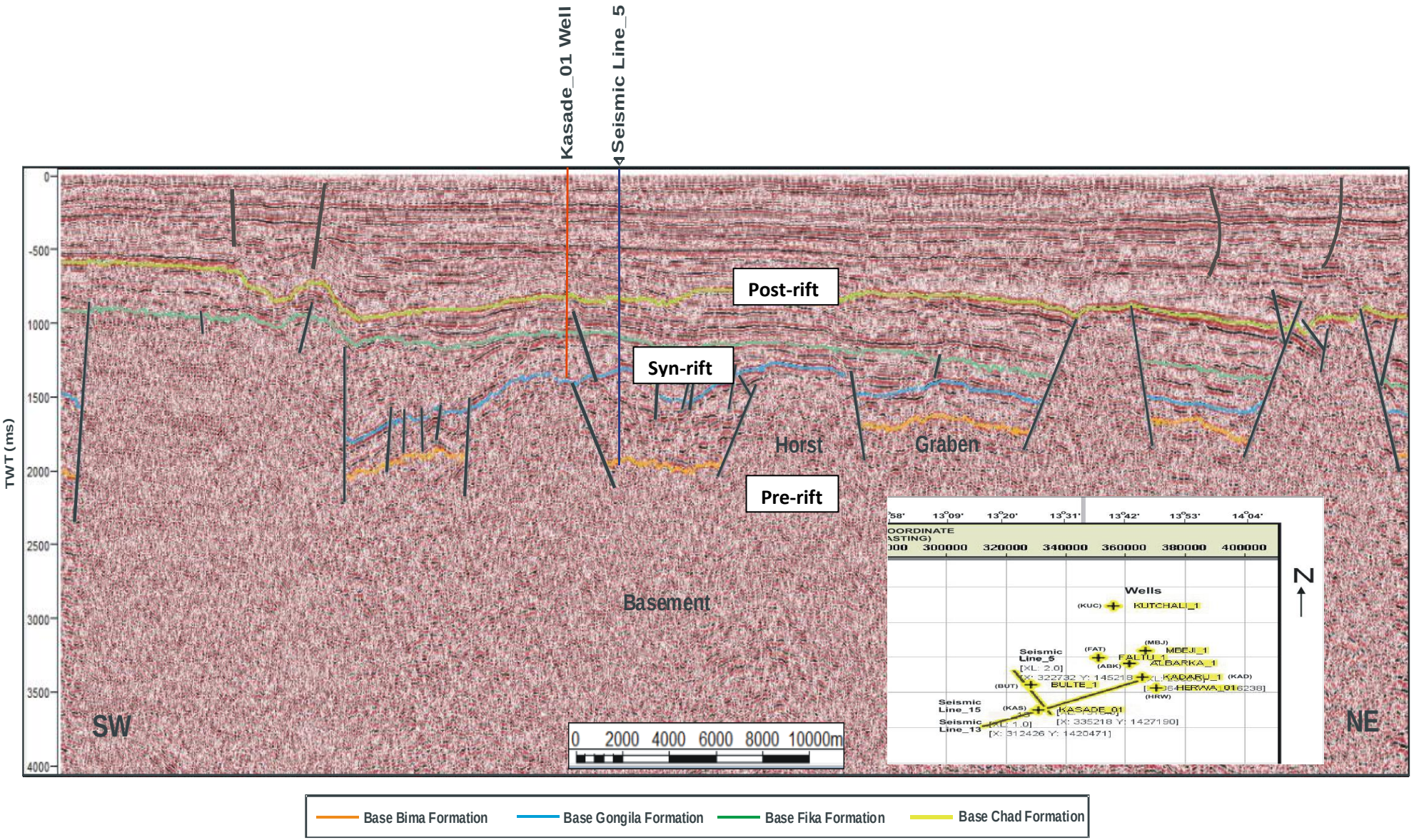

Figure 5.10. Interpreted NE-SW oriented seismic Line_13 showing stratigraphic horizons correlated from the well logs. Subsurface basin structure indicating horst and graben features with Kasade_01 (KAS) well bottomed on horst and basal facies infilled within grabens. (Inset figure is part of Fig 5.1) section showing preserved extensional geometry

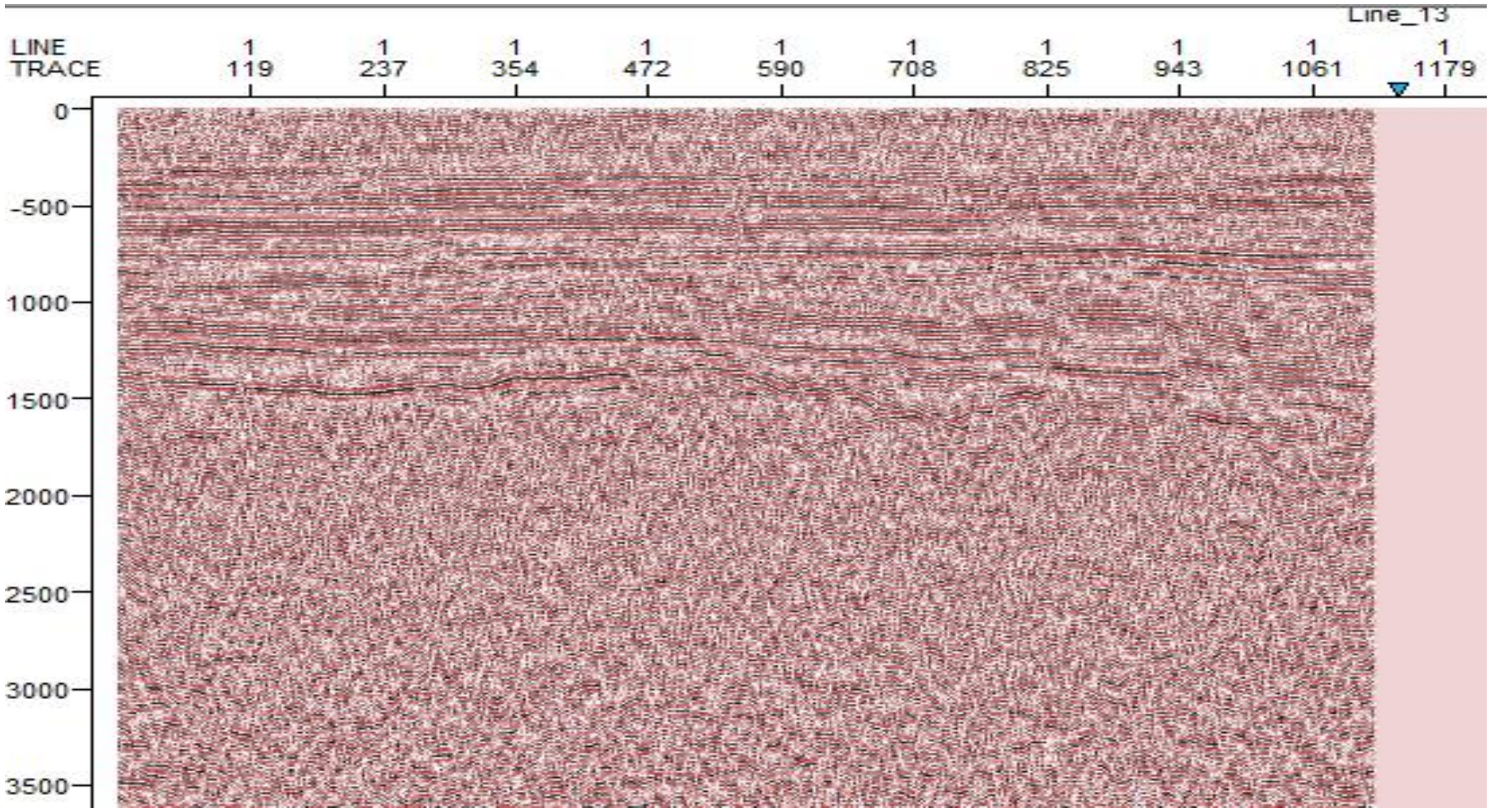

Fig 5.11: Uninterpreted seismic line_5. Note the position of intersection of the seismic line_13 on the right

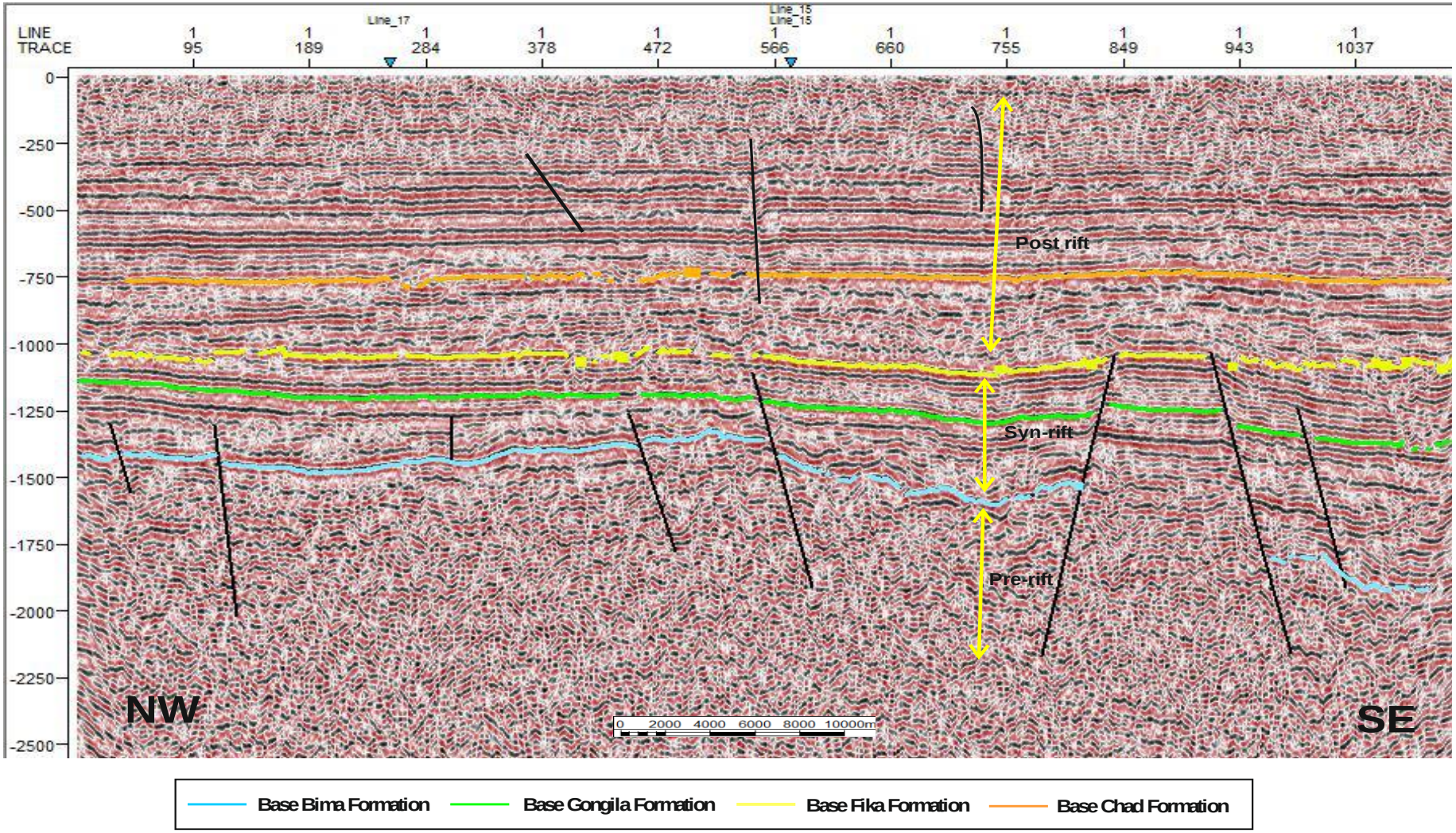

Fig 5.12: interpreted seismic line_5 showing stratigraphy and structures. Top of the seismic horizon is noisy and poorly processed to enable mapping of structures in the upper position. NW–SE oriented seismic Line_5, which perpendicular bisects seismic Line_13 as shown in Figure 5.10. Relative positions of the mapped seismic stratigraphic horizons from intersecting seismic line_13 are shown.

The base of Bima Formation terminated discordantly at the bottom flanks of the basement while having a concordant depositional relationship with the overlying seismic facies units. Internal seismic facies in Bima Formation is characterised by weak uneven amplitude reflectors distributed within the grabens. The overlying base of the Gongila Formation is characterised by sub-parallel to parallel configurations of stronger seismic reflectors marking the top of deeper horst faults mostly developed in the deeper basin depocenter and truncated at the lower flanks of the shallower horst faults**.** The seismic reflector representing the base of Fika Formation is characterised by strong and uneven configuration best developed in the south-western part of the area where it is folded and marked the top of the main shallow horst feature mapped in the seismic section. However, the Fika Formation was truncated at the middle of the horst and graben fault flanks in the north-eastern sector of the area (Fig. 5.10).

Concordant relationship exists between the Fika Formation and the strongest seismic reflectors, which characterised the overlying Chad Formation has continuous parallel amplitude reflections representing base of the Chad Formation. The characteristic strong seismic reflection is best developed in the north-eastern sector of the area where it marked the thickest seismic facies towards the Lake Chad as shown in Figure (5.10). Medium and small scale observations within the Chad Formation indicate potential sequences and parasequences as represented by strong and continuous reflections across the entire area. The seismic analysis shows that the top portion of the Chad Formation is relatively unaffected with faulting and folding in comparison with its base, which appeared folded due to the effect of shallow subsurface horst features.

5.5 Seismic time-structure maps

This section describes the results of further seismic stratigraphic and structural mapping in the north eastern Bornu basin. The seismic structural interpretation in the previous section is used towards the development of time structural maps of the subsurface from the two dimensional arrival times of the reflected seismic waves. Time structure maps are commonly used to study the subsurface structures from interpreted seismic sections. The seismic data location map Fig (5.13) shows the seismic lines used to produce the time-structure maps using Petrel software. Seismic time structure maps herein are produced based on six interpreted seismic sections (Figs 5.13) including the seismic - well log correlation, which analysed the stratigraphy for the north eastern Bornu basin already established in Isyaku et al., (2016).

Time-structure maps of the four stratigraphic formations consisting of the Bima, Gongila, Fika and Chad formations were used to highlight the chronological variations in stratigraphy and sediment accommodation related to the Cretaceous rift tectonics that affected the basin. Well log stratigraphy (Figs. 5.4 and 5.5) were used for the wells adjoining the seismic lines to constrain the stratigraphic units and to validate the stratigraphic variations observed on the time-structure and isochron maps. The interpreted seismic horizon units were correlated with the Kasade (KAS) well that intercepted the seismic line_13 and extended throughout the adjoining seismic sections. Thus, the seismic time-structure maps are constrained by the four formations and the faults mapped in interpreted seismic lines 5, 7, 8, 13, 14 and 15. The time-structure map analysis is also constrained by the lack of well data intersecting the rest of the seismic lines (Figs. 5.13 and 5.14). Individual horizons representing tops of the formations including the mapped seismic faults in the north-eastern Bornu basin are marked on the time seismic sections and posted on the seismic base map.

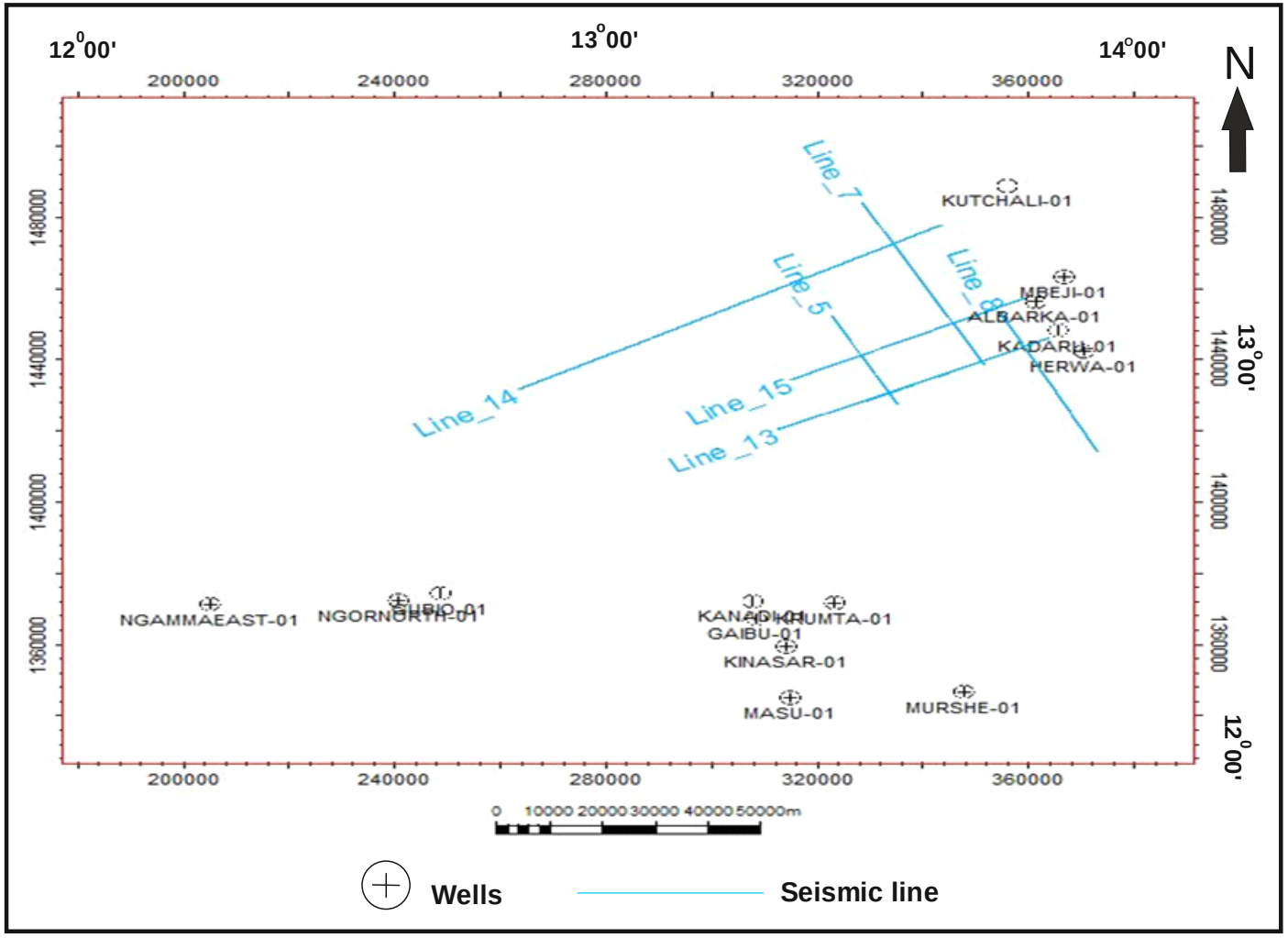

Fig 5.13: Layout of the well locations and those of the six seismic lines used to constrain the seismic time structure maps plotted using Petrel software.

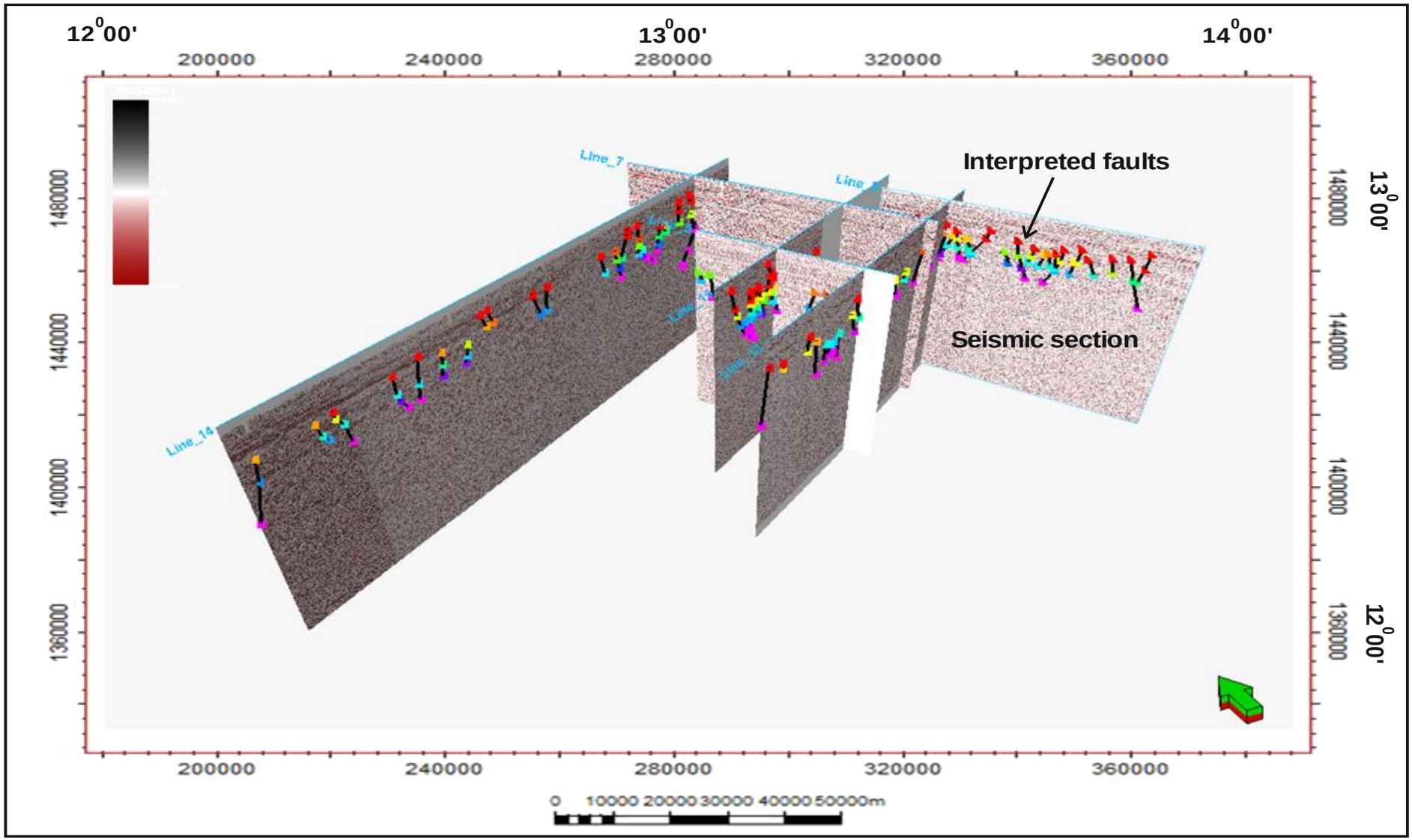

Fig. 5.14: The 6 seismic lines plotted in 3D window in Petrel software with the interpreted faults and stratigraphic horizons used in constraining the seismic time structure maps herein.

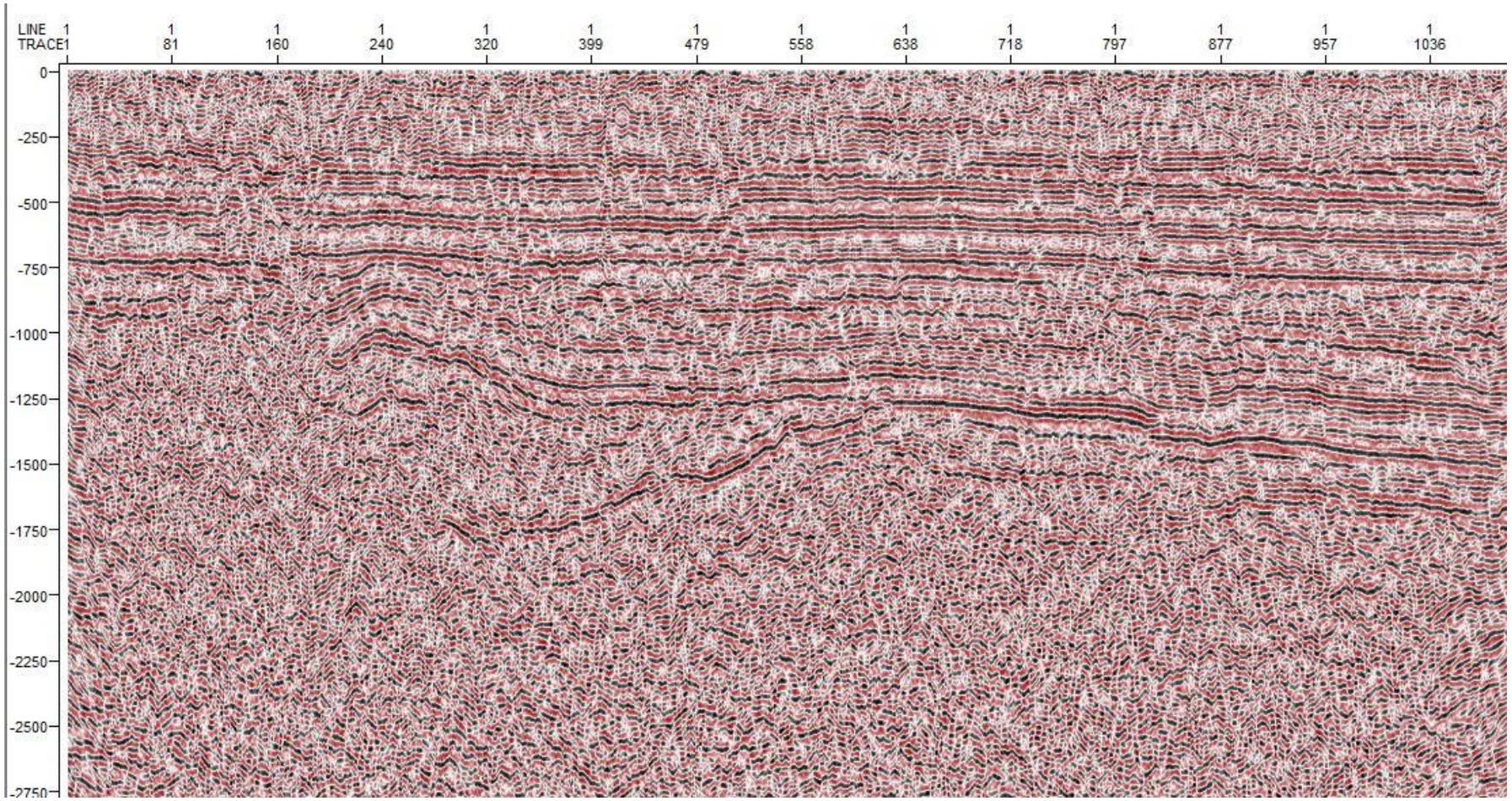

.

Figure 5.15: Uninterpreted Seismic Line 15.

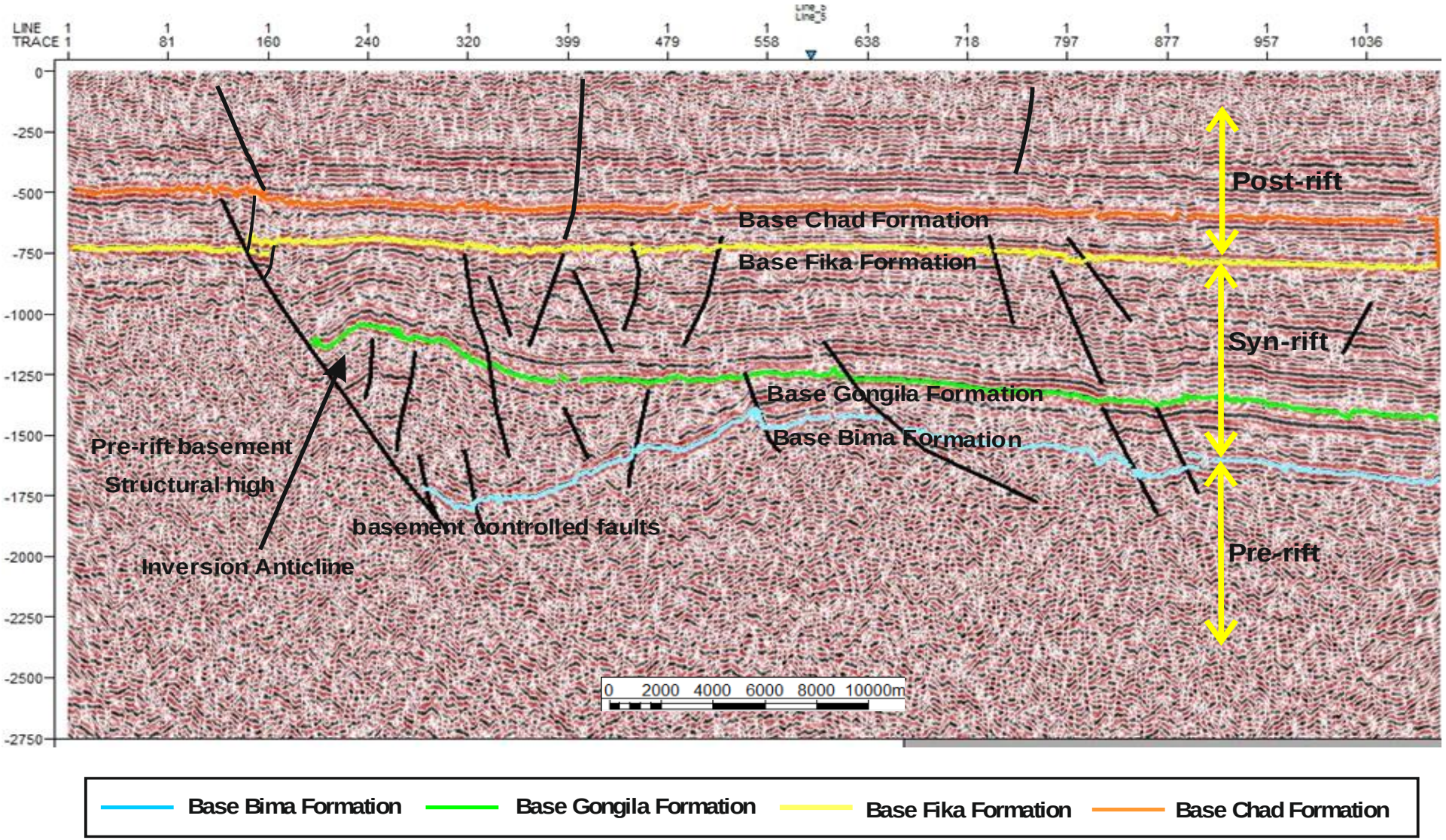

Fig 5.16: Interpreted seismic line 15 showing the structure and stratigraphy from pre-rift to post rift sedimentation. The main down-to-the-basin faults tending listric with depth and forming numerous synthetic and antithetic faults are indicated. Seismic section shows a “classic” rift geometry with simple extensional rollover anticlinal structure. Even where obvious, the compressional overprint is generally subtle compared to the extensional fault geometry,

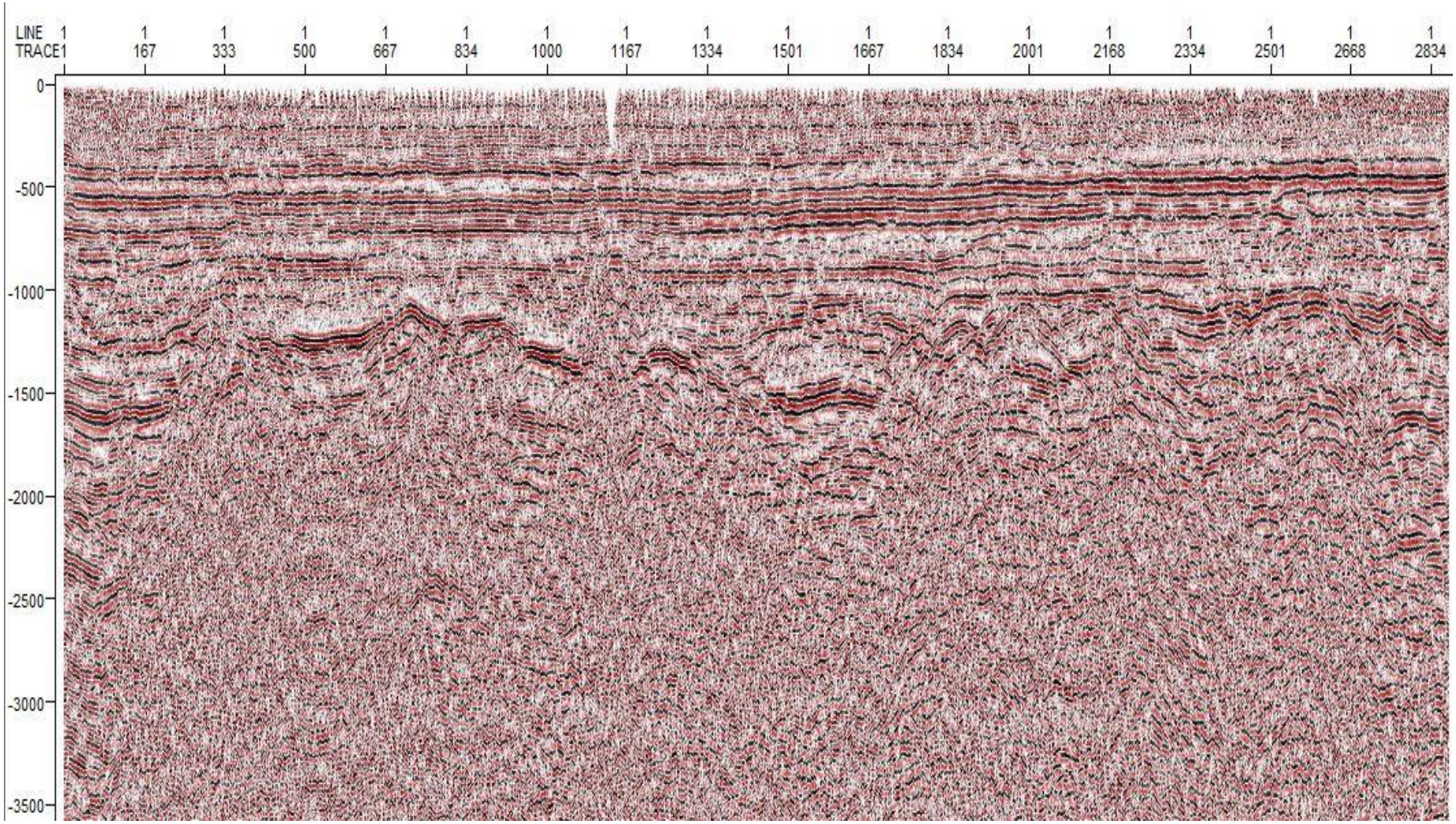

Fig 5.17: Uninterpreted seismic line 8

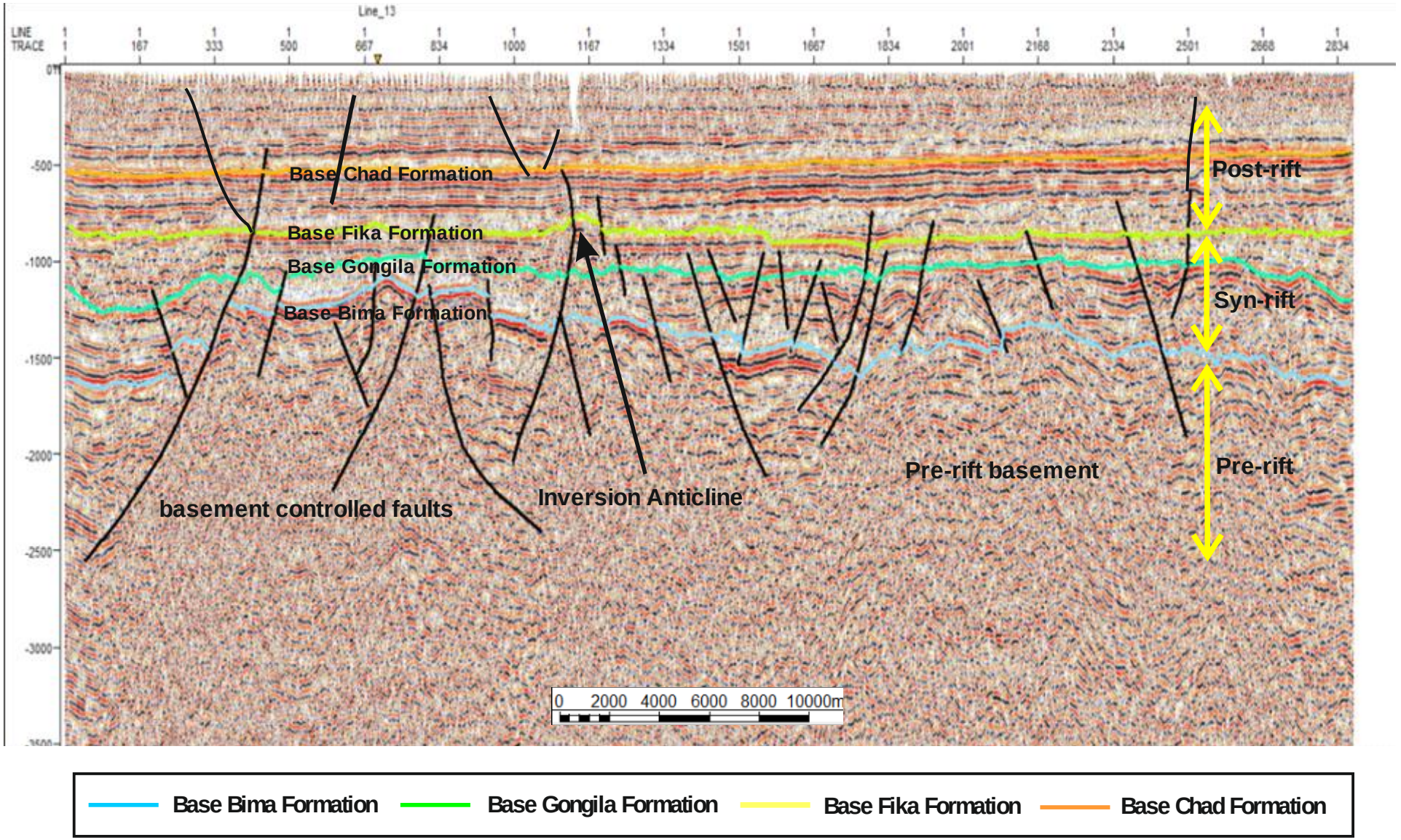

Fig 5.18: Interpreted seismic line 8 showing the structure and stratigraphy from pre-rift to post rift sedimentation. The main down-to-the-basin faults tending listric with depth and forming numerous synthetic and antithetic faults are indicated.

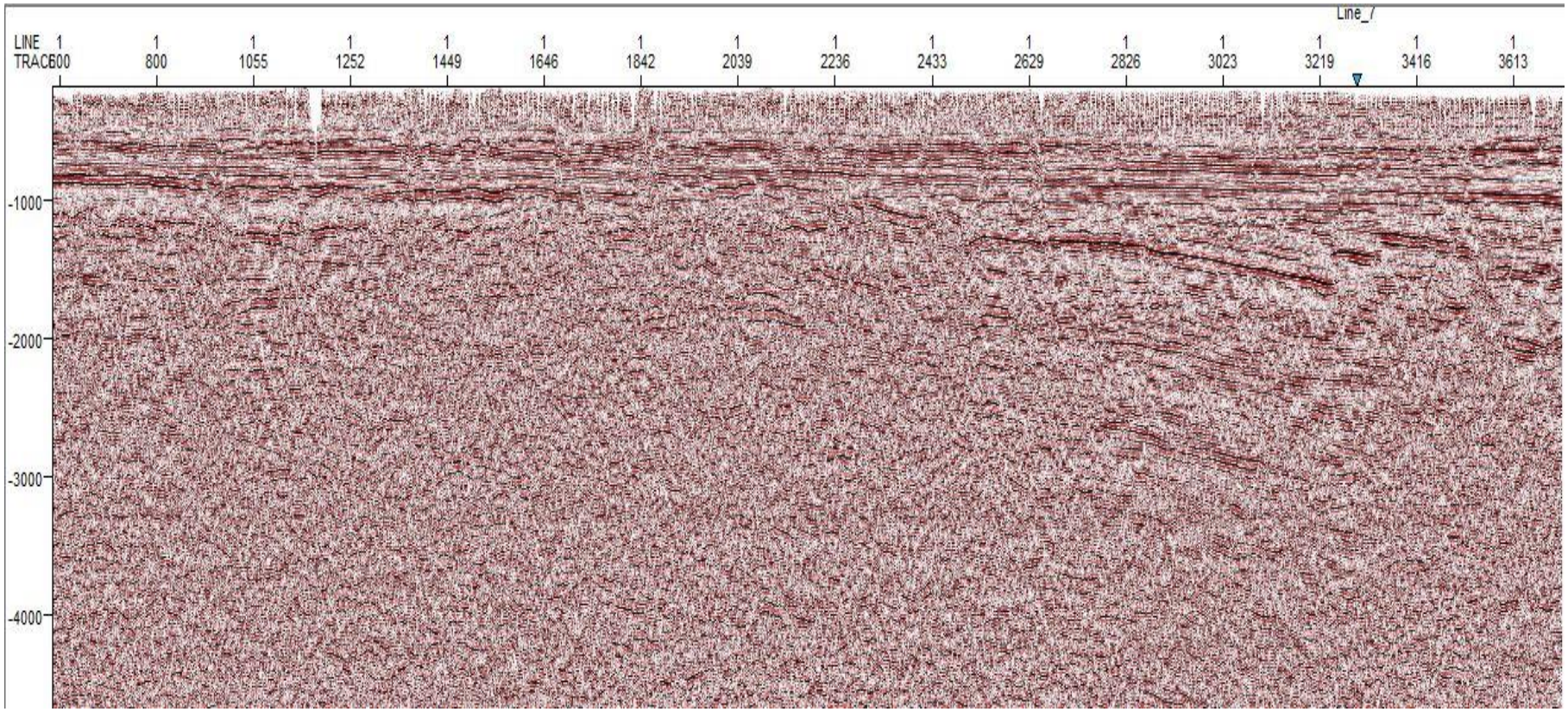

Fig. 5.19: Uninterpreted seismic line 1

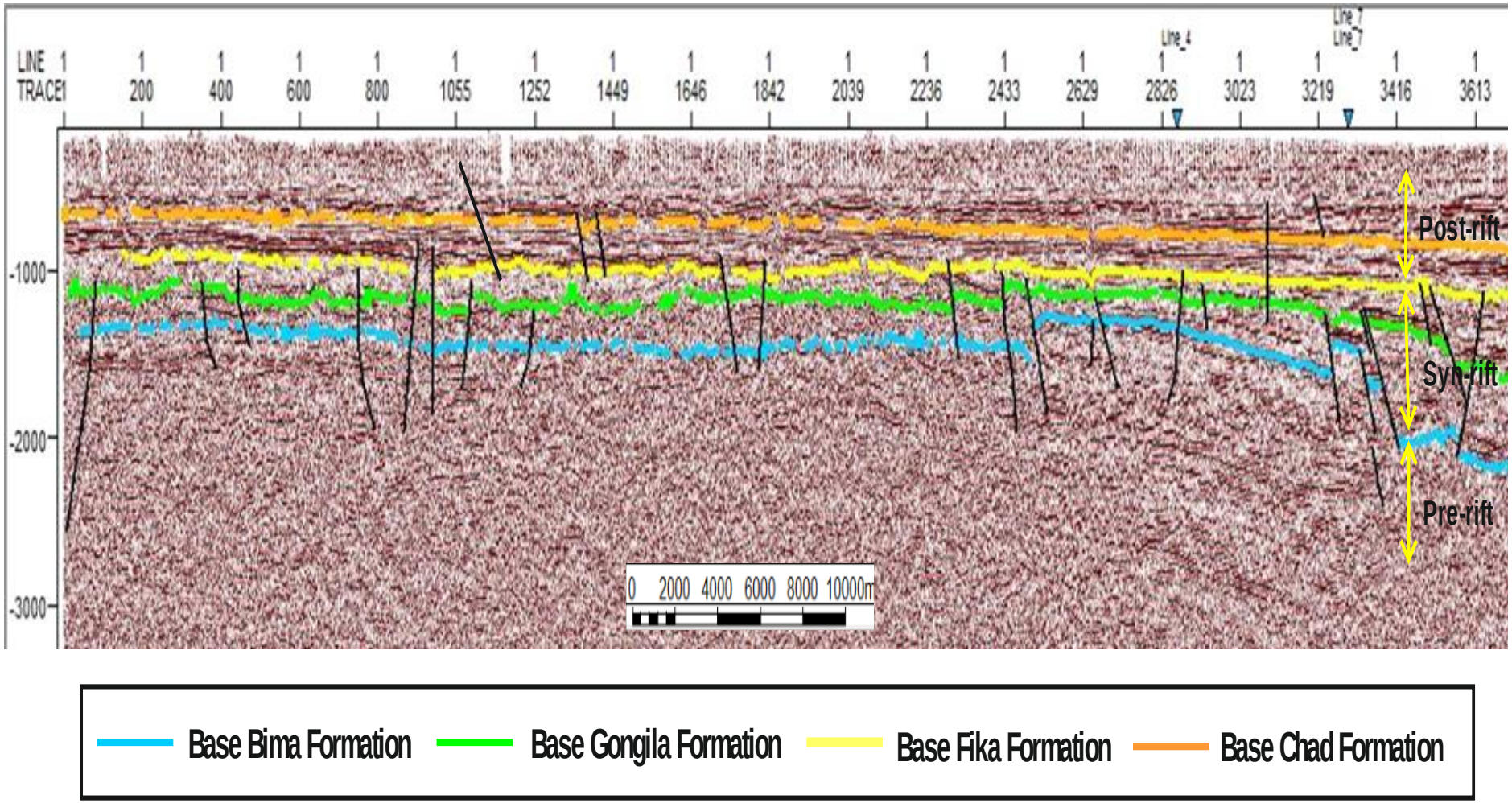

Fig. 5.20: Interpreted seismic line 14 showing seismic structure and stratigraphy. Poor processing and noise at the top horizons hinders resolution of faults

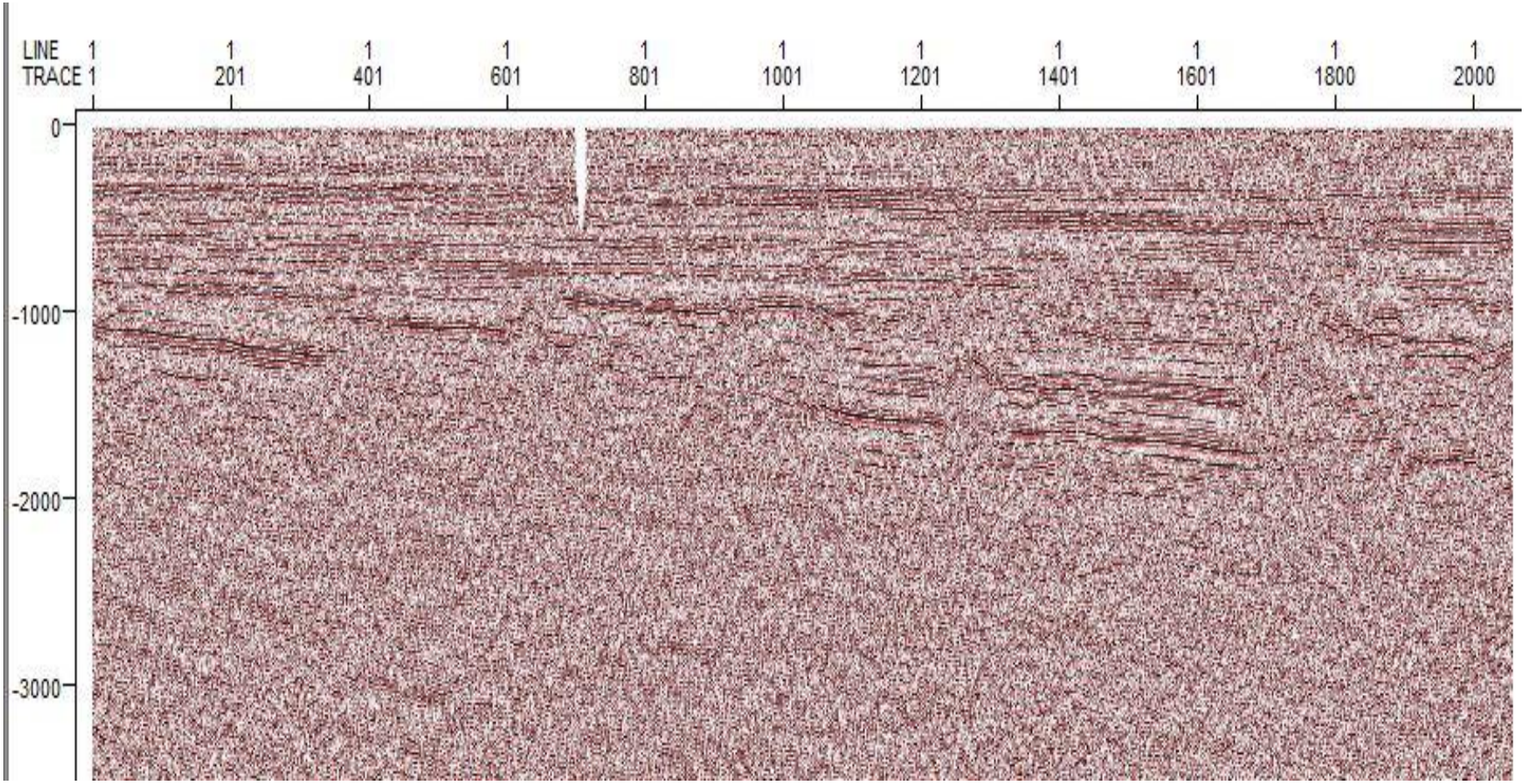

Fig. 5.21: Uninterpreted seismic line 7

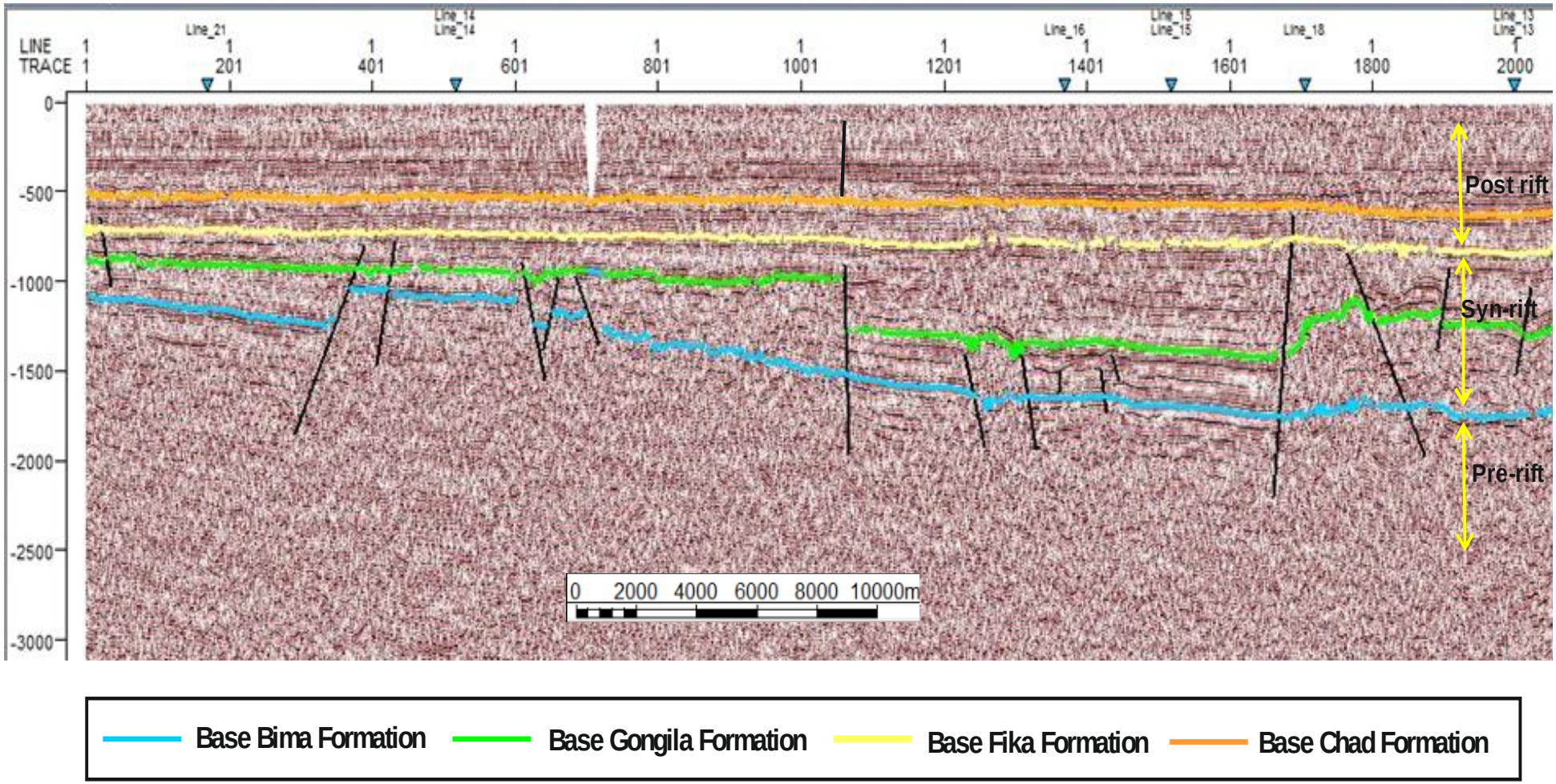

Fig. 5.22: Interpreted seismic line 7 showing seismic structure and stratigraphy

Seismic survey check shot data is not available for this research; as such, depths to the horizons plotted on the time structure maps are not presented since the time-structure maps were not converted to depth maps.

Arrival times of the seismic reflection directly below the shot number or the shot points are automatically used for constructing the contour maps using *Petrel software* by spatially plotting the points of equal arrival times. Contour closures are identified and interpreted to determine the shape of the subsurface structures. Results of the stratigraphic mapping as well as structural interpretations, which show the faults, structural styles and fault geometry, were used in the time structure maps for each formation. The subsequent interpretation of the time-structure maps help to deduce sedimentation including spatial distribution of potential source rock areas and sediment supply points. Red-yellow colours indicate lower TWT values, which represents the shallower subsurface depths while green-purple colours indicate higher TWT values that represent deeper subsurface depths.

The base of Cenomanian Bima Formation time-structure map in the north-eastern Bornu basin consists of predominantly sandstones. Seismic analysis of the contoured time structure map for this formation indicates that this horizon exhibits anticlinal structure trending NE-SW in the northern part of the map and dipping SE direction where the formation forms in a depocenter. The structure map displays general dipping towards the SE where the time contours steadily increase in SE direction. The time contours show a steady increase towards the SE direction, which characterises dipping bed in a downward closing synformal axis. The Bima Formation time structure map (Fig. 5.23) thus, shows an association of graben and half graben features in an undulating subsurface topography. Broadly, the area can be subdivided into two sub-basins bifurcated by an axial high showing a 1400 TWT. Three round high contours form closures forming ring contours in the central, south eastern and northern sectors

of the map respectively indicating structurally high area. A closed spaced contour concentration shows existence of a steep slope area. The axial highs are dissected by several bounding faults trending NE-SW and NW-SE.

Turonian Gongila Formation time-structure map shows a much less complex topography within the mapped area. The formation is bifurcated by the graben and axial high. The horizon map represents the topography of the mixed sandstones and shale formation. However, it shows the crest of the anticlinal structure that is located in the NW part of the map trending NNE-SSW and dipping steadily in the south and the east into a depocenter. The crest of the anticline in the central part of the map forms a 4-way structural closure with the time contours closing around it in all the four directions. A fault exists between the axial high and the depocenter southwards, which exerted control on sedimentation within the depocenter. The structurally lowest point in this formation shows a TWT of 1900 while the major structural high occurred at 800 TWT. The main axial high opens out towards the NW where the extent of the data discontinued. In the southern area of the basin, a structural low exist opening out southwards (Fig. 5.24).

Senonian Fika Formation time-structure map shows relatively shallower horizon topography in TWTT, in which the predominantly shale formation is deposited. The horizon map displays a much less complex topography formed in the early post rift stages. Nevertheless, the structural map also shows a main axial anticlinal structure dipping eastwards into a synformal downward closing syncline. Two adjacent low relief contours closing of the same TWT are observed within the deeper areas of the formation indicating occurrences of the depocenters of the same depth in the eastern boundary (Fig. 5.25). Discontinuity of the data constrained the extent of the anticlinal feature in the western part of the map. However, the crest of the anticline shows a potential 1-way structural closure.

Quaternary Chad Formation time-structure map displays the structural high relief blanketing the mapped area with the minor low relief structural area occupying a small portion and confined to the south east boundary of the map. This indicates that the undulating topography of the subsurface inherited from the underlying graben rift features are now covered with the post rift broad topmost horizon. The map shows the infilling of the gentle undulating topography and the isolation of the structural low. It can be seen that structurally high areas do not exist within this broad high. The absence of closely occurring time contours indicates the few occurrence of faults in this horizon. However, a 3-way structural closure is seen towards the crest of the anticline in the southern boundary (Fig 5.26).

The fault propagation scenario is demonstrated herein by the time structure mapping, showing faults from the synrift sequence traced into the post rift sequence.

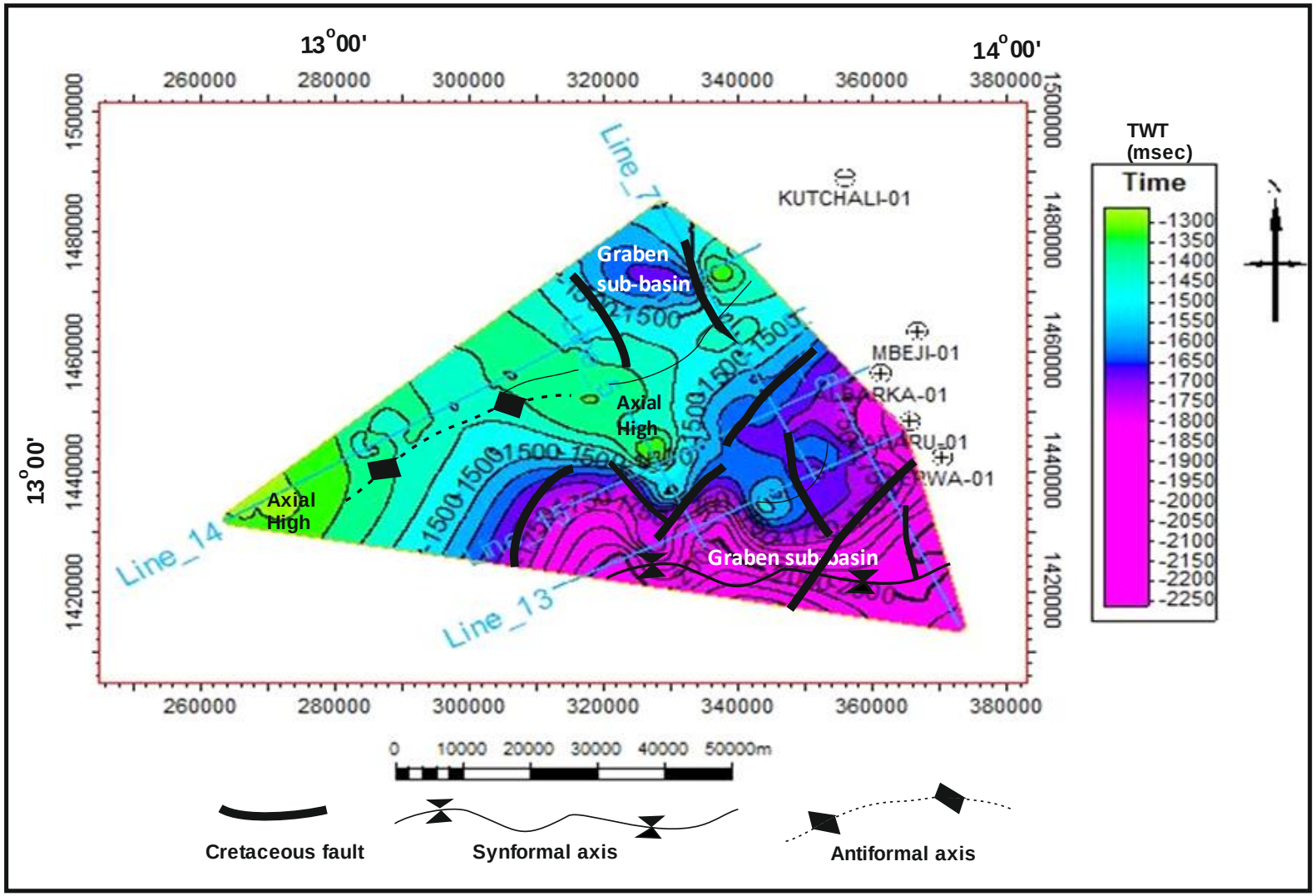

Fig. 5.23: Bima Formation Time-structure map showing more faults occurring in the synrift basal Formation. Due to the constraint on the extent of the seismic data, the faults at the synformal and anticlinal boundaries correlate with the Intrabasinal faults in the gravity and magnetic data showing basement control of the basement propagated faults with the synrift package. Compare this image with the GIS correlated surface and subsurface structural analysis map on Fig. 7.8.

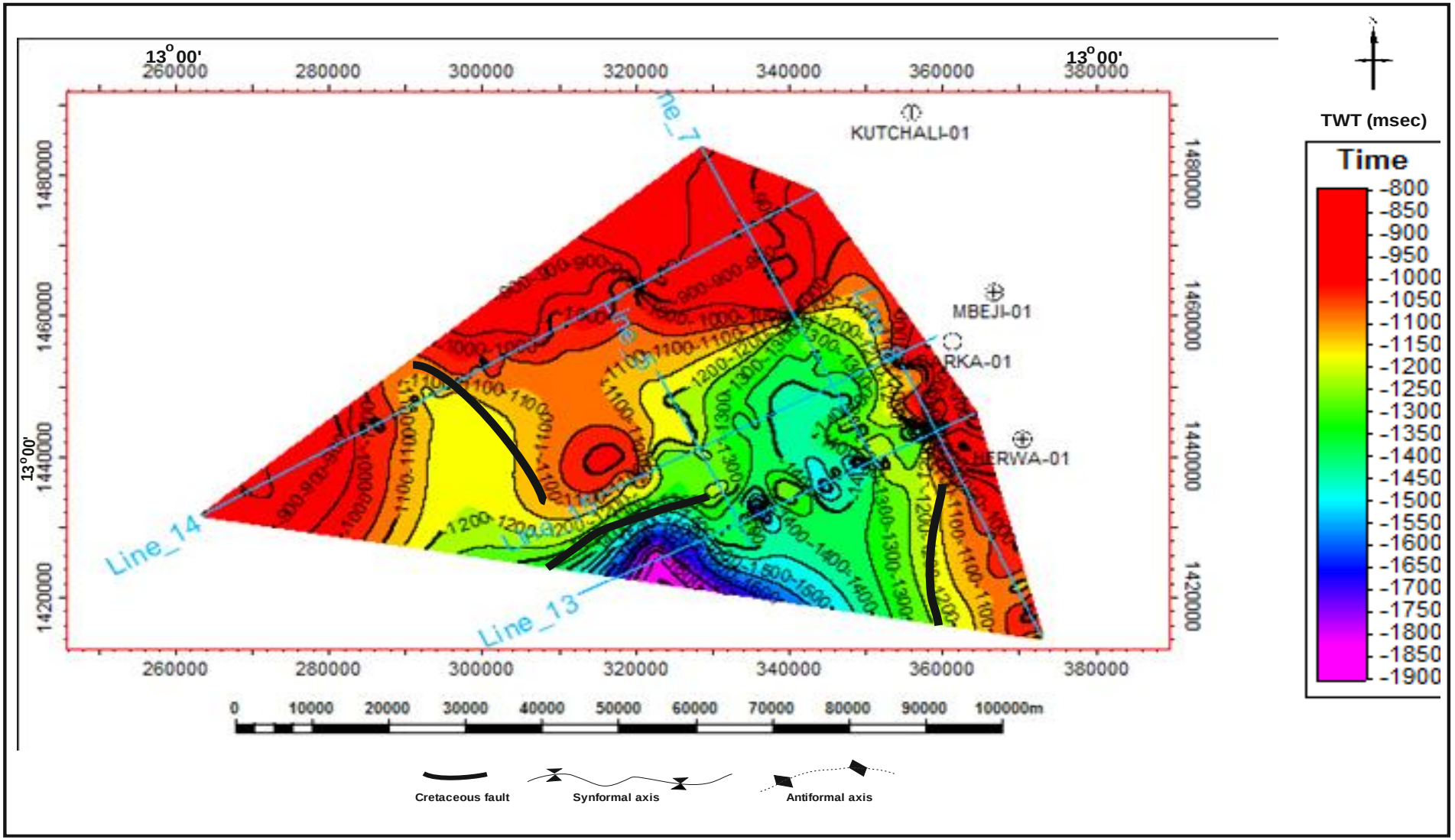

Fig 5.24: Gongila Formation Time-structure map showing fewer faults occurring in the synrift basal Formation. Due to the constraint on the extent of the seismic data, the faults at the synformal and anticlinal boundaries correlate with the Intrabasinal faults in the gravity and magnetic data showing basement control of the basement propagated faults with the synrift package. Compare this image with the GIS correlated surface and subsurface structural analysis map on Fig. 7.9.

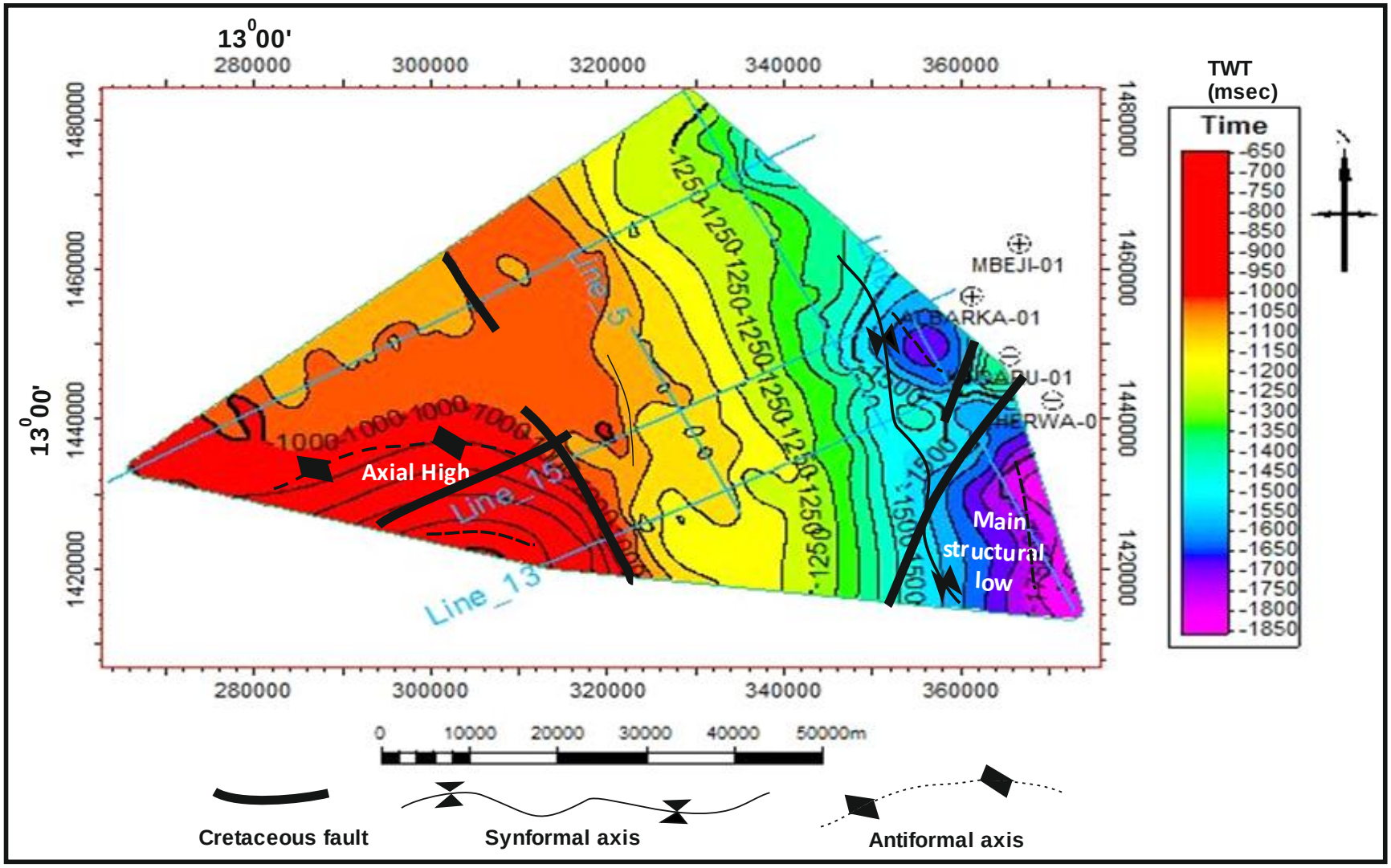

Fig 5.25: Fika Formation Time-structure map showing fewer faults occurring in the post rift Formation. Due to the constraint on the extent of the seismic data, the faults at the synformal and anticlinal boundaries correlate with the Intrabasinal faults in the gravity and magnetic data showing basement control of the basement-propagated faults with the synrift package. Compare this image with the GIS correlated surface and subsurface structural analysis map on Fig. 7.10.

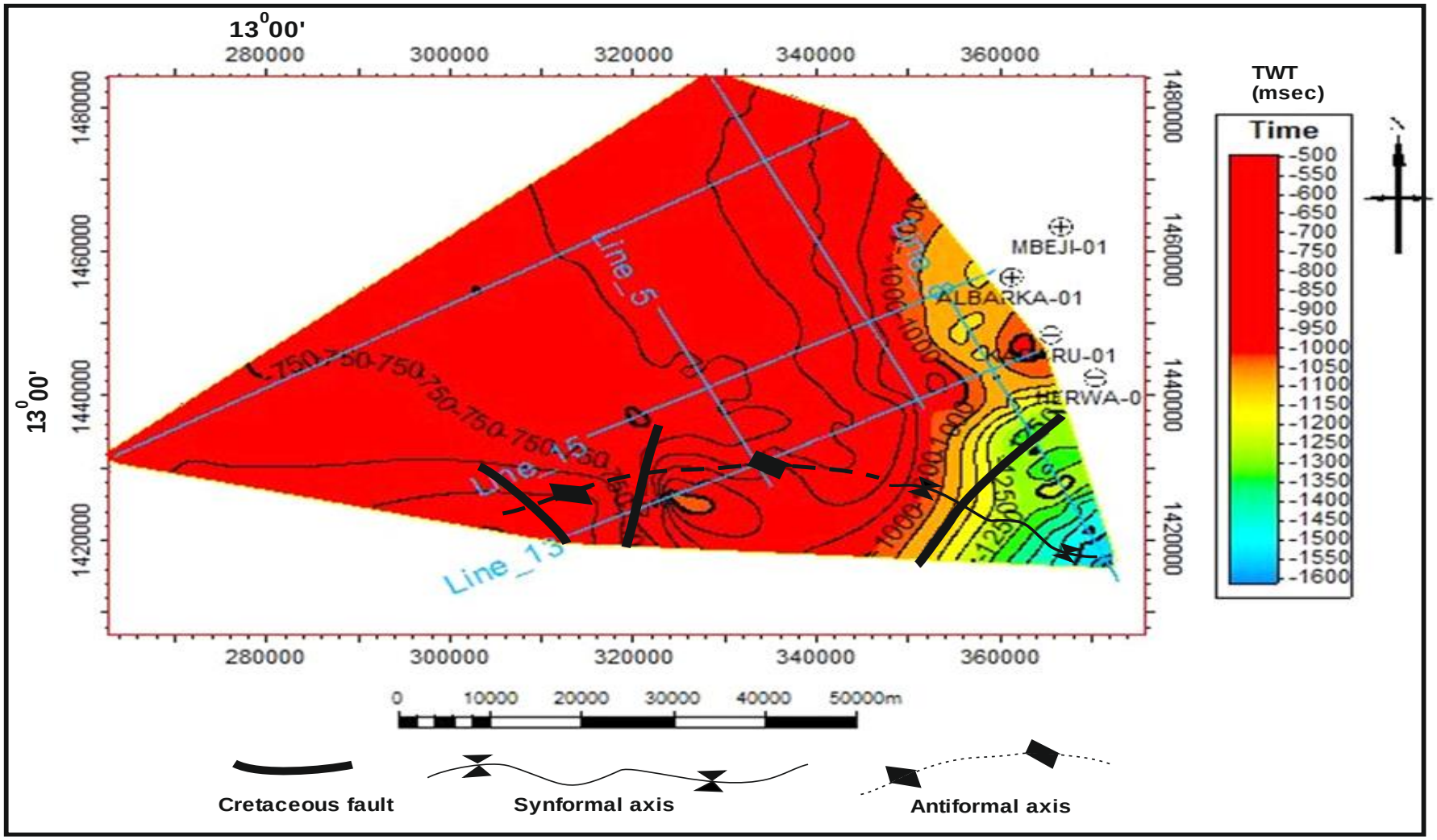

Fig 5.26: Chad Formation Time-structure map showing fewer faults occurring in the post rift Formation. Due to the constraint on the extent of the seismic data, the faults at the synformal and anticlinal boundaries correlate with the Intrabasinal faults in the gravity and magnetic data showing basement control of the basement propagated faults with the synrift package. Compare this image with the GIS correlated surface and subsurface structural analysis map on Fig. 7.11.

5.6 Rift architecture and stratigraphic development

The previous sections of this chapter have constrained the stratigraphic development of the north eastern Bornu basin using the 21 well log data and six adjoining seismic reflection data. In this section, the four stratigraphic horizons mapped within the north eastern basin from the integrated 2D seismic and combined well data analysis, have enabled the identification of the sedimentation history and distribution of sediments in the north eastern Bornu basin development during the pre-rift, syn-rift and post-rift geologic events. This section summarises the stratigraphic development in the north-eastern Bornu basin as it evolved from the Lower Cretaceous rifting to the Quaternary post rift tectonics and sedimentation. To establish the rift architecture of the north-eastern Bornu basin, the seismic time-structure analysis has identified the major chronostratigraphic horizons and the bounding faults of the grabens.

5.6.1 Pre-rift basement

The pre-rift geology is represented by the pre-Albian basement rocks of the Cratonic platform and the Pan African crustal consolidation rocks of McCurry (1971) and Benkhelil (1982), which include the migmatite and gneiss complex that constitute the Nigerian basement (Olade 1975). Pre-rift basement lineaments formed ancestor tectonic structures that influenced the formation of syn-rift faults in the basin. In this study, the pre-rift geology is identified as a seismically hard basement reflector in the lowest parts of the seismic sections, which reflects the pre-rift disconformity of the north-eastern Bornu basin. The reflectors below the interpreted basement top, which marks the base of the oldest uncomfortable sedimentary formation, are chaotic and non-coherent indicating that it is not composed of layered sediments but rather igneous or metamorphic rocks. The pre-rift disconformity is marked by seismic reflector terminations along bounding faults that are associated with the intra-graben

syn-rift sediments. Rift onset disconformity that separates the pre-rift and the syn-rift is subtle and cannot be resolved from the 2-D seismic data. Few moderately to steeply dipping basement involved normal faults associated with the basement rocks that might be part of regional faults related with the pre-rift tectonic phase extend into the syn-rift phase. The few pre-existing zones of weakness exist in the pre-rift crystalline basement were reactivated during the Cretaceous rifting several of which are high angle normal faults (Ajakaiye et al., 1986; Genik, 1992; Obaje, 2009) (Figs. 5.16 and 5.18).

5.6.2 Syn-rift geology

The 2-D seismic data analysis enables the identification of the sedimentation history within the syn-rift grabens, which marked the period of the rift basin formation. The syn-rift packages, within the grabens show prominent reflectors that begin from the boundary between the chaotic reflectors of the pre-rift basement. The syn-rift deposits are recognisable in the seismic sections by divergent reflectors that show syn-tectonic deposition in an active graben setting. Seismic and well log interpretations herein show that the early syn-rift is represented by the oldest sedimentary rock as the Cenomanian Bima Formation composed of sandstone that evolved from weathering of the basement rocks. The Turonian mixed continental, marine Gongila Formation composed of sand, and shale sequence when the rifting slowed down represents the late syn-rift stage. The continental fluvial depositional environment for the Bima Formation deposited directly on the basement during the syn-rift phase required incremental structurally controlled accommodation space during rifting for sediment supply. Progressive axial sediments supply predominated, with the deeper axial depocenters created by the rifts initially becoming completely infilled with sediments prior to the shallower rift margins (Fig. 5.10).

Few wells penetrated to the syn-rift sediments with the deepest level of 5000 m reached in Kadaru_1 (KAD) well (Fig. 5.4). The early syn-rift is a thick sequence that exists only in the grabens in the deepest part of the north eastern Bornu basin. The syn-rift sub-basin underwent higher compaction and subsidence over the more competent metamorphic and igneous basement rocks. The fault bounded syn-rift graben depocenters as imaged on seismic and revealed from the well interpretation supports features of the subsidence. The syn-rift packages show the presence of layering and reflection continuity that terminates at faults bounding grabens as well as having parallel and sub-parallel reflections depending on local accommodation spaces available during various phases of rifting. Deposition of the Bima Formation marking the syn-rift base is characterised by discontinuous reflectors that terminate against graben bounding faults while the syn-rift top represented by the base of Gongila Formation is characterised by relatively sub continuous reflectors. The syn-rift faults are part of extensive segments, whose initiation might have been influenced by the pre-rift extensional basement faults. Other synrift fault architecture is composed of the extensive synthetic faults that dip to the west as well as the eastward dipping antithetic normal faults (Figs 5.10, 5.16, 5.18).

5.6.3 Post-rift geology

The top of rift-related sediments comprising of the early post-rift Senonian Fika Formation represents the post-rift fill and the late post-rift Quaternary Chad Formation deposited over the syn-rift package. This stage marked the period when the palaeotectonic events ceased. Avbovbo et al., (1986) have recognised the presence of the Tertiary period of non-deposition beneath which most of the Cretaceous faults terminated. However, the syn-rift to post-rift boundary is easily defined by the change in fault growth beyond the top of synthetic and antithetic fault arrays that marked the end of the syn-rift phase. However, most of the faulting ceased during the early post-rift within the aggradational sequence and only a few faults continued further upwards into the late post-rift sequence. As represented on the time-structure maps (Figs 5.25, Fig. 5.26), the Fika Formation and Chad Formation show low relief subsurface topography. Fluvial - lacustrine environment of deposition had occurred in the late post-rift fill that demonstrates a lake-highstand interval succeeded from a deep-water lacustrine early post-rift sediments filling. The structural mechanism for the post-rift tectonic development represented by the change in fault growth to a post-Cretaceous. Chad Formation time-structure map shows a northeast retrogradational sequence following the early post-rift aggradational sedimentation in response to the fluctuating palaeolake levels.

5.6.4 Isochron thickness maps

Isochron maps showing the thickness maps of two individual stratigraphic intervals in the study area are generated from well tops of the individual stratigraphic horizons mapped from the GR well logs as presented in Section 5.3.1, which shows four Formations underlying the north-eastern Bornu basin. Hence, the interval isochron maps are constrained by the wells, which covered more area than the seismic data Fig. 5.1. The isochron maps generated between the mapped horizons indicate stratigraphic evolution and structural growth through time and space. Accordingly, the four stratigraphic horizons including Bima, Gongila, Fika and Chad Formations are remapped using petrel software and the isochron thicknesses between two proximal stratigraphic formations are generated. Hence, three isochron thickness maps are produced for thicknesses between Bima and Gongila Formations, Gongila and Fika Formations and Fika and Chad Formations.

Bima - Gongila (Cenomanian – Turonian) interval isochron map shows an overall southeast ward thickening of sediments indicating a broad synrift depocenters bounded by a broad northwest thinning of the sediments deposited in shallower environment. Thickness between the Bima - Gongila interval ranges from 50 m to 1300 m. The broad thick depocenter trends NE-SW with the thickest area of 1300 m coinciding with spatial location of the deepest wells drilled in the basin including Kinasar and Murshe as shown in Fig. (5.5). The overall structural geometry of the depositional styles show less folding with broad separation of graben depocenters and shallow horst areas bounded by rift faults (Fig. 5.27).

Gongila – Fika (Turonian – Senonian) interval isochron map, which defines the top of syn-rift and beginning of post-rift represented by the Fika Formation, is folded, and the folds define a series of crenulations that are typically located directly above interpreted rift horst and grabens bounded by faults. The map further indicates the westward

thinning of the deposits represented by the locations of the shallow Kasade and Bulte wells as shown in Fig. (5.4). The thickness between the Gongila Fika interval is 100 m – 2400.

Chad - Fika (Senonian – Quaternary) interval isochron map, which defines the top of Fika Formation, indicates an overall westward thinning bounded by a narrow south-eastern NE-SW trending thick post rift depocenter with maximum of 2000 m thickness as a result of a changes in the depositional axis during the basin evolution. Overall, the isochron map shows that the narrow thick depocenter is truncated by a series of amorphous to sub-circular isochron ‘thins’ around Faltu, Bulte and Kasade wells, which corresponds with the shallow wells that were herein demonstrated to have bottomed over bulging horsts in the basin as shown in Fig. (5.10). Conversely, the narrow thick flank represents positions of the deeper wells drilled. Thickness range of 200 m - 2000 m exist between this interval. Well log cross-sections and interpreted seismic sections indicate that these relative thickness variations are principally related to variable subsurface relief that dips broadly to the west. The thickest part of the isochron map is located southwards were the deep Kinasar well is drilled.

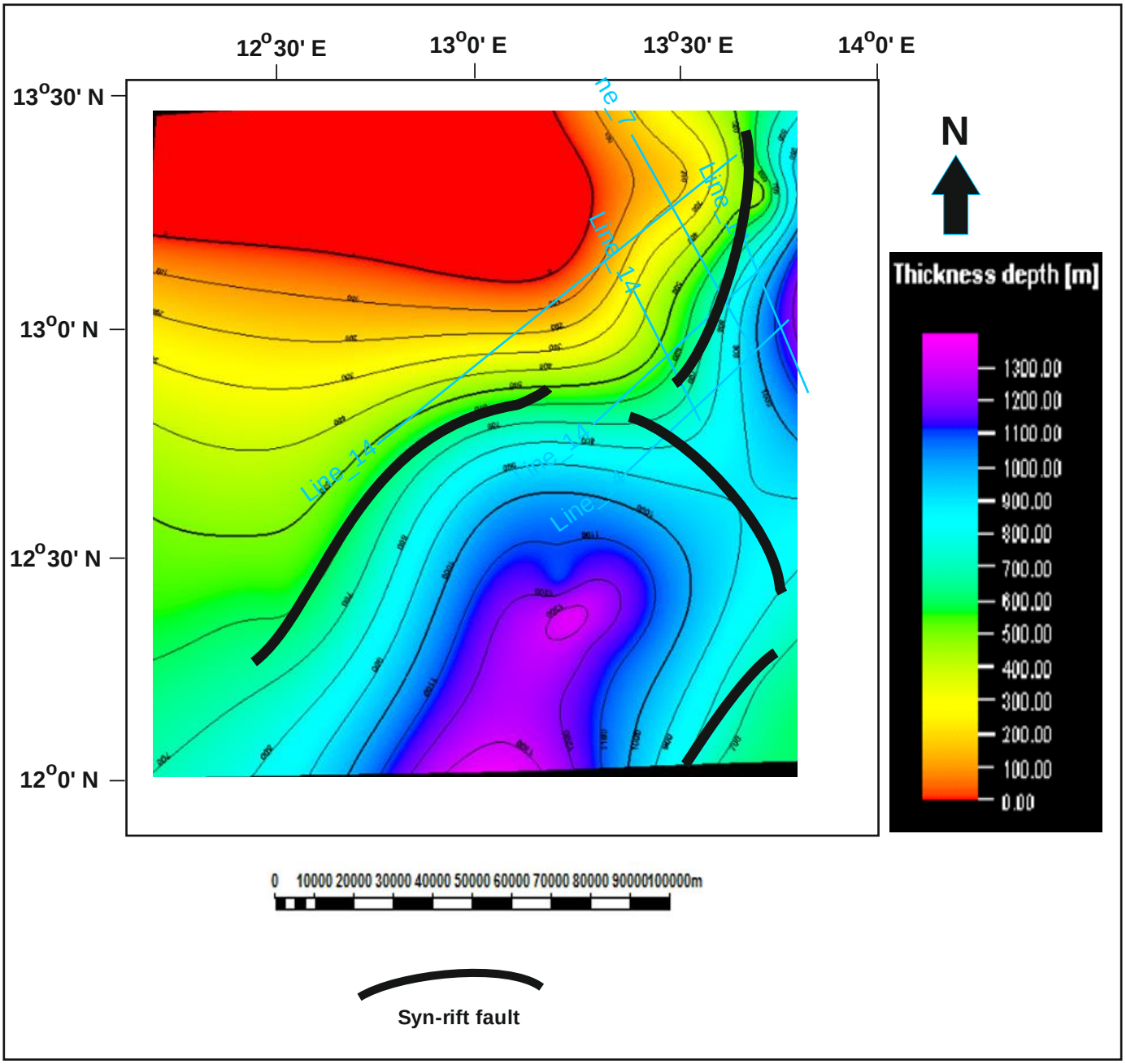

Fig. 5.27. Bima - Gongila (Cenomanian – Turonian) interval isochron map shows an overall southeastward thickening of sediments indicating a broad synrift depocenters bounded by faults. Bounding faults trends mainly NE-SW and NW-SE. Note the broad depocenter trending NE-SW corresponding to the trend of the Gubio-Munguno depression on the gravity map Fig. 6.7. This further emphasise the synergy between the different datasets showing validation.

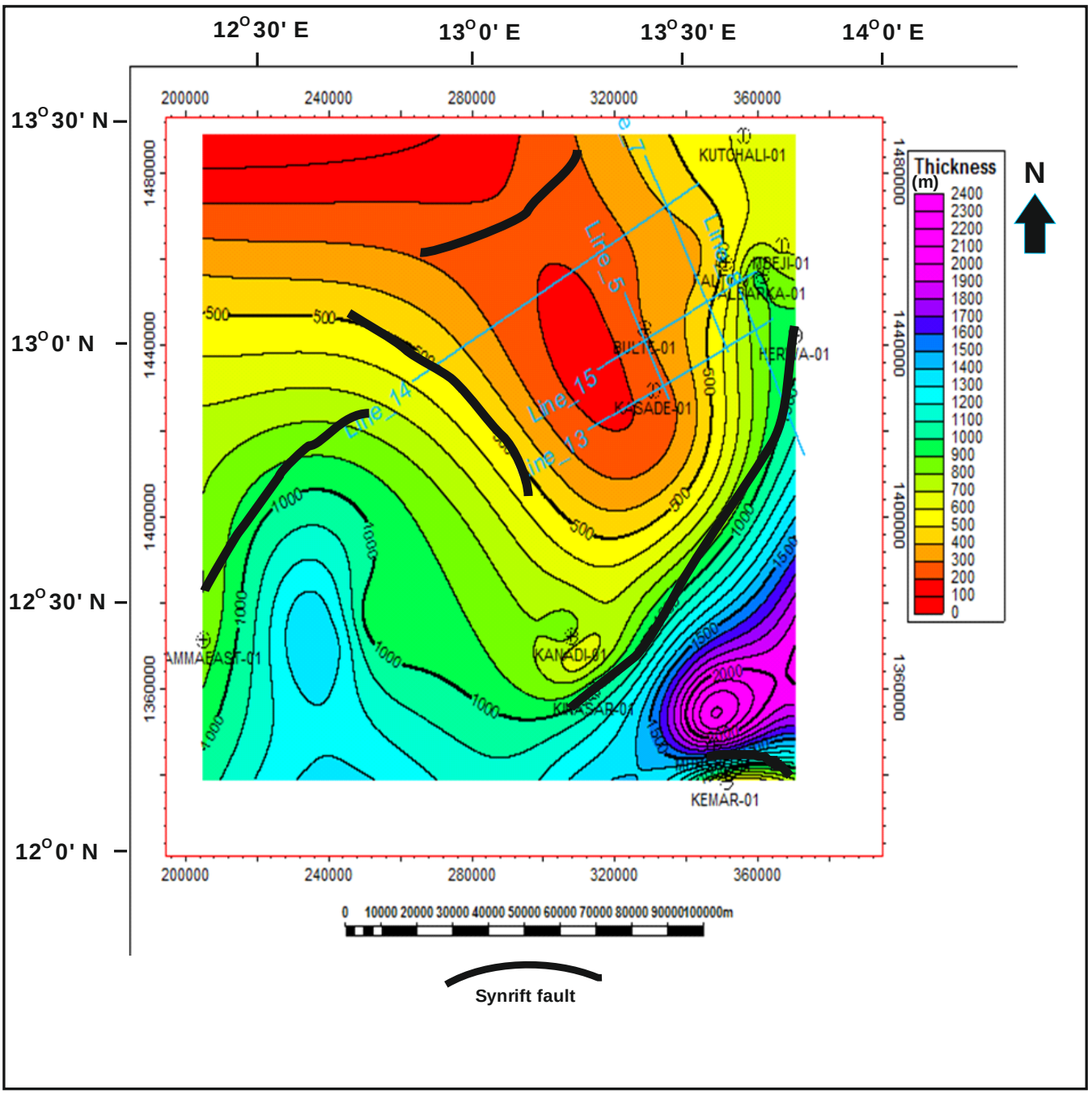

Fig. 5.28 Gongila - Fika (Turonian – Senonian) interval isochron map, showing defines the top of syn-rift and beginning of post-rift represented by the Fika Formation and bounding faults Bounding faults trends mainly NE-SW and NW-SE. Note the broad depocenter trending NE-SW corresponding to the trend of the Gubio-Munguno depression on the gravity map Fig. 6.7.

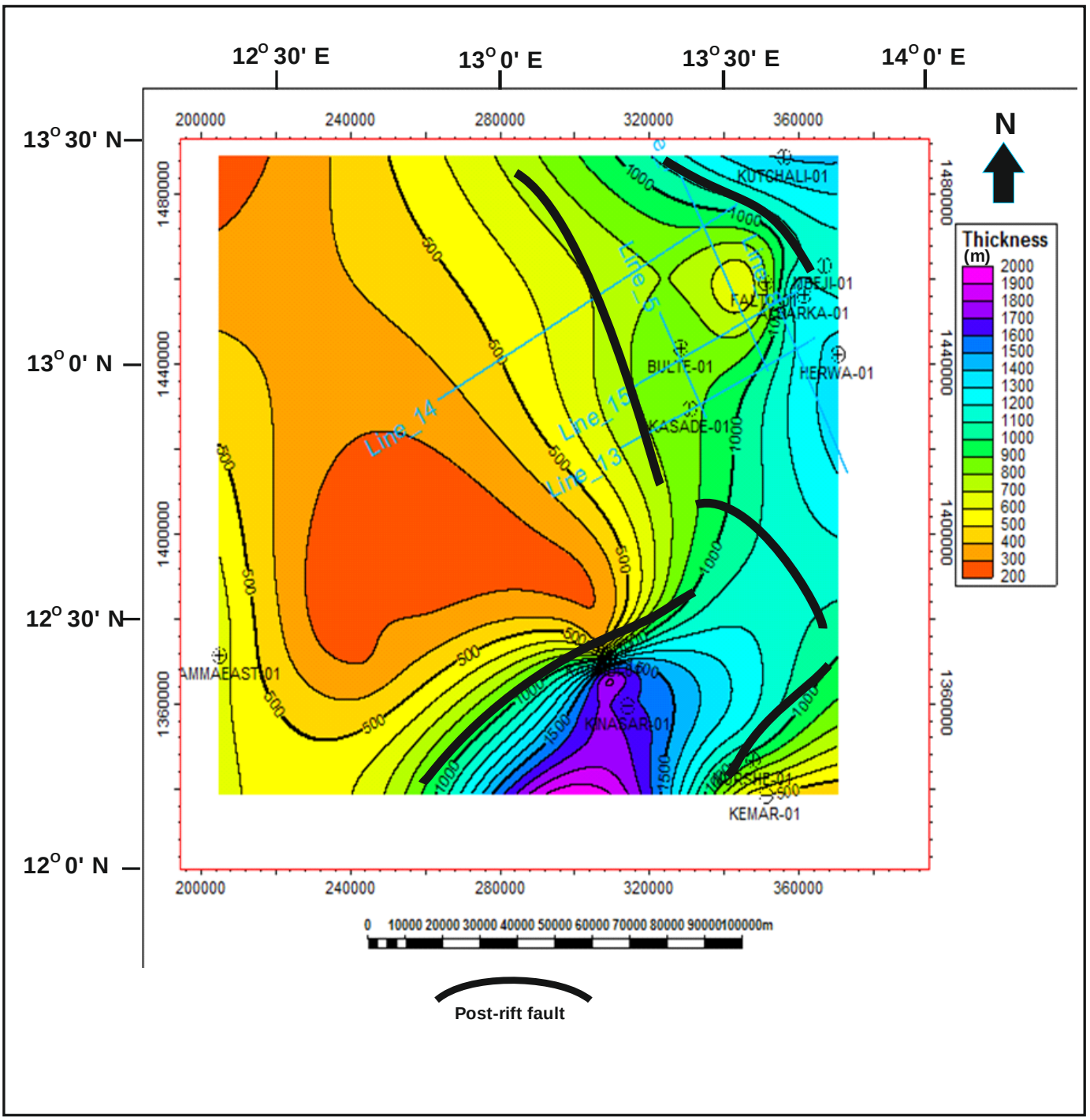

Fig. 5.29. Chad - Fika (Senonian – Quaternary) interval isochron map, which defines the top of Fika Formation, indicates an overall westward thinning and bounding faults, Bounding faults trends mainly NE-SW and NW-SE. Note the broad depocenter trending NE-SW corresponding to the trend of the Gubio-Munguno depression on the gravity map Fig. 6.7

5.7 Quaternary development of the north eastern Bornu basin

The thick Quaternary phase as interpreted in the post rift geology evolved from the influence of the prevailing climatic factors, which determined the sediments provenance in the entire Lake Chad Basin. The Lake Chad Basin is an internal drainage basin since rivers do not flow out of it. The Quaternary deposit represented by the topmost Chad Formation consists of mixed sand and clay deposit. However, the presence of thick Quaternary soils and surficial deposits in the north-eastern Bornu basin bordering the Lake Chad consist of aeolian sand, river alluvium, deltaic deposits and clay plains (Pullan, 1964). The perennial rivers that rise from the central northern Nigeria highlands in Adamawa, Cameroon and Central African Republic supplied 95% of the fluvial input while Yobe River, Komadugu River and meteoric additions supplied the rest of the fluvial supply in to the Lake Chad drainage basin. The Lake is deepest in the Chad and Niger countries at > 4 m and shallows southwards to < 2 m (Nwajide, 2013). In the northern area overlying the Chad Formation, occasional sand dunes occur within the mainly flat topography. The dunes are composed of quartzose sand. The sand dunes are rimmed with vegetation within the interdune depressions (Obi, 1995), which are herein identified in Fig (4.23).

The considerable thickness of the Quaternary as represented by the Chad Formation interpreted herein from the seismic and well log datasets was suggested earlier by Wright et al., (1985), that in the deeper parts of the basin the Chad Formation may be up to 1 Km in thickness. The African continent undergoes string uplifting relative to the other continents since Miocene (Bond, 1978), in agreement with Burke and Dewey (1974) that convection plumes in the mantle lifted areas in Africa and held the continental plate stationary. However, renewed subsidence in the Lake Chad basin in the Quaternary indicates that intracratonic basins once formed were reactivated by sediment loading if the surrounding basement areas are uplifted

and eroded (Burke, 1976), producing a basin-and-swell topography. The surrounding regional basements of Adamawa, Darfur, Tibesti, Hoggar and Air that are associated with several volcanic rocks provide the geodynamic processes affecting the lithospheric plates in the area. However, the basin uplift in Santonian with phases of intraplate compression has affected the basins within the WARS including the Bornu basin. However, the amount of subsidence was not rapid considering the large areal extent of the Lake Chad Basin such that the rate of uplift of the swells around the Lake Chad basin determines the thickness of sediment infill (Nwajide, 2013).

In the Bornu basin, development of the thick Quaternary sedimentation is related to the general uplifts in the Upper Benue Trough due to the Late Cretaceous folding (Benkhelil, 1988). The uplifts could have been associated with the beginning of the Late Tertiary - Quaternary volcanism in the African continent, including Jos and the Biu Plateaux that formed the main highlands bordering the Bornu basin in the south, are part of Younger Granites and volcanic rocks. Aeromagnetic anomalies indicate that a series of buried NE–SW lineaments of incipient rifts controlled the disposition of the individual anorogenic Younger Granite ring complexes in Nigeria (Ajakaiye et al., 1986). Thus, as indicated from the combined well log and seismic interpretation herein the structural model of the origin of the Chad basin, which lead to the development of the thick overlying Quaternary phase is based on development of faults and relative movements as suggested by Burke (1976). Following the African plate resting with respect to the mantle below during the Oligocene/Miocene (Burke and Dewey 1974), crustal areas including the continent overlying the thermal plumes became elevated. Volcanic intrusions occurred within the elevated areas, while erosion of the newly uplifted areas lead to increased intracontinental deposition including in the Lake Chad basin prior to the Quaternary. Later erosion from the watershed into the basin due to the thermal sag, episodic and sporadic uplift

deposited the early Quaternary sediments. Continuous loading response produced by outflow in the asthenosphere lead to subsidence and continued Quaternary sedimentation. The depositional environments for the stratigraphic succession in the north eastern Bornu basin is interpreted from the well log analysis Table (5.1), which indicates that depositional environments include marine, fluvial, deltaic and lacustrine. Continental sediments in the basin are mainly sourced from the basement rocks as well as volcanic intrusives forming various types of sediment particle sizes, sorting and lithologies. However, younger continental facies were derived from reworking of the older series.

Chapter 6:

Delineation of basement lineament structures from gravity and aeromagnetic data in north-eastern Bornu Basin

6.1 Introduction

In this Chapter, ground gravity and aeromagnetic data were used to analyse gravity and magnetic anomalies and interpret subsurface basement configuration and structural lineaments of the north-eastern Bornu basin. Gravity data is used to detect variations of subsurface rock mass distributions in the study area, which can be interpreted for potential geological conditions for hydrocarbon accumulation and tectonic analysis.

Many similarities exist between gravity and magnetic methods in the sense that both deal with theories of potential fields. However, as gravitational field requires magnitude of mass, the magnetic field requires magnitudes and the direction of magnetization. Gravity method is the measurement, which detects lateral variations of the gravitational field of the Earth caused by density contrast from one point to the other. Subsurface crustal density variations are detected from gravity anomaly maps, which indicate high and low Bouguer anomalies. The main objective of the gravity method in this study is to delineate the rim of the basin depocenters, lineaments and basement horst features in the study area. Use of the gravity data herein is justified because Bornu basin evolved through tectonic rifting in the Cretaceous, as such, anomalous gravity highs may indicate where basement rocks are closer to the surface or where basement rift features including horst and graben are located.

Magnetic method measures the anomalies due to the magnetic potential field of the earth inherent in the magnetic crust mineral components. The use of magnetic data herein is to delineate anomalies related to magnetic bearing rocks in the study area whose anomalous patterns could be used to indicate buried faults as well as locations

of the magnetic source basement rocks. Magnetic anomalies are more related to magnetic minerals in crystalline rocks and structures than from the lesser or non-magnetic overlying sediments. However, due to the high altitude of aeromagnetic surveys the effect of non-geological source magnetic materials are reduced or eliminated giving only measurements related to the basement relief and variations in magnetic susceptibility in rocks (Nettleton, 1976).

Hence, a combined analysis of magnetic and gravity data would constrain the underlying lineament patterns of the basement rocks in the study area to compare their relationships with the surface lineaments determined from remote sensing methods in Chapter 4 of this thesis. As this research involve both structural and tectonic evaluation of the Bornu basin, hence the gravity and magnetic datasets having wider geographic coverage than the well log and seismic datasets, provide contextual regional representation of the wider subsurface tectonic features in the basin than the localised well log and seismic data would provide (Fig. 7.1). This tectonic evaluation is presented in Chapter 7 of this thesis.

6.2 Data location and description

The gravity data used was freely obtained directly from the Bureau Gravimetrique International (BGI) France. The data was originally processed for drift, latitude, free-air and Bouguer corrections. Data analysis was carried out herein using *Geosoft Oasis Montaj* software. The gravity data consist of Bouguer anomaly values (z values) ranging from -58.9 mGal and -2.5 mGal with their corresponding axes (x, y) covering longitudes 8.00 – 14.00 and latitudes 11.00 – 13.00 degrees of the study area in the north-eastern Bornu basin.

Magnetic data used herein is part of the country-wide digital quality commercial aeromagnetic data acquired by Fugro in 2007 and commissioned by the Geological

Survey of Nigeria Agency (GSNA). Average flight elevation is 800 m above sea level with line spacing of 2000 metres and 0.1 seconds recording interval, using Scintrex (x3) CS3 Cesium Vapour magnetometer. The raw magnetic datasets were obtained as total magnetic intensity (TMI) values (z values) in Tesla units with their corresponding latitudes and longitudes (x, y coordinates). All digital data are based on the WGS84, UTM Zone 33N projection, which covers the study area in order to allow geospatial correlation with corresponding georeferenced map layers in GIS. For the purpose of direct subsurface correlation of geological features from the gravity and magnetic maps, the geographical location of the seismic and well log data covering Longitudes 12 – 14 degrees and Latitudes 11.5 – 13 degrees is focused for this analysis.

6.3 Data processing and filtering

The theories and equations of gravity and magnetic data processing and separation as contained in the *Geosoft Oasis Montaj 2007* software are adopted in this study. Details of the mathematical and theoretical background of gravity and magnetic methods in geophysical prospecting and data analysis can be found in Dohr (1981) and Dasgupta et al., (2013).

In this study, the potential field datasets were sorted in *Excel* spreadsheet formats and converted to CSV Comma Delimited files to enable importation into the *Oasis Montaj* environment, which is used throughout the gravity and magnetic data analyses herein. The gravity and magnetic values from the data base file are plotted into equally spaced or square grids according to their correct geographic coordinates by creating a regular and smooth multi coloured patterns. Minimum curvature (RANGRID) gridding method was suitable for the datasets because they fit the non-parallel survey method. Deep blue–green colour range represents positive anomalies while yellow-magenta colours represent negative anomalies. The colour display is used together with the colour legend bar to refer to different wavelength values of the signals corresponding to the magnetic and density variations. Combined contour and colour grid density prepared the magnetic (Fig 6.1) and gravity anomaly maps (Fig 6.2) ready for interpretation. The sedimentary cover in the study area is assumed as non-magnetic hence, anomalies observed are considered to be due to the underlying crystalline basement rocks. However, secondary magnetisation of the lacustrine sedimentary deposits in the study area or presence of concentration of potential local magnetic minerals in the clastic rocks may cause local intra sedimentary anomalies.

Various filters are applied for potential filed data analysis (Gibson and Millegan, 1998), however, in this study, conventional filters that directly relate the location of magnetic basement rock bodies that have contrasting density variation with the surrounding

sedimentary rocks are used to provide the theoretical basis for subsurface analysis. The concept of filtering as applied in this study is to retain and enhance the desired part of the potential field signals and suppress the unwanted portions. The process involves separating the shallow and deep components in the potential field data to sharpen and focus on the source of the anomalies observed in the original data. High pass filters, which retain higher frequency-shorter wavelength signals, are able to emphasize shallower sources in potential field data and generate the residual gravity anomaly map. Low pass filters that retain low frequencies-long wavelength signals are used to emphasize on deeper sources (Isles and Rankin 2013). In this study, to enhance the visualization of the Bouguer anomalies and TMI anomalies including their shapes and boundaries, upward continuation, downward continuation, low pass and high pass filters were applied to the datasets. Further details of the mathematical theories of these filters are presented in Miller and Singh (1994) and in Verduzco et al., (2004). Thus, the magnetic and gravity signatures in the basin suggest that lithological heterogeneities in the basement may be partially responsible for the anomalies. The elongated positive and negative anomalies in the north-eastern Bornu basin are associated with subsurface moderate to high susceptibility dense metamorphic rocks within the basement including migmatite and gneiss, which characterised the northern Nigerian Basement Complex.

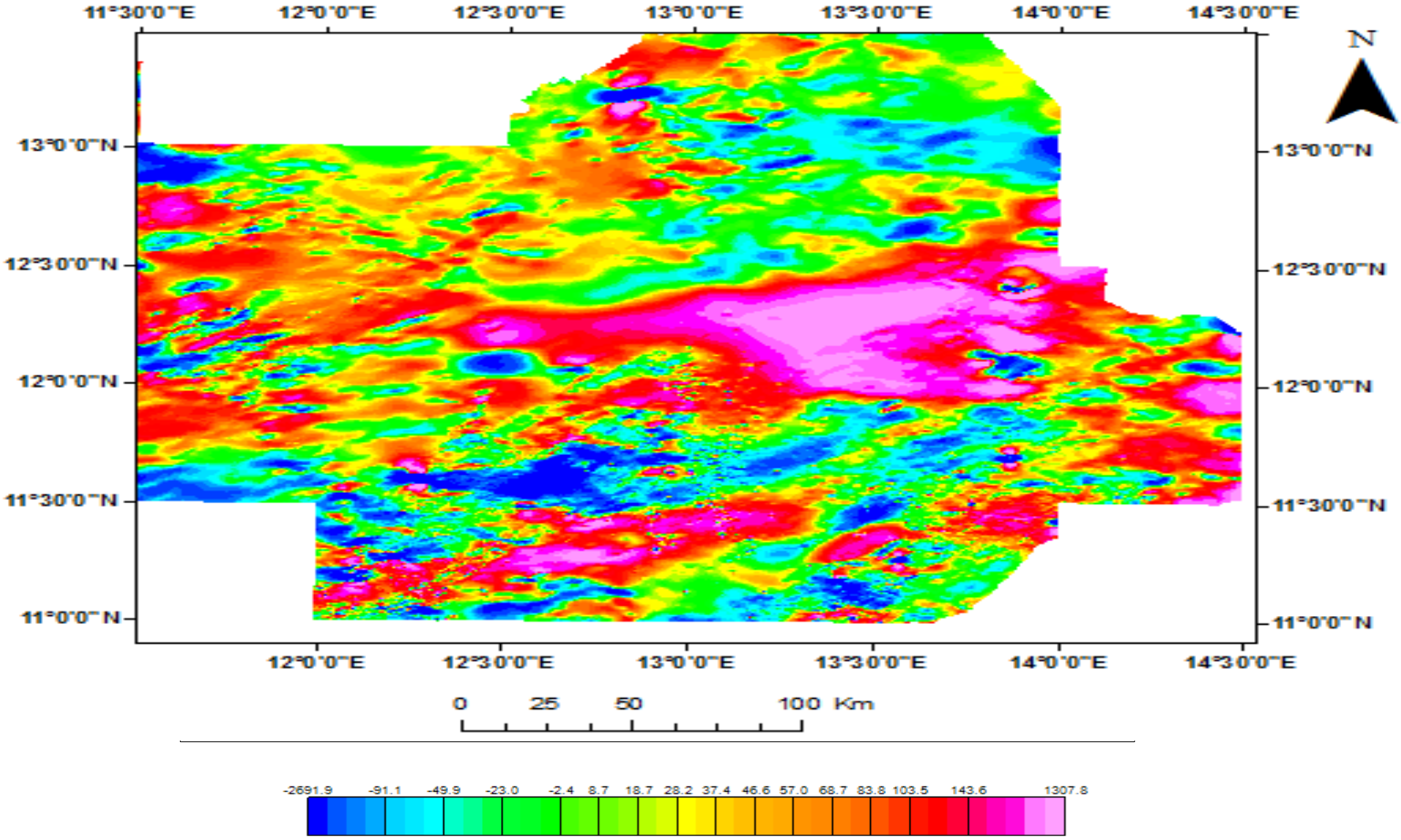

Figure 6.1. Total Magnetic Intensity map of the north-eastern Bornu basin processed from the raw data values. Based on the georeferenced coordinates, portions of this larger map can geospatially correlate with gravity map layer (Fig. 6.2) in GIS

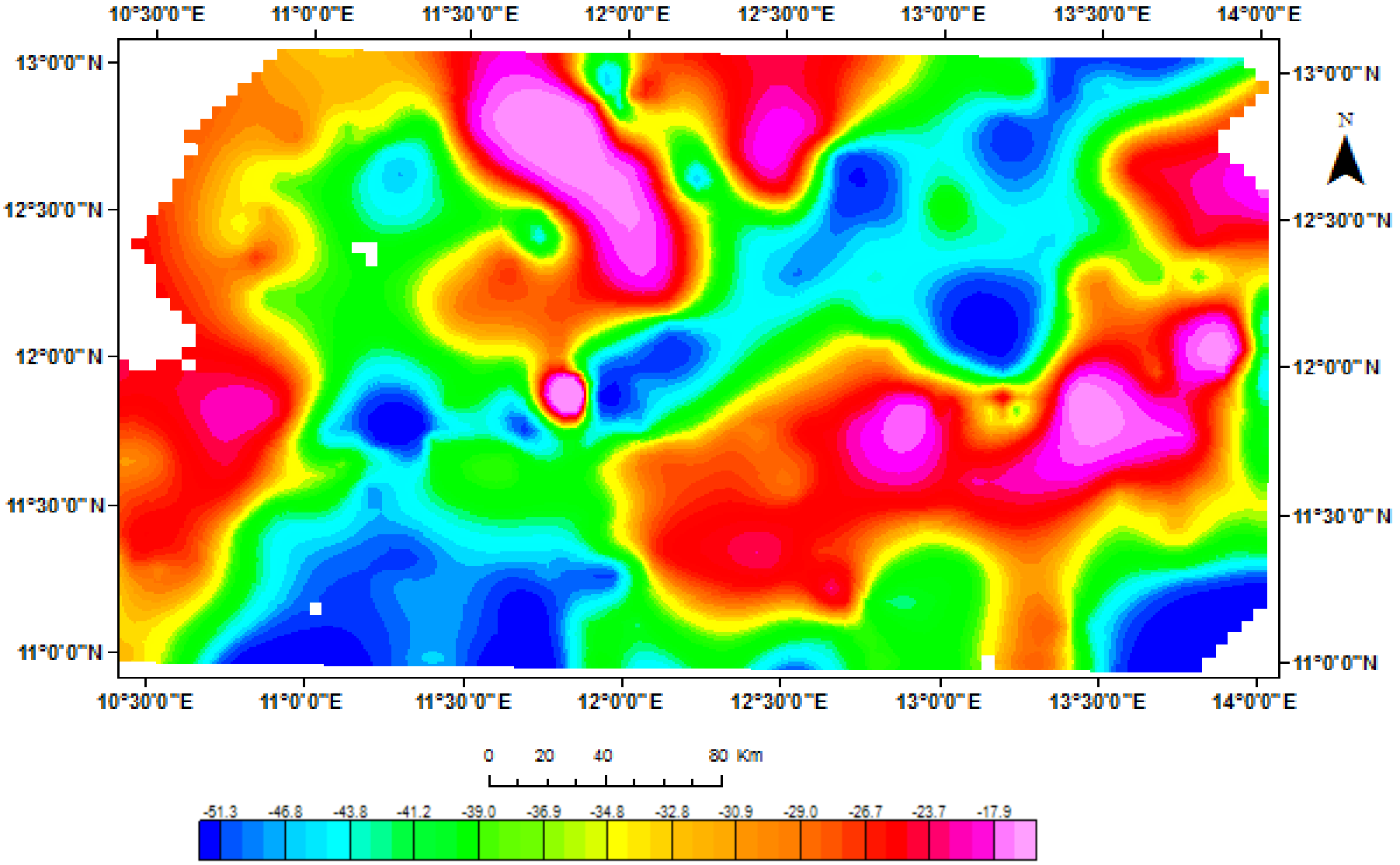

Figure 6.2 Bouguer gravity anomaly map of the north eastern Bornu Basin processed from the raw data value Figure 6.1. Based on the georeferenced coordinates, this map can geospatially correlate with the magnetic map (Fig. 6.1) layer in GIS

6.4 Regional and residual separation

Regional and residual anomalies separations of the gravity and magnetic datasets were applied since the anomalies observed were assumed to be from various depth sources and therefore should be separated. The regional–residual separation was achieved by band-pass filtering to produce deep regional and shallow residual components of the datasets. The long wavelength regional anomalies detect the geological structures in the deeper subsurface while the short wavelength residual anomalies detect the structures in the upper crustal levels. As such, in order to focus on the deep regional anomalies, the shallow residual components were subtracted from the Bouguer gravity and the TMI anomalies. The difference between the magnetic and gravity patterns in the north-eastern Bornu basin is the primary distinguishing characteristics.

The observed gravity anomalies reflect the lateral variations of basement rock density, where the vertical components of the gravity field indicating positive anomalies (highs) represent areas of relatively high density rocks while negative anomalies (lows) represent areas of relatively low density rocks. The aeromagnetic anomalies reflect lateral variations of the total magnetisation including induced and remanent magnetizations in the rocks since magnetizations from remanent components may be associated with the composition and geological history of rocks in the study area. In such situation, remanent magnetisation may orientate differently from the source components due to induced magnetization (Clark 1999). The broad anomalies, which reflect the deep-seated structural changes of the basement rocks were highlighted on the regional anomaly maps.

The different gravity and magnetic signatures indicate the assumption of some causative sources causing gravity and magnetic anomalies are disrupted possibly due to the difference between the contrasts of the physical properties and the decay rates

of the gravitational and magnetic fields. Residual magnetic anomalies reflect the contrast of the magnetic susceptibilities between the sedimentary and basement rocks while the gravity anomalies are strongly influenced by deeper sources within basement rocks (De Castro D.L. et al., 2016). Processed maps are converted into colour shaded relief images for the TMI map (Figure 6.3) and Bouguer gravity (Figure 6.4) is generated to present a 3-dimentional (3D) effect of the 2-dimentional (2D) data. For the gravity data, the relief images produced emphasize the topographic effect of the low data values representing basins or depocenters and high anomaly areas representing possible basement highs as well as their boundaries to be better defined. The shaded relief images enhance the visual extraction of gravity and magnetic lineaments in *ArcMap* software. Extracted lineaments were and plotted on Rose diagrams using *RockWorks* software.

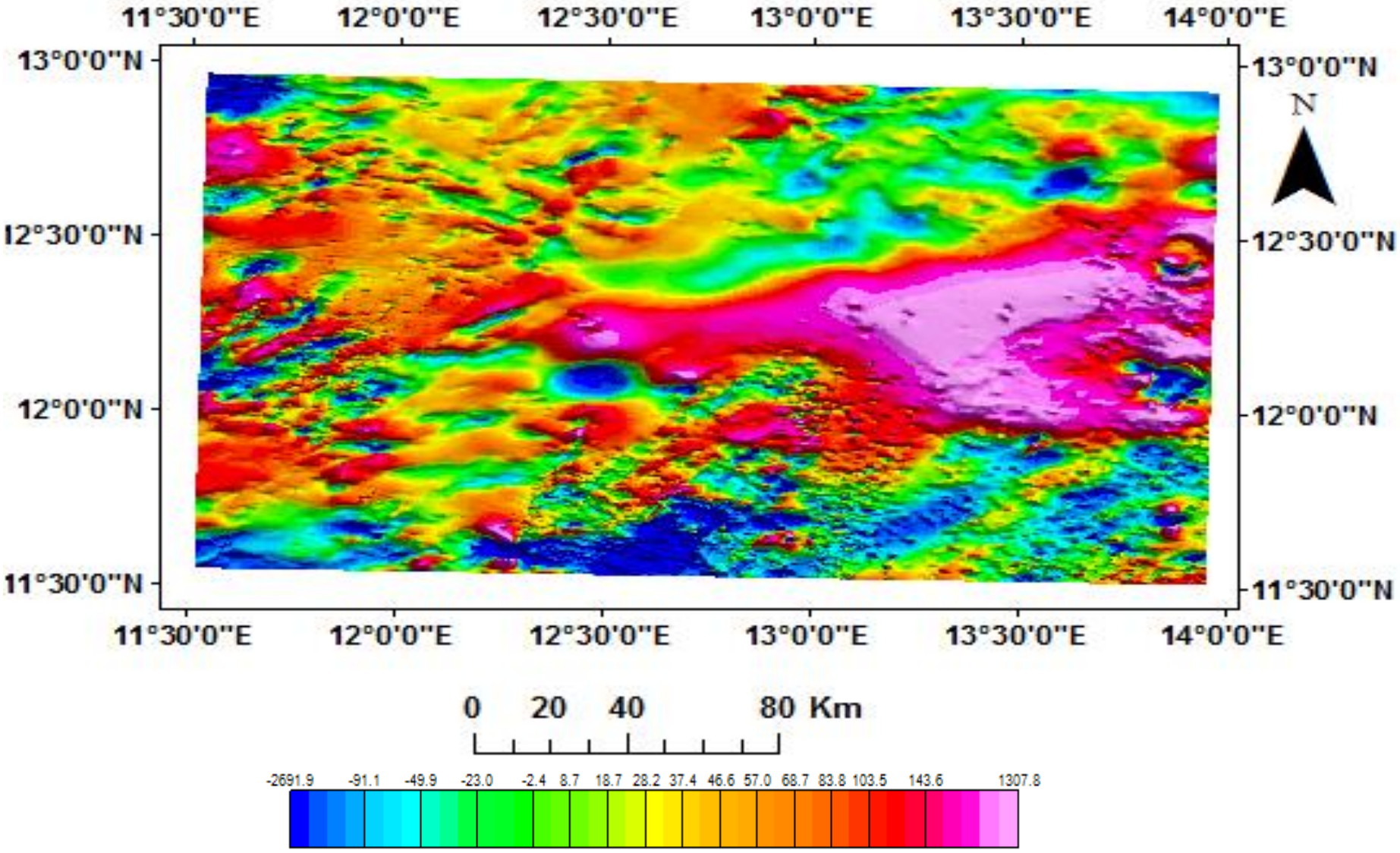

Fig. 6.3: Colour shaded relief image map of the regional magnetic anomaly. Map focused from Fig 6.1 to geospatially overlay with the gravity map on Fig s. 6.2 and 6.4 in GIS.

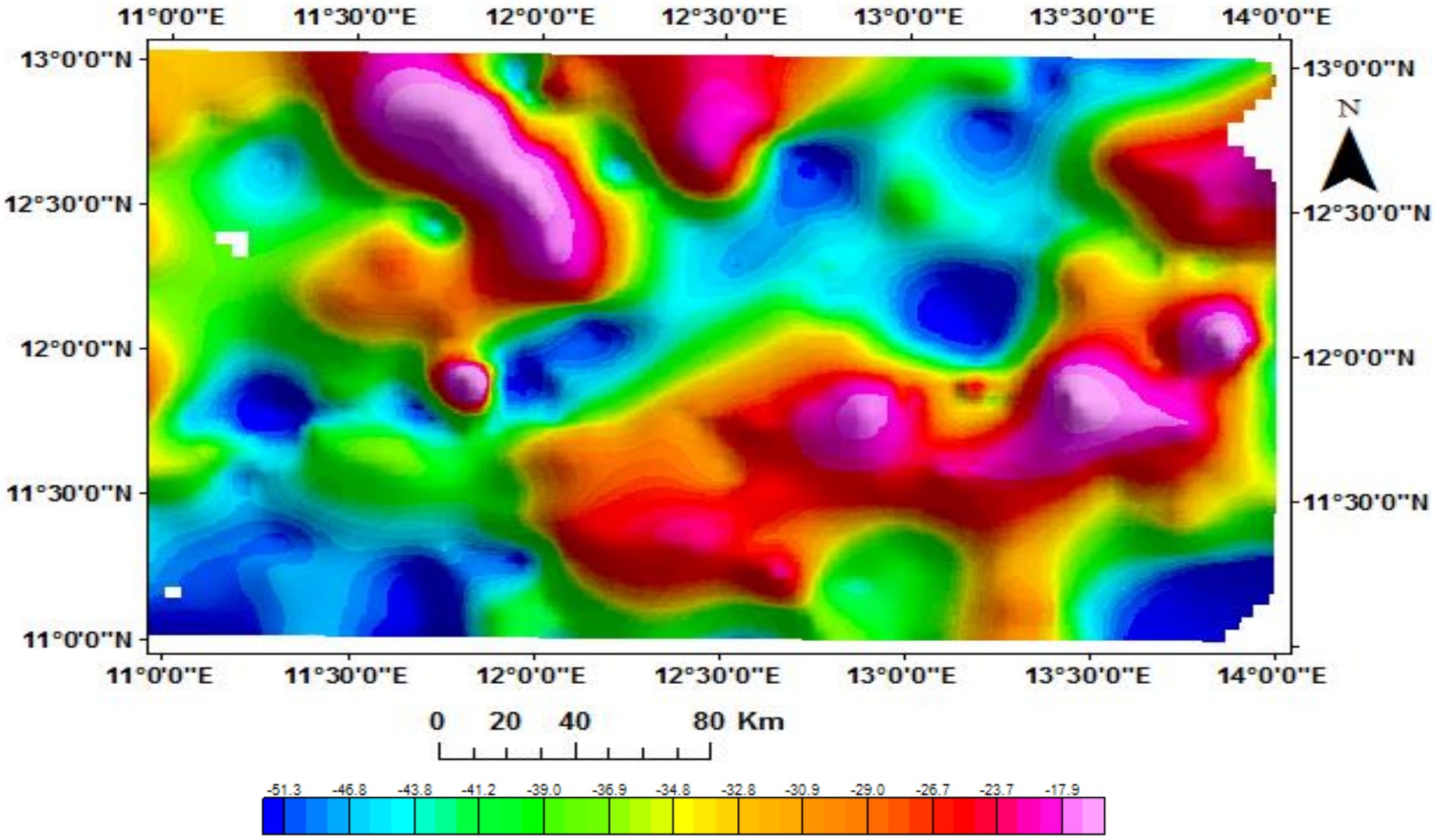

Fig. 6.4: Colour shaded relief image map of the regional gravity anomaly

6.5 Upward and Downward continuation

The regional/residual separation process is further enhanced through generating downward continuation of the datasets. Various simulated magnetic fields are modelled to enhance the regional anomalies by filtering and screening the short wavelengths and producing different patterns of the anomalies to depict the form of potential field if it were measured at higher or lower altitude. Downward continuation and low pass filters applied to the TMI grid emphasize the structural expressions of local structures and their boundaries while suppressing the effect of large regional magnetic anomalies (Figs. 6.5 – 6.6).

Downward Continuation filter applied emphasizes the deeper magnetic basement. However, the Downward Continuation filter is significantly affected by potential noise signals in the original datasets since it amplifies minimum variations in the signals. The filter is used to estimate the potential field closer to its source by sharpening them to improve the resolution of the underlying distribution of the potential fields (Trompat et al., 2003). Hence, in this study, Butterworth Low Pass filtering was used to suppress any potential noise in the datasets. The Low Pass filter, combined with the Downward Continuation filter, cuts off the short wavelength noise and attenuates the noise accentuated by downward continuing towards the source of the geological body that causes the anomaly. Downward continuation of the magnetic data is modelled at two different depth levels of 3 km and 5 km respectively based on the geothermal gradient for Bornu Basin, which range from 3.0 to 4.4 ^{o}C/100 m with an average of 3.4 ^{o}C/100 m (Nwankwo and Ekine 2009) (Figs. 6.5 – 6.6). Well data analysis indicated that depth to basement rocks in the area reached 5 km (Figs. 5.4 and 5.5). Geological considerations for the selections of the two downward continuation depth levels include; (1) 3 km downward continuation level represents the depth range for shallow upper crust to intermediate depth range with the potential of reflecting brittle crustal

conditions in the basin, hence this depth range has greater potential for higher lineament density useful for recognition of the shorter secondary lineaments. This residual depth level represents the Upper Cretaceous rocks with faults linked to the large-scale fault systems and potential for direct connection with the surface lineament systems (Fig. 6.5). (2) At 5 Km, the geothermal gradient in the basin is far less than the Curie temperature of potential magnetic minerals in the area as described by Nwankwo and Ekine (2009). Rocks in this intermediate to deep crustal depth are expected to have the potential to generate magnetic responses, which are sensitive to long wavelength signals. Long primary aeromagnetic lineaments with low population density can therefore be detected.

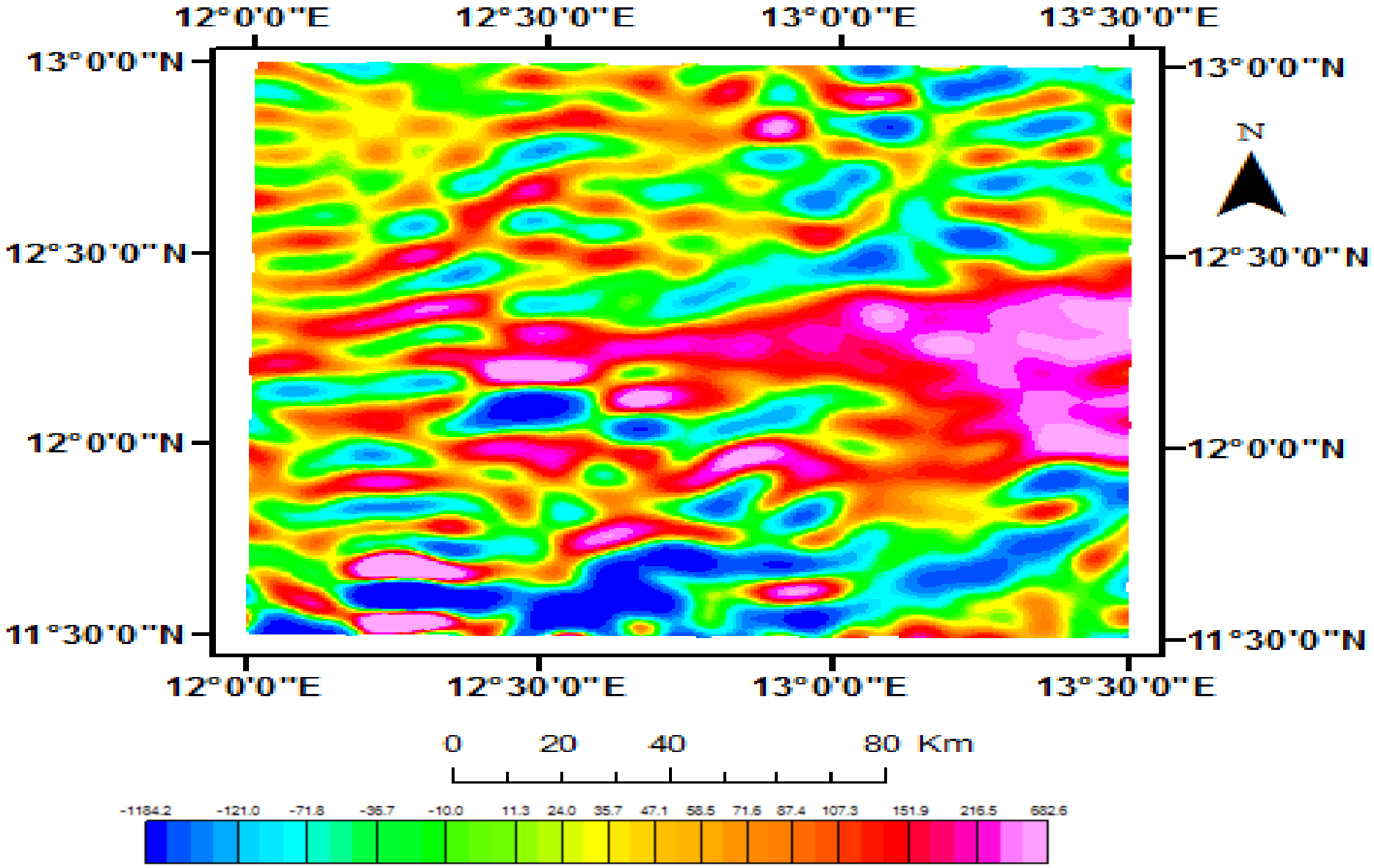

Figure 6.5. 3 km Downward Continuation of subset of the magnetic data showing anomalies becoming ductile closer to the sources.

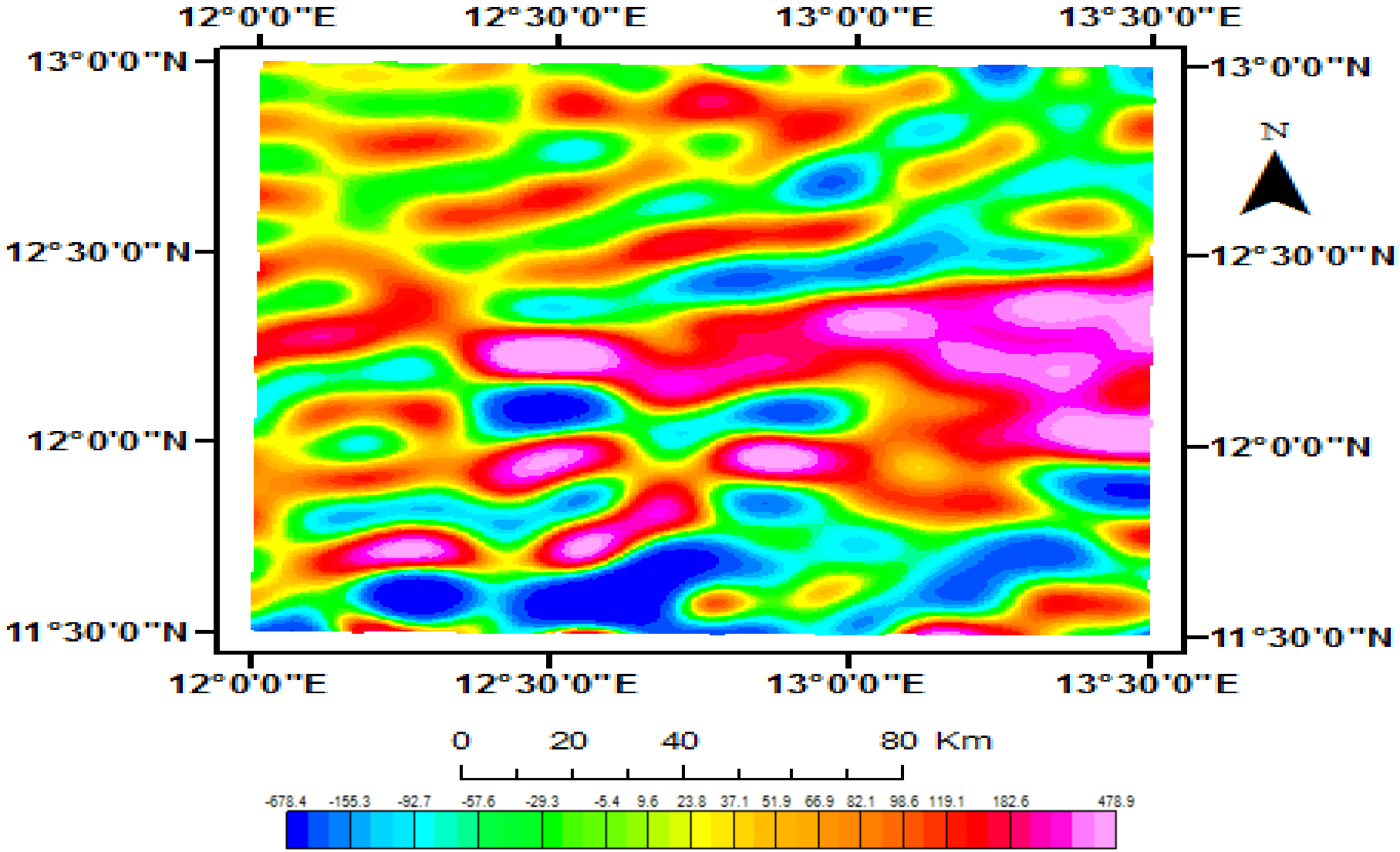

Figure 6.6. 5 km Downward Continuation subset of the magnetic data showing longer and sharpening of anomalies closest to the source

6.6 Results: Structural interpretation

6.6.1 Basement tectonic maps

The gravity and magnetic datasets are interpreted for regional structural and tectonic analysis of the north-eastern Bornu basin. Systematic approach to structural interpretation in this study uses the various map layers imported into GIS project, including TMI map, Bouguer gravity map and the two different downward continued maps of the TMI presented in Sections 6.4 and 6.5.

From the gravity map, qualitative interpretation indicated that the study area is tectonically comprised of high relief (positive anomalies) basement flanks mainly at the rims of the study area surrounding low relief (negative anomalies) depocenters, which indicate the undulating topography of the subsurface in the area. Notably, the high anomalies named herein from their geographical localities on the regional gravity map are the central E-W striking Bornu Yassu-Bida anomaly, Lau anomaly on the eastern rim, NW-SE striking adjoining parallel to sub-parallel Gazabure and Bololo anomalies on the northern rim and Kusur-Ai anomaly on the western rim of the study area. The source of the large positive anomalies can be interpreted as rock bodies, which could represent part of the Pan African crystalline basement system (Obaje, 2009) underlying the regional maps of the area (Fig. 6.7). A large central depocenter that trends NE-SW and smaller sub basins (mini basins) that trend E-W exist in the study area. The average width of the main axis of the central depocenter interpreted herein as the Gubio-Munguno depression is approximately 80 km and forms the largest depocenter in the study area. The central depression is bounded on the northwest and southeast sides by steep gravity contours that indicate sharp vertical displacements (Fig. 6.7). The faults that bound the main depocenter are longer than the faults that occur within the depocenter.

The crystalline basement rocks mainly on the north-western and south-eastern boundaries are defined by steep contours (Fig. 6.7). In comparison with locations of the gravity high anomalies, interpretation of the high magnetic anomalies shows that a thick, highly magnetic source body in the upper crust causes them. Coincidence of approximate locations of the magnetic high anomalies with the gravity high anomalies shows a broad region underlain by stiff crust and high-density basement.

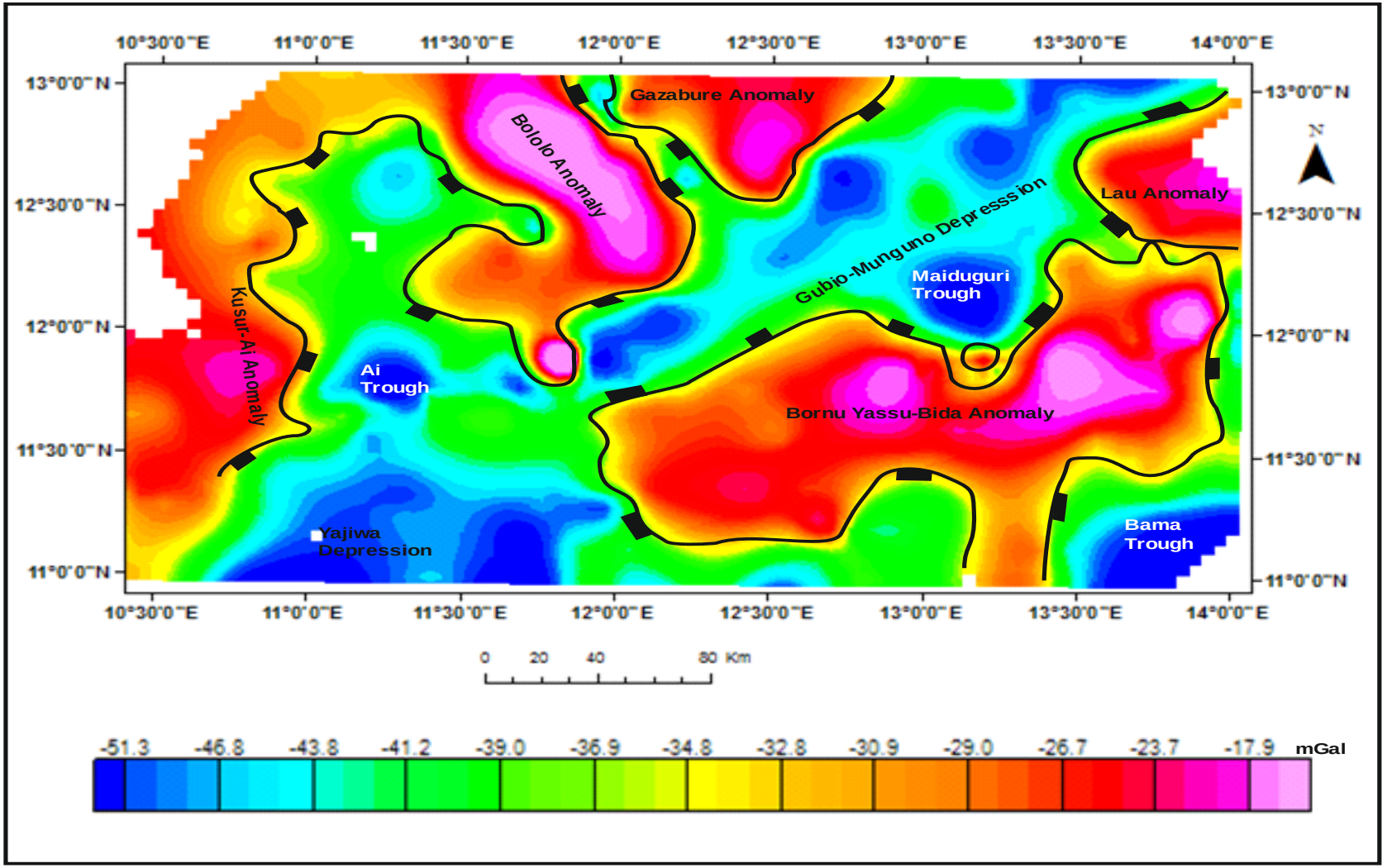

Figure 6.7. Basement relief tectonic map of the north-eastern Bornu Basin from regional gravity data

The underlying dense and magnetic basement in the north-eastern Bornu basin that form series of horsts surrounding depocenters are evidence of the Cretaceous rift features in the basin. The gravity interpretation also shows localised deeply rooted basement intrusives occurring at the rims of the study area and surrounding structurally low areas indicating the rift valley tectonic setting of the Bornu basin.

In the tectonic domain of the Gubio-Munguno depression (Fig. 6.7), the rift zone has a depth of about 160 km wide revealing the main central symmetrical graben consisting of secondary troughs. The low-density crustal blocks may represent the low-grade metasedimentary and/or granitic rocks underlying the basin. Thus, the central Gubio-Munguno graben is characterised by symmetrical structure where the underlying basement blocks are low density, low magnetic rocks where the gravity low is adjoined by higher density and magnetic basement horst rocks.

6.6.2 Gravity and magnetic lineaments maps

McClay and Bonora (2001) highlighted that a key objective of potential field data interpretation include mapping of structural lineaments. Subtle lineaments observed from enhanced potential field data can be mapped from alignments of local anomalies, aligned breaks, sudden change in anomalies and apparent discontinuities (Lyatsky, 2006). Accordingly, lineament trends mapped from the magnetic and gravity maps represent regional structures that controlled the basement pattern in the north-eastern Bornu basin. However, the regional lineaments interpreted herein are characterised as straight, curved or rounded features and must be regarded based on the context of the resolution of the potential field data, which may not completely resolve details such as sharp offsetting of the inferred geological structures. The lineaments mapped thus, represent broad deformation features and discontinuities that may not necessarily appear as discrete continuous structures.

In gravity lineament mapping, the disruption in the contour pattern due to the juxtaposition of blocks of rocks of different densities at various places along all edges of the rocks are mapped as lineaments. Lineaments are recognised from the steep or flattened gravity gradient and most of the lineaments are mapped along the gravity highs that terminate against them. The gravity and magnetic lineaments and discontinuities have strike lengths up to ~ 120 km.

Results of visual mapping and digitisation of regional (deep seated) and gravity and magnetic component maps herein indicate the dominant major structural trends in the area are NW-SE to NE-SW with secondary E-W, N-S, and NNE-SSW directions (Figs. 6.8 – 6.11).

The interpreted Bornu-Yassu - Bida High corresponds with the general elongated E-W axial trend of the entire Bornu basin. The three analogous high relief features occurring on the opposite side in the northern and western margin and extending westward including Bololo High with NW-SE strike, Kusur-Ai High with E-W strike and the Gazabure High have an overall N-S strike. The Bololo anomaly is bounded on the west side by an interpreted normal fault trending NW-SE. A parallel and opposite NW-SE trending fault on the east side separates the Bololo anomaly and the Gazabure anomaly representing a lithological boundary between the two adjoining basement structural highs. These parallel bounding faults are characterised by large throws and long strike lengths up to 60 km (Figs. 6.10 - 6.11). It is interpreted that the Bornu-Yassu - Bida High and the adjoining Gazabure and Bololo Highs representing crystalline horst masses have probably constrained the formation and shape of the enclosed elongated NE-SW Gubio-Munguno depression interpreted as part of the graben system of the Bornu basin.

Parallel faults trending NE-SW are delineated on interpreted gravity and magnetic maps bounding the large and extensive Gubio-Munguno depression occurring at the

sharp boundary between the eastern side of the Gazabure High with the western side of the Gubio-Munguno depression. A corresponding bounding fault at the eastern side separates the Gubio-Munguno depocenter and the Bornu Yassu – Bida High. In the central part of the area, an isolated roundish negative anomaly is shown, which could result from very low magnetic susceptibility sedimentary deposit in a mini basin is interpreted as the Maiduguri depression (Fig. 6.10). Tables 6.1 and 6.2 show the statistical characteristics of the gravity and magnetic lineaments respectively.

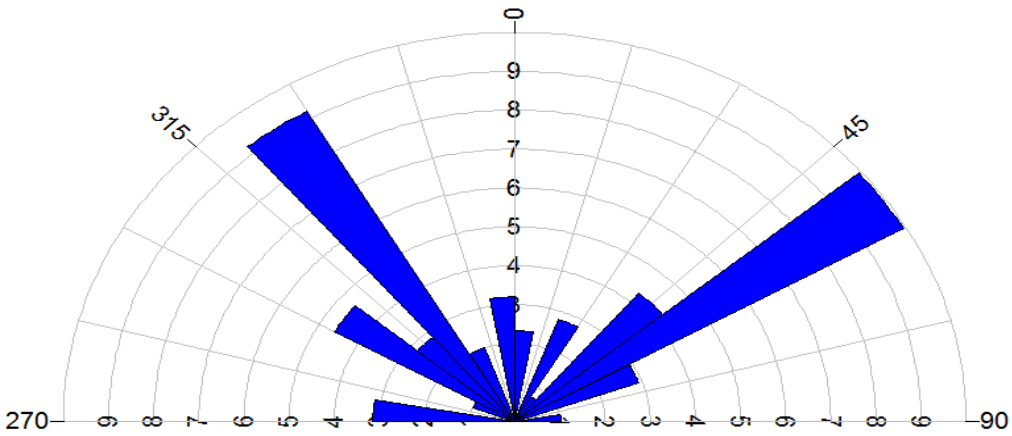

Fig 6.8: Rose diagram showing the trends of structural gravity lineaments mapped from Fig 6.10

Table 6.1: Statistical characteristics of the gravity lineaments mapped in the north-eastern Bornu basin. Metadata for the extracted lineaments are presented in Appendix C.

Statistical Summary	
Calculation Method:	Length
Class Interval:	10.0 Degrees
Min.Length Filtering:	Deactivated
Max.Length Filtering:	Deactivated
Azimuth Filtering:	Deactivated
Data Type:	Bidirectional
Population:	39
Total Length of All Lineations:	2,519,074.84
Maximum Bin Population:	7.0
Mean Bin Population:	2.79
Standard Deviation of Bin Population:	1.89
Maximum Bin Population (%):	8.97
Mean Bin Population (%):	3.57
Standard Deviation of Bin Population (%):	2.43
Maximum Bin Length:	250,444.12
Mean Bin Length:	89,966.96
Standard Deviation of Bin Lengths:	68,957.95
Maximum Bin Length (%):	9.94
Mean Bin Length (%):	3.57
Standard Deviation of Bin Lengths (%):	2.74
Vector Mean:	100.0 Degrees
	280.0 Degrees
Confidence Interval:	300.6 Degrees
	(80 Percent)
R-mag:	0.03

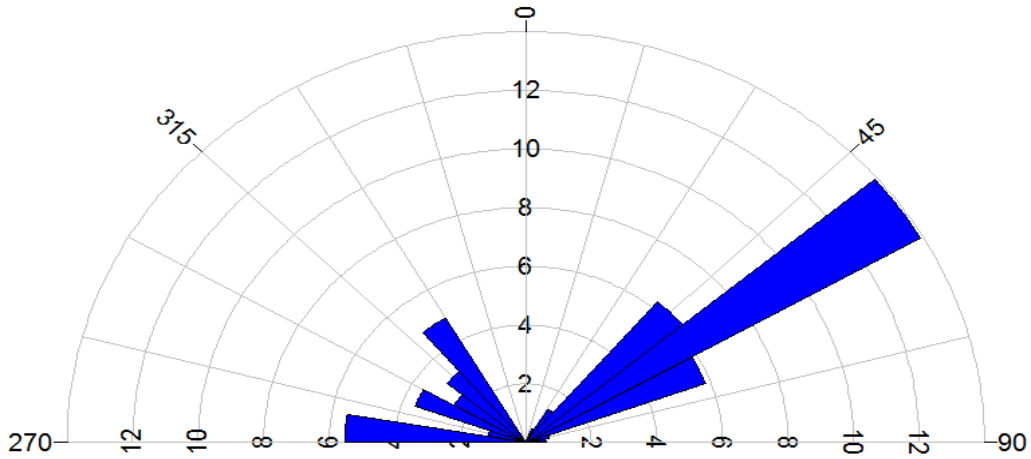

Fig 6.9: Rose diagram showing the trends of structural magnetic lineaments mapped from Fig 6.11

Table 6.2: Statistical characteristics of the magnetic lineaments mapped in the north-eastern Bornu basin. Metadata for the extracted lineaments are presented in Appendix C.

Statistical Summary	
Calculation Method:	Length
Class Interval:	10.0 Degrees
Min.Length Filtering:	Deactivated
Max.Length Filtering:	Deactivated
Azimuth Filtering:	Deactivated
Data Type:	Bidirectional
Population:	47
Total Length of All Lineations:	3,068,729.31
Maximum Bin Population:	7.0
Mean Bin Population:	3.62
Standard Deviation of Bin Population:	2.32
Maximum Bin Population (%):	7.45
Mean Bin Population (%):	3.85
Standard Deviation of Bin Population (%):	2.46
Maximum Bin Length:	427,260.53
Mean Bin Length:	118,028.05
Standard Deviation of Bin Lengths:	110,679.37
Maximum Bin Length (%):	13.92
Mean Bin Length (%):	3.85
Standard Deviation of Bin Lengths (%):	3.61
Vector Mean:	73.9 Degrees
	253.94 Degrees
Confidence Interval:	16.8 Degrees
	(80 Percent)
R-mag:	0.43

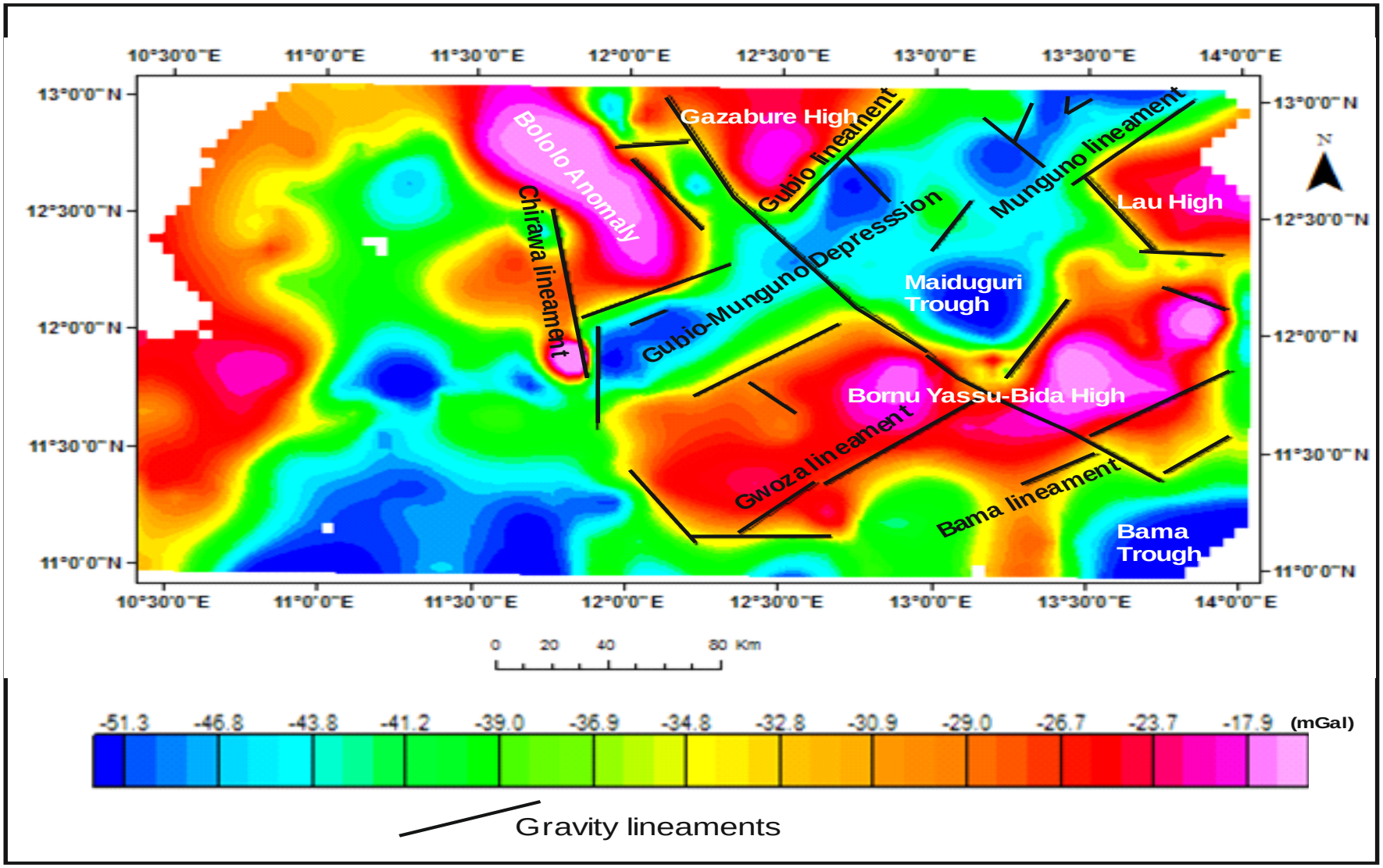

Figure 6.10. Principal gravity lineaments in the north eastern Bornu Basin. Rose diagram fig 6.8 shows the trends of the gravity lineaments

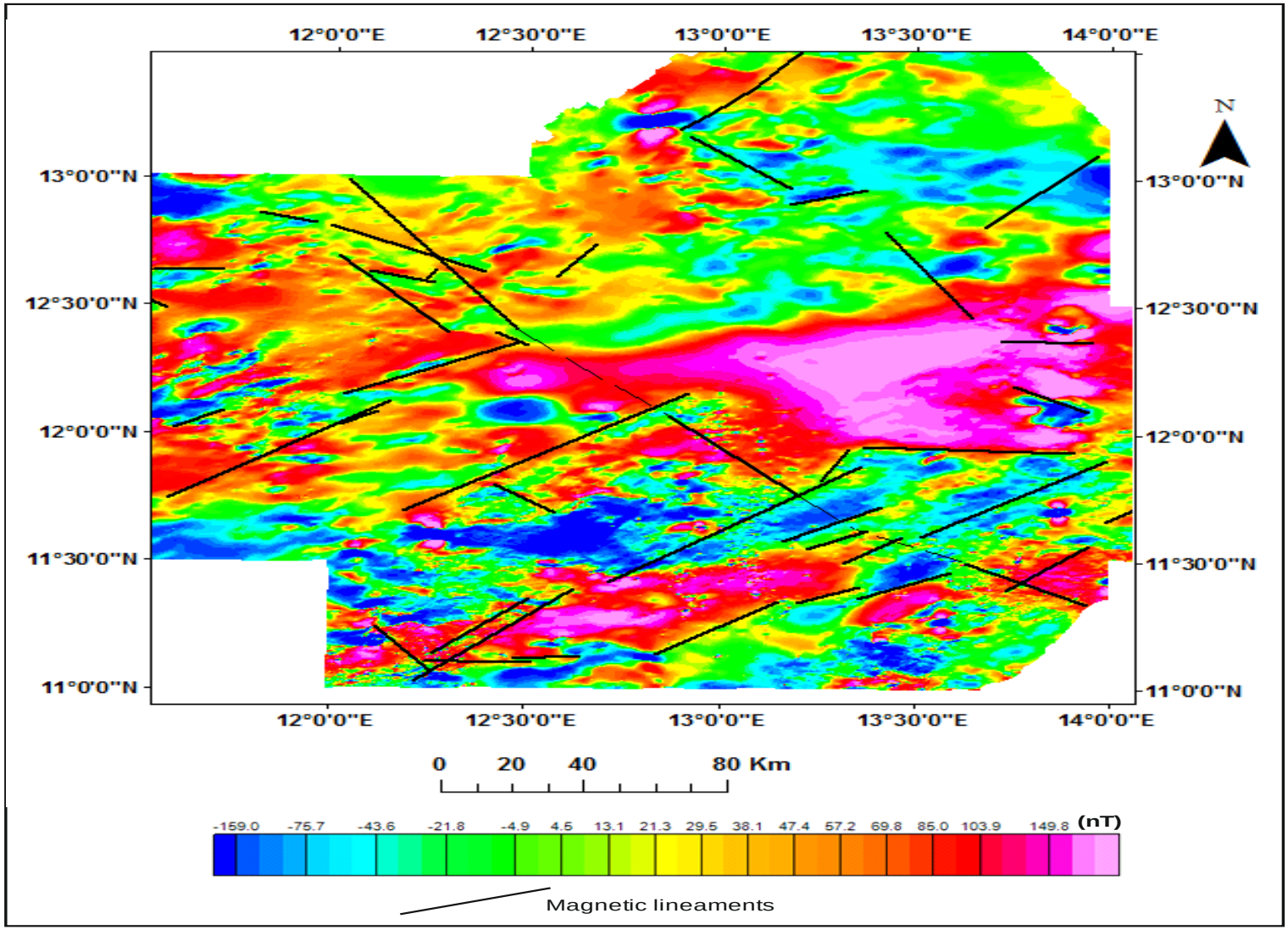

Fig. 6.11. Principal lineaments from magnetic map of the north-eastern Bornu Basin. Rose diagram fig 6.9 shows the trends of the lineament in the northeastern Bornu basin

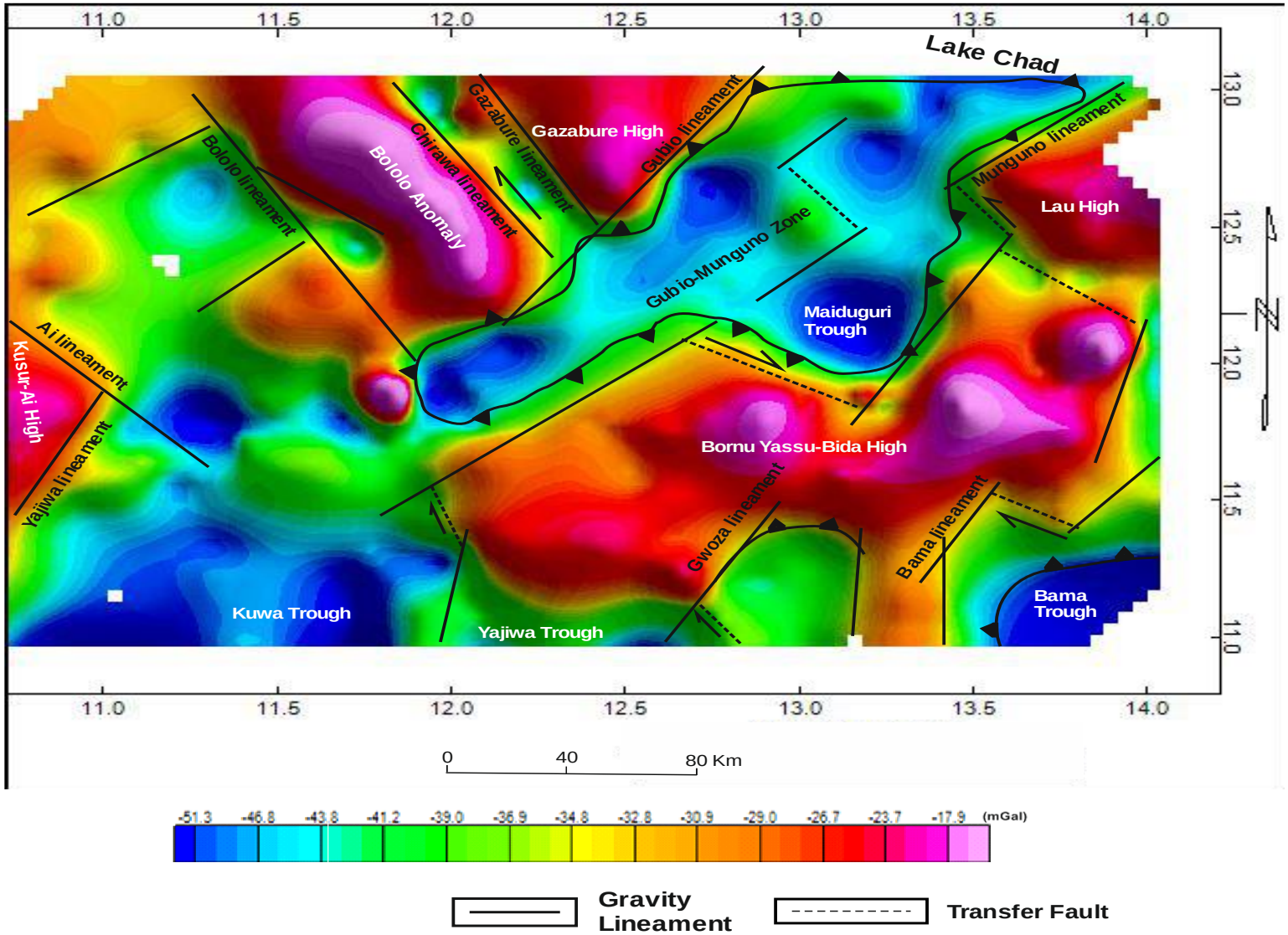

.

Fig 6.12. Gravity (basement) lineaments showing the main NE-SW normal faults in relation with the NW-SE faults forming transfer faults similar to the surface structural architecture.

.

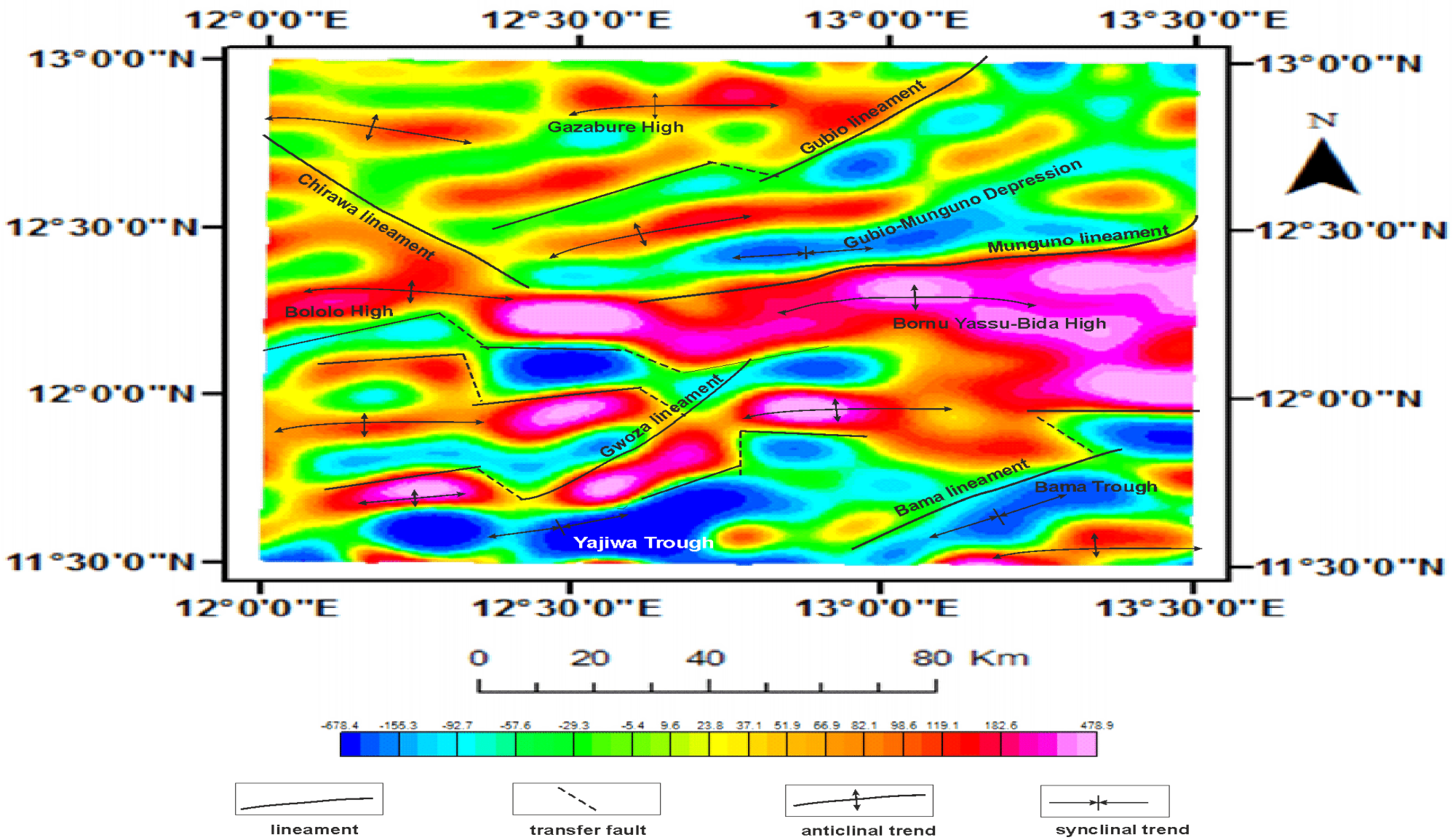

Fig 6.13 Magnetic basement lineaments showing the main NE-SW normal faults in relation with the NW-SE faults forming transfer faults from the 5 km downward continued magnetic data. The figure is a subset of Fig 6.11. Data is focused to smaller area for detail analysis.

6.7 Structural lineaments orientations

6.7.1 Major NE-SW trending lineaments

The dominant northeast – southwest (NE-SW) trending structural systems are continuous and linear in the north-eastern Bornu basin. Rose diagrams show that the NE-SW trend is more predominant in the magnetic data showing the overall magnetic lineaments predominantly trending NE-SW (Fig. 6.9) reflecting the magnetic basement truncations at the negative anomaly features. On the gravity map (Fig. 6.12), the Gubio lineament bifurcates the eastern side of the Gazabure High and the western side of the Gubio-Munguno depression. Its corresponding Monguno lineament is the most visible elongated lineament that bifurcates the central Gubio-Munguno depression, Lau High and the largest central Bornu Yassu – Bida High (Fig. 6.10). Gwoza lineament, Bama lineament and Yajiwa lineaments are parallel to sub parallel lineaments bifurcating elongated depressions in the southern area. Bama lineament occurs at the rim of the Bama depression and the Yajiwa lineament discernible on the magnetic maps bifurcates the Yajiwa depression (Fig. 6.10). In addition to these main parallel to sub parallel lineaments, several other shorter lineaments trending NE-SW are identified within the area corresponding to different deformation regimes.

6.7.2 Major NW-SE trending lineaments

Major parallel to subparallel NW-SE trending lineaments (Fig. 6.8 and Fig. 6.9) from aeromagnetic and gravity data and discontinuities identified are part of the regional deformation fabric in the basin. The lineaments identified are also commonly defined from the bounding anomalies described earlier. Gazabure lineament extends southeast and obliquely intersecting the Gubio lineament, which together they defined the Gazabure high. The Gazabure lineament extends southeast perpendicular to the Gubio – Munguno central depression. Chirawa lineament and its adjoining parallel

Bololo lineament engulf the Bololo High. Ai lineament occurring at the north-eastern rim of the Kusur-Ai High is apparent on the Bouguer gravity Figure (6.12) and the TMI map Figure (6.11). It is observed that the overall frequency of NW-SE trending lineaments appeared low on the magnetic maps compared to the lineaments from gravity map. However, the lengths and frequency of the NW-SE lineaments indicate that they are the second most dominant trends in this area. Apart from the major NW-SE trending lineaments identified, other short NW-SE trending lineaments are mapped on the Bouguer gravity and regional magnetic maps but are not apparent on the magnetic data downward continued through to 5 km (Fig. 6.13).

6.7.3 Other lineament trends

Several other minor lineaments trending E-W, N-S and NNE-SSW directions (Fig. 6.8 and Fig. 6.9), are interpreted mainly from the Bouguer gravity and the TMI maps. These minor groups of lineaments are not discernible at the deeper levels from downward continued map (Fig 6.13). Nevertheless, NNE-SSW lineaments are considered the third most dominant group in the study area. The N-S trending lineaments are detected only on the Bouguer gravity map but not identified on the TMI map. The E-W direction lineament trend in the study area appeared on all the magnetic maps Figures (6.8 - 6.9). The subsurface analyses of gravity and magnetic datasets are presented on larger scale to take account of the wider spectrum of the subsurface tectonic setting assuming that the local geological setting evolved from the broader subsurface deformation. The lineament trends indicate that different palaeotectonic movements have intensively affected the study area. Combined gravity and magnetic lineament map showing geospatial relation as assembled in GIS shown in (Fig. 6.14).

Generally, although the 2-D seismic datasets has low resolution, which could be due to inadequate processing or noise effects particularly at the upper seismic signals within the uppermost and post rift Chad Formation, few of the basement faults have been propagated upward through the overlying Cretaceous deposits by reactivation and rejuvenation and are reflected on the surface. In Section 7.4, detail geospatial correlations of subsurface structures have established relationships between the surface lineaments mapped in Landsat 7 ETM+ mosaic subset and the subsurface basement fault structures mapped from the gravity and magnetic data.

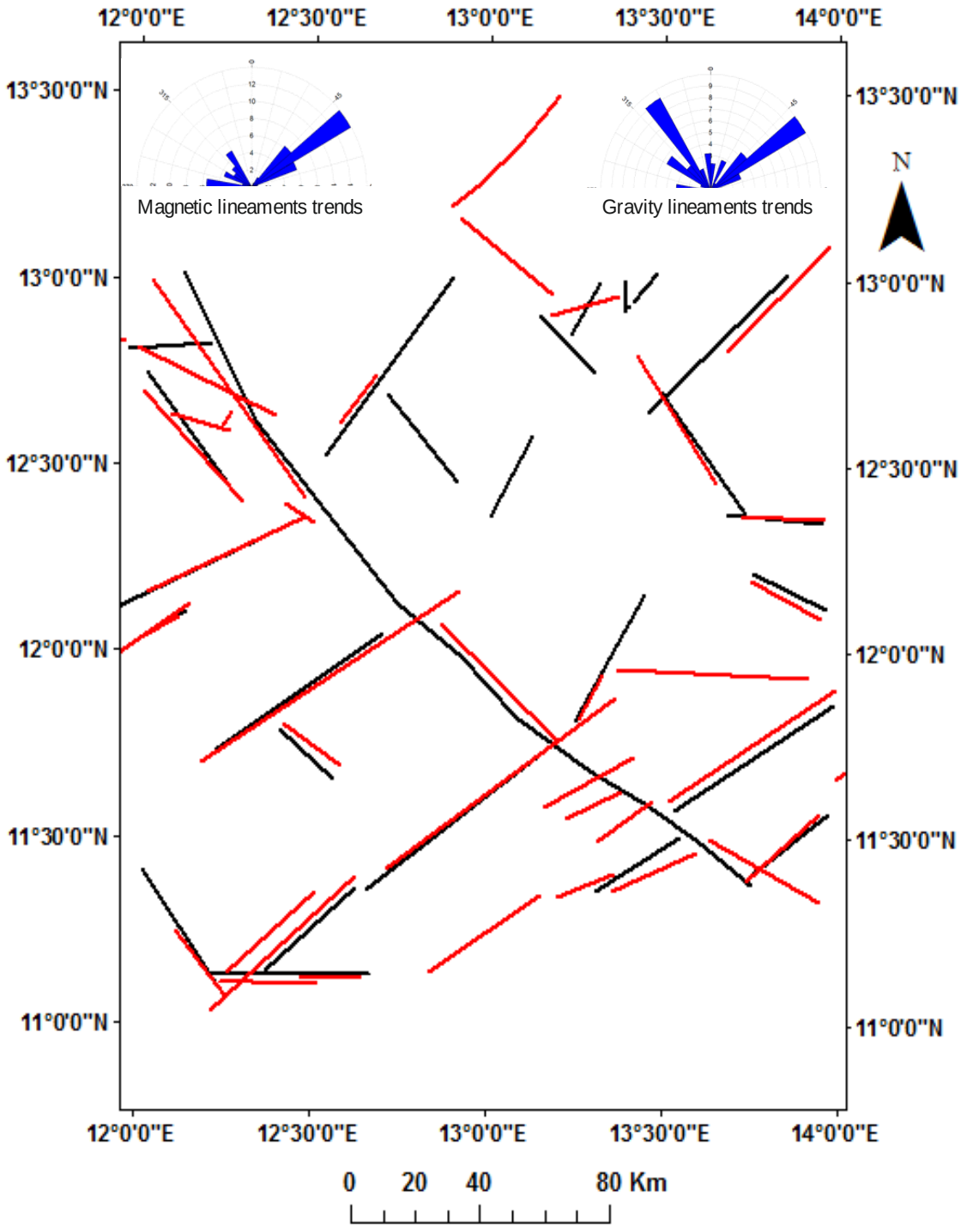

Fig. 6.14. Lineaments same as in Figs. 6.10 and 6.11. Combined herein to form subsurface (basement) lineaments map from gravity (black lines) and magnetic data (red lines) overlain for geospatial correlation in GIS. Insets are Rose diagrams for the individual lineaments from the two datasets.

Chapter 7:

Discussions on the tectono-lithostratigraphic analysis of evolution and hydrocarbon potential of the north-eastern Bornu basin from surface and subsurface geospatial correlation

7.1 Introduction

This chapter provides new insights into the evidence in support of the existing hypothesis of the rift mechanism due to the Cretaceous separation of South America and African continents and the resulting imprints in the Bornu basin. Existing tectonic models for the Bornu basin have been generalised with that of the south adjoining Benue Trough using simple active extensional models that explain migration of the rift axis arising from the Rift-Rift-Fail (RRF) junction. The triple RRF junction comprised of the Gulf of Guinea - South Atlantic - Benue Trough intercontinental separation under the influence of rise and cessation of mantle plumes as proposed by Grant (1971); Avbovbo et al., (1986); Binks and Fairhead, (1992), Genik, (1993) (Fig 2.1).

Previous tectonic interpretations of the regional tectonic framework show that structural trends characterising different tectonic phases controlled the tectonic development of the Bornu basin. In general, Genik (1992; 1993) identified several regional tectonic phases of evolution for the West and Central African Rift System (WCARS) (Fig 2.3). Initially, the Pan African (750 - 550 Ma) crustal consolidation phase established the main pre-existing lineaments and faults within the basement igneous and metamorphic rocks. The basement lineaments controlled the NE-SW rift trend in the Benue - Bornu rift axis of the WARS and the subsequent Cretaceous NW-SE rift trend in the Niger - Air axis (Ajakaiye et al., 1986) with similar trends in the CARS (Benkhelil, 1988). Palaeozoic - Jurassic (550 - 130 Ma) tectonic phase formed a stable platform that was invaded by transgressive sediments (Guiraud et al., 1987). Cretaceous (130 - 98 Ma) main rifting phase occurred in response to the initial

separation of the African and South American plates and the evolution of the WCARS. The opening of South Atlantic started with wrench faults extending from South America through the Gulf of Guinea into Africa. Intercontinental Romanche and Chain faults are controlled by the pre-existing openings formed during the Pan African Orogeny Cratchley et al., (1984). Extensional rifting of the Niger - Chad axis, followed Transtensional faulting in the WARS at the Benue - Bornu axis. All the WCARS basins were developed following a new rift phase in the Maastrichtian-Palaeogene (75-30 Ma). The last major tectonic rift phase existed from Palaeogene to Recent with uplift and erosion of volcanic masses in Cameroon - Nigeria border regions (Genik, 1992; 1993) (Fig. 2.2).

However, the existing models did not establish the influence of structural lineaments on the Cretaceous rifting in Bornu basin using correlated multiple subsurface data analysis to enable more understanding into the tectonic setting of the basin and its hydrocarbon prospectivity within the regional WARS framework. Additionally, the previous studies did not compare geophysical and the Earth Observation interpretation for the north-eastern Bornu basin to investigate association of the surface and subsurface structural patterns and the lithostratigraphy.

The methodology and analyses of the surface and subsurface lineaments and lithostratigraphy of the north-eastern Bornu basin are already presented in the previous Chapters 4, 5 and 6 in this thesis. In this chapter, various georeferenced map results of the surface and subsurface data analyses including lineament maps obtained from satellite observation and geophysical datasets overlays (Fig. 7.1, Appendix D) are geospatially integrated in a GIS to visualise and constrain the tectonic implications of the litho-stratigraphy and structures on the hydrocarbon prospectivity in the basin. The Figure (7.1), shows the spatial coverage of all the datasets used in this work, which shows that datasets are not disjointed or out of

place. However, the figure shows slight disparity only in extents of the geographical coverage of the regional gravity and magnetic datasets, which is an advantage for situating the geology identified from the constrained well log and seismic within the wider basement tectonic framework of the area. Thus, the chapter aims at constraining the rift setting in the Bornu basin in comparison with the regional tectonic framework of the West and Central African Rift System (WCARS) basins. Quaternary development of the Bornu basin in relation to the characteristics of surface lithology and landforms and their relationship with the structural setting of the basin is presented.

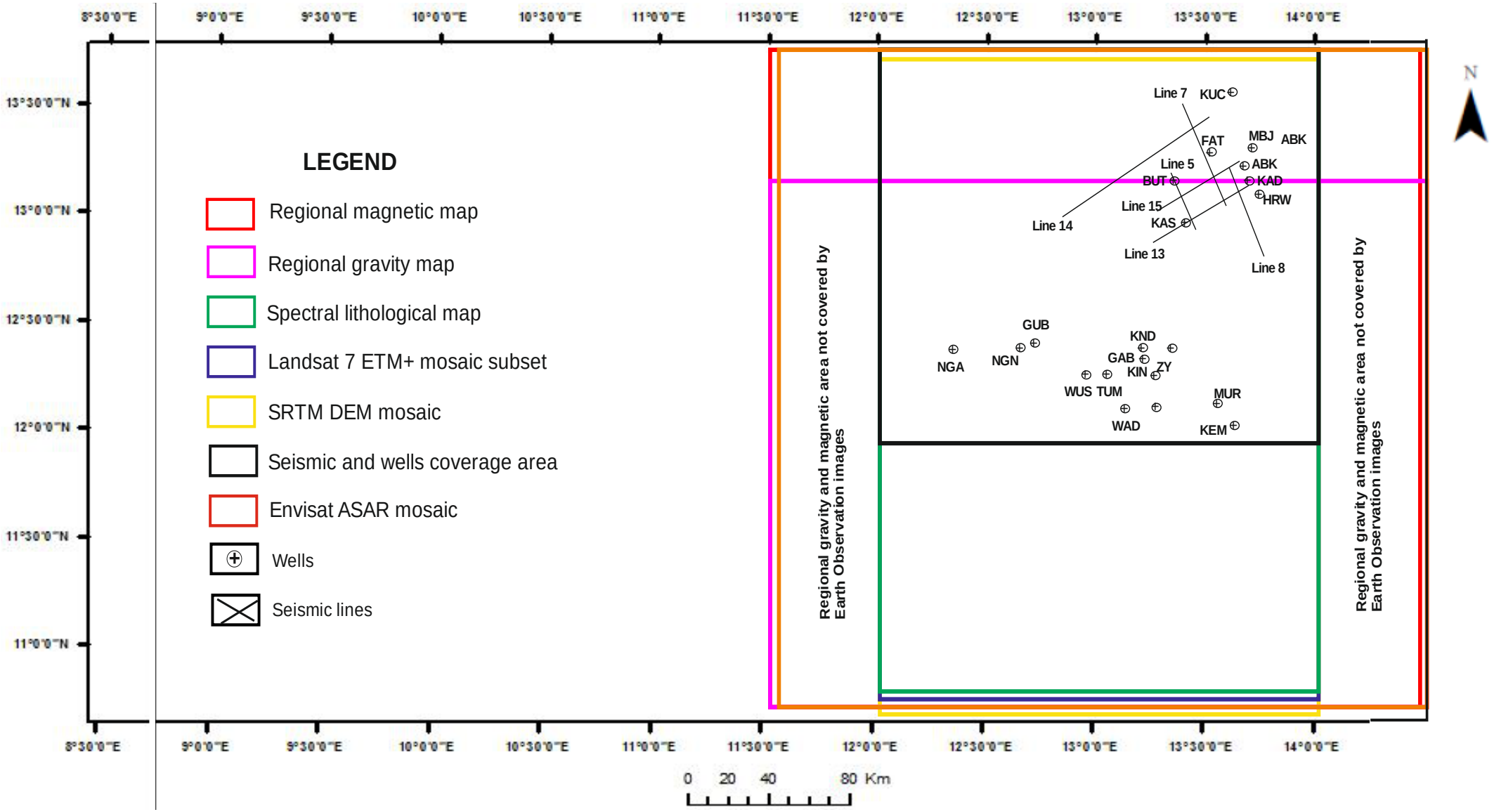

Fig. 7.1: GIS overlay map of the multiple datasets for georeferenced data correlation analysed herein showing extents of the datasets used in the north eastern Bornu basin within the outline of the entire limits of the Bornu basin as defined by Olugbemiro (1997). Insert are the wells and seismic lines as presented in fig. 5.1. Note that Earth Observation maps have exact outlines, while regional gravity and magnetic maps (which should be larger, for regional analysis) have small mismatch at upper portion of the gravity layer. However all seismic and well log data are covered within all maps. this allows for valid geospatial correlation of features.

7.2 *Combined subsurface expressions of structures and stratigraphy*

Delineations of the fault bounded subsurface structural highs indicate that they controlled the Late Cretaceous deposition in the basin. From previous studies, only discreet high angle short normal fault systems were mapped in the basin from seismic data by (Avbovbo et al., 1986; Genik 1992, and Okpikoro and Oluronniwo, 2010). The existing well log and 2-D seismic data for the north-eastern Bornu basin used for this research as well as additional segregated ditch cutting samples obtained from few wells were used variously by several workers to study the subsurface stratigraphy of the basin. Nonetheless, this study confirmed findings from the some previous studies including Okosun (1995); Olugbemiro et al., (1997) Obaje et al., (2004); Moumouni et al., (2007); and Obaje (2009) that suggested the non-occurrence of Gombe Formation and Kerri-Kerri Formation in the north-eastern part of the basin. The present study thus support the existence of four stratigraphic units including Bima, Gongila, Fika and Chad Formations in the north-eastern part of the Bornu basin as penetrated by the wells drilled within the basin (Figures 5.4 - 5.5, 5.10, 5.12, 5.16, 5.18, 5.20, 5.22 - 5.26).

Due to the lack of surface outcrops in the north-eastern part of the Bornu basin, previous studies simply generalised the geology of the south adjoining Gongola Basin in the Upper Benue Trough with the entire parts of the Bornu basin. Adepelumi et al., (2012); Avbovbo et al., (1986); Hamza and Hamidu (2012), identified the existence of Gombe Formation and Kerri-Kerri Formation in the southern part of the Bornu basin extending from the Benue Trough in the southern boundary and extending into the north eastern part. Earlier, Miller et al., (1968) and Burke (1976) initially suggested that the Kerri-Kerri Formation, which directly underlies the Chad Formation as well as the subsequent underlying Gombe Formation found in southern part of the basin, may have pinched out and have not extended towards the Lake Chad area in the north-

eastern region. Accordingly, stratigraphic interpretations herein show that sedimentation in the Bornu basin is not the same as that in the south adjoining Benue Trough.

Well sections in (Figs. 5.4 – 5.5), which showed the uppermost Chad Formation as the thickest layer was also indicated on seismic sections having strong seismic reflections representing possible internal sequences and parasequences. The possible existence of internal sequences and parasequences may support the findings that the Chad Formation can be further subdivided into upper, middle and lower layers (Miller et al., 1968; Isiorho and Nkereuwem, 1996). Adepelumi et al., (2012) used gamma ray log and resistivity log and identified seven stratigraphic successions that include an undefined basal Pre-Bima Formation, Gombe Formation and Kerri-Kerri Formation in the north-eastern area. Although, bedrock outcrops in the area were widely reported as scarce, integrated subsurface study using several different datasets to validate the subsurface stratigraphy were not previously carried out. The stratigraphic units in the north-eastern area as interpreted by Avbovbo et al., (1986) used disjointed 2-D seismic datasets. However, in this study, the integrated well log and seismic data analyses have indicated stratigraphic successions in the basin including their depths, thickness and lateral variations. The new Combined Log Pattern (CLP) method in Section (5.2.1) and (Appendix B), which utilises combined well log data analysis, validated with seismic stratigraphic analysis has established the synergistic relationship between the different well log and seismic datasets. The strength of the CLP method adapted from (Krassay, 1998) that used only GR log and Resistivity log is improved herein by including Bulk Density and Sonic logs to correlate corresponding responses between the several log types at same depths in order to increase facies predictability and improve reliability of stratigraphic correlation. Nevertheless, stratigraphy of the north-eastern Bornu basin in this study relied on the

background knowledge of the general stratigraphy of the entire basin obtained from field mapping, rock core and rock cuttings. This is a limitation of the CLP method especially in areas with previously unknown stratigraphy that need to be fully validated from the indirect subsurface measurement of the lithology using well log and seismic data. Moreover, the well log data is limited by quality as several data breaks are recorded in some of the wells. As seen in (Fig. 5.1), Masu and Krumta wells are so poor that they are not included in the analysis. The well log data is limited by geographical coverage as well, as the data is restricted only to the north-eastern part of the study area, which did not cover the entire study area to allow for wide coverage. However, basin architecture and subsurface topography as revealed by the well log sections consist of thick depocenters or mini basins flanked by low relief areas (Figs. 5.4 – 5.5). The depocenters identified on the seismic sections indicate basement controlled deposition. As interpreted from seismic Line_13, Kasade_01 (KAS) well, bottomed over a “bulging” horst feature, which accounts for the absence of the basal Bima Formation in the well. Absence of the Bima Formation in Kasade_01 (KAS) well and Bulte_01 (BUT) well is because the wells have not penetrated the basal Bima Formation that was mainly deposited within grabens (Fig. 5.10). The correlated well log interpretation has identified environments of deposition for the subsurface facies units in the north-eastern Bornu basin, which generally agrees with the inferences by Okpikoro and Olorunniwo (2010). Although intact rock core samples provide direct physical contact with the subsurface lithology, well log data used herein provides continuous indirect digital in-situ record of the subsurface than obtained from cores. Similarly, well log data provides more reliable continuous in-situ rock record with depth, for more accurate stratigraphic reconstruction than the segregated and disturbed samples of ditch cuttings used by previous workers including Hamza and Hamidu (2012) in the basin.

Similarly, the 2D seismic datasets are constrained by lack of spatial coverage compared to all the other datasets used in this work. This prevents structural continuity to be mapped and correlated with the other data. Another limitation that affected the seismic stratigraphic and structural analysis is the reduced spatial resolution of the 2D seismic data, which makes tying seismic reflections and smooth tracking of seismic horizons difficult.

The combined subsurface basement structural map interpreted from gravity and magnetic datasets displays a swarm of regional lineaments forming linear, curvilinear, anastomising intersections and alignments (Figs. 6.14, and 7.4). The subsurface lineaments correlations show lineament trends in several directions, however, the NE-SW and NW-SE trends remain predominant, reflecting regional pre-existing basement crustal structural origin. However, the map shows moderate alignments between the major gravity and magnetic lineaments with truncation occurring predominantly between NE-SW and NW-SE trending lineaments showing consistent relations, while the secondary trends are represented by N-S, E-W, NNW-SSE trends. There are indications of relationship between interpreted lineaments in the deeper subsurface with the outcropping Bama lineament zone (Figs. 7.2 – 7.3), due to the presence of the NW-striking lineaments adjacent to the Bama lineament zone where NW-striking basement transfer faults occurred.

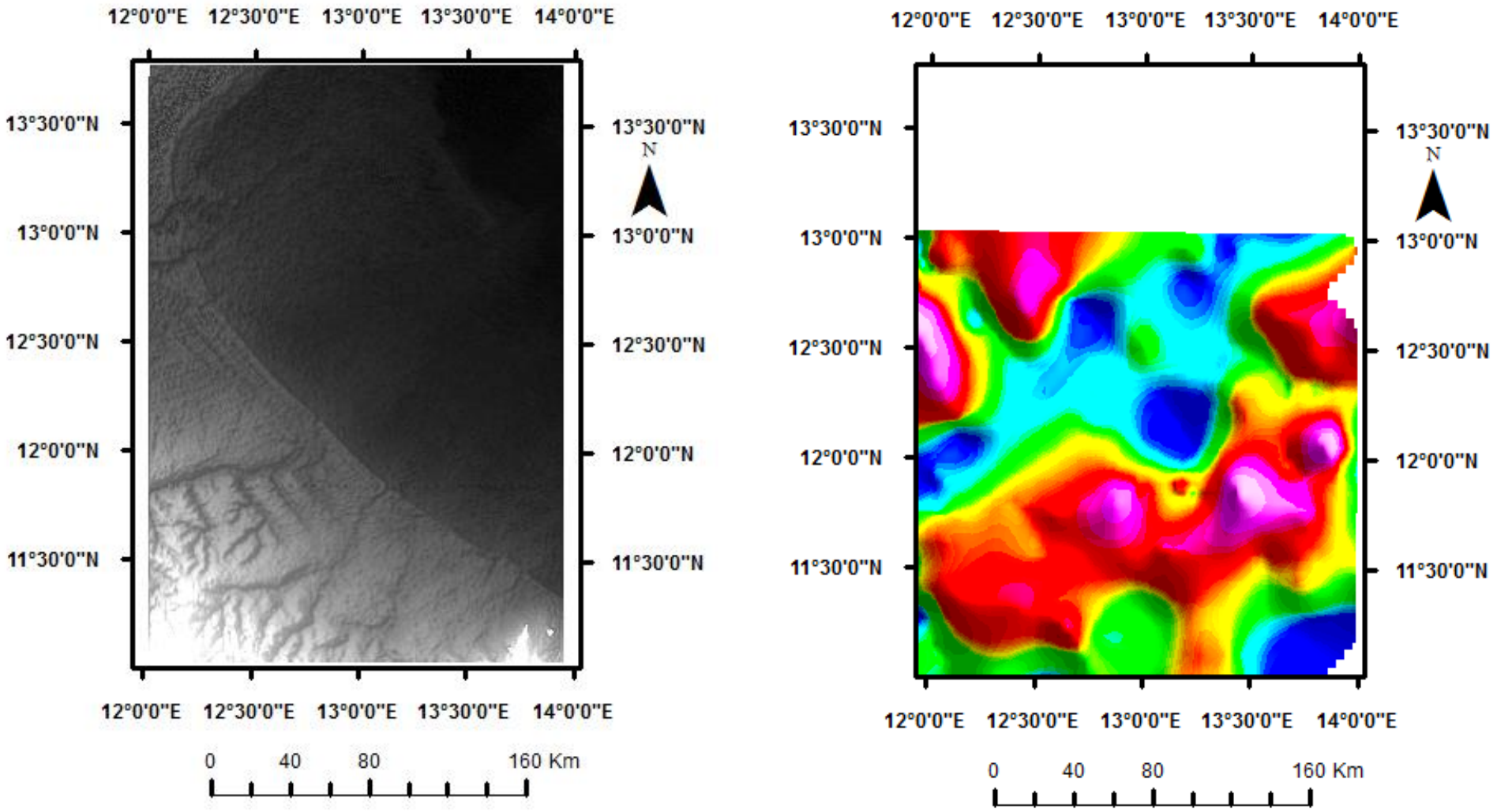

Fig. 7.2 a,b: Uninterpreted SRTM DEM hillshade same as Fig. 4.24 and the gravity anomaly map respectively compared for georeferencing of structures in GIS

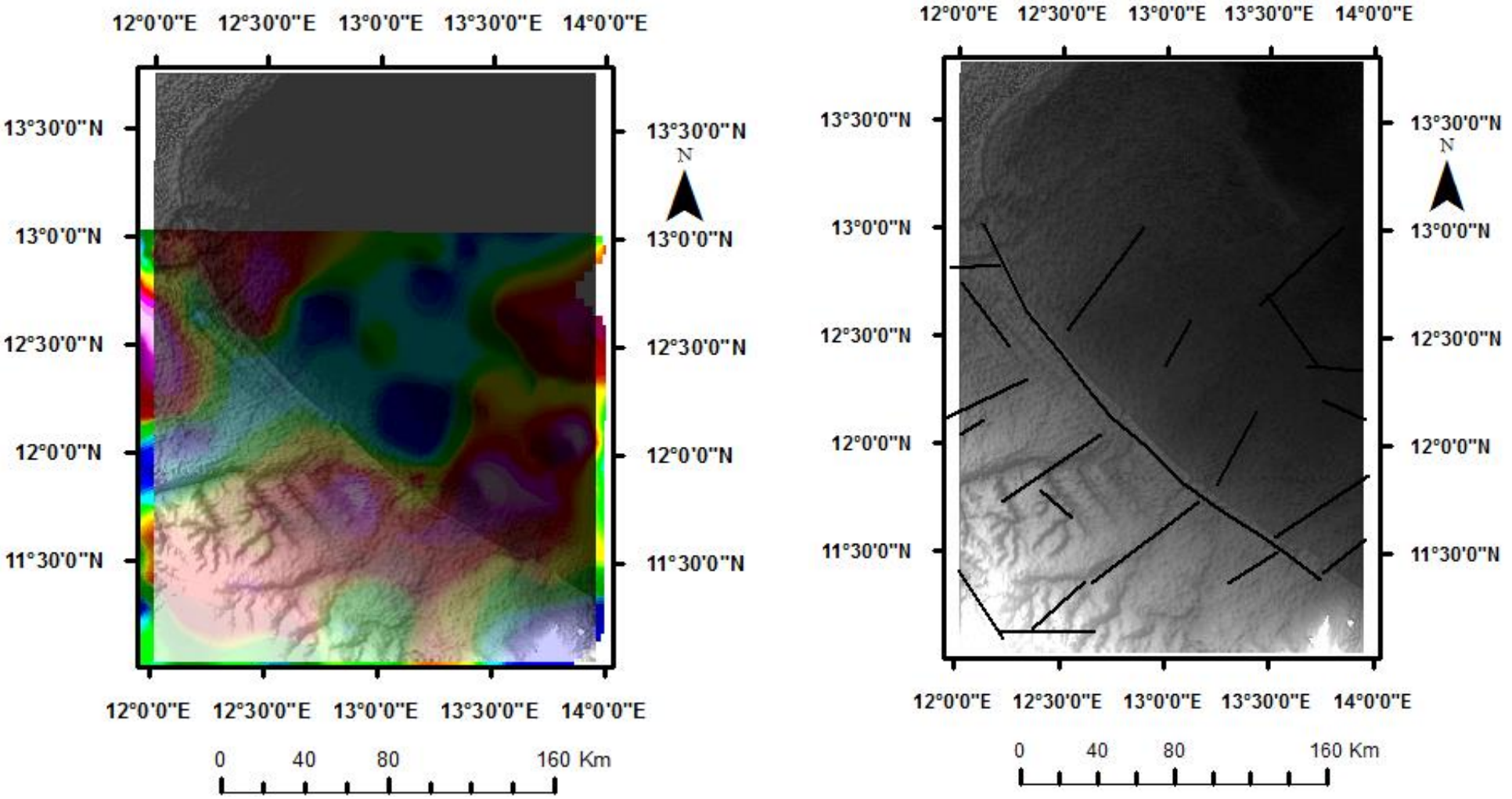

Fig. (7.3 a,b): (a) SRTM Dem hillshade overlain on gravity anomaly map in GIS showing alignment of the NW-SE trending Bama Beach Ridge with basement structural setting (b) Gravity lineament layer overlain on the SRTM DEM hillshade map showing correlation of the Bama Beach Ridge palaeoshoreline with the gravity lineaments. Geospatial boundary of the palaeo-rivers (Fig 4.23) in the southwestern boundary of the SRTM DEM corresponds with the structural boundary of the gravity high anomaly and the gravity lineaments.

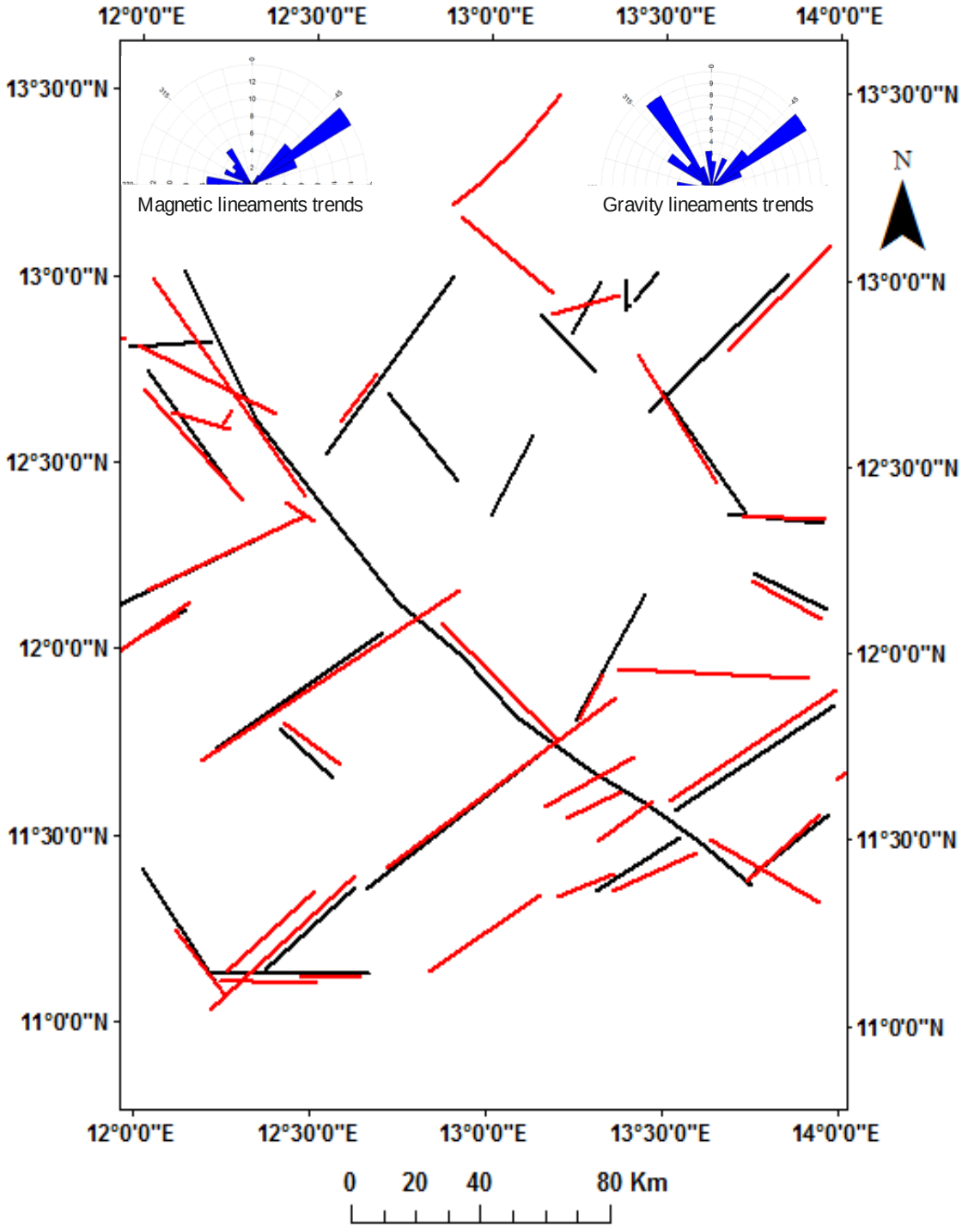

Fig. 7.4 Combined subsurface lineaments map derived from gravity (black lines) and magnetic data (red lines) showing subsurface (basement) structures in the study area. Insets are Rose diagrams for the individual lineaments from the two datasets. Same as Fig. 6.14.

7.3 *Development of new pre-rift to post-rift tectonic evolution model for the Bornu basin, from basement to surface perspective*

Review of our current understanding of the tectonic evolution and geological aspects of the Bornu basin within the context of the regional West and Central African Rift System (WCARS) basins following the Cretaceous separation of the African and South American continental plates is already presented in sections 2.1, 2.2, 2.3 and 7.1. This section however, demonstrates how this research improves our understanding of the tectonic development of the north-eastern Bornu basin using new integrated surface and subsurface data interpreted herein.

Extensional rifting played significant role in the tectonic development of the West African Rift System (WARS), which includes the Bornu basin during the Cretaceous (Grant 1971; Avbovbo et al., (1986); Genik, 1992; 1993). Accordingly, the Bornu basin tectonic system is traditionally thought of as having been affected by the rift extension without details on how; (1) the pre-rift basement controlled such tectonic movements, (2) roles of the pre-existing basement lineaments, (3) discovery, origin and role of transfer faulting, as well as (4) reactivation and upward propagation of faults**.** Thus, the significances of the effects of these four geological aspects were previously not determined. This led to many previous generalisations in geological interpretations, in part because of the use of specific single data and not a combination of multiple datasets in a geospatial analysis, which reduces uncertainty and enhances validity of geological interpretations.

The development of a new extensional basin model for the Bornu basin from pre-rift to post-rift tectonic regimes using the basement to surface perspective is suggested herein using inferences from results of the previous chapters of this thesis.

7.3.1 Role of pre-rift basement

The role of basement tectonics was neglected in previous tectonic evolution models of the Bornu basin as presented in Avbovbo et al., (1986); Genik, (1992) and Genik (1993). However, the tectonic analysis in this study shows that deformation in the basin was not entirely syntectonic as established in the previous studies. Evidences from this integrated approach indicate that rifting in the north-eastern Bornu basin shows more widespread basement control. The basement tectonics consisting of the rift related extensional faults formed parallel – sub-parallel and conjugate fault patterns in the basin as revealed from gravity and magnetic subsurface interpretations (Figs 6.10 – 6.13). McKeinzie, (1978) Pure Shear model of rifting supports the extensional setting in the north-eastern Bornu basin where ductile lower crustal thinning occurs below the rift surface, related to the stress field activated from the hot and buoyant mantle plume that initiated the rifting. This led to asthenospheric bending of the lithospheric layer and form dome shaped topographic elevation, over which radial fractures developed into rifts. The lithospheric layer that became thinned from below, thermally and mechanically began to propagate rifts from the upwelling dome. The pre-existing basement faulted blocks, were modified by the rifting in the Bornu basin and controlled to large degree, the subsurface topography and basin architecture (as revealed from gravity and magnetic subsurface interpretations (Figs 6.10 – 6.13))., which in turn controlled the subsequent structures that originated from the pre-existing pre-rift basement and subsequent sedimentary deposition.

However, combining gravity, magnetic, seismic and well datasets for the north-eastern Bornu basin herein allowed individualising vertical and lateral variations in the subsurface structure and lithostratigraphy of the basin. Evidence from combined well analysis showed wells having variable depths (Figs 5.4 – 5.5). However, tying a well to

the seismic revealed that low depth wells actually bottomed over basement horsts (Figs. 5.4 – 5.5). Similarly, the gravity and magnetic structural maps (Figs. 5.8 and 5.10) revealed that many different palaeotectonic movements have intensively affected the basement rocks underlying the basin. The extensional WARS segmented the basement rocks of the north-eastern Bornu basin into orthogonal blocks at various scales (Fig. 6.7). In seismic sections, spatial distribution of the individual graben sub-basins, formed during the Cretaceous rifting shows intimate structural relationships to the basement fault boundaries. Geometry of the basinal areas revealed in the gravity map are controlled by the continental scale basement fabric and associated faults, which probably rejuvenated and rotated the basinal areas to positions parallel to the basement axial directions (Fig.6.7). Individual basement blocks became asymmetric and bounded on both sides by the conjugate parallel to sub parallel NE-SW and NW-SE faults (Fig. 6.12).

The basement rocks of the north-eastern Bornu basin characterised by adjacent blocks bounded by fault zones commonly display mutually offsetting relationships. Adjoining sub-basins are commonly controlled in size and orientation by the basement fault zones with mainly three large blocks separated by the fault zones. Overlay of gravity and magnetic basement lineaments shows parallel relationship with various degrees of overlapping are evidence of extensional faulting that divided the main basin into sub-basins or depocenters where thick sedimentary deposits were overlaid.

The extensional faults that led to stretching and thinning of the continental crust formed broad active intra-continental rift. In addition to the various basement blocks identified from the gravity, magnetic and seismic interpretations, further evidence from the well log stratigraphic cross sections and isochron thickness maps (Figs. 5.27 – 5.29) validated presence of the sub-basins adjoining the structurally high areas.

Specifically, in (Fig. 6.12) the Gubio-Munguno Rift Zone lies along a dislocation zone between elevated basement flanks that are represented on the gravity map by the Bornu Yassu-Bida/Lau margin on the eastern side and by the Bololo/Gazabure margin to the west. The main Gubio-Munguno Rift zone is bifurcated by the largest Bornu Yassu-Bida NE-SW trending basement block and the Gubio block trending NE-SW parallel to the main basement structural fabric in the area. Similarly, NE-SW orientation of the Gubio-Munguno Rift Zone is in agreement with the major NE-SW structural trend of the lineaments in the area. Furthermore, the Gubio-Munguno Rift Zone encompasses several sub-basins including the Maiduguri Trough in the south, while the north-eastern end of the rift zone merges with the Bornu basin's NE axial drainage bordering the present day Lake Chad. The general trend of the Gubio-Munguno Rift Zone is perpendicular to the regional NW-SE extension direction that affected the Bornu basin as earlier indicated by (Genik, 1993) (Fig. 2.4). Well log cross sections (Figs, 5.4 – 5.5) and isochron maps Figs 5.27 – 5.29) showing the undulating subsurface topography and stratigraphic thickness, imply presence of the rift features in the area and the thickest overlying sediments were deposited over the rifted fault blocks. This structural arrangement is more prominently identified on the gravity map as well as on the magnetic maps (Figs. 6.11 and 6.12).

Thus, the Lake Chad - Gubio-Munguno rift axis is herein regarded as a down-to-the-east major graben structure having the greatest subsidence in the study area. Interpreted seismic sections 13, 14 and 15 (Figs. 5.13, 5.16, 5.18, 5.20) that run parallel to the axis of the Gubio-Munguno rift zone (Fig. 6.12) validate the gravity and magnetic maps by indicating the deepest continuous seismic reflector dipping toward the Lake Chad area. More so, the seismic lines 13, 14 and 15 display relatively more deformation in comparison to interpreted seismic lines oriented across the rift zone

(seismic lines 5 and, 8) (Figs. 5.13, 5.22). Similarly, the seismic stratigraphic horizons tend to thicken toward the downslope of the rift zone while the down-to-the-basin faults tend to become listric at depth beneath the Bima Formation (Fig. 5.18).

This implies that the Early Cretaceous rift extension originating from the basement rocks trending in NW-SE direction apparently provided the opening direction for the perpendicular main NE-SW trending Bornu basin rift zone. (Cratchley et al., 1984) suggested that sediments compression in the south adjoining Benue Trough into long folds parallel to the rift boundaries began in the Santonian into the southwest of the Benue Trough and reached the Middle Benue by the end of the Senonian. This occurred at the same time that marine deposition was continuing in the Upper Benue, the Gombe and Maiduguri troughs in the north-eastern Nigeria during an anticlockwise rotation of the basement blocks of Northern Nigeria during the Senonian as earlier suggested by Guiraud and Borsworth, (1997).

However, the inference that magnetic and gravity lows indicate buried rifts can be distorted by the potential basement causative sources this suggests that basement causative sources contribute in forming the anomaly patterns produced by the basin geometry. 2-D combined gravity and magnetic data modelling can help further resolve the limitations of the gravity and magnetic datasets, as the observed gravity anomalies may reflect the lateral variations of basement rock density. Similarly, the aeromagnetic anomalies reflect lateral variations of the total magnetisation may include induced and remanent magnetizations in the rocks.

7.3.2 Role of pre-existing (pre-rift) basement lineaments

Ajakaiye et al., (1986) proposed that basement lineaments controlled Cretaceous NW-SE rift trend in the adjoining Niger - Air axis and the NE-SW rift trend in the Benue - Bornu rift axis of the WARS. Predominance of the NE-SW and NW-SE faults systems resulted from the Early Cretaceous initial rift movements in response to the continental separation. However, from the integrated analysis carried out herein, it is deduced that, three additional regional stress regimes that might have affected the structural architecture of the north-eastern Bornu basin area include;

(1) The main NE-SW directed tensile stress from the breakup of the Gondwana, led to the propagation of sub-parallel NW trending Mesozoic rifts faults in the WCARS and subsequent opening up of the NE-SW Bornu basin, (2) Late Neocomian – Barremian NW-SE – directed tensile stress associated with the orthogonal opening of the main Benue Trough - Bornu basin rift. Consistency of the NE-trending lineaments in the Benue Trough - Bornu basin rift have already been established by Ajakaiye et al, (1986) and Guiraud et al., (2005) however, without details of the origin and orientation of the palaeotectonic stress directions from integrated data analysis. (3) Late Cretaceous - Quaternary fault reactivation and upward propagation of pre-rift lineaments into the post rift strata and formation of regional scale surface lineaments (Fig. 7.14). However, occurrence of the Quaternary surface lineaments at the fringes of the Bornu basin and the Lake Chad are already been established in Isiorho et al., (1992), without details of the origin and orientation of the neotectonic stress directions. Since each of these structures were generated in distinct time intervals under different tectonic conditions, a new tectonic model of evolution of the Bornu basin presented in this research defines the origin of the different fault set geometries than previously presented.

Aydogan et al., (2013); Dufréchou et al., (2014) Rodríguez et al., (2016) have carried out structural analyses of lineaments mapped from gravity and magnetic anomaly maps. Similarly, surface mapped lineaments can determine the kinematic and dynamic structural settings of basins (Solomon and Ghabreab 2006). Accordingly, inferences from the gravity, magnetic, Landsat 7 ETM+ and seismic datasets analysed in the previous chapters of this thesis, validate the two main faults trends, which dissected the basement blocks in the study area. The NE-SW related stress field most probably represents an older palaeo-stress field while the stress field related to the NW-SE fault set represents a younger one.

Consequently, development of the predominantly north-easterly and north-westerly trending fault lineaments in the north-eastern Bornu basin can be possibly explained using a deformation scenario with the б1 in the vertical direction and variable dominance of the horizontal stress directions. The maximum stress ($б_1$) probably generated the main fault zones perpendicular to the principal stress in a dip slip movement considering the extension direction of the secondary stress ($б_3$) in the NE-SW direction, which account for the shorter NW-SE transfer faults in the north-eastern Bornu basin. Genik, (1993) suggested that the Early Cretaceous phase in the region is characterised by the NW-SE trending faults and the Senonian - Palaeogene is characterised by NNW-SSE trending faults. Later complex association of several fold patterns and strike slip faulting resulted in NW-SE horizontal shortening due to the Late Santonian compression that corresponds with changes in the focal point of opening for the Atlantic Ocean and the major rifting and subsidence that followed the Campanian and Maastrichtian periods (Guiraud and Bosworth 1997).

From observations herein, a mechanism of deformation as it affected the north-eastern Bornu basin is associated with the lineaments rooted in the basement where

the normal faults are bordering the graben or pull apart structures. In the presence of the significant initial extension stress regime in the Bornu basin, the structures opened perpendicular to the maximum stress (б1) (Fig. 7.5) The б1 in the basin is perpendicular to the inferred extension direction as reflected by the basement tectonic deformation and consistent with findings of Fairhead (1988) and Guiraud and Maurin (1992). The apparent listric geometry of the normal faults as seen on seismic sections (Fig. 5.16 and Fig. 5.18), result from closely spaced low displacement faults. The principal compressive stress б1 acting vertically is less than the horizontal tensional stress particularly б2, which acted at right angle to the б1 in opposite NW-SE direction possibly during the Barremian (120 Ma) tectonic extension regime as later explained in section 7.3.3.1. Other secondary faults including E-W, N-S, NNE-SSW were formed gently dipping and rotating eastwards and westwards (Fig. 7.5). Dominant NE-SW structural trend form high angle normal faults observed throughout the study area are seen on both surface and subsurface maps forming orthogonal and conjugate relationship with the opposite NW-SE cross faults. Synthetic faults in close trends and at the vicinity of the main NE-SW faults are the NNE-SSW structures, which appear more prominently on the interpreted seismic sections and surface structural maps (Fig. 4.26). Interrelationships of the diversity of these lineament trends in different directions as observed on the surface structural maps and correlated on the subsurface gravity and magnetic maps, suggest that the Bornu basin was probably subjected to more than one stage of secondary deformation in different directions during the Cretaceous rifting. It is suggested herein that the pre-rift basement structures reflect reactivated faults formed in the Pan African orogenic basement prior to the Early Cretaceous palaeotectonic rifting between the South American and African tectonic plates.

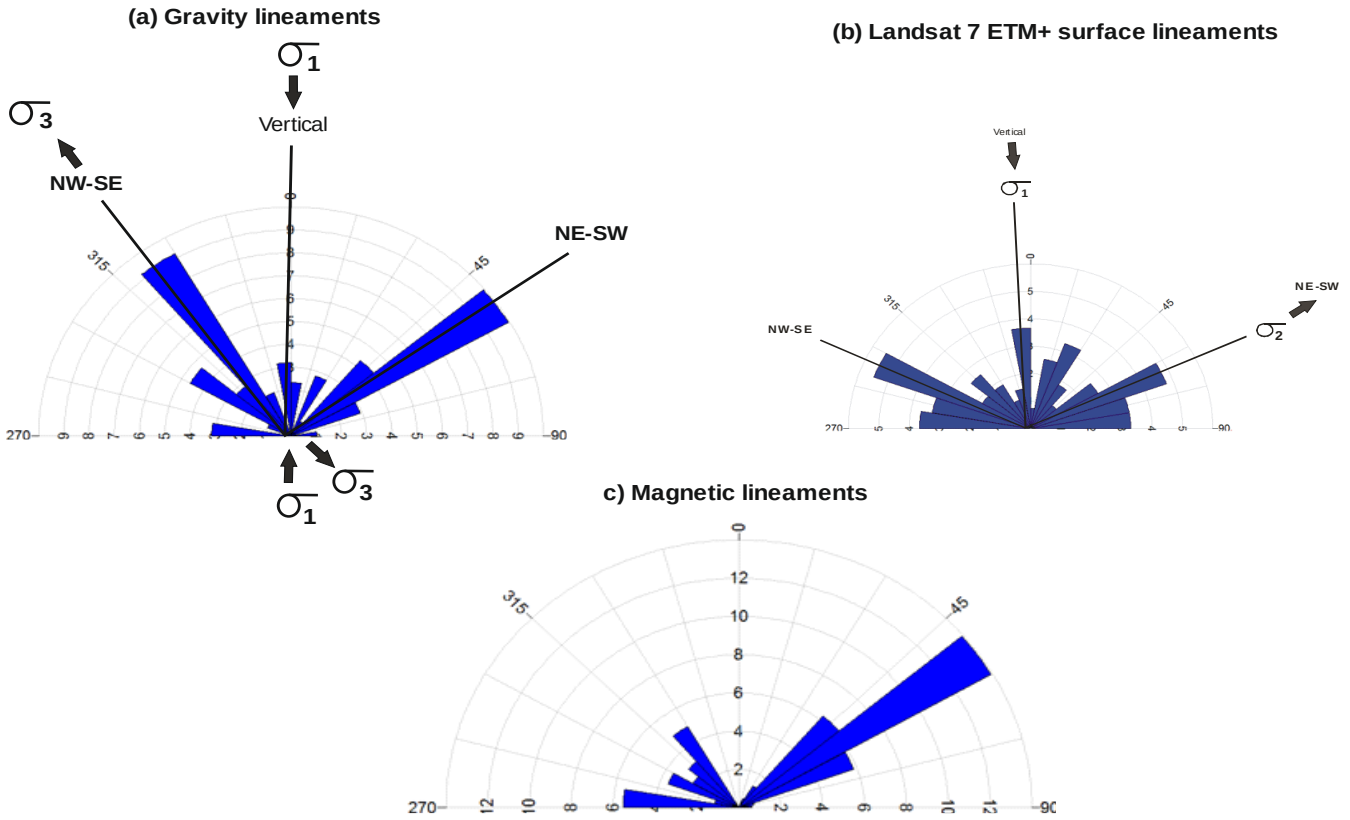

Fig 7.5 a-c: Stress analysis of the extensional rifting in the Bornu basin from the various datasets. Palaeotectonic extension regime showing parallel NW-SE oriented transfer faults that led to the formation of the oblique NE-SW rift. NE-SW neotectonic extension fractures led to the formation of the oblique NW-SE trending rift faults

7.3.3 Genesis and role of transfer faulting in the north-eastern Bornu basin

Cobbold et al., (2001) and Meisling et al., (2001) interpreted transfer zones based on lineament analysis of Bouguer-gravity anomaly maps. Accordingly, the interpretation of transfer fault zones mapped from the gravity map in the Bornu basin permits understanding of the rift architecture of the basin (Fig. 6.12). The alternative evolution model proposed herein explains the genetic relationship of the two main NE-SW and NW-SE structures with other secondary structural trends. The proposed model, (Fig. 7.14) further explains the characteristics of rift related underlying horst and graben system as interpreted from the seismic data and validated from gravity and well log cross sections. The conjugate NW-SE and NE-SW fault lineaments found to be cross cutting each other or terminating against each other suggest that they developed transfer zones between the normal faults within which the crustal extension is accommodated. With further extension, relay ramps developed to absorb the amount of differential displacements into the transfer faults, which transfer extension and tilt the predominant NE-SW eastwards (Fig. 7.6a).

The rotation of the eastern flank of the Bornu basin margin along the Lake Chad/Termit basin boundary during the Senonian, suggests an unequal action of a dominant stress field with the continuing maximum compressive stress oriented vertically and the near perpendicular extension direction of NE-SW. The б3 stress field is expected to locally rotate when approaching the NW-SE extensional faults with б1 rotating to vertical (Fig. 7.6b). However, there are no available regional structural analysis data in the nearby basins and this hypothesis only infers that the palaeo-stress field was extensional with б1 vertical and б3 horizontal in the contiguous Termit basin in Chad and Niger Republics.

In seismic, down-to-the-basin normal faults with associated subsidiary faults dipping in the opposite directions forming antithetic faults are herein identified in the north-eastern Bornu basin. The extensional planar and listric normal fault blocks and transtensional synthetic and antithetic normal fault blocks identified on the interpreted seismic sections (Figs. 5.16 and 5.18) show distributions of major faults at the flexural margins where the antithetic faults are abundant, while the minor faulting is abundant in central rift areas in the full grabens. Boundary fault margins and flexural margins indicate timing between the major and minor faults and suggest that the minor faults were inactive prior to cessation of activity on the main boundary fault. The synthetic faults, which are numerous in the half grabens were affected most by the extension with even mixture of the minor faults in the full graben areas. The extensional faults and cross faults mapped from gravity data were essential for rotation of the main basin axis during deformation.

The south-eastern thrust belt of the Bama depocenter and the Bornu Yassu - Bida high are oriented parallel to a transfer fault that separates the Bama lineament, with similar geometry occurring with the Gwoza lineament (Fig. 6.12, 6.13). According to Morley (1995), transfer zones and rift segments coincide with changes in structural styles as represented by major fault terminations. Accordingly, rift extension probably occurred initially as an association of isolated rift segments of the main extensional system in the basin. The transfer zones in the basin show that a change in geometry occurred that was active at the same time with the extension being transferred across the faults. This change in geometry in the basin representing different tectonic regimes that developed the NW-SE transfer faulting probably occurred in the Barremian (120) Ma between the Neocomian and Aptian – Albian tectonic events of Genik (1993) as illustrated in (Fig. 7.14). Intrabasinal faults found within the Gubio-Munguno

depression observed in the gravity map (Fig. 6.12) are part of minor fault systems in the basin. The Intrabasinal faults are formed at right angle to the extension vector, where the rifting results in the rotation of the basin axis. Such fault evolution supports a model wherein a nearly orthogonal rift generates transverse slip fault zones (transfer zones) and a subsequent rifting changes the mechanism of displacement to a relay ramp fault system (accommodation zones). Relay ramps in the north-eastern Bornu basin that developed between the two contemporaneous segments of the normal fault system represent the complex system of graben and horsts that are oblique to the main fault trend in the basin (Fig. 7.6a).

Thus, based on the structural analysis herein, it is proposed that the origin of the transfer faults are reactivated pre-existing structures, since without tectonic inheritance, it is most likely that all extensional faults in the basin should trend sub-perpendicular to the main NW-SE direction of the main extension. Similar geometries and interpretations have been reported elsewhere for the East African Rift System (Corti et al., 2007; Rosendahl, 1987). Similarly, in the N–S Kenyan Gregory rift, NW–SE to NNW–SSE oblique faults are pre-existing basement shear zones reactivated during rifting (Smith and Mosley, 1993). Similar observations were reported for the Malawi rift where pre-existing basement structures controlled the internal rift geometry (Ring, 1994). Parallelism of these NW-SE transfer zones with the elongated Bama lineament zone (Figs. 7.2 – 7.3) suggests that the Bama lineament zone may have played an important role on the orientation of the transfer fault axes. Basement transverse/transfer faults of which the NW-SE structures occur orthogonal to the main NE-SW structural trend in the basin are

the most significant tectonic structures and are originally identified herein in the north eastern Bornu basin (Figs. 6.12 – 6.13). However, geochronological analysis of structures in the Bornu basin is beyond the scope and objectives of this study, therefore, the age and timing of the lineaments on both the surface structural maps and basement maps are not determined quantitatively.

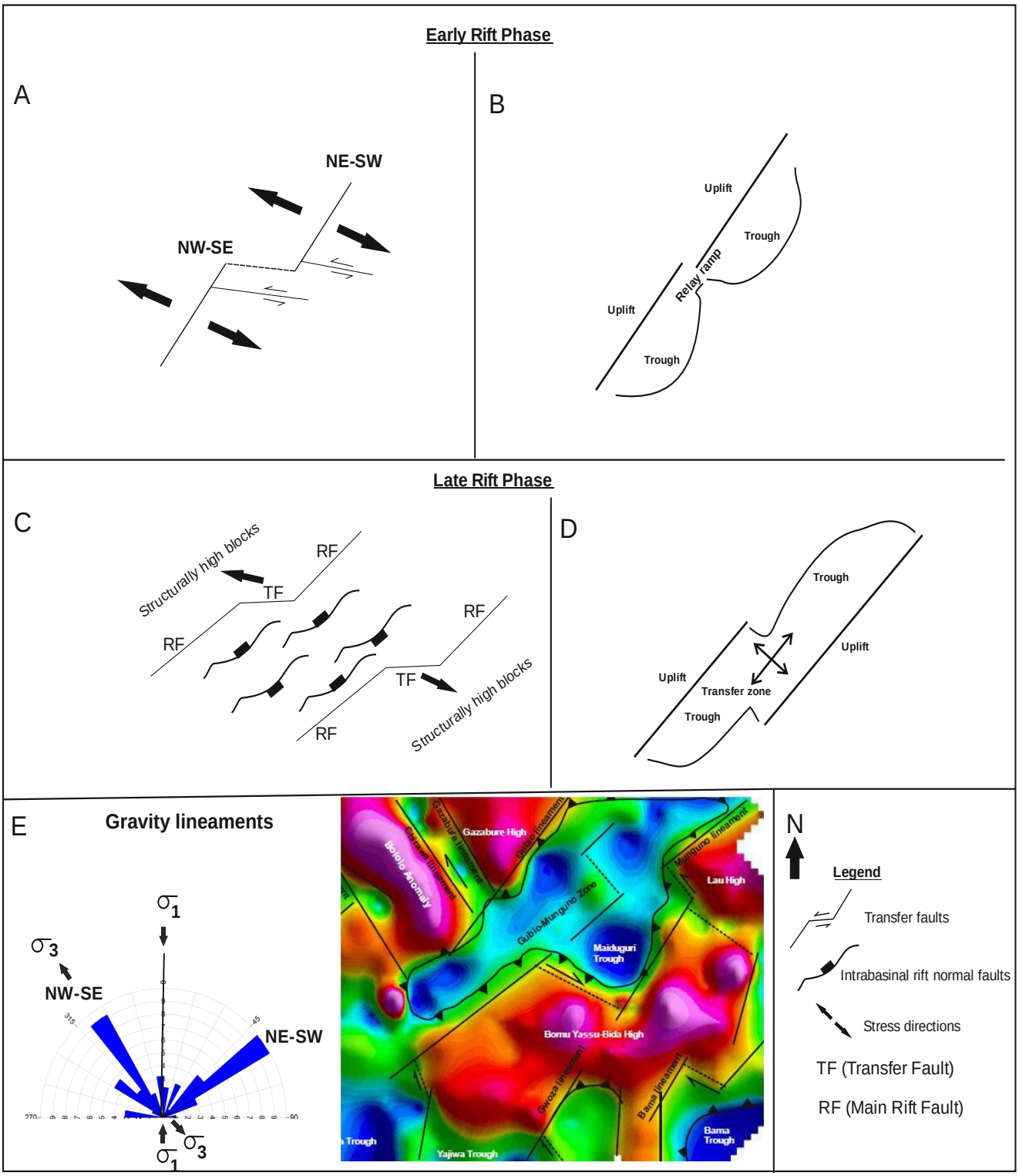

Fig. 7.6a. Sketch of the regional early syn-rift to late synrift stages of the north-eastern Bornu basin showing approximate structural architecture. This sketch shows how this work understands the basement control of the rift setting as well as the Intrabasinal transfer faulting. As the rift axis changes paleostress directions accommodation zones based on relay ramps are formed.

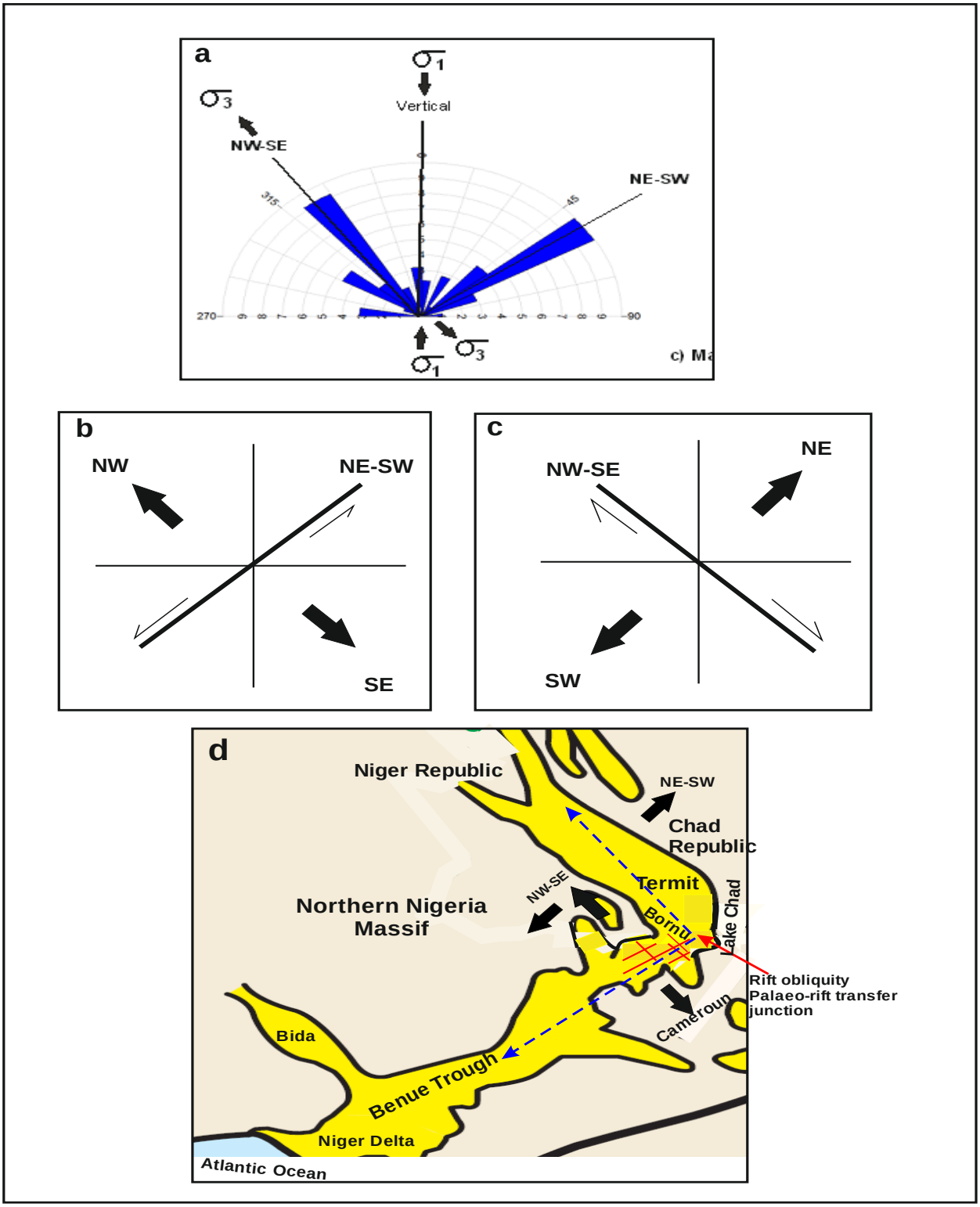

7.6b Sketch diagrams not to scale of fault kinematics and related stress fields in relation to the WARS tectonic framework with emphasis on the two phases of conjugate structural lineaments. with the directions of principal and secondary stress axes(a) All basement lineaments directions as mapped from gravity data, the NE-SW, NW-SE lineaments trends being dominant. (b) NW-SE initial extension direction that opened up the main NE-SW Bornu basin margin. (c) Later NE-SW extension direction that generated the secondary NW-SE lineaments (d) a simplified tectonic map of the Benue-Bornu-Termit rift syatem with few transfer faults shown in the Bornu basin as revealed from gravity, magnetic and Landsat data. Integrated kinematic and dynamic analyses of the two conjugate structural pairs indicating a continuation of NE-SW rift trend in the Benue trough and continuation of the NW-SE rift trend in the Termit basin hinged at the Bornu basin and forming a rift obliquity at a palaeo-transfer junction.

7.3.3.1 Bornu basin – Lake Chad boundary as an intracontinental pre-existing major palaeotectonic transfer fault junction - New insights into the Barremian (120 Ma) and Late Aptian – Early Albian (101 Ma)

Genik, (1993) described different Cretaceous - Recent phases of rifting due to the breakup of Gondwana and formation of the WCARS basins (Fig. 2.4). Since the rift basin represents a zone of lithospheric weakness within the African plate, changes in the plate stress and movement resulted in the deformation. Thus, plate tectonic processes that affect the African plate have been recorded by the tectonic settings of the WCARS basins, which reveal a poly-phase development. However, the Barremian (120 Ma) and Late Aptian – Early Albian (101 Ma) tectonic regimes in the Bornu basin are not identified in the previous studies.

As strike-slip faulting was predominant in the Benue Trough, while NE-SW extension occurred in the Termit basin during the Late Albian tectonic phase. It is suggested herein that the Bornu basin area, which is situated in between the two adjoining Benue Trough and Termit basin, was probably affected by a predominantly NW-SE short-lived extension, which occurred perpendicular to its main NE-SW basin rift trend. It is further understood herein that, Bornu basin's present tectonic location is actually situated at a palaeotectonic rift transfer junction that probably formed in Barremian (120 Ma) tectonic regime. The tectonic movement occurred when the principal compressive stress б1 acting vertically is less than the horizontal tensional stress particularly б2, which acted at right angle to the б1 in opposite NW-SE direction between the NE-SW striking south adjoining Benue Trough rift province and the NW-SE striking north adjoining Termit rift province due to the transfer faulting process (Fig. 7.6 a,b). Apparently, the three individual contiguous (Benue Trough-Bornu-Termit)

basins formed a continuous large graben structure of the continental WARS. The structural linkage between their different extension zones was probably achieved by means of an extension related continental scale palaeo-transfer fault that offers a new tectonic scenario for the extension mechanism and genetic relationship of the Bornu basin hinged between the two adjoining Benue trough and Termit basins (Fig.7.6b). During the Barremian deformation regime, the perpendicular extension fractures developed and opened up the NW-SE Bornu basin margin with several dispersed NE-SW lineaments perpendicular to the axial trend of the Bornu basin (Fig. 7.14). The NW-SE opening up of the Bornu basin margin continued during the Late Aptian – Early Albian 101 Ma, with the basal syn-rift continental deposition.

Evidence from the subsurface data interpretation, herein (Fig. 7.6a) shows that the tectonic style in the Bornu basin linked by a fault system separated by strike slip transfer faulting developed during the rifting process. From gravity maps, it is herein inferred, by analogy and from the occurrence of the extensional NE-SW striking basement bounding faults structures, that the opposite faults were connected to form the major bounding faults of the depocenters, thus determining their sense of symmetry. Geometric characteristics of the intracontinental transfer zone further suggest that intracontinental transfer faults evolved from the pre-rift basement structures. Burke and Dewey (1974) had proposed a possible intracontinental Chad (Bornu) – Chum – Yola triple junction centred at Chum in the Upper Benue Trough in north east Nigeria exist, which is about 600 km up the Benue Trough, where the Chad and Benue arms spread and later closed in the Cretaceous while the Yola arm failed (Fig. 2.3). Arguably, such setting can last through time only if there were continental transverse structures that accommodate the differential opening. As such, based on the present tectonic analysis, it is proposed that the Bornu basin rift domain is a

reactivated pre-existing tectonic margin that separates structurally contrasting Benue Trough domain and the Termit rift domain that was active during the earliest phase of the intercontinental rifting. This distinct separation and difference in structural trends between the adjoining Benue Trough and Termit rift segments further indicates the existence of a tectonic junction, which separates the two WARS provinces. This implies that a major transfer accommodation zone probably existed at the Bornu basin margin in between the two adjoining basins during rifting, that was responsible for the evolution of the perpendicular extension of the Termit rift zone because of the rift obliquity. The two main extensions, which produced the Benue Trough NE-SW rift extension and the NW-SE Termit rift, meet perpendicularly at the Bornu basin-Lake Chad junction. The NE-SW rift trend extends into the adjoining Birni Logoni basin in Cameroon while the NW-SE rift trend extends into the Termit basin in Niger and Chad (Figs. 2.3, 7.6b).

7.4 *Reactivation and upward fault propagation into the synrift to the post-rift sequence - Linking subsurface tectonic lineaments and lithostratigraphy to the surface*

The systematic integration of structural lineaments and lithostratigraphy for tectonic analysis herein is based on the proposition that surface geologic lineaments are correlative with subsurface structural features, which control basin development and distribution of potential fluids including oil and gas (Guo and Carol, 1995; Saadi et al., 2009). Lineament trends from the study area mapped from Landsat 7 ETM+, SRTM DEM, gravity, magnetics and seismic datasets are herein integrated using georeferenced correlations (Fig. 7.1). Although, the seismic and well datasets are constrained by lack of geographical coverage in comparison with the regional gravity, magnetic and Earth Observation datasets used herein for correlation. As such only structures that occur within the geographical coverage of the seismic data are mapped on the seismic time structure maps overlays.

Preliminary validation of the surface lineaments is carried out using automatic and manual digitisation lineament extractions. The lineament zones represent areas of weakness along which increased structural activity occurred. Correspondingly, the predominant NE-SW and NW-SE trends of the surface lineaments and lineament zones (Figs 4.26 and 4.28), which compare with predominant trends of the individual lineaments (Fig. 4.29) are herein regarded as fault zones outlined by series of continuous parallel to sub parallel and oblique structures. Lineaments correlation method includes comparison between the results obtained from computer assisted automatic lineaments extraction and visual extraction methods as established in Harris

et al., (2012) using GIS to validate their geospatial positions as well as their geologic trends (Fig. 4.30).

Lineaments correlation in spatial position is achieved by digitisation, overlaying and stacking of the various surface and subsurface lineament map layers in a GIS, Effectiveness of the integrated structural analysis method shows lineament systems interpreted from various datasets successfully delineated several previously unknown geologic faults in the north-eastern Bornu basin. Orientations of the fault lineaments detected are consistent with the results from previous studies reported by Avbovbo et al., (1986) and Genik, (1993). The lineaments trends also compared well with the previously known tectonic basement fracture patterns in the basin as established in Avbovbo et al., (1986) and Genik, (1992; 1993).

Results herein showing characteristics of post-rift deposition and secondary morphotectonic lineament trends indicate actions of subsequent local stress regime due to basement fault reactivation and upward propagation to surface, which may also in part account for the neotectonic deformation in the basin. This secondary deformation regime constrains the tectonic structure of the north-eastern Bornu basin against the generalised Benue Trough - Chad basin rift extension tectonic setting hypotheses of Cratchely et al., (1984); Avbovbo et al., (1986); Genik, (1992) and Genik, (1993). Overall surface structural geometry of the north-eastern Bornu basin as mapped from Landsat 7 ETM+ data is characterised by the two main groups of fault related lineaments structures. The NW-SE lineaments represent extension faults characterised as normal fault zones perpendicular to the NE-SW basin rift trend. The NW-SE group represents cross-faults, which trend at high angles and offset the main NE-SW fault elements of the basin essentially forming transfer zones. Similar tp the basement structural maps from the gravity and magnetic data, the surface lineament

interpretations demonstrate similar mutual offsetting relationships and lineament intersections. The NE-SW and NW-SE main surface lineament groups are generally longer than the secondary fault systems in the basin. However, the NE-SW trending lineaments probably reflect older subsurface lineaments that were later truncated by the younger NW-SE lineaments (Figs. 4.26, 4.28). This supports the understanding that the surface lineaments were formed by later tectonic reactivation and upward fault propagation during which the additional secondary faults in different directions were induced from the associated local stress regimes. Vertical fault movements controlled by the bounding rift faults are reflected by the patterns of the underlying basement blocks. The lineament architecture observed on the surface structural map (Figs. 4.30, 7.13), is similar with the patterns of corresponding subsurface transfer faults in the underlying basement blocks interpreted from gravity data (Fig. 6.12). The new tectonic model (Fig. 7.14) proposed herein incorporates surface lineament expressions of the basement structural evolution of the rifting process deduced from the integrated data analysis.

Insley et al., (1996) have demonstrated that structural continuity and trends of faults mapped from satellite imagery can be used to constrain the correlation of faults between seismic lines. However, the structural continuity and trends of faults herein interpreted from the satellite Earth Observation imageries are used to constrain the correlation of faults on GIS georeferenced seismic time-structure maps overlays. This scenario is reflected by the geospatial correlation between the optical Landsat 7 ETM+ derived surface lineaments and the contours of the time structure map for the topmost post rift Chad Formation in the north-eastern Bornu basin. The map shows that surface lineaments represent expressions of the post rift faults (Figs. 7.7b, 7.11). Additionally, correlations between faults in the synrift and post rift sequences from pre-

rift basement lineaments validate the basement upward structural propagation scenario (Figs. 7.7 - 7.12).

Seismic sections (Figs. 5.16 and 5.18) reveal that structural heterogeneities exist at basement level and associated faulting above, that suggests that the pre-rift basement morphology not only partially controlled syn-rift antithetic faulting but also had influence on the early post rift deposition due to the reactivation of the antithetic faults. Antithetic faults have relatively less control on the sediments deposition. In the synrift packages, the individual depocenters are recognizable where large and relatively symmetric basin developed.

The post rift faults that extend towards the surface from the upward continuation of the Cretaceous faults were reactivated as normal faults during the Quaternary neotectonic events. Major subsurface NE-SW Gubio - Munguno lineaments that bifurcates the main Gubio-Munguno depression in the north eastern part of the study area mark a zone of intense normal faulting during rifting and fault displacement contemporaneous with the basin sedimentary infilling (Fig. 6.12). Lineaments aligned with boundaries of the rift features form horst and graben or separate fault structures. Shorter parallel to sub-parallel subsurface lineaments that do not correspond with the surface lineaments along structural highs occur mainly within the sub-basin areas. The decrease in population of lineaments on the magnetic map downward continued to 5 km suggests that fewer lineaments represent unexposed deep-seated crustal structures. Longer subsurface lineaments represented by Bama, Gwoza, Munguno and Gubio lineaments represent the deep-seated basement structures (Fig. 6.13).

The major NW-SE trending Bama Beach Ridge (Figs. 4.24, 7.2a, 7.3a,b) appeared on all the corresponding satellite images used herein and identified as Bama lineament zone on the surface structural maps and is found to have a direct corresponding

subsurface structural expression in terms of geospatial correlation with the Bouguer gravity map and the gravity lineaments map (Fig. 7.2, 7.3). It is therefore suggested that surface lineaments in the basin must have undergone neotectonic post rift reactivation during displacement along the Bama ridge, which localised the formation of lateral ramps on its sides as evidenced from the truncation of the lineament features along its two sides.

Thus, it is inferred that the Bama ridge lineament zone would probably have facilitated subsequent reactivation of the upper crustal structures. The Bama Beach Ridge lineament zone is elevated relative to the adjoining flanks on its opposite sides thus forming a primary boundary along which the NE-SW lineament are truncated on its opposite sides. The close difference in altitudes of the two main palaeoshorelines (Bama Beach Ridge and Ngelewa Ridge) identified in the area interpreted herein from the SRTM DEM may preclude their tectonic origin (Figs. 4.24 – 4.25). However, the elevation of the prominent Bama Beach Ridge is higher at the south-eastern end than that at the north-western end. This change in elevation may however, indicate slight regional tectonic tilting with uplift of a few meters at the south-eastern end (Fig. 4.25). The differences in elevations of the Bama Beach Ridge (Fig. 4.24) are an indication that it could probably be related to a structural feature. This change in elevation may indicate slight regional tectonic tilting with uplift of a few metres at the southwestern end of the lake.

More so, from the central portion towards the north eastern sector of the study area an elongated topographic depression is clearly visible on the SRTM data but it is undetectable on the Envisat ASAR image mosaic and the Landsat 7 ETM+ mosaicked image subset. The NE trend of this depressed area on the SRTM DEM that is similar to the major trend of the lineaments in the basin and its geospatial correlation with the

Gubio-Munguno depression on the gravity map suggest a structural origin (Fig. 7.3a, 7.7 a - c). Thus, this graben like depression may have probably controlled the highest stand of the southern Lake Chad border represented by the Bama Beach Ridge palaeo-shoreline. Generally, from basement to surface combined perspective, there is a good systematic correlation of the lineaments in the north eastern Bornu basin (Figs. 7.7 – 7.12).

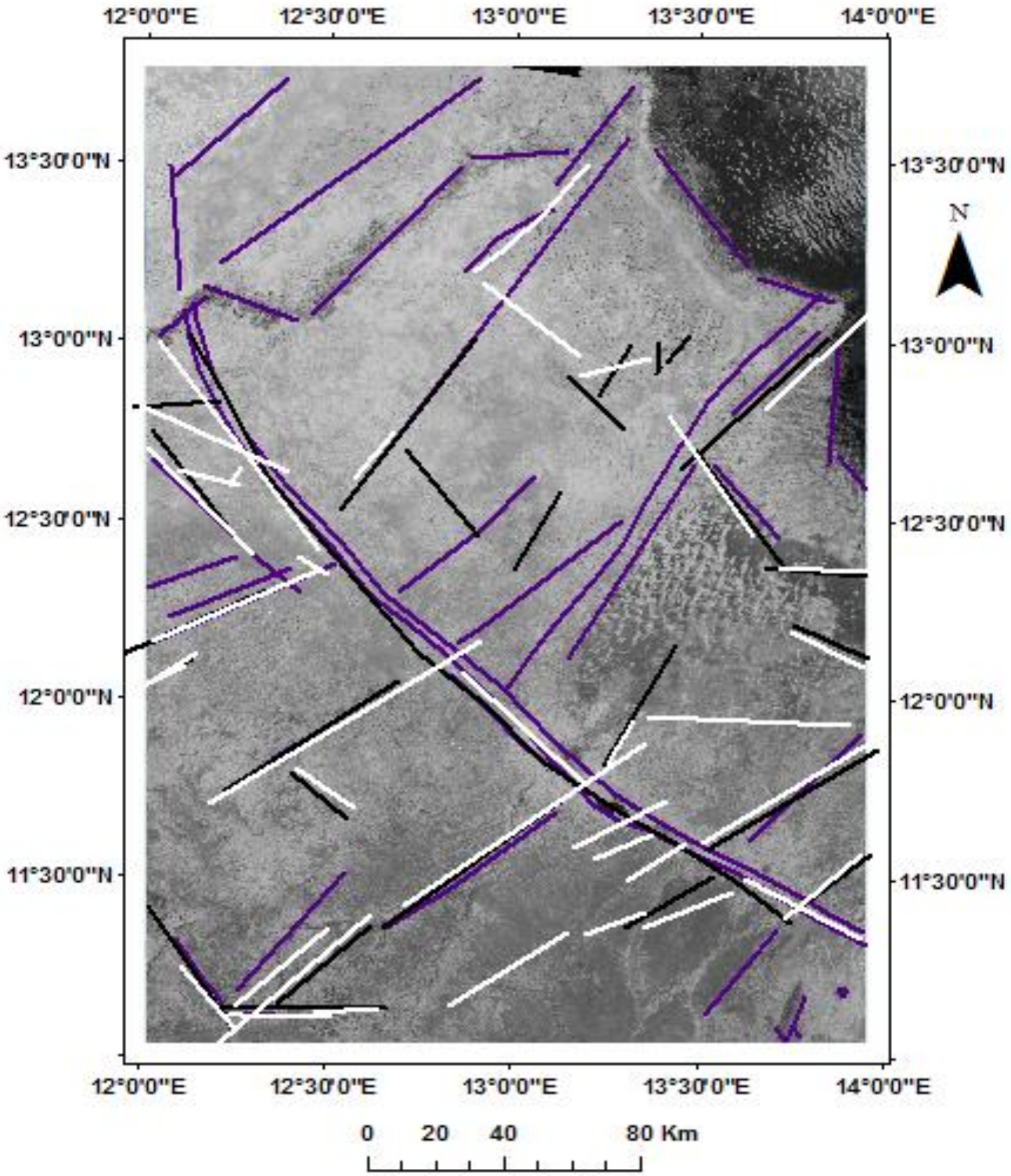

Fig. 7.7 a: Subsurface lineaments linked with surface lineaments using GIS. Landsat 7 ETM+ mapped lineaments (purple), magnetic lineaments (white), gravity lineaments (black) overlain on Landsat 7 ETM+ mosaic subset.

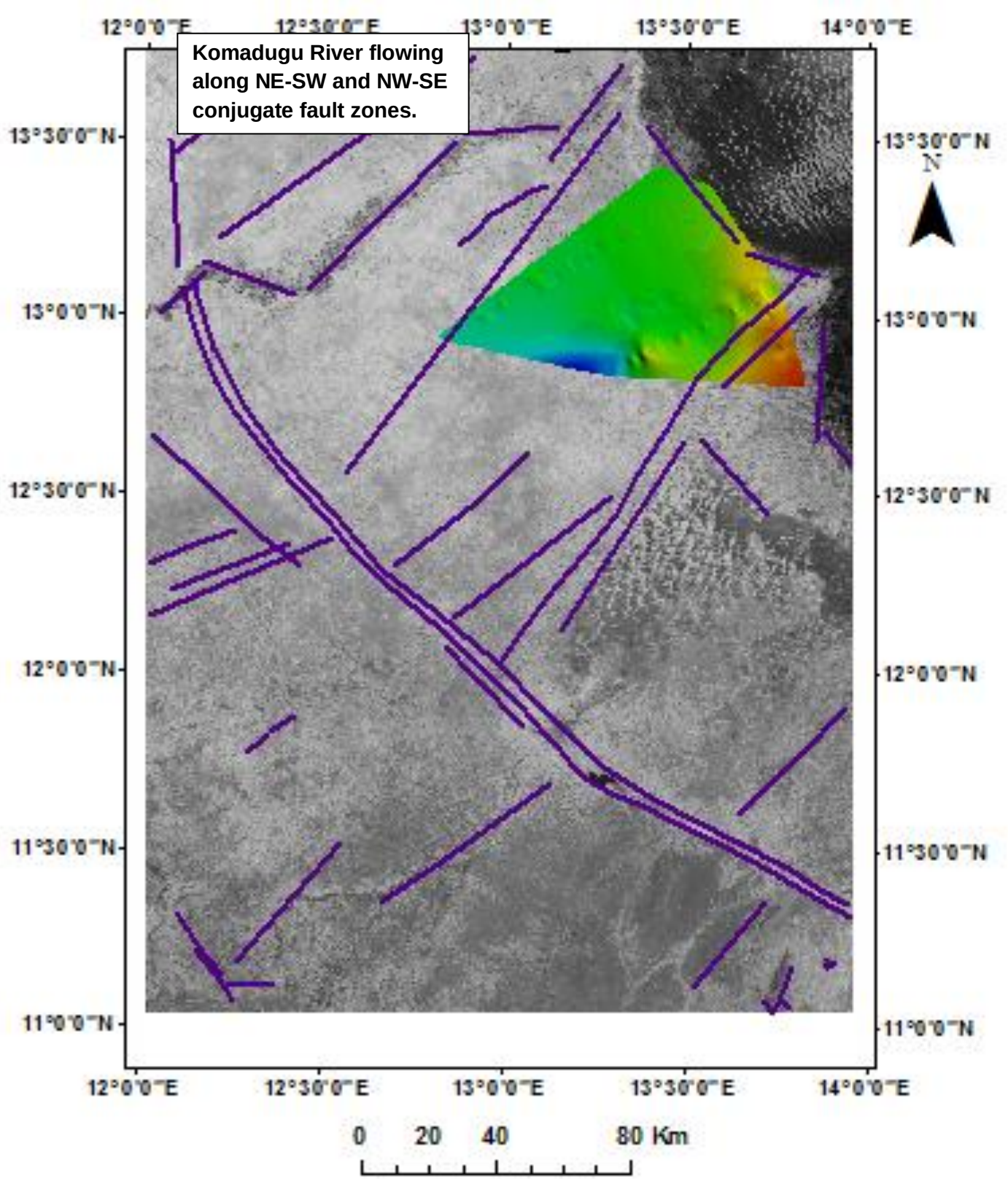

Fig. 7.7b.Landsat 7 ETM+ surface mapped lineaments and seismic time structure map mapped faults using GIS. Compare the insert Chad Formation time-structure map overlay with the Fig 5.26 showing detail description of the post-rift Chad Formation time-structure map. Komadugu River that empties into the Lake Chad apparently flows along the conjugate main NE-SW and NW-SE lineament structural alignments.

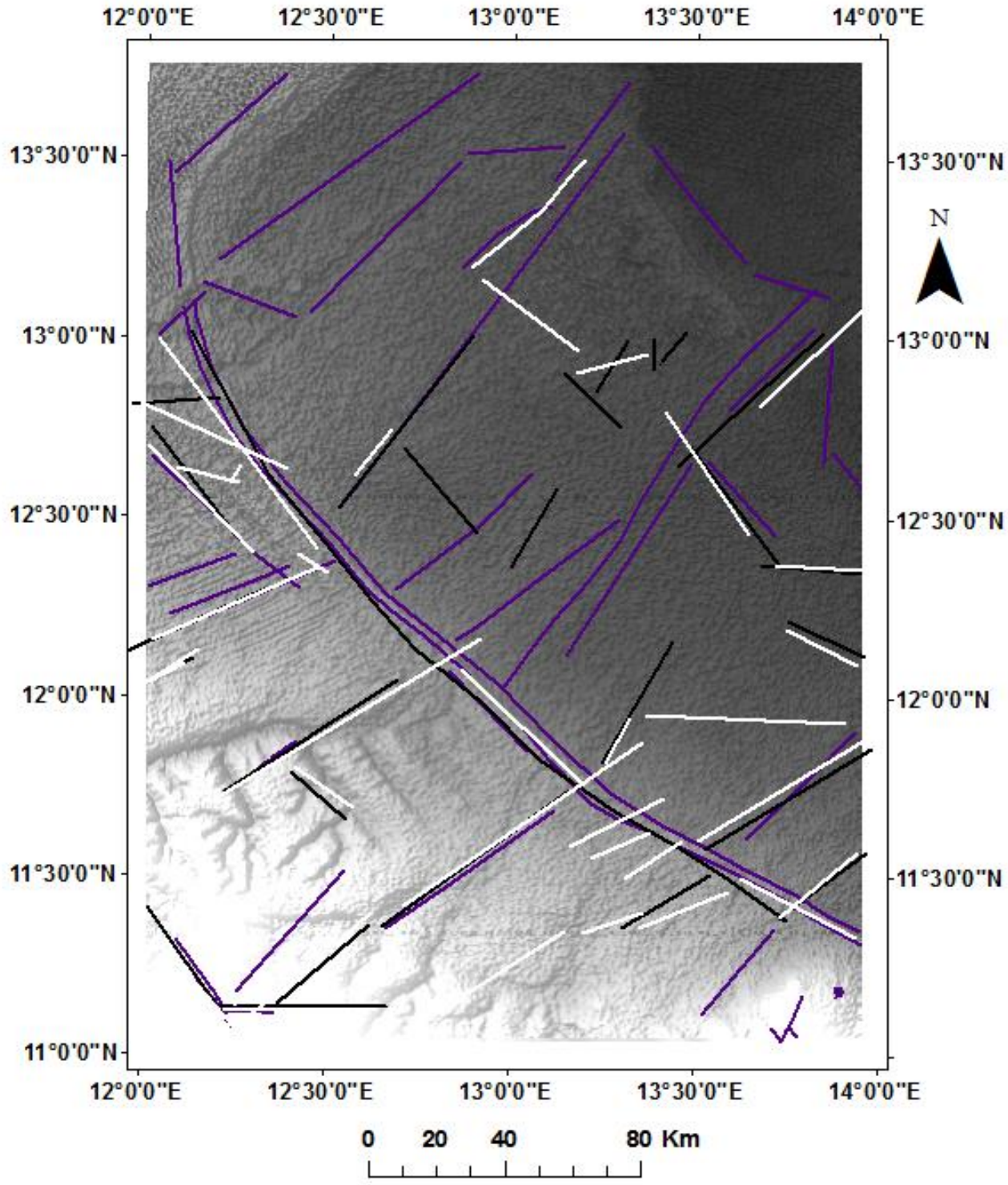

7.7 c. Landsat 7 ETM+ mapped lineaments (purple), magnetic lineaments (white), gravity lineaments (black) overlain on SRTM DEM hill-shade. Komadugu River that empties into the Lake Chad apparently flows along the conjugate main NE-SW and NW-SE lineament structural alignments.

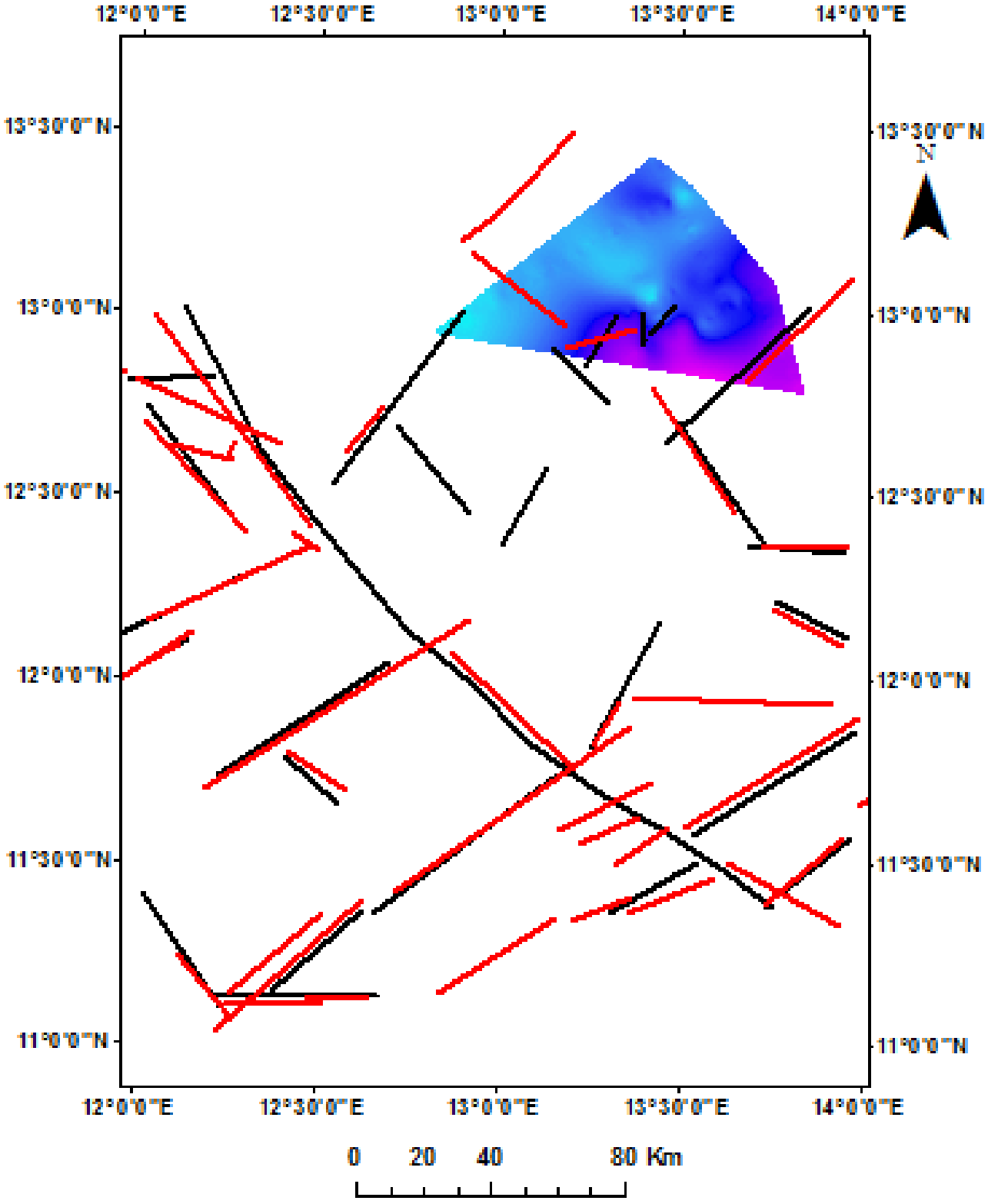

Fig. 7.8. Surface and subsurface faults linked from pre-rift basement gravity and magnetic data mapped lineaments using GIS. Compare the insert syn-rift Bima Formation time-structure map overlay with the Fig 5.23 showing detail description of the Bima Formation time-structure map and correlated subsurface gravity and magnetic lineaments with faults mapped from the seismic time structure map.

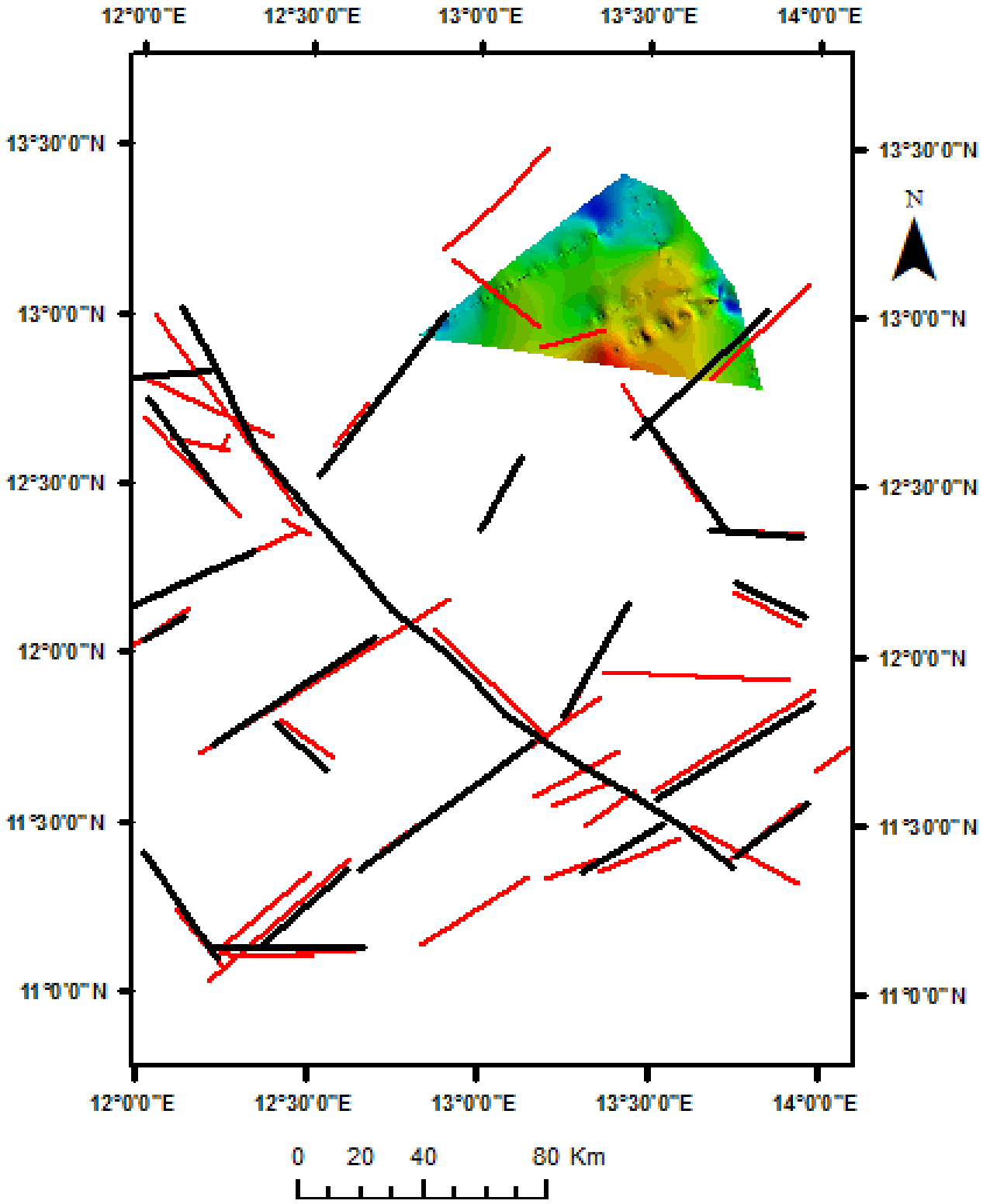

Fig. 7.9: Subsurface faults mapped from gravity and magnetic maps with Gongila seismic time structure map using GIS. Compare the insert syn-rift Gongila Formation time-structure map overlay with the Fig. 5.24. Showing detail description of the Gongila Formation time-structure map, correlated subsurface gravity, and magnetic lineaments with faults mapped from the seismic time structure map.

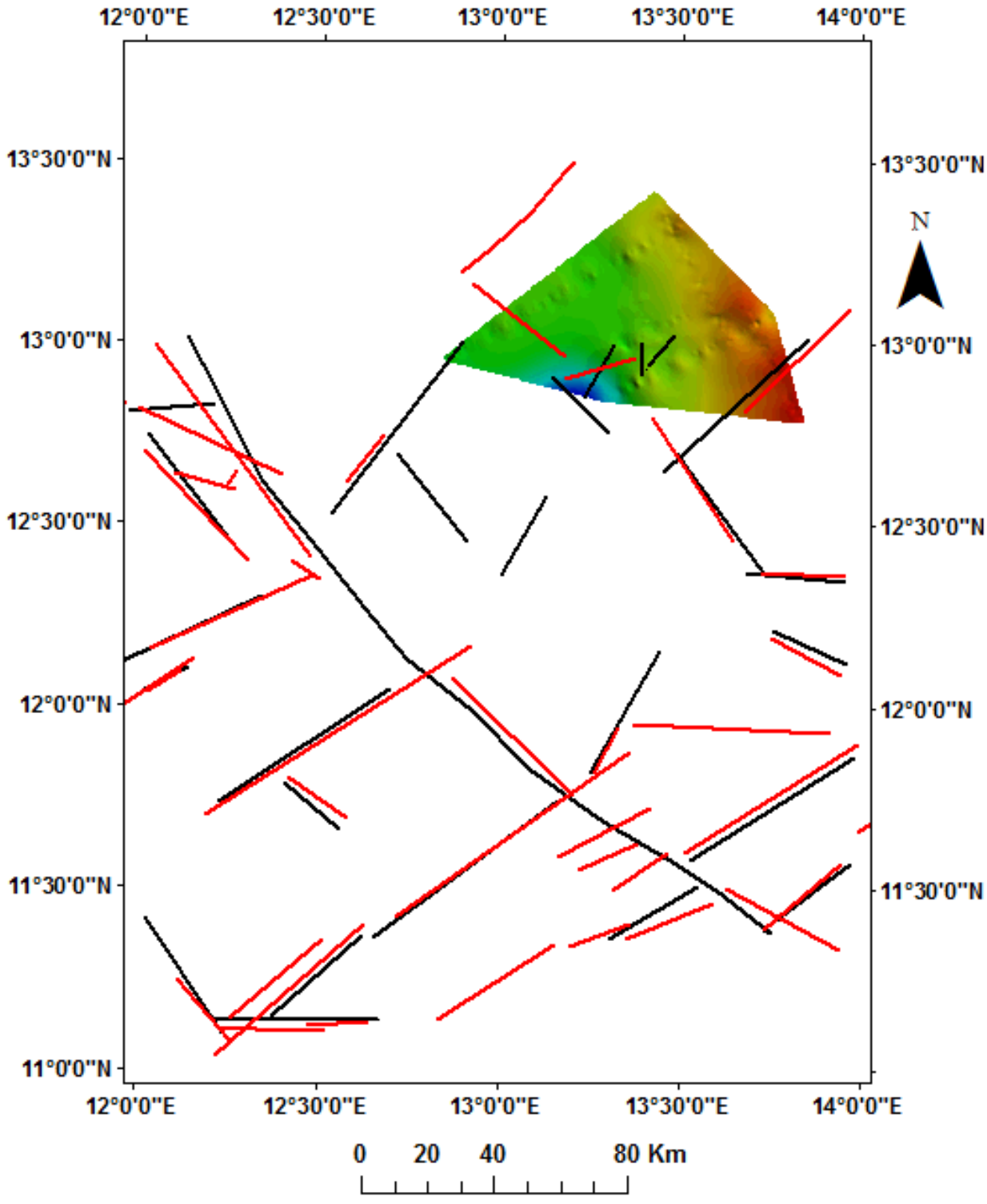

Fig. 7.10: Subsurface faults linked from basement gravity and magnetic with seismic mapped lineaments using GIS. Compare the insert post-rift Fika Formation time-structure map overlay with the Fig. 5.25 showing detail description of the Fika Formation time-structure map and correlated subsurface gravity and magnetic lineaments with faults mapped from the seismic time structure map.

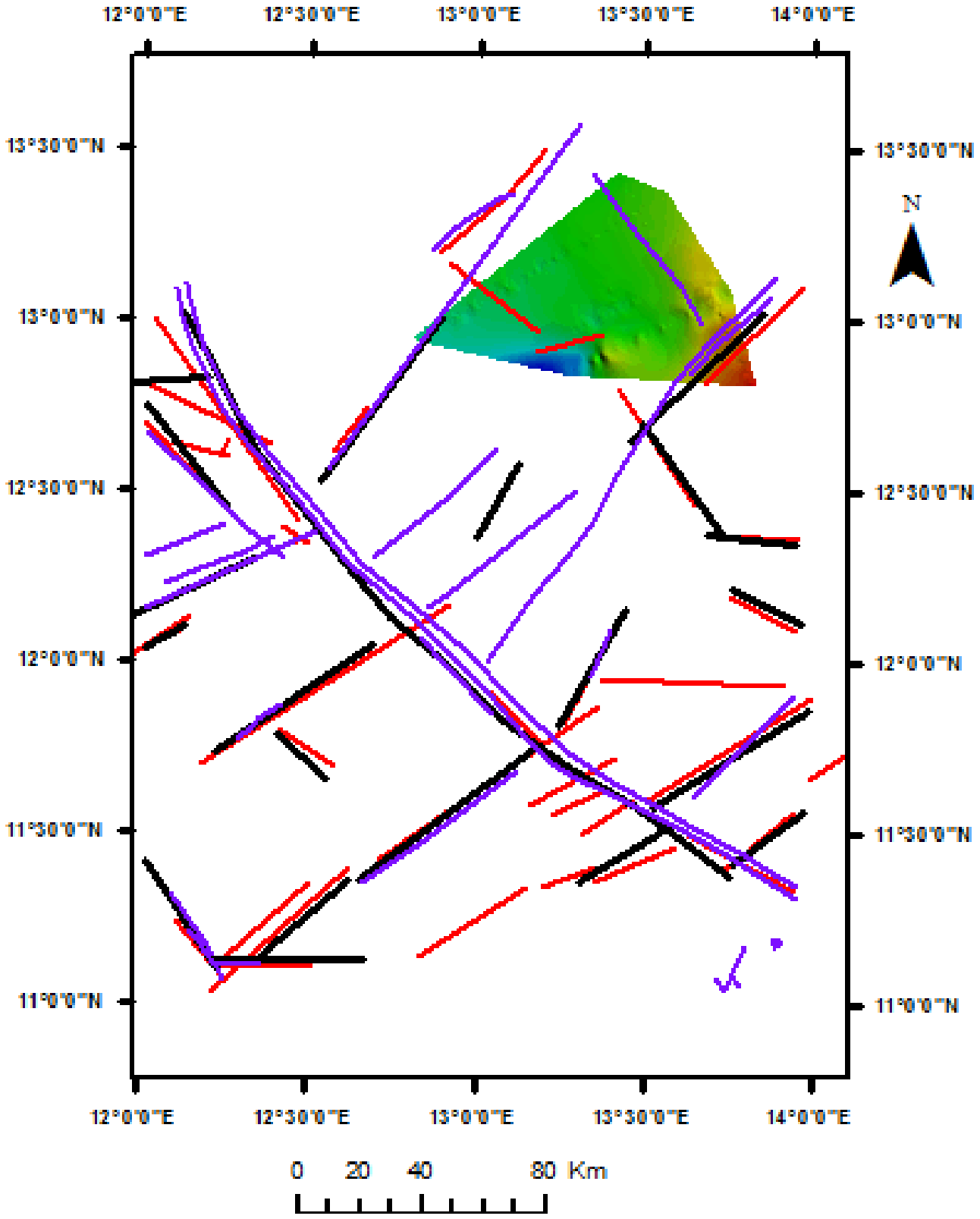

Fig. 7.11: Post rift surface mapped lineaments mapped from Landsat 7 ETM+ image mosaic and subsurface faults mapped from gravity and magnetic maps with Chad seismic time structure map-using GIS. Compare the insert syn-rift Chad Formation time-structure map overlay with the Fig. 5.26. Showing detail description of the Chad Formation time-structure map, correlated subsurface gravity, magnetic lineaments and surface lineaments with faults mapped from the seismic time structure map.

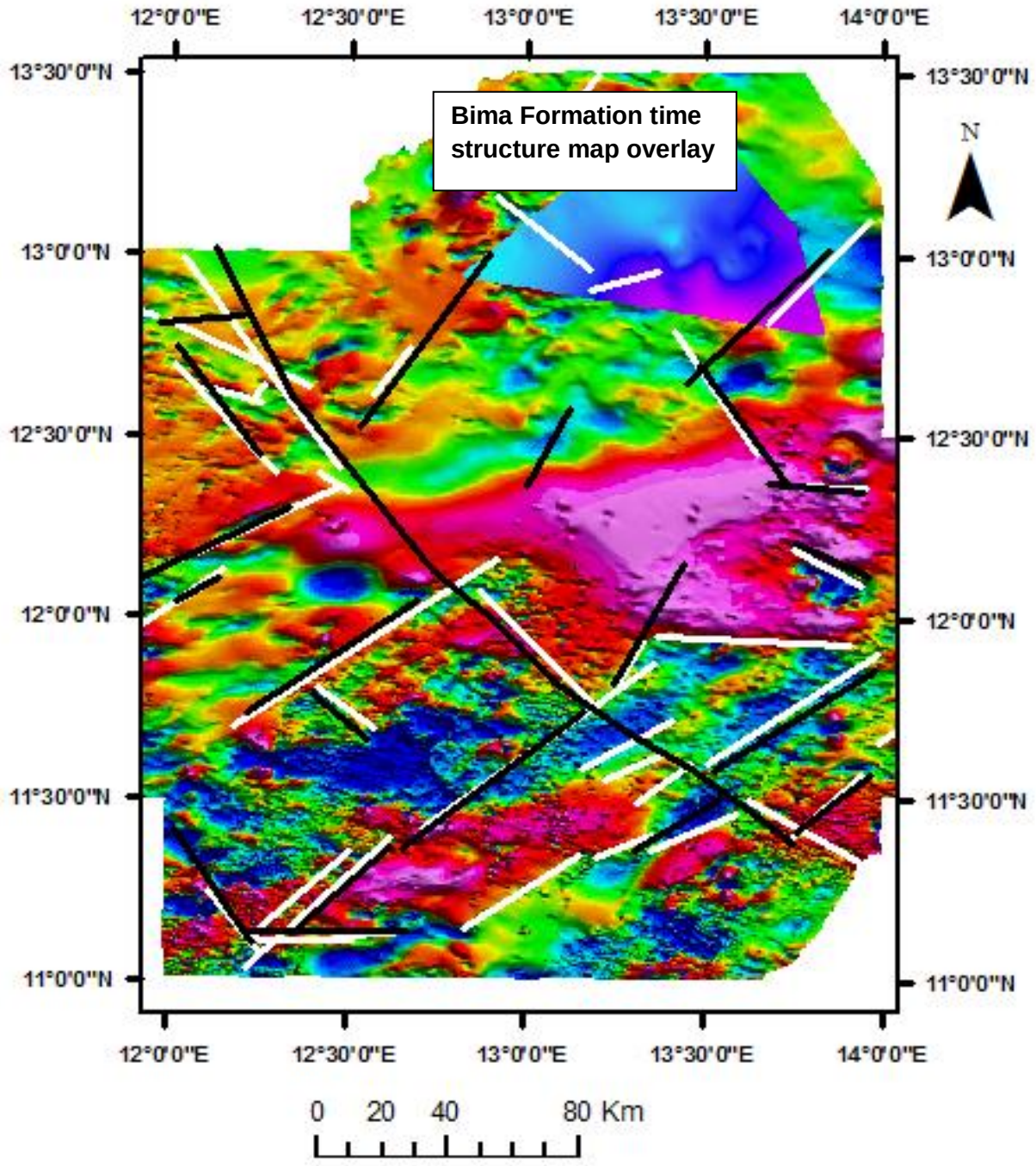

Fig. 7.12 a. Bima Formation time-structure map overlay with subsurface lineaments linked with surface lineaments using GIS. Magnetic lineaments (white), gravity lineaments (black) overlain on magnetic anomaly map. Compare the insert syn-rift Bima Formation time-structure map overlay with the Fig 5.23 showing detail description of the Bima Formation time-structure map.

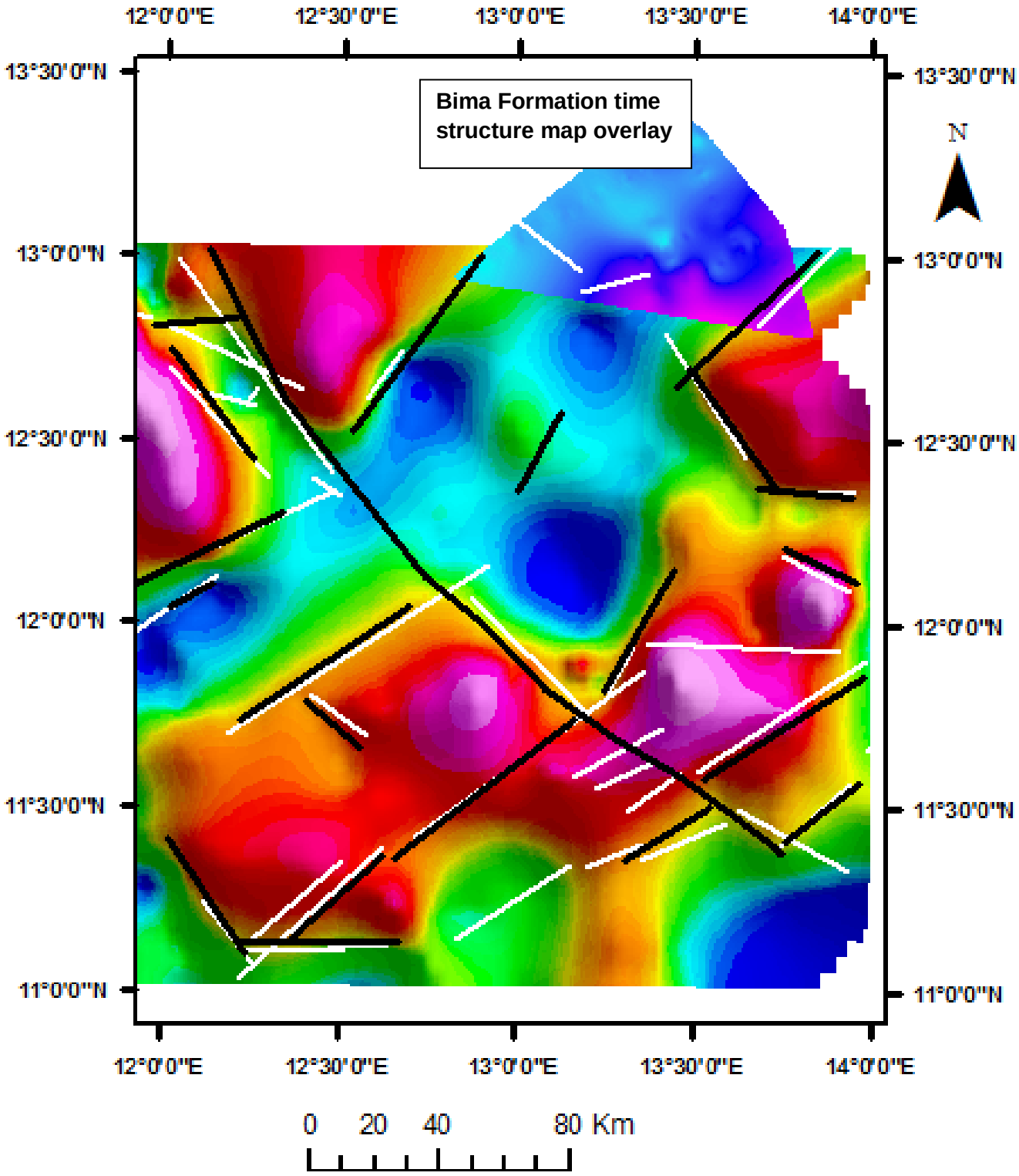

Fig. 7.12 b. Bima Formation time-structure map overlay with subsurface lineaments using GIS. Magnetic lineaments (white), gravity lineaments (black) overlain on gravity anomaly map. Compare the insert syn-rift Bima Formation time-structure map overlay with the Fig 5.23 showing detail description of the Bima Formation time-structure map.

The surface lineaments map (Fig. 4.26) overlain on the predictive spectral lithological (PSL) map of the area deduces their relationship with the surface lithological materials in which they occur (Fig. 7.13). Lineament zones are clearly spatially associated with the surface lithological boundaries. In the northern region, lineaments occurred at the rim of the Lake Chad characterised by intersecting NW-SE and NW-SE trending surface lineaments defined the south-western margin of the Lake Chad and correspond with the north-eastern margin of the Bornu basin. The trends of the lineaments correspond with the lineaments mapped by Isiorho et al., (1992). It is observed that the Komadugu River banks associated with lateritised silicate deposits flows along the conjugate NE-SW and NW-SE structural pattern (Fig. 7.7 a). The adjoining perpendicular NE-SW trending lineament zones formed series of structures running downslope towards the Bama Beach Ridge. More complexity of the lineament zones in the southern area is shown in the mainly fragmented appearance of the shorter NW-SE lineament zones, which are truncated or intersected by the longer NE-SW structures.

Spectral lithological analysis indicates that the surface deposits are more likely related to Quaternary - Recent deposition than they are from relics of the subsurface geology as mapped from the seismic and well log data. However, it has to be considered that the sandy sediments of probably fluvial origin may have been subjected to aeolian reworking under prevailing palaeoenvironmental conditions. The result of the spectral lithological mapping of the Quaternary – Recent drift sediments in the north eastern Bornu basin has agreed with earlier suggestion of the existence of undifferentiated deposits overlying the topmost Chad Formation in the basin by Isiorho and Nkereuwem (1996). As such, a new stratigraphy (Table 7.1) of the north eastern Bornu basin from subsurface to surface is proposed herein, utilising results of the

combined well log and seismic stratigraphic interpretation (Table 5.1) and the spectral lithological mapping.

Table 7.1: Stratigraphy of the north eastern Bornu basin from combined remote sensing and geophysical data interpretation

Period	**Formation**	**Maximum thickness (m)**	**Maximum Depth (m)**	**Lithology**	**Environment of deposition**
(Quaternary) - Recent	Post - Chad	1 - 6	6	Lateritised silicates clays, alluvial sands	Aeolian/fluvial
Quaternary	Chad	1711	1711	Mixed sand and clay (shale) sequence	Fluvial/ Lacustrine
Senonian	Fika	1349	3180	Shaly	Lacustrine
Turonian	Gongila	1621	3800	Alternating shaly and sandy sequence	Lacustrine
Cenomanian	Bima	1600	5000	Sandy	Continental

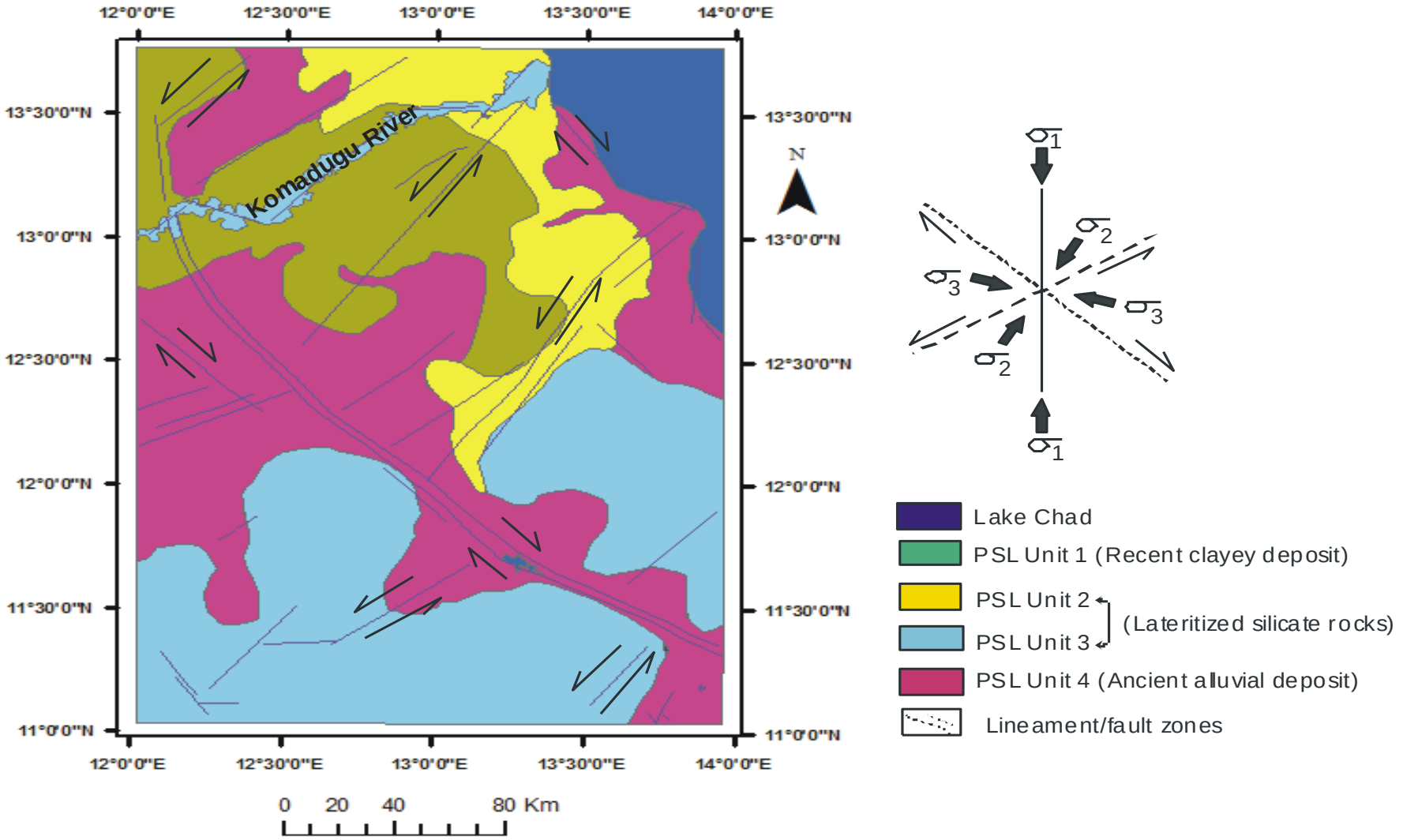

Fig 7.13. Major morphotectonic conjugate set of fault zones overlying the north eastern Bornu basin and the proposed model of deformation. Note the drainage structural alignment of the major River Komadugu in the north western part of the study area, which appears to be flowing along the conjugate NE-SW and NW-SE fractures. Similar structural architecture in the south western part of the study area involving river flowing along the NE-SW and NW-SE conjugate fractures are observed.

7.4.1 Tectonic reactivation and fault propagation – New insights into the Late Santonian (84 Ma) tectonic regime in the Bornu basin

Late Santonian corresponds to the first general compressional episode in the African–Arabian plate during the Alpine Cycle (Guiraud et al., 1987; Guiraud and Bellion, 1995). Late Santonian (84 Ma) folding and basin inversion exist in the Benue Trough and adjoining basins within the WCARS including the Termit basin (Genik, 1993). The Santonian compressional inversion affected parts of the Lake Chad basin, due to the change in relative plate motions during convergence between Africa and Europe Guiraud and Maurin, (1992) Petters and Ekweozor (1982); Genik, (1993) and Reynolds and Jones (2004). However, the geometry of inversion structures depends on the geometry of the original fault system. The rift geometry in the adjoining Chad-Bongor basin, the Niger-Termit basin and the Benue Trough have their basin-controlling faults more favourably orientated with respect to later compressional stress (Genik, 1993). As such, the intracratonic WCARS is a genetically linked system of initial extension and later compressional inversion.

Accordingly, later tectonic regime is herein suggested to have also affected the Bornu basin in the Late Santonian (84 Ma) after the Turonian – Early Santonian phase of Genik, (1993) (Fig 2.4). The Santonian inversion caused folding in the Benue, Yola and Bornu basins (Popoff et al., 1983; Benkhelil, 1988), as well as similar structuring in the southern Termit and Bongor basins. Avbovbo et al., (1986) contradicted, that the folds, which are mainly cut by the normal faults are uncommon in the south-eastern part of the Bornu basin. Similarly, from results of seismic interpretation herein, it can be deduced that the compressional overprint is generally subtle in the north-eastern Bornu basin compared to the pervasive Late Santonian folding and basin

inversion in the Benue Trough and adjoining basins within the WCARS including the Termit basin. Tectonically, the Santonian compressional stress was nearly orthogonal to the Early Cretaceous extension direction (Genik, 1993). The resulting inversion is best documented in the ENE–WSW orientated Benue Trough, Logone Birni, Bongor, Doba and Doseo basins (Fig. 2.3), (Petters and Ekweozor 1982; Fairhead 1988; Manga et al. 2001), However, some of the WCARS basins are affected by initial extensional tectonics with intermittent periods of less influential compressive tectonism and magmatism (Guiraud et al., 2005; Warren, 2009). During the Santonian to Early Campanian, igneous activity occurred in the Bornu basin, during which saucer-shaped sills and en-echelon sills were emplaced similar to the magmatic events documented in the Benue Trough (Torsvik et al., 2009). The structural setting for the adjoining Muglad basin in Sudan has however, been interpreted as purely extensional (Mohamed et al., 2000) as some structures are far less clearly the result of inversion. Similarly, inversion is least pronounced in the NW-SE oriented Termit-Lake Chad, Muglad, Melut and other Sudan basins, where extensional rift geometries are commonly preserved with little or no direct evidence of compressional reactivation (El Hassan et al., 2017).

Thus, from these regional considerations, the Santonian episode, which is a plate scale tectonic event that resulted in large scale inversion or folding of adjoining basins in the WCARS, is suggested herein to be least recorded in the Bornu basin where extensional geometries are commonly preserved with little or no direct evidence of compressional reactivation (Warren, 2009). Earlier, Genik (1992; 1993) described that the regional rifting slowed to the point of being a sag and peaked in the Santonian, with a marked tectonic pulse at around 85 Ma. The regional stress regime suddenly changed due to variations in the spreading rate and direction between the Equatorial

and Southern Atlantic plates (Binks and Fairhead, 1992) and/or by a N-S compression between the African and European plates (Guiraud,et al., 1987). More so, due to the tectonic setting of the Bornu basin located in between the Benue Trough and Termit basins with different tectonic regimes during the Santonian inversion, which affected the Benue Trough more than the Termit basin, it is suggested, that the Late Santonian inversion had subtle effect in the Bornu basin as extension features where more prevalent. Few compression folds/anticlines interpreted herein from seismic data (Figs. 5.16, 5.18) represent the subtle imprints of the Santonian inversion regime. Unlike the widespread rift extensional faulting, the inversion overprints are therefore restricted features in the Bornu basin. Moreover, due to the scope of this research, the geographic restriction of the folds and the paucity of associated compressive features are difficult to explain, since data from the south-eastern Bornu basin are not available.

Subsequent to the change in extension direction to NW-SE due to the change in relative plate motions similar during the Barremian (120 Ma) – Early Albian (101 Ma) as indicated by Genik, (1993) (Fig. 2.4). It is suggested herein that the Late Santonian tectonic episode that affected the Benue Trough re-oriented the structural arrangement anticlockwise and merged into the shallow warping of the Manga pattern in the Termit basin after the rifting slow-down in the Bornu basin (Fig. 7.6b). The regional stress regime suddenly changed due to variations in the spreading rate and direction between the Equatorial and Southern Atlantic plates (Binks and Fairhead, 1992) and/or by a N-S compression between the African and European plates (Guiraud,et al., 1987). This arrangement was achieved from a change in plate motions around 84 Ma in the onset of the collision with the Eurasian plate. This episode is part of the plate scale event, resulting in inversion or folding of most of the E–W to ENE–

WSW trending basins in response to NE oriented shortening also registered in Eurasia (Tokarski, 1973).

These tectonic events that were previously lacking in the Genik (1993) and Avbovbo et al., (1986) models are described in the new evolution model of the Bornu basin developed herein from the results of combined surface and subsurface interpretation of lineaments in this research (Fig. 7.14).

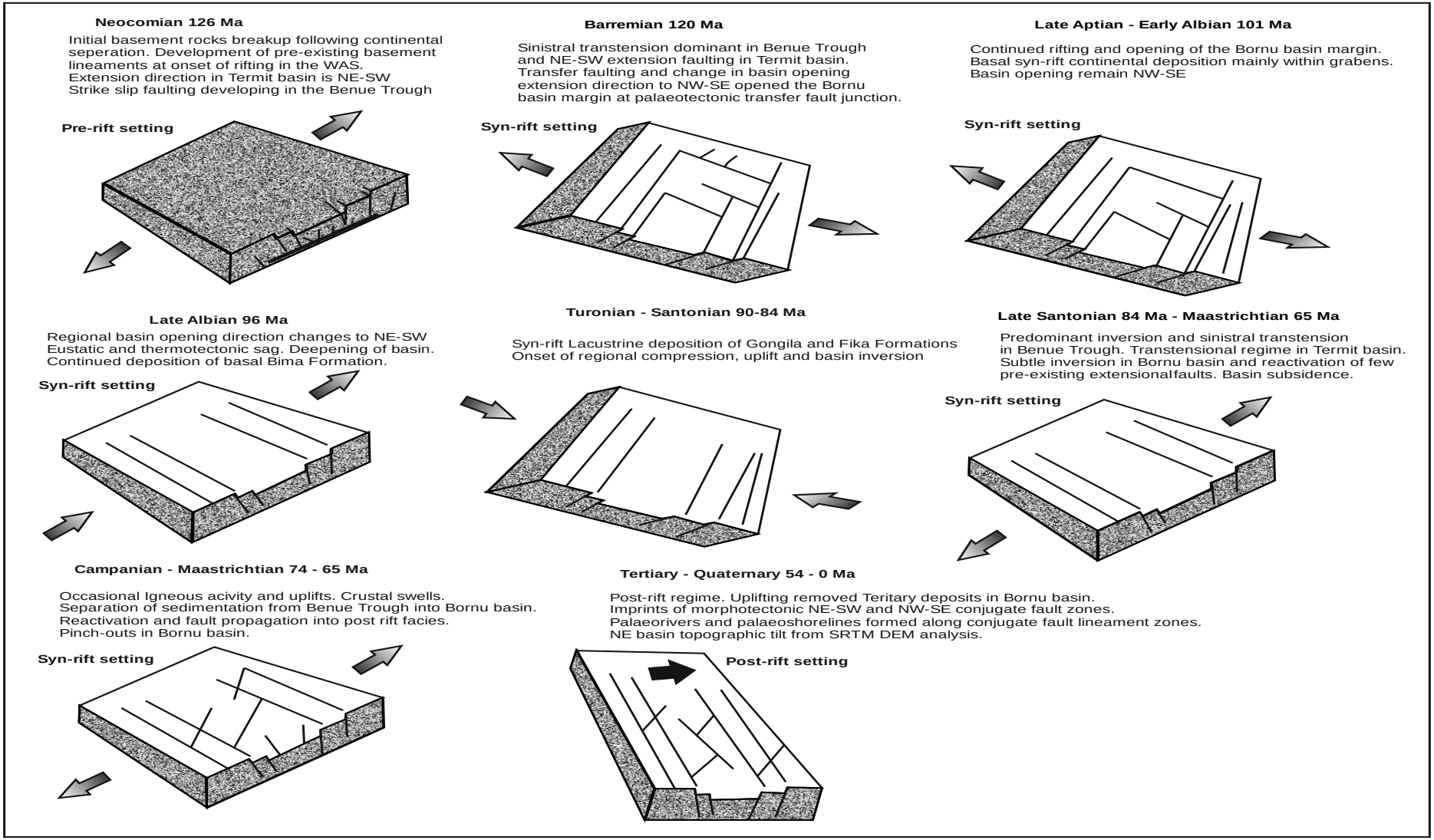

Fig. 7.14: showing the proposed pre-rift to post-rift tectonic evolution model with additional Barremian 120 Ma, Late Santonian Inversion (84) Ma tectonic events and Early Aptian – Late Albian (101) Ma events as they affected the Bornu basin within the context of the regional WCARS. (Genik 1993) to include the new tectonic phases that affected the Bornu basin from the integrated data analysis herein improves the existing model given in Fig 2.4

7.5 *Potential petroleum systems from the syn-rift to post rift evolution in the Bornu basin*

Rift basins contain a significant proportion of the world's hydrocarbon reserves and in recent years the focus of exploration in Nigeria for example, is shifting from the deep waters or passive margin basins to the under-explored inland rift basins (Obaje 2009). Exploration for oil and gas have been intense within the regional West and Central Africa Rift System (WCARS) and commercial discoveries have been recorded elsewhere within the south-western sector of the Lake Chad Basin. Bornu basin is one of the most explored inland basins in Nigeria and its hydrocarbon potentials have been identified (Avbovbo et al., 1986; Genik, 1992, 1993; Olugbemiro, 1997; Moumouni et al., 2007; Obaje, 2009; Anakwuba and Chinwuko, 2012; Hamza and Hamidu, 2012; Adepelumi et al., 2012).

However, petroleum system represents the natural framework through which all related hydrocarbon deposits are linked by origin and occurrence through providing the link between the distribution of oil and gas and the stratigraphic development and tectonic evolution of a basin (Magoon and Dow 1994a). Although, the petroleum system analyses of the basin are inadequate, the basin is understood to have most of the important factors required for oil and gas prospectivity. These include; geological age of the basin (Burke, 1969), considerable sediment thickness (Petters, 1978 and Okosun, 1995), potential source rock geochemistry (Petters and Ekweozor (1982); Alalade and Tyson (2010), potential reservoir rocks and structural styles, Avbovbo *et al.* (1986); Okosun, (1995) and potential trapping mechanisms (Agagu and Ekweozor, (1980), and Avbovbo *et al.,* (1986).

Although, petroleum exploration within the Bornu basin has produced only minor gas shows in two wells out of twenty-three exploratory wells drilled from 1976 until 1996.

This lack of exploration success does not necessarily signify overall hydrocarbon deficiency but highlights the need for better understanding of the basin's structural complexity and evolution. Previous studies on the basin's structural geology using mainly single data types were largely inadequate. Published sedimentology and stratigraphy of the north-eastern Bornu basin by various authors using core, single type wireline log and/or biostratigraphic data have not attempted to integrate the datasets with seismic data, which is a common practise in basin analysis for regional tectono-stratigraphic validation. Thus, the tectono-stratigraphic architecture, thickness and continuity of reservoirs within the sub-basins of the north eastern Bornu basin are poorly understood.

Several of the world's petroleum producing basins have evolved through syn-rift to post-rift evolution as documented by Kingston *et al*., (1983) and Sladen (1997). However, previous studies of the petroleum systems in the Bornu basin remain narrow in perspective and not presented within the context of the regional rift tectonic evolution of the basin from integrated data analysis. Hence, the identification of common rift-related petroleum system types can contribute to the stimulation of further exploration in the basin.

This section presents the significance of this research by evaluating the petroleum prospectivity of the syn-rift and post-rift phases of the basin. However, evaluations of the organic matter maturation, petroleum geochemistry, as well as the quantitative evaluation of the petrophysical properties of the rock facies described in the research are totally beyond the scope of this research as such only inferences drawn from relevant previous studies are discussed herein. However, evaluation of trapping mechanisms and seal, which relates to the structural architecture of sedimentary basins, is within the scope of this research and is therefore considered in more detail for the study area. Additionally, the subsurface facies distributions and their

identification as potential source rocks and reservoir rocks, which are within the scope of this research are discussed herein. This section thus, presents the fundamental components of the petroleum system in the Bornu basin within the context of the previous studies and how the structural and lithostratigraphic analyses carried out in this research constrain the petroleum prospectivity in the north-eastern Bornu basin.

7.5.1 *Petroleum system analysis of the Bornu basin*

(Hamza and Hamidu, 2012) have identified two potential petroleum systems including, Lower Cretaceous Petroleum System and Upper Cretaceous Petroleum System in the basin from organic matter analyses of ditch cuttings obtained from few wells. The synrift sediments comprising of sandstones and lacustrine deposits represent the Lower Cretaceous Petroleum System while the marine shales, deltaic sandstones and carbonates represent the Upper Cretaceous Petroleum System. However, reported igneous intrusives in the southern Bornu basin may have destructive effect on the organic matter in the basin if the intrusion is post-primary migration due to the possibility of degradation of the organic matter to generate gas or even graphite (Okpikoro and Oluronniwo, 2010). This petroleum system classification is inadequate since it does not specify the significance of the tectonic regimes on the rock facies in the basin.

Alternatively, Doust and Lijmbach (1997) proposed that petroleum charge systems could be correlated with the main stages in a basin evolution (Fig. 7.15). Accordingly, the potential petroleum systems of the Bornu basin can be linked closely to the phases of the basin development from syn-rift to post rift as described in Sections 7.3, 7.4. The pre-rift to post rift model of tectonic evolution for the Bornu basin developed in this research can be examined on the basis that the long duration of overall

extensional and strike-slip strains may have facilitated high porosity and permeability to be maintained in the rock facies with effects on fluid migration. Additionally, the distribution of fault systems is key for geometric basin analysis of distribution of traps in the basin.

7.5.2 *Pre-rift - syn-rift petroleum system*

Early syn-rift continental Bima Sandstone and Marine Gongila Formation are strongly oil prone due to the widespread development of organic-rich source rocks in this tectonic rift regime. Evidence of oil-generating, organic-rich sediments exists in both the Bornu basin and the Upper Benue Trough (Olugbemiro et al., 1997; Akande et al., 1998; Obaje et al., 2004; Alalade and Tyson, 2010, 2013; Habib and Xie, 2012; Adegoke et al., 2014; Boboye and Nzegwu, 2014). Potential reservoir rocks in the petroleum system are suggested to be within both the Bima Sandstone and the intercalating sandy facies in the Gongila Formation (Okpikoro and Olorunniwo, 2010; Boboye and Abimbola, 2009). This study interpreted significant thickness and depths of the potential reservoir rocks (Table 5.1), with the Bima Sandstone mainly contained within the grabens. Blocky nature of the gamma ray and resistivity logs for the Bima Sandstones (Appendix B) indicate reservoir homogeneity, uniform composition, good sorting and permeability provided by the sandstone facies. The Cretaceous period witnessed the deposition of the transgressive sandstones unconformably on the pre-rift Precambrian basement in the Bornu basin (Avbovbo et al., 1986). Relationship of the Cretaceous Bima Formation with organic matter makes it a suitable reservoir with high possibility of hydrocarbons migration into the transgressive sand above the disconformity. The Bima Sandstones are potential reservoir rocks while the

compaction features over the horsts and fault closures against them are suitable structural traps (Fig. 5.16).

It is also shown in this study, that the north-eastern Bornu basin contains several sub-basins bounded by basement highs as defined by the Bouguer gravity anomalies interpreted in this study. A sub-basin penetrated by Herwa (HRW) – Kuchalli (KUC) wells in N-S cross section (Fig. 5.4) is a large area spanning approximately 72 km containing up to 5 km depth of continental-shallow marine and lacustrine rocks of the syn-rift Bima Formation and Gongila Formation, overlying the Precambrian basement. Hydrocarbon trapping styles are provided by the antithetic fault closures herein interpreted in the basin (Fig. 5.18). Migration and expulsion of the potential hydrocarbon would be easier from half grabens filled with thicker sediments than from fully uplifted horst blocks due to the extensional movement of pre-existing pre-rift basement fault blocks. It can be deduced from the seismic analysis in Fig (5.18) that the various structures in the north-eastern Bornu basin grew and propagated differently due to the synrift extension architecture that controls local variations in sediment facies distribution and thickness.

The Cretaceous extensional structures, which are classified as potential hydrocarbon traps in the WARS include the horsts, compactional anticlines (particularly in the southern Termit basin), formed over the basement and roll-over normal faults (Genik, 1993). Other potential hydrocarbon traps in the basin include stratigraphic traps from interfingering sandstones (Petters and Ekweozor, 1982) and combination traps from juxtaposed sandstone and shale sequences against faulted blocks and graben and horst (Obaje et al., 2004), which are present in the syn-rift Gongila Formation consisting of mixed sandstones and shales or clays. Depth of burial of the potential source rocks, which is more favourable in the syn-rift tectonic regime, affects the basin's potential hydrocarbon migration and accumulation. According to Hunt, (1995),

minimum burial depth of 2000 m is necessary for expulsion and migration of hydrocarbon from source rocks. This burial depth is obtained in the north-eastern Bornu basin as interpreted in the wells (Figs. 5.4 and 5.5) and seismic data (Table 5.3), the isochron thickness map for the Bima – Gongila stratigraphic interval as well as from the Gongila – Fika isochron thickness map (Figs. 5.27 – 5.28). However, the potential source rocks often located at the required depths are within grabens and trapped by the horst fault blocks that makes lateral migration less preferred than vertical upward migration (expulsion) of the potential hydrocarbon.

The major syn-rift faults having significant influence on the sediment deposition tend to create more accommodation when the rate of sediment supply was high. Lineaments from the various data types in this study show predominant NE-SW trend parallel to the dominant trend of the central Gubio – Munguno depression representing a central graben with parallel bounding faults on both edges (Fig. 6.11). However, interpreted seismic lines and interpreted gravity cross section across the central graben indicate the existence of intra-basinal horst and graben system inside the main depression. From the wells cross sections (Figs. 5.4 – 5.5), the southern margin of the HRW - KUCH wells sub-basin is dissected by a NE striking steeply dipping normal fault. A shallow NE dipping basin floor as penetrated by the shallower Albarka (ABK) – Kuchalli (KUC) wells of approximately 3 km depth, marks the northern margin of the HRW-KUCH wells sub-basin. There is no seismic coverage in the Tuma (TUM) – Murshe (MUR) sub-basin, which coincides with E-W trending Bouguer gravity low of the Maiduguri Trough in the southern margin of the Gubio-Munguno depression (Fig. 7.12b). The Maiduguri Trough is bifurcated from the Gubio-Munguno depression by the main Munguno lineament. Clay facies of the Gongila Formations are likely to offer good intraformational seals for the Cretaceous sequence, Clay facies occurring at sequence boundaries can act as seals to the underlying Bima Sandstone reservoirs.

Seal risk is minimised where antithetic faults occur on either side of uplifted horsts with relatively minor hanging wall graben that provide optimum trapping configuration of up-dip stratigraphic pinchout (Figs. 5.16, 5.18).

7.5.3 *Syn-rift to Early Post rift petroleum system*

The hydrocarbon source rocks in this tectonic rift regime in the basin are the Turonian – Campanian post rift Fika Shales (Hamza and Hamidu, 2012) and the clayey facies of the syn-rift Gongila Formation (Anakwuba and Chinwoko, 2012; Obaje et al., 2004). Although, the Cretaceous tectonic movements that affected the basin may cause juxtaposition of the stratigraphic sequence to develop juxtaposed sandstone against shale due to block faulting. These movements can manifest where uplifted horst blocks became exposed to extensive erosion and reworking of the potential source rocks, which would reduce their thickness and diminish their potential as good source rocks. Tectonic processes responsible for the block faulting could result in poor development or subsequent removal of the source rocks, while preserving considerable thickness of the Fika and Gongila potential source rocks on the other side of the horst block.

Presence of full graben and half graben controlled by movements of the basement sub-blocks in the north-eastern Bornu basin improved favourability for deposition and preservation of the potential source rocks. A good example of this circumstance is in the adjoining prolific Termit basin in Chad Republic where subsurface data indicate that hydrocarbon discovery were part of the half grabens, antithetic and synthetic faults (Genik, 1992; 1993), which are also mapped herein from the seismic datasets in the north-eastern Bornu basin (Fig. 5.18). The extensional regime of the Termit basin was contemporaneous with the Bornu basin.

The propagation of pre-rift structures into the post-rift regimes results in neotectonic expression of lineaments and manifestations of potential oil and gas trapping or migratory mechanisms in basins. Extensional stress generated faults form steep fault planes, which have more potential of opening to produce migration pathways (Okpikoro and Oluronniwo, 2010). Surface manifestations of the subsurface structures identified herein could be reliable in locating areas of favourable subsurface architecture regarding the petroleum habitat. Accordingly, the correlations of the surface and subsurface structures in the north eastern Bornu basin suggest that the syn-rift structures having been reactivated and propagated upward into the post rift regime as demonstrated in Section 7.4, may act as the loci for the development of potential oil and gas traps.

Hydrocarbon charge risk is enhanced in the Bornu basin due to the post-rift Santonian compression event that had wide-ranging effects significant for exploration in the WARS basins by creating hydrocarbon-trapping folds. However, inversion can also destroy or modify any previous structural trap geometries developed during rift extensional faulting and cause remigration of earlier hydrocarbon accumulations (Cooper and Warren, 2010). However, (El Hassan et al., 2017) describe that subtle inversion overprint such as that determined in the Bornu basin in this study (section 7.4.1) is favourable for preserving extensional fault trap geometry that prevents hydrocarbon remigration or losses especially if the extension predates the source rock maturation and so the earliest migrated hydrocarbon could be trapped. The structures would remain buried rather than uplifted and partly eroded, thus preserving seals as occurred elsewhere (Cooper and Warren, 2010).

Accordingly, the post rift Fika Shale source rock and the potential source clay facies in the underlying syn-rift Gongila Formation may have been preserved within generating windows relative to the earlier extensional potential trap geometry with the structures

fully buried rather than uplifted and eroded. Similar favourable conditions were suggested to be partly responsible for several large discovered hydrocarbon fields of adjoining Muglad and Melut basins in Sudan within the WCARS (Schull, 1988, Mohamed et al., 2000; Idris and Yongdi 2004). In these basins large extensional structures are oriented NNW-SSE, which is approximately related to the initial extension trend in the Bornu basin and therefore least favourable for reactivation during the Santonian compressional event. Additionally, the subtle Santonian inversion may have created the 4-way dip structural closure in the Gongila Formation time-structure map that is independent of a fault sealing (Fig. 5.24).

Potential source rocks require temperature and pressure at depth necessary for potential hydrocarbon generation. Critical minimum depth of 1400 m burial for source rocks is necessary for the generation of hydrocarbon to commence (Tissot et al., 1987). Accordingly, such a depth in the north-eastern Bornu basin has been established from the combined well log interpretation (Figs. 5.4 and 5.5), with maximum burial depth of the potential source rocks of Fika Shales and Gongila Formation being 3180 m and 3800 m respectively (Table 5.1). Similarly, the Gongila – Fika isochron thickness interval show the required thickness of the stratigraphic regime (Fig. 5.28). This implies sufficient depth of burial hence, a favourable condition for hydrocarbon generation from the Upper Cretaceous source rocks in the basin. The blocky shape of the gamma ray and resistivity signatures for the Fika Shale shows homogeneity of porosity and mineralogical composition of the shale rock (Appendix B). Additionally, depths within this formation were variable due to the basement topographic configuration, which control the depositions within graben and shallower troughs as well as orientations of the bounding faults.

Petters and Ekweozor, (1982) indicated that organic geochemical data analysis for the total organic carbon content (TOC) of the Bornu Basin is similar with that in the Benue

Trough and Anambra Basin in southern Nigeria. The basins have high total organic carbon content (TOC) greater than 0.5% determined from their Turonian-Santonian shale samples. The shales in Fika Formation and Gongila Formations are mature and provide good potential source rocks for both oil and gas due to their low n-alkane ratio and marine fossil facies contents. The rift nature of the Bornu basin provides good geothermal gradient for the organic matter maturity. Heat flow values in the basin range from 63.6 – 105.6 mWm^{-2}, which correlates with other petroliferous basins of the world (Nwankwo, et al., 2012). Hamza and Hamidu (2012) obtained TOC values with average of 0.74 wt % belonging to low liptinite and high victrinite-inertinite organic facies from the potential source rock Fika Shale is mainly Type III Kerogen, and correlates with mainly gas prone potential as obtained by Petters (1978).

The shale components of the source rocks that are present in the syn-rift and post rift tectonic regimes are suitable seal rocks for oil and gas (Avbovbo et al., 1986). The accommodation space created during rift extension can also control source rock distributions as illustrated in the adjoining CARS basins (Genik, 1992). Extensional faulting can also control source maturation in fault-controlled depocenters (Cooper and Warren 2010). The extensional structures in the Bornu basin were already formed relative to the maturation of source rocks and peak migration and structures remained fully buried rather than uplifted and partly eroded, thus preserving seals and keeping source rocks intact.

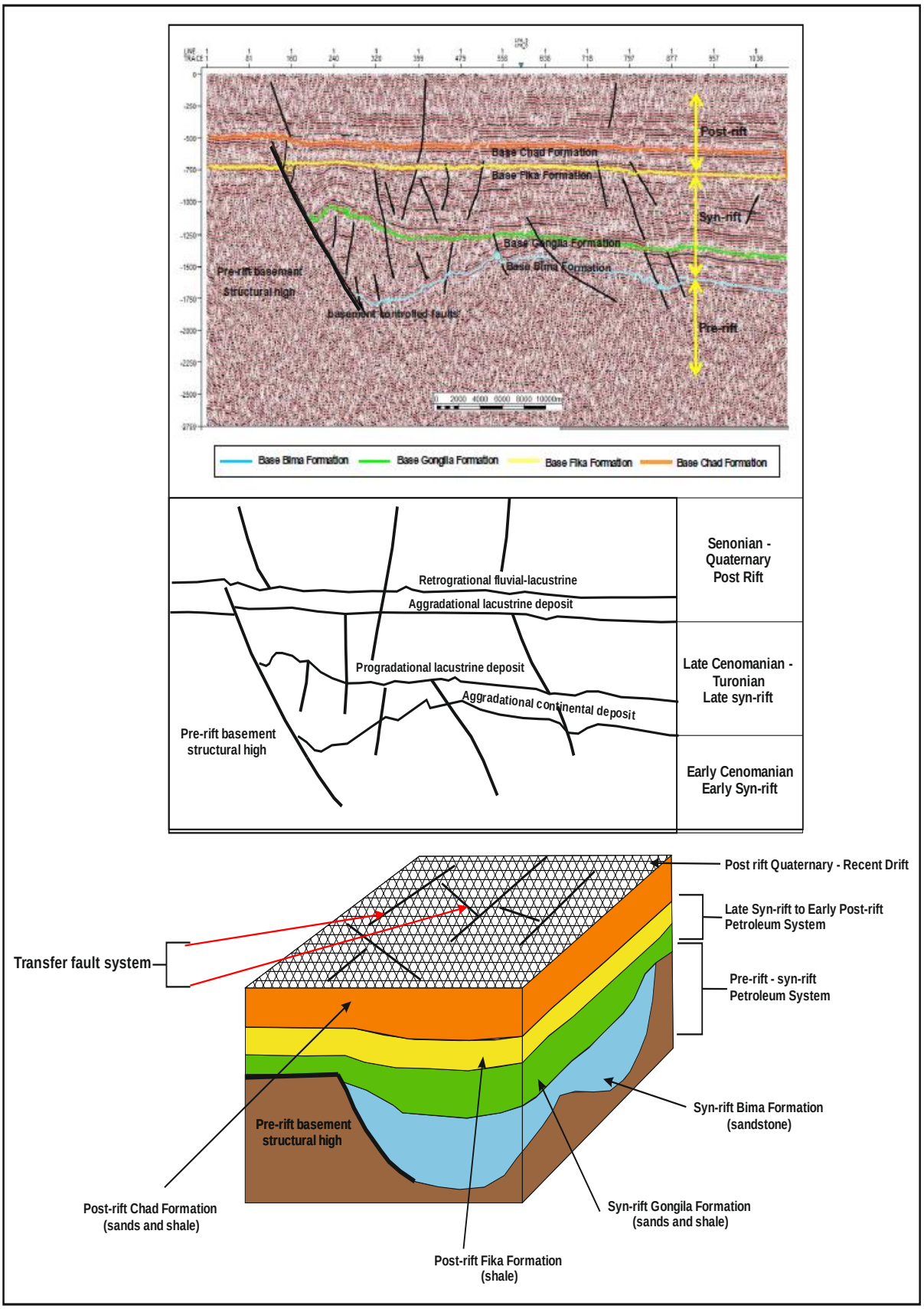

7.15. A schematic diagram showing the two petroleum systems identified from pre-rift to post-rift in the Bornu basin using the seismic data interpreted in this study and their relation to stages of basin evolution. Enlarged seismic section selected for this analysis is same as Fig 5.12. Also in Appendix B. Conceptual model is derived from the seismic section above with other information derived from gravity Figs. 6.12 and Landsat images 4.26 and 4.28 analyses.

7.5.4 *Petroleum exploration potentials of lineaments and spectral lithological mapping*

Synopsis of petroleum exploration potentials of lineaments and applications of lineaments and spectral mapping is already presented in section 3.7 of this thesis. This section presents synthesises of the applications of lineaments and spectral mapping in petroleum exploration from the results obtained in the preceding chapters in this thesis. Accordingly, in regions with poor rock exposures, where opportunities for field geological mapping are limited such as in the Bornu basin, the use of data with regional coverage is required to generate geological and structural maps. Thus, Earth Observation data applications are effective in providing a reliable and cost effective alternative for generating regional geological maps through identifying and mapping surface lithology and structures that can be correlated with subsurface structures to deduce hydrocarbon-trapping features (Gunn et al., 1997). Several oil and gas traps are formed during the Cretaceous - Tertiary rift evolution of the WCARS basins. Such traps are mainly extensional, transtensional and transpressional structural traps (Genik, 1992).

However, the origin and relationship of surface and subsurface lineaments are vital to the understanding of the processes associated with the extensional basin margins. As such, any potential oil and gas structural traps in the basin, if they exist, will likely be associated with the main structural groups. However, if hydrocarbon deposits were trapped in the study area by the outcropping propagated surface structures, hydrocarbon seepage may have been likely. However, the study area is more gas prone than oil as reportedly discovered in two wells drilled and no hydrocarbon seepage is reported in the area. More so, although the seismic data coverage is limited, only few subsurface structures are mapped as propagated and expressed on

the surface maps (Fig. 7.7b). This shows that the upward fault propagation is not widespread in the basin.

In this study, mapping of surface features using EO datasets indicate the predominant NE-SW and NW-SE lineaments that are herein proven to be expressions of the subsurface geological structures that might signify existence of the main potential structural trapping architecture for hydrocarbon migration and accumulation in the basin. Surface lineaments represent manifestations of subsurface controlling mechanisms for potential hydrocarbon traps. The subsurface transfer faults and their corresponding surface transfer zones are important features that indicate the distribution of hydrocarbon reservoirs. According to Morley, (1995), transfer zones are associated with topographic breaks provide entry points for large fluvial systems that form reservoir or source rocks in basins.

The spectral lithological boundaries mapped herein are shown to be intimately related to the surface lineaments in the north eastern Bornu basin. The Predictive Spectral Lithologic (PSL) mapping in the north eastern Bornu basin demonstrates high relevance for surface lithological classification in the semi-arid region where bedrock is covered with thick Quaternary sediment cover. Although, direct mapping of the obscured bedrock geology for hydrocarbon exploration in the basin remains difficult. Field validation of the spectral lithologic map remains indispensable. However, even the “boots on the ground” can be constrained in mapping the subtle lithologic variability in every ground cover in the study area. Thus, the traditional field outcrop mapping in this area will likely lead to under-sampling and extrapolation that lead to generalisations. Nonetheless, the spectral mapping remains an integral reconnaissance tool needed to constrain fieldwork.

7.6 *Tertiary non-deposition in the north-eastern Bornu basin*

Review of the Tertiary geology of the Bornu basin from previous works have been presented in sections 2.1, 2.2, .2.3.2, 2.3.3, 5.6.3, and 5.7 in this thesis.

Petters and Ekweozor (1982), Genik (1993), Reynolds and Jones (2004) and (Guiraud and Maurin 1992), observed that due to change in relative plate motions, specifically convergence between Africa and Europe, compressional inversion occurred locally in Santonian following a widespread unconformity. There were two cycles of renewed extension and subsidence in Late Cretaceous and Early Tertiary time, and finally regional uplift in Miocene, particularly in western Africa. Cycles of renewed extension and subsidence in the Late Cretaceous–Early Tertiary followed the widespread Santonian unconformity and later regional uplift in West Africa.

In the Bornu basin, the Tertiary is represented by Kerri-Kerri Formation, which is a flat lying NE dipping sedimentary layer that thins out beneath the overlying Chad Formation (Burke, 1976). This implies that the existence of the Tertiary formation is restricted in the southern part of the Bornu basin. This earlier finding is validated herein from the combined well log and seismic interpretation as the Tertiary deposition is not mapped in the north-eastern Bornu basin. The absence of the Tertiary sedimentation in the north-eastern Bornu basin is reportedly due to the existence of a depositional barrier formed by a granitic ridge (Barber and Jones, 1960). The absence of Tertiary sediments in the north-eastern Bornu basin was earlier supported by Miller et al., (1968) and Burke, (1976). The rift extensional movements in the Bornu basin were terminated during the Early Tertiary with the uplift of sediments and erosion of the early Tertiary reliefs of the south adjoining Benue Trough (Benkhelil, 1982).

It is herein supported that a Tertiary uplift existing near the north-eastern Bornu basin bordering the Maiduguri trough (Fig. 6.12) may have provided the barrier that

prevented the continuous deposition of Tertiary sediments from the Upper Benue Trough to the north-eastern Bornu basin, which explains why there is no Tertiary depositional record in the north-eastern Bornu basin. Additionally, this research validated that the Bornu Yassu – Bida high that borders the Maiduguri depocenter represents the uplifted mass that prevented the continuous deposition of the Tertiary Kerri Kerri Formation into the north-eastern basin, particularly in the Gubio- Munguno main depocenter, where the wells and seismic sections are located (Fig. 7.12b). This explains why the well log and seismic interpretations did not indicate presence of the Tertiary deposit in the basin. The Tertiary non-deposition is possibly due to a pinch out of the Tertiary Kerri-Kerri Formation that extends from the Benue trough but pinched out near the Maiduguri area before the deposition reached the north-eastern Bornu basin (Fig. 7.16).

The development of this event is interpreted herein to mark the end of the Cretaceous rifting and the beginning of a renewed rapid subsidence followed by sedimentation in the Quaternary in response to the crustal uplift and erosion of the basement areas that surround the Lake Chad Basin. The renewed subsidence accounts for the thick Quaternary sediments accommodation. As such, this research disagrees with findings in Olabode et al., (2015), Adepelumi et al., (2012) and Okpikoro and Olorunniwo, (2010) that indicated the presence of Tertiary sediments in the north eastern Bornu basin. However, the absence of the Tertiary deposit from the north-eastern Bornu basin as interpreted in the wells and seismic data analysis in this research is in agreement with Hamza and Hamidu 2012, Olugbemiro et al., 1997; Obaje et al., (2004); Boboye and Abimbola, (2009); Alalade and Tyson, (2010) as reviewed in section 2.3.2 of this thesis as well as presented in Isyaku et al., (2016). Stratigraphic analysis herein showing lack of Tertiary sediments in the north-eastern Bornu basin validated by the quantitative analysis of integrated well log and seismic data

interpretation is more reliable than by use of well log data in isolation as presented in Olabode et al (2015), the result of which is not validated by any other method.

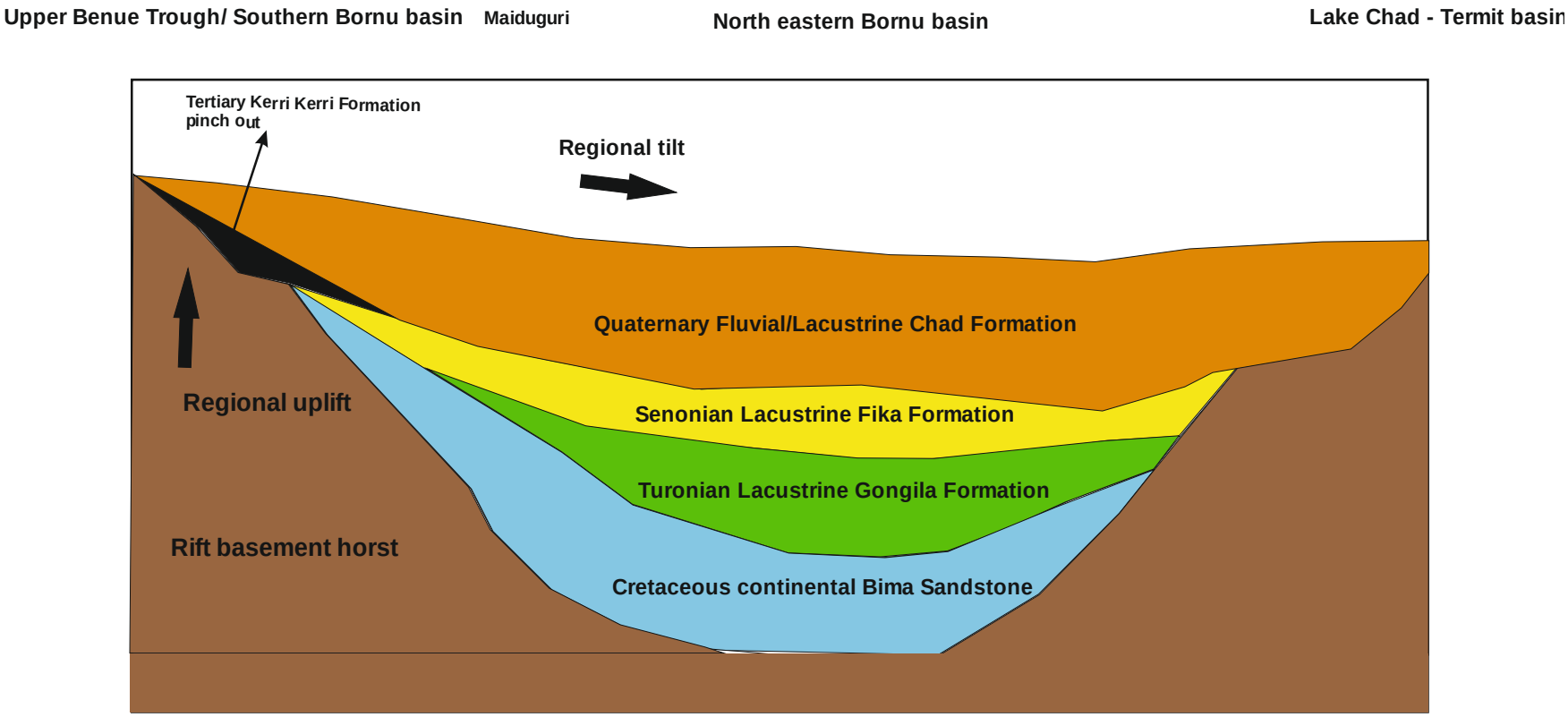

Fig. 7.16. Conceptual model showing schematic geological cross-section of the study area (drawn not to scale) based on the combined well log and seismic data analyses in this research. The regional uplift provided the barrier that prevented the continued deposition of the Tertiary and erosion that removed the formation in the north eastern Bornu basin. The slight regional tectonic tilting from the uplift of a few meters is derived from analysis of Fig. 4.25 due to the differences in elevations of the Bama Beach Ridge itself as well as the elevation difference between the Bama Beach Ridge and Ngelewa Ridge in the SRTM image Fig. 4.24.

Chapter 8:

Conclusions, summary and suggestions for future work

Combined application of remote sensing and geophysical data to study lithology and structures is common and practised since decades ago in various environments for hydrocarbon exploration and as standard procedures in the oil industry. Examples of similar previous works were acknowledged in section 1.1, sections 3.4 - 3.7 and other relevant sections in this thesis.

However, quite a few published works that specifically and inclusively combined well logs (inclusive of gamma ray, resistivity, bulk density, sonic logs), seismic, gravity, magnetic, Landsat 7 ETM+, SRTM DEM and Envisat radar data in GIS for geospatial lithostructural and tectonic studies are published. More so, development of these existing scientific techniques in the north - eastern Bornu basin to improve our existing knowledge regarding stratigraphy, lithology, structures and tectonic development of the basin is new.

In this thesis, the different data types were integrated to study geologic structures, tectonics, and lithostratigraphy of the north-eastern Bornu basin, with emphasis on significance of lineaments. Surface and subsurface geometry of the tectonic lineaments are investigated in the basin using integrated geophysical methods and satellite remote sensing datasets. From the interpretations, the subsurface structural lineaments and their surface manifestations have constrained the tectonic setting of the area within the regional rift setting. The datasets have also revealed basement configuration from aeromagnetic, gravity, seismic and well log, while subsurface stratigraphy and surface spectral lithological material of the basin were identified. This section presents a summary of the major findings and conclusions from Chapters, 4, 5, 6 and 7 of this thesis concerned with:

- Optical – radar - DEM integration for surface lithostructural analysis,
- Seismic – well log integration for subsurface stratigraphy and structure analysis,
- Gravity – magnetic data integration for basement structural analysis, as well as
- Discussions on surface and subsurface GIS correlation for tectonic and hydrocarbon evaluation.

Additionally, this summary presents the major findings on the tectonic setting and possible influence of the basin setting on the hydrocarbon potential within the context of regional tectonic setting presented in the literature review in Chapter 2. This section therefore addresses the specific objectives set in Chapter 1 by answering the earlier stated research questions and the hypothesis proposed.

1. Regarding Research Question 1: *How does combined optical, radar and DEM remote sensing/Earth Observation datasets apply for geomorphic, lithological and structural mapping in regions with flat topography and lack of bedrock outcrops*?

Geological remote sensing/Earth Observation data analysis utilising combined optical, radar and DEM imageries has proved applicable in lithostructural mapping of topographically flat semi-arid basins.

The hitherto surface structural mapping constraints due to flat topography and lack of continuous bedrock exposures in the north-eastern Bornu basin has been addressed by the combined use of Landsat 7 ETM+, Envisat ASAR and SRTM DEM images. The remote sensing/Earth Observation datasets proved useful in detecting surface and near surface structural lineaments over the large area. The georeferenced correlated spatial positions and trends of the lineaments described equally agreed with

previous studies and conform to the regional trends within the contiguous West African Rift System (WARS) basins. The effectiveness of the integrated method offers validation between the different remote sensing datasets used.

Radar imageries and SRTM DEM scenes analyses correlate with the result of optical Landsat 7 ETM+ data analysis validating the morphological characteristics in the basin. Although lineaments are detected from geological remote sensing analysis due to the variability of structurally related surface geomorphological features, this research finds that structures are better detected from the Landsat 7 ETM+ images and the SRTM DEM hill shade image mosaic than from the Envisat ASAR images. The geospatial positions and trends of structures are in good agreement with the results obtained from geophysical analyses particularly regarding lineaments and structural control of the Bama Beach Ridge palaeoshoreline, which is discernible on all the three types of Earth Observation datasets used herein. The remote sensing/Earth Observation method presents a cost effective approach for structural mapping in the north eastern Bornu basin than the traditional field traverse, which proved ineffective from previous studies in the basin. The stratigraphy of the north eastern Bornu basin is updated herein (Table 7.1) with the inclusion of the drift Quaternary to Recent Post - Chad deposits mapped from the spectral mapping method developed herein.

Validation of lineament mapping using combined automatic and manual methods

An effective methodology for mapping and tracing of morphotectonic lineaments has been developed in the north-eastern Bornu basin. The methods utilized automatic extraction using the LINE algorithm in *PCI Geomatica* from Landsat 7 ETM+ image mosaic subset as well manual tracing and digitisation in ArcMap to delineate surface lineaments and basement lineaments. GIS *ArcMap* software

highlighted the lineaments density area used for mapping the lineaments zones. A comparison made between the automatically mapped surface lineaments and lineament zones as well as basement lineaments from gravity and magnetic maps show good GIS correlation revealing the predominant NE-SW and NW-SE structural trends. While the visual tracing method is good for small scale observation, the automatic method is good for large scale mapping. Similarly, this study revealed that lineament zones, which group individual lineaments occurring closely together in parallel, intersecting or cross cutting relationships, reflected the same predominant NE-SW and NW-SE trends of the individual lineaments mapped from the various datasets. As such, comparison and correlation of the results of the different lineament maps offers validation of the different methods. The close agreement in geospatial locations and trends of the surface lineaments from the two methods in (Fig. 4.30) offer validation of the two lineament mapping results. The methodology involving lineament mapping and GIS correlation between manual digitised lineaments and the lineament zones mapped from the automatic method is an original approach to surface lineament mapping.

Despite the indispensable importance of traditional field geological mapping in establishing the preliminary understanding of the basin's geologic setting, field surveys have so far failed to identify and characterise the surface lineaments in the study area. This is due to the paucity of bedrock outcrops, flat topography and extensive surficial cover sediment that conceal the deformational features and make them ambiguous in the field. This problem was approached by the analyses of lineaments and lineament zones from remote sensing/Earth Observation images in this study. The spectral and spatial resolution of the Landsat 7 ETM+ composite image subset RGB and infrared (30 m) bands correlated with the 30 m resolution C-band Envisat ASAR images is superior for lineament identification in the area than the ASAR images.

Spectral lithological mapping in the semi-arid terrain achieved using supervised optical Landsat 7 ETM+ image classification.

A new detailed surface lithological map is generated for the Bornu basin using colour combination images from composite RGB band combination and band ratio Landsat 7 ETM+ images as base maps. The area is reportedly devoid of continuous bedrock exposures, hence, outcrop mapping is constrained by thick surficial cover having flat topography particularly throughout the north-eastern part of the Bornu basin. Thus, there is inadequate knowledge of the surficial lithologic units in the area. Consequently, in the absence of any published geological base map of the north-eastern Bornu basin, 7-4-1 RGB Landsat 7 ETM+ band combination image, which relatively gave the best highlight of the geological features provided the base knowledge of the spectral appearance of the various surficial deposits in the area. However, the composite image shows little spectral variation of the different lithological materials, but provided the basis for end-member training pixels selection, which form the basis for the supervised classification used.

Classical algorithm of the *Spectral Angle Mapper* in *ENVI* provided the capability to visually discriminate the subtle lithological variability in the north-eastern Bornu basin. However, mineralogical compositions of the mapped classes were determined using band ratios of the different band wavelengths to deduce their corresponding lithology. Accordingly, the surficial lithological materials are found to be more related to Quaternary deposition than they are likely sourced from the bedrock. Other geomorphic landforms including palaeodunes, palaeoshorelines and palaeodrainage were identified in the study area. The Predictive Spectral Lithological (PSL) map generated, thus, serves as a new drift geological base map for the north-eastern Bornu basin. Important preliminary validation of the spectral mapping is given by the geospatial alignment of surface lineaments along boundaries of the spectral

lithologies and the separation of the non-lithological materials in the area including the Lake Chad and the structurally aligned vegetation. Developing on the SAM approach for spectral lithological mapping herein using combined image band combination, image band ratio and SAM supervised classification to infer on surface lithology is an original approach.

2. Regarding Research Question 2: *What synergistic relationship exists in subsurface multiple data correlation to identify subsurface stratigraphy and structure?*

Integration of gravity and magnetic data as well as seismic and well log analysis validated the subsurface stratigraphy of the north-eastern Bornu basin, which influence the distribution of facies bearing potential hydrocarbon.

This study has demonstrated the effectiveness of geospatial data correlation and supports the objective of multi-source data integration. The present study, which utilised combined data analysis, has provided a detailed stratigraphic interpretation of the available subsurface data for the north-eastern Bornu basin. A new stratigraphy of the north-eastern area has been constrained within the general context of the Cretaceous – Recent sedimentary deposition in the Bornu basin.

Therefore, this study provided alternative method for stratigraphic studies in the basin characterised with flat topography and lack of bedrock outcrops and disputed the generalisations made from previous studies. Stratigraphic facies interpretation using cores and outcrop data, which were often affected by completeness of sections are most likely subjected to generalisation. However, subsurface facies characterisation from well log data allows for enhanced correlation of inferred strata from the continuous data. The following is specifically concluded:

A new subsurface stratigraphic classification consisting of Bima Formation, Gongila Formation, Fika Formation and Chad Formation is proposed herein for the north-eastern Bornu basin, while, Gombe Formation and the Tertiary Kerri-Kerri Formation were not deposited in the study area due to pinchout, uplift and erosion of the Tertiary sediments at the structural high along the Maiduguri depocentre. The stacking patterns of individual sedimentary formations were deduced from the combined well log analysis. Bima Formation and Fika Formation are characterised by aggradational stacking pattern. Gongila Formation is characterised by progradational stacking pattern, while Fika Formation is characterised by retrogradational stacking pattern. Subsurface thickness variation in the north-eastern Bornu basin revealed distinct depositional pattern of the formations in deep depocenters or mini basins flanked by shallower depth depositional centres. Depositional pattern in the area was controlled by the basement tectonic features consisting of horst and graben and associated faults, which originated from the Cretaceous rifting and basin evolution. The basal Bima Formation and Gongila Formation were deposited within the grabens, while the overlying formations are relatively unaffected by basement structures. The uppermost Chad Formation representing the thickest in the north-eastern area supports the existence of internal sequences representing further stratigraphic subdivisions within the formation. Thickness of the Chad Formation increases eastward towards the Lake Chad.

The close agreement in the computed two-way-time velocities of the sonic log and the seismic data correlation proved the synergistic relationship between the different data sets. In addition, synergistic analysis of multiple well log types herein presented provides more reliable interpretation of the subsurface well log stratigraphy.

This integrated study using combined multiple subsurface data analysis provides a new insights into the local stratigraphy in the north-eastern Bornu basin,

since the area is characterised with thick sediment cover and devoid of continuous bedrock outcrops necessary for any reliable field geological mapping. Effectiveness of the Combined Log Pattern (CLP) method proposed herein is therefore based on the synergistic relationship between the various physical properties measured by the different logging methods. The new CLP method has demonstrated that use of multiple log types increases the reliability of well log analysis for geological interpretation than using any single or dual combination of well log data. This combined well log analysis inclusive of gamma ray, resistivity, bulk density and sonic logs tied with seismic data is a novel approach for subsurface stratigraphic analysis in the basin.

The time structure maps for the subsurface seismic stratigraphy that are validated by the combined well log analysis and isochron thickness maps offer new insights into the subsurface stratigraphy and structure of the area. Structural closures determined from the time-structure map contours, which may be fault assisted or opened closures have direct bearing on the hydrocarbon trapping architecture in the basin. This seismic time structure data analysis using GIS technique to demonstrate fault propagation from pre-rift through syn-rift into post-rift sequence and their correlation with the gravity, magnetic mapped lineaments with surface structural lineaments is a novel approach.

3. Regarding Research Question 3: *What geotectonic relationship exists between the surface and subsurface structural lineaments in the Bornu basin and how does it influence petroleum prospectivity of the basin?*

The complimentary use of combined satellite Earth Observation image interpretation with multiple geophysical data has proved to be effective in correlating surface and subsurface tectonic structures in the Bornu basin.

Geometry of the north-eastern Bornu basin is clearly delineated on the interpreted surface and subsurface maps as a fault bounded basin characterised with structural highs and graben sub-basins. The axial eastern margin of Bornu basin is interpreted herein as the juncture at which the regional transverse NE-SW structural trend of the Bornu basin is oriented anticlockwise into the NW-SE trend of the Termit basin in Chad and Niger. As such, the two genetically related Bornu and Termit basins are likely to share a single depocenter at their shared palaeotectonic junction located beneath the Lake Chad. This relationship may have significant influence on the hydrocarbon distribution between the producing Termit basin and the Bornu basin. Moreover, there is no significant structural barrier between the two adjoining basins other than the obliquity of their predominant axial trends, which provides axial structural closure.

The hitherto unknown transfer fault structures and lineament zones in the basin are herein described. Transfer fault system detected for the first time in the north-eastern Bornu basin formed during the Early Cretaceous rifting may have reactivated and propagated to the surface to be indirectly detected as lineaments zones. The tectonic relationship of the transverse/transfer fault lineaments that defined the WARS extension as it affected the Bornu basin shows that the Bornu basin – Lake Chad boundary is a palaeotectonic transfer fault junction where the fault obliquity occurred

with a change in tectonic extension direction into the Termit basin. Barremian, Late Aptian – Early Albian and Late Santonian tectonic phases as they affected the Bornu basin are herein identified, where strike slip faulting was predominant in the Benue trough and NE-SW extension occurred in the Termit basin, the Bornu basin, which is situated in between the two adjoining basins was affected by a predominantly NW-SE short-lived extension, which occurred perpendicular to the main NE-SW basin rift trend. Surface and subsurface structural maps in the north-eastern Bornu basin show that the basement structures and their corresponding morphological expressions have good geospatial correlations. This is evident in the systematic linkages demonstrated herein between subsurface faults mapped in gravity, magnetic and seismic datasets with the surface lineaments mapped from Landsat 7 ETM+ imageries. Thus, this study emphasises on the synergistic and systematic use of multiple data for enhanced reliability of geological interpretations. It is found that the transverse basement structures played significant role in controlling the basement block configuration and were responsible for the geometry of elongated sub-basins during the Cretaceous rifting. Similarly, pre-existing pre-rift basement lineaments influenced the later reactivation and upward propagation of faults into the syn-rift and the post rift strata.

Convergence of the surface transverse NE-SW and NW-SE lineament zones at the Bama Beach Ridge surface lineament zone indicates the surface lineament zones were formed from reactivation of the Early Cretaceous basement deformation and upward propagation of the lineaments. More so, the structural correlation of the Bama Beach Ridge palaeoshoreline mapped from SRTM DEM, Landsat 7 ETM+ and Envisat ASAR images with underlying subsurface gravity and magnetic lineaments is thought to reflect initial existence of an irregular Pan African orogenic basement crustal structure in the basin, which controlled sedimentation and the southwestern axial margin of the Lake Chad shoreline. More so, the difference in topographic

elevations of the Bama Beach Ridge palaeoshoreline and its topographic elevation above the adjoining Ngelewa palaeoshoreline besides the Lake Chad shore indicate north-east ward structural tilting of the basin. The drainage mapping shows structural alignment of the major River Komadugu in the area, which appears to be flowing along the conjugate NE-SW and NW-SE fractures corresponding to the structural grain of the basin. Similar structural architecture in the south-western part of the study area involving river flowing along the NE-SW and NW-SE conjugate fractures is observed. As already acknowledged severally in this thesis, the fact that combining remote sensing and geophysical datasets analysis is a common approach, the development on the existing geospatial correlation of surface and subsurface geological features using combined datasets inclusive of Landsat 7 ETM+, SRTM DEM, seismic time-structure maps, gravity and magnetics map layers for the Bornu basin is a new approach to structural tectonic analysis.

A comparison between characteristics of the known oil trapping structures in the contiguous producing Termit basin in Niger and in Chad indicated additional consideration for further exploration in the tectonically linked north-eastern Bornu basin.

Occurrence of hydrocarbon associated with antithetic faults, graben features in several of the WARS basins in Chad, and Niger indicates that areas adjacent to the basin structures characterised by similar structures may provide same trapping mechanisms. Identification of the potential hydrocarbon systems in the Bornu basin from the syn-rift to post rift stratigraphic facies in the basin enhanced by the syn-rift to post rift antithetic and synthetic faulting identified, are mapped in the basin for the first time. Most of the discovered hydrocarbon accumulations in the Termit and Tenere basins in Chad and Niger are trapped in similar structural traps. Geographical

locations of all the wells drilled so far in the Bornu basin falls within the coordinate location of the interpreted NE-SW trending Gubio – Munguno rift zone identified on gravity maps. Additionally, this study has revealed other sub basins that were not delineated including Maiduguri trough and the Bama trough identified on gravity maps. Lineaments analysis in the Bornu basin show that the NW-SE trend, which corresponds with axial trend of the Termit basin strongly influenced the NW-SE trending faults as the predominant structures in the Termit basin. The structural closure provided by the intersecting predominant NE-SW and NW-SE fault lineaments in the Bornu basin might provide potential traps where they occur in the reservoir rocks. The predominance of extension features rather than compressional features in the north eastern Bornu basin, show that the Santonian inversion only had subtle effect on the basin as such most hydrocarbon trapping features are presumed to be preserved. The identification in the north-eastern Bornu basin, of similar structural trapping mechanism and shared tectonic setting that relates to those in the contiguous hydrocarbon producing Termit basin in Chad is an original contribution to our existing knowledge of the basin.

Research limitations

1. Although, surface data analysis segment of this research present alternative method to field survey specifically, in areas constrained by access, flat topography and ambiguity of lineament field identifications, field validation can be guided to ascertain their field occurrences.
2. The Predictive Spectral Lithological (PSL) mapping is constrained by the exclusive reliance on remote sensing spectral measurement, which offers improved prediction of the sedimentary deposits in the north-eastern Bornu basin for potential field survey. However, the field sampling of the surficial

materials would be required to ascertain their compositions and sediment provenances. Similarly, relative age and stratigraphy of the spectral lithological units cannot be determined from the PSL method.

3. The slight disparity only in extents of the geographical coverage of the regional gravity and magnetic datasets is an advantage for situating the geology identified from the constrained well log and seismic within the wider basement tectonic framework of the area.
4. The historical/legacy 2-D seismic data used in this study has reduced resolution for resolving fine fault geometries that would allow a more robust structural analysis. Structural correlation is constrained by the amount of seismic data available where only six seismic lines are available. More seismic data coverage in positions covered by the well data will enhance seismic-well data correlation and may indicate other structures from the time structure map layers used in the GIS for geospatial correlation with the surface lineament layers.

Recommendations for further work

Based on the inferences and limitations deduced from this research, the following are recommended:

1. Lineament extraction on the Level 1 Envisat ASAR images is difficult where lineaments are not easily discernible, as such, higher nominal processed level ASAR data may provide improved spectral resolution. User friendly, commercial processing software may produce better quality pre-processing result and fine textural details of the ASAR data.
2. Given that the basin is not an active oil and gas producing basin that would permit the use of SAR interferometry to detect subsidence due to hydrocarbon extraction, the InSAR technique may however, be useful in investigating effects of

local subsidence where excessive draw down of groundwater is reported in the area .

3. 3D seismic data modelling can resolve detail fault geometries and continuity including the identified synthetic and antithetic faults detected on the 2D seismic. Relative timing of the deformation in the basin as well as fault control on sedimentation and inversion can be better resolved in 3D seismic data.

4. Although aspects of the methodology presented in this study are variously applied by several workers in analogous basins and in the oil and gas industry. Nevertheless, the methods developed in the geological environment of the north eastern Bornu basin has improved our understanding of the basin and it can be applicable to regions of similar geologic setting where multiple surface and subsurface datasets necessary for the integrated study are available.

5. Fault control on sedimentation, relative timing of deformation from seismic and well logs may be used to evaluate the gravity and magnetic derived lineaments as fault related features.

Bibliography

Abafoni, J. D., A.S. Arabi, I.I. Funtua (2014). Luminescence chronology of the Bama Beach Ridge, Chad Basin, north eastern Nigeria. *Quaternary International* 338, 42-50.

Abdelsalam, M.G., Stern, R.J. and Berhane, W.G. (2000a). Mapping gossans in arid regions with Landsat TM and SIR-C images: The Beddaho alteration zone in northern Eritrea. *Journal of African Earth Sciences*, 30(4), p.903–916.

Abdelsalam, M., Robinson, C., El-Baz, F. and Stern, R. (2000b). Applications of orbital imaging radar for geologic studies in arid regions: the Saharan testimony. *Photogrammetric Engineering and Remote Sensing*, 66, p.717–726.

Abdullah, A., Nassr, S. and Ghaleeb, A. (2013). Landsat ETM-7 for Lineament Mapping using Automatic Extraction Technique in the SW part of Taiz area, Yemen. *Global Journal of Human Social Science, Geography, Geo-Sciences, Environmental and Disaster Management*, 13(3).

Abdul-Qadir, A.M. (2013) Supervised Classification for Lithologic Discrimination in Shaikh Ibrahim Area, NW Iraq Using Landsat Images. *Arabian Journal for Science and Engineering*, 39(1), p.437–451.

Abrams, M. and Hook, S.J. (1995). Simulated Aster data for geologic studies. *IEEE Transactions on Geoscience and Remote Sensing*, 33(3), p.692–699.

Abrams, M.J., Rothery, D.A. and Pontual, A. (1988). Mapping in the Oman ophiolite using enhanced Landsat Thematic Mapper images. *Tectonophysics*, 151(1-4), p.387–401.

Adams K. D and Steven G. Wesnousky (1998). Shoreline processes and the age of the Lake Lahontan highstand in the Jessup embayment, *Nevada. GSA Bulletin*; v. 110; no. 10; p. 1318–1332;

Adeigbe, O.C. and Abimbola, A.F. (2013) The Cretaceous -tertiary Clastic rocks weathering indices: A case study of Maastrichtian?-Paleocene rock Succession, Bornu Basin Northeastern Nigeria. *International Journal of Engineering Sciences and Research Technology*, 2(2), p.122–130.

Adepelumi, A.A., Alao, O.A., Ako, B.D. And Oseikpe, R.E. (2012). Modeling of Hydrocarbon Potential and Thermal Maturity of Gongila Shale, Chad Basin, Northeastern Nigeria. *Oil Shale*, 29(2), p.151.

Adegoke, A.K., Abdullah, W.H., Hakimi, M.H. and Sarki Yandoka, B.M. (2014) Geochemical characterisation of Fika formation in the Chad (Bornu) basin, northeastern Nigeria: Implications for depositional environment and tectonic setting. *Applied Geochemistry*, 43, p.1–12.

Agagu, O.K, and Ekweozor, C.M., (1980): Petroleum Geology of Senoniam sediment in Anambra syncline, Southern Nigeria, (abs.). AAPG Bulletin 64: 668.

Ajakaiye, D. E., Hall, D. H., Miller, T. W., Verheigen, P. J. T., Awad, M. B and Ojo, S. B. (1986). Magnetic Anomalies and Tectonic Trends in and around the Benue Trough. Nature. 319, 582 – 584.

Akande, S.O., Ojo, O.J., Erdtmann, B.D., Hetenyi, M., (1998). Paleoenvironments, source rock potential and thermal maturity of the Upper Benue rift basins, Nigeria: implications for hydrocarbon exploration. Org. Geochem. 29, 531-542.

Alalade, B. and Tyson, R.V. (2010). Hydrocarbon Potential of the Late Cretaceous Gongila and Fika Formations, Bornu (Chad) Basin, Ne Nigeria. *Journal of Petroleum Geology*, 33(4), p.339–353.

AL Fastawi, Y.A. and Van Dijk, P.M. (1990). Lineament and Geomorphic Analysis of Remote Sensing Data as an Aid to Hydrocarbon Exploration, Sirt Basin, Libya. *ITC Journal Bulletin de l'ITC* (2), p.137–144.

Anakwuba, E. and Chinwuko, A. (2012). Re-Evaluation of Hydrocarbon Potentials of Eastern Part of the Chad Basin, Nigeria: An Aeromagnetic Approach *AAPG Annual Convention and Exhibition*. Long Beach, California: AAPG.

Anakwuba, E.K., Onwuemesi, A.G., Chinwuko, A.I. and Onuba, L.N. (2011) The interpretation of aeromagnetic anomalies over Maiduguri – Dikwa depression, Chad Basin Nigeria: A structural view. *Archives of Applied Science Research*, 2011(34), p.499–508.

Arlegui, L.E. and Soriano, M.A. (1998) Characterizing lineaments from satellite images and field studies in the central Ebro basin (NE Spain). *International Journal of Remote Sensing*, 19 (16), p.3169–3185.

Asquith, G.B. and Gibson, C. R. (1982) *Basic well log analysis for geologists American 761 Association of Petroleum Geologists, Methods in Exploration Series No. 3.*. AAPG.

Athanasios, A. (2012). *A methodology for the rapid identification of neotectonic features using geographical information systems and remote sensing: a case study from Western Crete, Greece. Unpublished PhD thesis, University of Portsmouth.*

Avbovbo, A.A., Ayoola, E.O. and Osahon, G.A. (1986) Depositional and structural styles in Chad Basin of northeastern Nigeria. *AAPG Bulletin*, 70(12), p.1787–1798.

Aydogan, D., Pinar, A., Elmas, A., Bal, O. and Yuksel, S. (2013). Imaging of subsurface lineaments in the southwestern part of the Thrace Basin from gravity data. *Earth, Planets and Space*, 65(4), pp.299-309.

Baars, D.L. (1995) Basement tectonic configuration in Kansas. *Kansas geological Survey Bulletin*, 237 [Online]. Available at: http://www.kgs.ku.edu/Publications/Bulletins/237/Baars1/.

Barber, W. and Jones, D.G. (1960). The Geology and Hydrology of Maiduguri, Bornu Province (Unpublished Records) Geological Survey of Nigeria.1958, P1-20

Benkhelil, J. (1982) Benue trough and Benue chain. *Geological Magazine*, 119 (02), p.155.

Benkhelil, J. (1987) Cretaceous deformation, magmatism, and metamorphism in the lower Benue trough, Nigeria. *Geological Journal*, 22(S2), p.467–493.

Benkhelil, J., (1988). Structure et évolution géodynamique du bassin intracontinental de la Bénoué, (Nigéria) [Thèse d'Etat]. Univ. Nice. and Bull. Cent. Rech. Explor. Prod. Elf Aquitaine, 12: 29–128.

Binks, R.M. and Fairhead, J.D. (1992). A plate tectonic setting for Mesozoic rifts of west and central Africa. *Tectonophysics*, 213(1-2), p.141–151.

Boboye, O.A. and Abimbola, A.F. (2009) Hydrocarbon potential of the Lithostratigraphic units in late Cenomanian-Early Paleocene Shale, southwestern Chad Basin. *World Applied Sciences Journal*, 7(5), p.567–573.

Boboye, O., A., and Akaegbobi, I., M. (2012). Sedimentological and Palyno-environmental appraisal of the late quaternary sediments, north-eastern Bornu Basin. Quaternary International 262, 14-19.

Boboye, O.A., Nzegwu, U.A., (2014). Evaluation of bio-molecular signatures and hydrocarbon potential of upper Cretaceous Shale, NE Nigeria. J. Afr. Earth Sci.

Bond, G. (1978). Evidence for Late Tertiary uplift of Africa relative to North America, South America, Australia and Europe. J. Geol., v. 86, p. 47-65.

Bueno, J.F., Honório, B.C.Z., Kuroda, M.C., Vidal, A.C. and Leite, E.P. (2014). Structural and stratigraphic feature delineation and facies distribution using seismic attributes and well log analysis applied to a Brazilian carbonate field. *Interpretation*, 2(1), p.SA83–SA92 [Online]. Available at: http://www.yourknowledge.com.br/public/cms/mat/2/published-interpretation.pdf [Accessed: 15 July 2016].

Burke, K.C. (1969), Seismic areas of the Guinea coast where Atlantic fracture Zones reach Africa. *Nature* 222: 655 – 677.

Burke, K. (1976). The Chad Basin: An active intra-continental basin. *Tectonophysics*, 36(1-3), p.197–206.

Burke, K. and Dewey, J. F. (1974). Two plates in Africa during the Cretaceous. Nature, Lond. 249,313-315.

Caran, S.C., Woodruff, Jr, C.M. and Thompson, E.J. (1982). Lineament Analysis and Inference of Geologic Structure — Examples from the Balcones/Ouachita Trend of Texas. *Transactions of the Gulf Coast Association of Geological Societies*, XXXI, p.59–69.

Carter, J.B. (1963). The geology of parts of Adamawa, Bauchi and Bornu provinces in northeastern Nigeria. *Geol. Surv. Nigeria Bull*, 30.

Chaabouni, R., Bouaziz, S., Peresson, H. and Wolfgang, J. (2012). Lineament analysis of south Jenein area (southern Tunisia) using remote sensing data and geographic information system. *The Egyptian Journal of Remote Sensing and Space Science*, 15(2), p.197–206.

Chinwuko, A.I., Onwuemesi, A.G., Anakwuba, E.K., Onuba, L.O. and Nwokeabia, N.C. (2012) Interpretation of Aeromagnetic anomalies over parts of upper Benue trough

and southern Chad Basin, Nigeria. *Advances in Applied Science Research*, 2012(33), p.1757–1766.

Chambers, J.; Weller, A.; Gunn, D.; Kuras, O.; Wilkinson, P.; Meldrum, P.; Ogilvy, R.; Jenkins, G.; Gibson, Andy; Ford, J.; Price, S. (2008). Geophysical anatomy of the Hollin Hill landslide, North Yorkshire, UK. *Near Surface 2008*: 14th European Meeting of Environment. and Engineering Geophysics, Krakow, Poland.

Chavez, P.T. and Kwarteng, A.Y. (1989). Extracting spectral contrast in Landsat Thematic Mapper image data using selective principal component analysis. *Photogrammetric Engineering and Remote Sensing,* 55(3), p.339–348.

Chukwunonso, O.C., Godwin, O.A., Kenechukwu, A.E., Ifeanyi, C.A., Emmanuel, I.B. and Ojonugwa, U.A. (2012) Aeromagnetic interpretation over Maiduguri and environs of southern Chad Basin, Nigeria. *Journal of Earth Sciences and Geotechnical Engineering*, 2(2012), p.77–93.

Clark, D.A. (1999). Magnetic petrology of igneous intrusions: Implications for exploration and magnetic interpretation. *Exploration Geophysics*, 30(2), p.5.

Cobbold, P.R., Meisling, K.E., Mount, V.S., (2001). Reactivation of an obliquely-rifted margin, Campos and Santos basins, southeastern Brazil. AAPG Bull. 85, 1925e1944.

Cooper, M., Warren, M.J., (2010). The Geometric Characteristics, Genesis and Petroleum Significance of Inversion Structures, vol. 335. Geological Society Special Publications, pp. 827-846.

Cortés, A.L., Maestro, A., Soriano, M.A. And Casas, A.M. (1998). Lineaments and fracturing in the Neogene rocks of the Almazán Basin, northern Spain. *Geological Magazine*, 135(2), p.255–268.

Corti, G., vanWijk, J., Cloetingh, S., Morley, C.K., (2007). Tectonic inheritance and continental rift architecture: numerical and analogue models of the East African Rift System. Tectonics 26.

Cratchley, C.R., Louis, P. and Ajakaiye, D.E. (1984). Geophysical and geological evidence for the Benue-Chad basin Cretaceous rift valley system and its tectonic implications. *Journal of African Earth Sciences (1983)*, 2(2), p.141–150.

Crippen, R.E., (1989). Selection of Landsat TM band and band-ratio combinations to maximize lithologic information in color composite displays. In*: Proceedings of the Seventh Thematic Conference on Remote Sensing for Exploration Geology* II, pp. 912–921.

Dasgupta, S.N., Aminzadeh, F. and Rector, J.W. (2013). *Geophysics for petroleum engineers*. United Kingdom: Elsevier Science.

De Castro, D., R. Branco, G. Martins, and N. de Castro (2002). Radiometric, magnetic, and gravity study of the Quixada batholith, central Cear ´ a´ domain (NE Brazil): evidence for Pan-African/Brasiliano extensioncontrolled emplacement, J. South Am. Earth Sci., 15, 543–551,.

De Castro D. L., Francisco H. B, Reinhardt A. F and Roberta M. V. (2016). Geophysical evidence of pre-sag rifting and post-rifting fault reactivation in the Parnaíba basin, Brazil. *Solid Earth*, 7, 529–548.

Dohr, G. (1981). *Applied Geophysics: Introduction to Geophysical Prospecting*. 2nd ed. Stuttgart: Ferdinand Enke.

Dou, L., Xiao, K., Cheng, D., Shi, B. and Li, Z. (2007). Petroleum geology of the Melut basin and the great Palogue field, Sudan. *Marine and Petroleum Geology*, 24(3), p.129–144.

Doust, H. and Lijmbach, G.W.M. (1997). Charge constraints on the hydrocarbon habitat and development of hydrocarbon systems in Southeast Asia Tertiary basins. *Proceedings of the Petroleum Systems of SE Asia and Australasia Conference.* IPA 97-OR-16. Indonesian Petroleum Association.

Drury, S.A. (2001). *Image interpretation in geology*. 3rd ed. United Kingdom: Routledge.

Dufréchou, G. and Harris, L.B. (2013). Tectonic models for the origin of regional transverse structures in the Grenville province of SW Quebec interpreted from regional gravity. *Journal of Geodynamics*, 64, p.15–39.

Dufréchou, G., Harris, L. and Corriveau, L. (2014). Tectonic reactivation of transverse basement structures in the Grenville orogen of SW Quebec, Canada: Insights from gravity and aeromagnetic data. *Precambrian Research*, 241, pp.61-84.

Dunbar, J.A. and Sawyer, D.S. (1989). How pre-existing weaknesses control the style of continental breakup. *Journal Geophysical Research*, 94(B6), p.7278–7292.

Durand, A. (1982): Oscillations of the Lake Chad over the past 50,000 years. New data and hypothesis. Paleoclimatology, Vol.39. PP 37-53.

Drake N. and C. Bristow (2006). Shorelines in the Sahara: geomorphological evidence for an enhanced monsoon from palaeolake Megachad. *The Holocene* 16, 6 pp. 901 – 911.

Edet, A.E., Okereke, C.S., Teme, S.C. and Esu, E.O. (1998). Application of remote-sensing data to groundwater exploration: A case study of the Cross River State, southeastern Nigeria. *Hydrogeology Journal*, 6(3), p.394–404.

El Hassan W. M., Abdalla G. F., Mohamed Z. A. (2017). Inversion tectonics in Central Africa Rift System: Evidence from the Heglig Field. *Marine and Petroleum Geology 80. pp293 -306.*

Ellis, D.V., and Singer, J.M. (2008). Well Logging for Earth Scientists. Second Editions. Springer, Netherlands.

Evans, D., (1988). Multi-sensor classification of sedimentary rocks. *Remote Sensing of the Environment* 25, 129–144.

Fairhead, J.D. (1988). Mesozoic Plate Tectonic Reconstructions of the Central South Atlantic Ocean: The Role of the West and Central African Rift System. *Tectonophysics*, 155, 181-191.

Ferretti, A. (2014). Satellite InSAR Data: Reservoir Monitoring from Space, EAGE Publications.

Gasse, F., (2000). Hydrological changes in the African tropics since the Last Glacial Maximum. *Quaternary Science Reviews,* 19, 189-211.

Gardner, G.H.F., Gardner, L.W., and Gregory, A.R., (1974). Formation velocity and density – The diagnostic basics for stratigraphic traps: Geophysics, 39, 770-780.

Gad S. and T. Kusky (2006). Landsat TM data and field studies in the central highlands of Eritrea Lithological mapping in the Eastern Desert of Egypt, the Barramiya area, using Landsat thematic mapper (TM), Journal of African Earth Science 44 (196-202).

Gad, S. and Kusky, T. (2007). ASTER spectral ratioing for lithological mapping in the Arabian–Nubian shield, the Neoproterozoic Wadi Kid area, Sinai, Egypt. *Gondwana Research, 11*(3), 326-335.

Gannouni, S. and Gabtni, H. (2015). Structural Interpretation of Lineaments by Satellite Image Processing (Landsat TM) in the Region of Zahret Medien (Northern Tunisia). Journal of Geographic Information System, 7, 119-127.

Gay, Jr., S.P. (2012). Joints, Linears, and Lineaments – The Basement Connection *AAPG Rocky Mountain Section Meeting*. Grand Junction, Colorado: AAPG Search and Discovery Article #41083.

Gaffey, S.J. (1987). Spectral reflectance of carbonate minerals in the visible and near infrared (0.35–2.55 microns): calcite, aragonite, and dolomite. *American Mineralogist* 71, 151–162.

Genik, G.J. (1992). Regional framework, structural and petroleum aspects of rift basins in niger, Chad and the Central African Republic (C.A.R.). *Tectonophysics*, 213(1-2), p.169–185.

Genik, G.J. (1993). Petroleum geology of Cretaceous-Tertiary rift basins in Niger, Chad, and Central African Republic. *AAPG Bulletin*, 77, p.1405–1434.

Gibson, R.I. and Millegan, P.S. (eds.) (1998) *Geologic applications of gravity and magnetics: Case histories*. Tulsa, OK: Published jointly by the Society of Exploration Geophysicists and the American Association of Petroleum Geologists.

Girouard, G., Bannari, A., El Harti, and A., Desrochers, A., (2004). Validated spectral angle mapper algorithm for geological mapping: comparative study between QuickBird and Landsat-TM. In: XXth ISPRS Congress, Geo-imagery Bridging Continents, Istanbul, Turkey, pp. 12-23.

Ghoneim E., C. Robinson and F. El-Baz (2007). Radar topography data reveal drainage relics in the eastern Sahara, International Journal of Remote Sensing, 28:8, 1759-1772.

Grandjean, G., Paillou, P., Baghdadi, N., Heggy, E., August, T. and Lasne, Y. (2006). Surface and subsurface structural mapping using low frequency radar: A synthesis of the Mauritanian and Egyptian experiments. *Journal of African Earth Sciences*, 44(2), p.220–228.

Grant, N.K. (1971). South Atlantic, Benue trough, and gulf of guinea Cretaceous triple junction. *Geological Society of America Bulletin*, 82(8), p.2295.

Guiraud, R. and Bellion, Y., (1995). Late Carboniferous to Recent geodynamic evolution of the West Gondwanian Cratonic Tethyan margins. In: Nairn, A., Dercourt, J., Vrielynck, B. (Eds.), The Ocean Basins and Margins, Vol. 8: The Tethys Ocean. Plenum Press, New York, NY, pp. 101-124.

Guiraud, R., Bellion, Y., Benkhelil, J. and Moreau, C. (1987). Post-Hercynian tectonics in northern and western Africa. *Geological Journal*, 22(S2), p.433–466.

Guiraud, R. and Maurin, J. C. (1992). Early Cretaceous rifts of western and central Africa: An overview. *Tectonophysics*, 213(1-2), p.153–168.

Guiraud, R. and Bosworth, W. (1997). Senonian Basin Inversion and Rejuvenation of Rifting in Africa and Arabia: Synthesis and Implications to Plate-Scale Tectonics. Tectonophysics, 282, 39-82.

Guiraud, R., Bosworth, W., Thierry, J., Delplanque, A., (2005). Phanerozoic geological evolution of Northern and Central Africa: an overview. *Journal of African Earth Sciences* 43, 83–143.

Gunn, P.J., Maidment, D. and Milligan, P.R. (1997). Interpreting aeromagnetic data in areas of limited outcrop. *Journal of Australian Geology and Geophysics*, 17(2), p.175–185.

Guo, G. and Caroll, H.B. (1995). *A new methodology for oil and gas exploration using remote sensing data and surface fracture analysis*. Bartlesville, Oklahoma: US National Petroleum Technology Office Report. DOE/PC/91008-0163.

Guo, G. and George, S.A. (1999). *An Analysis of Surface and Subsurface Lineaments and Fractures for Oil and Gas Exploration in the Mid-Continent Region*. Tulsa, Oklahoma: US Department of Energy.

Guo, G., George, S.A. and Lindsey, R.P. (1997). Analysis of surface lineaments and fractures for hydrocarbon exploration and production optimization in the mid-continent region *SPE Annual Technical Conference and Exhibition*. San Antonio Texas: Society of Petroleum Engineers.

Habib, M., Xie, C., (2012). Nigeria's inland basins: investment opportunities and environment. J. Petrol. Gas Explor. Res. 2, 202-211.

Harbord, (n.d.). Electromagnetic spectrum showing wavelength ranges Retrieved from http://geology.wlu.edu/harbor/geol260/lecture_notes/notes_rs1.html.

Hamza, H. and Hamidu, I. (2012). Hydrocarbon resource potential of the Bornu basin northeastern Nigeria. Global Journal of Geological Sciences. *Global Journal of Geological Sciences*, 10(1).

Harris, J.R., Schetselaar, E. and Behni, P. (2012). Remote predictive mapping: An approach for the geological mapping of Canada's arctic. *Earth Sciences*.

Herron, D. A. (2011). First steps in seismic interpretation. *SEG, Geophysical Monograph*, 16.

Herron, D. A. (2014). Tutorial: Tying a well to seismic using a blocked sonic log. *Interpretation*, 2(2), p.SD1–SD7.

Hubbard B. E. T. J. Mack, and A. L. Thompson (2012). Lineament Analysis of Mineral Areas of Interest in Afghanistan, Open-File Report 2012–1048 *USGS Afghanistan Project Product No. 233* U.S. Department of the Interior U.S. Geological Survey.

Hung, L.Q., Batelaan, O. and De Smedt, F. (2005). Lineament extraction and analysis, comparison of LANDSAT ETM and ASTER imagery. Case study: Suoimuoi tropical karst catchment, Vietnam</title>. *Remote Sensing for Environmental Monitoring, GIS Applications, and Geology V*.

Hunt, J. M. (1995). *Petroleum geochemistry and geology*. New York, NY: W.H.Freeman and Co.

Igbokwe, O.A. (2011). *Stratigraphic Interpretation of Well-Log data of the Athabasca Oil 817 Sands Alberta Canada through Pattern recognition and Artificial Intelligence. 818 Unpublished MSc Thesis Westfälische Wilhelms-Universität Münster (WWU)*.

Idris, K. M. and Yongdi, S., (2004). Lateral Seal – A major exploration risk in the faulted traps of the Cretaceous petroleum system – central Muglad Basin, Sudan; American Association of Petroleum Geologists Bulletin, 88, Supplement,

Insley, M., E X. Murphy, D. Naylor and M. Critchley (1996). The use of satellite imagery in the validation and verification of structural interpretations for hydrocarbon exploration in Pakistan and Yemen. From Buchanan, R G. and Nieuwland, D. A. (eds), 1996, Modem Developments in Structural Interpretation, Validation and Modelling, *Geological Society Special Publication* No. 99, pp. 321-343.

Inzana, J., Kusky, T., Higgs, G. and Tucker, R. (2003). Supervised classifications of Landsat TM band ratio images and Landsat TM band ratio image with radar for geological interpretations of central Madagascar. *Journal of African Earth Sciences*, 37(1-2), p.59–72.

Isiorho, S.A. and Nkereuwem, T.O. (1996). Reconnaissance study of the relationship between Lineaments and fractures in the southwest portion of the lake Chad Basin. *Journal of Environmental and Engineering Geophysics*, 1(1), p.47–54.

Isiorho, S.A., Taylor-Wehn, K.S. and Nkereuwem, T.O. (1992). The relationship between Lineaments and fractures in Chad Basin. *Symposium on the Application of Geophysics to Engineering and Environmental Problems 1992*, p.509–518.

Isles, D.J. and Rankin, L.R. (2013). *Geological interpretation of aeromagnetic data*. Collingwood Australia: Australian Society of Exploration Geophysicists.

Isyaku A. A., D. Rust, R. Teeuw, M. Whitworth (2016). Integrated well log and 2-D seismic data interpretation to image the subsurface stratigraphy and structure in north-eastern Bornu (Chad) basin. *Journal of African Earth Sciences* 121, 1-15.

Jensen, J.R. (1996) *Introductory Digital Image Processing*. Prentice Hall Series in Geographic Information Science ed.

Jensen, J.R. (2000). *Introductory digital image processing: A remote sensing perspective*. 2nd ed. Upper Saddle River, NJ: Prentice Hall.

Karnieli, A., Meisels, A., Fisher, L. and Arkin, Y. (1996). Automatic extraction of geological linear features from digital remote sensing data using a Hough Transform. *Photogrammetric Engineering and Remote Sensing*, 62, p.525–531.

Kodikara, G. R. L., P.K. Champati ray, P. C. R.S. Chatterjee (2016). Spectral mapping of morphological features on the moon with MGM and SAM. *International Journal of Applied Earth Observation and Geoinformation*. Volume 44, February 2016, Pages 31-41.

Kassenaar, J.D. (1989). *Automated Classification of Geophysical Well Logs.Unpublished 826 MSc Thesis University of Waterloo, Ontario Canada*. [Online]. Available at: Retrieved from 827 ftp://earthfx.com/software/vlw3/brochure/MultiWell%20Papers/Kassenaar%20Thesis. 828 pdf.

Kaymakci, N., Özmutlu, Ş., Van Dijk, P.M. And Özçelik, Y. (2010). Surface and subsurface characteristics of the Çankırı basin (central Anatolia, turkey): Integration of remote sensing, seismic interpretation and gravity. *Turkish Journal of Earth Sciences*, 19(1), p.100–79.

Kenea, N.H. (1997) Improved geological mapping using Landsat TM data, southern red sea hills, Sudan: PC and IHS decorrelation stretching. *International Journal of Remote Sensing*, 18(6), p.1233–1244.

Kenneth, H. and Alan, H. (2003). *Interpretation of Shaly Sands* [Online]. Available at: http://www.lps.org.uk/docs/heslop_shaly_sands.pdf.

Khatiwada, M., Keller, G.R. and Marfurt, K.J. (2013). A window into the Proterozoic: Integrating 3D seismic, gravity, and magnetic data to image subbasement structures in the southeast Fort Worth basin. *Interpretation*, 1(2), p.T125–T141.

Kim, G.-B., Lee, J.-Y. and Lee, K.-K. (2004b) Application of representative elementary area (REA) to lineament density analysis for groundwater implications. *Geosciences Journal*, 8(1), p.27–42.

Kingston, D.R., Dishroon, C.P. and Williams, P.A. (1983). Global basin classification system. *American Association of Petroleum Geologists' Bulletin,* **67** (12), 2175–2193.

Komolafe, A. A., Z. N. Kuria, T. M. Noomen and Y. B. A. Adeleye (2012). Integrated Remote Sensing and Geophysical Investigations of the Geodynamic Activities at Lake

Magadi, Southern Kenyan Rift. *International Journal of Geophysics* Volume 2012 (2012), Article ID 318301.

Koike, K., Nagano, S. And Ohmi, M., (1995). "Lineament Analysis of Satellite Images Using A Segment Tracing Algorithm (STA)", Computers and Geosciences, Vol. 21, No. 9, 1091-1104.

Koike, K., Nagano, S. and Kawaba, K. (1998). Construction and analysis of interpreted fracture planes through combination of satellite-image derived lineaments and digital elevation model data. *Computers and Geosciences*, 24(6), p.573–583.

Krassay, A. A. (1998). Outcrop and drill core gamma-ray logging integrated with sequence 832 stratigraphy: examples from Proterozoic sedimentary successions of northern 833 Australia. *AGSO Journal of Australian Geology and Geophysics*, 17(4), p.285–299.

Kruse, F.A., Lefkoff, A.B., Boardman, J.W., Heidebrecht, K.B., Shapiro, A.T., Barloon, P.J. and Goetz, A.F.H. (1993). The spectral image processing system (SIPS)—interactive visualization and analysis of imaging spectrometer data. *Remote Sensing of Environment*, 44(2-3), p.145–163.

Kusky, T.M. and Ramadan, T.M. (2002). Structural controls on Neoproterozoic mineralization in the South Eastern Desert, Egypt: an integrated field, Landsat TM, and SIR-C/X SAR approach. *Journal of African Earth Sciences*, 35(1), p.107–121.

Laake, A., Al-Alawi, H. and Gras, R. (2006). Integration of remote sensing data with geology and geophysics – Case study from Bahrain, GEO 2006, Manama, March 2006.

Laake, A. and Cutts., A. (2007). The role of remote sensing data in near-surface seismic characterization, First Break, Vol. 25, pp. 51 – 55.

Laake, A., Strobbia, C. and Cutts, A. (2008). Integrated approach to 3D near surface characterization in desert regions. *First break*, 26, p.109–112.

Laake, A., Sheneshen, M., Strobbia, C., Velasco, L. and Cutts, A. (2011). Integration of surface/subsurface techniques reveals faults in Gulf of Suez oilfields, Petroleum Geoscience, Vol. 17, 2011, pp. 165–179.

Laake A. and M. Insley (2004). Applications of satellite imagery to seismic survey design. *The Leading Edge*. 1062-1064.

Leech, D.P., Treloar, P.J., Lucas, N.S. and Grocott, J. (2003). Landsat TM analysis of fracture patterns: A case study from the coastal Cordillera of northern Chile. *International Journal of Remote Sensing*, 24(19), p.3709–3726.

Lenov, Y.G. (1991). Intraplate tectonics in the light of tectonic layering of the earth crust. *Geotectonics*, 25(6), p.459–472.

Leverington, D.W. and Moon, W.M. (2012). Landsat-TM-Based Discrimination of Lithological Units Associated with the Purtuniq Ophiolite, Quebec, Canada. *Remote Sensing*, 4(12), p.1208–1231.

Lillesand, T.M., Kiefer, R.W. and Chipman, J.W. (2004). *Remote sensing and image interpretation*. 5th ed. New York, NY: Wiley, John and Sons.

Lillesand, T.M., Kiefer, R.W. and Chipman, J.W. (2007). *Remote sensing and image interpretation*. 6th ed. United Kingdom: Wiley, John and Sons.

Lyatsky, H.V. (2006). Frontier next door: geology of hydrocarbon assessment of sedimentary basins offshore western Canada. *RECORDER (Canadian Society of Exploration Geophysicists)*, 31(4), p.66–75.

Mabee, S.B., Hardcastle, K.C. and Wise, D.U. (1994). A method of collecting and analyzing Lineaments for regional-scale fractured-bedrock aquifer studies. *Ground Water*, 32(6), p.884–894.

Madibboyina, J.C. (2011). Subsurface facies analysis using electrologs - A case 835 study on Krishna Godavari Basin Rajahmundry. In: Rao, N. (ed.) *the 2nd South Asian Geoscience 836 Conference and Exhibition, GEOIndia2011*. New Delhi.

Magoon, L.B. and Dow, W.G. (1994*a)*. The Petroleum System. *In:* Magoon and Dow, W.G. (eds) *The Petroleum System – from source to trap.* American Association of Petroleum Geologists' Memoir, **60**, 3–24.

Mahny A.S., and Turner B.J. (2007). A comparison of four common atmospheric correction methods. Photogramm. Eng. Remote Sens. 73:361–368.

Mahapatra, P. and Hanssen, R. (2011). *Tiger capacity building facility II training course on active and passive microwave remote sensing next ESA SAR Toolbox (NEST) a cookbook TIGER capacity building facility II training course on active and passive microwave remote sensing*. Delft: Delft University of Technology.

Mah, A., Taylor, G.R., Lennox, P. and Balia, L. (1995). Lineament Analysis of Landsat Thematic Mapper Images, Northern Australia. *Photogrammetric Engineering and Remote Sensing*, 61(6), p.761–773.

Manga, C. S., Loule, J. P. and Koum, J. J (2001). Tectonostratigraphic evolution and prospectivity of the Logone Birni Basin, North Cameroon – Central Africa. *American Association of Petroleum Geologists Bulletin,* 85, Supplement, 1-6.

Marghany, M. (2012). Fuzzy B-spline algorithm for 3-D lineament reconstruction. *International Journal of Physical Sciences*, 7(15).

Marshak S. (2009). Essentials of Geology, W. W. Norton and Company, 3rd ed).

Masoud, A. and Koike, K. (2006). Tectonic architecture through Landsat-7 ETM+/SRTM DEM-derived lineaments and relationship to the hydrogeological setting in Siwa region, NW Egypt. *Journal of African Earth Sciences*, 45(4-5), p.467–477.

Meisling, K.E., Cobbold, P.R., Mount, V.S., (2001). Segmentation of an obliquely rifted margin, Campos and Santos basins, southeastern Brazil. AAPG Bull. 85, 1903e1924.

McClay, K. and Bonora, M. (2001). Analog models of restraining stopovers in strike-slip fault systems. *AAPG Bulletin*, 85.

McCurry, P. (1971). Pan-African Orogeny in northern Nigeria. *Geological Society of America Bulletin*, 82(11), p.3251.

McKeinzie, D. (1978). Some remarks on the development of sedimentary basins. *Earth and Planetary Science Letters*, 40(1), p.25–32.

Miller, H.G. and Singh, V. (1994). Potential field tilt—a new concept for location of potential field sources. *Journal of Applied Geophysics*, 32(2-3), p.213–217.

Misra, A., Gupta, R.P. and Sen, A.K. (2007). Using ASTER TIR radiance and surface emissivity data to map lithology and silica abundance in metamorphic terrain. *IEEE*, 1640–1643.

Miller, R.E., Johnston, R.H., Olowu, J.A.I. and Uzoma, J.U. (1968). Ground-water hydrology of the Chad Basin in Bornu and Dikwa Emirates, northeastern Nigeria, with special emphasis on the flow life of the artesian system. *USGS Water Supply Paper 1757-1*.

Mohammed, A., K, P., Kumanan, C.J. and Ramasamy, S. (2010). Significance of surface Lineaments for gas and oil exploration in part of Sabatayn Basin -Yemen. *Journal of Geography and Geology*, 2(1).

Mohamed, A.Y., Illiffe, J. E., Ashcroft, W.A. and Whiteman, A.J. (2000). Burial and maturation history of the Heglig field area, Muglad Basin, Sudan. Journal of Petroleum Geology, 23, 107-128.

Morelli, M. and Piana, F. (2006). Comparison between remote sensed lineaments and geological structures in intensively cultivated hills (Monferrato and Langhe domains, NW Italy). *International Journal of Remote Sensing*, 27(20), p.4471–4493.

Morley, C.K. (1995). Developments in the structural geology of rifts over the last decade and their impact on hydrocarbon exploration. *Geological Society, London, Special Publications*, 80(1), p.1–32.

Mostafa, M.E. and Bishta, A.Z. (2005). Significance of lineament patterns in rock unit classification and designation: a pilot study on the Gharib-Dara area, northern Eastern Desert, Egypt. *International Journal of Remote Sensing*, 26(7), p.1463–1475.

Mostafa, M.E. And Zakir, F.A. (1996). New enhancement techniques for azimuthal analysis of lineaments for detecting tectonic trends in and around the Afro-Arabian Shield. *International Journal of Remote Sensing*, 17(15), p.2923–2943.

Moumouni, A., Obaje, N.G., Nzegbuna, A.I. and Chaanda, M.S. (2007). Bulk geochemical parameters and biomarker characteristics of organic matter in two wells (Gaibu-1 and Kasade-1) from the Bornu basin: Implications on the hydrocarbon potential. *Journal of Petroleum Science and Engineering*, 58(1-2), p.275–282.

Nettleton, L.L. (1976). *Gravity and magnetics in oil prospecting*. New York, NY: McGraw-Hill Inc.,US.

Nwankwo, C.N. and Ekine, A.S. (2009). Geothermal gradients in the Chad Basin, Nigeria, from bottom hole temperature logs. *International Journal of Physical Sciences*, 4(12), p.777–783.

Nwankwo, C.N., Emujakporue, G.O. and Nwosu, L.I. (2012). Evaluation of the petroleum potentials and prospect of the Chad Basin Nigeria from heat flow and gravity data. *Journal of Petroleum Exploration and Production Technology*, 2(1), p.1–6

Nwajide, C. S. (2013). Geology of Nigeria's sedimentary basins. CSS Bookshops Ltd, Lagos.

Obi, G. C. (1995). Soda-bearing evaporates of the Yusufari District, SW Chad Basin, northeast Nigeria. J. Mining and Geol., v. 31, p. 99-104.

Obaje, N.G. (2009) *Geology and mineral resources of Nigeria*. Germany: Springer.

Obaje, N.., Wehner, H., Hamza, H. and Scheeder, G. (2004). New geochemical data from the Nigerian sector of the Chad basin: Implications on hydrocarbon prospectivity. *Journal of African Earth Sciences*, 38(5), p.477–487.

O'Driscoll, E.S.T. (1981). The double helix in global tectonics. *Tectonophysics*, 63(1-4), p.397–417.

Okosun, E.A. (1995). Review of the geology of Bornu Basin. *Journal of Mining and Geology*, 31(2), p.113–122.

Okpikoro, E. and Olorunniwo, M. (2010). The application of seismic-log sequence stratigraphy in mapping stratigraphic traps and reservoirs' facies in Afam channel area, niger delta. *Global Journal of Geological Sciences*, 8(1).

Olabode S. O. Adekoya J. A, Ola P. S. (2015). Distribution of sedimentary formations in the Bornu Basin, Nigeria. *Petroleum Exploration and Development*, 42 (5): 674–682.

Olade, M.A. (1975) Evolution of Nigeria's Benue trough (Aulacogen): A tectonic model. *Geological Magazine*, 112(06), p.575.

O'Leary, D.W. (1977) Remote sensing for lineaments. *Earthquake Information Bulletin*, 9(1), p.14–18.

Olugbemiro R.O. (1997). Hydrocarbon Potential, Maturation and Paleoenvironments of the Cretaceous series in Bornu Basin, NE Nigeria. Ph.D. Thesis, Institut und Museum fur Geologie and Palaontologie der Universitat Tubingen, Germany, 14, 150.

Olugbemiro, R.O., Ligouis, B. and Abaa, S.I. (1997). The Cretaceous Series in the Chad Basin, Ne Nigeria: Source Rock Potential and Thermal Maturity. *Journal of Petroleum Geology*, 20(1), p.51–68.

Pana, D., Waters, J. and Grobe, M. (2001). *GIS compilation of structural elements in Northern Alberta, Release 1.0*. Alberta Geological Survey: EUB Earth Sciences Report.

Peña, S.A. and Abdelsalam, M.G. (2006). Orbital remote sensing for geological mapping in southern Tunisia: Implication for oil and gas exploration. *Journal of African Earth Sciences*, 44(2), p.203–219.

Peterson, J.A. (1985). *Geology and petroleum resources of central and east-central Africa Open-File Report 85-589*. Missoula, Montana: United States Department of the Interior Geological Survey.

Petters, S.W. (1978). Stratigraphic evolution of the Benue trough and its implications for the upper Cretaceous Paleogeography of West Africa. *The Journal of Geology*, 86(3), p.311–322.

Petters, S.W. and Ekweozor, C.M. (1982). Petroleum Geology of the Benue Trough and Southeastern Chad Basin, Nigeria. American Association of Petroleum Geologists Bulletin, 66, 1141-1149.

Popoff, M., Benkhelil, J., Simon, D. B. and Motte, J. J., (1983). Aproche géodynamique du fossé de la Bénoué (NE Nigéria) á partir des donrées de terrain et de télédétection. *Bulletin Centre Exploration-Production. Elf-Aquitaine*, 7(1) 323-337.

Pullan, R. A. (1964). The recent geomorphological evolution of the south central part of the Chad Basin. J. West African Sci. Assoc., v. 9, p. 115-139.

Prabaharan, S., Ramalingam, M., Subramani, T. and Lakshumanan, C. (2013). Remote sensing and GIS tool to detect hydrocarbon prospect in Nagapattinam sub basin, India. *Geotechnical and Geological Engineering*, 31(1), p.267–277.

Qaoud, N. (2014). Utilization of space-borne imagery for Lithologic mapping: A case study from um had area, central eastern desert, Egypt. *Journal of Geography and Geology*, 6(2).

Rahnama M. and R. Gloaguen (2014). TecLines: A MATLAB-Based Toolbox for Tectonic Lineament Analysis from Satellite Images and DEMs, Part 2: Line Segments Linking and Merging. *Remote Sens*., 6, 11468-11493.

Railsback, L.B. (2011). [Online]. Available at: Synthetic 873 log responses to lithologies. Retrieved from 874 www_gly_uga_edu_railsback_11111figs_8180ExampleLog_pdf.pdf.

Reynolds, D.J. and Jones, C.R. (2004). Tectonic Evolution of the Doba and Doseo basins, Chad: Controls on Trap Formation and Depositional Setting of the Three Fields Area, Chad. *American Association of Petroleum Geologists Bulletin*, 88, Supplement, 15-16.

Ramadan, T.M., Abdelsalam, M.G. and Stern, R.J. (2001). Mapping gold-bearing massive sulfide deposits in the Neoproterozoic Allaqi suture, southeast Egypt with Landsat TM and SIR-C/X-SAR images. *Photogrammetric Engineering and Remote Sensing*, 67, p.491–497.

Richards, J.A., Jia, X. and Xiuping, J. (2005). *Remote sensing digital image analysis: An introduction*. 4th ed. Berlin: Springer-Verlag Berlin and Heidelberg GmbH and Co. K.

Ring, U., (1994). The influence of pre-existing structure on the evolution of the CenozoicMalawi rift (East African Rift System). Tectonics 13, 313–326.

Rodríguez, A., Christiansen, R., Suvires, G., Lince Klinger, F. and Martinez, M. (2016). Structural features of the southern Tulum Fault System, western central Argentina, through gravimetric data and geomorphologic analyses. *Journal of South American Earth Sciences*, 72, pp.159-168.

Rosendahl, B.R., (1987). Architecture or continental rifts with special reference to East Africa. Annual Review of Earth and Planetary Sciences 15, 445–503.

Rowan, L.C. and Mars, J.C. (2003). Lithologic mapping in the Mountain Pass, California area using Advanced Spaceborne Thermal Emission and Reflection Radiometer (ASTER) data. *Remote Sensing of Environment*, 84(3), p.350–366.

Saadi, N.M., Aboud, E. and Watanabe, K. (2009). Integration of DEM, ETM+, geologic, and magnetic data for geological investigations in the Jifara plain, Libya. *IEEE Transactions on Geoscience and Remote Sensing*, 47(10), p.3389–3398.

Saadi, N.M., Watanabe, K., Imai, A. and Saibi, H. (2008). Integrating potential fields with remote sensing data for geological investigations in the Eljufra area of Libya. *Earth, Planets and Space*, 60(6), p.539–547.

Saadi, N.M., Zaher, M.A., El-Baz, F. and Watanabe, K. (2011). Integrated remote sensing data utilization for investigating structural and tectonic history of the Ghadames basin, Libya. *International Journal of Applied Earth Observation and Geoinformation*, 13(5), p.778–791.

Sabins, F.F. (1996). *Remote Sensing: Principles and Interpretation*. 3rd ed. New York, NY: W.H. Freeman and Co.

Sabins, F.F. (1997) Remote Sensing—Principles and Interpretation. 3rd Edtion, W.H. Freeman, New York, 494 pp.

Sabins, F.F. (1998a). Remote sensing for petroleum exploration, Part 2: Case histories. *The Leading Edge*, p.623 – 626.

Sabins, F.F. (1998b). Remote sensing for petroleum exploration, Part 1: Overview of imaging systems. *The Leading Edge*, 17(4), p.467–470.

Sabins, F.F., (1999). Remote sensing for mineral exploration. Ore Geology Reviews 14, 157–183.

Sabins, F., and Wender, L., (1991). Geologic Interpretation of Satellite Images, Saudi Arabia. In: Proceedings—Middle East Oil Show, vol. 7, 213p.

Sandwell, D.T. and Smith, W.H. (2009). Global marine gravity from retracked Geosat and ERS-1 altimetry: Ridge segmentation versus spreading rate, Journal of Geophysical, Vol 17, pp 165-179.

Schaefer, A. (2005). Klastische Sedimente. *Elsevier, Spektrum Akad. Verl.*

Schull, T.J., (1988). Rift basins of interior Sudan*: petroleum exploration and discovery. AAPG 72, 1128e1142.*

Servant, M. (1983). Se´quences continentales et variations climatiques: e´volution du bassin du Tchad au Cenozoı¨que Supe´rieur. Travaux et Documents de l'ORSTOM, 159.

Sharma, M.P., Kujur, A. and Sharma, U. (2012). Identification of groundwater prospecting zones using Remote Sensing and GIS techniques in and around Gola block, Ramgargh district, Jharkhand India. *International Journal of Scientific and Engineering Research*, 3(3).

Sladen, C. (1997). Exploring the lake basins of east and southeast Asia. *In:* Fraser, A.J., Matthews, S.J. and Murphy, R.W. (eds) *Petroleum Geology of Southeast Asia.* Geological Society, London, Special Publications, **126**, 49–76.

Smith, M., and Mosley, P., (1993). Crustal heterogeneity and basement influence on the development of the Kenya rift, East Africa. Tectonics 12, 591–606.

Solomon, S. and Ghebreab, W. (2006). Lineament characterization and their tectonic significance using Landsat TM data and field studies in the central highlands of Eritrea. *Journal of African Earth Sciences*, 46(4), pp.371-378.

Sultan, M., Arvidson, R.E. and Sturchio, N.C. (1986). Mapping of serpentinites in the Eastern Desert of Egypt by using Landsat thematic mapper data. *Geology*, 14(12).

Sultan, M., Arvidson, R.E., Sturchio, N.C. and Guinness, E.A. (1987). Lithologic mapping in arid regions with Landsat thematic mapper data: Meatiq dome, Egypt. *Geological Society of America Bulletin*, 99(6), p.748.

Teeuw, R.M., McWillian, N., Whiteside, M. and Zukowskyj, P.M. (2005). *Geographical Information Sciences and fieldwork*. London: Royal Geographical Society.

Thiemeyer, H., (1992). On the Age of Bama Ridge, a New 14C Record From Konduga Area. Zeitschrift Fur Geomorphologie, N.F. 36, Borno State, N.E. Nigeria, pp. 113 - 118.

Thannoun R. G. (2013). Automatic Extraction and Geospatial Analysis of Lineaments and their Tectonic Significance in some areas of Northern Iraq using Remote Sensing Techniques and GIS. *International Journal of Enhanced Research in Science Technology and Engineering.* Vol. 2 Issue 2.

Thurmond, A.K., Abdelsalam, M.G. and Thurmond, J.B. (2006). Optical-radar-DEM remote sensing data integration for geological mapping in the afar depression, Ethiopia. *Journal of African Earth Sciences*, 44(2), p.119–134.

Tissot, B.P., Ungerer, P. and Pelet, R. (1987). Thermal history of sedimentary basins, maturation indices, and Kinetics of oil and gas generation. *AAPG Bulletin*, 71.

Torsvik, T.H., Rousse, S., Labails, C. and Smethurst, M.A. (2009). A new scheme for the opening of the South Atlantic Ocean and the dissection of an Aptian salt basin. *Geophysical Journal International*, 177, 1315–1333.

Tokarski A. (1973). Geological possibilities for Chad oil in Nigeria. Occasional Paper No. 3, Department of Geology Ahmadu Bello University Zaria, Nigeria publication. Published by Gaskiya Corporation, Zaria.

Trompat, H., Boschetti, F. and Hornby, P. (2003). Improved downward continuation of potential field data. *Exploration Geophysics*, 34(4), p.249.

Tso, B., Mather, P.M. and Tso, T. (2009). *Classification methods for remotely sensed data, Second edition*. 2nd ed. Boca Raton: Taylor and Francis.

Umar, T. (1999): Geologie petroliere du secteur Nigerian du basin du Lac Tchad. Unpublished Ph. D. Dissertation. Universite de pau et des pays de l' adour. Centre Universitaire de Recherche Scientifique Laboratoire de Geodynamique et Modelisation des Bassins Sedimentaires: 425pp

Van Der Meer, F., Vazquez-Torres, M. and Van Dijk, P.M. (1997). Spectral characterization of ophiolite lithologies in the Troodos Ophiolite complex of Cyprus and its potential in prospecting for massive sulphide deposits. *International Journal of Remote Sensing*, 18(6), p.1245–1257.

Vesnaver, A., Ralph B., Robert L. and Christopher L. (2009). Painting the near surface using geology, geophysics, and satellites. *Geophysics*, Vol. 74, No. 3.

Verduzco, B., Fairhead, J.D., Green, C.M. and MacKenzie, C. (2004). New insights into magnetic derivatives for structural mapping. *The Leading Edge*, 23(2), p.116–119.

Warren M. J. (2009). Tectonic Inversion and Petroleum System Implications in the Rifts of Central Africa. *AAPG Search and Discovery* Article #90171 CSPG/CSEG/CWLS GeoConvention 2009, Calgary, Alberta, Canada, May 4-8.

Weng, Q. (2010). Advances in Environmental Remote Sensing: Sensors, Algorithms, and Applications, CRC Press/Taylor and Francis.

Wise, D.U., Funiciello, R., Parotto, M. And Salvini, F. (1985). Topographic lineament swarms: Clues to their origin from domain analysis of Italy. *Geological Society of America Bulletin*, 96(7), p.952.

Won-In, K. and Charusiri, P. (2003). Enhancement of thematic mapper satellite images for geological mapping of the Cho Dien area, Northern Vietnam. *International Journal of Applied Earth Observation and Geoinformation*, 4(3), p.183–193.

Wright, J.B. (1976). Fracture systems in Nigeria and initiation of fracture zones in the south Atlantic. *Tectonophysics*, 34(3-4), p.T43–T47.

Wright, J. B. Hastings, D. A., Jones, W. B., and Williams, H. R., (1985). Geology and Mineral Resources of West Africa. Geprge Allen and Unwin, London, 187p.

Yassaghi, A. (2006). Integration of Landsat imagery interpretation and geomagentic data on verification of deep-seated transverse fault lineaments in SE Zagros, Iran. *International Journal of Remote Sensing*, 27(20), p.4529–4544.

Zakir, F.A., Qari, M.H.T. and Mostafa, M.E. (1999). Technical note a new optimizing technique for preparing lineament density maps. *International Journal of Remote Sensing*, 20(6), p.1073–1085.

Zeinalov, G.A. (2000). Importance of remote-sensing data in structural geologic analysis of oil and gas-bearing regions of Azerbaijan. *Natural Resources Research*, 9(4), p.307–313.

APPENDICES:

APPENDICES:

Appendix A: Earth Observation images

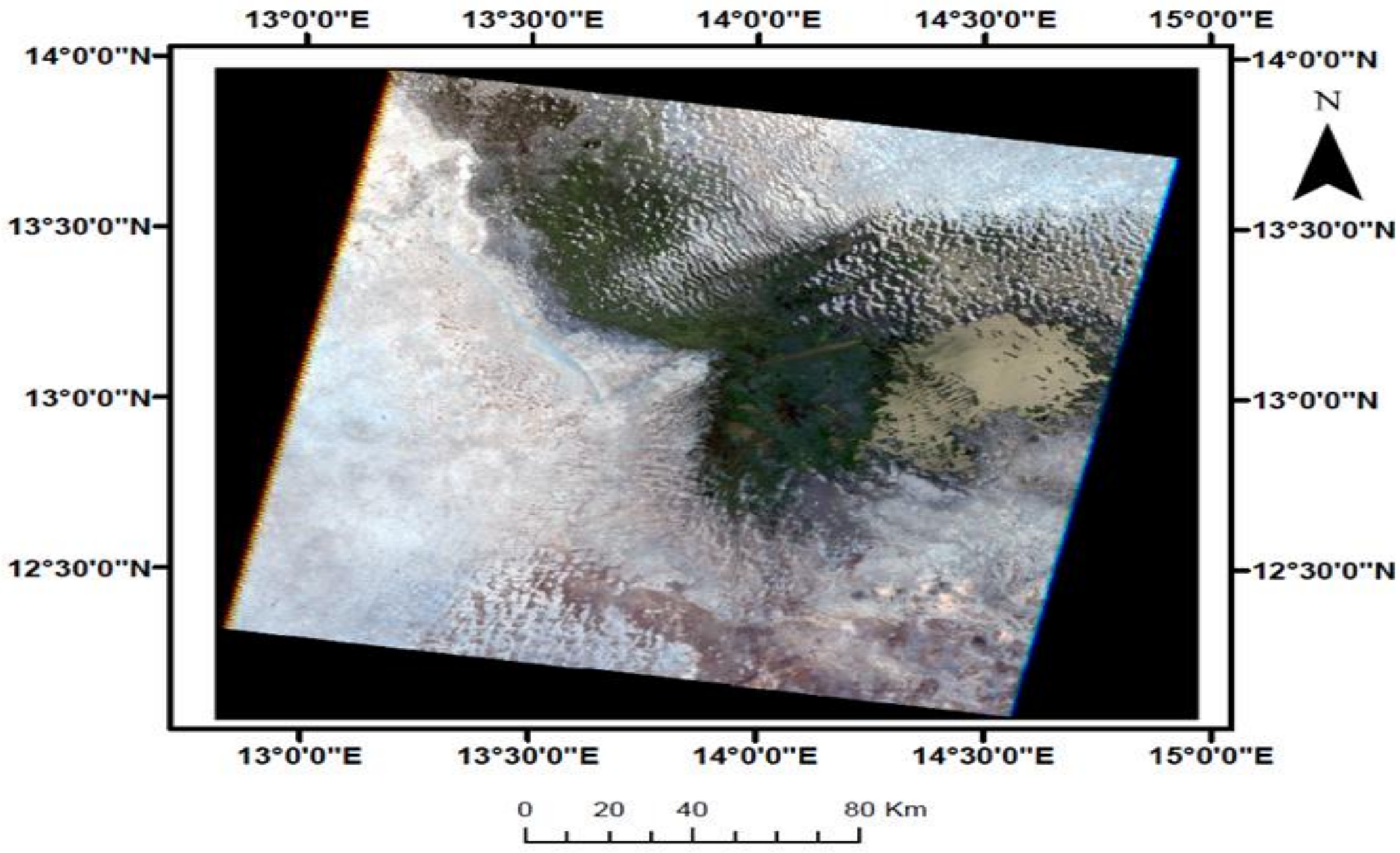

Coordinate system: WGS 1984 UTM zone 33N
Projection: Transverse Mercator

Fig 4.1: Linear stretched RGB 321 Landsat 7 ETM+ composite image. Path/Row: 185/051 of the study area showing Lake Chad.

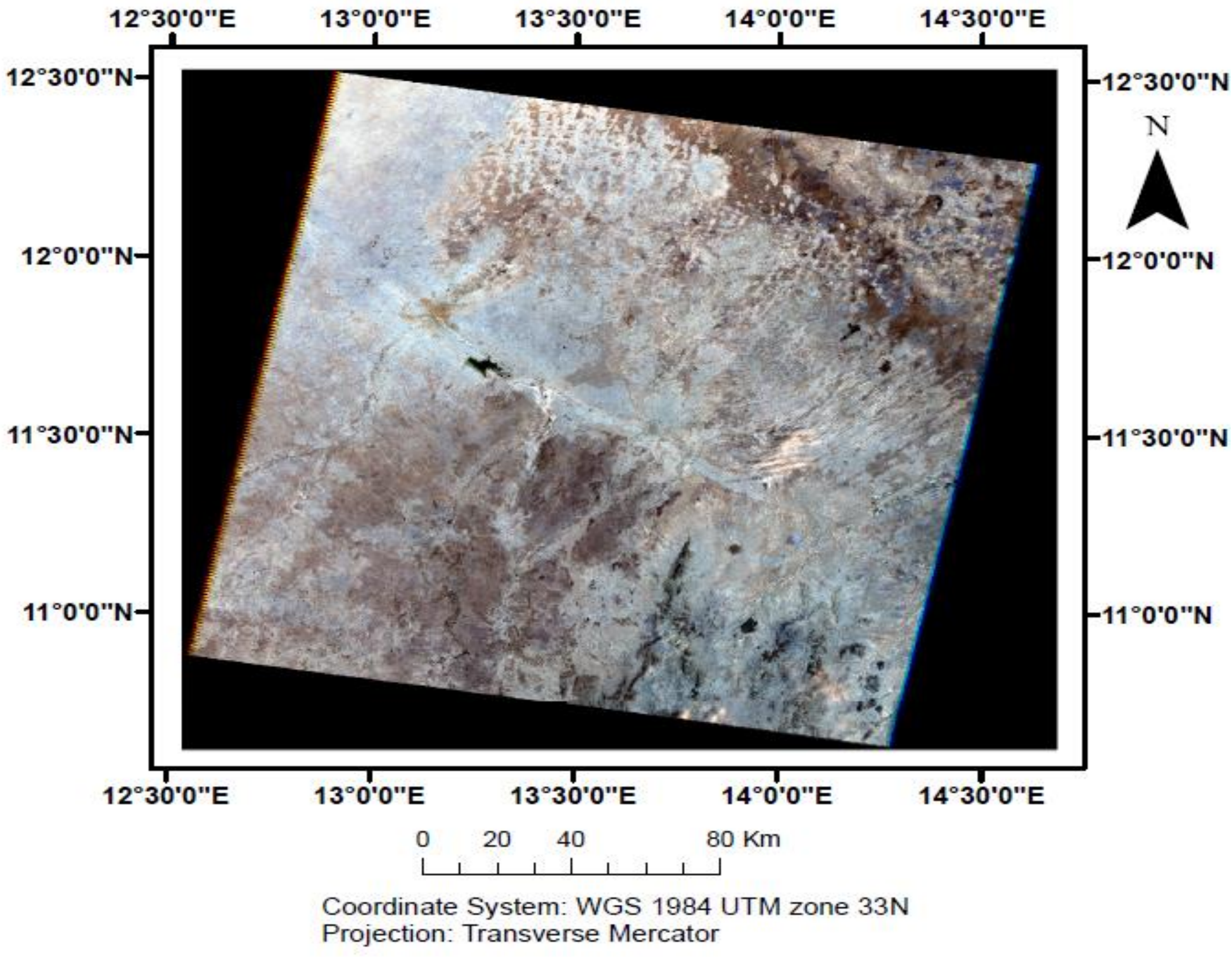

Fig 4.2: Linear stretched RGB 321 Landsat 7 ETM+ composite image. Path/Row: 185/052 of the study area showing Alau Lake along the NW-SE strectched Bama Beach Ridge paleoshoreline.

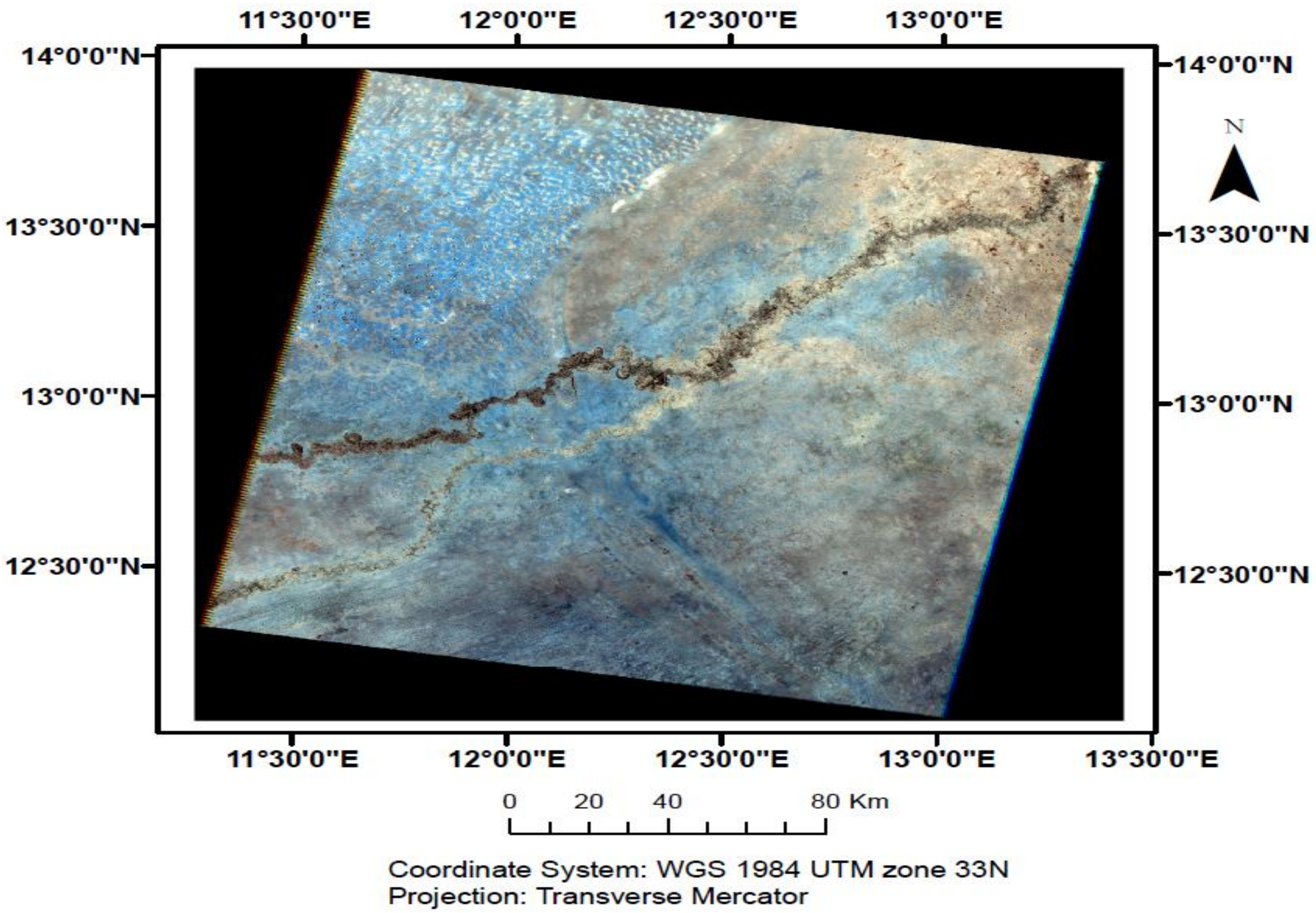

Fig. 4.3: Linear stretched RGB 321 Landsat 7 ETM+ composite image. Path/Row: 186/051 of the study area.

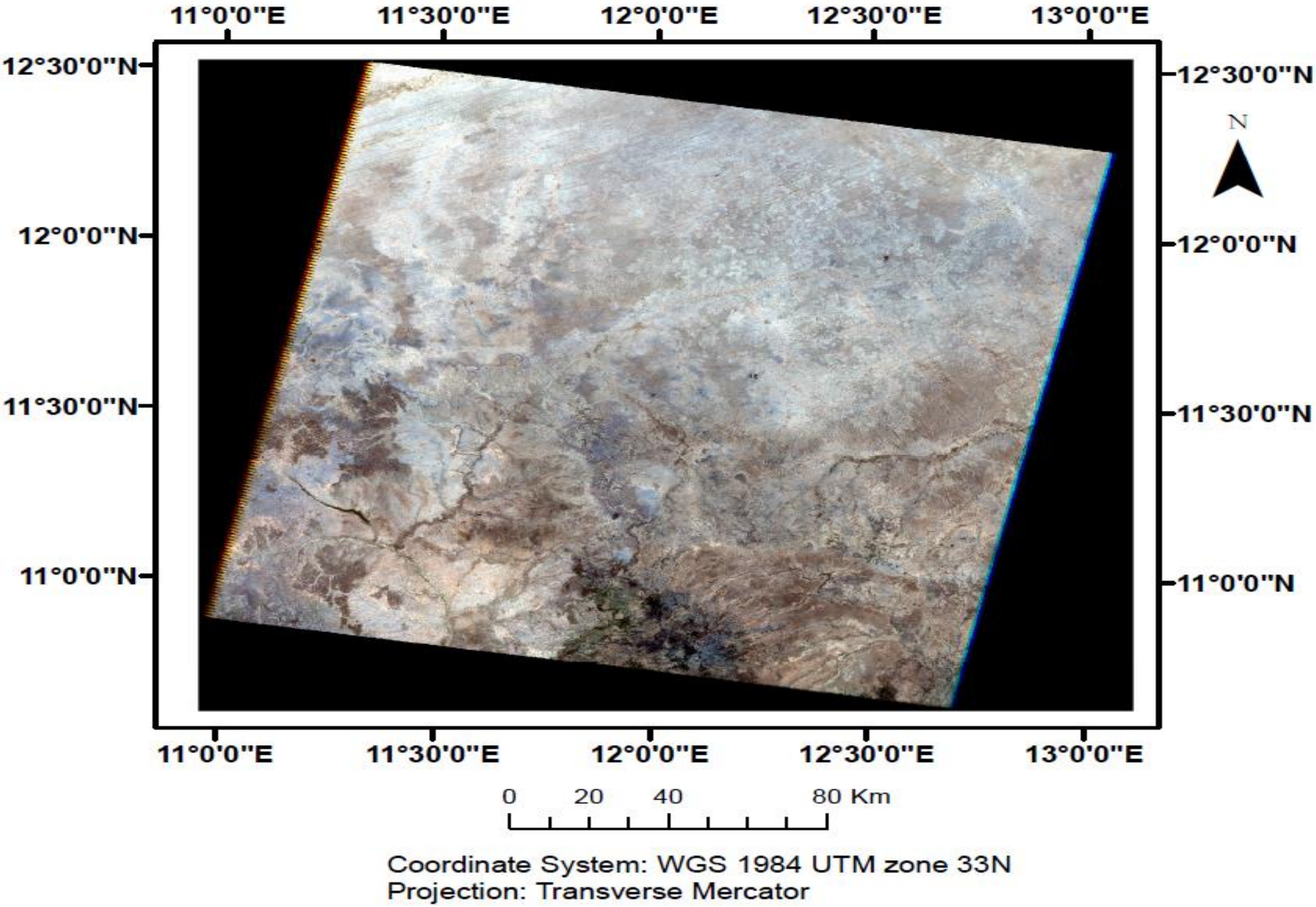

Fig 4.4: Linear stretched RGB 321 Landsat 7 ETM+ composite image. Path/Row: 186/052 of the study area.

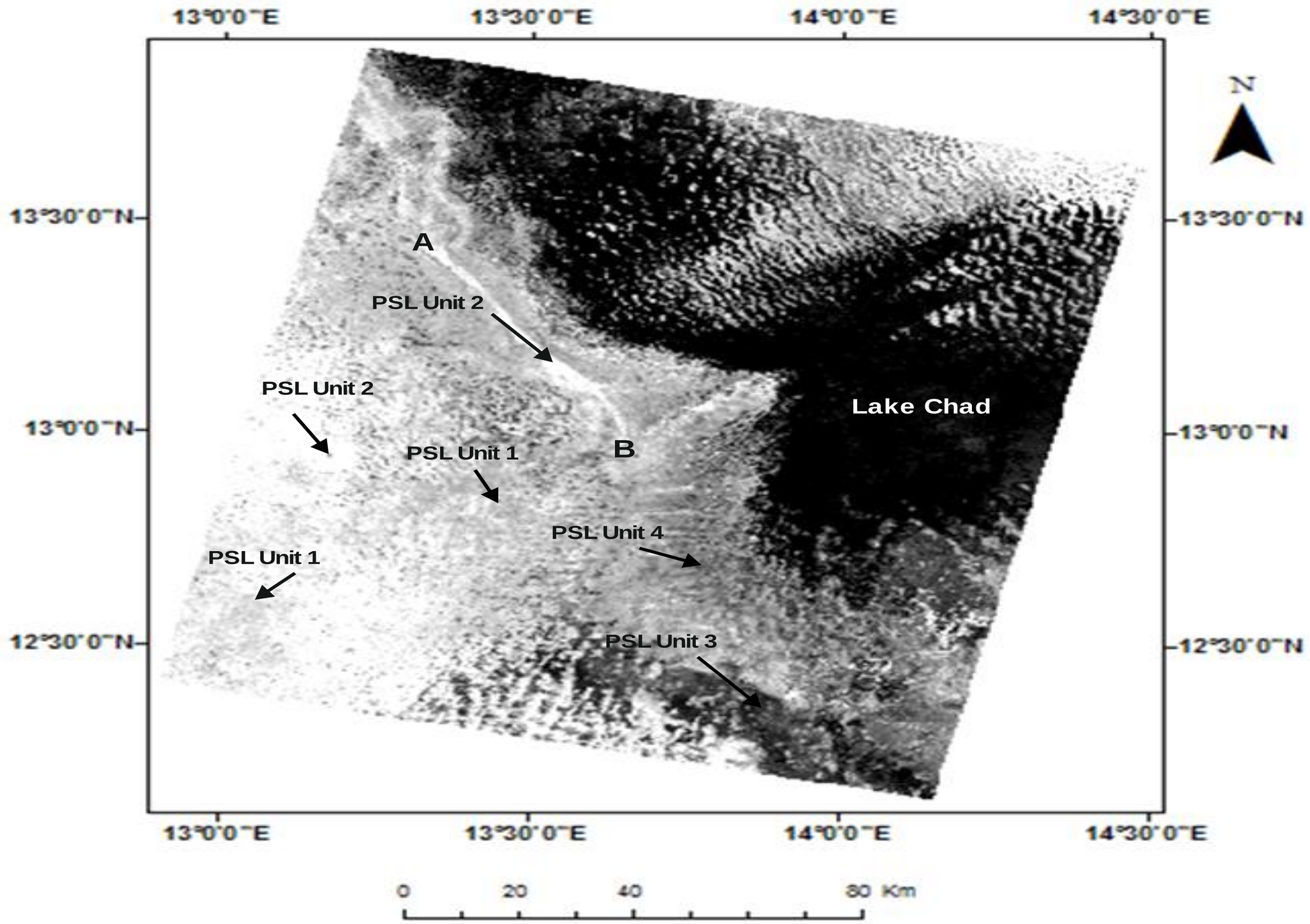

Fig. 4.14: Band ratio 3/1 image for the 185/051 path/row Landsat 7 ETM+ image showing the different spectral responses of the lithological compositions in different contrasts.

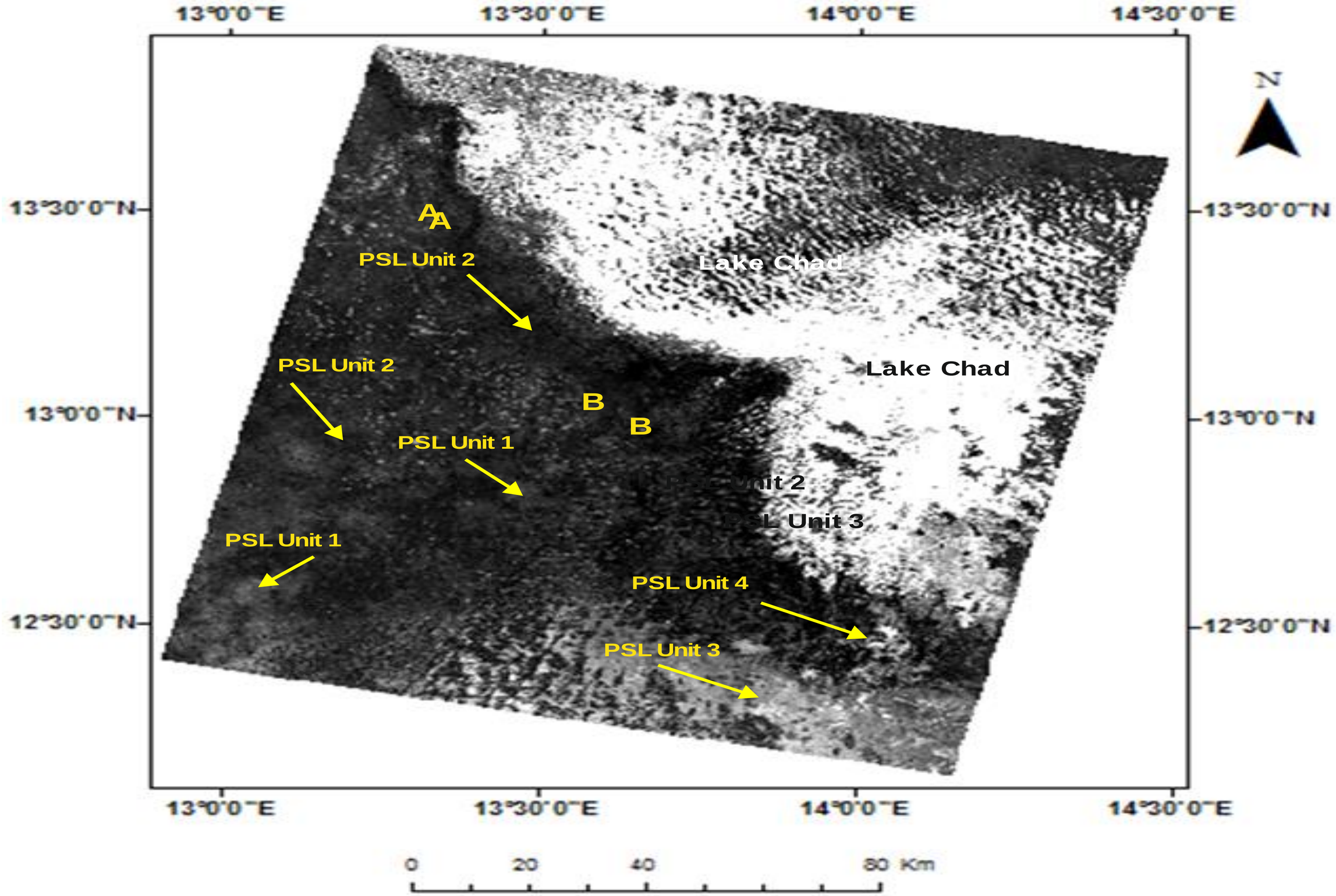

Fig. 4.15: Band ratio 5/7 image for the 185/051 path/row Landsat 7 ETM+ image showing the different spectral responses of the lithological compositions in different contrasts.

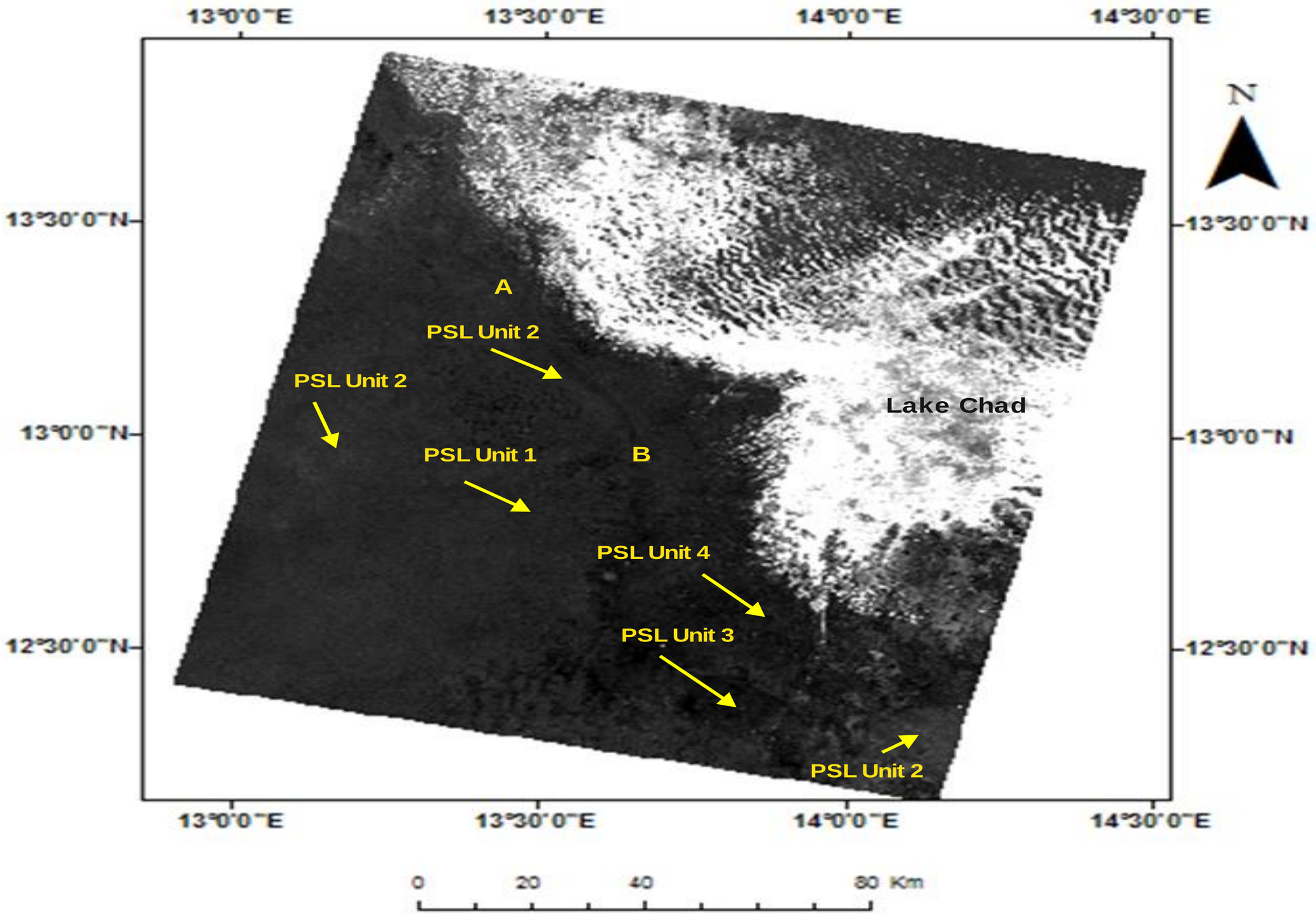

Fig. 4.16: Band ratio 5/4 image for the 185/051 path/row Landsat 7 ETM+ image showing the different spectral responses of the lithological compositions in different contrasts

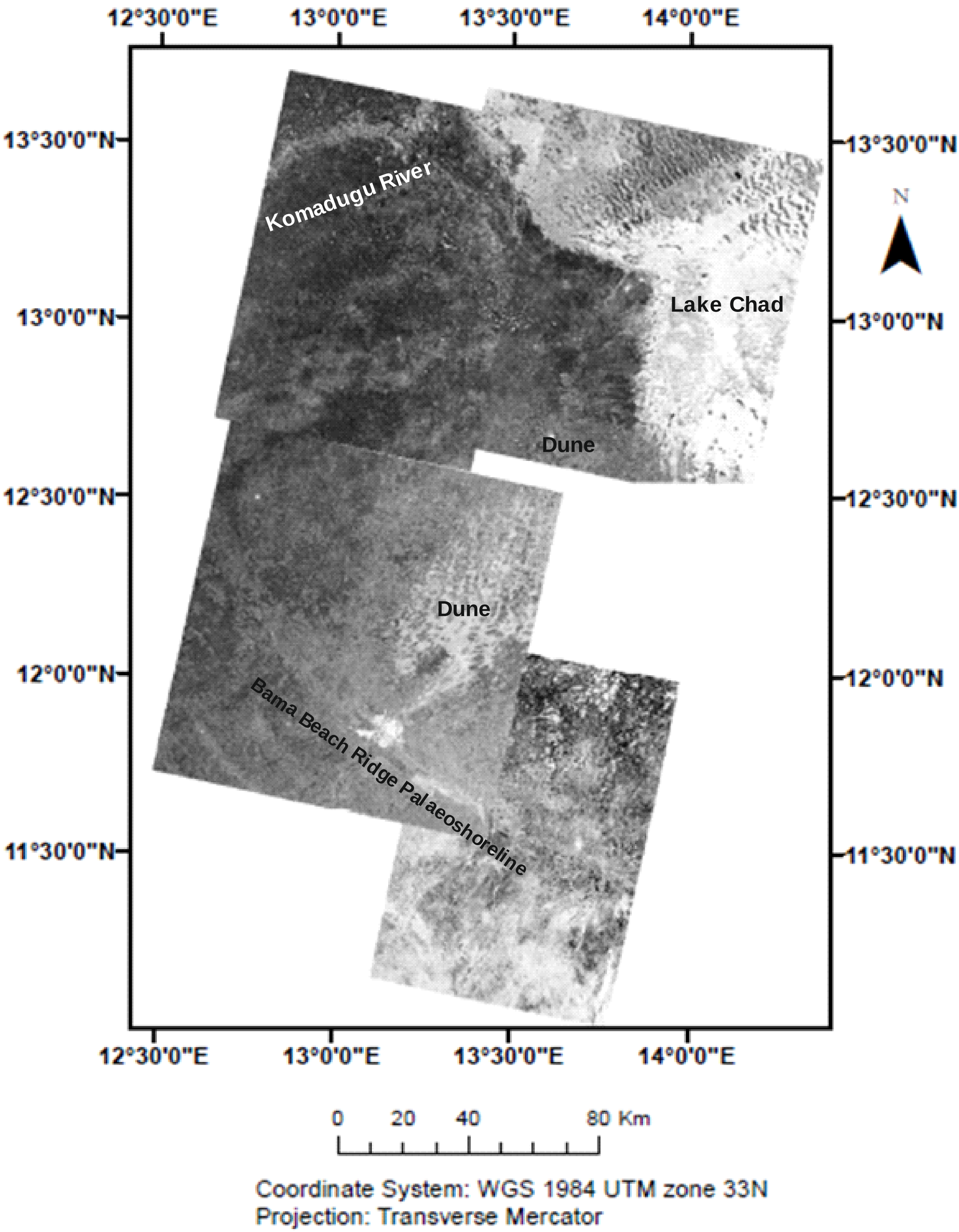

Fig 4.5: Calibrated, speckle filtered, geometrically and radiometrically corrected mosaic of 4 raw (Level 1) Envisat ASAR images. Showing the geomorphic features mapped in the area, hoqwever lineaments are difficult to be discernible.

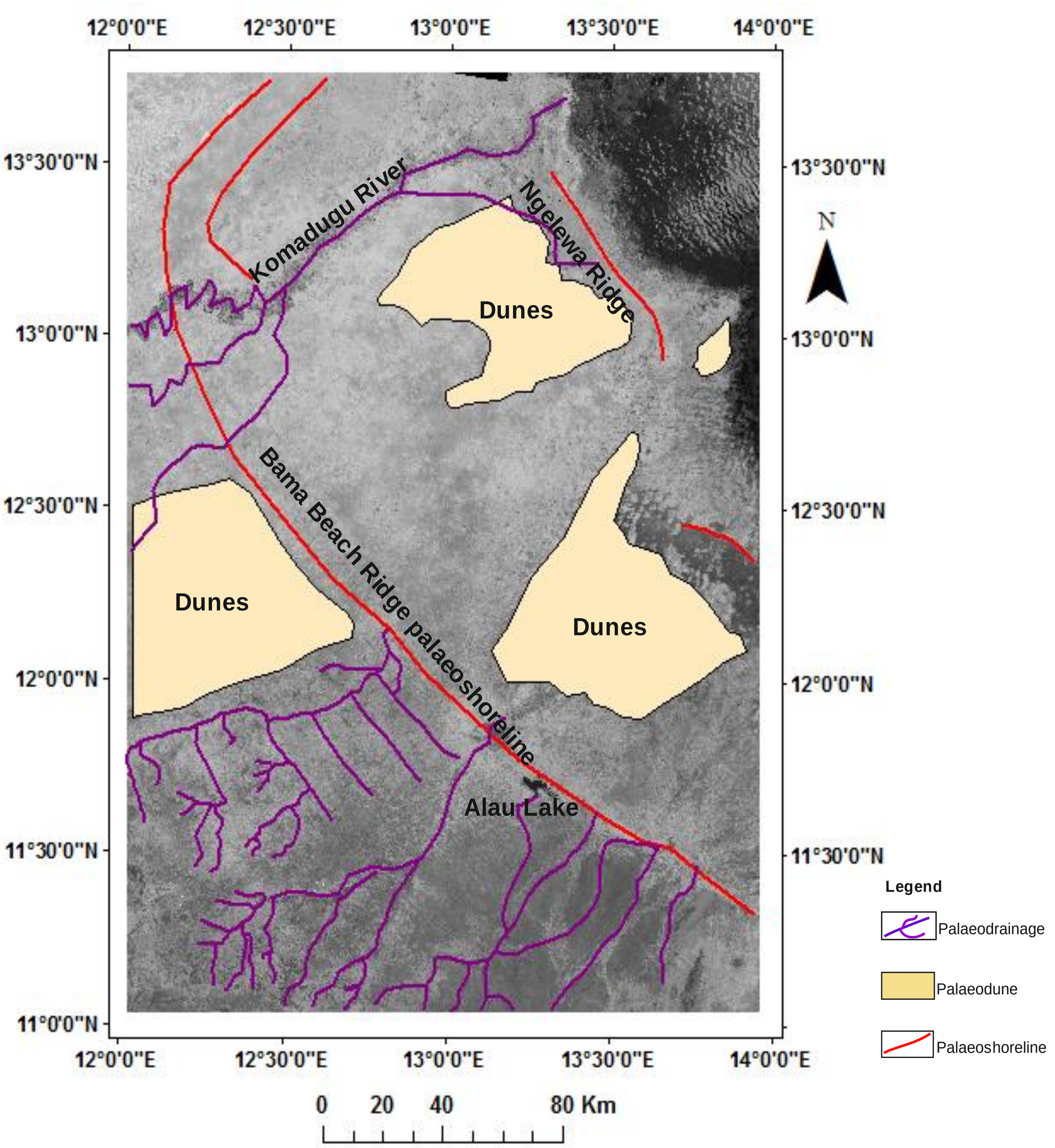

Fig. 4.23: Surface landforms identified in the north-eastern Bornu basin including palaeoshorelines, dunes and palaeodrainage features. The different map layers are overlain using GIS on the Landsat 7 ETM + mosaic image subset.

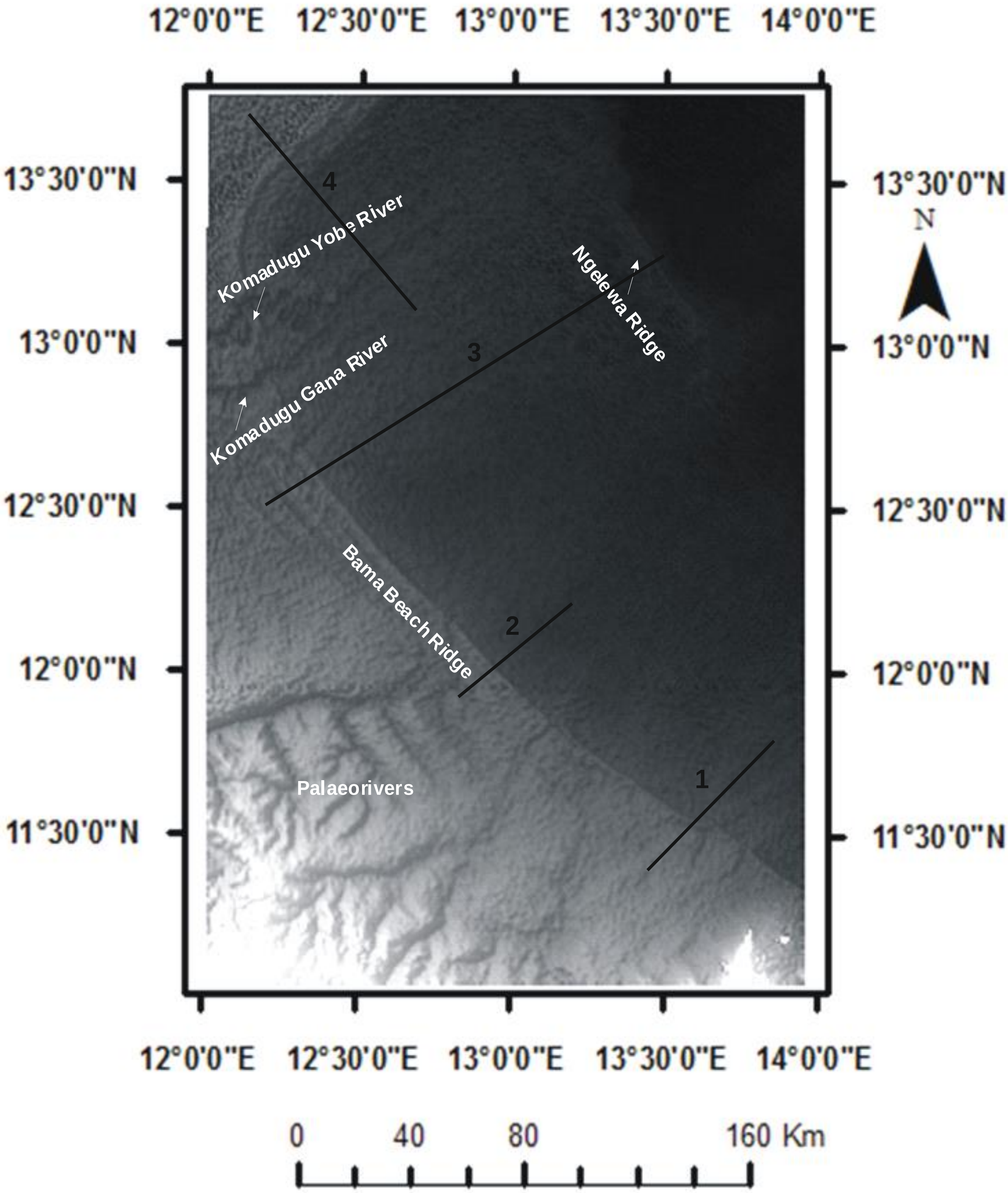

Fig.4.24. SRTM DEM Hill shade relief image showing the subsurface expressions of the palaeoshorelines and palaeodrainage features

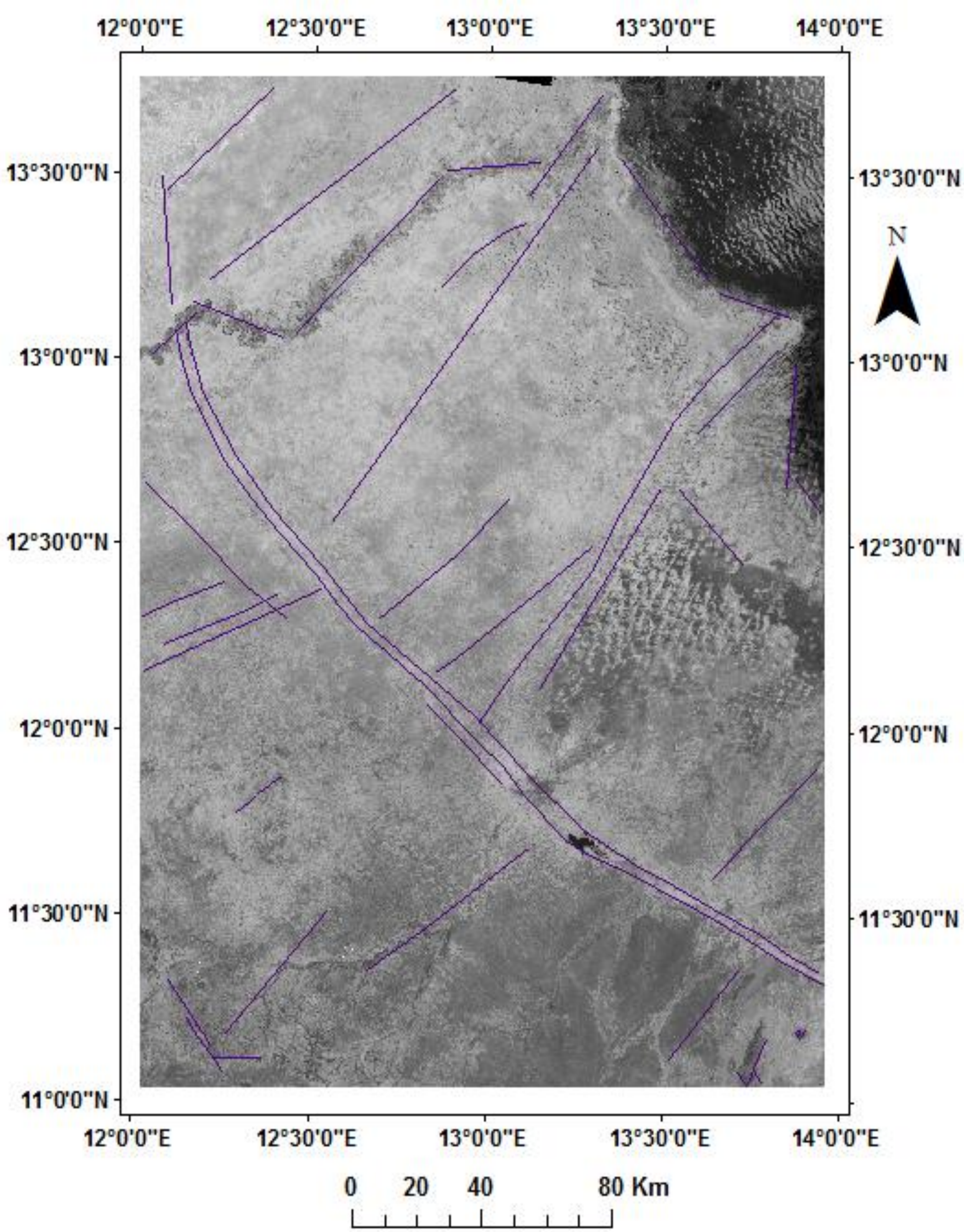

Fig 4.26: Manual GIS digitisation of surface lineaments in the north eastern Bornu basin mapped from the Landsat 7 ETM+ mosaic image subset and overlain on the raster image. Dune areas identified are masked out during the manual mapping (lineaments are shown in purple colour)

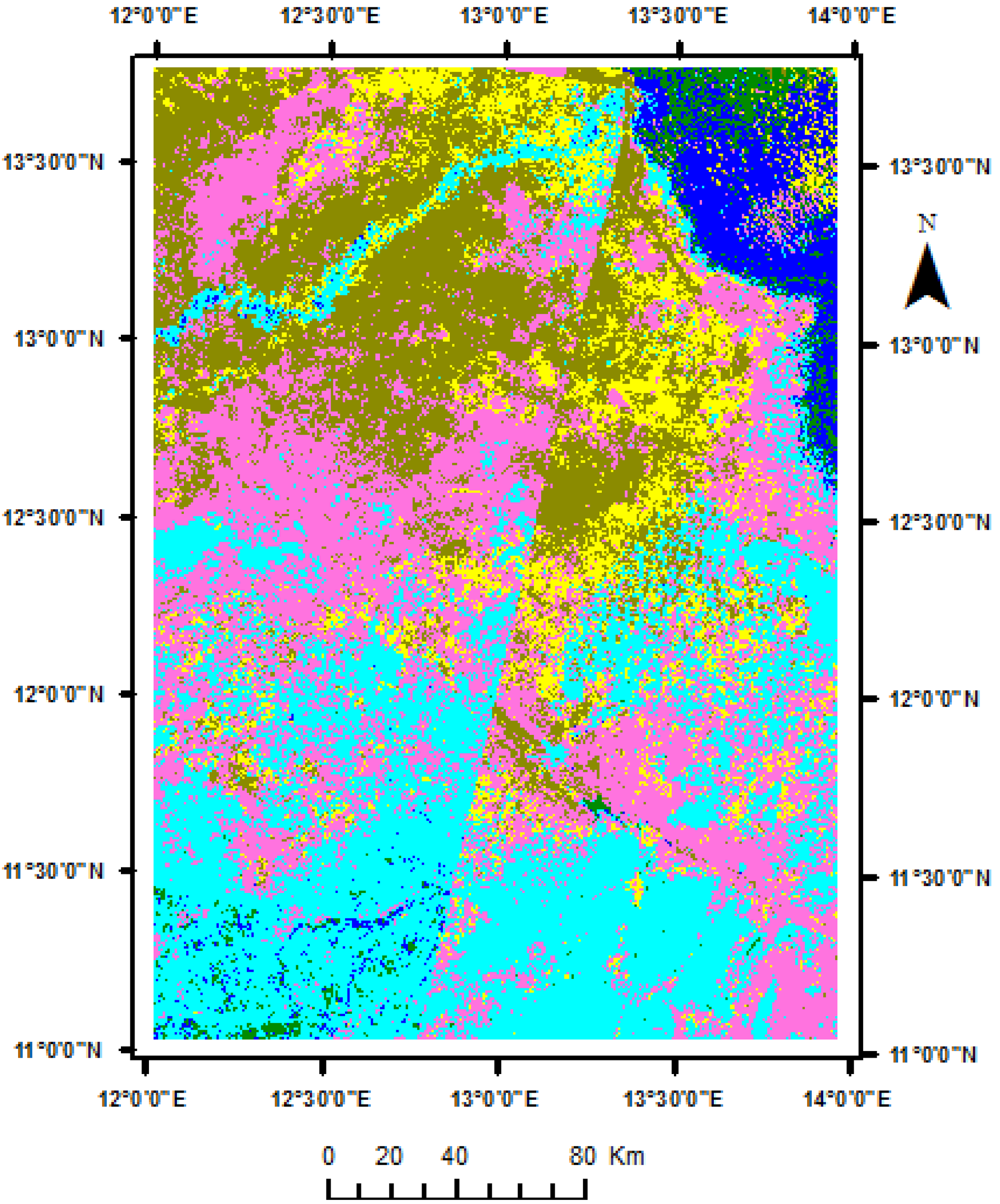

Fig. 4.21 b. Result of the SAM classification of various surface lithological materials in the north eastern Bornu basin processed from Fig. 4.21 (a). Note image edge mosaicking artefact that repeatedly appear after the SAM processing but disappear on the mosaic image subset Fig. 4.26. Artefact does not affect accuracy of the spectral mapping as it is removed in GIS digitisation of final spectral map Fig. 4.21 c..

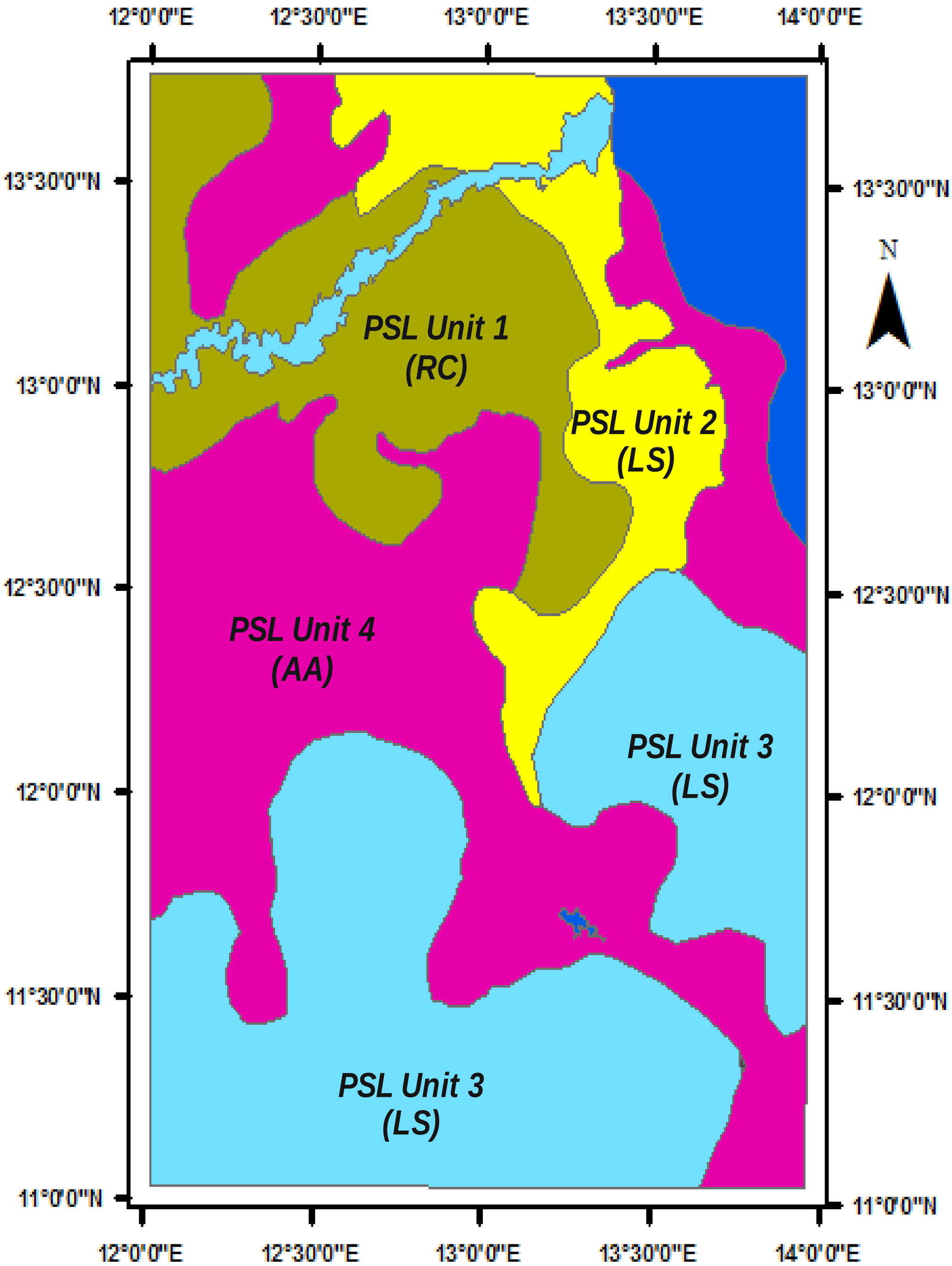

Fig. 4.21 c. Digitised version of the SAM classification map showing the surficial geological map of the north eastern Bornu basin produced from Fig. 4.21 (b,) after all image processing edge artefacts are removed

Appendix B: Seismic and well log

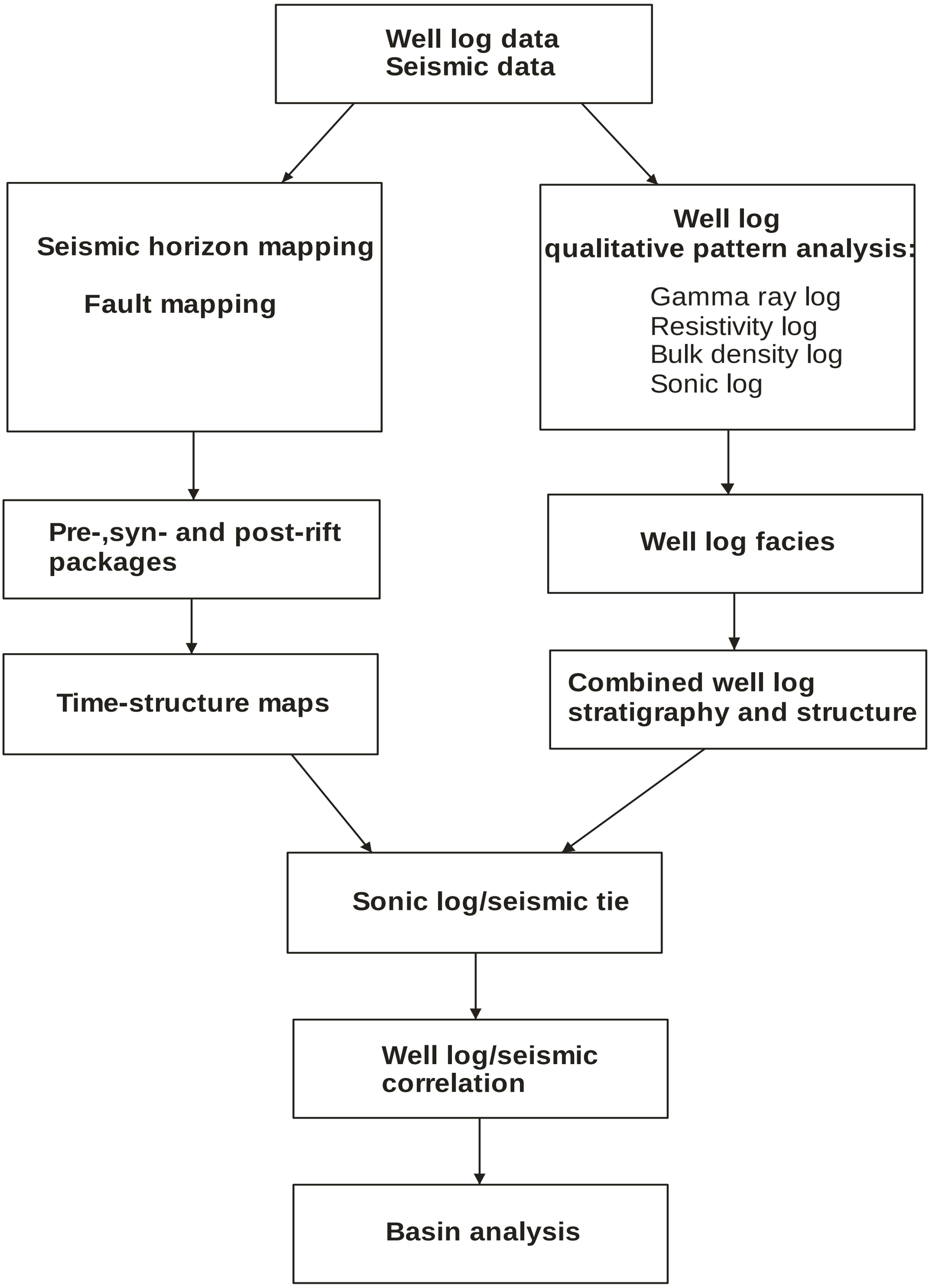

Workflow for the combined seismic and well log data analysis

Well log stratigraphic correlation:

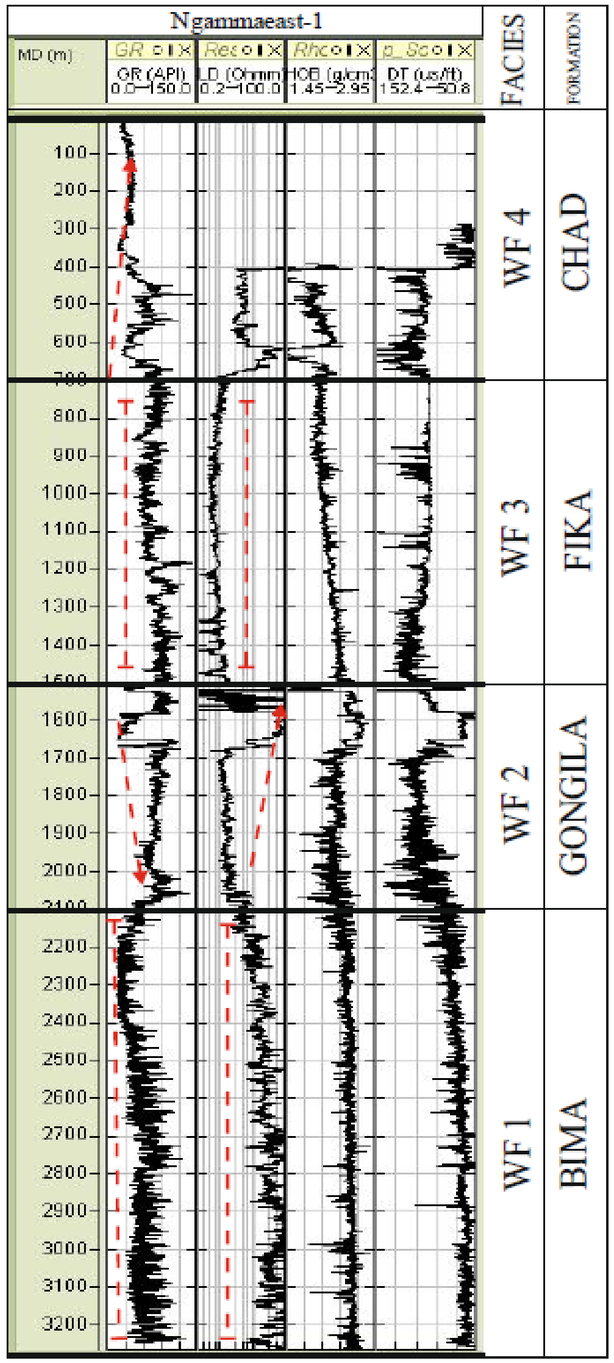

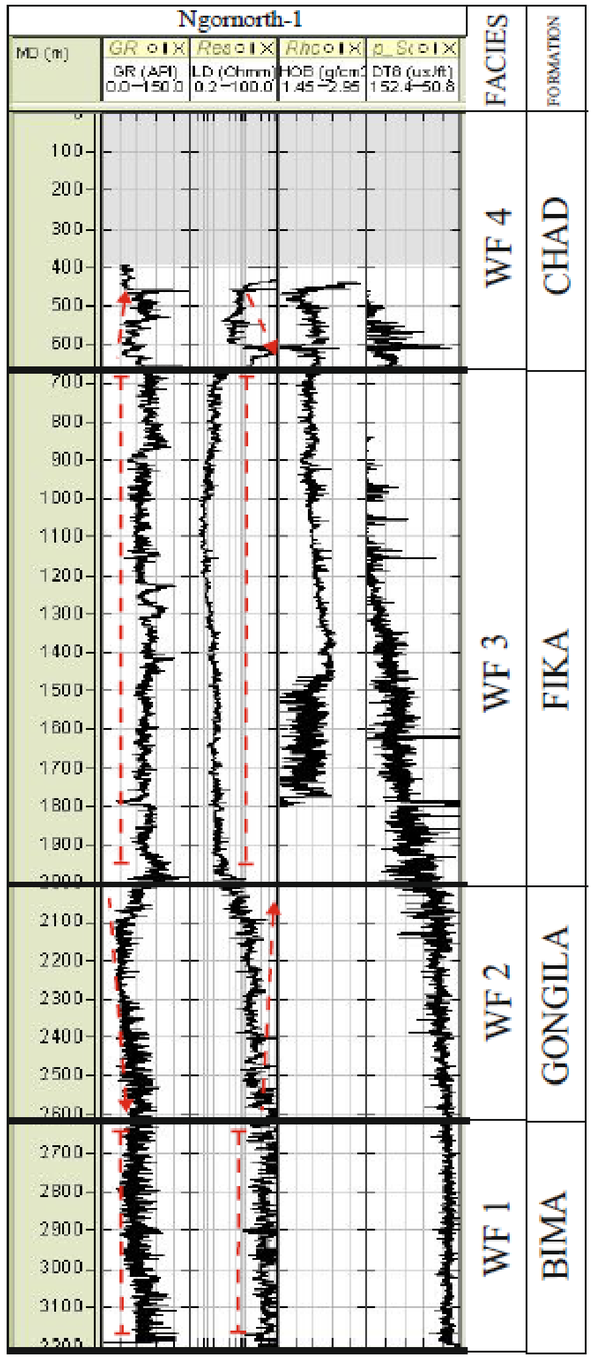

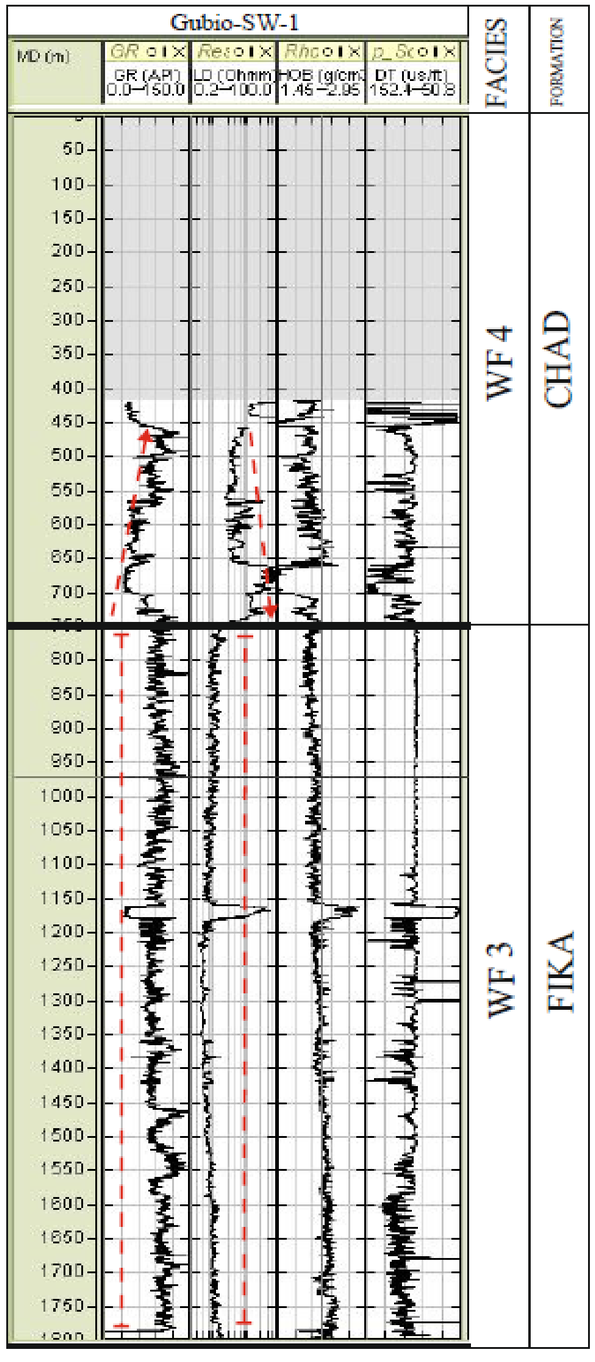

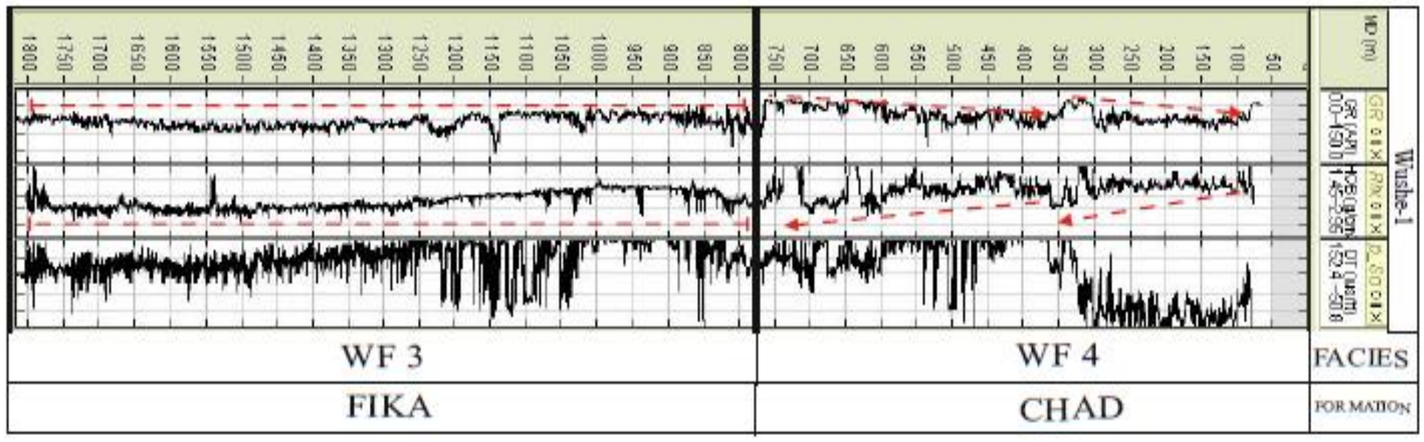
Wushe-1
WF 3
WF 4
FACIES
FIKA
CHAD
FORMATION

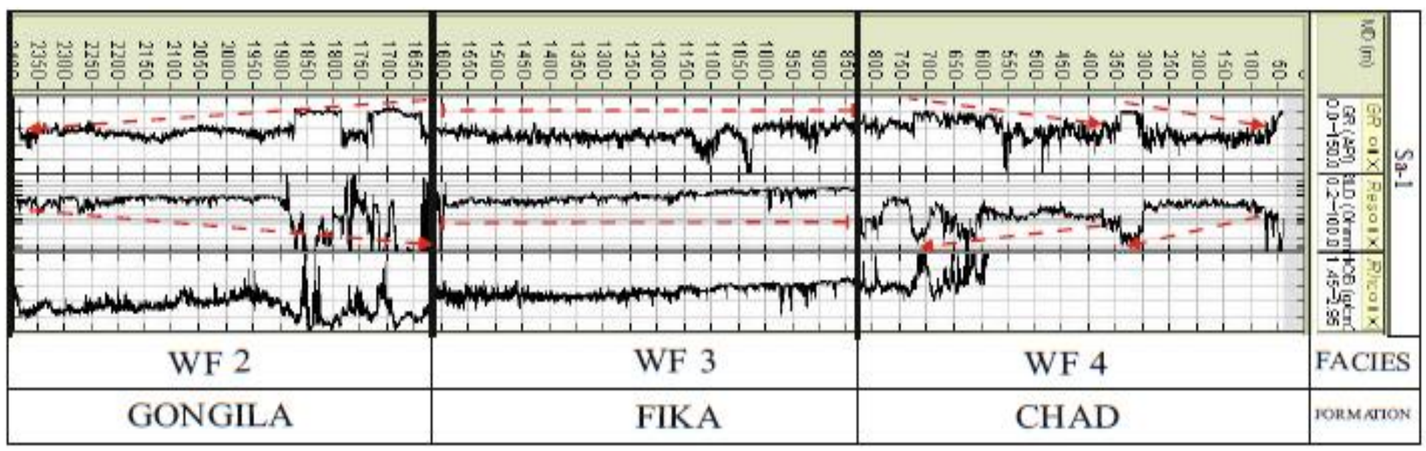
Sa-1
WF 2
WF 3
WF 4
FACIES
GONGILA
FIKA
CHAD
FORMATION

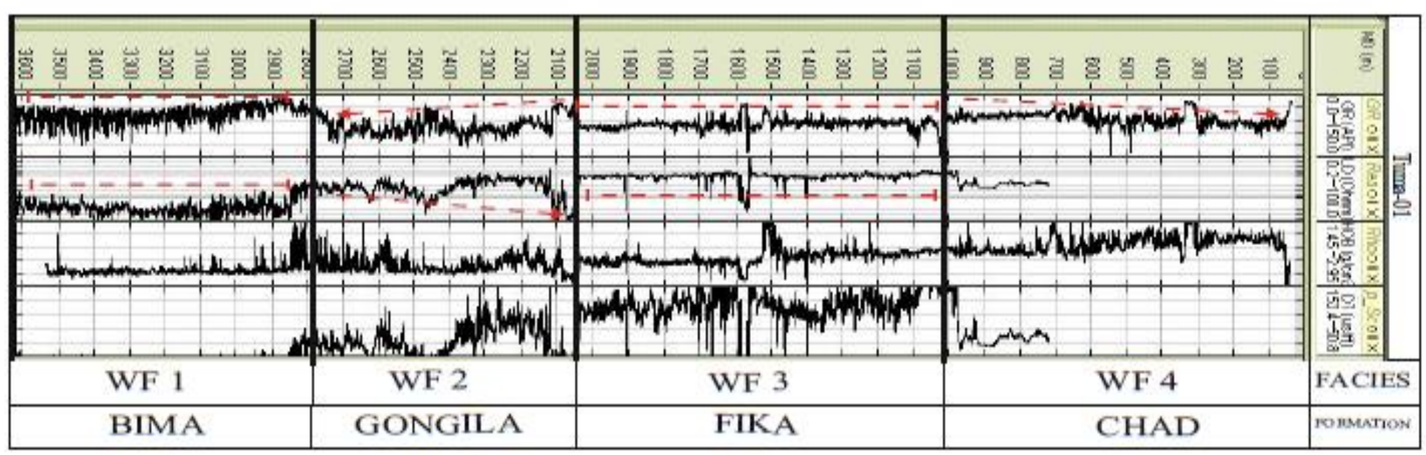
Tuma-01
WF 1
WF 2
WF 3
WF 4
FACIES
BIMA
GONGILA
FIKA
CHAD
FORMATION

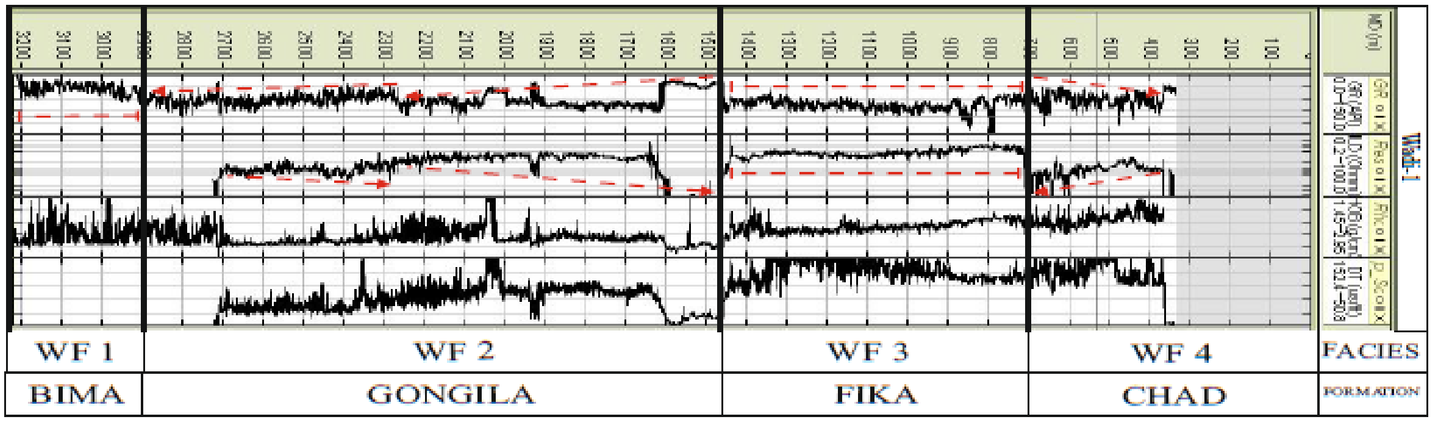
Wadi-1
MD (m)
GR (API)
LD (Ohmm)
RHOB (g/cm3)
DT (us/ft)
0.0–150.0
0.2–100.0
1.65–2.55
152.4–50.8
WF 1
WF 2
WF 3
WF 4
FACIES
BIMA
GONGILA
FIKA
CHAD
FORMATION

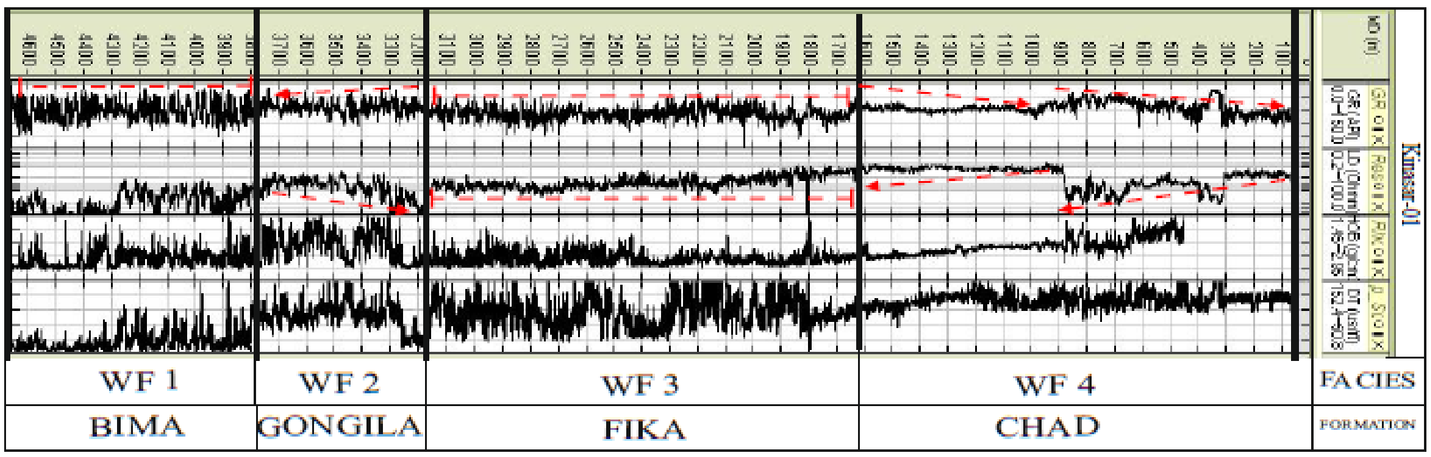
Kimasar-01
MD (m)
GR (API)
LD (Ohmm)
RHOB (g/cm3)
DT (us/ft)
0.0–150.0
0.2–100.0
1.65–2.55
152.4–50.8
WF 1
WF 2
WF 3
WF 4
FACIES
BIMA
GONGILA
FIKA
CHAD
FORMATION

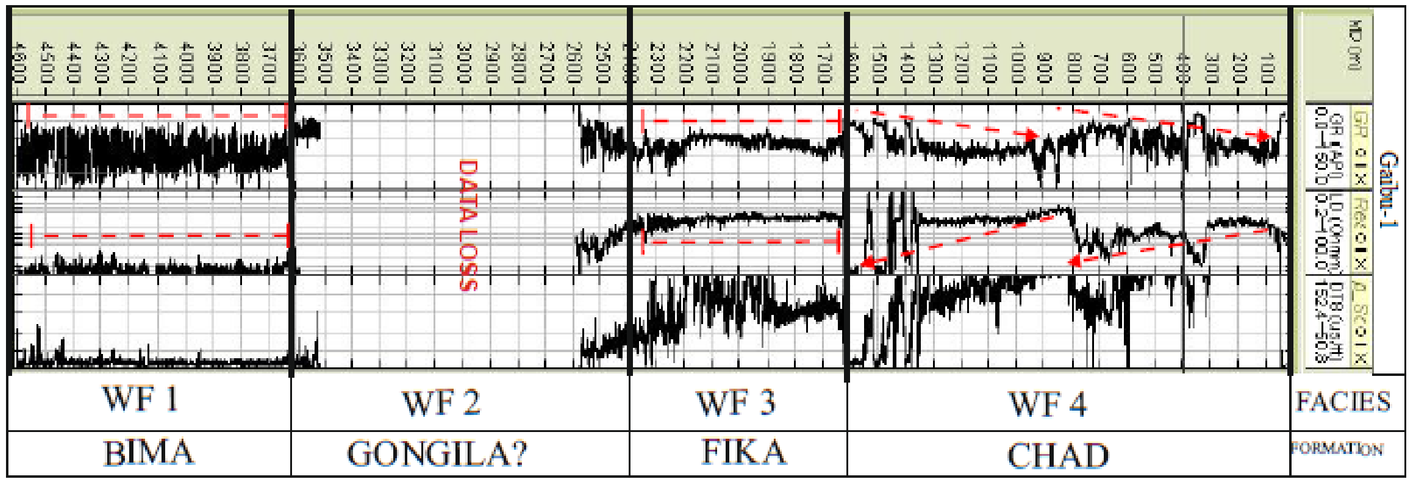
Gaibu-1
MD (m)
GR (API)
LD (Ohmm)
DTB (us/ft)
0.0–150.0
0.2–100.0
152.4–50.8
DATA LOSS
WF 1
WF 2
WF 3
WF 4
FACIES
BIMA
GONGILA?
FIKA
CHAD
FORMATION

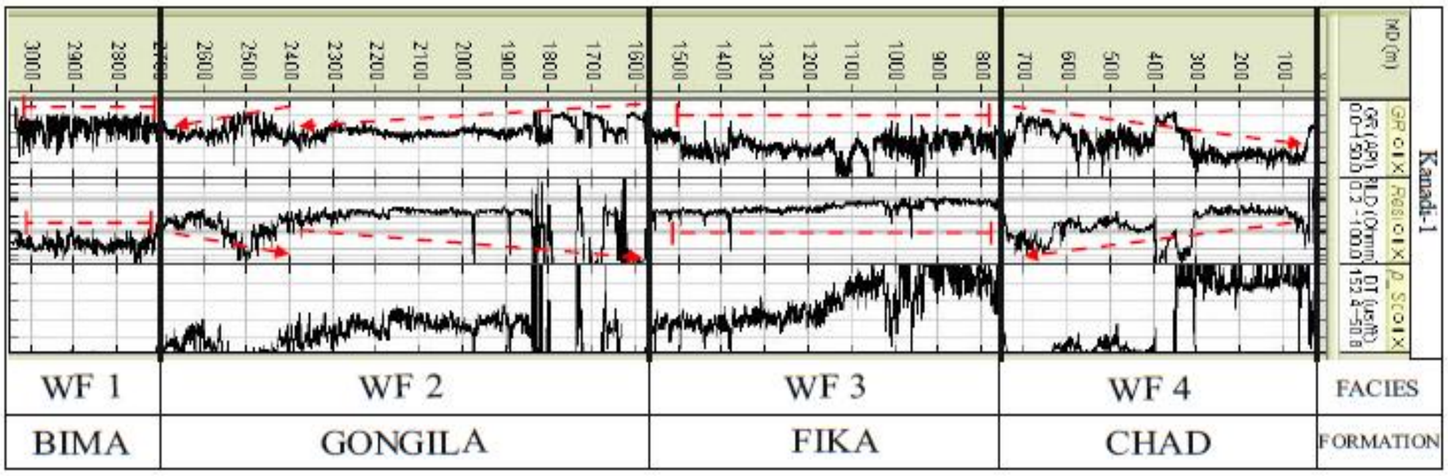
Kanadi-1
MD (m)
GR (API) 0.0-150.0
RLD (Ohmm) 0.2-1000.0
DT (us/ft) 152.4-50.8
WF 1
WF 2
WF 3
WF 4
FACIES
BIMA
GONGILA
FIKA
CHAD
FORMATION

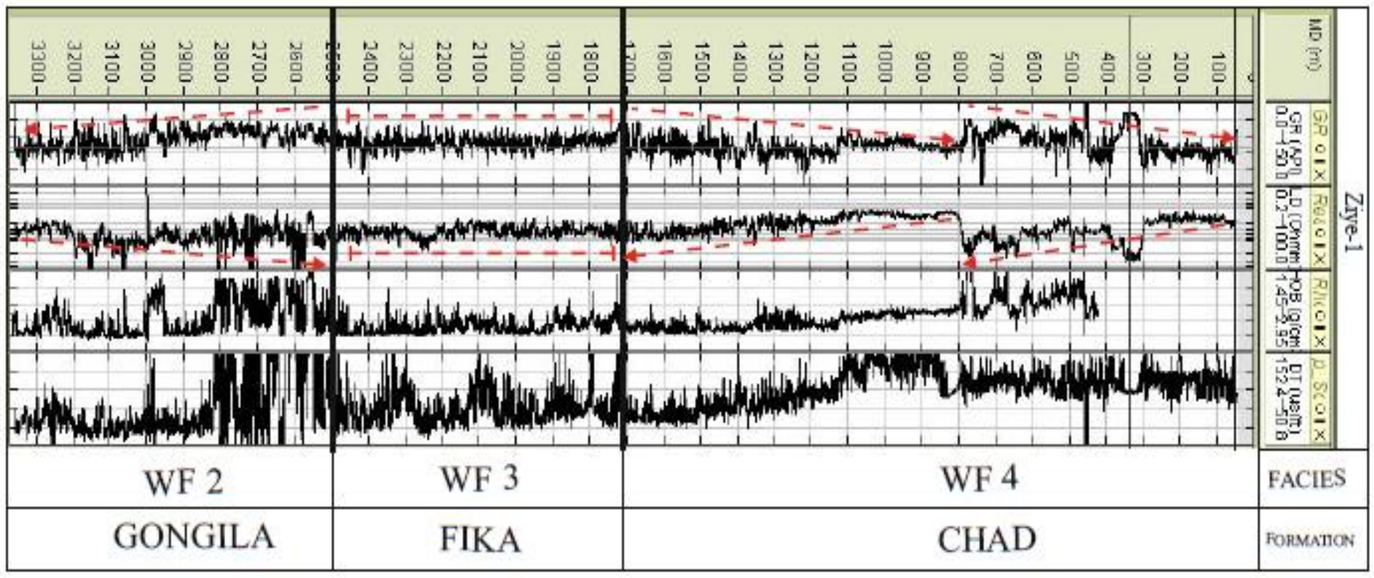
Zaye-1
MD (m)
GR (API) 0.0-150.0
RLD (Ohmm) 0.2-1000.0
RHOB (g/cm3) 1.95-2.95
DT (us/ft) 152.4-50.8
WF 2
WF 3
WF 4
FACIES
GONGILA
FIKA
CHAD
FORMATION

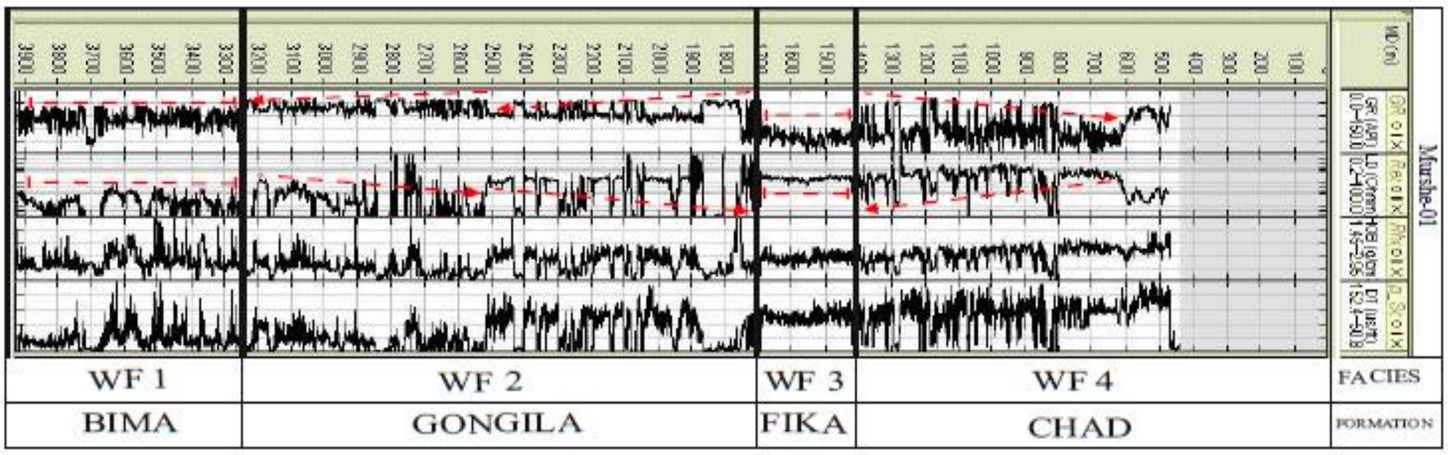
Mursie-01
MD (m)
GR (API) 0.0-150.0
RLD (Ohmm) 0.2-1000.0
RHOB (g/cm3) 1.95-2.95
DT (us/ft) 152.4-50.8
WF 1
WF 2
WF 3
WF 4
FACIES
BIMA
GONGILA
FIKA
CHAD
FORMATION

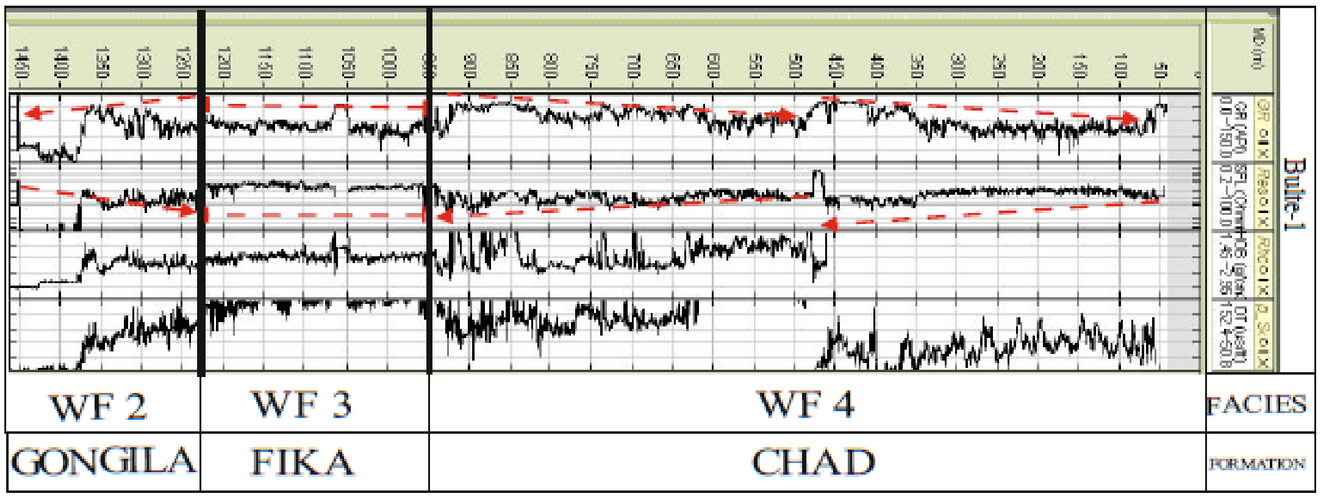
Bulle-1
WF 2
WF 3
WF 4
FACIES
GONGILA
FIKA
CHAD
FORMATION

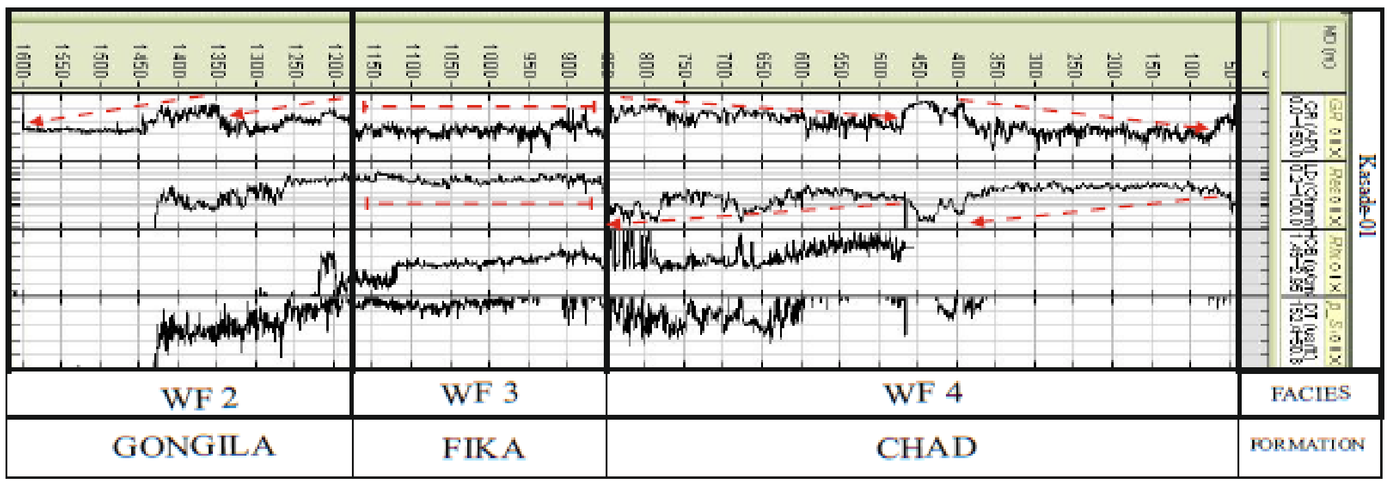
Kasade-01
WF 2
WF 3
WF 4
FACIES
GONGILA
FIKA
CHAD
FORMATION

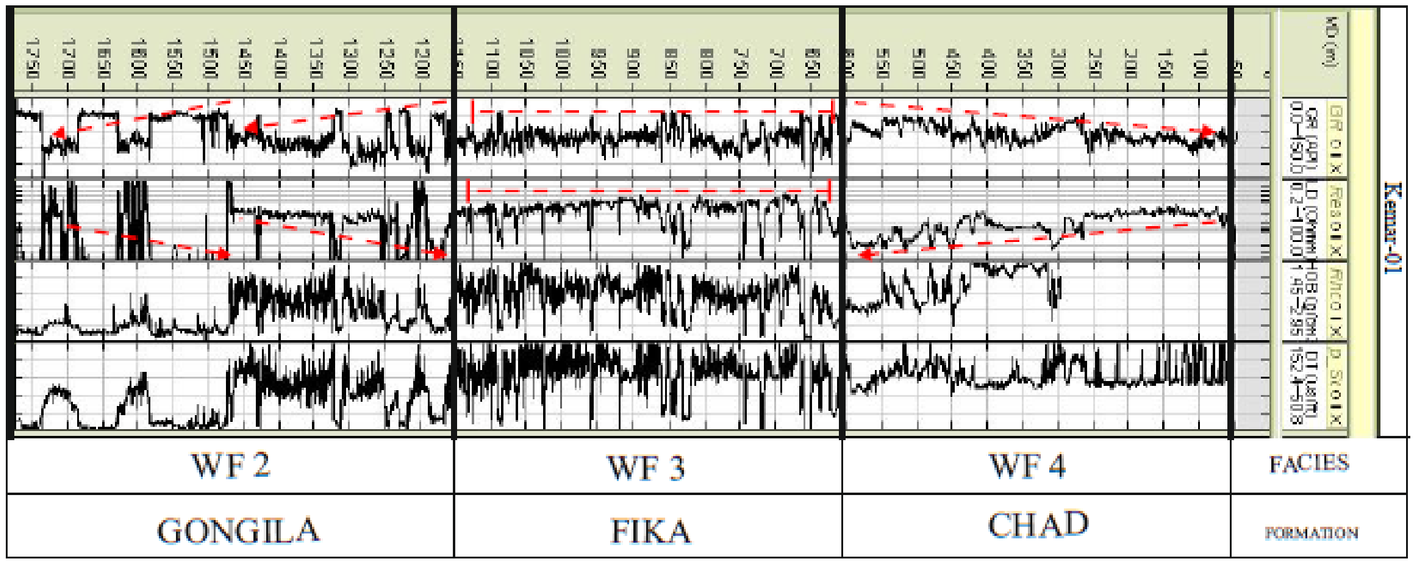
Kemar-01
WF 2
WF 3
WF 4
FACIES
GONGILA
FIKA
CHAD
FORMATION

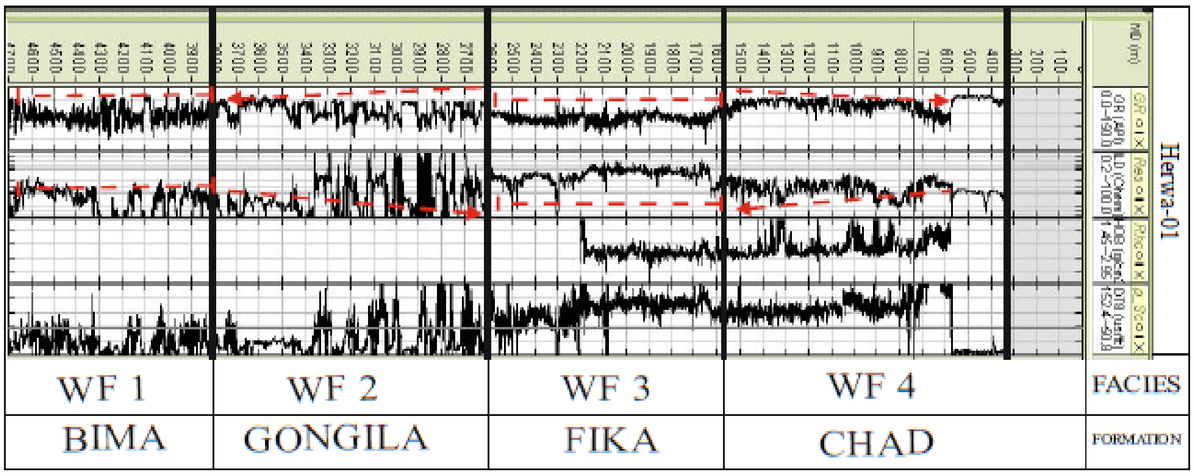
Herwa-01
WF 1
WF 2
WF 3
WF 4
FACIES
BIMA
GONGILA
FIKA
CHAD
FORMATION

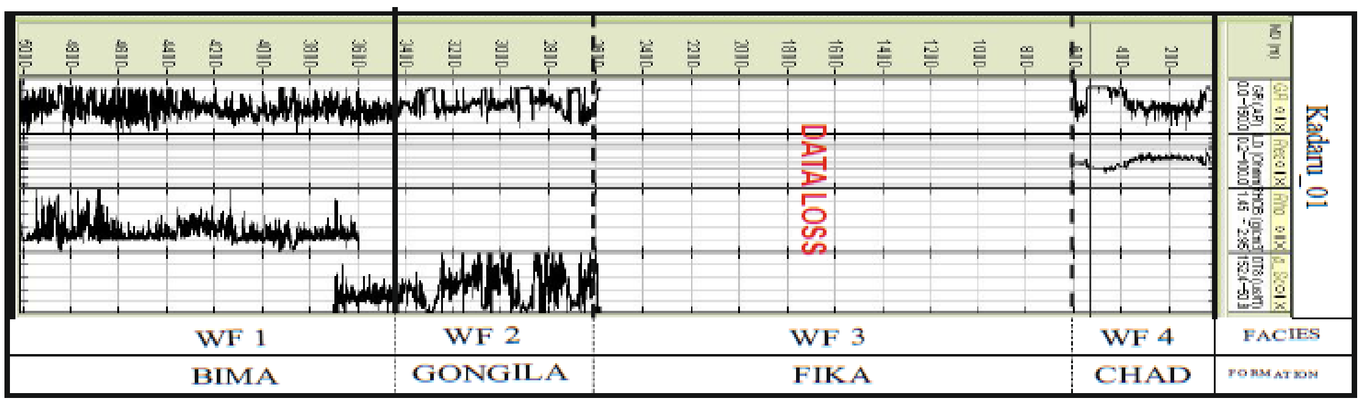
Kadaru_01
DATA LOSS
WF 1
WF 2
WF 3
WF 4
FACIES
BIMA
GONGILA
FIKA
CHAD
FORMATION

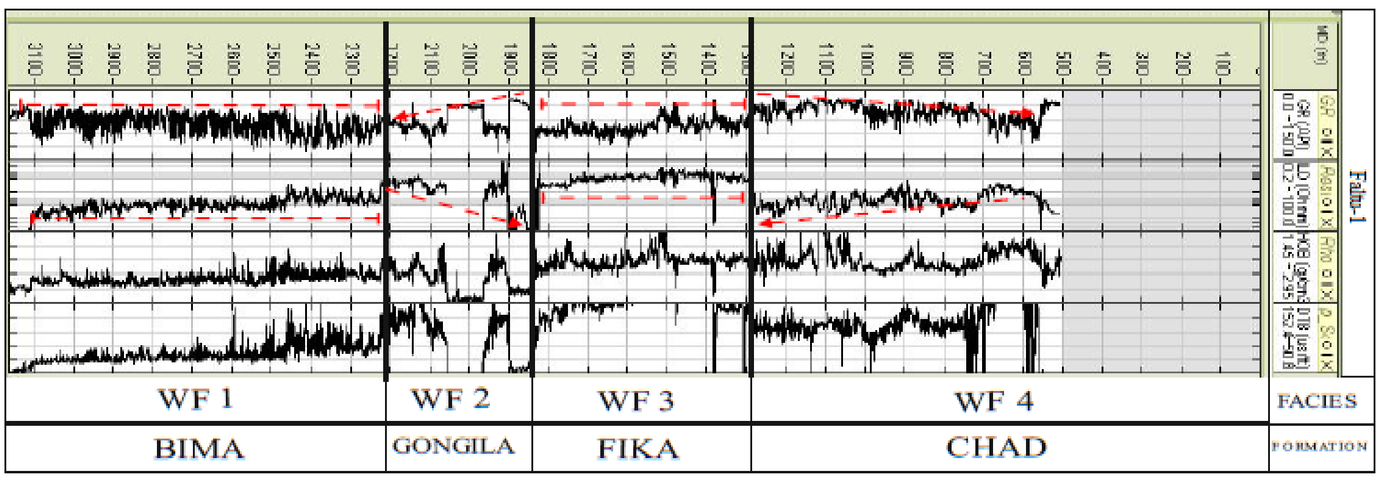
Faibu-1
WF 1
WF 2
WF 3
WF 4
FACIES
BIMA
GONGILA
FIKA
CHAD
FORMATION

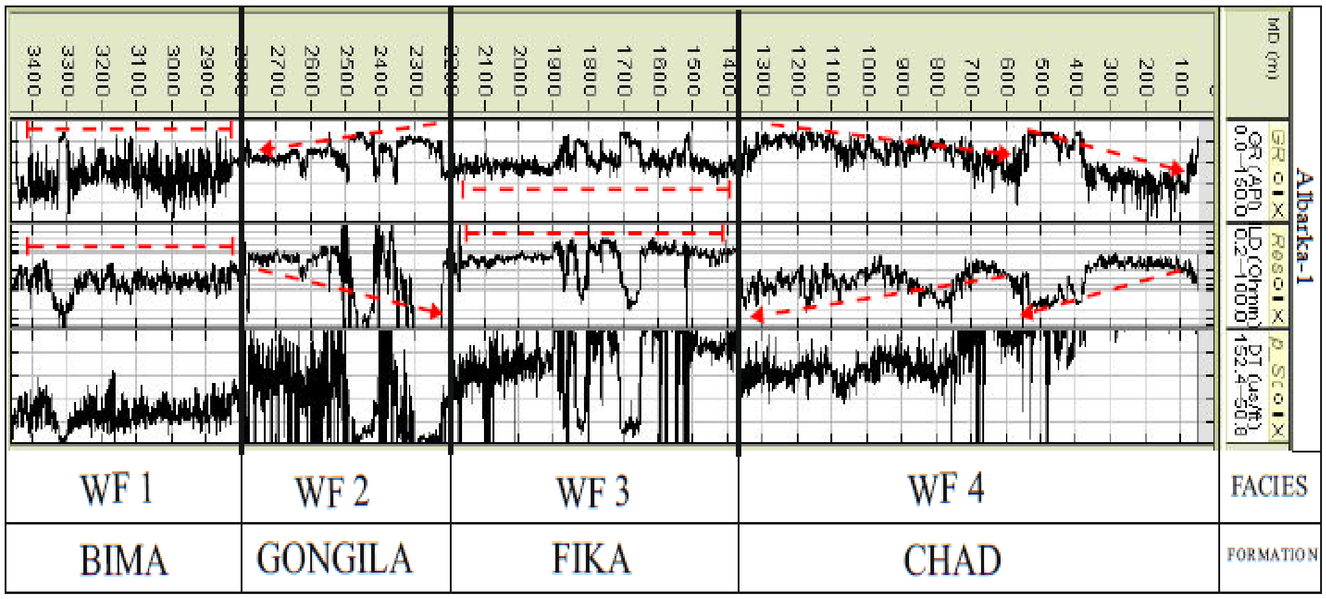
Albarka-1
MD (m)
GR (API)
0.0 - 150.0
ILD (Ohmm)
0.2 - 1000
DT (us/ft)
152.4 - 50.8
WF 1
WF 2
WF 3
WF 4
FACIES
BIMA
GONGILA
FIKA
CHAD
FORMATION

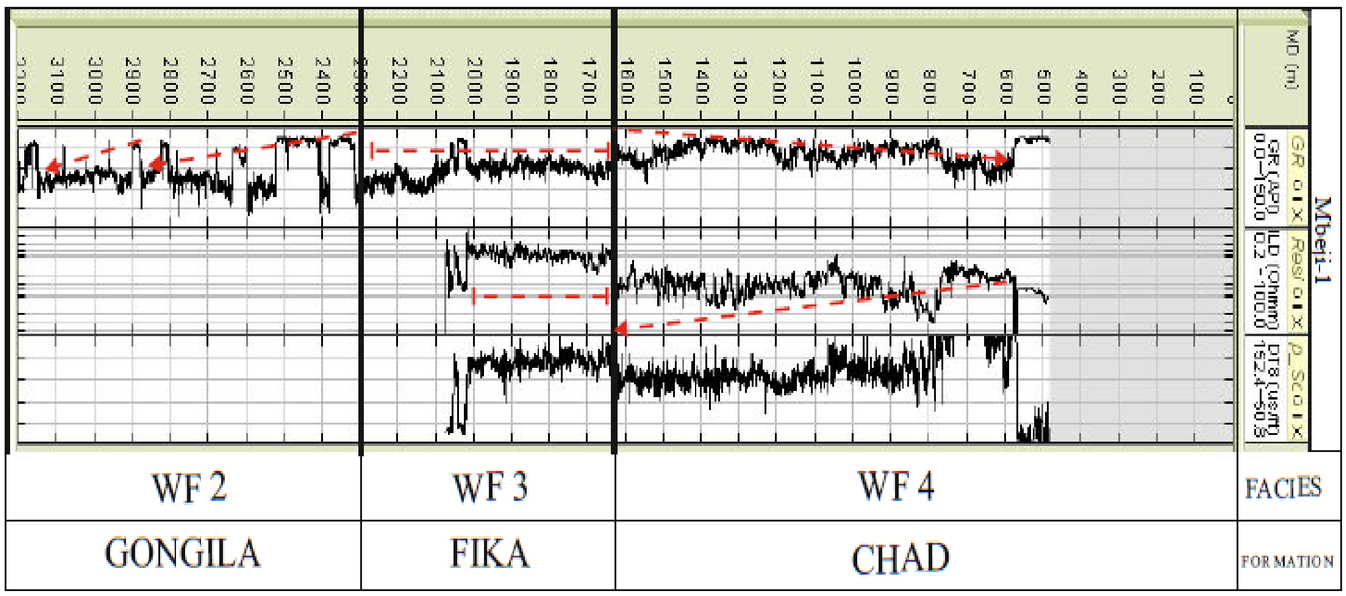
Mberi-1
MD (m)
GR (API)
0.0 - 150.0
ILD (Ohmm)
0.2 - 1000
DT (us/ft)
152.4 - 50.8
WF 2
WF 3
WF 4
FACIES
GONGILA
FIKA
CHAD
FORMATION

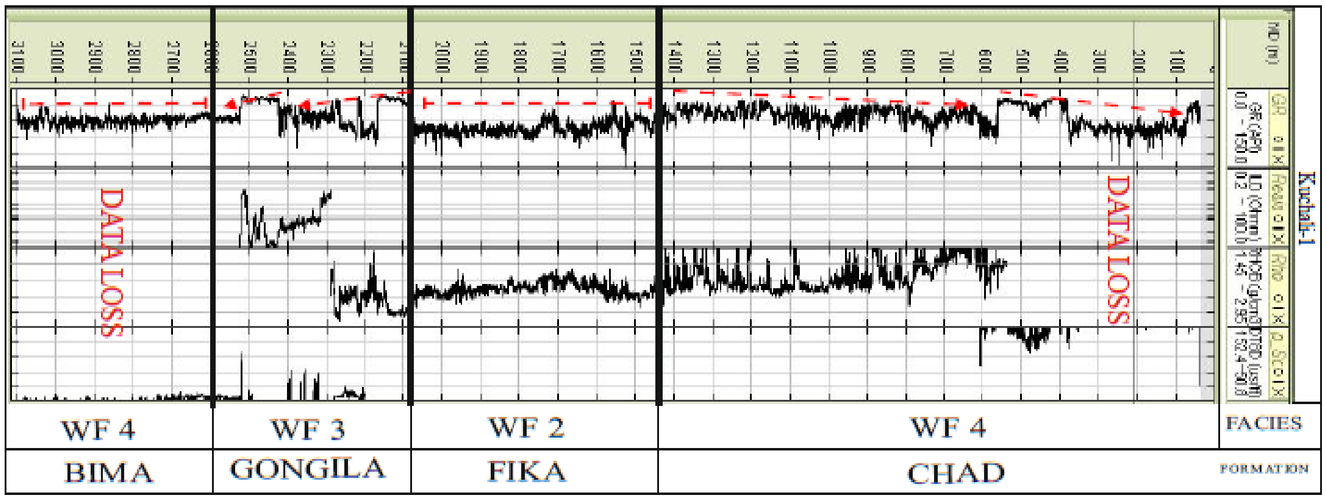
Kuchali-1
MD (m)
DATA LOSS
DATA LOSS
WF 4
WF 3
WF 2
WF 4
FACIES
BIMA
GONGILA
FIKA
CHAD
FORMATION

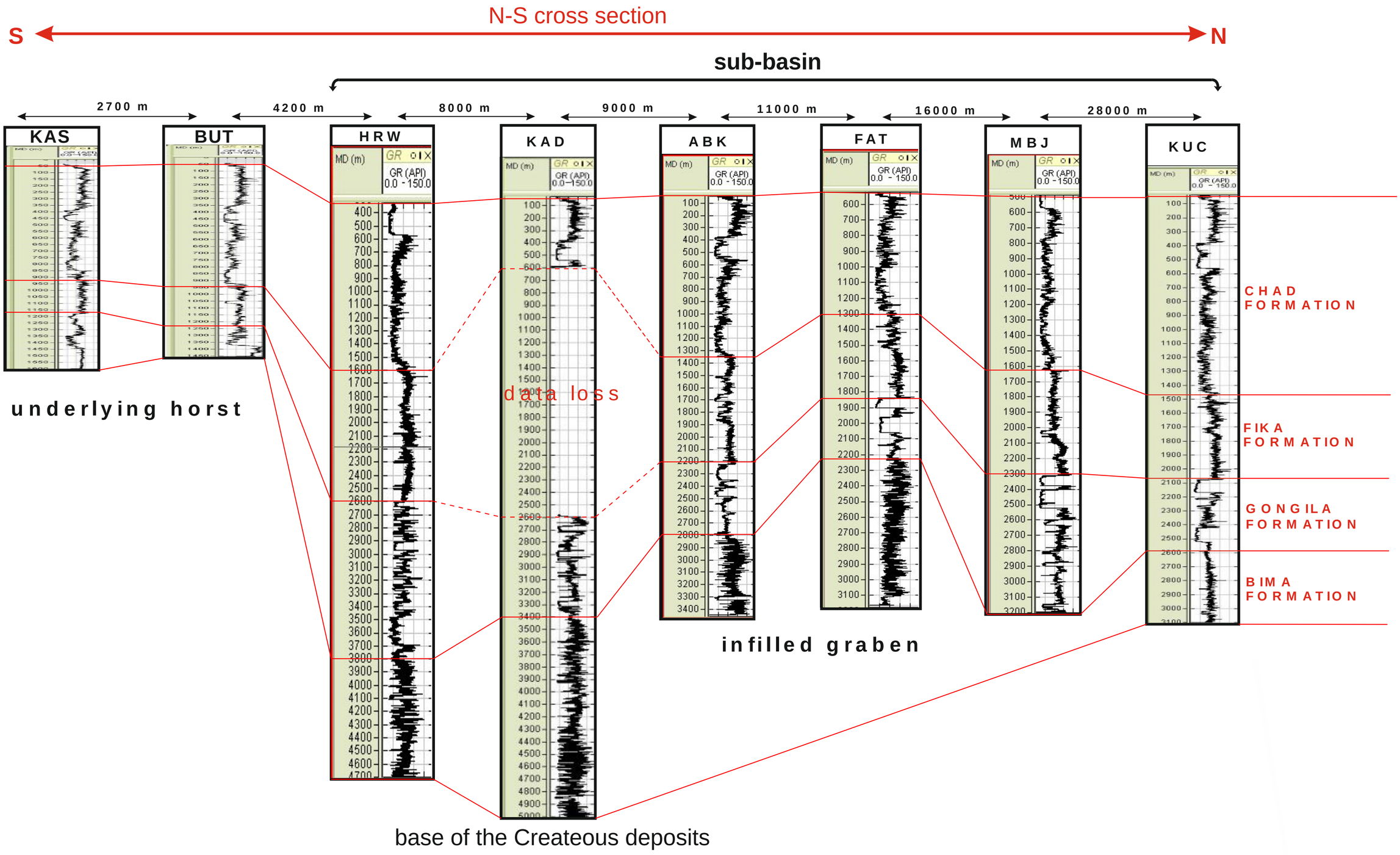

Figure 5.4. N–S oriented cross section of wells as shown in Figure 5.1, showing interpreted subsurface stratigraphic correlation and basin structure. Wells Abbreviations: KAS (Kasade), BUT (Bulte), HRW (Herwa), KAD (Kadaru), ABK (Albarka), FAT (Faltu), MBJ (Mbeji), KUC (Kuchalli) wells.

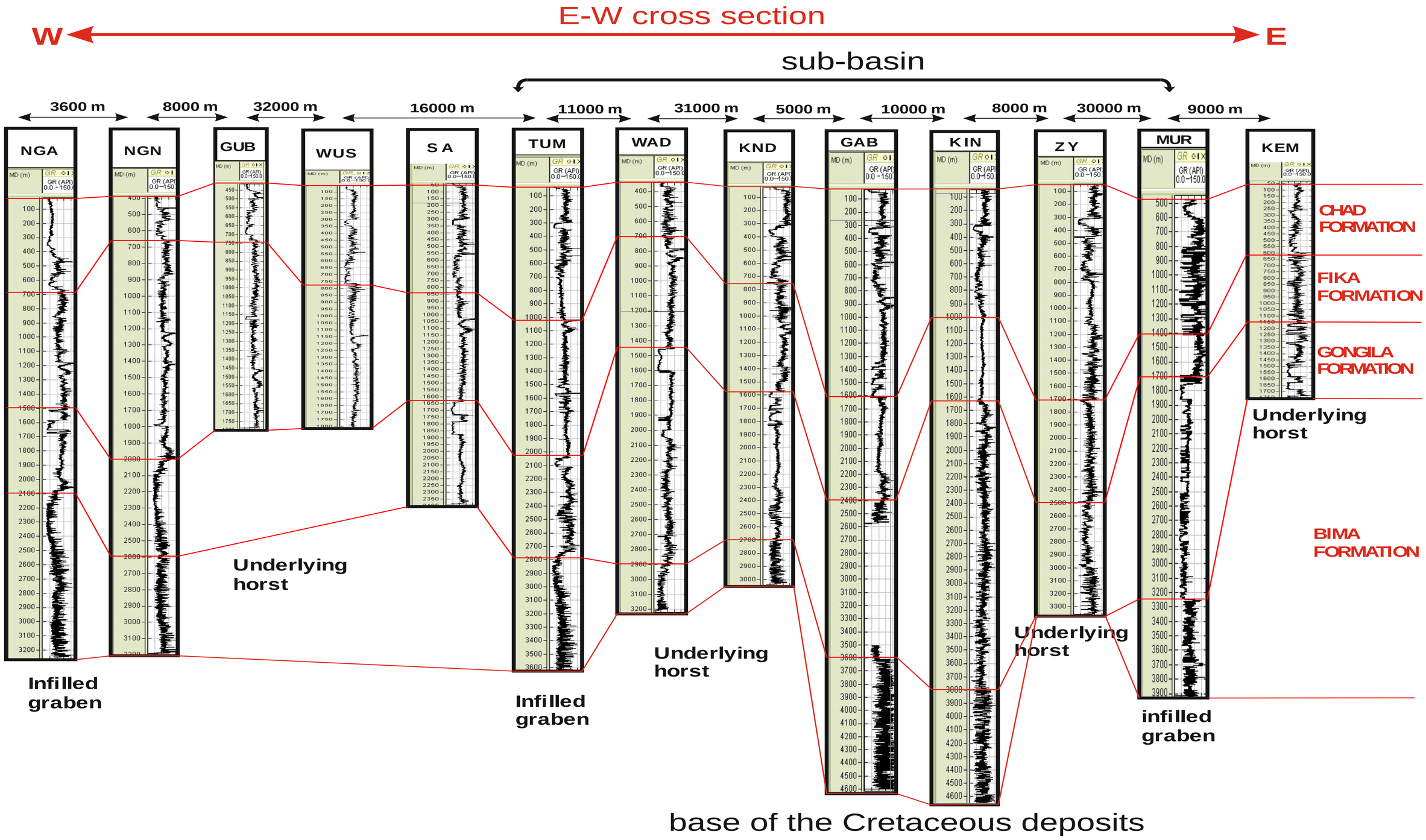

Figure 5.5. W-E oriented cross section of wells as shown in Figure 5.1, showing stratigraphic correlation and basin structure. Wells abbreviations: NGA (Ngammaeast), NGN (Ngornorth), GUB (Gubio), WUS (Wushe), SA (Sa), TUM (Tuma), (WAD (Wadi), KND (Kanadi), (GAB (Gaibu), KIN (Kinasar), ZY (Ziye) MUR (Murshe), KEM (Kemar).

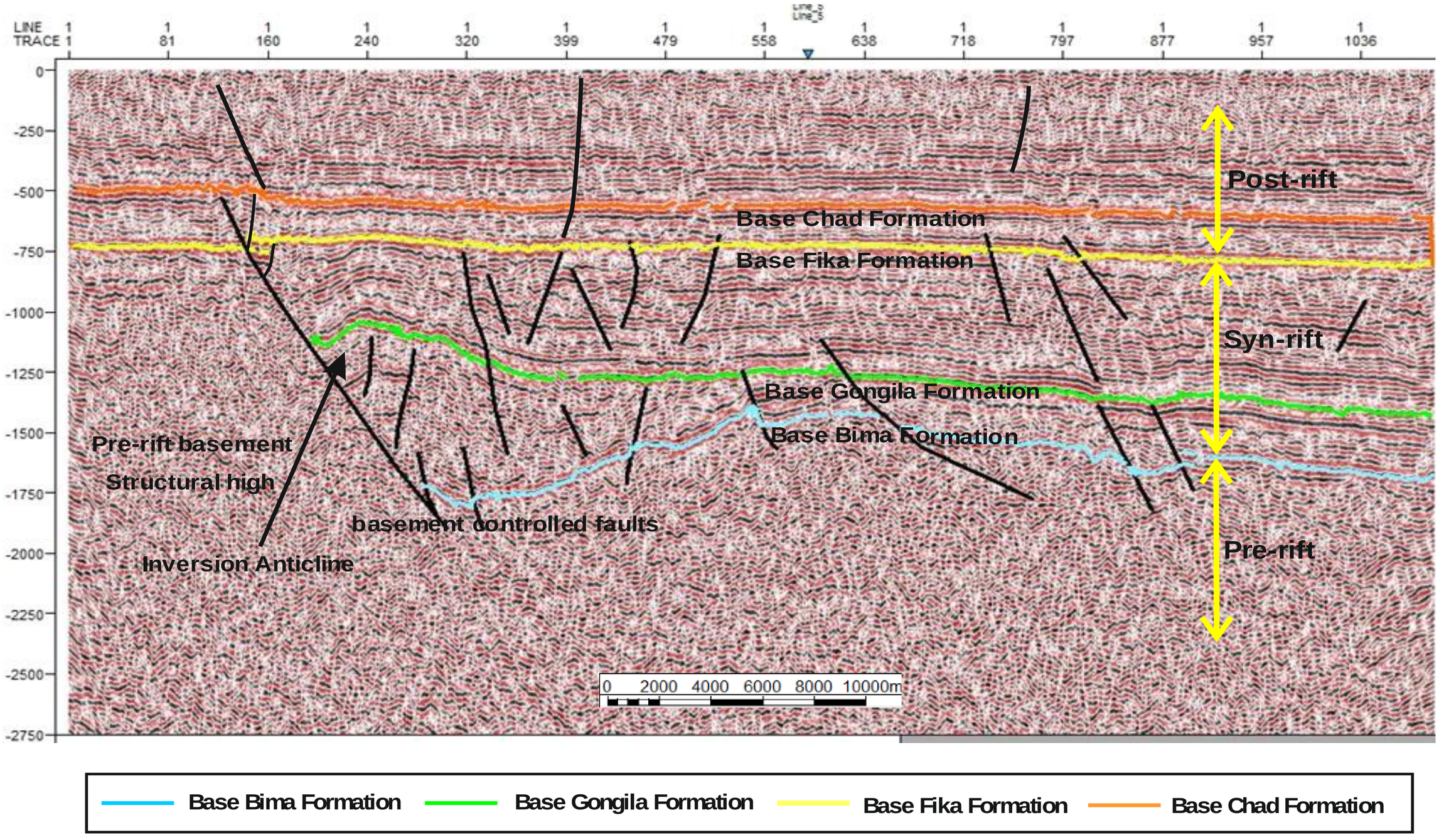

Fig 5.16: Interpreted seismic line 15 showing the structure and stratigraphy from pre-rift to post rift sedimentation. The main down-to-the-basin faults tending listric with depth and forming numerous synthetic and antithetic faults are indicated. Seismic section shows a “classic” rift geometry with simple extensional rollover anticlinal structure. Even where obvious, the compressional overprint is generally subtle compared to the extensional fault geometry,

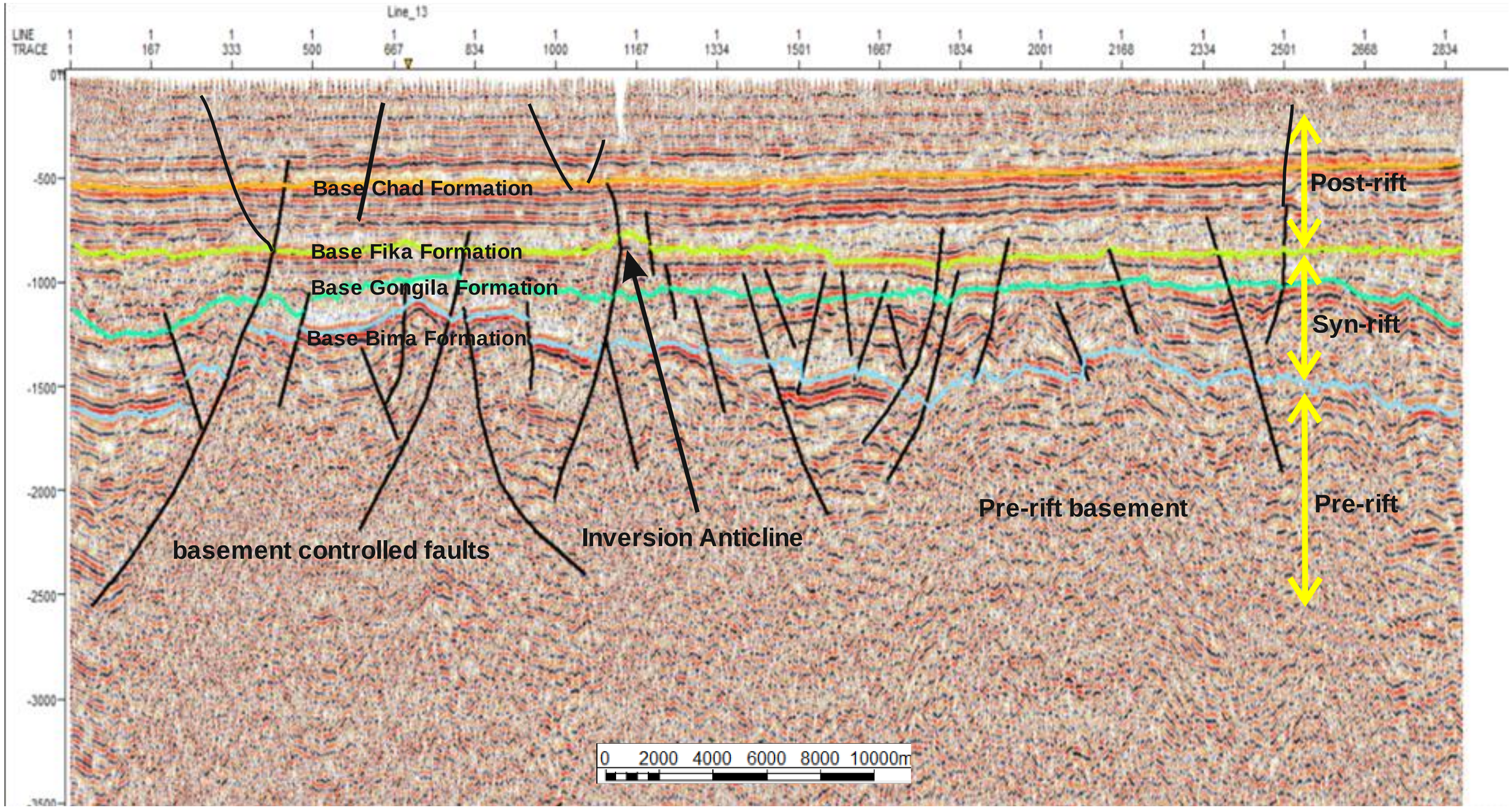

Fig 5.18: Interpreted seismic line 8 showing the structure and stratigraphy from pre-rift to post rift sedimentation. The main down-to-the-basin faults tending listric with depth and forming numerous synthetic and antithetic faults are indicated.

APPENDIX C: GRAVITY AND MAGNETIC

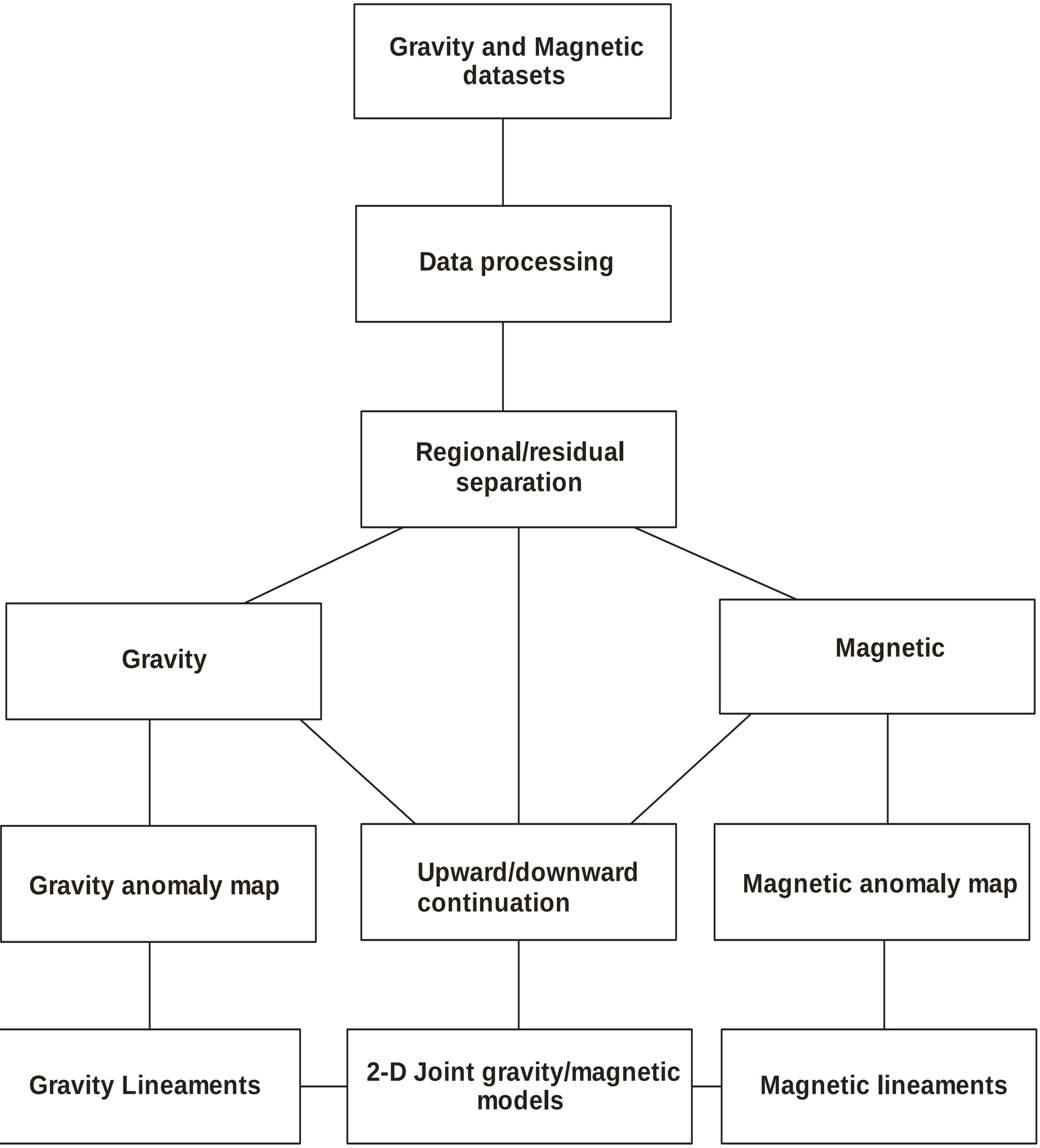

Workflow for the combined gravity and magnetic data analysis

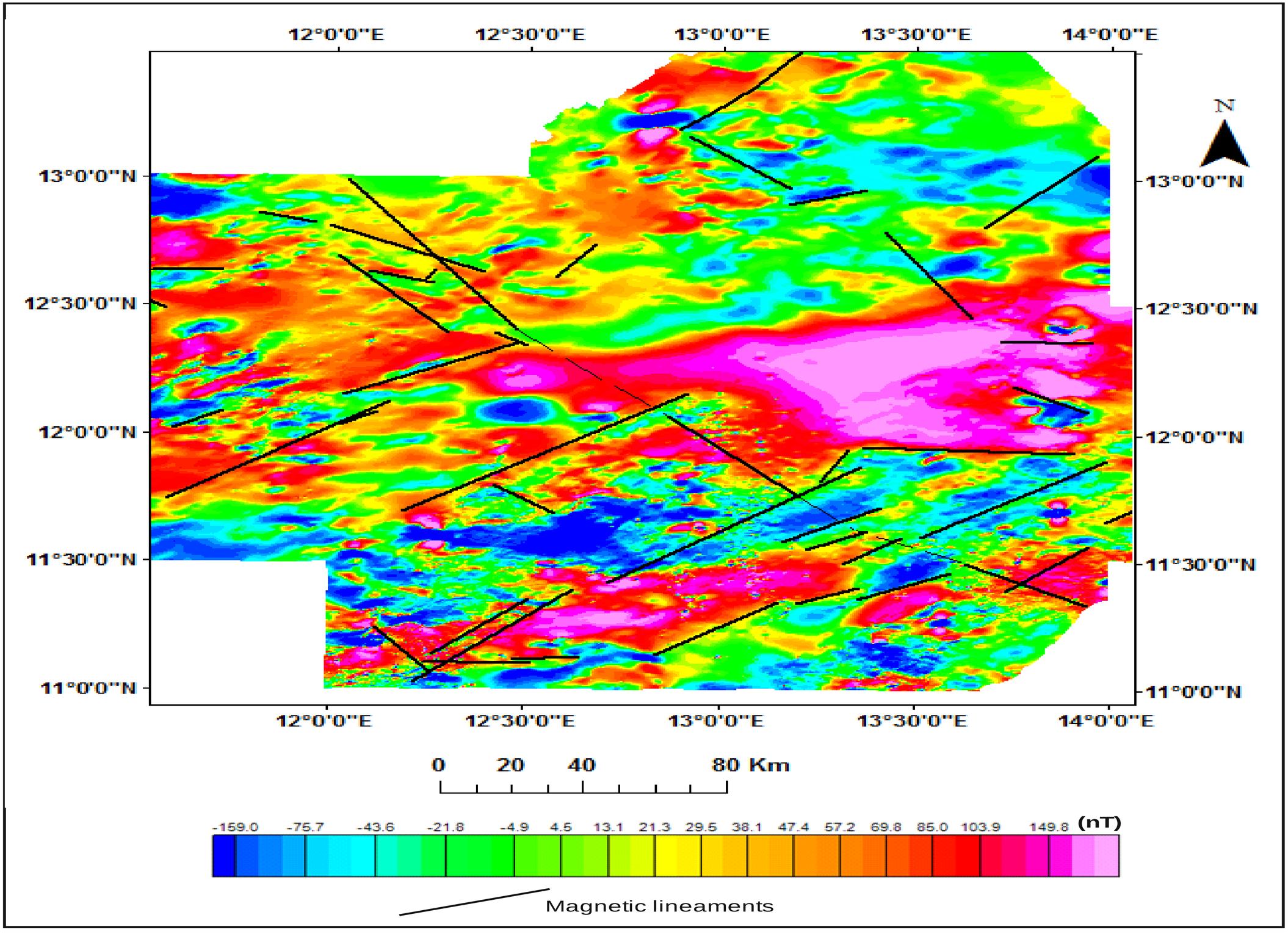

Fig. 6.11. Principal lineaments from magnetic map of the north-eastern Bornu Basin. Rose diagram fig 6.9 shows the trends of the lineament in the north-eastern Bornu basin

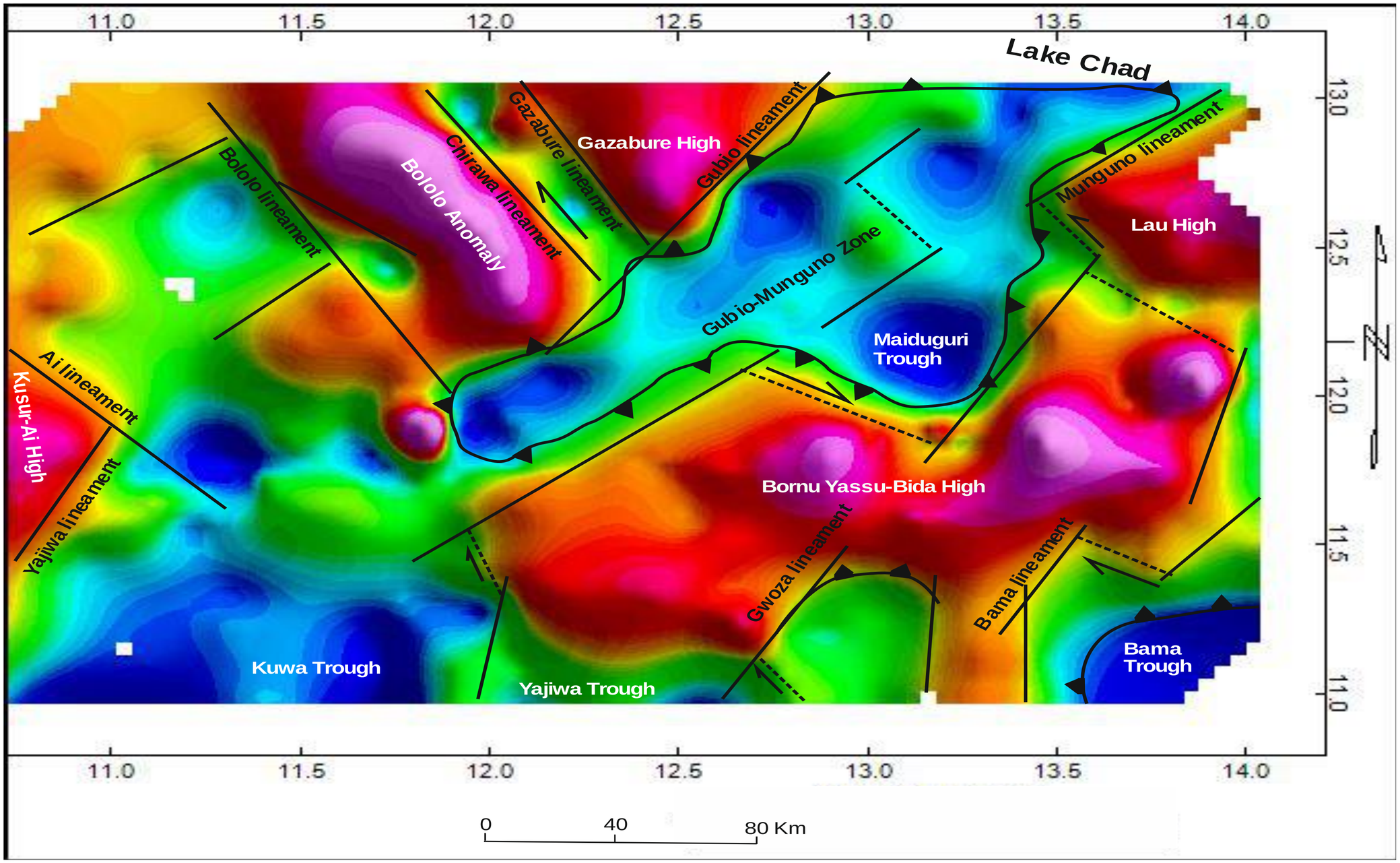

Fig 6.12. Gravity (basement) lineaments showing the main NE-SW normal faults in relation with the NW-SE faults forming transfer faults similar to the surface structural architecture.

Gravity lineaments metadata

1	2	3	4	Bearing	Length	Midpoint-X		Midpoint-Y	
XY_UTM_METERS		XY_UTM_METERS		XY_UTM_METERS		XY_UTM_METERS	TEXT	LINEAR_METERS	XY_UTM_METERS
330545.626652	1344189.873283	309114.33379	1306883.548671	210	43024.0	319829.98	1325536.71		
243970.096222	1256759.362469	299706.300023	1298559.217165	53	69668.9	271838.2	1277659.29		
249053.797002	1332759.850423	197195.359952	1298363.948298	236	62228.4	223124.58	1315561.9		
386990.183986	1339868.336862	364514.051122	1350555.517685	295	24887.6	375752.12	1345211.93		
174790.251648	1263131.916752	198294.548349	1227981.431572	146	42284.9	186542.4	1245556.67		
187770.386675	1440524.361525	196501.654137	1424252.453981	152	18466.5	192136.02	1432388.41		
196501.654137	1424252.453981	210789.182712	1395677.396831	153	31947.9	203645.42	1409964.93		
210789.182712	1395677.396831	227061.090256	1375436.73135	141	25970.4	218925.14	1385557.06		
227061.090256	1375436.73135	241745.494625	1357180.444837	141	23429.1	234403.29	1366308.59		
241745.494625	1357180.444837	254048.644231	1342099.164675	141	19463.1	247897.07	1349639.8		
254048.644231	1342099.164675	273495.558125	1326224.132925	129	25103.8	263772.1	1334161.65		
273495.558125	1326224.132925	290958.09305	1307967.846412	136	25263.3	282226.83	1317095.99		
290958.09305	1307967.846412	313580.013294	1292092.814662	125	27636.4	302269.05	1300030.33		
313580.013294	1292092.814662	332630.051394	1280980.292437	120	22054.3	323105.03	1286536.55		
332630.051394	1280980.292437	347314.455763	1271058.397593	124	17722.2	339972.25	1276019.35		
347314.455763	1271058.397593	363983.2391	1257961.496399	128	21198.5	355648.85	1264509.95		
363983.2391	1257961.496399	361851.895159	1259277.517893	302	2504.9	362917.57	1258619.51		
217324.404116	1304438.683538	233675.686819	1289992.404645	131	21818.8	225500.05	1297215.54		
157219.622144	1336417.123829	210446.376327	1361168.406814	65	58700.2	183833.0	1348792.77		
175139.368043	1332547.353568	188246.569974	1339812.654665	61	14986.1	181692.97	1336180.0		
176170.231452	1410899.610083	201191.245972	1377485.926746	143	41743.6	188680.74	1394192.77		
387624.195359	1278964.955481	364499.127408	1261526.493962	233	28963.2	376061.66	1270245.72		
385920.80821	1365398.378182	356514.901299	1368176.124682	275	29536.8	371217.85	1366787.25		
375121.06445	1439252.505222	331613.538227	1398743.755821	227	59446.3	353367.3	1418998.13		
315079.692659	1256320.467502	341538.078909	1272195.499252	59	30855.5	328308.89	1264257.98		
240622.776774	1257394.794	212894.387984	1232841.41156	228	37036.9	226758.58	1245118.1		
361807.33783	1368227.401511	335666.452215	1404634.140992	324	44819.6	348736.9	1386430.77		
339532.884108	1280252.959431	389274.650258	1311473.855206	58	58728.1	364403.77	1295863.41		
245431.881901	1231712.469975	195726.802755	1231821.474293	270	49705.2	220579.34	1231766.97		
163437.342912	1330878.50164	162445.153428	1281930.487078	181	48958.1	162941.25	1306404.49		
147562.311162	1387102.572422	159137.855147	1307396.683843	172	80542.1	153350.08	1347249.63		
296126.149957	1391468.206153	282632.372969	1367655.658528	210	27370.0	289379.26	1379561.93		
170583.312065	1417714.925313	196195.029956	1419831.596213	85	25699.0	183389.17	1418773.26		
298186.503002	1427623.564466	315119.870202	1410690.197266	135	23947.4	306653.19	1419156.88		
250958.283546	1404406.330531	272588.014305	1377815.65235	141	34277.0	261773.15	1391110.99		
326364.684359	1430203.257125	326364.684359	1430004.819228	180	198.4	326364.68	1430104.04		
316951.97725	1437442.389562	307757.688029	1421633.503778	210	18288.1	312354.83	1429537.95		
334718.919817	1440062.313302	327178.279736	1431331.045839	221	11536.7	330948.6	1435696.68		
325236.234185	1438006.49669	325077.483867	1428481.47764	181	9526.3	325156.86	1433243.99		

Magnetic lineaments data

1 2 3 4 Bearing Length Midpoint-X Midpoint-Y

XY_UTM_METERS	XY_UTM_METERS	XY_UTM_METERS	XY_UTM_METERS	TEXT	LINEAR_METERS	XY_UTM_METERS
279962.924793	1467091.447645	291869.198605	1478005.531974	47	16151.7	285916.06	1472548.49
291869.198605	1478005.531974	302121.823277	1490242.535614	40	15964.4	296995.51	1484124.03
302121.823277	1490242.535614	304767.661902	1493219.104067	42	3982.5	303444.74	1491730.82
273816.641667	1456473.697243	302180.031727	1434036.985703	128	36164.7	287998.34	1445255.34
176382.702023	1345499.023253	225426.458081	1367646.280005	66	53812.6	200904.58	1356572.65
192965.32545	1294844.376589	273322.548794	1345547.030977	58	95016.0	233143.94	1320195.7
263328.096384	1232171.074159	298385.458165	1254991.4323	57	41830.5	280856.78	1243581.25
385069.746117	1279002.417822	361851.895159	1259277.517893	230	30465.4	373460.82	1269139.97
250414.723537	1263120.726716	321521.636584	1313391.660591	55	87082.5	285968.18	1288256.19
267634.198746	1335881.058055	304146.771771	1300426.820479	134	50893.7	285890.49	1318153.94
178180.5997	1438336.418347	225170.69368	1373407.538489	144	80148.8	201675.65	1405871.98
247309.748375	1409946.569901	236064.934219	1395725.187291	218	18129.9	241687.34	1402835.88
317828.299405	1320597.836563	310353.900062	1307305.096767	209	15250.0	314091.1	1313951.47
328140.03432	1415308.137446	352871.653943	1377585.317678	147	45107.3	340505.84	1396446.73
184850.042292	1244649.620817	200328.198249	1225520.207559	141	24607.1	192589.12	1235084.91
235898.191264	1293484.91163	218435.656339	1306026.186713	306	21499.4	227166.92	1299755.55
240716.92486	1260696.632078	195980.667032	1220888.046043	228	59883.7	218348.8	1240792.34
175306.798776	1332414.498955	186025.40098	1338157.250975	62	12160.1	180666.1	1335285.87
363971.277705	1348112.218802	385190.88376	1336803.964791	118	24044.7	374581.08	1342458.09
223718.679492	1230488.816888	242345.383412	1231335.485248	87	18645.9	233032.03	1230912.15
200698.562828	1232479.224488	228241.742914	1256291.772113	49	36409.7	214470.15	1244385.5
175117.314045	1405410.266745	206174.346349	1372149.186988	137	45506.5	190645.83	1388779.73
386334.764173	1366695.445057	360873.223455	1367984.636992	273	25494.2	373603.99	1367340.04
356269.464247	1416895.168841	388019.527747	1448248.356547	45	44621.6	372144.5	1432571.76
346505.640928	1267393.302148	320311.83854	1256201.404764	247	28484.6	333408.74	1261797.35
198388.687965	1229380.213665	202357.445903	1229314.067699	91	3969.3	200373.07	1229347.14
202357.445903	1229314.067699	208575.166672	1229115.629803	92	6220.9	205466.31	1229214.85
208575.166672	1229115.629803	228767.545598	1228805.405224	91	20194.8	218671.36	1228960.52
337813.089002	1282700.360159	390102.489915	1315806.667246	58	61888.7	363957.79	1299253.51
384580.296987	1252907.488188	350363.870915	1271531.766756	299	38956.7	367472.08	1262219.63
443285.599658	1285461.413844	408757.405601	1289231.733885	276	34733.4	426021.5	1287346.57
303307.507201	1254425.726773	321166.91792	1261093.240108	70	19063.4	312237.21	1257759.48
316086.90776	1271094.510111	332835.066257	1282762.658447	55	20411.9	324460.99	1276928.58
306085.637758	1277682.648287	323389.422365	1285699.539321	65	19070.7	314737.53	1281691.09
299576.87474	1281254.530431	327437.555461	1296018.309958	62	31530.7	313507.22	1288636.42
389885.961608	1289013.452199	427390.724118	1314810.378792	55	45520.2	408638.34	1301911.92
127034.57219	1300224.642156	189740.947603	1342293.476293	56	75510.8	158387.76	1321259.06
219317.0137	1371865.132659	228101.197935	1366150.121229	123	10479.7	223709.11	1369007.63
119304.313674	1388639.749541	126765.578597	1382607.237476	129	9594.9	123034.95	1385623.49
173279.421624	1418421.309105	216300.757667	1398101.268464	115	47578.8	194790.09	1408261.29
199314.473694	1394026.676982	202595.313589	1399106.687142	33	6047.3	200954.89	1396566.68
123220.154839	1399437.41697	142905.194209	1399331.583425	90	19685.3	133062.67	1399384.5
381404.615653	1319166.200872	322270.122384	1321944.331428	273	59199.7	351837.37	1320555.27
128935.827729	1331308.836268	142826.48051	1338293.850238	63	15548.0	135881.15	1334801.34
183793.98432	1398558.612695	202050.270833	1393637.352853	105	18908.0	192922.13	1396097.98
169360.934621	1419936.988785	152956.735146	1424170.330585	284	16941.6	161158.83	1422053.66
301820.435651	1427424.712094	322987.144651	1433245.557069	75	21952.5		

APPENDIX D: Integrated data analysis work flow

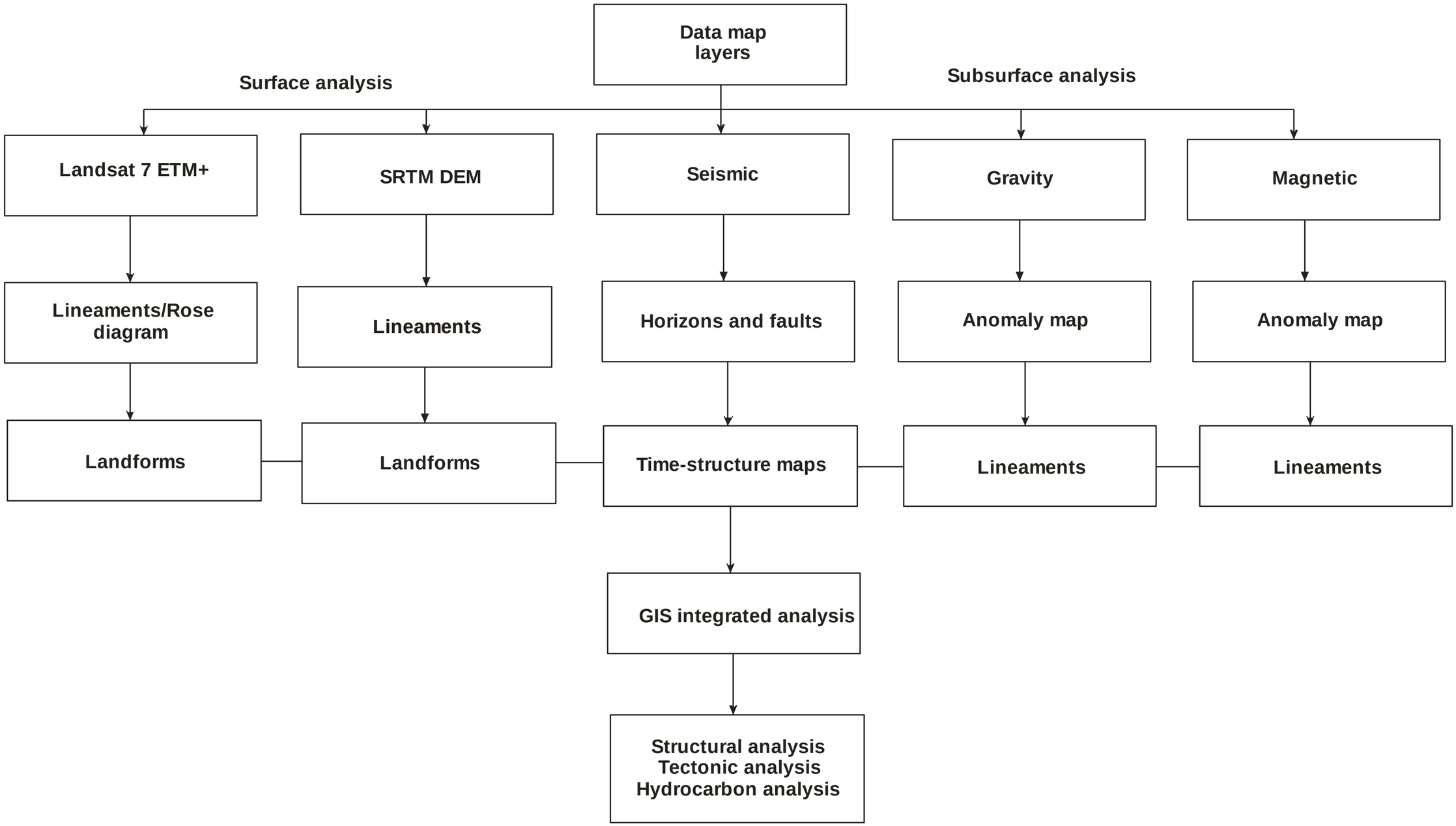

Workflow for the integrated data analysis

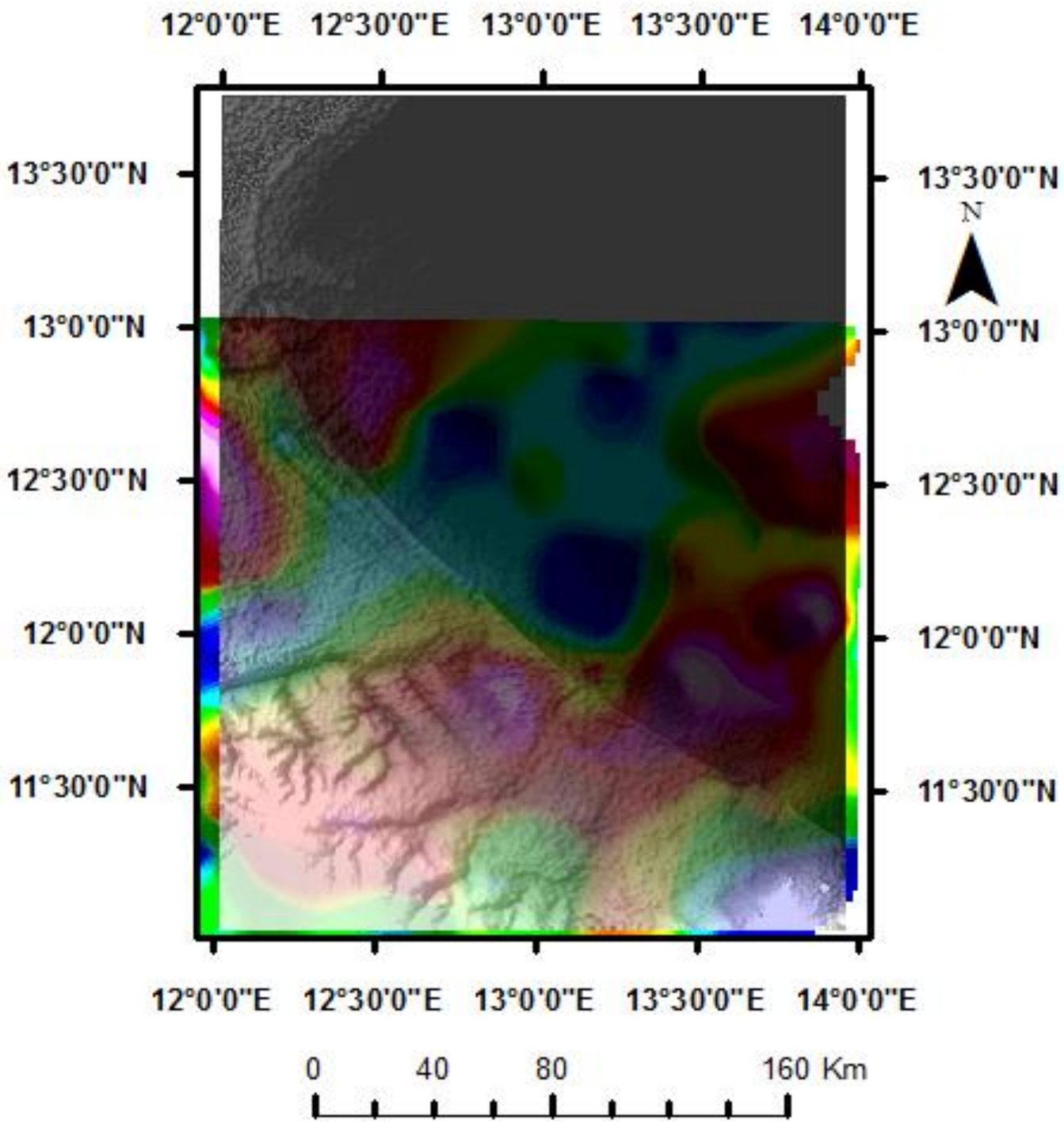

Fig. (7.3 a): (a) SRTM Dem hillshade overlain on gravity anomaly map in GIS showing alignment of the NW-SE trending Bama Beach Ridge with basement structural setting

FORM UPR16

Research Ethics Review Checklist

Please include this completed form as an appendix to your thesis (see the Postgraduate Research Student Handbook for more information

Postgraduate Research Student (PGRS) Information			**Student ID:**	472846
PGRS Name:	AMINU ISYAKU ABDULLAHI			
Department:	SEES	**First Supervisor:**	DR DEREK RUST	
Start Date: (or progression date for Prof Doc students)		**SEPTEMBER 2012**		
Study Mode and Route:	Part-time ☐ Full-time ☒	MPhil ☐ PhD ☒	MD ☐ Professional Doctorate ☐	

Title of Thesis:	Lithostratigraphy and tectonic evolution of the north- eastern Bornu basin, from integrated surface and subsurface interpretation
Thesis Word Count: (excluding ancillary data)	49,188

If you are unsure about any of the following, please contact the local representative on your Faculty Ethics Committee for advice. Please note that it is your responsibility to follow the University's Ethics Policy and any relevant University, academic or professional guidelines in the conduct of your study

Although the Ethics Committee may have given your study a favourable opinion, the final responsibility for the ethical conduct of this work lies with the researcher(s).

UKRIO Finished Research Checklist:
(If you would like to know more about the checklist, please see your Faculty or Departmental Ethics Committee rep or see the online version of the full checklist at: http://www.ukrio.org/what-we-do/code-of-practice-for-research/)

a) Have all of your research and findings been reported accurately, honestly and within a reasonable time frame?	YES ☒ NO ☐
b) Have all contributions to knowledge been acknowledged?	YES ☒ NO ☐
c) Have you complied with all agreements relating to intellectual property, publication and authorship?	YES ☒ NO ☐
d) Has your research data been retained in a secure and accessible form and will it remain so for the required duration?	YES ☒ NO ☐
e) Does your research comply with all legal, ethical, and contractual requirements?	YES ☒ NO ☐

Candidate Statement:

I have considered the ethical dimensions of the above named research project, and have successfully obtained the necessary ethical approval(s)

Ethical review number(s) from Faculty Ethics Committee (or from NRES/SCREC):	None

If you have *not* submitted your work for ethical review, and/or you have answered 'No' to one or more of questions a) to e), please explain below why this is so:

Signed *(PGRS)*:	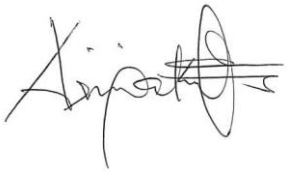	**Date:** 12/09/18